Bond Behaviour and Tension Stiffening of Flat Stainless Steel Rebars with Continuous or Alternate Rib Pattern Embedded in Concrete

Aanhechtingsgedrag en 'tension stiffening' van inoxen wapeningsstrippen met uniforme of wisselende ribconfiguratie in beton

Dorleta Ertzibengoa Gaztelumendi

Promotor: prof. dr. ir. S. Matthys
Proefschrift ingediend tot het behalen van de graad van
Doctor in de Ingenieurswetenschappen: Bouwkunde

Vakgroep Bouwkundige Constructies
Voorzitter: prof. dr. ir. L. Taerwe
Faculteit Ingenieurswetenschappen en Architectuur
Academiejaar 2012 - 2013

UNIVERSITEIT
GENT

ISBN 978-90-8578-545-3
NUR 955
Wettelijk depot: D/2012/10.500/71

Supervisor

Prof. dr. ir. Stijn Matthys

Research Institute

Magnel Laboratory for Concrete Research
Department of Structural Engineering
Faculty of Engineering and Architecture
Ghent University, Belgium

Other members of the examination committee

Prof. dr. ir. Geert De Schutter (secretary)
Ghent University – Faculty of Engineering and Architecture

Ir. Laurent Faivre
Aperam Isbergues R&D (France)

Prof. dr. ir. Marisa Pecce
Università del Sannio (Italy) – Faculty of Engineering

Prof. dr. ir. Luc Taerwe (chairman)
Ghent University – Faculty of Engineering and Architecture

Prof. dr. ir. Philippe Van Bogaert
Ghent University – Faculty of Engineering and Architecture

Prof. dr. ir. Joost Walraven
Delft University of Technology (The Netherlands) – Faculty of Civil Engineering and Geosciences

Research funding

This doctoral research project was funded by Aperam Stainless & Electrical Steel Europe (Project number A08-TT-0062 “Bond of flat inox rebars in concrete”)

Did you hear about the rose that grew from a crack in the concrete?
Proving nature's law is wrong it learned to walk without having feet
Funny it seems, but by keeping its dreams, it learned to breathe fresh air
Long live the rose that grew from concrete when no one else ever cared

Tupac Shakur

To Lity and Achike

Aitatxo eta Amatxori

Acknowledgements

It has been a long journey... not always easy but certainly challenging journey with this book as final destination. A journey that would not have been possible without the support and contribution of several people. First of all, I am very grateful to my supervisor Prof. Stijn Matthys for his support, guidance and trust during all my doctoral research. I so much appreciate his always smart suggestions and the useful discussions we had related to the research topic. I would also like to thank Prof. Luc Taerwe, director of the Magnel Laboratory for Concrete research, who gave me the opportunity of becoming part of the "Magnel Team". I would like to acknowledge Aperam Stainless & Electrical Steel Europe (represented by Aperam Isbergues R&D) for the financial support to this project. I am also grateful to Matière® for their collaboration in the project and in developing the alternate rib pattern in flat reinforcement members. Special thanks as well to Ir. Gonzalo De Dios for his collaboration in the development of the finite element model.

With respect to the experimental work, I am very grateful to the technical staff of the Magnel Laboratory who contributed and assisted during the testing program. Without them this work would have not been possible. My thank words as well to the members of the Structural Research Group for their always useful suggestions and collaborations. Special acknowledgments to Marijke, Christel and Viviane: thank you for your friendly and unconditional help. To other members of the "Magnel Team": thanks so much for making this experience so unique.

For their support and encouragement in a more personal way, I would like to thank my family and close friends. Pantxike eta Maite, mila esker laguntasunak distantziarik ez duela erakusteagatik: benetan gertu sentitu zaituztet. To the Gentse Corralito Units, thanks so much for making me feel at home in the distance. Laura, moitas grazas pola túa amizade e apoio, e por ensinarme que "compartir es vivir"! I am infinitely grateful to my parents and my brother for their unconditional support, not only with this project but also during my entire life. Aitatxo eta Amatxo, mila esker beti nire ondoan izateagatik, zuen babesagatik eta bizitza honetan exenplu izateagatik. Oso harro nago zuetaz. Maite zaituztet. Haritz eta Txell, mila esker, moltes gràcies, momentu garrantzitsuenetan laguntzeko prest eta "hor" egoteagatik. Us estimo molt. To the rest of my family in the Basque Country, eskerrik asko zuen maitasunagatik. And to my family in Nigeria, thank you so much, dalu, for your warm welcome and love.

Finally, special words to Lity and Achike. Lity, thanks so much for your endless support and encouragement. You know that this book is also yours. And thank you so much for your love and for sharing your life with me, for showing me that there is another way of looking at life, that each day "*a new day has come*" and that "*everything has solution*". Afurunginanya nkem. And to Achike, thanks for allowing mama to make her closed defense!! "*It wasn´t easy…but it was worthy*". Thank you for each of your smiles: you make me so happy… Maite zaitut.

Table of contents

List of abbreviations and symbols

1 Abbreviations

2D	*2 dimensional*
3D	*3 dimensional*
AAF	*Alloy adjustment factor*
AASHTO	*American Association of State Highway and Transportation Officials*
ACI	*American Concrete Institute*
AISI	*American Iron and Steel Institute*
ALM	*Automatic laser measurement*
B	*Bar rupture*
CMM	*Classical coverage method*
CR	*Completely ribbed*
CS	*Carbon steel*
EC2	*Eurocode 2*
EXP	*Experimental*
FE	*Finite element*
FEM	*Finite element model*
HSHC	*High strength high chromium*
k	*Characteristic*
LCC	*Life cycle cost*
LVDT	*Linear variable data transducer*
MC2010	*Model Code 2010*
MC90	*Model Code 1990*
PO	*Pull out failure*
R	*Ribbed*
RC	*Reinforced concrete*
REGR	*Regression*
S	*Smooth*
SC	*Splitting of concrete*
SCC	*Self compacting concrete*
SS	*Stainless steel*
TC	*Traditional concrete*
UV	*Ultra violet*

2 Symbols

Roman letters

a	*Side length of a flat reinforcement*	mm
A_c	*Area of concrete*	mm²
A_{flat}	*Area of a flat reinforcement*	mm²
A_{gt}	*Ultimate elongation*	%
a_m	*Mean rib height*	mm
A_r	*Aspect ratio*	-
A_{round}	*Area of a round reinforcement*	mm²
A_s	*Are of steel reinforcement*	mm²
$a_{s,i}$	*Average rib height of a portion i*	mm
b	*Side length of a flat reinforcement*	mm
c	*Rib spacing*	mm
c_1	*Rib spacing for the first surface configuration level*	mm
$c_{1,ef}$	*Effective rib spacing for the first surface configuration level*	mm
c_2	*Rib spacing for the second surface configuration level*	mm
$c_{2,ef}$	*Effective rib spacing for the second surface configuration level*	mm
c_c	*Concrete cover*	mm
c_m	*Minimum concrete cover*	mm
c_{max}	*Maximum concrete cover*	mm
c_{min}	*Minimum concrete cover*	mm
$c_{min,dur}$	*Minimum concrete cover needed for durability reasons*	mm
$Cr_{equivalent}$	*Chromium equivalent alloying composition of SS*	%
$\mathrm{d}x$	*Differential length of the embedded reinforcement*	mm
d_τ	*Ratio between the standard deviation and the mean value of the bond stress*	-
E_c	*Secant modulus of elasticity of concrete*	N/mm²
e_i	*Average gap between two adjacent rib rows*	mm
E_s	*Modulus of elasticity of steel*	N/mm²
F	*Force*	N
F'/s'_a	*Bond stiffness for the first ascending branch*	kN/mm
F''/s''_a	*Bond stiffness for the second ascending branch*	kN/mm
f_b	*Bond strength*	N/mm²
$f_{b,ref}$	*Reference bond strength*	N/mm²
f_c	*Compressive strength of concrete*	N/mm²
$f_{c,cub150}$	*Compressive strength of concrete determined from compression test to cubes of 150mm side length*	N/mm²
f_{ck}	*Characteristic compressive strength of concrete*	N/mm²
f_{cm}	*Mean compressive strength of concrete*	N/mm²

F_{cr}	*Load at first cracking*	kN
$F_{cr,exp}$	*First cracking load obtained experimentally*	kN
f_{ct}	*Tensile strength of concrete*	N/mm^2
$f_{ct,fl}$	*Flexural tensile strength of concrete*	N/mm^2
$f_{ct,sp}$	*Splitting tensile strength of concrete*	N/mm^2
f_{ctm}	*Mean concrete tensile strength*	N/mm^2
F_{max}	*Maximum measured force*	N
f_R	*Relative ribbed area*	-
F_R	*Area of the longitudinal section of one rib*	mm^2
h	*Rib height*	mm
h	*Narrower side of a flat reinforcement*	mm
h_1	*Rib height for the first surface configuration level*	mm
h_2	*Rib height for the second surface configuration level*	mm
k_1	*Coefficient considering bond properties of the reinforcement*	-
k_2	*Coefficient considering the distribution of strain*	-
k_3	*Coefficient defining the maximum crack spacing*	-
k_4	*Coefficient defining the maximum crack spacing*	-
k_{m}	*indicator of material type*	-
k_{sh}	*Coefficient dependent on bar shape*	-
k_{sz}	*Coefficient dependent on bar size*	-
k_t	*Empirical factor to assess the mean strain over the transfer length*	-
l	*Reinforced concrete member length*	mm
l'	*Bar length corresponding to the crack opening*	mm
l''	*Bar length detached from the concrete*	mm
l_b	*Embedment length*	mm
$l_{b,TOT}$	*Total bond length*	mm
l_d	*Development length*	mm
l_p	*Length of a reinforced concrete part originated from first cracking*	mm
l_R	*Length of the ribbed zone of one time the alternate pattern*	mm
l_S	*Length of the smooth zone for one time the alternate pattern*	mm
l_t	*Transfer length*	mm
n	*Number of samples*	-
n_C	*Number of samples of the considered group T, for the two-tailed t-test*	-
$Ni_{equivalent}$	*Nickel equivalent alloying composition of SS*	%
n_T	*Number of samples of the considered group T, for the two-tailed t-test*	-
r	*Radio*	mm
R_a	*Arithmetic average of absolute roughness*	µm
R_m	*Ultimate tensile strength of steel*	N/mm^2
R_p	*Maximum surface roughness peak height*	µm
$R_{p0,2}$	*Tensile stress at an elongation of 0,2%*	N/mm^2

R_{sk}	*Surface skewness*	µm
R_t	*Maximum height of the surface roughness profile*	µm
R_v	*Maximum surface roughness valley depth*	µm
R_z	*Average distance between highest peak and the lowest peak based on s highest peaks and lowest valleys*	µm
s	*Slip*	mm
s_1	*Slip at maximum bond stress*	mm
s_2 , s_3 , s_4	*Slip values at different bond stress-slip curve points*	mm
s_a	*Bar slip at the active end*	mm
$s_{a,fb}$	*Slip at the active end at the moment of bond strength*	mm
$s_{a,Fm}$	*Active end slip at the moment of maximum force*	mm
s_a'	*Measured slip at the active end, including the bar deformation* Δl_s	mm
S_{dev}	*Standard deviation of the bond strength*	N/mm²
$s_{r,m}$	*Mean crack spacing*	mm
$s_{r,max}$	*Maximum crack spacing*	mm
$s_{rm,50\%y,exp}$	*Mean cracking space at approximately 50% of the yielding stress, obtained experimentally*	mm
s_τ	*Standard deviation of the bond stress*	N/mm²
t_t	*shear stress in DIANA*	N/mm²
u	*Reinforcement perimeter*	mm
w	*Wider side of a flat reinforcement*	mm
w_d	*Design crack width*	mm
w_{lim}	*Limited crack width*	mm
w_m	*Mean crack width*	mm
$w_{m,flat\_alternate}$	*Mean crack width for flat rebars with an alternate rib pattern*	mm
$w_{m,flat\_CR}$	*Mean crack width for completely ribbed flat rebars*	mm
$w_{m,Ø}$	*Mean crack width given by the model codes for round ribbed bars*	mm
$w_{m,pred}$	*Predicted mean crack width*	mm
$w_{rm,50\%y,exp}$	*Mean cracking width at approximately 50% of the yielding stress, obtained experimentally*	mm
x	*Distance starting from the active end*	mm
X_C	*Mean value of the considered group C, for the two-tailed t-test*	
x_R	*Section corresponding to the transfer length*	-
$x_{R,\ cracking}$	*Section corresponding to a first crack*	-
x_S	*Symmetry section*	-
X_T	*Mean value of the considered group T, for the two-tailed t-test*	
$\Delta c_{dur,st}$	*Reduction of concrete cover to be applied if SS is used for reinforcement*	mm
Δl	*Length of a part from a rib subdivided in p parts*	mm
Δl_s	*Deformation of the bar along the gauge length of the slip measurement device*	mm
Δu_t	*Shear slip in DIANA*	mm

Greek letters

$Ø$	*Reinforcement diameter*	mm
α	*Significance level of the two-tailed t-test*	-
α	*Rib face angle*	°
α_s	*Relation between the modulus of elasticity of steel and concrete*	-
β	*Rib angle with respect to the reinforcement axis*	°
β_1	*Coefficient taking into account bond characteristics of the reinforcement*	-
β_2	*Coefficient taking into account duration of the loading*	-
β_t	*Coefficient related to the applied load*	-
γ	*Confidence level for CMM*	-
δ_c	*Displacement of the concrete*	mm
δ_s	*Displacement of the steel*	mm
ε_c	*Concrete strain*	-
ε_{cm}	*Mean concrete strain*	-
$\varepsilon_{cr,I}$	*Steel strain at the point of zero slip (uncracked section) at the moment where the first crack occurs*	-
$\varepsilon_{cr,II}$	*Steel strain at the crack when first cracking occurs*	-
ε_{ct}	*Ultimate tensile strain of concrete*	-
ε_I	*Strain at uncracked phase*	-
ε_{II}	*Strain at fully cracked phase*	-
ε_m	*Average strain of reinforced concrete*	-
ε_s	*Steel strain*	-
ε_{sm}	*Mean steel strain*	-
ζ	*Tension stiffening coefficient*	-
λ	*Empirical factor modifying the parameters involving bond differences between the round and flat ribbed rebars tested*	-
λ	*Statistical coefficient*	-
ρ_s	*reinforcement ratio*	-
σ	*Actual stress of the reinforcement*	N/mm^2
σ_c	*Concrete stress*	N/mm^2
σ_C	*Standard deviation of the considered group C, for the two-tailed t-test*	
σ_{cm}	*Mean concrete stress*	N/mm^2
σ_{cr}	*Tensile stress at first cracking*	N/mm^2
$\sigma_{cr,exp}$	*First cracking stress obtained experimentally*	N/mm^2
$\sigma_{cr,n}$	*Stress at which the last crack occurs*	N/mm^2
σ_{ct}	*Concrete tensile stress*	N/mm^2
σ_s	*Steel stress*	N/mm^2
σ_T	*Standard deviation of the considered group T, for the two-tailed t-test*	
σ_y	*Yielding stress of the reinforcement*	N/mm^2

τ	*Bond stress*	N/mm²
τ_1	*Bond stress at which the change in the bond stiffness occur*	N/mm²
τ_b	*Mean bond stress along the bond length*	N/mm²
τ_f	*Frictional stress*	N/mm²
τ_m	*Mean shear strength*	N/mm²
τ_{max}	*Maximum bond stress*	N/mm²
$\bar{\tau}$	*Statistical mean bond stress*	N/mm²
$\hat{\tau}_{0,05}$	*Estimated characteristic value for a fractile of 5%*	N/mm²
φ	*Parameter giving the number of smooth zones within the embedded length*	-
χ	*Parameter dependent on the geometrical and material properties of reinforced concrete*	-
ψ	*Proportion of the smooth zone length with respect to a single alternate pattern length*	-

Summary

The good performance of reinforced concrete relies to a great extent on the bond interaction between the reinforcement and the concrete, hence with the force transfer between the two materials. The understanding of the bond mechanism involved at the interface between the two materials as well as the knowledge of the bond capacity developed by a given reinforcement is of great importance for the correct design of reinforced concrete elements. The bond behaviour of a reinforcement embedded in concrete is characterized by the bond strength developed and by the bond stress-slip relationship, whereas the slip expresses the relative displacement between the steel and the concrete. Thus, the slip at which the bond stresses develop for a given reinforcement, will determine the stiffness of the bond behaviour involved.

The bond characteristics of standard round ribbed reinforcement have been extensively studied by several researchers and the bond mechanisms involved in the interaction between the two materials are well known. However, in the last years other alternative reinforcement materials are being investigated, most of them related to corrosion resistant materials as epoxy coated rebars, galvanized steel reinforcements, rebars made of fibre reinforced polymer materials, and stainless steel (SS) reinforcement.

This thesis focuses on the understanding of the bond behaviour developed by stainless steel flat rebars when embedded in concrete as well as on their tension stiffening behaviour and the cracking characteristics. Furthermore, flat SS rebars are tested with two different surface configuration concepts: (1) the traditional continuously ribbed or continuously smooth rebar and (2) alternate surface configurations combining smooth and ribbed zones within a single reinforcement. According to the literature available, the bond behaviour of flat SS rebars has not been previously studied: not for the completely ribbed configuration, neither for the alternate rib pattern. Furthermore, no literature has been found regarding bond behaviour of round rebars with an alternate surface configuration.

The interest of applying flat rebars has emerged based on the optimization of the rebar surface in contact with the concrete as well as on the reinforcement optimization for shallow slabs, for which the concrete cover dimensions play a key role. For a given cross sectional area of the reinforcement (for a given reinforcement ratio), a flat rebar will provide greater surface contact between steel and concrete as larger perimeters are always involved for flat rebars. The larger contact areas will, in theory, lead to higher load bearing capacity for the flat rebars provided the same bond strength as a round bar is developed by the flat rebar. Furthermore, replacement of round rebars by strips might allow a reduction of the overall concrete thickness. The latter benefit is of main importance when dealing, for example, with shallow slabs.

The application of stainless steel in replacement of carbon steel is basically motivated from a corrosion protection point of view. As a result, the application of SS will allow for a relaxation of some design parameters as concrete cover, crack width or concrete mix design. Existing national standards and design guides, allow for a reduction of the minimum concrete cover required for durability purposes if SS reinforcement is applied. The mayor drawback on the application of SS reinforcement is its high cost price in comparison to the carbon steel. However, a selective use of SS (application of SS only in those parts of the structure that are vulnerable to environmental conditions) as well as the right choice of the SS type to be applied (right quality/price ratio, without over-specification) will lead to a cost effective structure if a Life Cycle Cost analysis is performed.

On the other hand, an optimal surface configuration of the reinforcement containing an alternate rib pattern combining ribbed and smooth areas, within the same reinforcing element may improve the cracking behaviour and tension stiffening of a reinforced concrete structure that has been reinforced with this type of rebars. The innovation is based on the idea of altering the bond behaviour in the proximity of a crack, so to distribute and flatten strains and stresses at the location of the crack. This is obtained by the alternate rib pattern, through partial detachment of the bar with respect to the concrete or through a somewhat less stiff bond behaviour.

The bond behaviour of stainless steel flat rebars that are completely smooth, completely ribbed and that combine smooth and ribbed areas has been tested by means of 126 pull out tests performed to concrete cubes centrally reinforced. Carbon steel round and flat rebars have also been tested for reference, and both traditional and self compacting concrete (TC and SCC, respectively) have been applied. The bond behaviour has been analyzed in terms of developed bond strength and bond stress-slip relationship, and statistical tools have been applied for a reliable analysis when comparing the test results. Moreover, failure aspect analysis has been conducted by epoxy injection technique and by means of visual and microscope inspection. The experimentally observed bond behaviour has been compared to existing bond models, and where necessary, adaptations have been proposed in order to analytically predict the bond behaviour of flat SS rebars. Mean and characteristic values of the proposed bond models are given for design purposes.

Bond affecting parameters differ depending on the bar surface configuration:

- For completely smooth flat rebars, influence of steel material is important as chemical bond forces are of great importance for this type of reinforcement. Furthermore, microroughness influence played a secondary role, as material type (CS or SS and TC or SCC) and bar geometry appeared more deterministic for the developed bond behaviour. The bar geometry influence was observed when comparing round and flat rebars, the latter with different aspect ratios. A higher bond strength has been observed for smooth round rebars compared to smooth flat rebars, although higher forces were needed for pulling out of the flat rebars given the higher perimeter involved.

- For completely ribbed flat rebars, the differences observed regarding reinforcement material have been considered insignificant given the variability of the test results. In the same way, yet opposite as observed for round ribbed rebars, application of SCC instead of TC seem not to affect the bond performance of flat ribbed rebars. On average, lower bond strength has been observed for flat rebars compared to round rebars, although higher forces were needed for pulling out of the flat rebars given the higher perimeter involved. Observed differences regarding developed bond strength are closely related to the different relative rib areas of the tested reinforcements.

- For flat rebars with an alternate rib pattern, differences regarding material type (CS or SS and TC or SCC) have limited to no influence on the bond strength, as also observed for completely ribbed flat rebars. The addition of smooth areas within the bond length results in a different bond stress-slip behaviour in comparison to the completely ribbed configuration. When the smooth area is positioned in between two ribbed zones, higher bond strength values have been recorded, although a less stiff behaviour is observed as the maximum bond stress is reached at considerably higher slip values. Furthermore, a slope change in the ascending branch of the bond stress-slip behaviour has been observed for the alternate patterns. The change in the slope is related to a secondary bond mechanism of the smooth zone, which implies a second rib level configuration within the bond length. The larger the smooth zone, the less stiff the second ascending branch.

The observed bond behaviour of the flat reinforcement differs in comparison with round bars, as discussed above. This restricts the applicability of existing bond models. To obtain an accurate analytical prediction of the bond behaviour of the flat reinforcement, adaptations to the existing bond models are proposed, taking the constitutive model of the fib Model Code as a reference.

- For completely smooth flat rebars, the degradation of the bond has been modelled as a logarithmic descending branch which derives asymptotically towards the remaining frictional forces. This instead of a constant branch after reaching the maximum bond stress.

- For completely ribbed flat rebars, the proposed bond model is in line with the bond stress-slip relationship generally accepted for round rebars. However, curve defining parameters have been modified according to the applied reinforcement.

- For flat rebars with an alternate rib pattern, the bond model adapted for completely ribbed flat rebars is not suitable for predicting the bond behaviour of alternate patterns. This is due to the non-uniform ascending branch of the bond stress-slip relationship. Consequently, an adapted bond model has been proposed comprising two different ascending branches.

The influence of confinement reinforcement on the bond behaviour has also been analyzed. The results show, that if pull out type of failure is governing, the addition of confinement does not significantly influence the bond strength developed by the rebar. However, the capacity of confinement reinforcement to avoid splitting type of failure has been demonstrated by the experimental program.

The tension stiffening and cracking behaviour developed by flat SS rebars has been studied by means of 16 tensile tests performed on axially loaded reinforced concrete prisms. The study includes the influence of different alternate rib configurations (with ribbed zones between 50 mm and 150 mm, and smooth zones of 10 mm or 20mm), on the mean crack spacing, the maximum and the mean crack width and the crack pattern.

Results showed that, regarding reinforcement geometry, first cracking occurs at lower steel stress levels for flat elements than for round bars. However, the round bars develop less tension stiffening effect than the flat elements do. On the other hand, round bars develop better crack behaviour than flat members do as they have smaller crack widths and less crack spacing (more but thinner cracks). Results regarding influence of material type on tension stiffening behaviour and developed crack pattern are not consistent and no conclusions have been derived in this sense. Tentatively and focussing at serviceability stress levels, the influence remains rather limited. When alternate patterns are compared to completely ribbed surface configurations, the cracking behaviour improves for all of the tested alternate configurations in comparison to the completely ribbed rebar, and best results are obtained when a limited number of smooth areas are applied. Furthermore, first cracking always occurred at higher tensile stress when an alternate pattern is applied.

The existing tension stiffening and mean crack width predicting design equations (as developed for round bars) have been used for analytical verification. Based on Eurocode 2 and the fib Model Code, adapted analytical models have been derived for the cracking behaviour of flat reinforcement with continuous or alternate rib configuration.

In addition to the experimental and analytical study and for a better understanding and analysis of the bond and tension stiffening behaviour of flat SS rebars embedded in concrete, also a numerical analysis has been applied by means of Finite Element Modelling (FEM). Three different approaches have been used in the numerical modelling: (1) a phenomenological approach based on defining the interface between the steel and concrete by means of a given bond stress-slip relationship; (2) a semi-detailed mixed approach combining the phenomenological approach at ribbed zones of the alternate pattern and a geometrically detailed smooth zone; and (3) detailed geometrical modelling of the rebar with alternate rib configuration. FEM results, using approaches (2) or (3), confirmed the secondary bond mechanism of the smooth zone, in the bond behaviour observed for the alternate patterns. Regarding tension stiffening behaviour and cracking pattern, FEM results confirmed that concrete structures reinforced with rebars containing alternate patterns might develop better cracking behaviour than the completely ribbed rebars. Best results are obtained with a limited number of smooth zones.

The application of stainless steel flat rebars with an alternate rib pattern combining smooth and ribbed areas for reinforcement of concrete proved to be of interest based on the obtained results. Further fundamental research on the bond mechanisms observed in this study will allow to further optimize the rib configuration obtained so far and to develop flat rebars with an improved relative rib area. Also, to gain knowledge on the overall structural behaviour of reinforced concrete structures reinforced with this type of rebars, further research is needed.

Samenvatting

De werking van gewapend beton gaat uit van een goede aanhechting tussen het beton en de wapening, zodat er een efficiënte krachtsoverdracht is tussen beide. Kennis van de aanhechtingsmechanismen en de hechtsterkte tussen wapeningsstaal en beton is dan ook van essentieel belang voor het ontwerp van elementen in gewapend beton. Het constitutief gedrag van de aanhechtingsinterface wordt uitgedrukt door het verband tussen de schuifspanningen en de slip die optreden in deze interface. De optredende slip is de onderlinge vervorming van de wapening en het beton. De hoeveelheid slip waarmee de schuifspanningen zich opbouwen bepaalt de stijfheid van de aanhechtingsinterface.

De aanhechtingskarakteristieken van traditionele ronde wapeningsstaven met verbeterde hechting (geribde staven) zijn uitgebreid gedocumenteerd in de wetenschappelijke literatuur. De laatste jaren is er evenwel een toenemende interesse in alternatieve wapeningsstaven voor beton. Deze relateren meestal tot een verbeterde corrosieweerstand, zoals epoxy gecoate staven, gegalvaniseerde wapeningsstaven, niet-metallische wapening op basis van vezelcomposietmaterialen en inox (SS: stainless steel) wapeningsstaven.

Dit doctoraatswerk bestudeert het aanhechtingsgedrag van inox wapeningstrippen in beton, evenals bij uitbreiding het scheurgedrag en de tension stiffening. De bestudeerde inox wapeningstrippen gaan uit van twee verschillende opvattingen: (1) een traditionele oppervlaktetextuur gekenmerkt door een volledig glad of geribd oppervlak, en (2) een alternatieve oppervlaktetextuur gekenmerkt door een combinatie van gladde en geribde zones, een zogenaamde wisselende ribconfiguratie. Het aanhechtingsgedrag van inox wapeningsstrippen met volledige of wisselende ribconfiguratie is, uitgaande van de beschikbare literatuur, nooit eerder onderzocht. Dit is evenmin het geval voor ronde wapeningsstaven met wisselende ribconfiguratie.

De interesse in wapeningsstrippen is gerelateerd tot hun groter contactoppervlakte tussen wapeningsstaaf en beton, voor een gegeven wapeningsdoorsnede (voor een gegeven wapeningspercentage). Dit komt door de grotere omtrek van de strippen t.o.v. een equivalent ronde staaf, en laat toe om hogere aanhechtingskrachten te realiseren. De vervanging van ronde staven door strippen laat bovendien toe de totale dikte van het betonelement in zekere mate te reduceren. Dit laatste voordeel is vooral van belang voor slanke elementen.

De vervanging van staal door inox gebeurt vanuit het standpunt van corrosiebescherming. De toepassing van inox wapening laat dan ook toe bepaalde ontwerpparameters minder streng te nemen, zoals de betondekking, de scheurwijdte en het ontwerp van de betonsamenstelling. Huidige ontwerpnormen of richtlijnen laten inderdaad een reductie toe van de minimum betondekking gedefinieerd voor duurzaamheid, indien inox wapening

wordt toegepast. Daar tegenover staat de hogere kostprijs van inox wapening in vergelijking met staalwapening. Niettemin, is een kostefficiënte toepassing mogelijk, bij selectieve toepassing van inox wapening (in de zones van de constructie die het meest blootgesteld zijn aan nadelige klimaatvoorwaarden) en bij een juiste keuze van het type inox (juiste prijs/kwaliteit verhouding, zonder overspecificatie). Deze kostefficiëntie blijkt ook bij toepassing van LCC (life cycle cost) analyse.

Door het optimaliseren van de oppervlaktetextuur van de wapening, op basis van een wisselende ribconfiguratie, kan het scheurgedrag en de tension stiffening verbeterd worden voor betonelementen gewapend met deze wapeningstypes. Deze innovatie rond wapeningstrippen met wisselende ribconfiguratie is gestoeld op het aanhechtgedrag in de onmiddellijke omgeving van een scheur. Deze mikt op het afvlakken van de spanning in de wapening ter hoogte van de scheur, door de aanwezigheid van een wisselende ribconfiguratie, met meer lokale onthechting ter hoogte van de scheur of door een iets minder stijf aanhechtingsgedrag.

Het aanhechtingsgedrag van inox wapeningsstrippen met volledig glad, volledig geribd of wisselend geribd oppervlak, is experimenteel bestudeerd aan de hand van 126 pull-out proeven op betonkubussen met een centrisch geplaatste wapeningsstrip. Ronde stalen wapeningsstaven en stalen wapeningstrippen zijn eveneens beproefd, bij wijze van referentie. De proeven zijn zowel uitgevoerd met traditioneel beton (TC: traditional concrete) als zelfverdichtend beton (SCC: self compacting concrete). Het aanhechtingsgedrag is onderzocht in termen van hechtsterkte en schuifspanning-slip gedrag. Statistische analyse is gebruikt om proefresultaten onderling te vergelijken op significantie van de invloed van proefparameters. Daarnaast is een epoxy injectie techniek toegepast om het breukaspect nader te bestuderen door middel van visuele en microscopische inspectie. Het experimenteel vastgesteld aanhechtingsgedrag is vergeleken met bestaande aanhechtingsmodellen. Aanpassingen aan de modellen zijn voorgesteld om het aanhechtinggedrag van de wapeningsstrippen analytisch te voorspellen. Zowel gemiddelde als karakteristieke waarden van de voorgestelde modellen zijn gegeven, voor ontwerpdoeleinden.

Bepalende parameters voor het aanhechtingsgedrag bleken verschillend te zijn naargelang de toegepaste oppervlaktetextuur:

- Voor volledig gladde strippen is het type wapeningsmateriaal (staal of inox, type inox) belangrijk, gezien het belang ervan voor de chemische aanhechtingskrachten die bepalend zijn voor het aanhechtingsgedrag van gladde strippen. De microruwheid van de gladde strippen bleek van secundair belang. Dit in tegenstelling tot het type wapeningsmateriaal (staal of inox) of het type beton (TC of SCC). De invloed van de geometrie volgt uit de vergelijking tussen ronde staven en strippen, voor deze laatste met toepassing van verschillende verhouding van de zijdelingse afmetingen van de strip. Een hogere aanhechtingsterkte wordt bekomen bij ronde staven, indien uitgedrukt als een spanning. Bij de strippen kan evenwel een hogere aanhechtingskracht opgebouwd worden (door de grotere omtrek voor eenzelfde wapeningsdoorsnede).

Voor volledig geribde strippen is de invloed van het type wapeningsmateriaal niet significant, in acht genomen de proefresultaten en hun variatie. Hetzelfde geldt voor het betontype (TC of SCC), dit in tegenstelling tot ronde staven waar SCC een iets hogere hechtsterkte geeft. Gemiddeld genomen wordt een lagere hechtsterkte waargenomen voor strippen in vergelijking met ronde staven. Bij de strippen kan evenwel een hogere aanhechtingskracht opgebouwd worden (door de grotere omtrek voor eenzelfde wapeningsdoorsnede). Het waargenomen verschil in aanhechtsterkte staat in relatie tot de verschillende relatieve riboppervlaktes voor de in het onderzoek beschikbare wapeningsmateriaal.

- Voor strippen met wisselende ribconfiguratie is de invloed van het type wapeningsmateriaal en het type beton van weinig tot geen invloed op de aanhechtsterkte, analoog zoals vastgesteld voor de volledig geribde strippen. De toepassing van een wisselende ribconfiguratie resulteert in een verschillend schuifspanning-slip gedrag, ten opzichte van volledig geribde strippen. Als de gladde zone zich centraal tussen twee geribde zones situeert, wordt een hogere hechtsterkte vastgesteld, evenwel een minder stijf aanhechtingsgedrag. De maximale schuifspanning doet zich immers voor bij een duidelijk grotere slip. Bovendien wordt een knik waargenomen in de helling van de stijgende tak van het schuifspanning-slip diagram. Dit specifieke gedrag is te relateren aan een secundair aanhechtingsmechanisme dat ontstaat door de toevoeging van een gladde zone in de aanhechtingslengte. Hoe groter de gladde zone, hoe lager de waargenomen stijfheid van het geknikte gedeelte van de stijgende tak in het schuifspanning-slip diagram.

Het waargenomen aanhechtingsgedrag van de wapeningsstrippen verschilt, zoals hierboven beschreven, in vergelijking met ronde staven. Dit uit zich dan ook bij het toepassen van bestaande modellen. Om tot een goede analytische modellering van het aanhechtingsgedrag van de wapeningsstrippen te komen, zijn dan ook aangepaste aanhechtingsmodellen voorgesteld. Hierbij is het aanhechtingsmodel van de fib Model Code telkens als basis genomen.

- Voor de volledig gladde strippen wordt het aanhechtingsmodel verbeterd door af te stappen van een constante schuifsterkte na het bereiken van de maximale schuifsterkte. Hierbij kan worden uitgegaan van een logaritmisch dalende tak die asymptotisch overgaat in de schuifspanning bij wrijvingsslip van de strip.

  Voor de volledig geribde strippen zijn geen wijzigingen aangebracht aan het verloop van het schuifspanning-slip model, doch zijn evenwel aangepaste modelparameters voorgesteld voor de wapeningstrippen.

- Voor de strippen met wisselende ribconfiguratie bleek het model voor volledig geribde staven niet toepasbaar. Dit vanwege het geknikt verloop van de stijgende tak van het schuifspanning-slip diagram. In lijn hiermee, is een aangepast model voorgesteld voor strippen met wisselende ribconfiguratie.

De invloed van inrijgwapening op het aanhechtingsgedrag is mee opgenomen in het toegepast proefprogramma. Hieruit blijkt dat, indien het breukaspect gekenmerkt wordt door pull-out, de inrijgwapening weinig invloed heeft. Daarentegen is experimenteel aangetoond dat de inrijgwapening belangrijk is om splijtbreuk tegen te gaan.

Het tension stiffening en scheurgedrag van de wapeningstrippen is nader onderzocht door middel van 16 trekproeven op axiaal in trek belaste gewapend betonprisma's. Hierbij is het gedrag nagegaan van verschillende wisselende ribconfiguraties (met geribde zones tussen 50 mm en 150 mm en met gladde zones van 10 mm of 20 mm), o.a. met betrekking tot gemiddelde scheurafstand, gemiddelde en maximale scheurwijdte en het scheurpatroon. Resultaten tonen aan dat eerste scheurvorming gebeurt bij een lagere kracht voor wapeningstrippen in vergelijking met ronde staven. De ronde staven vertonen evenwel minder tension stiffening dan de strippen. Daar tegenover staat het beter scheurgedrag van de ronde staven, gekenmerkt door meer – evenwel fijnere – scheuren. De invloed van het type wapeningsstaaf en het type beton bleek niet altijd eenduidig, waardoor op dit gebied moeilijk besluiten kunnen getrokken worden. Tentatief en met focus op het gedrag bij een gebruiksbelastingsniveau, lijkt de invloed meestal eerder beperkt. Indien strippen met wisselende ribconfiguratie vergeleken worden met volledig geribde strippen, wordt steeds een beter scheurgedrag vastgesteld. De beste resultaten worden hierbij bekomen, voor de geteste configuraties, met een kleine gladde zone (10 mm) in het wisselende ribpatroon. Bovendien ligt ook de eerste scheurlast steeds hoger bij de strippen met wisselende ribconfiguratie.

De bekomen tension stiffening resultaten en het scheurgedrag zijn verder afgetoetst aan bestaande modellen (die zijn ontwikkeld voor ronde staven). Hierbij zijn, op basis van Eurocode 2 en de fib Model Code, aangepaste analytische modellen uitgewerkt voor de beschrijving van het scheurgedrag van de wapeningstrippen met volledige of wisselende ribconfiguratie.

Aanvullend op het experimenteel en analytisch onderzoek en om verdere inzichten op te bouwen in het aanhechtingsgedrag, de tension stiffening en het scheurgedrag, is eveneens een numerieke berekening toegepast aan de hand van een eindige elementen modellering. Drie verschillende benaderingen zijn hierbij toegepast: (1) een fenomenologische benadering die het gedrag van de aanhechtingsinterface oplegt aan de hand van een schuifspanning-slip model; (2) een semi-gedetailleerde benadering, waarbij de fenomenologische benadering wordt toegepast op de geribde zones en waarbij de gladde zone geometrisch wordt gemodelleerd; en (3) een geometrische benadering, waarbij de vorm van de wapening als een geheel geometrisch in detail wordt gemodelleerd. Resultaten van de numerieke berekening, bij toepassing van benadering (2) of (3), bevestigen het waargenomen secundaire aanhechtingsmechanisme bij wisselde ribconfiguratie. Met betrekking tot tension stiffening en scheurgedrag bevestigt de numerieke analyse de betere resultaten die bekomen worden voor een wisselende ribconfiguratie, in vergelijking met volledig geribde strippen. Dit positief effect is meer uitgesproken bij toepassing een beperkte gladde zone (10 mm) in het wisselende ribpatroon.

Op basis van de uitgevoerde experimentele, analytische en numerieke studie, blijkt de toepassing van inox wapeningsstrippen met een wisselde ribconfiguratie, waarbij gladde en geribde zones elkaar afwisselen, interessant. Een verdere fundamentele uitdieping van de in deze studie waargenomen aanhechtingsmechanismen, kan toelaten de ribconfiguratie verder te optimaliseren en wapeningstrippen te ontwikkelen met een verbeterde relatieve riboppervlakte. Onderzoek is eveneens noodzakelijk om een ruimere kennis op te bouwen rond de toepassing van dit type wapening en om verdere inzichten te verwerven in het constructief gedrag van betonelementen gewapend met inox wapeningsstrippen.

Chapter 1 Introduction

As an introduction of this thesis, the scope and the research significance of the performed study are discussed in this chapter. By looking to the title of the thesis, some innovative aspects of the subject can already be highlighted: "*Bond behaviour and tension stiffening of flat stainless steel rebars with continuous or alternate rib pattern embedded in concrete".* In the following 1) the reasons why *stainless steel* has been chosen for this research, 2) where the idea of using *flat reinforcement* comes from and 3) the theoretical reasoning for applying *alternate rib pattern* within a single reinforcement rebar are given.

Furthermore, it is also the objective of this chapter to introduce the main goal of this work and to give a brief description of the topics or research aspects studied and included in each chapter of this book.

1 Why stainless steel

Avoiding premature deterioration of reinforced concrete (RC) structures due to corrosion of the reinforcement is an important aspect of the design. When chloride ingress and/or carbonation take place, corrosion of the reinforcement occurs in the presence of moisture and oxigen and the durability of the structure is then being impaired [1]. As a result of the corrosion reaction, rust forms and occupies a volume of up to 6-7 times that of the original metal, hence generating internal stresses. These stresses might exceed the tensile strength of the concrete, causing cracking and spalling of the concrete, which leads to further corrosion and loss of bond between the concrete and the steel [2]. As a consequence, the interest on applying non corrodible reinforcement has increased. Although initially more expensive than the standard carbon steel (CS), the use of stainless steel (SS) leads to cost savings when the life cycle analysis of the RC structure is considered. Elimination of rebar coatings, cement inhibitors and concrete sealers, reduction of concrete cover, and considerable reduction of maintenance and repairing costs are the main advantages of using SS reinforcement in terms of long term cost reductions [3][4]. Studies have demonstrated that the replacement of CS rebars with SS in structural elements with high risk of corrosion, provides a satisfactory solution from the corrosion point of view [5]. However, while research has been focused on corrosion resistance, very little information is available about the bond strength of SS reinforcement and its compliance with bond requirements defined in design guides and codes. Alhborn et al. [6] indicate that bond strengths of SS rebars were found to be lower than that of standard carbon steel reinforcement for No. 6 bars (~Ø19 mm) and higher for No. 4 bars (~Ø12 mm). In any case, obtained values were always higher than the predicted ones and therefore no modifications were suggested when estimating the development length of SS rebars following ACI 318 [7]. Results from other investigations are variable, ranging from 10% lower bond strength when testing SS compared to an equivalent CS rebar [8] up to 25% higher bond strength values [9].

An example of the concrete cover reduction if SS reinforcement is used for reinforcing of a reinforced concrete structure is given in Figure 1-1. According to Eurocode2 [10], when defining the minimum concrete cover needed for durability aspects, a concrete cover reduction is possible when using SS. Different existing design guides and standards give values of this cover reduction. According to [11] , for example, a maximum concrete cover of 30 mm is needed when SS is used for reinforcement (considering the most aggressive environment and for the highest structural class). In the example illustrated in Figure 1-1 replacement of flat CS reinforcement by flat SS, leads to a reduction of concrete thickness by 10%.

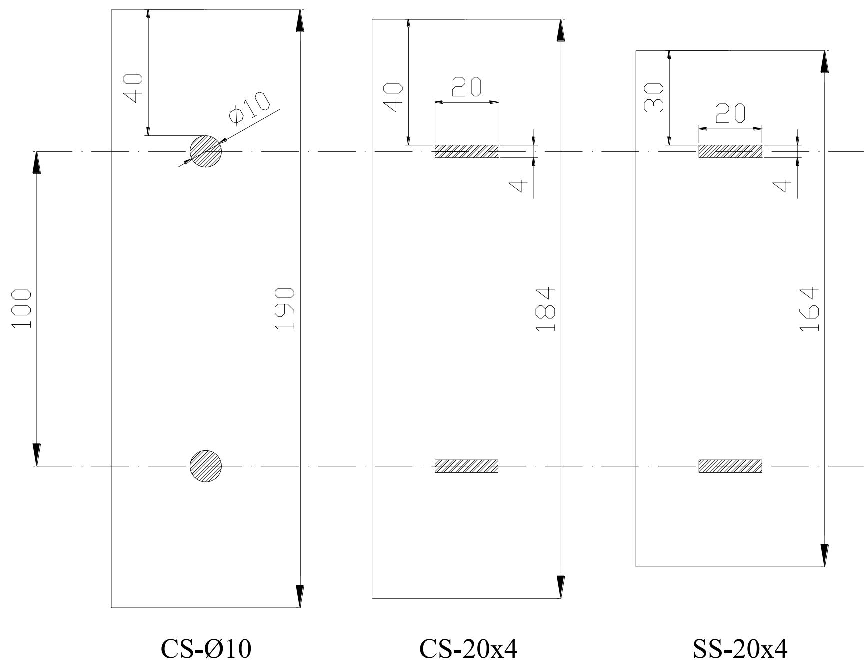

Figure 1-1 Concrete thickness reduction example as consequence of replacing a) round reinforcement by flat elements and b) CS by SS. Dimensions in mm

2 Why flat

On the other hand, an interest in applying flat rebars as reinforcement elements has emerged. The idea is based on the optimization of the rebar surface in contact with the concrete as well as on the reinforcement optimization for shallow slabs.

Given a round cross section with radius r (area $A_{round} = \pi r^2$ and perimeter $u_{round} = 2\pi r$) and a flat cross section with side lengths a and b (area $A_{flat} = ab$ and perimeter $u_{flat} = 2(a+b)$), for a comparable cross sectional area $A_{round} = A_{flat}$, the flat section has always a larger perimeter (Table 1-1). Figure 1-2 gives an example of the larger perimeter involved when a flat strip with aspect ratio of 5 (b equals 5 times a) is used instead of a round bar. Given $A_{round} = A_{flat}$, the perimeter of the strip is 50% larger than for the round bar. As a consequence, 50% larger contact surface per unit length is involved in the case of the flat element.

As the bond interaction between concrete and its reinforcement is one of the most important parameters when evaluating the effectiveness of a concrete structure, a larger contact surface per length unit (for comparable cross sectional area of the reinforcement) will lead, in principle, to a higher bond interaction between the two components of the RC system.

According to the literature available to the author, few studies have been conducted related to the bond behaviour of flat rebars when embedded in concrete. Abrams [12] in 1913, studied different parameters affecting the bond interaction between the steel and the concrete, among which the geometry of the rebar. The study concluded that for a similar bond strength to be achieved, more steel was needed if round bars were used. In other words, for a comparable bond strength development, where similar contact areas were involved ($u_{round} \approx u_{flat}$ and same embedment length), larger surface areas, and therefore more material, was used in the case of round bars ($A_{round} > A_{flat}$).

Table 1-1 Perimeter ratio between flat and round reinforcement for different aspect ratios

Aspect ratio	***1***	***5***	***10***
u_{flat} / u_{round}	1,13	1,51	1,96

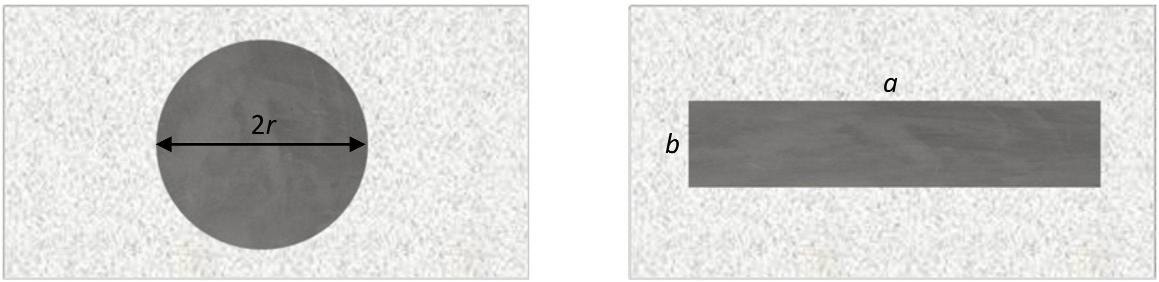

Figure 1-2 Example of the larger perimeter involved when a flat strip is used instead of a round bar for $A_{round} = A_{flat}$.

Furthermore, the use of flat reinforcing elements in replacement of round bars will optimize the total thickness of an RC member. An example is illustrated in Figure 1-1: for a constant lever arm of 100 mm without changing the concrete cover (40 mm), when replacing a round rebar of Ø10 mm by a flat rebar of 20 x 4 mm^2 (comparable cross section area), the total concrete thickness will be reduced 3,5%. This reduction gains importance when dealing, for example, with shallow slabs for which minimum concrete thickness is required.

A further advantage of using flat reinforcements in the case of intersecting reinforcing elements to be welded is the greater area of contact available for the weld. This is the case for example, when a reinforcement mesh is applied or overlapping reinforcement.

Furthermore, flat rebars can be bent around sharper angles (compared to round bars) in a selected direction without fear of cracking or similar damage to the reinforcement. The energy requirement for bending is also reduced [13]. The storage and transport of flat strips is also considered to be more optimal in terms of minor space occupied compared to round bars.

3 Why alternate rib pattern

When the concrete tensile stress in a reinforced concrete structure reaches the tensile strength of the concrete, cracking will occur. At a cracked section the steel will be the only active material (the concrete stress at that section will drop to zero). At increasing loads, the tensile stresses carried by the steel at the cracked section will increase, provoking an elongation of the bar at that section. With increasing loads, the relative slip between the two materials will also increase, resulting in an enlargement of the crack opening and as a consequence a further elongation of the bar. Sufficient bond capacity should be available to bridge cracks and for exchange of forces between the concrete and the steel.

For concrete structures reinforced with standard bars, which are completely ribbed throughout the entire length, the embedded length of the bar is larger than the transfer length of the bar. Thus, when a crack appears (see Figure 1-3a), the steel areas at both sides of the cracked section remain attached to the concrete as far as the tensile stresses do not develop shear stresses that are larger than the debonding stresses. The bar length corresponding to the crack opening, *l’*, will be the part of the bar carrying the total tensile stress of the structure at that section (see σ_s graph in Figure 1-3a). As mentioned, these high tensile forces concentrated at a short *l’* length, will lead to an important elongation of the bar at that section and consequently to an opening of the crack width.

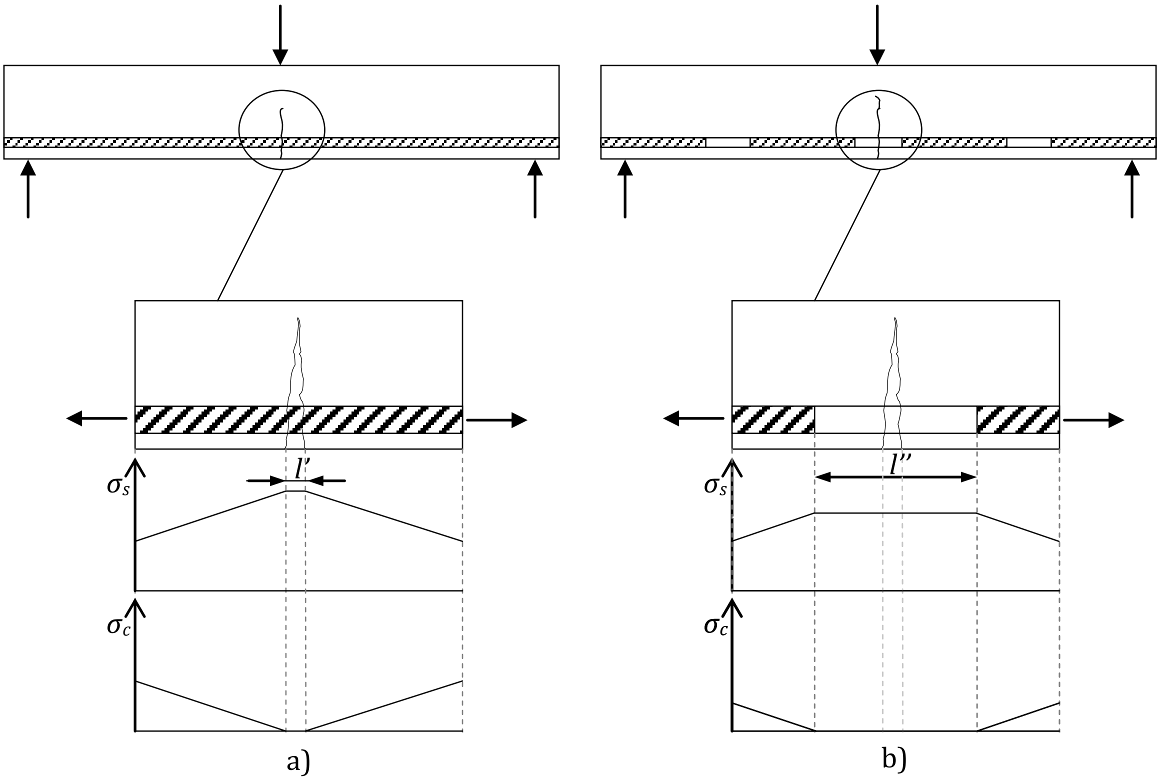

Figure 1-3 Stress situation at a cracked zone of a tensile member. a) Applying completely ribbed reinforcing bar; b) applying an alternate rib pattern combining smooth and ribbed zones

If at the zones surrounding a crack, the steel is partially detached from the concrete (as it is the case at a cracked section) or if bond stiffness is altered, larger steel length might be available to carry the tensile stresses at the crack, and therefore, stress and deformations will be more distributed (flattened) leading to a smaller crack opening. Furthermore, the area around the crack will be immune for new cracks to appear as the concrete will play a less active role at that zone. The concept [14] deals with the idea of combining ribbed areas (necessary for the appropriate transfer of forces between steel and concrete) with smooth areas within the same reinforcing bar: an alternate rib pattern.

If a steel bar with an alternate rib pattern is used for the reinforcing of a concrete structure submitted to tensile forces, when a crack appears coinciding with or close to a smooth area (see Figure 1-3b), the tensile stresses borne by the steel at the cracked section and at the surroundings might be high enough for the debonding of the smooth area to occur. In this way the length of the bar detached from the concrete is not only the one corresponding to the crack opening but larger: *l''* > *l'* in Figure 1-3b. Thus, the tensile stresses at the cracked section, carried only by the bar, will be distributed and flattened within the entire length *l''*. As a consequence, smaller crack opening might be expected as far as this favourable strain distribution can be achieved with limited increase in crack spacing as the latter also has an influence on the crack opening.

Hence, large smooth zones or a large amount of smooth zones may negatively influence the bond behaviour of the whole system, given the poorer bond characteristics of smooth bars compared to ribbed ones. It is necessary to find an optimal relation between ribbed and smooth zones which will derive in an improved cracking behaviour of the structure, without any diminishing of the overall bond capacity of the system.

4 Problem statement and aim of the thesis

The use of *flat stainless steel* reinforcement elements for reinforcing concrete structures is attractive, especially in the cases where a limited or reduced concrete thickness is desired and where aggressive environments are foreseen. Furthermore, the application of *alternate rib patterns* combining smooth and ribbed areas within a single reinforcement, can potentially result in a more favourable cracking behaviour of the structure. However, the interest on this type of reinforcement will only successfully result in practical applications if the structural behaviour of concrete structures reinforced with flat SS rebars with an alternate rib pattern is sufficiently understood.

Structural reinforced concrete combines the good compression resistance of the concrete with the good tensile performance of steel, making the 2 material's system to work properly if appropriate transfer of forces between the concrete and the steel can be established. This transfer allows for the two materials to work together and relies on the good *bond* interaction between the steel and the concrete. Thus, the author believes that the first step in proving of the applicability of the mentioned innovation (flat – SS – alternate rib pattern) should be in the direction of assessing the bond behaviour of the new reinforcing elements when embedded in concrete. Furthermore, the cracking behaviour developed by a concrete structure reinforced with this reinforcement type in a tensile situation should be analyzed as the application of the alternate rib pattern relates to an improvement in the cracking behaviour.

Although some literature is available regarding bond behaviour of SS reinforcement, and little about bond of flat reinforcement, no research has been conducted so far regarding the bond behaviour of flat SS reinforcements when embedded in concrete. Furthermore, the idea of combining smooth and ribbed areas within the same reinforcing element is novel and has not been studied so far according to the literature available to the author.

The main objective of this research project is to study the bond and the cracking behaviour developed by flat stainless steel rebars with continuous and alternate rib pattern when embedded in concrete. At the same time, the applicability of existing design models and equations is verified, and adapted models are proposed for the analytical description of the observed bond and cracking behaviour. This thesis finally aims to give first steps in proving the applicability of the new rebars for the reinforcement of concrete structures.

5 Outline of the thesis

Following this first chapter where a contextualization of the subject has been given, Chapter 2 and Chapter 3 deal with the literature review. Chapter 2 analyzes stainless steel as material for reinforcement of concrete. Different stainless steel grades are introduced, and their main material properties are presented. Existing national standards and design guides are analyzed and the economic aspect of applying stainless steel reinforcement is also briefely studied.

Chapter 3, on the other hand, compiles information regarding the bond behaviour of reinforcement when embedded in concrete, giving details on the bond phenomena, the most influencing factors and the most used test set-ups for testing the bond interaction between the two materials. A compilation of existing bond models is included in this chapter as well as a study result regarding bond of stainless steel reinforcement. Also, an introduction to tension stiffening is given in this chapter.

The following 3 chapters, are related to the 3 testing programmes conducted within this research. Chapter 4 deals with the study of bond behaviour of flat stainless steel rebars which are continuously smooth or continuously ribbed. Test results and the following discussion are presented together with an analytical study. New bond stress-slip models are proposed for predicting the bond behaviour of the flat reinforcement. Chapter 5 is similar to Chapter 4 and deals with the test programme performed in order to analyze the bond behaviour of flat rebars with an alternate rib pattern. Emphasize is given on the understanding of the behaviour of the combined surface configuration. Both experimental and analytical work are presented, and a bond model for alternate rib configurations is proposed. The third testing programme is discussed in Chapter 6 and is focused on the analysis of the tension stiffening and cracking behaviour of tensile members. The behaviour of both continuously ribbed and alternate rib patterns are analyzed (experimentally and analytically). Adapted modelling of the crack width is proposed to cover the cracking behaviour of flat rebars with an alternate rib pattern.

Chapter 7 deals with the numerical modelling work performed for a better understanding of the test results and the behaviour of flat stainless steel rebars when embedded in concrete. This is done on the basis of a non-linear finite element model of the performed tests.

Finally, in Chapter 8 the main concluding remarks obtained from this study are presented. Suggestions for further research are also given in this last chapter.

6 References

[1] Cigna R., Andrade C., Nürnberger U., Polder R., Weydert R., Seitz E. (2003) *Corrosion of steel in concrete structures – final report.* European Commission, COST Action 521

[2] Markeset G., Rostam S. and Klinghoffer O. (2006) *Guide for the use of stainless steel reinforcement in concrete structure.* Norwegian Building Research Institute, Project report 405

[3] McGurn J.M. (1998) *Stainless steels reinforcing bars in concrete*. Proceedings of the International Conference on Corrosion and Rehabilitation of Reinforced Concrete Structures, Orlando

[4] Knudsen A. (1998) *Cost effective enhancement of durability of concrete structures by intelligent use of stainless steels reinforcement*. Proceedings of the International Conference on Corrosion and Rehabilitation of Reinforced Concrete Structures, Orlando

[5] Garcia-Alonso M.C., Escudero M.L., Miranda J.M., Vega M.I. et al (2007) *Corrosion behaviour of new stainless steels reinforcing bars embedded in concrete*. Cement and Concrete Research 37: 1463-1471

[6] Alhborn T.M., DenHartigh T.C. (2003) *Comparative Bond Study of Stainless and High-Chromium Reinforcing Bars in Concrete*. Transportation Research Record 1845: 88-95

[7] ACI (2004) ACI 318-05 *Building code requirements for structural concrete*. American Concrete Institute, USA

[8] Aal Hassan A.A.A. (2003) *Bond of reinforcement in concrete with different types of corroded bars*. Master Thesis, Theses and dissertations -Paper 133, Reyerson University, Toronto

[9] Johnson J.B. (2010) *Bond strength of corrosion resistant steel reinforcement in concrete*. Master Thesis, Virginia Polytechnic and State University, Blacksburg, Virginia

[10] CEN (2004) Eurocode 2: EN 1992-1-1: *Design of concrete structures - Part 1-1: General rules and rules for buildings.* European Committee for Standardization, Brussels

[11] CIMBéton (2006) *Béton armé d'inox. Le choix de la durée*. Collection Technique Centre d'information sur le ciment et ses applications, T.81. France

[12] Abrams D. A. (1913) *Tests of bond between concrete and steel*. Bulletin 71, University of Illinois, Illinois

[13] Clapson J. et al (1994) *Concrete reinforcement, reinforced concrete and methods of reinforcing concrete*. International Patent application: WO 94/23151

[14] Matière M. (2010) *Method for producing a reinforced concrete part, and thus-produced part*. International Patent application: WO 2010/067023 A1

Chapter 2 Stainless Steel Reinforcement

1 The corrosion problem in concrete: a brief introduction

The general corrosion process of a metal can be defined as the destruction of the metal at its free surface due to an interaction with its environment at a certain temperature. In the case of reinforced concrete, during the hydration process of cement, some soluble alkaline products (i.e. NaOH, KOH, $Ca(OH)_2$) are formed which are responsible of the high alkalinity of young concrete mixtures, resulting in pH values possibly higher than 13 [1][2][3][4]. This alkaline environment is a safe situation for steel reinforcement: a thin stable rust layer is formed protecting the steel from further corrosion. As long as the film totally encloses the steel surface, a continuous and destructive corrosion process is inhibited. Such condition is known as passivation. However, this passivity may be destroyed by chlorides penetrating through the concrete, or due to the carbonation process originated by CO_2 penetration into the concrete. Carbonation of concrete will occur, when the penetration of the atmospheric CO_2 will neutralize the alkaline products by forming their corresponding carbonates, leading to a reduction of the pH values. At a typical threshold pH value of 8 to 9 an overall depassivation of steel will occur [1][5]: corrosion forming electro-chemical reactions will then start in the presence of oxygen and moisture. Carbonation leads to a rather slow and uniform corrosion process, without any locally accelerated steel destruction. A much more local, quick and potentially more dangerous way of depassivation is the chloride initiated corrosion. Due to the porous nature of the concrete, chlorides and in general aggressive negative ions can easily penetrate the concrete specimen and reach the steel reinforcement surface, destroying locally the passive film, and creating acid corrosion pits that may substantially reduce the cross section of the steel bar. As a result of the corrosion reaction, rust forms and occupies a volume of up to 6-7 times [3] that of the original metal, hence generating internal stresses. These stresses might exceed the tensile strength of concrete: cracks will form and spalling of the concrete cover may occur. Cracks and spalling expose the steel to the environment and thus increase the vulnerability of the concrete against water and oxygen penetration and increase the corrosion rate. When loss of bond between the steel and concrete occurs, and when increased stresses are carried by the remaining cross sections, structural failure is likely to happen. Premature deterioration and collapse of concrete buildings and infrastructural provisions due to corrosion of reinforcement is one of the most challenging difficulties to be overcome in reinforced structures. Repair and maintenance works in public transport infrastructures, for example, are causing significant delays and inconveniencies both for industry and for the general public and they are now recognized as an important cost for the society. It has been estimated that Western Europe spends 5 billion euro yearly for repair of corroding concrete infrastructures [6].

During the last decades there has been an increasing interest and applied effort for addressing the corrosion problem of reinforced structures. Mainly five different strategies have been studied and applied:

- Developing very dense and strong types of concrete to protect the reinforcement against ingress of corrosive substances, particularly chlorides, in combination with sufficient concrete covers
- Inhibiting corrosion through passive (corrosion inhibitors) or active protection (cathodic protection/prevention)
- Developing coatings to the concrete surface or to the carbon reinforcement (particularly epoxy or zinc)
- Applying non-metallic reinforcements (fiber-reinforced polymers –FRP)
- Applying high alloyed steel types with higher threshold values for corrosion initiation: stainless steel reinforcement

This section presents an extensive study regarding stainless steel (SS) reinforcement, giving basic definitions and classifications, analyzing material properties, studying existing design guides and standards, and assessing durability and economical aspects. An example of an existing SS applied project's cost effectiveness is also included.

Figure 2-1 Reinforcement corrosion in reinforced concrete column at the coast side, Nieuwpoort, Belgium

2 General considerations

Stainless steel, highly alloyed steel, is the term used to describe an extremely versatile family of engineering materials, which are distinguished primarily for their corrosion and heat resistant properties. All stainless steels contain principally iron, a minimum of 10,5% chromium and a maximum of 1,2% carbon [7]. At this level, chromium reacts with oxygen and moisture in the environment to form a protective, adherent and coherent oxide passivating film that envelops the entire surface of the material. The passive layer on stainless steels exhibits a remarkable property: when damaged it self-repairs as chromium in the steel reacts rapidly with oxygen and moisture in the environment to reform the protective layer. Increasing the chromium content confers greater corrosion resistance (see Figure 2-2). This resistance may be further improved, and a wide range of properties provided, by the addition of 8% or more nickel. The addition of molybdenum further increases corrosion resistance (in particular, resistance to pitting corrosion), while nitrogen increases mechanical strength and reduction of carbon enhances resistance to intergranular corrosion.

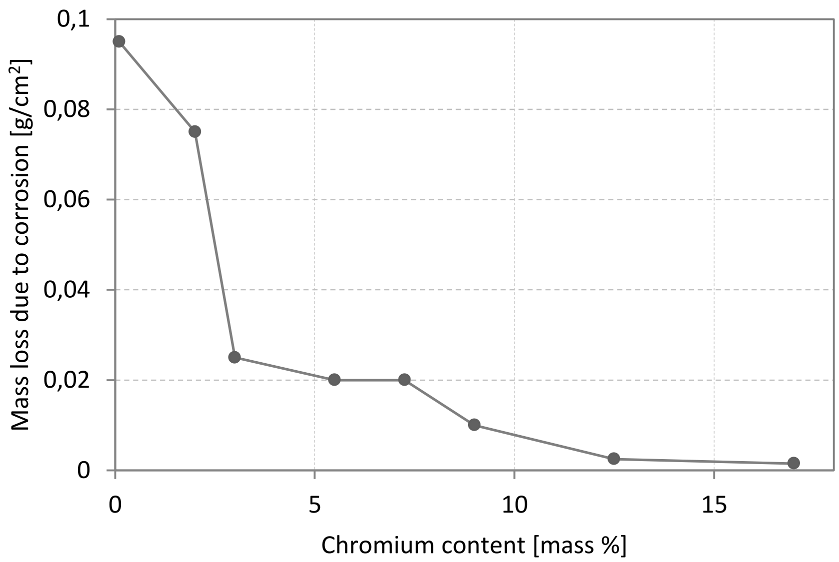

Figure 2-2 Mass loss of the reinforcement due to corrosion depending on the chromium content of the material, exposed to industrial air. Binder and Brown in [8]

The combination of the chromium percentage together with mainly nickel and carbon content of the steel determines the nature and the proportion of the metallurgical phases present in their microscopic structures and consequently, defines the stainless steel type or grade.

2.1 Stainless steel types

The stainless steel family tree has several branches, which may be differentiated using several criteria: depending on their areas of application, by the alloying elements used in their production, or by the metallurgical phases present in their microscopic structures. As stated before, changing the balance of the alloying elements (chromium, nickel, molybdenum, nitrogen, titanium and others) will influence the microscopic structure and consequently, properties such as corrosion behaviour, mechanical and physical properties and weldability. Members of the stainless steel family are most often grouped by metallographic structure: ferritic, martensitic, austenitic and combined types. The metallographic structure refers to the arrangement of atoms within the crystal structure of the steel and it is Body Centered Cubic (BCC) for the ferritc SS, Face Centered Cubic (FCC) for the austenitic SS and Body Centered Tetragonal (BCT) for the martensitic SS (see Figure 2-3).

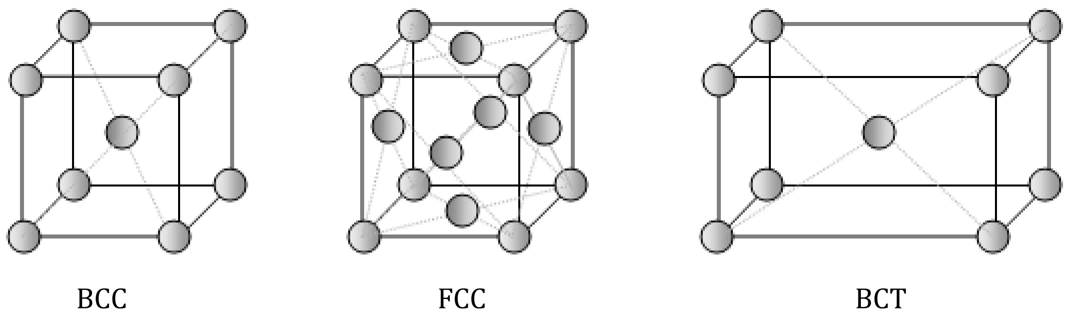

Figure 2-3 BCC, FCC and BCT crystal structures of ferritic, austenictic and martensitic SS, respectively

Figure 2-4 shows the so-called Schaeffler diagram and represents in a schematic way how the variability in the composition of the alloying elements influences on developing different metallurgical phases and corresponding SS types. The diagram compiles the influence of different alloying elements simplified as chromium equivalent and nickel equivalent and defined as follows:

$$Cr_{equivalent} = \%Cr + 2\ \%Si + 1{,}5\ \%Mo + 5\ \%V + 5{,}5\ \%Al + 1{,}75\ \%Nb + 1{,}5\ \%Ti + 0{,}75\ \%W \qquad (2\text{-}1)$$

$$Ni_{equivalent} = \%Ni + \%Co + 0{,}5\ \%Mn + 0{,}3\ \%Cu + 25\ \%N + 30\ \%C \qquad (2\text{-}2)$$

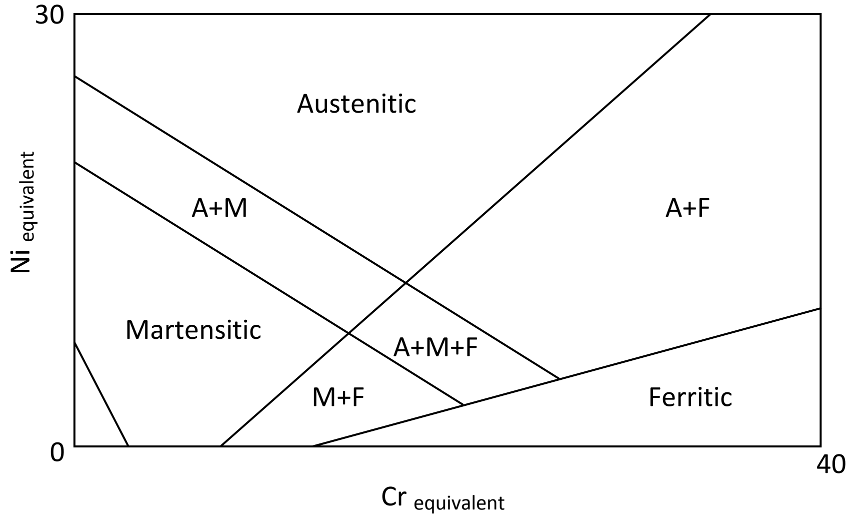

Figure 2-4 Schematic representation of the Schaeffler diagram

In the following, the effect of each alloying element is analyzed separately [9]:

- CHROMIUM. Chromium is by far the most important alloying element in stainless steel production. A minimum of 10,5% chromium is required for the formation of a protective layer of chromium oxide on the steel surface. The strength of this protective (passive) layer increases with increasing chromium content. Chromium prompts the formation of ferrite within the alloy structure and is described as ferrite stabilizer.

- NICKEL. Nickel improves general corrosion resistance and prompts the formation of austenite (it is an austenite stabilizer). Stainless steels with 8-9% nickel have a fully austenitic structure and exhibit superior welding and working characteristics over ferritic stainless steels. Increasing nickel content beyond 8-9% further improves both corrosion resistance (especially in acid environments) and workability.

- MOLYBDENUM (AND TUNGSTEN). Molybdenum increases resistance to both local (pitting, crevice corrosion) and general corrosion. Molybdenum and tungsten are ferrite stabilisers which, when used in austenitic alloys, must be balanced with austenite stabilisers in order to maintain the austenitic structure. Molybdenum is added to martensitic and ferritic stainless steels to improve high temperature strength.

- NITROGEN. Nitrogen increases strength and enhances resistance to localised corrosion. It is austenite former.

- COPPER. Copper increases general corrosion resistance to acids and reduces the rate of work-hardening (e.g. it is used in cold-headed products such as nails and screws). It is an austenite stabilizer.

- CARBON. Carbon enhances strength (especially, in hardenable martensitic stainless steels), but may have an adverse affect on corrosion resistance by the formation of chromium carbides. It is an austenite stabilizer.

- TITANIUM (AND NIOBIUM & ZIRCONIUM). Where it is not desirable or, indeed, not possible to control carbon at a low level, titanium or niobium may be used to stabilize stainless steel against intergranular corrosion. As titanium (niobium and zirconium) have greater affinity for carbon than chromium, titanium (niobium and zirconium) carbides are formed in preference to chromium carbide and thus localized depletion of chromium is prevented. These elements are ferrite stabilizers.

- SULPHUR. Sulphur is added to improve the machinability of stainless steels. As a consequence, sulphur-bearing stainless steels exhibit reduced corrosion resistance.

- CERIUM. Cerium, a rare earth metal, improves the strength and adhesion of the oxide film at high temperatures.

- MANGANESE. Manganese is an austenite former, which increases the solubility of nitrogen in the steel and may be used to replace nickel in nitrogen-bearing grades.

- SILICON. Silicon improves resistance to oxidation and is also used in special stainless steels exposed to highly concentrate sulphuric and nitric acids. Silicon is a ferrite stabiliser.

2.1.1 Ferritic stainless steel

Ferritic stainless steel has properties similar to mild steel but with the improved corrosion resistance. The most common of these steels are 12% and 17% chromium containing steels, with 12% used mostly in structural applications and 17% in housewares, boilers, washing machines and indoor architecture. Currently, ferritic SS are rated in the lower range of corrosion resistance for reinforcement [6][10].

2.1.2 Austenitic stainless steel

Austenitic SS consist of chromium (16-26%), nickel (6-12%) and iron. Other alloying elements (e.g. molybdenum) may be added or modified according to the desired properties to produce derivative grades. The austenitic group contains more chemical composition variations that are used in greater quantities, than any other category of stainless steel and it is the most widely used type of stainless steel [11]. The range of applications of austenitic stainless steel includes housewares, containers, industrial piping and vessels, architectural facades and constructional structures. Austenitic stainless steels are rated in the higher range of corrosion resistance for reinforcement [6][10]. There is also a low Ni content (3-4%) austenitic SS in the market to which manganese is added for keeping the austenitic structure.

2.1.3 Martensitic stainless steel

They contain carbon (0.2-1.0%), chromium (10.5-18%) and iron. Their corrosion resistance may be described as moderate (their corrosion performance is poorer than other stainless steels of the same chromium and alloy content). Because of their low ductility, they are not considered as appropriate material for reinforcement of concrete structures [6], and therefore, not further investigated in this work.

2.1.4 Austeno-ferritic stainless steel

Also known as *duplex* stainless steel, they consist of chromium (18-26%) nickel (4-7%), molybdenum (0-4%), copper and iron. These stainless steels have a microstructure consisting of austenite and ferrite, which provides a combination of the corrosion resistance of austenitic stainless steels with improved strength. Duplex steels are mostly used in petrochemical, paper, pulp and shipbuilding industries. As reinforcement, they become very attractive at high chloride based corrosive environments at high temperatures. Currently these steels are rated in the very high range of corrosion resistance [6][10].

2.2 Classification of stainless steels: EN 10088:2005 and others

Traditionally stainless steels have been classified according to one of the following systems [11][12]:

- The American Iron and Steel Institute (AISI) in which ferritic and martensitic steels are classified, as 400 series alloys (i.e. 403 represents a ferritic stainless steel) and the austenitic steels are classified as 300 series alloy (i.e. 304 or 316). Besides identifying the generic group type these steel grades provided no other information regarding chemical composition or physical and mechanical properties.
- Traditionally UK standards, such as BS 6744 [13], have followed the AISI classification.
- The German or DIN classification is based on the concept of a material number such as 1.44xx. Where “1” stands for steel and the following two digits (“44” in this case) gives partial information about the alloying elements’ composition, and the last two digits stand for the individual material identification.
- The French classification is based on a unique material number for a given steel. As an example, X18Cr8Ni3Mo would be an austenitic stainless steel with a nominal alloy composition of 18% chromium, 8% nickel and 3% molybdenum. This nomenclature has the advantage of providing nominal compositions for each type of steel.

In 1995 a new European standard EN 10088-1:1995, nowadays superseded by EN 10088:2005 [7], was issued that provided a uniform method of classification for stainless steels. This standard adopted and combined together both the German and French systems. Thus, every stainless steel now has a generic number that identifies its grouping and an individual material number referred to its nominal alloy composition. The designation system can be understood for the following example of a stainless steel classified as:

- Material number: 1.4436
- Material name: X3CrNiMo 17-13-3

The material number has the following components: *1*, denotes steel; *44*, names one group of stainless steels[1]; *36*, stands for the individual material identification (given by the EN commission). The material name complies: *X*, which denotes high alloyed steel (whit content in an alloying element of at least 5%); *3* indicates the nominal percentage of the carbon content (in this case 0,03%); *CrNiM,* are the chemical symbols of the main alloying elements; *17-13-3* represents the nominal percentage of the main alloying elements.

This designation system appears to be longer and heavier than the AISI one. However, it provides understanding information about the alloy composition and therefore material type within the classification.

Table 2-1, Table 2-2 and Table 2-3 give the chemical composition for the most used stainless steel types regarding concrete reinforcement. Note that an upper boundary of the composition is given for most of the alloying elements. Although mostly austenitic SS is recommended, ferritic and austeno-ferritic types are also advisable according to [13],[14] and [15]. In the last column of these tables the available material grades for each SS type is given. These grades refer to the mechanical properties of the SS and are further explained in Section *3.2 Mechanical properties*.

[1]

40: stainless steel with Ni<2,5% without Mo, without special additions; *41*: stainless steel with Ni<2,5% with Mo, without special additions; *43*: stainless steelwith Ni≥2,5% without Mo, without special additions; *44*: stainless steel with Ni≥2,5% with Mo, without special additions; *45*: stainless steel with special additions such as Ti, Nb or Cu.

Table 2-1 Ferritic stainless steel – chemical composition according to EN10088-1:2005 [7]

Steel designation		***% by mass***											***Grades***
Steel name	*Steel №*	*C*	*Si*	*Mn*	*P*	*S*	*N*	*Cr*	*Mo*	*Ni*	*Ti*	*Others*	
X3CrNb 17	*1.4511*	≤0,050	≤1,000	≤1,000	≤0,040	≤0,015	-	16,0 to 18,0	-	-	-	12xC to 1,00	InE235
X2CrNi 12	*1.4003*	≤0,030	1,000	0,500 to 1,500	0,040	0,015	0,003	10,5 to 12,5	-	0,300 to 1,000	-	C+N≈0,030	InE500

Table 2-2 Austenitic stainless steel – chemical composition according to EN10088-1:2005 [7]

Steel designation		***% by mass***											***Grades***
Steel name	*Steel №*	*C*	*Si*	*Mn*	*P*	*S*	*N*	*Cr*	*Cu*	*Mo*	*Ni*	*Others*	
X5CrNi 18-10	*1.4301*	≤0,070	≤1,000	≤2,000	≤0,045	≤0,030	≤0,110	17,0 to 19,5	-	-	8,0 to 10,5	-	InE235,InE500, InE650
X2CrNiN 18-10	*1.4311*	≤0,030	≤1,000	≤2,000	≤0,045	≤0,030	0,120 to 0,220	17,0 to 19,5	-	-	8,0 to 11,5	-	InE235,InE500, InE650
X5CrNiMo 17-12-2	*1.4401*	≤0,070	≤1,000	≤2,000	≤0,045	≤0,030	≤0,110	16,5 to 18,5	-	2,000 to 2,500	10,5 to 13,5	-	InE235,InE500, InE650
X2CrNiMoN 17-13-3	*1.4429*	≤0,030	≤1,000	≤2,000	≤0,045	≤0,015	0,120 to 0,220	16,5 to 18,5	-	2,500 to 3,000	10,5 to 13,5	-	InE235,InE500, InE650
X3CrNiMo 17-13-3	*1.4436*	≤0,050	≤1,000	≤2,000	≤0,045	≤0,030	≤0,110	16,5 to 18,5	-	2,500 to 3,000	10,5 to 13,5	-	InE235,InE500, InE650
X6CrNiMoTi 17-12-2	*1.4571*	≤0,080	≤1,000	≤2,000	≤0,045	≤0,030	-	16,5 to 18,5	-	2,000 to 2,500	10,5 to 13,5	Ti: 5xC to 0,700	InE235,InE500, InE650
X1CrNiMoCu 25-20-5	*1.4539*	≤0,020	≤0,700	≤2,000	≤0,030	≤0,010	≤0,150	19,0 to 21,0	1,200 to 2,000	4,000 to 5,000	24,0 to 26,0	-	InE235, InE500
X8CrMnCuNB 17-8-3	*1.4597*	≤0,100	≤2,000	6,5 to 8,5	≤0,040	≤0,030	0,150 to 0,300	16,0 to 18,0	2,000 to 3,500	≤1,000	≤2,000	B: 0,0005 to 0,0015	InE235,InE500, InE650

Table 2-3 Austeno-ferritic (duplex) stainless steel – chemical composition according to EN10088-1:2005 [7]

Steel designation		***% by mass***											***Grades***
Steel name	*Steel №*	*C*	*Si*	*Mn*	*P*	*S*	*N*	*Cr*	*Cu*	*Mo*	*Ni*	*Others*	
X2CrNiMoN 22-5-3	1.4462	≤0,030	≤1,000	≤2,000	≤0,035	≤0,015	0,100 to 0,220	21,0 to 23,0	-	2,500 to 3,500	4,500 to 6,500	-	InE500,InE650, InE800

3 Material properties

3.1 Corrosion resistance

3.1.1 Resistance to chloride attack and carbonation

As opposed to carbon steel (CS) which is protected by a passive film only in alkaline environments, the protective film which forms on stainless steel is stable in alkaline to neutral and slightly acid environments [6]. Consequently, stainless steels do not suffer general widespread corrosion as consequence of the carbonation process. Moreover, stainless steel reinforcement has a much higher corrosion resistance against chloride attack and can withstand much higher chloride contents compared to the normal carbon steel.

However, also stainless steels can be subjected to localized corrosion if the chloride content in the concrete resulting from seawater or de-icing salts exceeds a certain critical value (Figure 2-5). Such threshold values depend on the chemical composition and microstructure of the stainless steels, surface finishing and the presence of welding scale, the pH-value of the concrete solution and environmental conditions (humidity and temperature). It has been observed that chloride induced corrosion on a not sufficient resistant type of stainless steel, develops differently than for CS. On stainless steel the attack does not spread in the same way as on CS, but grows more like a pinhole. This might lead to a quick reduction in the cross section and consequently in the load bearing capacity if the stainless steel is not highly enough alloyed with respect to the environment.

Depending on the actual corrosion attack, ferritic or austenitic steel as well as ferritic-austenitic (duplex) steel can be used. These steels used as concrete reinforcement will not corrode at all provided they are selected in accordance with the expected conditions. Existing design guides and standards [6][12][13][14][15][16][17] give instructions about the SS grade to be used for each service condition. See section 4.2 of this chapter. Figure 2-5 gives a schematic example of the steel type to be selected depending on the chloride content and alkalinity of the concrete, at ambient temperature (20 °C).

Different studies have been conducted for the investigation of stainless steel corrosion when embedded in concrete [18] - [25]. These researches range from basic electrochemical tests to the reinforcement elements (without embedding them into concrete), or laboratory scale induced current accelerated corrosion tests, up to real aggressive ambient exposure tests for large periods of time. In most of the investigations chloride ions have been added to the concrete mix so that the aggressive environment was created and accelerated. Different variables like time and type of exposure, concrete cover, concrete quality, stainless steel grade or percentage of chlorides concentration have been extensively assessed. For all the investigations, carbon steel has been taken as reference, but also other corrosion resistant reinforcing elements have been studied for comparison, as epoxy coated rebars or galvanized steel reinforcement. Generally, results show that spalling of the concrete occurs when carbon steel was used, even for the least unfavourable testing conditions, and the carbon steel elements show high corrosion levels. With increasing aggressiveness of the environment and reducing concrete cover and/or concrete quality, spalling of the concrete and pitting corrosion also occurred for some of the corrosion resistant reinforcement, like epoxy-coated bars or tested ferritic stainless steel. Very high corrosion resistivity has been found for austenitic and austeno-ferritic stainless steels. For example, they show lack of corrosion and no cracks after 7 years of embedment in concrete with 4,8% of chloride by weight of cement, exposed to the environment of Eastern Saudi Arabia (high salinity, humidity, intense temperatures and strong, persistent drying winds) [25].

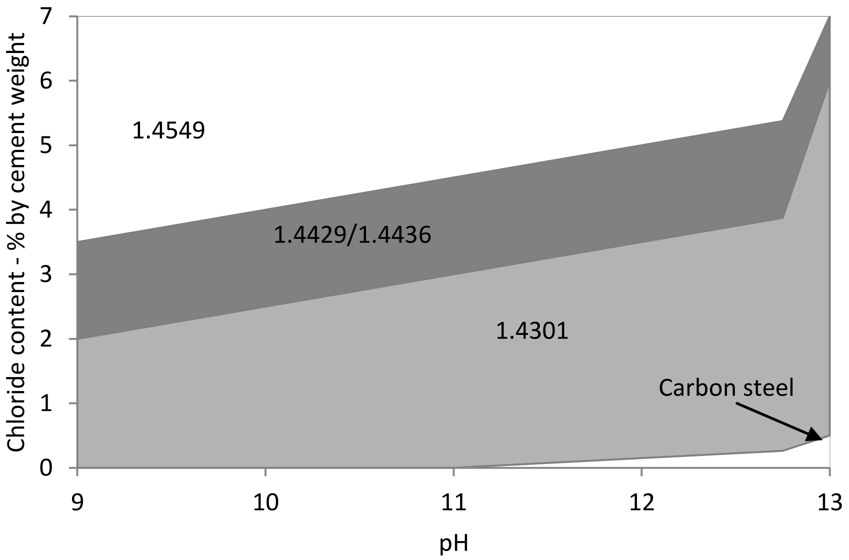

Figure 2-5 Schematic representation of fields of applicability of different stainless steels in chloride containing environments and for different levels of concrete alkalinity, at ambient temperature (20°C) [26]

3.1.2 Resistance to galvanic corrosion

When two dissimilar metals (with different electrode potentials) are connected electrically and immersed in a conductive solution, an electrolyte, an electric current will generate going from the anode to the cathode. As a rule, the less noble material, the anode, is attacked, whilst the more noble metal, the cathode, is essentially protected from corrosion. This phenomenon is called galvanic corrosion. This might be the case when combining in the same structure both carbon and stainless steel. Carbon steel, a very active low potential material, will corrode provided it is in electric contact with the more noble (higher electrode potential) stainless steel in case they are immersed in a conductive electrolyte like sea water.

However, when stainless steel is cast into concrete, the cathodic reaction is a very slow process, since no catalytic activity takes place on a stainless steel surface. A research project conducted by [25] has indicated that the cathodic reaction is inhibited on stainless steel embedded in concrete, as compared to the cathodic reaction on carbon steel reinforcement in galvanic contact with corroding carbon [28]. Publications of Pedeferri et. al [26] and Jägi et. al. [29] provide also results, which confirmed the above mentioned findings. In other words, connection between stainless steel and carbon steel should not promote significant galvanic corrosion, as long as both metals are in the passive conditions: their potentials will be more or less the same when embedded in concrete [30]. However, [17] remarks, that in areas where the existing concrete has high chloride levels or low alkalinity, the carbon steel may already be active (depassivated) and thus vulnerable to galvanic corrosion with the SS reinforcement. The fact that stainless steel is a far less effective cathode in concrete than carbon steel, makes stainless steel a useful reinforcement material for application in repair projects provided the SS reinforcement is not in contact with already corroding carbon steel.

3.2 Mechanical properties

Ferritic, austenitic and duplex grades of steels show early plastic deformation in tensile tests, and continue to sustain increasing load with increasing strain. Figure 2-6 gives the stress-strain relationship for different types of stainless steels.

For the stainless steel to meet the requirements for use as reinforcement, a cold working process is normally applied, which will increases the strength of the steels. For the austenitic types, however, cold working results in a reduction of the elongation from 40% to 20-25%. For small dimensions (<Ø16 mm) also warm working may be used for increasing the strength, resulting in mechanical properties similar to those obtained by cold working. Another way of increasing strength is addition of nitrogen (0.15-0.2%). This is however not sufficient to reach the required strength and must therefore be combined with either cold or warm working [6].

To characterize the yield strength of such strain hardening materials, a proof strength is defined and determined as the tensile stress ($R_{p0,2}$) at an elongation of 0,2 %. The ultimate tensile strength is defined at the maximum load the tested reinforcement can withstand. As listed in Table 2-4, stainless steels can be produced as ribbed bars within the normal range of strength and deformability required for application in concrete. The material grades to be used as reinforcement are defined considering their proof strength; thus grades InE235, InE500, InE650 and InE800 are defined for 235 N/mm^2, 500 N/mm^2, 650 N/mm^2 and 800 N/mm^2 of characteristic proof strength at 0,2% of strain, respectively. The modulus of elasticity (E-modulus) for SS relevant for reinforcement is about 200-220 GPa, in the same range as for carbon steel reinforcement (210 GPa). Owing to their excellent mechanical properties in the as-rolled conditions, duplex steels are of particular interest as material for reinforcement. For example, the duplex steel of type 1.4462 as cold rolled, has a proof strength of 950 N/mm², tensile strength of 1059 N/mm² and elongation of 14 % for 10 mm bars.

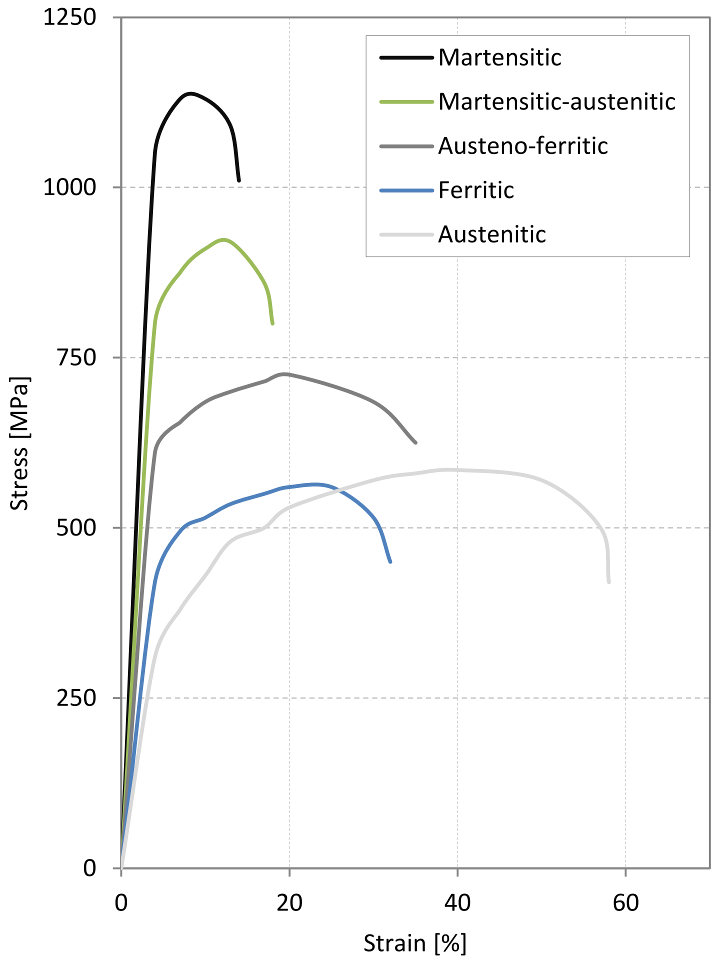

Figure 2-6 Tensile stress-strain relationship for different stainless steel grades [31]

Table 2-4 Mechanical properties of stainless steel reinforcement according to [15] and [32]

Steel grade	***0,2 % Proof strength $R_{p0,2}$ (N/mm²)***		***Ratio $R_m/R_{p0,2}$***		***Total elongation at maximum force A_{gt} (%)***	
	Fractile value*	***Minimum value***	***Fractile value*****	***Minimum value***	***Fractile value*****	***Minimum value***
InE235	235	220	1,15	1,12	8	7
InE500	500	475	1,10	1,08	5	4
InE650	650	625	1,10	1,08	5	4
InE800	800	775	1,10	1,08	5	4

* 0,05 fractile

** 0,10 fractile

3.3 Physical properties

Important physical properties of stainless steel to be considered in relation to application in concrete are: density, thermal conductivity, coefficient of thermal expansion and magnetic permeability. In Table 2-5 typical values of these parameters at ambient temperature for different types of stainless steel in the annealed condition are collected. From the structural point of view, the most important physical property is the coefficient of linear thermal expansion [33]. The coefficients of thermal expansion of ferritic steel and concrete are more or less the same (~11 x 10^{-6}/°C). In comparison, the coefficient of thermal expansion of austenitic stainless steel is significantly higher (up to 18 x 10^{-6}/°C). If a concrete structure with austenitic reinforcement is exposed to high temperatures, tensile stresses will be produced in the uncracked concrete as a consequence of the different thermal coefficient of steel and concrete. This may, in theory, cause some minor defects in the contact zone and expansion cracking. However, there are no practical evidence or laboratory results supporting this assumption [33]. On the other hand, compared to carbon steels, the higher coefficients of thermal expansion for the austenitic steels, and the lower thermal conductivitiy, may give rise to greater welding distortions (see section *3.4 Weldability*).

Ferritic stainless steels are (ferro-)magnetic, as are carbon steels. The magnetic behaviour of the various types of austenitic steel varies, but they have low magnetic permeabilities compared to other ferrous steels and are generally considered to be non-magnetic. Finally, because of the ferritic phase present in their micro-structure, duplex type of SS are also considered magnetic.

Table 2-5 Physical properties of different stainless steel grades, from [6] and [33]

Stainless steel type	***Density (kg/m³)***	***Thermal conductivity (W/m °C)***	***Coefficient of thermal expansion (10^{-6}/ °C)***	***Magnetic***
Carbon steel	7800	40	11	Yes
Ferritic SS	7700-7900	23	11-12	Yes
Austenitic SS	7800-8000	12-15	16-18	No
Duplex SS	7700-7800	20	13	Yes

3.4 Weldability

In the presence of chlorides the corrosion resistance of stainless steel in concrete can be adversely influenced in the region of the weld and the heat affected zone [34]. This is because welding results in the formation of high temperature oxides on the surface of the steel, often referred to as heat tint, or welding scale, and these oxides do not remain as stable (passive) as the oxide layers on the bare stainless steel when exposed to chloride environments. An investigation of the effect of welding on the corrosion resistance of carbon steel and stainless steel reinforcement types 1.4301 and 1.4436 has been conducted [35]. The effect of ingress of chlorides as well as cast-in chlorides was investigated. The study showed that the stainless steel reduced the chloride threshold level from 10 times, in the not-welded case, to three to six times that of the carbon steel as welded, due to the combined effect of oxidation and insufficient compaction of concrete around the weld.

The corrosion resistance can be reinstated by the complete removal of all heat tint scale after welding. This is not easily done under conditions prevailing on construction sites. Where bars need to be joined alternative methods of connection, such as lapping or mechanical couplers, can be used. If welding is unavoidable then a post cleaning process should form part of the welding procedure qualification. The quality procedures should also include accelerated testing to demonstrate that the cleaning process reinstates the corrosion resistance of the stainless steel surface. However, welding in factory conditions, where welding condition can be closely controlled, can be carried out successfully.

All stainless steel can be welded either to themselves or to carbon steel provided that necessary precautions are taken [12][36]. However, the welding method and type of weld should be considered. Welding of reinforcement can be made by resistance welding as well as metal arc welding. As most materials used for reinforcement have been strengthened by cold working, reduction of strength at the weld is possible depending on the heat input applied.

In comparison with carbon steel, the higher thermal expansion of austenitic stainless steel coupled with its lower value of thermal conductivity, increases the possibility of distortion occurring during the welding process. However, the higher electrical resistance of stainless steel is an advantage because it results in the generation of more heat for the same current. Together with the low heat conductivity this can be advantageous when resistance welding processes are used. When welding the duplex stainless steels, it is the cooling rate which controls the microstructure, therefore the heat input should be controlled in conjunction with the material thickness to obtain the correct weld structure.

Because stainless steel concrete reinforcing bars have different chemical compositions it is important to select welding electrodes or wires which result in welds with identical or better composition to those of the bars. That provides weld filler with corrosion resistance properties as nearly identical to the base metal. Proper weld rod selection not only preserves corrosion resistance properties, but is also important in achieving optimum mechanical properties.

4 Constructing with stainless steel reinforcement

4.1 Existing standards and design guides

For the construction of a reinforced concrete structure using SS as reinforcement material, there exist some standards and design guidelines which establish different parameters and recommendations that will allow for an effective and secure structure to be constructed. First of all, the aforementioned European Standard *EN 10088:2005 Stainless Steel* [7], presents stainless steel generalities such as the classification of stainless steel grades according to their chemical composition. However, this standard does not include any specific information regarding design of reinforced concrete structures using stainless steel for reinforcement.

According to the information available to the author, three national standards or norms have been published regarding SS rebars for concrete reinforcement: 1) the British Standard *BS 6744:2001 Stainless steel bars for the reinforcement of/and use in concrete – Requirements and test methods* [13]; 2) the American Standard *A955/A955M-04 Specification for Deformed and Plain Stainless Steel Bars for Concrete Reinforcement* [14]; and 3) the French Norm *XP A 35-014: 2003 Reinforcing steels – Plain, indented or ribbed stainless steel bars and coils* [15]. Similar requirements are defined in the three documents, as classification and designation; fabrication process; standard sizes, dimensions, mass and tolerances; surface geometry; mechanical and physical properties; conditions of supply and product identification, among others. Furthermore, the British and the French documents give guidance on grade selection to prevent corrosion depending on the environmental and service-life conditions.

At present a common European Standard on Corrosion resistant (stainless) reinforcing steels [32] is under preparation. This standard specifies the requirements for the chemical composition, mass per unit length, dimensional, mechanical, technological and shape properties of bars and coils (wire rod and wire) of reinforcing stainless steel, smooth of grade InE235 and smooth, ribbed or indented of grades InE500, InE650 and InE800, with a nominal diameter between 5 mm and 50 mm. The designation of reinforcing stainless steels covered by this standard consists of the indication of the specified proof strength of the product (see Table 2-4).

Besides the national standards, some other design guides and recommendation documents produced by different associations or research institutes are available at the moment:

- *Guidance on the use of stainless steel reinforcement* by the Concrete Society of UK. Technical Report No. 51. 1998 [12]

- *Le choix de la durée* by CIMbéton (Centre d'information sur le ciment et ses applications), France. Technical Report T.81. 2006 [16]
- *BA 84/02 Use of stainless steel reinforcement in highway structures* by the Highway Agency of UK. Volume 1 Section 3 Part 15 of the Design Manual for Roads and Bridges. 2002 [17]
- *Guide for the use of stainless steel reinforcement in concrete structures* by the Norwegian Building Research Institute. Project report 405. 2006 [6]
- *Structural properties of stainless steel rebar* by Euroinox (The European Stainless Steel Development Association). 2000 [37]
- *Recommendations for design and construction of concrete structures using stainless steel bars (draft version)* by the Japan Society of Civil Engineers. 2009 [38]

The model code MC2010 [39] is not specific regarding the use of stainless steel reinforcement, though some possible effects that might have to be considered in the design or the detailing with stainless steel reinforcement are briefly provided. Regarding Eurocode 2 [40], the possible concrete cover reduction in case of applying SS reinforcement, as has been explained in section *4.3.2 Concrete cover*, is mentioned.

A compilation of the data obtained from reviewing the aforementioned documents is given in Sections 4.2 till 5.1.

4.2 Selection of the appropriate type of stainless steel

When considering the adoption of SS reinforcement, selecting the most suitable SS type essentially means considering the design/service life required for the structure, the nature of the environment and the degree of corrosion resistance required, the mechanical properties of the reinforcement at ambient, low and elevated temperatures, the bar availability (grade, diameter and length) and both initial and life cycle cost. Provided that the mechanical properties and the bar availabilities are fulfilled according to the existing standards regarding stainless steel reinforcement [13][14][15], the choice of material type depends mostly both on the design service life and the environmental aggressiveness. For the cost to be kept at the lowest, over-specification of material type should be avoided.

Table 2-6 gives a summary of recommendations on SS to be selected for reinforcing of concrete according to existing standards and guidance reports. The recommendation is given for an appropriate corrosion resistance choice and for a good quality/price ratio, where over-specification of material type is avoided. The two French documents (the norm XP A35-014 [15] and the Technical Report T81 from CIMBéton [16]) are the only ones recommending ferritic SS type in case of low risk of chloride contamination and for low thermal variability at rural or urban areas. All the rest of the analyzed documents ([6][12][13][14][17][37][38]) state that if the use of SS is necessary, then only austenitic or ferritic-austenitic (duplex) steel grades should be applied for the durability of the structure to be guaranteed.

Table 2-6 Recommendation on the choice of SS reinforcement for different service conditions

Steel designation according to EN 10088-1 [7]		***Type***	***Type of exposure/ service condition/examples of applications***	***Recommended by****
SS Nº	***SS name***			
1.4511	*X3CrNb 17*	Ferritic	• For rural or urban environment, out of chloride contamination, with important thermal seasonal differences • For concrete permanently submerged in (non sea) water	2-3
1.4301	*X5CrNi 18-10*	Austenitic	• For rural or urban environment, submitted to seasonal chloride contamination • Every construction in non-aggressive environment where a reduction of the concrete cover is required. For moderate design service life (50-100 years) • Cryogenic use	1-2-3-4-5-6
1.4311	*X2CrNiN 18-10*	Austenitic	• For rural or urban environment, submitted to seasonal chloride contamination • Every construction in non-aggressive environment where a reduction of the concrete cover is required	2-3
1.4597	*X8CrMnCuNB 17-8-3*	Austenitic		
1.4401	*X5CrNiMo 17-12-2*	Austenitic	• For rural or urban environment, submitted to seasonal chloride contamination, in wet and polluted zones • Marine environment with moderate temperature and relative humidity and moderate to long service life design (50-200 years)	2-4
1.4429	*X2CrNiMoN 17-13-3*	Austenitic	• For rural or urban environment, submitted to seasonal chloride contamination, in wet and polluted zones • For visible structure elements (bridging joints, dowel bars…) • Marine environment with moderate temperature and relative humidity and moderate to long service life design (50-200 years)	1-2-4-5-6
1.4436	*X3CrNiMo 17-13-3*	Austenitic	• For rural or urban environment, submitted to seasonal chloride contamination, in wet and polluted zones. For visible structure elements (bridging joints, dowel bars…) • Marine environment with moderate temperature and relative humidity and moderate to long service life design (50-200 years) • Cryogenic use	1-2-4-5-6

1.4571	*X6CrNiMoTi 17-12-2*	Austenitic	• For rural or urban environment, submitted to seasonal chloride contamination, in wet and polluted zones • Marine environment with moderate temperature and relative humidity and moderate to long service life design (50-200 years)	2-4
1.4539	*X1CrNiMoCu 25-20-5*	Austenitic	• Structures submitted to winter de-icing salts • Marine structures permanently immersed • Highly aggressive chemical environments • Containers for waste water or brackish effluent water	2-3
1.4462	*X2CrNiMoN 22-5-3*	Austeno-ferritic	• Offshore structures and platforms • Splash zone of marine structures exposed to freezing • Structures submitted to winter de-icing salts • Leisure public buildings like public swimming pools • Highly aggressive chemical environments • Marine environment with high temperature and relative humidity, exposed to high chloride concentrations and long design service life (200-300 years)	1-2-3-4-5-6
** Recommendation given for an appropriate choice of corrosion resistance and quality/price ratio, by:* *1: BS 6744:2001 [13]* *2: AFNOR XP A35-014 [15]* *3: CIMBéton [16]* *4: Norwegian Buiding Reserch Institute [6]* *5: Concrete Sciety of UK [12]* *6: The Highway Agency of UK [17]*				

4.3 Concrete section design

The improved corrosion resistance provided by SS in comparison to CS, allows room for considerable changes in the design for durability compared to current designs based on carbon steel reinforcement.

4.3.1 Concrete mix

Having solved the corrosion problem through the selection of an appropriate SS grade, considerations adopted regarding concrete mix design for protection of carbon steel reinforcement can now be relaxed according to [6], that proposes two possible changes in the mix design: 1) optimization of type and quantity of pozzolanic additives regarding concrete durability and cost and 2) an increase in the water-cement ratio up to 0,45, leading to a reduction in plasticizers and ensuring workability of the concrete. However, [36] states that it is not recommended that concrete mix designs are relaxed although there is certainly no need to adopt more onerous mix designs.

4.3.2 Concrete cover

For the design of a reinforced concrete structure a minimum concrete cover, c_{min}, should be provided for ensuring a safe transfer of bond forces between the reinforcement and the concrete, for the protection of the steel against corrosion and for an adequate fire resistance of the structure. Eurocode2 [40] defines the minimal concrete cover as given by Equation 2-3 where the term $\Delta c_{dur,st}$ stands for reduction of concrete cover to be applied to the minimum concrete cover needed for durability reasons, $c_{min,dur}$, because of the use of stainless steel. Eurocode2 allows each Country to give the value of $\Delta c_{dur,st}$ in its corresponding National Annex; however it recommends a value of 0 mm if no other specification is given. Specified values of $c_{\mathrm{min,dur}}$ as given by Eurocode2 are summarized in Table 2-7, depending on the environmental condition and structural class of the structure.

$$c_{min} = \max\{c_{min,b};\ c_{min,dur} + \Delta c_{dur,\gamma} - \Delta c_{dur,st} - \Delta c_{dur,add};\ 10\text{ mm}\} \tag{2-3}$$

Table 2-7 Minimum concrete cover related to durability aspects based on exposure and structural class of the structure [40]

Environmental Requirement for $c_{min,dur}$ (mm)							
Structural Class*	***Exposure Class****						
	X0	*XC1*	*XC2/XC3*	*XC4*	*XD1/XS1*	*XD2/XS2*	*XD3/XS3*
S1	10	10	10	15	20	25	30
S2	10	10	15	20	25	30	35
S3	10	10	20	25	30	35	40
S4	10	15	25	30	35	40	45
S5	15	20	30	35	40	45	50
S6	20	25	35	40	45	50	55

* Exposure Class and Structural Class are according to Table 4.1 and Table 4.3N in Eurocode2, respectively

Analyzed design guides agree on applying a reduction of concrete cover regarding durability aspects in specific situations if stainless steel is used, although the size of the reduction varies from one to another. The Technical Report T.81 from CIMBéton [16] provides the most specific information giving the value of $\Delta c_{\mathrm{dur,st}}$ for each Exposure and Structural Class following the same structure as in Table 2-7. Thus, even for the most demanding environmental and service condition the maximum concrete cover to be applied for durability reasons is limited to 30 mm. The Technical Report no. 51 of the Concrete Society of UK [12] states that a minimum concrete cover of 40 mm can be used in a highly corrosive environment. The Norwegian Building Research Institute in their "Guide for the use of stainless steel reinforcement in concrete structures" [6] states that the concrete cover needed for structural reasons should not be modified, and should be taken equal to, at least, 30 mm + 5mm of tolerance. It later states that no additional corrosion protection is needed if SS reinforcement is applied. Regarding fire protection, although SS is more tolerant to high fire-induced temperatures (loosing strength only at higher temperatures than carbon steel), no change in concrete cover is recommended in this guide when SS is used. EuroInox, in the paper called "Structural properties of stainless steel bar" [37] advises a reduction of 10 to 15 mm on nominal concrete cover for most applications in which SS has been applied. In the Design Manual for Road and Bridges of UK [17] it is stated that the concrete cover for durability can be relaxed to 30 mm where SS reinforcement is used irrespective of the concrete quality or exposure condition. However, extra 10 mm cover should be applied if the 30 mm cannot be realistically maintained.

4.3.3 Crack width

According to article 7.3.1 in Eurocode2 [40] cracking shall be limited to an extent that will not impair the proper functioning or durability of the structure or cause its appearance to be unacceptable. Thus for reinforced members using carbon steel exposed to X0 and XC1 environmental conditions, Eurocode2 specifies a maximum crack width value of 0,40 mm (which is the one considered acceptable from appearance point of view). However, for more aggressive environments, the value is limited to a maximum crack width of 0,30 mm. Nevertheless, for general use, typically a crack width in the range of 0,10 to 0,20 mm is generally required. Most of the analyzed documents, [6][16][17][37], relax the latter value to an average of 0,35 mm (ranging between 0,30 and 0,40 mm) when stainless steel is used. On the contrary, the UK Concrete Society report [12] recommends that crack width calculations are carried out to the requirements of the existing codes for carbon steel.

4.4 Selective use of stainless steel

Technically it is possible to design reinforced concrete structures entirely out of stainless steel; however, this will not usually be necessary as it is rare for all the reinforcement in a structure to be exposed to aggressive environment. Furthermore, the complete substitution of carbon steel with stainless steel is unlikely to be cost-effective. However, [17] recommends full substitution with stainless steel reinforcement for major components of new structures where future repair and maintenance works would be very disruptive to traffic and therefore, very costly. In this case, the total use of stainless steel in that component can be justified by a whole life cost benefit analysis. Generally, the most cost optimal solution is to use SS reinforcement only in the most exposed zones/parts of the structure where the possibility of chloride attack is likely: bridge joints, splash zones of marine structures, the inter-tidal zone of structures placed in seawater, areas of structures beneath joints in slabs where water runoff can occur, areas of structures subject to splashing with road water containing chlorides (i.e. de-icing salts), exposed faces of a building close to the shoreline, seawalls, etc. In these locations stainless steel can be used whilst other areas of the structure which are not subject to chloride contamination can remain reinforced with carbon steel.

Recently a number of very large and prestigious bridges in highly corrosive marine environments have adopted SS reinforcement in the most outer horizontal and vertical reinforcement layer of the most exposed parts of the structure. The remaining layers of the reinforcement are ordinary carbon steel reinforcement. This is the case, among others, for the Stonecutters Bridge and the Shenzhen Corridor (both in Hong Kong) where duplex stainless steel grade 1.4462 has been used, five bridges in the M4 motorway in the UK where 1.4301 austenitic SS has been applied selectively, or the Schaffhausen Bridge in Switzerland where duplex SS 1.4462 for the pylon legs and the austenitic SS 1.4301 in the longitudinal beams have been used.

Figure 2-7 The Stonecutters Bridge – Hong Kong (top left), The Shenzhen Corridor – Hong Kong (top right), The Bray Bridge – M4 UK (bottom left) and Schaffhausen Bridge – Switzerland (bottom right)

4.5 Stainless steel in repair works

SS reinforcement is since the 1980's introduced into repair projects. As stainless steel is a much poorer cathode than carbon steel, SS reinforcement can be beneficial in those repair cases where ordinary carbon steel has corroded to such an extent that local replacement or added reinforcement is needed as part of a repair [6]. However, [17] remarks that the latter is a good solution provided that the SS is not in contact with carbon steel in areas where the existing concrete has high chloride levels or low alkalinity. At these locations, the remaining carbon steel may already be active and thus vulnerable to galvanic corrosion with SS reinforcement.

A growing application area for SS is repair and renovation of historic buildings where very long design lives are required [6][12]. For example SS reinforcement has been used in the repair of several cathedrals including Winchester and Durham in the UK, or Sydney and Newcastle in Australia. Furthermore, for the repairing of zones with a low concrete cover where control of cracking is required, stainless steel welded mesh reinforcement is being extensively used.

5 The cost of using stainless steel reinforcement

The often-stated barrier to the use of stainless steel reinforcement is the high initial cost. The difference in comparison to carbon steel relates to the higher alloying elements contained in SS; nickel and molybdenum are particularly expensive and those SS grades having high contents of those elements are more costly than the less alloyed ones. Typically the price of stainless steel is comprised of two components, the base price and the Alloy Adjustment Factor (AAF) [31]. The base price represents the manufacturers cost for producing the material in a certain size, finish, profile etc. The AAF is a charge for the alloys used (e.g. nickel, molybdenum) to produce the specific grade, as this varies considerably according to the grade (and the specific composition). In order to get an idea of the cost level related to the material, relative cost ratios are given in Table 2-8. Ratios in the first column are taken from [42] and date back to 2007. The second column summarizes actual (May 2011) market data obtained from *MEPS (INTERNATIONAL) ltd* [41] which is a leading independent supplier of steel market information. Finally the third column gives the AAF values provided by [31] for the SS grades.

Because of the increase of the nickel market price, the duplex 1.4462 SS is more cost effective in comparison to the austenitic 1.4401 grade (being the duplex one more corrosion resistant than the austenitic one). This phenomenon has increased the use of the 1.4462 SS grade.

Table 2-8 Stinless steel price ratios and indexes

Steel grade	***Price index in comparison to unalloyed CS [42]***	***Price index in comparison to unalloyed CS [41]***	***AAF (euro/ton) [31]***
Unalloyed	1	1	-
Ferritic 1.4003	4,9		460
Austenitic 1.4301	5,5	6	1787
Austenitic 1.4401	8-11	9	2738
Duplex 1.4462	12		2028

If stainless steel is to be used in a cost-effective way, then it is important that:

- The most appropriate stainless steel grade is used (without any over-specification of material grade if this leads to an increase on the cost)
- Stainless steel is used where it is needed (a selective use of SS is applied, as discussed in section 2.3.3. According to [17] the total substitution of CS by SS could add 50% to the overall initial cost of a structure. Partial replacement, however, may add as little as 3% for a structure with few vulnerable elements)
- Relaxations of other design parameters due to the use of SS are considered (i.e. reduction of concrete section, reduction of the minimum amount of reinforcement needed due to a relaxation of the accepted maximum crack opening [6][16][37]).

5.1 LCC: Life Cycle Cost

Increasing attention is being given to the concept of whole project cost assessments, by not only considering the initial cost of a structure, but also the additional costs that may occur during its entire life. The estimation technique is defined as life cycle costing (LCC) and it was developed for identifying and quantifying all costs, initial and ongoing, associated with a project over a given period. In relation to material selection, LCC enables potential long-term benefits to be assessed against short-term expenditure. Initial material costs are evaluated together with their direct and indirect implications. Direct effects compile initial outlay, maintenance and its frequency, repair and possible replacements. Disruption costs, which are the indirect implications, may include costs related to the closing of a transport road like the need of designing and managing a new itinerary as a traffic flow solution, cost of lost production of people delayed because of repair works, wasted fuel, late delivery of vehicular freight, etc. Regarding initial costs, in comparison to the price of carbon steel, SS rebars are currently more expensive as stated before. However, the cost of cutting and bending, transporting and fixing SS reinforcement remains the same as for CS [12]. Despite higher initial costs, the use of stainless steel can be economically justified as demonstrated by several life cycle coast analysis, as reported by [12][33][43]. This is the case for the Schaffhausen bridge crossing the Rhine river, subjected to frequent splashing by de-icing salts, where SS was used for the skin layer of reinforcing steel in the most vulnerable exposed areas of the longitudinal beams and at the bottom of the pylon. The selective use of SS for the area of the reinforcement outlined, increased the initial cost of the structure from 9.76 to 9.81 million Euro, which represents an addition of only 0,5% to the total initial bridge cost. The total life cycle cost analysis resulted in a cost reduction of 13% using SS instead of CS for the selected exposed zones. The selective use of SS was considered by the designers to be highly cost effective [12][43].

6 Conclusions

The design and application of stainless steel reinforcement for development of new reinforced concrete structures, as well as for repair works requires adequate knowledge of the environmental conditions and the service life requirements of the structure, but also knowledge about different stainless steel grades and their properties. From the overview presented in this chapter, it can be concluded that ferritic, austenitic and duplex stainless steel grades fulfil requirements regarding physical and mechanical properties presented in the existing standards for reinforced concrete.

Extensive research has been conducted regarding corrosion resistance of stainless steel in concrete. Studies demonstrated that duplex stainless steel containing Mo is the most corrosion resistant SS grade, followed by austenitic SS (with Mo firstly, and without Mo secondly); ferritic grade is considered to be the SS grade with lowest corrosion resistivity among the alloyed steels. The latter, however, still improves substantially the corrosion behaviour of the reinforced structure compared to carbon steel.

Due to the higher price of the stainless steel material itself, the selection of the appropriate stainless steel grade and the selective use of the non-corrodible material play a key role in the design of the concrete structures reinforced with stainless steel. Furthermore, existing design guides allow for relaxations in concrete design when SS is applied as reinforcement: reduction of the minimum concrete cover, relaxation of the maximum crack opening and concrete mix design optimization are some of the proposed benefits. Life Cycle Cost analysis carried out considering the entire life of a reinforced structure demonstrates that the intelligent application of SS as reinforcement is a cost effective approach in designing structures that will be submitted to aggressive environments and for long periods of time. The initial increased cost of the project related to the elevated cost of SS will be compensated with the decrease in maintenance and repair costs, as well as decrease of indirect costs related to disruptions caused by the repair and maintenance works. Moreover, selective use of SS yields a relatively small increase of the initial total building cost.

7 References

[1] Van den Bergh K. (2009) *Study of the corrosion of reinforcing steel in concrete by means of electrochemical methods.* Doctoral Thesis, Vrije Universiteit Brussel, Brussels

[2] Volkwein A. (2003) *Corrosion protection by concrete.* COST 521: 8-17

[3] Broomfield J.P. (2003) *Corrosion of steel in concrete*. Ed. E&FN Spon, ISBN: 978-0419196303

[4] Chess P.M. (1998) Cathodic protection of steel in concrete. Ed. E&FN Spon, ISBN: 978-0419230106

[5] Cigna R., Andrade C., Nürnberger U., Polder R., Weydert R., Seitz E. (2003) *Corrosion of steel in concrete structures – final report.* European Commission, COST 521

[6] Markeset G., Rostam S. and Klinghoffer O. (2006) *Guide for the use of stainless steel reinforcement in concrete structure.* Norwegian Building Research Institute, Project report 405

[7] CEN (2005) EN 10088:2005 *Stainless steels - Part 1: List of stainless steels.* European Committee for Standardization, Brussels

[8] Edelstahl-Vereinigung (1989) *Nichtrostende Stähle*. Verlag Stahleisen, Düsseldorf

[9] International Stainless Steel Forum. *The stainless steel family* at www.worldstainless.org (consulted on 02/06/2012)

[10] Guiraud P. (2005) *Stainless steel rebar, the choice of a long lasting quality*. 10th DBMC International Conference on Durability Materials and Components. Lyon

[11] European Federation of Corrosion (1996) *Stainless Steel in Concrete*. European Federation of Corrosion Publications Number 18

[12] Concrete Society of UK (1998) *Guidance on the use of stainless steel reinforcement*. Concrete Society Technical Report 51. UK

[13] British Standards (2001) BS 6744:2001 *Stainless steel bars for the reinforcement of and use in concrete – Requirements and test methods*. British Standards Institution, UK

[14] ASTM (2005) A 955/A 955M – 05 *Specification for deformed and plain stainless steel bars for concrete reinforcement*. American Society for Testing and Materials, USA

[15] AFNOR (2003) XP A35-014 *Reinforcing steels – Plain, indented or ribbed stainless steel bars and coils.* Association Française de Normalisation, France

[16] CIMBéton (2006) *Béton armé d'inox. Le choix de la durée*. Collection Technique, Centre d'information sur le ciment et ses applications, T.81. France

[17] UK Highway Agency (2002) BA 84/02 *Use of stainless steel reinforcement in highway structures*. Design Manual for Roads and Bridges Volume 1, Section 3, Part 15. UK

[18] Garcia-Alonso M.C., Escudero M.L., Miranda J.M., Vega M.I. et al (2007) *Corrosion behaviour of new stainless steels reinforcing bars embedded in concrete*. Cement and Concrete Research 37: 1463-1471

[19] Castro H., Rodriguez C., Belzunce F.J., Canteli A.F. (2003) *Mechanical properties and corrosion behavior of stainless steel reinforcing bars*. Materials Processing Technology 143-144: 134-137

[20] WJE Engineers Architects Materials Scientists (2006) *Corrosion resistance of alternative reinforcing bars: an accelerated test*. Final report WJE No. 2006.0773

[21] Treadeway K.W.J. (1978) *Corrosion of steel in concrete construction*. Materials Preservation Group, Symposium of the Society for Chemistry Industry, London

[22] Callaghan B.G. (1993) *The use of 3Cr12 as reinforcing in concrete*. Construction and Building Materials, Vol 7 (3): 131-136

[23] Flint G.N., Cox R.N. (1988) *The resistance of stainless steel partly embedded in concrete to corrosion by seawater*. Concrete Research 40: 13-27

[24] Page C.L., Bamforth P., Figg J.W. (1996) *Corrosion of reinforcement in concrete construction*. Proceedings of the 4th International Symposium on Corrosion of reinforcement in concrete construction, Cambridge, 662-669

[25] Rasheeduzzafar, Dakhil F.H., Bader M.A., Khan M.M. (1992) *Performance of resisting steels in chloride-bearing concrete*. ACI Materials Journal 439-448

[26] Pedeferri P. et al (1998) *Behaviour of stainless steel in simulated concrete*. Repair and Rehabilitation of reinforced structures: state of the art. American Society of Civil Engineering publication. ISBN: 978-0784402993: 192-206

[27] The Danish Corrosion Centre (1990) *Materials for corrosion cell cathodes*. Internal report as part of BRITE contract 102D

[28] Klinghoffer O., Frolund T., Kofoed B. et al (1999) *Practical aspects of application of austenitic stainless steel, AISI 316, as reinforcement in concrete*. Proceedings from EUROCORR, European Corrosion Congress: 121-134

[29] Jäggi S., Elsener B., Böhni H. (1999) *Oxygen reduction on passive steel in alkaline solutions*. Book Proceedings from EUROCORR, The European Corrosion Congress

[30] Knudsen A. (1998) *Cost effective enhancement of durability of concrete structures by intelligent use of stainless steels reinforcement*. Proceedings of the International Conference on Corrosion and Rehabilitation of Reinforced Concrete Structures, Orlando

[31] Outokumpu. *Mechanical properties of stainless steel grades* at www.outokumpu.com (consulted on 02/06/2012)

[32] CEN (2005) *Corrosion resistant (stainless) reinforcing steels*. Preliminary European standard ECISS/TC 19/SC 1/WG6, draft 2/11/2005, European Committee for Standardization, Brussels

[33] Nürnberger U. (2005) *Stainless steel in concrete - a survey*. Otto Graf Journal 2005: 111-138

[34] Nürnberger U., Beul W., Onuseit G. (1993) *Corrosion behaviour of welded stainless reinforced steel in concrete*. Otto Graf Journal 1993: 225-259

[35] Sørensen B., Jensen P.B., Maahn E. (1990) *The corrosion properties of stainless steel reinforcement*. Corrosion of reinforcement in concrete, Warwickshire, UK: 601-610

[36] Bauer A.E., Cochrane D.J. (1999) *The practical application of stainless steel reinforcement in concrete structures*. Proceedings of the Euro Inox Conference, The European Stainless Steel Development Association, Brussels

[37] Gedge G. (2000) *Structural Properties of stainless steel rebar*. Symposium of Structural Applications of Stainless Steel in Building and Architecture: Proceedings of the Euro Inox Conference, The European Stainless Steel Development Association, Brussels

[38] Japan Society of Civil Engineers (2009) *Recommendations for design and construction of concrete structures using stainless steel bars*. Draft version. Japan Society of Civil Engineers, Japan

[39] fib (2010) *Model Code 2010 – First complete draft*. fib Bulletin 55. International Federation for Structural Concrete, Switzerland

[40] CEN (2004) Eurocode 2: EN 1992-1-1 *Design of concrete structures - Part 1-1: General rules and rules for buildings*. European Committee for Standardization, Brussels

[41] MEPS International Ltd. (2012) at www.meps.co.uk (consulted on 02/06/2012)

[42] Arminox (2007) *Stainless steel reinforcement – state of the art report*. Arminox Stainless, Denmark

[43] EuroInox (1997) *Life cycle cost case study, river crossing highway bridge (Schaffhausen Bridge, Switzerland)*, The European Stainless Steel Development Association, Switzerland

[44] fib (2000) *Bond of reinforcement in concrete. State of the art report*. fib Bulletin 10. International Federation for Structural Concrete, Switzerland

[45] McGurn J.M. (1998) *Stainless steels reinforcing bars in concrete*. Proceedings of the International Conference on Corrosion and Rehabilitation of Reinforced Concrete Structures, Orlando

[46] fib (2009) *Corrosion protection of reinforcing steel*. fib Bulletin 49. International Federation for Structural Concrete, Switzerland

Chapter 3 Bond Interaction Between Reinforcement and Concrete

1 Bond phenomena

Structural reinforced concrete combines the good compression resistance of the concrete with the high tensile capacity of steel, making the two material's system to work properly if appropriate transfer of forces between concrete and steel is satisfied. This transfer allows for the two materials to work together and relies on the good bond interaction between steel and concrete. If this bond degradates, steel strains will differ from concrete strains and consequently a relative displacement between the steel and the concrete does occur. If the reinforcement significantly slips with respect to the concrete, the ability to transfer the tension forces from the concrete to the steel will be strongly reduced. The slip is expressed as the displacement of the steel compared to the undeformed concrete (see Figure 3-1). For reinforced concrete structures subjected to moderate loading, the bond stress capacity of the system exceeds the demand and there is relatively small displacement between the reinforcing steel and the surrounding concrete. However, for systems subjected to severe loading, localized bond demand may exceed capacity, resulting in localized damage and significant displacement between the reinforcing steel and the surrounding concrete [1].

According to the literature, the resistant mechanism upon which the steel to concrete bond is based is made up of three components: chemical adhesion, friction and mechanical interaction (bearing interaction) between the two elements [2][3][4].

For low bond stress values bond efficiency is mostly assured by chemical adhesion. This chemical adhesion is constituted by chemical bonds developed during the curing process of concrete [4]. For smooth reinforcing elements, this bond component is the one dominating their bond behaviour. However, this chemical adhesion is also accompanied by a secondary component which deals with the micromechanical interaction due to the microscopically rough steel surface [3].

Bond of ribbed rebars depends primarily on the bearing of the ribs against the surrounding concrete. However, friction resistance between rebar and concrete along the rib's face plays an important role in developing bond strength by helping to avoid the concrete between the ribs from sliding. The force due to friction (F) vectorially adds to the bearing component (B) of bond acting in the rib. The vertical component of the resultant (R) bond force is the radial pressure (r) exerted on the surrounding concrete. The horizontal component of the resultant is the effective bond stress (τ) (see Figure 3-2).

When the chemical adhesion for smooth reinforcements and the bearing forces for ribbed bars are broken, frictional forces related to the contact between the two materials while slipping will still remain for both reinforcement types.

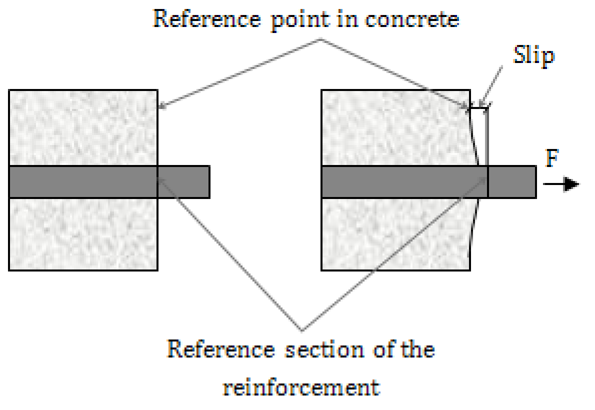

Figure 3-1 Relative bar displacement (slip). Based on [3]

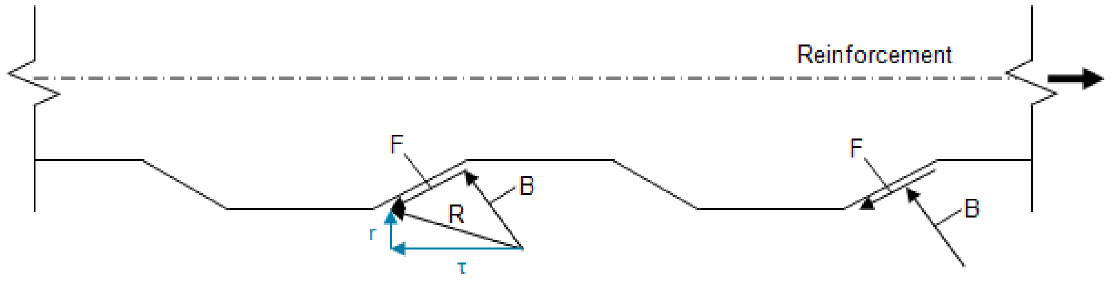

Figure 3-2 Bond forces acting in a rib

2 Bond characteristics

2.1 Bond response: bond stress-slip relationship

The bond response between the concrete and a bar subjected to a pull out force is typically characterized by giving the relationship existing between the bond stresses and the relative displacement presents at the steel-concrete interaction. According to the extensive research conducted in characterizing this bond stress-slip law, four main stages are differentiated [3]. Figure 3-3 schematically represents these four stages and they are individually explained in the following (within this context it should be mentioned that Stages 1 to 4 refer to local bond behaviour, while global behaviour results from the superimposition of the various stages):

- Stage 1: it corresponds to the stage where the concrete remains uncracked and where low values of bond stress are developed (bond stresses lower than 80% of the tensile strength of the tested concrete). The bond efficiency at this first stage is mainly assured by chemical adhesion, although micromechanical interaction may also be present due to the microroughness characteristics of the steel to be tested. Although the bar does not slip at this stage, a certain displacement occurs due to the localized shear deformations of concrete close to the interface. For smooth bars for which the bond is assured mainly by the chemical adhesion, the sliding of the bar will follow this stage (only friction forces will remain, Stage 4a).

- Stage 2: it relates to the stage where the first cracking occurs; the bond stress increase and the chemical adhesion breaks down. For ribbed or deformed reinforcement the ribs induce large bearing stresses in the concrete and microcracks will originate in front of the ribs allowing the bar to slip. However the wedging action of the ribs remains limited and there is no concrete splitting.

- Stage 3: at increasing bond stress (bond stress values higher than three times the tensile strength of the concrete), cracks spread radially due to the increased wedging action which is enhanced by the crushed concrete stuck in front of the ribs. Note that depending on the provided confinement the stiffness of this stage varies: for light confinement the stiffness of this stage is lower than when appropriate confinement is provided (see the two different Stage 3 branches in Figure 3-3). In the case of light transverse reinforcement or reduced concrete cover, this stage ends as soon as the concrete splitting cracks reach the outer surface of the specimen. Afterwards a sudden failure occurs (Stage 4b). In the case of sufficient transverse reinforcement or large concrete cover, splitting is prevented by the confining action provided by the transverse reinforcement or the large concrete cover. At increasing bond stresses the slip will also increase until a peak related to the maximum bond stress will be reached. Afterwards the force transfer will be by means of friction: due to the contact between the tips of the ribs and the concrete ones the concrete keys have been sheared off (Stage 4c).

- Stage 4: this last phase is mostly dependant as described before on the reinforcement type or applied confinement and concrete cover. Stage 4a deals with the friction forces present for a smooth bar once the chemical adhesion forces are broken. Stage 4b is related to the sudden splitting occurring for low confinement situations and Stage 4c represents the friction forces remaining for ribbed bars with confinement and where pull out type of failure occurs.

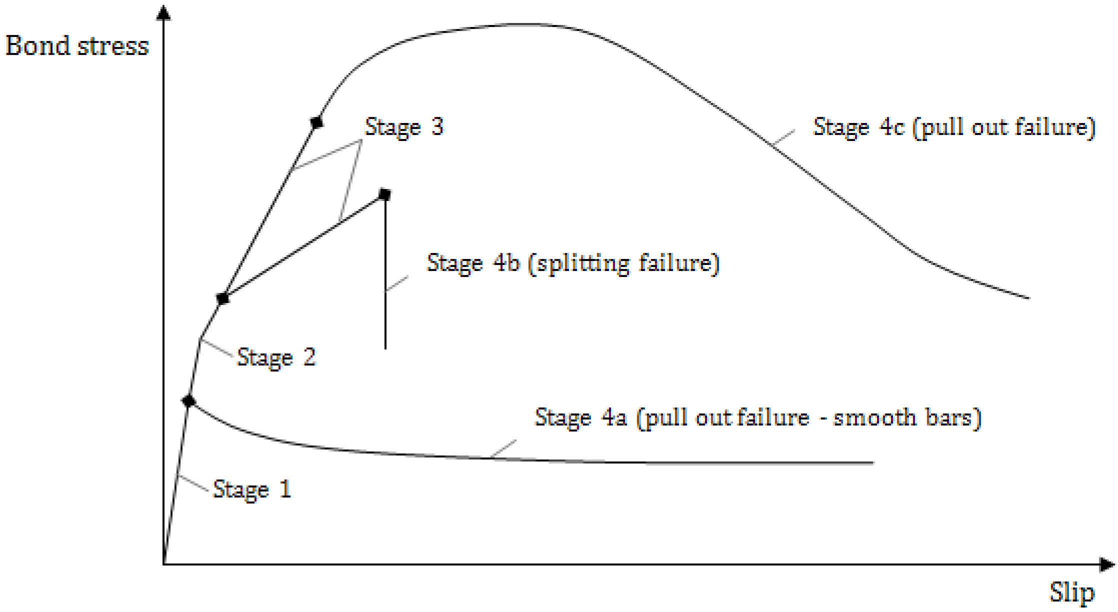

Figure 3-3 Different local bond-stress slip laws; and stages involved (based on [3])

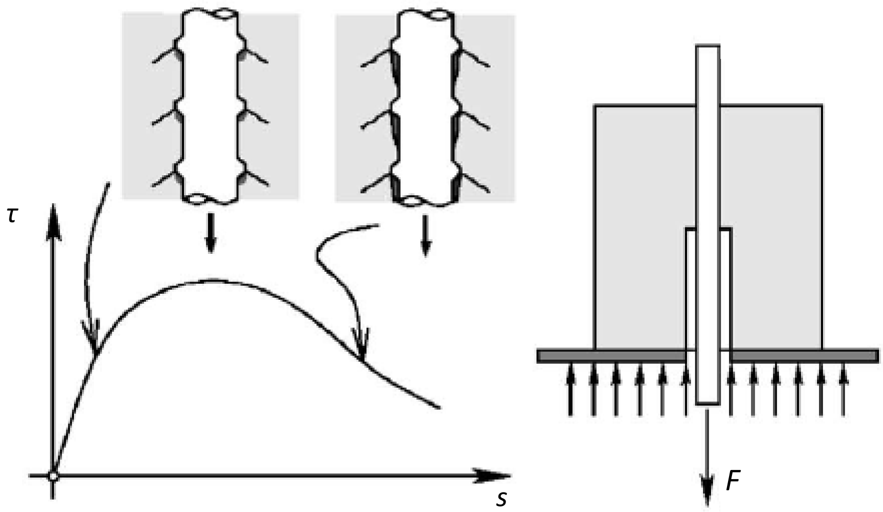

Figure 3-4 Schematic drawing of the bond-stress slip response for a short anchored bar; pull out type of failure (from [5])

Many relationships and models have been proposed in literature for defining the bond stress-slip behaviour. These are derived from studying the differential equations governing the behaviour of a single bar embedded in concrete.

Assuming that the concrete cover is large enough and/or severe confining action is applied to the concrete surrounding the bar, splitting cracks do not reach the concrete surface, and there is no splitting failure; the bond fails owing to bar pull out. Under these circumstances, bond can be modelled by considering the concrete as continuum and by introducing a bond stress-slip relationship at the interface [3].

The differential equations governing the behaviour of a single bar embedded in concrete are summarized in the following, where symmetry with respect to the bar axis, and negligible radial dimension have been assumed:

1) Strain-slip relation. From the definition of the slip between steel and concrete and for a differential length dx of the reinforcement, the slip strain relation in Equation 3-1 is obtained:

$$-\mathrm{d}s(x)/\mathrm{d}x = \varepsilon_s - \varepsilon_c \qquad (3\text{-}1)$$

where, ds(x) is the differential slip between the two materials; ε_s and ε_c stand for average steel and concrete strains, respectively; and dx is a differential length of the embedded steel.

2) Stress equilibrium in the differential steel length, see Figure 3-5. Equation 3-2 is obtained:

$$\mathrm{d}\sigma_s\ A_s = -\tau(s)\ \mathrm{d}x\ u \qquad (3\text{-}2)$$

where, σ_s is the steel stress; A_s the cross section of the steel reinforcement; $\tau(s)$ stands for the bond stress as a fuction of the relative slip; and u represents the perimeter of the reinforcement.

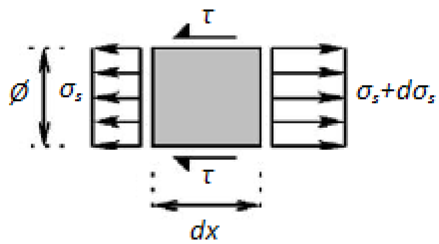

Figure 3-5 Simplified state of stress in a differential bar length

3) Reinforced concrete equilibrium, or steel-concrete force transfer. Given by Equation 3-3:

$$d\sigma_s / dx \ A_s = - \, d\sigma_{cm} / dx \ A_c \tag{3-3}$$

where, σ_{cm} represents the mean concrete stress at the concrete section $A_{c.}$

4) The derivation of Equation 3-1, and combining it with Equations 3-2 and 3-3 gives Equation 3-4, which is a second order differential equation that can be solved for a given bond stress-slip law, $\tau=\tau[s(x)]$, and assuming certain stress-strain relationships for the steel and the concrete, $\sigma_s = \sigma_s\ (\varepsilon_s\ )$ and $\sigma_c = \sigma_c\ (\varepsilon_c)$, respectively.

The solution of the differential equation will be a relation between the slip and the distance x starting from the active end (see Figure 3-6 for a pull out situation), which will allow to calculate the value of the slip at each point of the embedment length.

$$s'' - \chi \ \tau[s(x)] = 0 \tag{3-4}$$

where, $s'' = d^2s/dx^2$ and χ is a parameter dependent on the geometrical and material properties of the steel and the concrete, which is known for a given situation.

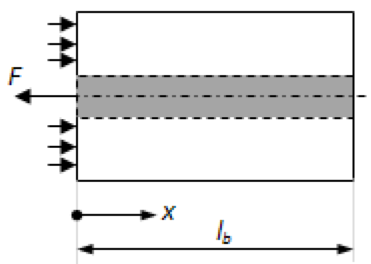

Figure 3-6 Bar pull out with concrete in compression

The local bond stress-slip law $\tau=\tau[s(x)]$, has been studied by several authors. Several models have been developed in order to predict the bond stress-slip behaviour, dependant on different factors like concrete compressive strength, concrete cover and bar diameter among others. Due to the complexity of the τ-s relationship, most authors defined the behaviour by multiple equations representing the bond stress situation for different slip values. Other authors only focused on the relationship for low slip values, until the maximum bond stress has been reached, or in the prediction of the bond strength value, without considering the slip at which this occur. Bond stress-slip equations included in design models and standards, are based on the ones available in literature but often show a level of simplification [6]. Table 3-1 summarizes available bond models from both design guidelines and individual author's research results. Due to the different bond behaviour developed by smooth bars compared to ribbed ones, bond stress-slip relationships have been defined depending on the surface configuration. In Table 3-1 a distinction is made between models available for ribbed rebars and smooth rebars.

Note that in the following table a summary of the models is given in terms of maximum bond stress definition (τ_{max}), slip value at which the latter is reached (s_1), and the bond-stress slip relationship curve defining equations. The summary is presented in terms of models available for pull out type of failure. However, some of the models also provide curve defining parameters for other conditions. The Model Codes MC90 [8] and MC2010 [10] refer to good or "other" bond conditions in terms of the inclination of the rebar and its position to the bottom of the formwork. However no specific details are given indicating for which situation bond should be considered as good or "other". Regarding round ribbed bars, the MC90 also provides curve defining parameters in case of unconfined concrete (splitting failure). In the same way, the MC2010 differentiates between pull out and splitting type of failure, and the latter is subdivided depending on the presence of transverse stirrups or not. Regarding smooth rebars, difference is made between cold drawn wires or hot rolled rebars in both Model Codes. Eurocode2 [54] does not provide a definition of the bond stress-slip relationship, but gives the definition of the maximum bond stress, dependant on the design value of the tensile strength of the concrete and two parameters that are dependent on the bar diameter and on good or poor bond conditions (defined according to the bar inclination and the position of the bar within the formwork). Huang et al. [12] developed a full bond model differentiating between normal strength and high strength concrete, good and "other" bond conditions, and whether yielding of the rebar occurs or not. Orangun et al. [41], Darwin & Zuo [9][17] and Al-Jahdali et al. [18] defined the maximum bond stress depending on the presence (or absence) of transverse reinforcement. In this summary only the definitions given for no transverse reinforcement are presented. On the other hand, Desnerck [6] defines the maximum bond stress separately if traditional concrete is applied or if self compacting concrete is used. Barbosa et al. [15] presented maximum bond stress equations depending on the concrete compressive strength values: one equation for specimens with compressive strength lower or equal to 50 N/mm^2 and another one for the case of f_c > 50N/mm^2.

Table 3-1 Summary of the bond stress-slip models available in literature

Reference	***Definition of τ_{max}***	***s_1***	***Curve shape***	***Remarks***
		Ribbed rebars		
MC90 [8]	$\tau_{max} = 2,5\ \sqrt{f_{ck}}$	1 mm	Eq. 3-5 to 3-8 $\alpha = 0,4$	Good bond conditions and pull out failure
MC2010 [10]	$\tau_{max} = 2,5\ \sqrt{f_{ck}}$	1 mm	Eq. 3-5 to 3-8 $\alpha = 0,4$	Good bond conditions and pull out failure
Eurocode2 [54]	$\tau_{max} = 2,25\ \eta_1\eta_2\ f_{ctd}$	-	-	$\eta_1 = 1$ for good bond conditions η_2 dependant on Ø
Eligehausen [11]	-	1 mm	Eq. 3-5 to 3-8 $\alpha = 0,4$	For pull out failure
Huang et al. [12]	$\tau_{max} = 0,45\ f_c$	1 mm	Eq. 3-5 to 3-7 and Eq. 3-9 $\alpha = 0,4$	For normal strength concrete, good bond conditions, and when yielding of the rebar does not occur
Soroushian [13]	$\tau_{max} = (20\text{-}Ø/4)\sqrt{(f_c/30)}$	1 mm	Eq. 3-10 and Eq. 3-6 to 3-8 $\alpha = 0,5$	-
Harajli [14]	$\tau_{max} = 2,57\ \sqrt{f_c}$	0,15c	Eq. 3-5 to 3-8 $\alpha = 0,3$	-
Orangun et al. [41]	$\tau_{max} = [(0,1 + 0,268(c_c/Ø) + 4,4\ (Ø/l_b)]\ \sqrt{f_c}$	-	-	Without transverse confinement
Darwin & Zuo [9][17]	$\tau_{max} = [(1,44 l_b(c_{c,min} + 0,5Ø) + 56,3A_s)\ (0,1c_{c,max}/c_{c,min} + 0,9)]\ f_c^{1/4}$	-	-	Without transverse confinement
Al-Jahdali et al. [18]	$\tau_{max} = (-0,88 + 0,324(c_c/Ø) + 5,79(Ø/l_b)\ \sqrt{f_c}$	-	-	Without transverse confinement
Desnerck [6]	$\tau_{max} = (1,94 + 0,29\ c_c/Ø)\sqrt{f_c}$, TC $\tau_{max} = (1,76 + 0,51\ c_c/Ø)\sqrt{f_c}$, SCC	$0,0032c^2 + 0,041$	Eq. 3-5 to 3-8 $\alpha = 0,3$	-
Barbosa et al. [15]	$\tau_{max} = 0,77e^{0,115Ø}e^{0,029fc}$, $f_c \leq 50\text{N/mm}^2$ $\tau_{max} = 2,52e^{0,114Ø}e^{0,006fc}$, $f_c > 50\text{N/mm}^2$	-	-	-
		Smooth rebars		
MC90 [8]	$\tau_{max} = 0,3\sqrt{f_{ck}}$	0,1 mm	Eq. 3-11 to 3-12 $\alpha = 0,3$	For good bond conditions, and hot rolled rebars
MC2010 [10]	$\tau_{max} = 0,3\sqrt{f_{ck}}$	0,1 mm	Eq. 3-11 to 3-12 $\alpha = 0,3$	For good bond conditions, and hot rolled rebars

Feldam et al. [21]	τ_{max} =[(0,19-0,07k_{sz}+0,05k_{sh})$\sqrt{R_y}$ + (-2,7 10^{-5} + 4,0 $10^{-5}k_{sz}$ -3,0 $10^{-5}k_{sh}$)$R_y l_b$] $\sqrt{f_c}$	0,01 mm	Eq. 3-13	Only the descending logarithmic curve defined.
Kankam [16]	-	-	Eq. 3-14	No maximum bond stress value defined

Ribbed rebars:

$$\tau(s) = \tau_{max} (s/s_1)^{\alpha} \qquad 0 \leq s \leq s_1 \qquad (3\text{-}5)$$

$$\tau(s) = \tau_{max} \qquad s_1 \leq s \leq s_2 \qquad (3\text{-}6)$$

$$\tau(s) = \tau_{max} - (\tau_{max} - \tau_f)((s\text{-}s_2)/(s_3\text{-}s_2)) \qquad s_2 \leq s \leq s_3 \qquad (3\text{-}7)$$

$$\tau(s) = \tau_f \qquad s \geq s_3 \qquad (3\text{-}8)$$

$$\tau(s) = \tau_f - \tau_f((s\text{-}s_3)/(s_4\text{-}s_3)) \qquad s_3 \leq s \leq s_4 \qquad (3\text{-}9)$$

$$\tau(s) = \tau_{max} (s/s_1)\, e^{(1-(s/s_1)^{\alpha})/\alpha} \qquad 0 \leq s \leq s_1 \qquad (3\text{-}10)$$

Note that s_1 relates to the slip at which the maximum bond stress is reached, s_2 stands for the slip at which the maximum bond stress starts to decrease, s_3 is related to the slip when only the frictional forces remain and s_4 is the slip at which the frictional forces dissappear.

Smooth rebars:

$$\tau(s) = \tau_{max} (s/s_1)^{\alpha} \qquad 0 \leq s \leq s_1 \qquad (3\text{-}11)$$

$$\tau(s) = \tau_{max} \qquad s \geq s_1 \qquad (3\text{-}12)$$

$$\tau(s)= (\beta_0 + \beta_1 \log s) \sqrt{f_c} \qquad s_1 \leq s \leq s_2 \qquad (3\text{-}13)$$

$$\tau(s) = (41{,}7\text{-}0{,}2f_s)s^{0,8} \qquad s \geq 0 \qquad (3\text{-}14)$$

Regarding the bond stress-slip definition for round ribbed rebars given by the different models, a 4 branches curve is presented by all of them and are based on the definition given for the first time by Eligehausen [11]: a first ascending branch until the maximum bond stress is reached (s_1, τ_{max}), followed by a plateau at maximum bond stress until s_2, with a third decreasing branch until the frictional bond forces (τ_f) are reached at a slip s_3, followed by a fourth branch related to the frictional forces. For most of the analyzed models, this fourth branch is a plateau that remains constant at increasing slips. However, the model proposed by Huang et al. represents the last branch as a descending branch until no bond forces are remaining at a slip value of s_4. Figure 3-7 gives the bond stress-slip relationship for the different models (pull out failure) for the case of round ribbed rebar with diameter 10 mm and a clear rib spacing of 7 mm (as for the reference rebars tested during the experimental program, Chapter 4), and for a characteristic compressive strength of the concrete of 50 N/mm^2 (corresponding to a mean compressive strength of 58 N/mm^2 according to [54], and taken from the mean values registered during the experimental program. See Chapter 4).

Note that the only difference between the two Model Codes is that the maximum bond stress plateau is 50% shorter according to MC2010. The maximum bond stress value given by the Model Codes is conservative if comparison is made to the other analyzed bond models, with differences of up to 32% compared to Huang et al. Regarding the first ascending branch (bond stress-slip relationship for slip values until ~1 mm, see Figure 3-8), the Model Codes and the models given by Huang et al. and Harajli use the same definition. Huang et al. and the Model Codes fix the value of the parameter α at 0,4. However given the higher maximum bond stress value given by Huang et al. the stiffness of the ascending branch is higher for the model given by Huang et al. On the other hand, although similar maximum bond stress values are given by Harajli and the Model Codes, Harajli gives an α value of 0,3, which makes the initial stiffness (slip values lower than 0,1 mm) of the bond behaviour stiffer. Soroushian gives a different definition for the first ascending branch (see Equation 3-10). It can be observed from Figure 3-8, that although less stiff behaviour is developed by the Soroushian definition for slip values until approximately 0,05 mm, it further develops a stiffer behaviour than the one given by Equation 3-5. For the slip values, s_1 is defined by most of the analyzed models by a fixed value (1 mm). However, Harajli and Desnerck provide s_1 dependant on the clear rib spacing of the rebar. In the same way, only Harajli gives s_2 dependant on the clear rib spacing (fixed value of 2 mm (MC2010) or 3 mm are adopted by the other models). Only the model presented by Soroushian fixes the value of s_3 (10,5 mm), other analyzed models give this parameter equal to the clear rib spacing of the reinforcement. Finally, regarding the fourth branch, Harajli, Huang et al. and the Model Codes give the frictional stress dependant on the maximum bond stress. However, only the model given by Huang et al. considers the fourth branch as a descending branch until no bond forces remain at a slip value s_4 equal to 3 times the clear rib spacing. Soroushian fixes the frictional bond stress value at 5 N/mm^2.

Regarding smooth rebars, both Model Codes give the same definition for the bond stress-slip relationship: a first steep ascending branch until a slip value of 0,1 mm (for good bond conditions and hot rolled bars), followed by a plateau that keeps constant at increasing slips (τ_{max} = τ_f). The other available bond stress-slip relationship given by Feldman, represents the behaviour of smooth rebars as a peak occuring at 0,01 mm followed by a logarithmic descending branch (see Equation 3-13) until frictional forces are reached at a slip value of 10 mm. Feldman defines the maximum bond stress and the frictional one dependant on several factors, like bar diameter, roughness, shape, bond length and compressive strength of the concrete. Figure 3-9 and Figure 3-10 give the comparison between the bond stress-slip relationship given by the Model Codes and the one given by Feldman for slip values until 14 mm and 1 mm, respectively. Note that for the plotting of the graphs, the definition of Feldman has been given twice: taking as maximum bond stress value the maximum stress value given by the Model Codes for a characteristic compressive strength of 50 N/mm^2 (lower graph) and taking as frictional bond stress value the one given by the Model Codes (upper curve). Finally, Kankam gives the relationship between the bond stress and the slip dependant on the stress of the steel rebar (f_s). This model does not provide information regarding maximum bond stress or slip values and is not further considered in this work.

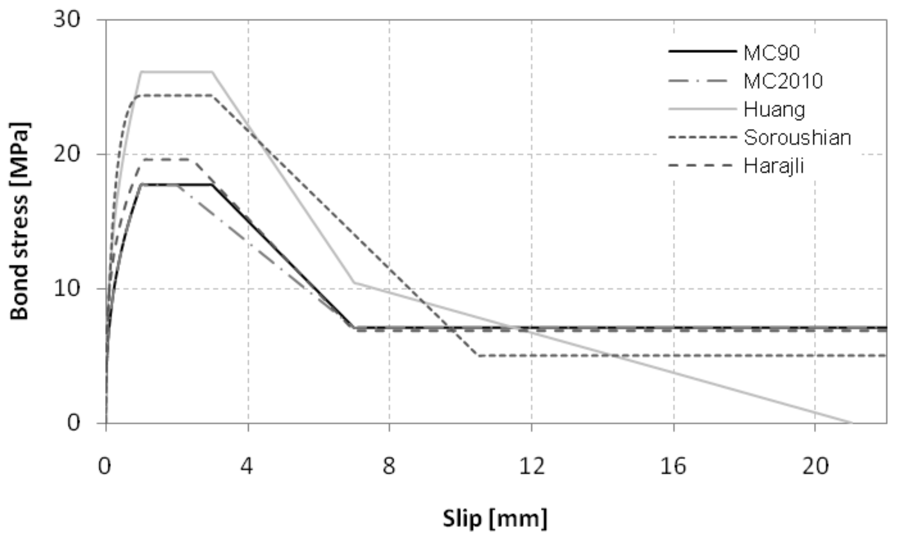

Figure 3-7 Bons stress-slip relationship for ribbed rebar models. Slip values until 22 mm

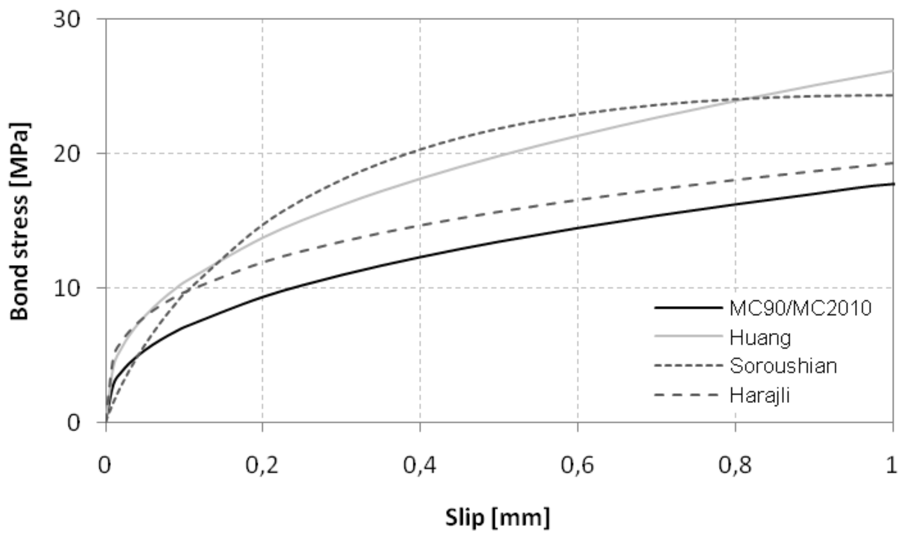

Figure 3-8 Bons stress-slip relationship for ribbed rebar models. Slip values until 1 mm

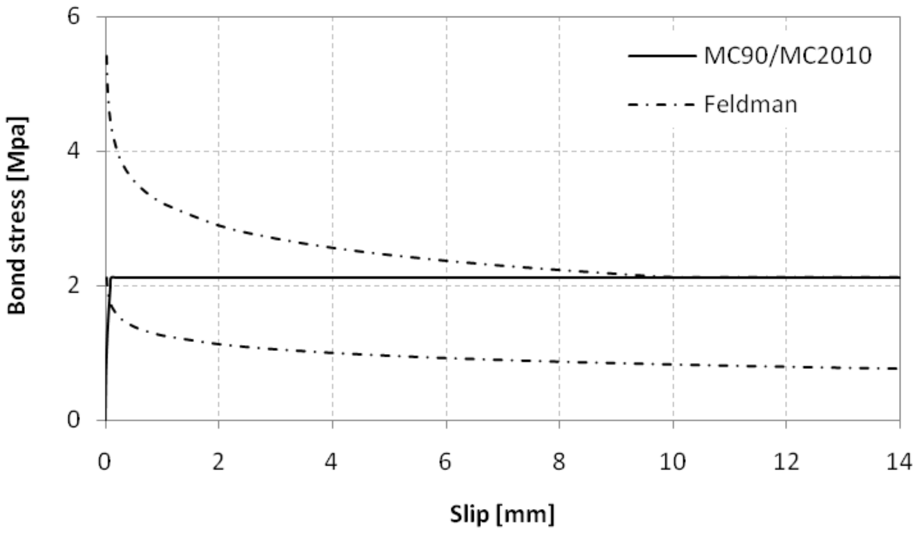

Figure 3-9 Bons stress-slip relationship for smooth rebar models. Slip values until 14 mm

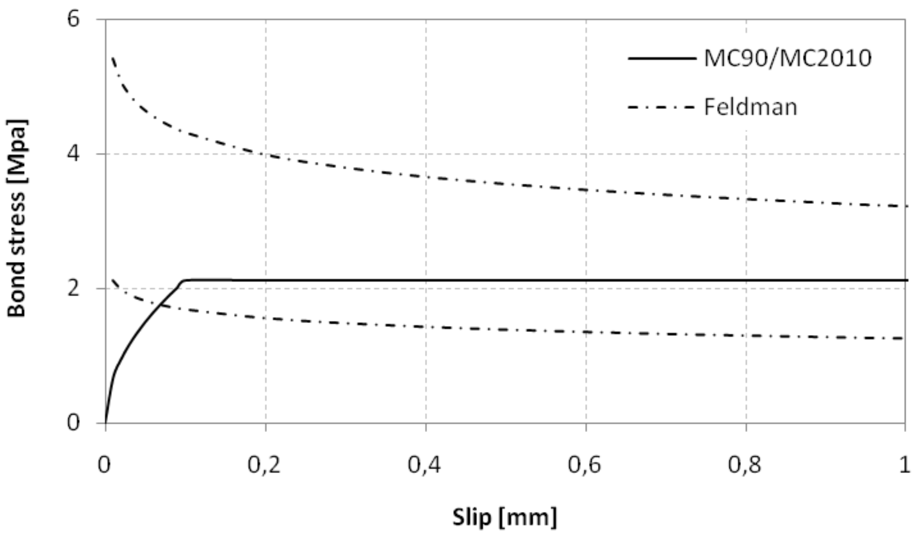

Figure 3-10 Bons stress-slip relationship for smooth rebar models. Slip values until 1 mm

According to the literature available to the author, no models have been developed regarding stainless steel flat rebars when embedded in concrete. Furthermore, no literature has been found regarding bond-slip laws for alternate patterns combining ribbed and smooth areas within the same reinforcing element.

The existing bond stress-slip relationships (both in literature and in standards) that are relevant for this work are further devloped and studied in Chapters 4 and 5, analyzing the applicability of the existing equations for prediction of the bond behaviour of the rebars studied in this thesis.

2.2 Modes of bond failure

A more detailed explanation of the observed bond failure types is given in this section. For a reinforced concrete structure, the bond failure will depend on a variety of physical and mechanical factors, such as confining pressure, concrete cover, transverse reinforcement or concrete toughness. Depending on the type of interaction between the bar and the concrete, two types of bond failure have been traditionally defined: pull out failure and splitting failure [3].

In the pull out, bond failure is due mostly to the shearing off of the concrete keys cast between each pair of ribs (see Figure 3-11-a) and the failure is by its nature related to a "local mechanism" even in the whole bar is involved (short anchorages). In other words, longitudinal cracks (parallel to the bar axis) will be formed locally between two consecutive ribs. At increasing loads, the cracks will continue growing, and each crack will join the crack formed between the following rib pair. Thus, a large crack, parallel to the bar axis, will be formed along the whole bond length allowing the bar to be pulled out. The concrete splitting remains limited to a cracked core around the bar. The bar that is being pulled out will drag the part of the concrete that has been sheared off.

The radial components of the bond forces are resisted by the tensile stress hoops developing in the surrounding concrete (see Figure 3-12). When the tensile capacity of the concrete is reached by the stress ring, the hoop breaks and longitudinal cracks appear. If the radial cracks reach the outer surface of the structural element the breaking of the tensile stress hoop will create longitudinal cracks (parallel to the bar axis) at the outer surface of the concrete: a splitting type of failure occurs and the bond capacity vanishes almost instantaneously. See Figure 3-12.

Also in pull out tests a limited splitting may occur and short hairlike radial cracks will appear, although ultimate bond behaviour is predominantly accompanied by pull out. A mixed failure (see Figure 3-11-b) has been observed for flat ribbed rebars tested in this work as it is further explained and visually demonstrated by the epoxy injection procedure applied for bond failure analysis (see Figure 4-15-d, in Chapter 4 of this work).

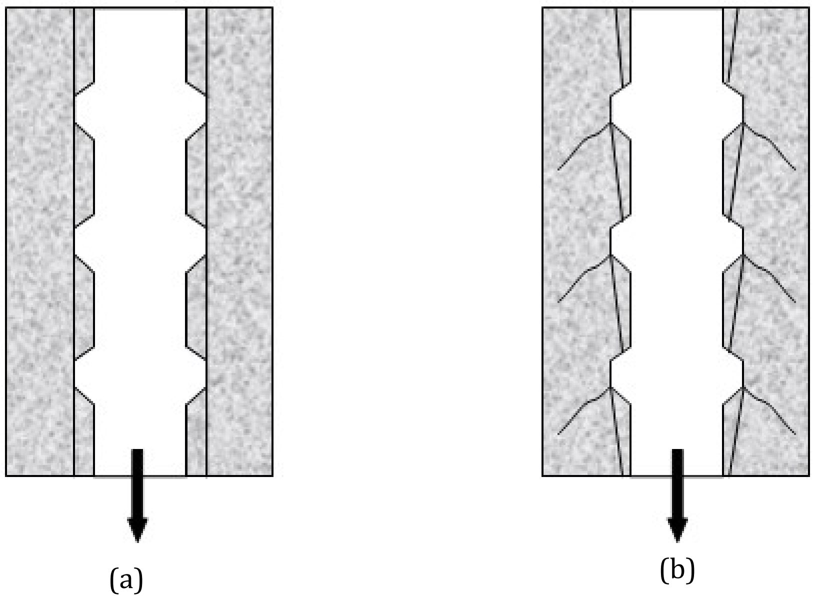

Figure 3-11 Modes of bond failure: (a) pull out type; (b) mixed type: pull out accompanied by radial cracks and crushing and/or shearing off in the concrete underneath the ribs

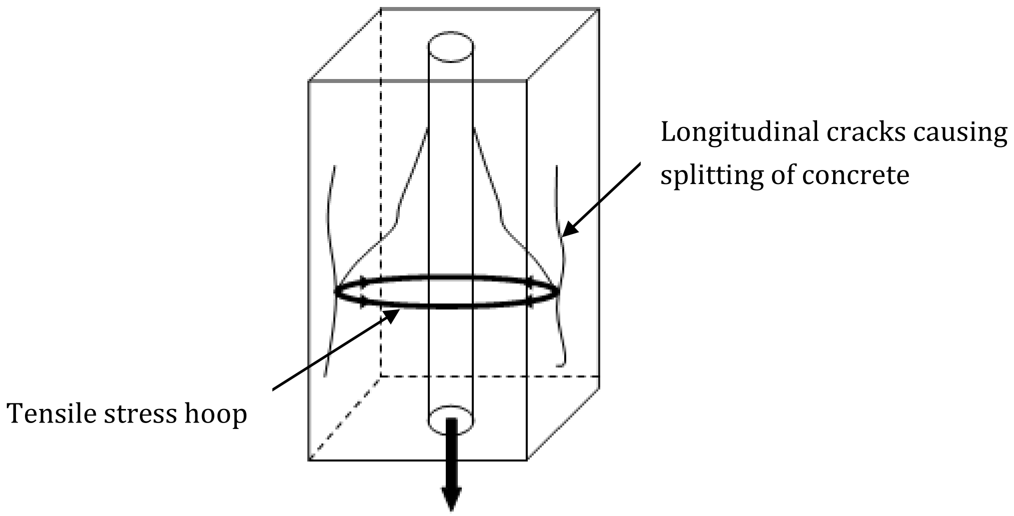

Figure 3-12 Schematic representation of how the radial components of the bond forces are balanced against tensile stress hoops, which might cause splitting type of failure if the radial cracks reach the surface of the concrete

3 Factors influencing the bond behaviour of reinforcement in concrete

Bond behaviour of reinforcement when embedded in concrete is dependent on a variety of different factors, parameters and testing conditions. It can be said that the bond behaviour basically depends on the reinforcing unit (material, shape, surface configuration, size, type, etc.), on the concrete (type, strength) and on the stress state in both the reinforcing unit and the surrounding concrete [3]. The latter factor can be conditioned by several technological aspects, as concrete cover, distance between reinforcements, casting direction, load history and transverse confinement, among others. Environmental aspects like corrosion or temperature are also conditioning the bond capacity of the reinforcement.

Extensive research regarding aspects influencing bond interaction is available in literature. In the following a summary is presented which compiles different factors influencing the bond behaviour that are most relevant for this work.

Regarding influence of reinforcement material, special focus is put in this work to possible differences in the bond behaviour between carbons steel and stainless steel reinforcement: available literature summary is presented separately in Section 4 of this chapter.

3.1 Concrete strength

Bond action between the concrete and the reinforcement is dependent on both compressive strength and tensile strength of the concrete as during loading ribs induce multiaxial stresses in the concrete and shear in the interface. Compressive strength of concrete f_c, is directly related to the pull out type of failure, while tensile strength, f_{ct}, plays a major role in the case of splitting type of failure [3].

Traditionally the square root of the concrete compressive strength has been used to describe the relationship between concrete compressive strength and the bond strength developed by the bar, with the bond strength varying linearly with $\sqrt{f_c}$ [7]. This is the case, for example, for the bond model given by the fib Model Code 1990 [8], where the maximum bond stress for the bond stress-slip law definition is given only dependent on the square root of the characteristic compressive strength of the concrete.

However more recently a move to replace the dependency of the bond strength on the compressive strength from the square root to the fourth root has emerged. Darwin et al. [9] defined the bond strength dependant on the fourth root of the compressive strength as it better characterizes the behaviour of specimens with high compressive strength (up to 100 N/mm^2), keeping the characterization of specimens with lower compressive strength as good as when applying the square root.

On the other hand, the draft version of the new Model Code 2010 developed by fib [10], considers that the maximum bond stress in the case of splitting type of failure is better characterized when the fourth root of the characteristic compressive strength of the concrete is considered. The dependency on the square root is still kept for the case in which pull out type of failure occurs.

3.2 Confinement

The degree to which the concrete surrounding the bar is confined, contributes to the ultimate bond strength of the bar. The confinement can be provided by several ways, as for example, providing enough concrete cover surrounding the reinforcement or applying extra transverse reinforcement in form of stirrups. In the following both ways are analyzed.

3.2.1 Bar spacing and concrete cover

As stated before, the radial component of the bearing forces results in tension stresses surrounding the bar. If the cover of the bar is insufficient, tension stresses will spread to the surface of the concrete resulting in a longitudinal crack along the bar and thus a loss of bond will occur rapidly. A similar reduction in bond is seen when bars are spaced closely within the concrete [7]. Figure 3-13 gives ans schematic drawing of how the concrete cover and the bar spacing influence on the splitting behaviour developed by the reinforcement. The grey areas in the drawing are meant to be understood as the area in which the radial component of the bearing forces acts.

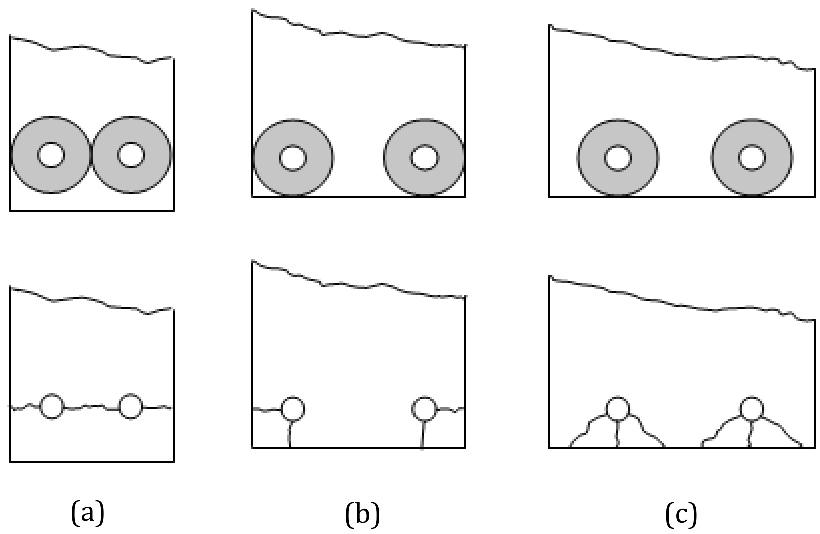

Figure 3-13 Schematic drawing of typical splitting failure surfaces. a) side cover and half the bar spacing both less than bottom cover; b) side cover equal to bottom cover, both less than half the bar spacing; c) bottom cover less than side cover and half the bar spacing. Based on [19]

As investigated by several authors [6][9][20], with increasing concrete cover, higher loads can be achieved before splitting occurs, leading to an increase of the bond strength of the reinforcement. According to Darwin et al [9], for example, the bond strength increases linearly with respect to the product $l_b(c_{min} + 0{,}5Ø)$, where l_b stands for the embedment length, c_m is the minimum of the cover or half of the clear spacing between bars and Ø is the diameter of the bar. On the other hand, Desnerck [6] related the results of his experiments to the concrete cover-to-bar diameter ratio, $c_c/Ø$. The results show a clear trend, both for traditional concrete and self compacting concrete: the bond strength increases with increasing of the ratio. Furthermore, Desnerck developed, by analytical regression of test results, bond strength prediction equations dependant on the $c_c/Ø$ ratio as given by Equation 3-15 for traditional concrete and by Equation 3-16 for self compacting concrete.

$$f_b = (1{,}940 + 0{,}291\, c_c/Ø)\, \sqrt{f_{cm}} \quad \text{for TC} \tag{3-15}$$

$$f_b = (1{,}762 + 0{,}514\, c_c/Ø)\, \sqrt{f_{cm}} \quad \text{for SCC} \tag{3-16}$$

In the case of smooth reinforcements, where bond capacity is developed mostly by chemical adhesion between the reinforcement and the concrete, bearing forces are not present, and therefore no relevant radial forces will develop surrounding the concrete. Thus, the influence of the concrete cover (or clear space between reinforcing bars) is limited. This lack of influence can be observed for example from the test results obtained by Feldman et al. [21], where several concrete diameters where tested keeping constant the bar diameter for smooth bars. No influence of the concrete cover was observed on the developed bond strength (see Table 3-3 in Section 3.4 of this chapter).

3.2.2 Transverse reinforcement

Once the radial component of the bond forces become large enough so that the compensating tensile stress hoops overcome the tension capacity of the concrete, splitting of the concrete along the longitudinal axis of the bar will occur, unless there is adequate confinement provided to resist the tensile forces. Transverse reinforcement is typically provided in form of shear and torsion stirrups in beams and columns, which surround the longitudinal bars [7]. The transverse reinforcement enables more ribs on the bar in tension to carry the existing load, creating a more uniform bond stress distribution over the bar, avoiding tensile stress peaks that could cause splitting cracks to develop abruptly.

Effort has been put in investigating how to control splitting and on to evaluate the minimum transverse reinforcement, in order to prevent an abrupt loss of bond at the onset of splitting. Giuriani et al. [22] defined the minimum reinforcement as a stirrup ratio which takes into account at the same time the yielding of the stirrup and a prefixed value of the crack width (as required for instance by durability aspects), considering crack cohesion, which contributes to the confining effect [3].

On the other hand, Darwin et al. [23] stated that once the point where a pull out failure governs over a splitting failure is past, increasing the confinement has little to no effect on the bond capacity developed by the rebar. This effect is also confirmed in this work, when extra stirrups are added to avoid the splitting tendency observed for the tested flat ribbed reinforcement. This is further discussed in Chapter 5 of this work.

3.3 Bar surface configuration

Regarding surface configuration of the reinforcement bar, the main distinction should be made between ribbed and smooth bars. As already discussed in this chapter, the bond mechanism governing for each of the surface textures is different: mechanical interaction between the ribs of the reinforcement and the concrete dominates the bond capacity of ribbed bars, while chemical adhesion and remaining friction are the main bond forces present when reinforcing with smooth bars. Thus, the two surface types are studied separately in the following.

3.3.1 Ribbed reinforcement

For an optimal mechanical interaction between the ribs of the rebar and the concrete to take place, optimal geometrical parameters should be present at the reinforcement. In the following the main influencing parameters are considered.

3.3.1.1 Relative rib area

For the bearing forces to be transferred in an effective way, an appropriate combination of rib height, rib spacing and bar diameter is necessary. It is believed that the best bond performance of ribbed samples is obtained when these three geometrical parameters are combined effectively. The so-called *bond index* or *relative rib area* (f_R) is a coefficient that considers the above mentioned parameters. It is defined as the area of the projection of a rib normal to the bar axis, divided by the perimeter area of the bar between two ribs, see Equation 3-17.

The existing standard EN ISO 15630 [24] gives the general formula (Equation 3-18) and a set of simplified formulas for the calculation of the relative rib area.

$$f_R = \frac{projected\ rib\ area\ normal\ to\ the\ axis}{nominal\ bar\ perimeter \times centre\ to\ centre\ rib\ spacing} \tag{3-17}$$

$$f_R = \frac{1}{\pi \emptyset} \sum_{i=1}^{n} \frac{\frac{1}{m}\sum_{j=1}^{m} F_{R,i,j} \sin \beta_{1,j}}{c_i} \tag{3-18}$$

where, Ø is the nominal diameter of the bar, c_i stands for the clear rib spacing between two ribs, n is the number of rows of transverse ribs on the circumference; m is the number of different transverse rib inclinations per row, β stands for the transverse rib angle and gives the inclination between the ribs and the longitudinal axis of the reinforcement, and $F_R = \sum_{i=1}^{p}(a_{s,i}\,\Delta l)$ is the area of the longitudinal section of one rib (see Figure 3-14) where $a_{s,i}$ is the average height of a portion i of a rib subdivided in p parts of length Δl.

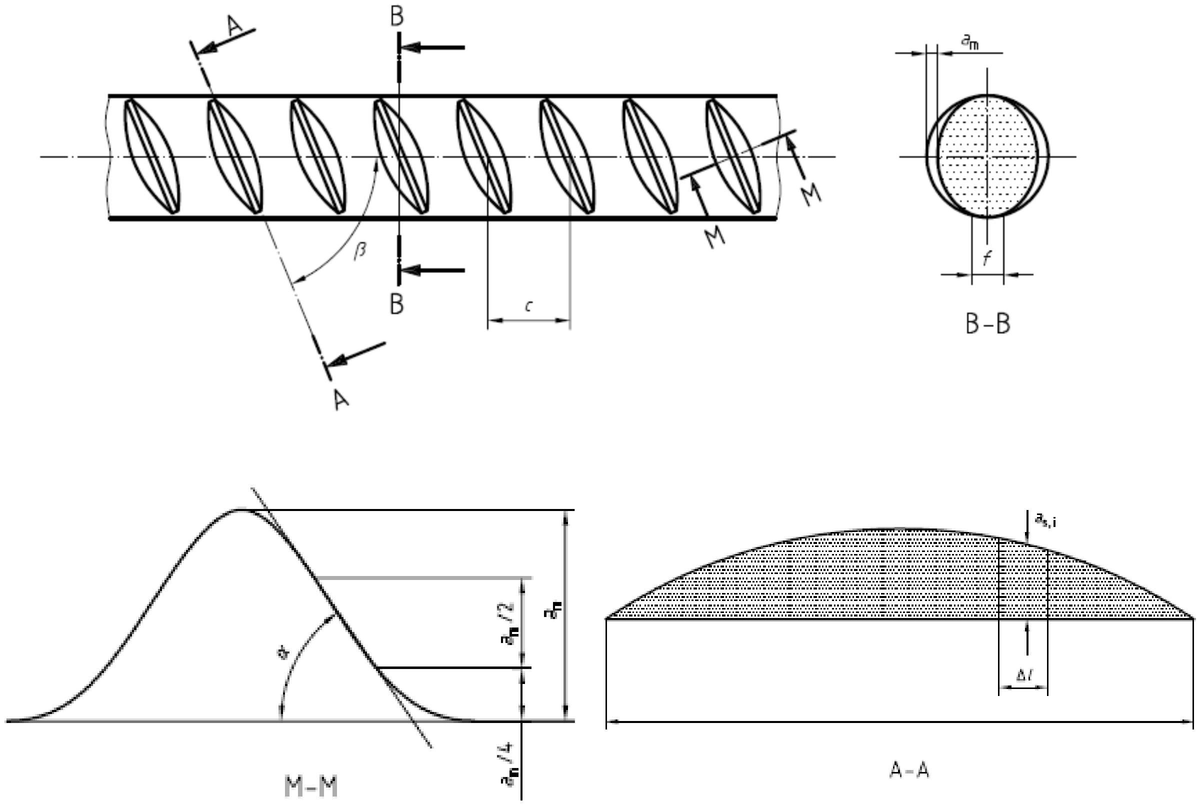

Figure 3-14 Geometrical parameters involved in the calculation of relative rib area. Figure given as in EN ISO 15630 [24]

In general, as the relative rib area increases, the bond strength also increases [9][25][26][27]. Figure 3-15 shows the results obtained by Rhem (taken from [3]): the bond stress at a slip of 0,1 mm normalized by the concrete compressive strength is represented versus the relative rib area of each tested bar. Bar diameters ranging between 8 and 32 mm were tested. The results showed a linear relation between the bond strength and the relative rib area. However, fib Bulletin 10 - Bond of reinforcement in concrete [3], recommends relative rib area values of between 0,05 and 0,10 for a good compromise in terms of ultimate bond strength, splitting tendency, industrial requirements and good service load performance (limited crack opening and cover splitting).

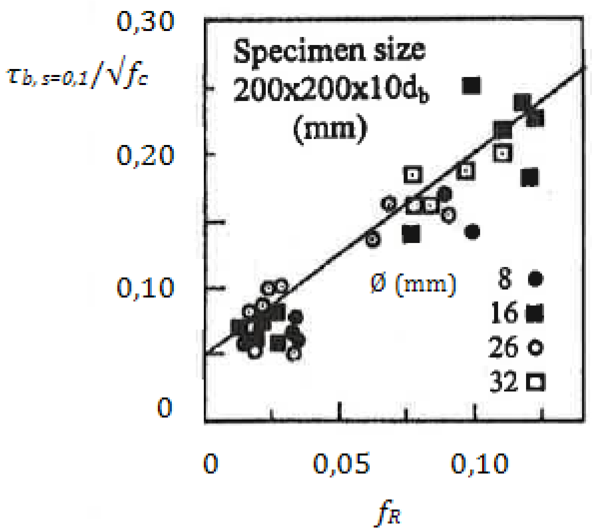

Figure 3-15 Effect of the relative rib area on the bond stress by Rehm. From [3]

3.3.1.2 Rib face angle

Another geometrical aspect that has been demonstrated that influences the bond behaviour of the reinforcement when embedded in concrete is the rib face angle (represented as α in Figure 3-14). The rib face angle influences the concrete area to be crushed in front of each rib, and therefore, directly influences the relative movement between the reinforcement and the concrete, the slip between them [28]. According to several investigations [2][28][29], the bond stiffness (bond stress to slip ratio) improves with increasing the rib face angle values. However, it has also been observed that after a certain value of this angle no improvement of the stifness is achieved. The latter phenomenon can be clearly observed in Figure 3-16, where the load slip behaviour of 5 reinforcements is plotted. The figure represents the test results obtained by Hamad et al. [29] for eccentric pull out tests performed to specially machined bars. The rib spacing, the rib height and the bar diameter were kept constant, and the only variable was the rib face angle, ranging from 30° to 90°. The average compressive strength of concrete was 22,4 N/mm^2. It can be clearly seen that the bond performance improved when increasing the rib face angle from 30° to 45° and from 45° to 60°. However, for samples with 75° and 90° of rib face angle, the initial stiffness of the bond capacity was similar to the one of 60° with decreased load values at increasing slips.

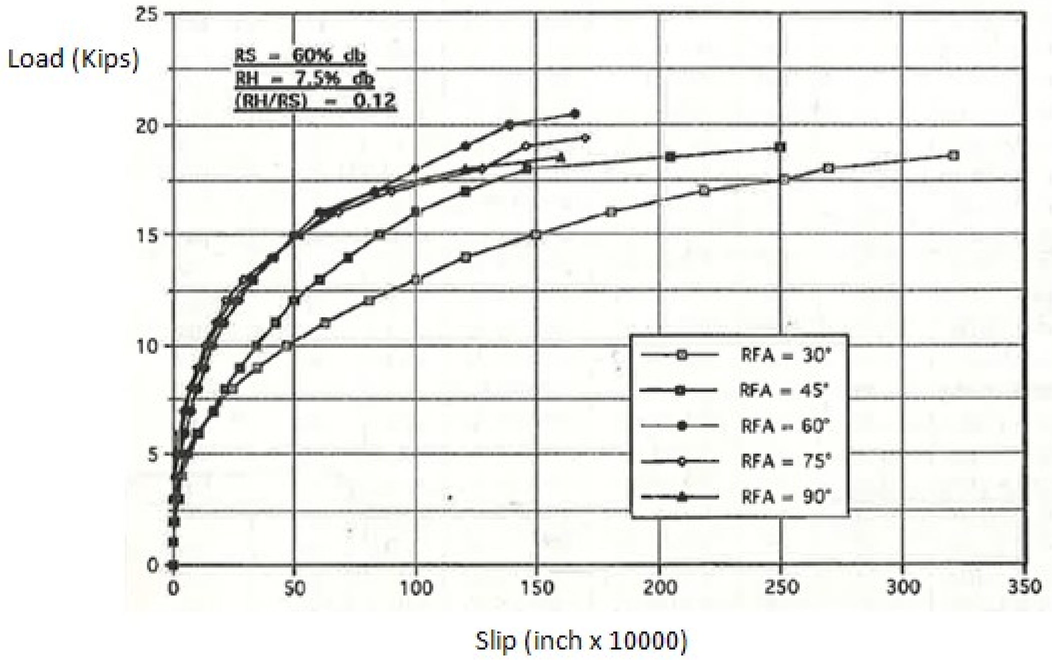

Figure 3-16 Load-slip curves for bars with different rib face angle values. From [29]. (1 Kips = 4448,22 N; 1 inch = 25,4 mm)

3.3.2 Smooth reinforcement

For smooth bars, the bond efficiency is mainly assured by chemical adhesion, although micromechanical interaction may also be present due to the microroughness characteristics of the steel to be tested. Once the chemical adhesion is broken, the sliding of the bar will follow where only friction forces will remain (see Stage 1 and Stage 4a in Figure 3-3). The bond stress-slip law present for smooth bars, therefore, differs from the one for ribbed bars. The chemical adhesion is able to develop bond strength values that are much lower than the bond capacity developed by the bearing forces present for ribbed bars. E.g. Mo et al. [30] concluded from pull out tests on smooth and ribbed reinforcements with a nominal diameter of 12,7 mm, that the bond strength of smooth rebars was only 28,6% of the deformed rebars. This phenomenon is also observed in this work, where differences of the bond strength and bond stress-slip relationships developed by ribbed and smooth bars are analyzed for both round and flat samples (see Chapter 4).

Furthermore, some parameters affecting the bond behaviour of the reinforcement when embedded in concrete have a more relevant effect when working with smooth samples. This is for example the case for the bar diameter. The bond strength decreases with increasing bar diameter as shown in Figure 3-17 [3]. The Poisson effect is also more relevant in the case of smooth samples: when the force transfer mechanism is based predominantly on friction (after the chemical bond is broken), the local transverse deformation of the bar cannot be disregarded, since the surface microroughness and the transverse reduction of bar diameter may have the same magnitude, leading to reduced frictional bond stresses [3].

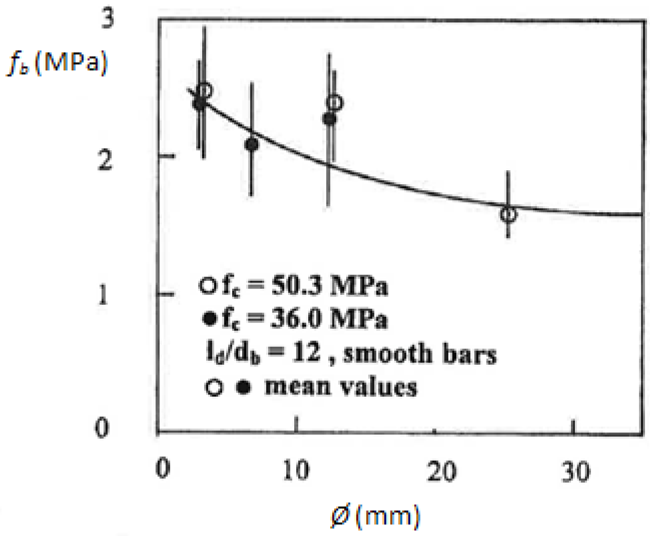

Figure 3-17 Size effect for smooth bars. From [3]

3.4 Bar geometry

According to the literature available to the author, few studies have been conducted related to bond behaviour of flat rebars when embedded in concrete. Abrams [31], in 1913, studied different parameters affecting the bond interaction between the steel and the concrete, among which the geometry of the rebar: flat rebars were compared to round bars. Smooth samples were tested and two different flat rebar aspect ratios were tested.

Bond tests were performed to specimens with an average compressive cube strength of concrete of 12,75 N/mm^2 and an embedment length of around 200 mm. The research conducted by Abrams allows for a comparison between the bond capacity of round smooth bars of a nominal diameter of 25,4 mm (1 inch) and two flat rebars with cross sections of 25,4 x 12,7 mm^2 (1 x ½ inch^2) and 50,8 x 6,35 mm^2 (2 x ¼ inch^2), respectively.

The study concluded that for similar bond strength to be achieved, more steel was needed if round bars were used. In other words, for a comparable bond strength development, where similar contact areas are involved ($u_{round} \approx u_{flat}$), larger surface area, and therefore more material was used in the case of round bars ($A_{round} > A_{flat}$). From the same study it has been concluded that for comparable cross sectional areas within the flat rebars, higher bond strength results were obtained for the elements with smaller aspect ratio (defining the aspect ratio as the ratio between the wider and the narrower side lengths of a given flat reinforcement). Table 3-2 summarizes the main geometrical properties of the tested bars together with giving the bond strength values obtained in this research.

Table 3-2 Tested rebars properties and test results by Abrams [31]

Rebar/Geometry	***Area (mm²)***	***Perimeter (mm)***	***Aspect ratio (-)***	***f_c (N/mm²)***	***f_b (N/mm²)***
Round – Ø 1 inch	506,7	79,8	-	12,75	3,03
Flat - 1 x ½ inch²	322,6	76,2	2	12,75	3,16
Flat - 2 x ¼ inch²	322,6	114,3	8	12,75	2,02

Feldman et al. [21] conducted an extensive research for assessing the bond behaviour of smooth reinforcements. Both round bars and squared bars were analyzed by means of pull out tests conducted for different bar cross sections, different embedment lengths and several confinement pressures by means of different concrete specimen diameters. Low cylinder compressive strength concrete was used for casting of the specimens (in average $f_c \approx 13{,}7$ N/mm²). Table 3-3 summarizes the main parameters involved in the experiments as well as the test results obtained in terms of normalized bond strength (normalized according to the squared root of the compressive strength of the concrete).

Test results in terms of developed bond strength show very similar or slightly better behaviour for squared samples. However, direct comparison becomes complex as different cross sections and different perimeters are involved, and drawing out conclusions in terms of which reinforcement shape performed better is difficult.

Table 3-3 Testing parameters and test results by Feldman [21]

Rebar/Geometry	***Area (mm²)***	***Perimeter (mm)***	***Embedment length (mm)***	***Concrete diameter (mm)***	***f_c (N/mm²)***	***$f_b/\sqrt{f_c}$ ($\sqrt{N}$/mm)***
Round – Ø16 mm	201,1	50,3	192	75	14,2	0,43
			192	100	18,6	0,35
			192	150	14,3	0,41
			192	200	14,4	0,32
Squared – ■16 mm	256,0	64,0	192	75	17,8	0,51
			192	100	14,2	0,32
			192	150	14,2	0,41
			192	200	18,3	0,42
Round – Ø32 mm	804,2	100,5	384	200	14,1	0,25
			768	200	13,5	0,20
Squared – ■32 mm	1024,0	128,0	384	200	12,8	0,27
			768	200	13,0	0,29

3.5 Corrosion

Rusting and corrosion are both two environmental aspects affecting the bond capacity of the reinforcement when embedded in concrete. A difference is made between rust and corrosion as follows: bar rusting refers to the initial bar rusting owing to steel exposure to the environment as it cools down from the rolling temperature (naturally or by water quenching) or to atmospheric conditions (humidity, pollution...). It consists of a thin layer of iron oxide (0,3-1,5 g/dm^2) which protects the bar against corrosion. On the other hand, corrosion is related to the destabilization of this protective layer which occurs in embedded steel when chloride ions or/and gases like oxygen and carbon dioxide penetrate the porous concrete and reach the steel surface.

Regarding influence of bar rusting on the bond behaviour developed by the bar, conducted results showed that bond strength is generally helped by the presence of residual rust and that the loss of section is too small to be significant [3].

On the other hand, severe steel corrosion in reinforced concrete leads to losses in the structural performance of the structure, mainly caused by three factors: losses in the mechanical performance of steel due to the decrease in its cross section area, splitting and spalling of the concrete section and loss of bond between the reinforcement and the concrete [32].

Several researches [32][33][34][35][36] have performed bond tests to specimens previously submitted to accelerated corrosion laboratory procedures. Overall results show that bond strength increases with the corrosion degree up to a maximum, after which increasing corrosion causes a significant reduction of bond strength [3]. A study performed by Fang et al. [32], for example, showed that for deformed bars, bond strength was very sensitive to corrosion levels (defined as weight of reinforcement lost due to corrosion within the bond length, in percentages) and generally decreased with increasing the corrosion level: with 4% of corrosion the bond strength was reduced around 40% and with 9 % of corrosion developed on the bar the bond strength was only 33% of the uncorroded specimens (see Figure 3-18). However, it was also observed that for low corrosion values (lower than 0,5%), the bond strength increased compared to the uncorroded samples.

In the same study, it was observed that for smooth samples, higher corrosion values are favourable to the bond strength development. Bars comprising corrosion levels up to 2-4%, developed bond strength 2,5 times higher than the one developed by the non corroded bar. However, at higher corrosion levels, the bond strength decreased rapidly.

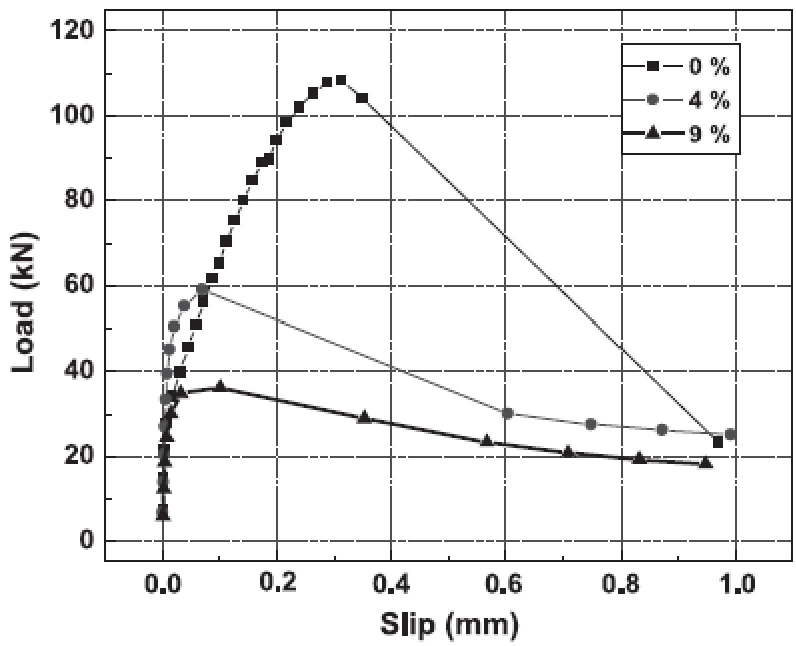

Figure 3-18 Load slip relationship for deformed bars tested with 0%, 4% and 9% of corrosion levels. From [32]

As a consequence of the unfavourable effect of severe corrosion on the good structural performance of reinforced concrete, several approaches related to the use of non corrodible reinforcement have been undertaken in order to avoid or reduce corrosion. This is the case for stainless steel reinforcement, which is discussed in Chapter 2 of this work.

4 Bond behaviour of stainless steel reinforcement in concrete

Although extensive research has been conducted in terms of assessing and verifying the corrosion resistance of SS reinforcement when embedded in concrete, as discussed in section *3.1 Corrosion resistance* of Chapter 2, little literature is available regarding bond interaction between SS reinforcing bars and concrete. Furthermore, the available literature only refers to round SS rebars and no research studies have been found regarding bond behaviour of flat SS rebars. In the following a description of the found works is presented.

4.1 Alhborn et al.

Alhborn et al. [37] from Michigan Technological University investigated the bond behaviour of two types of stainless steel (austenitic 1.4406 and ferro-austenitic 1.4462, corresponding to the American AISI denomination of 316LN and 2205, respectively). Both of them were compared to A615 Gr. 60 carbon steel reinforcement (corresponds to carbon steel reinforcement of grade 60 according to the ASTM specification A615 [38], which deals with a bar with a minimum yielding strength of 60 ksi, ~420 N/mm^2). The relative rib area, calculated according to ACI 408.3 [39], ranged from 0.0865 up to 0.1728 depending on the bar size and material. See Table 3-4.

Beam-end type of bond tests were performed and the used test specimen was designed according to ASTM A944 [40]; a schematic representation of the specimen is given in Figure 3-19. Bond lengths varying from 101,6 mm (4 in) up to 304,8 mm (12 in) were applied and two different bar diameters were tested: No.4 and No.6 bar sizes according to the American standards (equivalent to 12,7 mm and 19,05 mm of nominal diameter, respectively). A clear concrete cover of 38,1 mm (1,5 in) was applied for all tests, selected so that the bond failure would be by cracking of the concrete caused by the circumferential tensile stresses the bar sliding out of the concrete (splitting type of failure). As illustrated in Figure 3-19, externally the bar at the active end (where the force was applied) extended 1016 mm and 50,8 mm at the passive end. Regarding the embedded part of the reinforcement, 25,4 mm (1 in) of unbonded zone was kept at the active side of the specimen to reduce tensile stresses along the front face that do not exist in a full beam. Immediately after which the bonded length followed; a variable unbonded length (varying according to the applied bond length) was kept at the passive end of the specimen. No transverse reinforcement was included. The average compressive cylinder strength of the tested specimens was ~38 N/mm^2 . The load was applied at a rate of 138 N/mm^2 per minute, which corresponds to a loading rate of 0,30 kN per second for bars with a diameter ~13 mm, and 0,65 kN/s for bars with a diameter ~19 mm.

Load at failure and slip at the same instant where measured and recorded. In the study, bond failure was defined as the load to cause a passive end displacement of 0,05 mm, and this force value was considered as the maximum load for calculation of the bond strength. A compilation of the bond strength results obtained is given in Table 3-5.

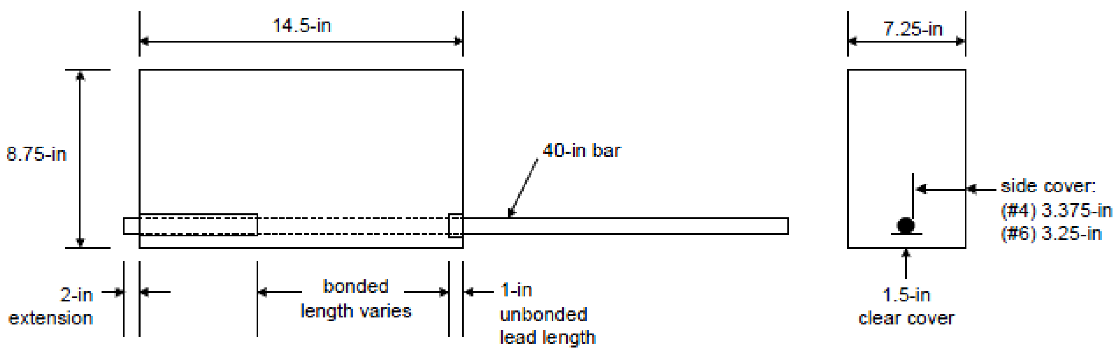

Figure 3-19 Beam-end test specimen, by Alhborn et al [37]. Note, 1 in = 25,4 mm

Table 3-4 Relative rib area values for tested bars [37]

	No.4			***No.6***		
Bar material	A615	1.4406	1.4462	A615	1.4406	1.4462
Relative rib area	0,0992	0,1083	0,0865	0,1728	0,1008	0,1156

Test results showed different trends depending on the bar size. For smaller sizes, No.4 bars (~13 mm of bar diameter), all of the highly alloyed steels develop higher bond strength than the standard carbon steel bar for any of the tested bond length. Moreover, the OJB equation [41] was used for prediction of the bond strength; the experimentally obtained bond strength values were up to 55% higher than the predicted ones for SS bars (for carbon steel a maximum of 18% of increase was observed). On the other hand, for higher bar sizes, No.6 bars (~19 mm of bar diameter), bond strength developed by carbon steel was always higher than the one developed by 1.4462 stainless steel, for any of the tested bond lengths. In the case of the austenitic 1.4406 SS, lower bond strength was developed, compared to carbon steel, for short bond lengths (6 and 8 in of bond length, 152,4 and 203,2 mm, respectively); for larger bond lengths (254,0 and 304,8 mm, corresponding to 10 and 12 in, respectively) higher bond strength was developed by the corrosion resistant rebar. In any case, the predicted values using the OJB equation [41] were always lower than the experimentally obtained ones, for any of the tested material and for all the tested conditions. Regarding failure type, similar crack patterns and failure modes were observed in all the cases: on the face of the specimen with the smallest concrete cover, the crack followed the bar axis up to the point where the bar was debonded, and then continued to each side of the specimen ("Y" form cracking).

Furthermore, statistical tools were applied for a more accurate test result analysis and comparison and concluded that there was no statistical reason to assume that the experimental bond strength obtained for SS reinforcement was less than the A615 bar experimental bond strength for all bonded lengths. As a final conclusion, Alhborn et al. stated that no modifications are needed when estimating the development length of tested highly alloyed materials as a one-to-one replacement for A615 Gr. 60 reinforcement, No.4 and No.6 bars.

Table 3-5 Main test results [37]

Material	*Diameter (mm)*	*Bond length (mm)*	*Bond strength (N/mm²)*
A 615 Gr. 60	~ 13	101,6	7,44
		139,7	6,59
		203,2	5,89
	~ 19	152,4	9,06
		203,2	8,33
		254,0	7,35
		304,8	6,10
1.4406	~ 13	101,6	9,03
		139,7	9,07
		203,2	7,80
	~ 19	152,4	7,67
		203,2	7,38
		254,0	7,40
		304,8	6,76
1.4462	~ 13	101,6	9,64
		139,7	8,01
		203,2	7,76
	~ 19	152,4	6,95
		203,2	6,74
		254,0	6,22
		304,8	5,83

However no analysis of the influence of the relative rib area on the developed bond strength was performed in this study. Analyzing the data presented in the paper, the higher relative rib area value for No.6 A615 carbon steel bar (compared to No.4 of the same material type), might explain the difference observed on the bond behaviour between No.4 and No.6 bars, regarding developed bond strength of highly alloyed materials in comparison to A615 carbon steel bar.

4.2 Jhonson

The study [42] consisted of the characterization of the bond strength of different corrosion resistant reinforcements when embedded in concrete, where among others, two austenitic stainless steels (1.4406 and another not classified austenitic SS called N32 (similar in composition to 1.4597 but with increased manganese percentage)), one duplex SS (1.4462) and one carbon steel core with 1.4404 SS clad (called NX) reinforcements were tested. Reference elements carbon A615 Gr. 60, No.4 and No.6, were also tested for comparison. Both pull out and beam-end tests were performed for each bar type (except for 1.4462 for which only beam-end tests were conducted). The full test matrix is presented in Table 3-6 (other corrosion resistant rebars that are not made of SS were also tested in the study, but they are omitted in this table). The test specimen consisted (for both performed test types) on a concrete prism (228,60 x 285,75 x 609,60 mm^3) with the reinforcement embedded eccentrically on it. The bar extended at both sides out of the concrete prism, and the bond length was limited by a PVC bond breaker tube which was placed at both active (76,20 mm long plastic tube) and passive end (the length of the plastic tube at this side varied as the bond length also varied from test to test) of the specimen. A Linear Variable Data Transducer (LVDT) was placed at the passive end for recording continuously the relative displacement between the steel and concrete (slip). Extra reinforcement in form of stirrups was applied to resist the shear forces developed in the specimens during testing. Compressive cylinder strength of the concrete at 28 days was on average ~41 N/mm^2.

Table 3-6 Test matrix by Jhonson [42]

	Pull out test				***Beam-end test***			
Bar type	*Bar size (AISI)*	*Bar size (mm)*	*Number of tests*	*Relative rib area*	*Bar size (AISI)*	*Bar size (mm)*	*Number of tests*	*Relative rib area*
A615	No.4	~ Ø13	4	0,080	No.4	~ Ø13	4	0,079
	No.6	~ Ø19	4	0,095	No.6	~ Ø19	4	0,097
1.4406	No.4	~ Ø13	6	0,079	No.4	~ Ø13	4	0,076
	No.6	~ Ø19	6	0,085	No.5	~ Ø19	4	0,089
N32	No.4	~ Ø13	6	0,095	No.4	~ Ø13	4	0,093
	No.5	~ Ø16	6	0,085	No.5	~ Ø16	4	0,060
1.4462	-	-	-	-	No.5	~ Ø16	4	0,090
	-	-	-	-	No.6	~ Ø19	4	0,081
NX	No.5	~ Ø16	6	0,060	No.5	~ Ø16	4	0,056
	No.6	~ Ø19	6	0,085	No.6	~ Ø19	4	0,063

Test results were presented in form of: 1) numerical values of average maximum recorded load and average slip at maximum load stage (for each test type and each tested bar and size) and 2) normalized load-slip graphs. Table 3-7 compiles the main test results obtained. Pull out test results showed that for both 1.4406 and N32 austenitic SS, higher maximum loads (27% and 22% higher loads, respectively) were recorded at a similar slip value in comparison to A615 carbon steel bar for a bar size of ~Ø13 mm. For ~Ø19 mm bars, and pull out tests, 1.4406 and NX reinforcements reached 22% and 17% higher load values, respectively, compared to A615. Furthermore, the higher values were reached at considerably lower slip values (up to 58% smaller slip for NX reinforcement). Note that due to the differences in bar diameter, not all the tested specimens are comparable to the reference. Regarding beam-end tests, for the smallest bar size (No.4, ~Ø13 mm), higher maximum loads (up to 25% higher) were recorded for 1.4406 and for N32 austenitic SS than for carbon A615 steel. However, the slip at which these values were reached are significantly larger (9 times larger) than for carbon steel, showing a less stiff bond capacity of SS bars. Finally, beam-end tests performed for No.6 reinforcements (~Ø19 mm) showed lower maximum load values for 1.4462 and NX (5% and 25% lower, respectively) than for carbon steel with the same diameter. The slip values at which these loads were registered, were similar in comparison to A615 for 1.4462 duplex SS and 3 times higher for NX.

In summary, regarding pull out tests, up to 27% higher bond strength values were developed by SS reinforcements, regardless of the bar diameter. However the bond strength to slip ratio (bond stiffness) was higher for the CS when diameter 13 mm bars were tested and higher for SS reinforcement when diameter 19 mm rebars were applied. For beam-end tests, only smaller rebars (Ø 13 mm) developed higher bond strength than the CS (up to 25% higher), but the latter was reached at higher slip values. Regarding diameter 19 mm rebars, CS developed higher bond strength and at lower slip values.

Regarding the effect of the relative rib area, a trend is observed related to an increase of the peak load (and therefore, an increase of the bond strength) with increasing relative rib area values. This influence is more pronounced for specimens that failed by pull out than for specimens that failed by splitting of concrete.

Table 3-7 Main test results [42]

Material	*Test type*	*Diameter (mm)*	*Bond length (mm)*	*Bond strength (N/mm²)*	*Slip at peak load (mm)*	*Bond strength/slip (N/mm³)*
A 615 Gr. 60	Pull out	~ 13	133,3	10,46	0,20	52,30
		~ 19	133,3	15,26	1,63	9,36
	Beam-end test	~ 13	101,6	13,51	0,20	67,55
		~ 19	101,6	20,02	0,81	24,72
1.4406	Pull out	~ 13	133,3	13,32	0,30	44,40
		~ 19	133,3	18,67	1,32	14,14
	Beam-end test	~ 13	101,6	16,29	1,96	8,31
N32	Pull out	~ 13	133,3	12,83	0,38	33,76
	Beam-end test	~ 13	101,6	16,94	1,83	9,26
1.4462	Beam-end test	~ 19	101,6	19,14	0,84	22,79
NX	Pull out	~ 19	133,3	17,95	0,69	26,01
	Beam-end test	~ 19	101,6	15,04	2,67	5,63

Bond strength tests results were compared to predicted values according to the ACI 318 [43] design code. For all the tested reinforcement types and sizes, the predicted values were lower than the ones derived from test results. Consequently, Jhonson concluded that all corrosion resistant reinforcement types tested could be considered for use in bridge decks as top mat reinforcement.

4.3 Aal Hassan

Bond behaviour of corrosion resistant reinforcements was tested at Reyerson University, Toronto [44], by pull out tests to centrally embedded bars. Besides standard carbon steel, epoxy coated bars and one type of SS bars were tested. Although denomination of the used SS grade is not specified in the work, according to the given composition, it can be concluded that an austenitic stainless steel grade was used, similar in composition to 1.4401 (X5CrNiMo 17-12-2). Test specimens (Figure 3-20) consisted of concrete cylinders with diameter 100 mm and height 200 mm, with a Ø20 mm reinforcement bar centrally embedded. The entire embedded length (160 mm) was in direct contact with the concrete (no unbonded zones) and the bar extended 300 mm outside the concrete cylinder. Four different concrete types were tested: 1) normal Portland cement (NPC) based concrete with a water/cement ratio of 0,32, and compressive cylinder strength at 30 days of 26 N/mm^2; 2) NPC based concrete with a water/cement ratio of 0,52 and compressive cylinder strength of 14 N/mm^2 at 30 days; 3) fly ash (FA) concrete mixture with 0,32 of water/cement ratio and compressive cylinder strength at 30 days of 33 N/mm^2; and 4) silica fume (SF) concrete mixture with water/cement ratio of 0,32 and compressive cylinder strength of 26 N/mm^2 at 30 days.

A LVDT, placed at the active end, was used for the recording of the relative displacement between the steel and the concrete. Maximum registered loads, the corresponding bond strength and the slip value at maximum load are given as test results. Furthermore, the continuous slip and load measurements allowed for plotting of the bond stress-slip relationships. No data was provided regarding relative rib area of the applied reinforcement.

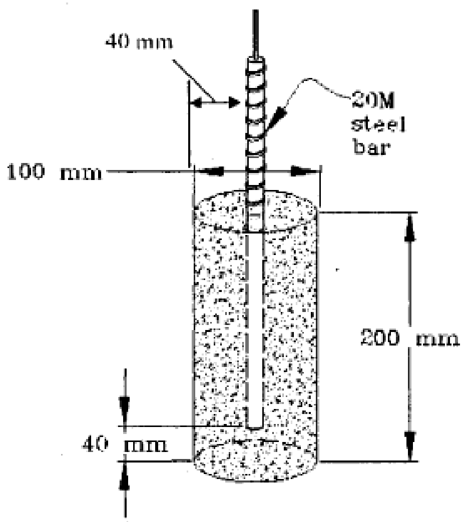

Figure 3-20 Test specimen by Aal Hassan [44]

Test results (see Table 3-8) showed better performance for standard carbon steel bars than for stainless steel bars for all the tested concrete types. The closest results were obtained for normal Portland cement with a water/cement ratio of 0,32, for which the SS rebar developed 0,88 times the bond strength developed by the standard carbon steel for the same condition. Bond stress-slip relationships for carbon steel, epoxy coated reinforcement and stainless steel rebar when embedded in normal Portland cement concrete with a water/cement ratio of 0,32 are given in Figure 3-21. The biggest differences between both materials were found when embedded in fly ash concrete; in this case the bond strength developed by SS was 0,78 times the one of carbon steel. Focusing on the stainless steel itself, best results in terms of bond strength were obtained when embedded in normal Portland cement with a water/cement ratio of 0,32 as illustrated in Figure 3-22. Note that individual test results are plotted in Figure 3-21 and Figure 3-22, whereas the numerical analysis has been performed based on average values (out of 3 tests performed per reinforcement and concrete type).

The results obtained in this research differ from the previous two studies in terms of the bond strength developed by the SS rebar, which is always lower than the one of CS. However, no data is provided regarding relative rib area of the applied rebars, which is an important influencing factor.

Table 3-8 Main test results [44]

Material	***Concrete type***	***w/c ratio***	***Diameter (mm)***	***Bond length (mm)***	***Bond strength (N/mm^2)***	***Slip at peak load (mm)***
Carbon steel	NPC	0,32	20	160,0	6,67	0,90
	NPC	0,52	20	160,0	3,91	0,79
	FA	0,32	20	160,0	5,45	0,69
	SF	0,32	20	160,0	5.93	0.72
1.4401	NPC	0,32	20	160,0	5,84	0,87
	NPC	0,52	20	160,0	3,24	0,66
	FA	0,32	20	160,0	4,26	0,46
	SF	0,32	20	160,0	5,04	0,62

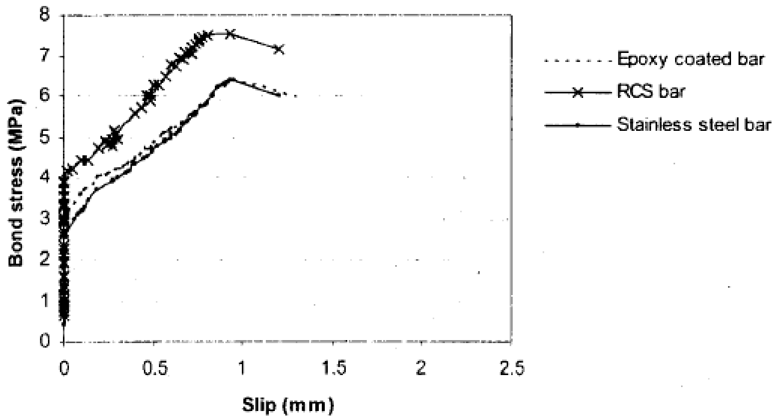

Figure 3-21 Bond stress-slip relationship recorded for different tested reinforcement types embedded in normal Portland cement with a w/c ratio of 0,32, by Aal Hassan [44]

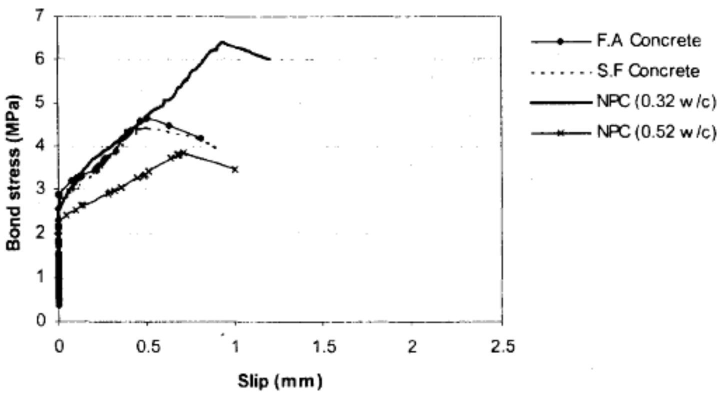

Figure 3-22 Bond stress-slip relationship recorded for SS embedded in different types of concrete, by Aal Hassan [44]

4.4 Jayasankar

During the National conference on Advances in Bridge Engineering of India in 2006, Jayasankar [45] presented several aspects related to the so-called Nuovinox reinforcement which consisted on carbon steel core reinforcement with SS (austenitic 1.4404) clad which is obtained by a metallurgical bond between the two materials during the hot rolling process (see Figure 3-23). Results obtained from a comparative study of the bond strength of different corrosion resistant reinforcements were given in this paper, where a purely SS (material grade not specified) reinforcement was also analyzed. No extensive data was provided related to specimen dimensions or test set up. Obtained bond strength values (average of performed 3 tests) were 4,70 N/mm^2 for Nuovinox, 4,35 N/mm^2 for stainless steel and 3,72 N/mm^2 for carbon steel. Thus, better bond capacity of SS reinforcement when embedded in concrete compared to carbon steel was reported.

Figure 3-23 Samples of Nuovinox provided by Stelax Industries Ltd., West Glamorgan, U.K. (thickness of cladding over carbon steel core varied from 5 to 10 mm)

4.5 Analysis of the compiled data

Test data obtained from the literature allow for a comparative analysis of the bond behaviour developed by stainless steel rebars when embedded in concrete (Table 3-9). Each test average result for SS has been divided by the corresponding average test result of carbon steel (for the same test type and same bar diameter), obtaining a bond strength ratio $f_{b,SS}/f_{b,CS}$. Figure 3-24 to Figure 3-26 give the values of the calculated ratio in relation to the bar diameter or relative rib area for each tested material type and test condition. The black line crossing at bond strength ratio value of 1 corresponds to carbon steel. Thus, values above the line can be interpreted as higher bond capacity than carbon steel bars and values below the line as lower developed bond strength values for SS. As given by Figure 3-24, a trend is observed in the influence of bar diameter: the smaller the bar diameter the better performance of the SS in comparison to carbon steel. Furthermore, it can be concluded that the influence of the bar diameter is stronger than the influence of the SS type, as for the same SS type different results (higher or lower bond strength than the corresponding carbon steel) are obtained depending on the bar diameter. However, note that the relative rib area is not constant for the data points included in this graph, which might have influenced the comparison.

The influence of the relative rib area can be seen in Figure 3-25 and Figure 3-26. The bond strength ratio between SS and CS has been plotted vs. the relative rib area ratio, the latter defined as the relative rib area of SS divided by the relative rib area of CS for the same testing condition (diameter and test set-up): $f_{R,SS}/f_{R,CS}$. Note that test results of austenitic SS 1.4401 are not plotted as the values of the relative rib areas are not specified in the work

[44]. Similar as observed for the bar diameter, the relative rib area appears to be a more deterministic influencing factor than the SS type on developed bond capacity.

A trend is observed regarding relative rib area ratio: the lower this ratio, the lower is also the bond strength developed by the SS in comparison to CS (see Figure 3-25), which confirms the effect of the relative rib area in the developed bond strength. However, if only relative rib areas are considered that are recognized as optimum for both steel materials (values between 0,05 and 0,10)[2], and the relative rib area ratio is calculated accordingly, 89% of the analyzed SS rebars develop higher (up to 27% higher) bond strength values than the CS rebars, regardless of the SS type (see Figure 3-26).

Table 3-9 Summary of the data obtained from literature

SS type	***Bar diameter (mm)***	***Relative rib area***	***$f_{b,SS}/f_{b,CS}$***	***Author***
1.4401	~20	nda*	0,82	Aal Hassan [44]
	~20	nda*	0,88	
	~20	nda*	0,85	
	~20	nda*	0,78	
1.4406	~13	0,108	1,19	Alhborn [37]
	~13	0,108	1,18	
	~13	0,108	1,14	
	~19	0,101	0,84	
	~19	0,101	0,88	
	~19	0,101	1,01	
	~19	0,101	1,11	
	~13	0,079	1,27	Jhonson [42]
	~19	0,086	1,22	
	~13	0,076	1,21	
1.4462	~13	0,086	1,27	Alhborn [37]
	~13	0,086	1,04	
	~13	0,086	1,14	
	~19	0,116	0,77	
	~19	0,116	0,81	
	~19	0,116	0,85	
	~19	0,116	0,95	
	~19	0,081	0,95	Jhonson [42]
N32	~13	0,095	1,23	Jhonson [42]
	~13	0,093	1,25	

* nda: no data available

[2] According to fib Bulletin 10 *Bond of reinforcement in concrete* [3], the generally accepted values of 0,05 to 0,10 of relative rib area represent a good compromise in terms of ultimate bond strength, splitting ability, industrial requirements and good service-load performances (limited crack opening and cover splitting). Note that these values are given for CS. However, given the insignificant material influence observed in the experimental program conducted in this work (see Chapter 4) these values are also assumed for SS reinforcement.

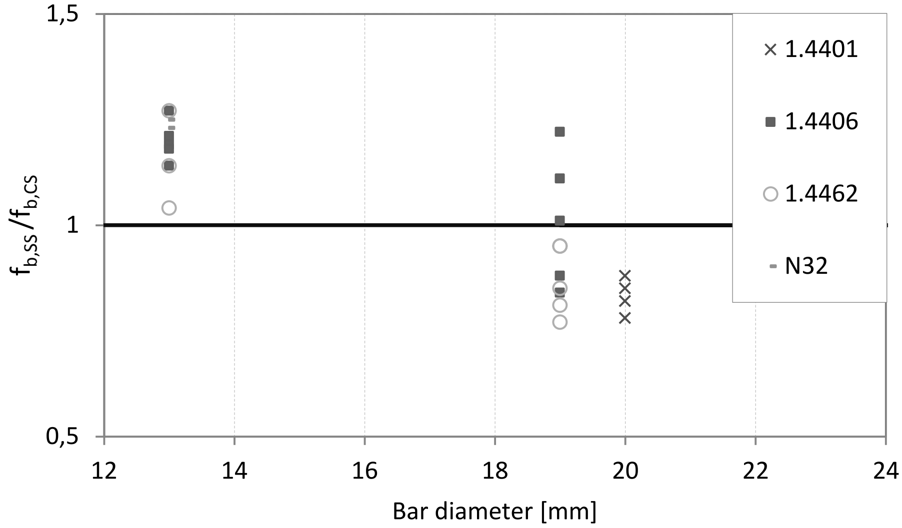

Figure 3-24 Bond strength ratio for analyzed stainless steel grades depending on the bar diameter

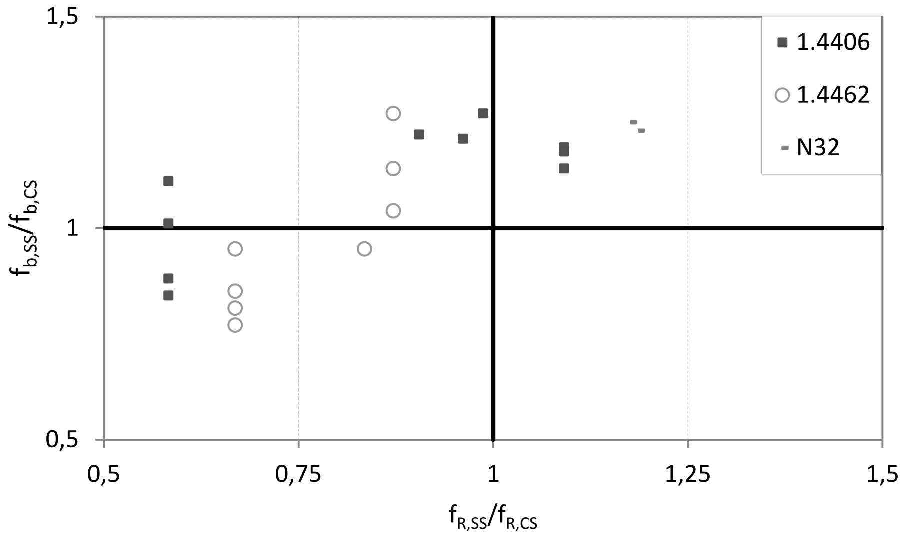

Figure 3-25 Bond strength ratio for analyzed stainless steel grades depending on the relative rib area ratio

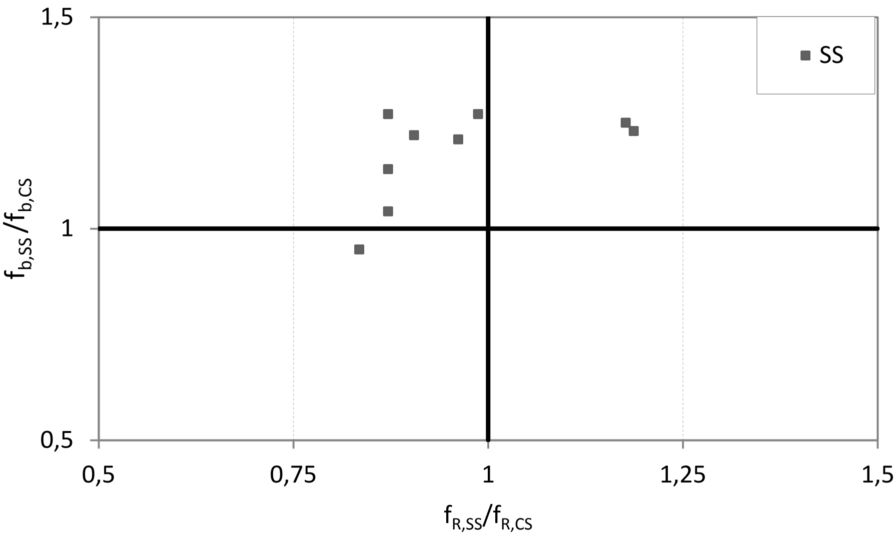

Figure 3-26 Stainless steel bond strength ratio vs. relative rib area ratio, for relative rib areas between 0,05 and 0,10

4.6 Bond interaction of SS according to standards

Existing standards regarding stainless steel reinforcement [46][47][48] agree that, provided the geometrical requirements of the reinforcement are fulfilled, the correct transfer of forces between reinforcement and concrete (good bond interaction) is guaranteed (if other design parameters are correctly applied). As an example, the definition of the rib pattern given by the French norm XP A35-014 [48] is presented by Figure 3-27, Figure 3-28, Table 3-10 and Table 3-11. Rib height (h), rib spacing (c), transverse rib flank inclination (α) and the transverse rib angle to the bar axis (β) are the parameters to be considered.

On the other hand, no information is given in the standards regarding bond strength values or bond-stress slip relationship developed by SS reinforcement.

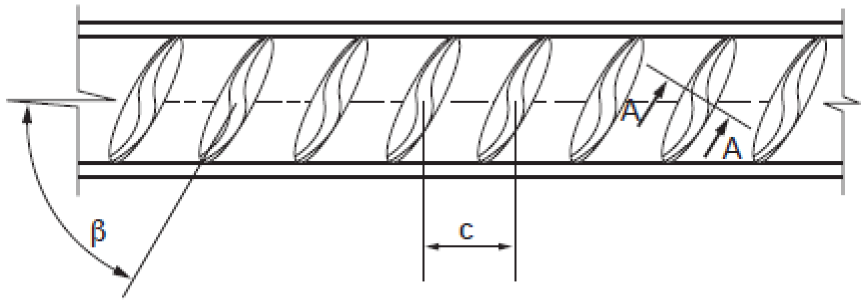

Figure 3-27 Schematic drawing of stainless steel rib geometry [15]

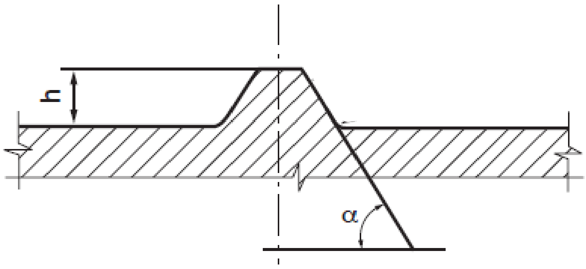

Figure 3-28 Rebar rib from A-A section from Figure 3-27 [15]

Table 3-10 Rib geometry design parameters [15]

Parameter	***h***	***c***	***α***	***β***
Value	Table 3-11	Table 3-11	≥ 45°	from 35° to 75°

Table 3-11 Rib height and rib spacing for each diameter size [15]

Nominal diameter (mm)	***h (mm)***		***c (mm)***	
	min	*max*	*min*	*max*
6	0,39	0,90	4,1	6,1
8	0,52	1,20	5,0	7,0
10	0,65	1,50	5,5	7,5
12	0,78	1,80	6,1	8,3
14	0,91	1,90	7,1	9,7
16	1,04	2,00	8,2	11,0
20	1,30	2,25	10,2	13,8
25	1,63	2,50	12,7	17,2
32	2,08	3,20	16,3	22,1
40	2,60	4,00	20,4	27,6
50	3,25	5,00	25,1	34,5

5 Pull out and beam-end test set-ups for bond behaviour characterization

There are several methods for testing the bond behaviour of reinforcement when embedded in concrete. Most of them deal with obtaining of the bond stress-slip relationship, which at the same time gives a value of the bond strength developed by the reinforcement when embedded in concrete. The test set-ups for bond behaviour characterization can be divided into two groups [3]: the one dealing with short specimens and the one related to long specimens. Although different test set-ups have been built up within each of the mentioned groups, the most relevant testing specimens and test set-ups are briefly explained in the following: the pull out test and the beam-end test. A comparison between the developed bond strength and the bond stress-slip relationship of both test set-ups is also included in this section.

5.1 Pull out test

As most of the test set-ups dealing with short specimens, the pull out test is devised to simulate a uniform bond stress distribution along a single bar; therefore, short anchorages are adopted ($l_b/Ø \leq 5$). For limiting the anchorage length, only a limited portion of the bar is in direct contact to the concrete, and the remaining portion is “debonded” by means of plastic tubes, rounds of tape or thin paraffin layers [3]. Generally there is no transverse reinforcement and bond is supposed to fail because of pulling out of the bar (shear-off of the concrete).

One of the most adopted test set-ups is the one defined in the 1970’s by RILEM in their guidelines [37]. It is also the test set-up used in the experimental work performed in this study for the characterization of the bond behaviour (Chapter 4 and Chapter 5). It can be considered as an improvement of the test set-up developed in the early sixties by Rhem [3], as the bonded length is moved from the central region of the specimen to the top (avoiding arch effects observed for Rehm’s test set-up), and as a rubber pad is inserted between the bearing plate and the specimen for reducing the friction between the two elements (one of the weak points of Rehm’s test set-up).

The test specimen is a cube of concrete and the steel bar is embedded in its axis. The bar to be tested extends beyond the two sides of the specimen; the tension is applied to the longer end. According to RILEM recommendations, concrete specimen’s side length is at least 10 times the steel bar diameter (10Ø) and the effective embedment length of the bar corresponds to 5 times the bar diameter (5Ø). The other part of the bar does not adhere as it is covered by a plastic tube. The unbonded length is located near the bearing plate, so to avoid its influence. The bar length at the passive end of the specimen should be at least 50 mm and the one at the active end 300 mm. Both the load applied to the lower extremity of the bar, as well as the relative displacement of the steel to the concrete are measured for obtaining the bond stress-slip relationship. Figure 3-29 gives a schematic drawing of the test set-up as given by RILEM in [37]. A detailed drawing of the test set-up used for bond characterization of the reinforcements studied in this work is given in Figure 4-4, page 106 (Chapter 4).

As the concrete specimen is bearing against a surface while the bar is being pulled, the entire concrete is in compression. This is one of the disadvantages of the pull out test as it does not represent the real situation in a typical flexural member [26]. The compression in the concrete might increase the bond strength by resisting the tensile splitting forces caused by the bearing of the reinforcement ribs. However, pull out tests are often considered as an easy, simple and with low concrete volumes needed way of testing the bond behavior of reinforcement. Furthermore, it allows for making comparison of the bond characteristics between different type of reinforcements.

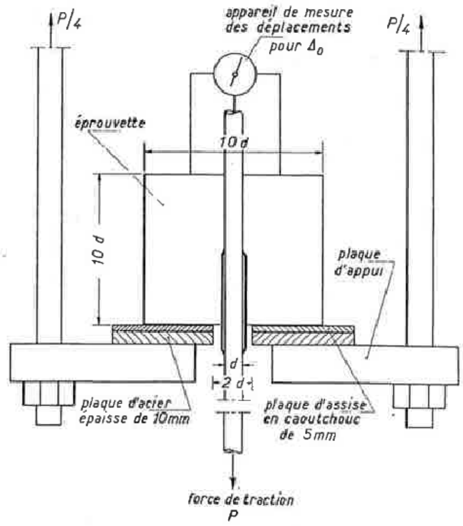

Figure 3-29 Pull out test set-up according to RILEM (from [37])

5.2 Beam-end test

The beam test is considered to be a “long specimen” type of test method for characterization of the bond behaviour of reinforcement when embedded in concrete, and allows (similar to the pull out test) to obtain the bond stress-slip law governing the bond capacity of the rebar. The main conceptual difference in comparison to the previously described pull out test, is that in the beam test the concrete part surrounding the bar to be tested is in tension, which allows for a more realistic situation regarding flexural members.

One of the most used test set-ups is again the one given by RILEM in its recommendations for testing the bond of reinforcing steel [50]. As described by the recommendations, the object of the bond test is to determine the conventional bond characteristics of the steel used as reinforcement in reinforced or prestressed concrete structures. However, the test is not suitable for testing prestressing tendons.

The principle of the test deals with a test beam comprising two parallelepipedal reinforced concrete blocks, interconnected at the bottom by the bar to be investigated and at the top by a steel hinge. The beam is loaded in simple flexure by two equal forces symmetrically placed with regard to the mid-span section of the beam (see Figure 3-30 and Figure 3-31). Both half beams are reinforced by auxiliary reinforcement for avoiding excessive splitting. The bond length specified for the test is equal to ten times the nominal bar diameter (10Ø). This bond length is located in the central zones of the two concrete blocks. The remaining bar areas are enclosed in plastic tubes which prevent any adhesion of the bar to the concrete. The dimensions of the test specimen vary depending on the size of the bar to be tested. Figure 3-30 gives an schematic drawing of the test specimen to be used for testing bars with nominal diameter inferior to 16 mm; the test set-up to be used for testing of bars with nominal diameter equal or larger than 16 mm is given by Figure 3-31.

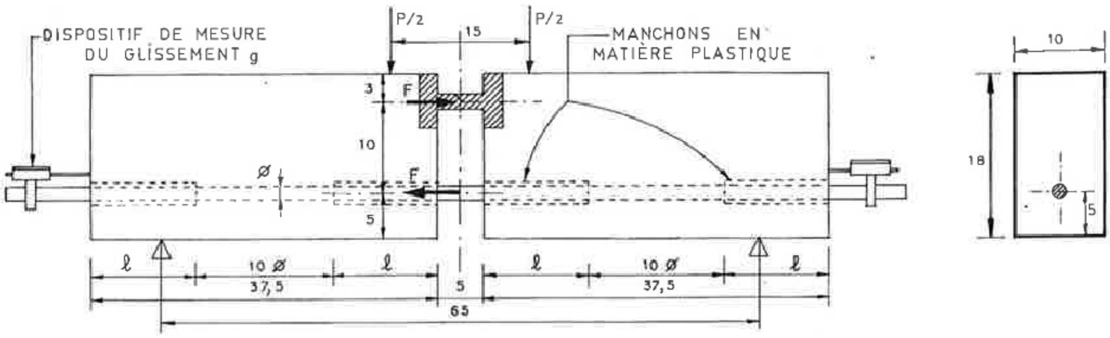

Figure 3-30 Beam test according to RILEM for Ø < 16mm. From [50]

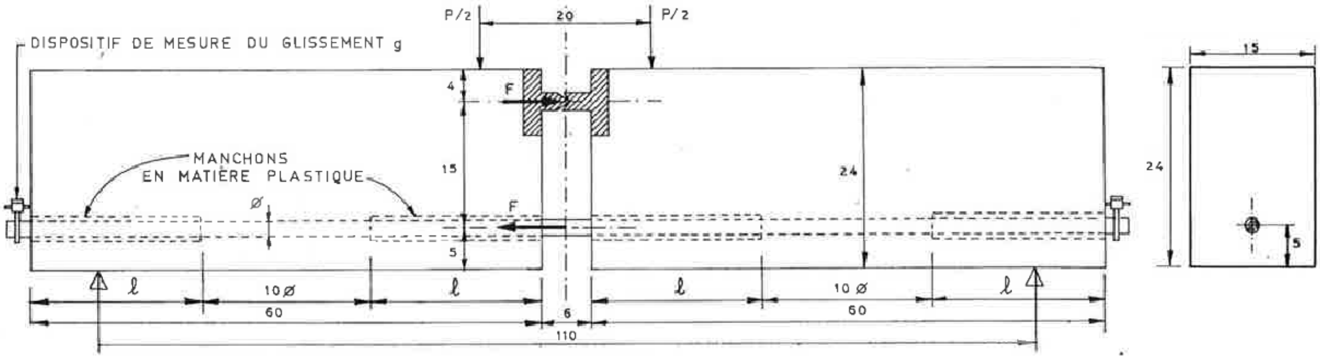

Figure 3-31 Beam test according to RILEM for Ø ≥ 16mm. From [50]

5.3 Pull out vs. beam-end test

Following the publication of the RILEM pull out (PO) and beam-end (BE) test set set-ups in 1970, Soretz [51] conducted a research for comparing both bond testing methods in 1972. The bond behaviour of carbon steel rebars with diameter 8, 16 and 30 mm embedded in traditional concrete with an average cube compressive strength of 31,5 N/mm² was analyzed, by both test set-ups. The bond stress at slip values of 0,01 mm, 0,1 mm and 1 mm was recorded and an average bond stress was calculated (τ_m). Furthermore, the bond stress at bond failure was also recorded (τ_r). The ratio of these bond stresses comparing both test set-ups are considered for the analysis. Table 3-12 gives the $\tau_{m,PO}/\tau_{m,BE}$ and $\tau_{r,PO}/\tau_{r,BE}$ ratios obtained from the average test results for all the tested diameters. Analysis of the given ratios allows for the following conclusions: pull out test is more favourable regarding bond stress at failure for any of the tested bar diameter, and this trend is more pronounced for increasing rebar diameter. E.g. for a diameter equal to 30 mm, 54 % higher maximum bond stress values were registered when tested with PO test set-up, than when tested with the BE test. However, regarding bond stress values at small slip, the results are variable: ~9% higher bond stress for the BE test for diameter 8 mm rebars, almost equal for diameter 16 mm and ~16% higher for the PO test for diameter 30 mm rebars.

Table 3-12 Bond stress comparison between PO and BE test set-ups [51]

Bar diameter (mm)	$\boldsymbol{\tau_{m,PO}/\tau_{m,BE}}$ ***(-)***	$\boldsymbol{\tau_{r,PO}/\tau_{r,BE}}$ ***(-)***
8	0,92	1,07
16	0,97	1,25
30	1,16	1,54

More recently, De Almeida et al. (2008) [52] conducted a research where steel rebars (diameter 10 and 16 mm) were embedded in both traditional and self compacting concrete. Specimens were tested by both pull out and beam-end test set-ups following RILEM recommendations. Two different concrete cylinder compressive strengths at 28 days were applied: 30 and 60 N/mm². Maximum bond stress values and slip at which these maximum values occurred were recorded. A summary is given in Table 3-13, in terms of PO/BE ratio for both parameters.

Analysis of the ratios allow for the following conclusions: regarding maximum bond stress values not a clear trend is observed between both test set-ups: an average ratio of 1,01 is observed. However, regarding slip at which the maximum bond stress occurred: the slip values are always higher for the pull out test set-up, with a more pronounced difference for decreasing bar diameter and increasing concrete compressive strength. A stiffer behaviour is therefore observed for the BE test set-up. Note that specimens with 30 N/mm² of compressive strength failed by pull out while the ones with 60 N/mm² failed by splitting of the concrete. The differences between the two test set-ups regarding the slip values at maximum bond stress are more significant when splitting type of failure occurs than for a pull out type of failure.

Table 3-13 Bond stress and slip comparison between PO and BE test set-ups [52]

Compressive strength (N/mm²)	*Concrete type*	*Bar diameter (mm)*	$s_{r,PO}/s_{r,BE}$ (-)	$\tau_{r,PO}/\tau_{r,BE}$ (-)
30	TC	10	2,41	1,10
		16	1,13	1,18
	SCC	10	3,32	0,86
		16	2,16	0,80
60	TC	10	12,77	0,92
		16	7,68	1,07
	SCC	10	19,00	0,95
		16	3,11	1,26

Both investigations, therefore, concluded that higher maximum bond stress values are obtained when pull out type of failure occurs. Furthermore, for small diameters (8 mm and 10 mm) the stiffness of the bond stress-slip ascending branch is higher for the beam-end test set up. For larger diameters, test results show different trends regarding stiffness of the ascending branch.

6 Bond in serviceability limit state: tension stiffening phenomena

6.1 Transversely cracked concrete

In reinforced concrete members that are subjected to tensile forces, primary cracks (transverse cracking) can form if the stress in the concrete reaches the tensile strength of the concrete (f_{ct}), see Figure 3-32. In the case of an axially loaded concrete prism where the load is applied to the steel reinforcement, these tensile stresses in the concrete are attributable to the load transfer from the steel to the concrete, via bond action. Furthermore, since the concrete strain depends on the steel strain through the relative displacement between steel and concrete (slip), see Equation 3-1, the analysis of transverse cracking in concrete has to be based on bond modelling and on the control of the concrete strain in tension [3].

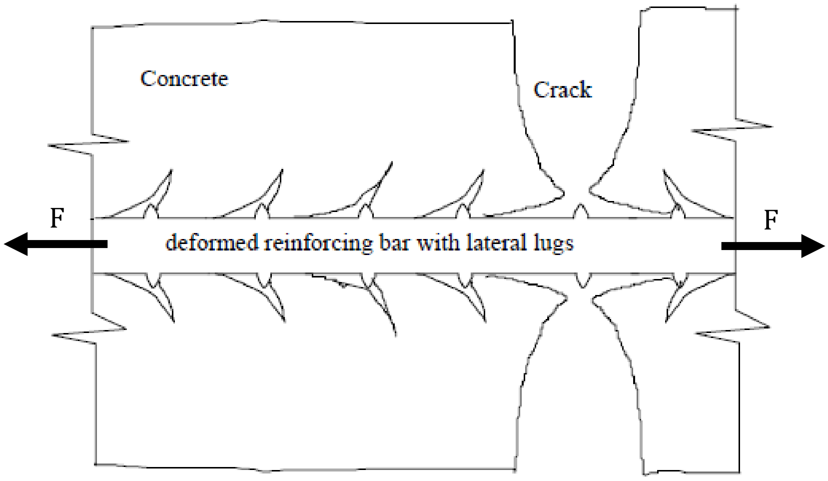

Figure 3-32 Transverse cracking in an axially loaded reinforced concrete member (deformations exaggerated for clarity). From [53]

Figure 3-33 gives the steel, concrete and the bond stresses existing for a transversally cracked prism that is axially loaded. It can be observed that at cracked sections, the steel is the only active material carrying the stresses. Thus, the bond interaction between the steel and the concrete is broken at cracked sections, and the bond stresses are zero at these points. On the other hand, for each of the uncracked parts of the concrete (in between the cracks), the bond stresses are developed symmetrically (though with opposite signs) at each half of the uncracked part, being the symmetry axis the middle point of the uncraked part (see τ_b diagram in Figure 3-33).

In the following, the cracking process for an axially loaded prism is analyzed, from the uncracked state to the crack stabilizing phase.

6.1.1 Cracking phases

The most typical problem where concrete appears transversally cracked is represented by a reinforced concrete member subjected to uniaxial tension (see Figure 3-33 and Figure 3-34) where the load is applied on the steel rebar. Being the length of the reinforced concrete member equal to l, because of the existing symmetry, only half member, $l/2$, is analyzed in the following taking the axis reference as shown in Figure 3-34.

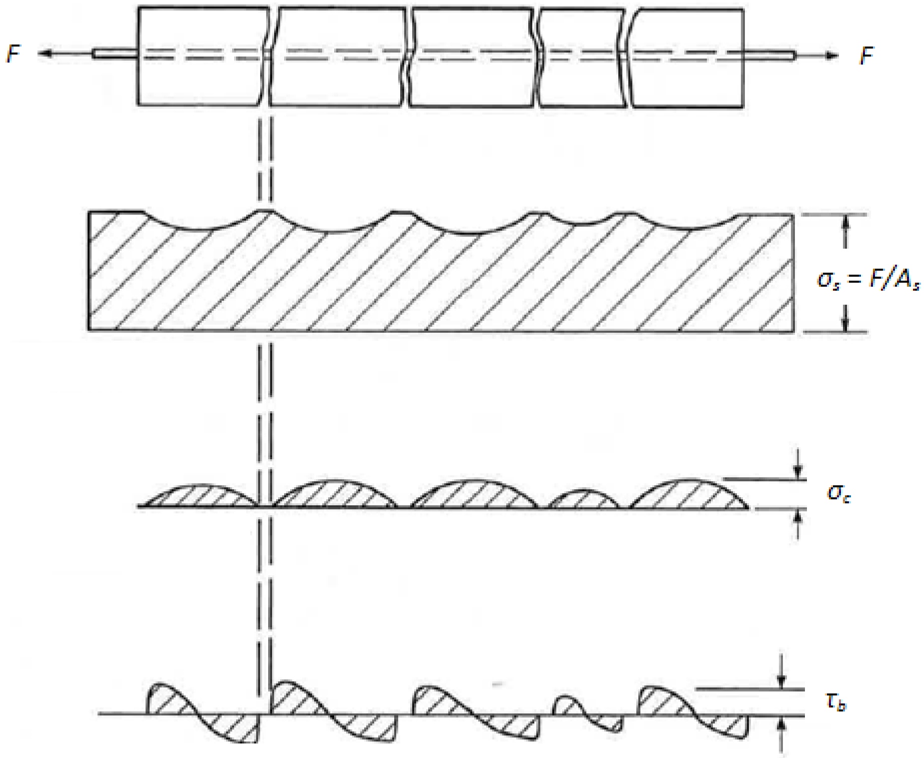

Figure 3-33 Axially loaded prism. Steel, concrete and bond stresses in a transversally cracked prism. From [19]

6.1.1.1 Uncracked member

For an uncracked reinforced concrete member, traditionally two typical behaviours are referred to in the literature: long-member and short member behaviours.

For long member behaviour, the bond efficiency and the anchorage length favour load transmission between the bar and the concrete, with the formation of an ineffective region (from x_R to x_S in Figure 3-35-a) characterized by uniform and equal strains in both steel and concrete, with no bar slip. On the contrary, in short members, the strains in the bar and in the concrete are never identical ($\varepsilon_s > \varepsilon_c$) and bar slip is zero only in the mid-span section, due to symmetry [3]. See Figure 3-35-b. In other words, for a long member behaviour, the transfer length is shorter than the mid-span length ($l/2$), whereas for a short member, the transfer length is larger than the mid-span length.

As plotted in Figure 3-35, for a long member, the maximum concrete strain is reached at x_R, which refers to the transfer length. For a short member, on the contrary, the maximum concrete strain is reached at the symmetry section (x_S).

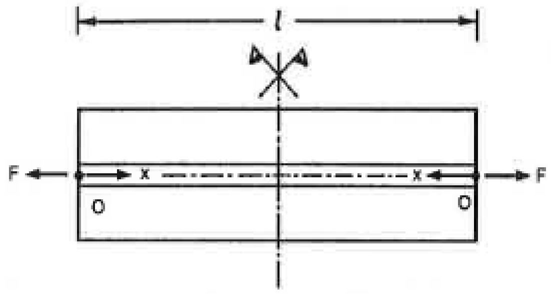

Figure 3-34 Reinforced concrete member subjected to uniaxial tension. From [3]

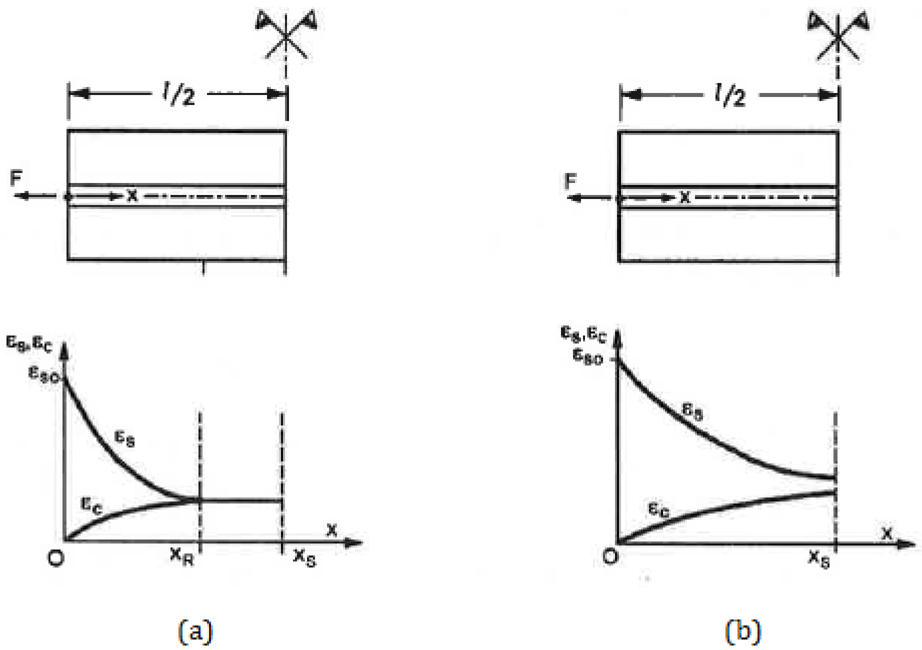

Figure 3-35 Typical strain distribution in a reinforced concrete member subjected to uniaxial tension: a) long member behaviour; b) short member behaviour. From [3]

6.1.1.2 First cracking

Assuming that the load is monotonically increasing, the section x_R moves toward the symmetry section and the concrete strain at x_R increases (at increasing loads). Two situations may occur:

a) The concrete strain reaches the ultimate tensile strain ($\varepsilon_c \geq \varepsilon_{ct}$) of the concrete at a x_R < $l/2$. In this case, the section corresponding to x_R will be the section where the first crack will appear ($x_{R,cracking}$). This is the typical behaviour for a long member. See Figure 3-36.

b) x_R reaches the section corresponding to the symmetry (x_S) before the concrete strain reaches the tensile strength of the concrete. In order to cause the member to crack, a greater load should be applied for the concrete strain to increase. Since, x_R cannot increase beyond $l/2$ because of symmetry, the first crack will appear at the symmetry section (x_S), when the concrete strain at that section reaches the ultimate tensile strain. This case can be defined as cracking of a short member. See Figure 3-37.

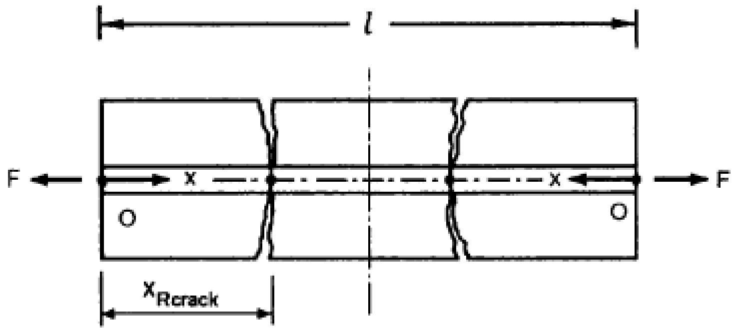

Figure 3-36 First cracking of a long member

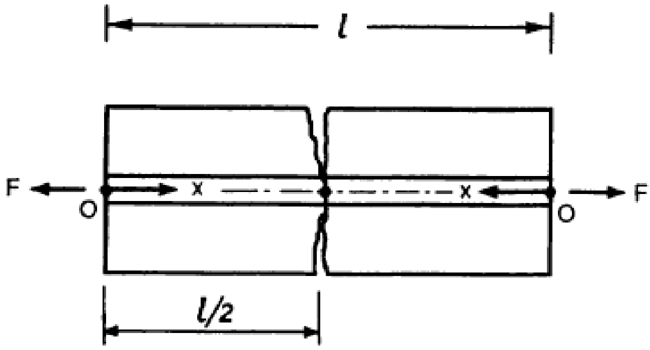

Figure 3-37 First cracking of a short member

6.1.1.3 Secondary cracking

After the formation of the first primary crack(s), each subdivision or part (p) of the reinforced concrete member is in a situation similar to the original (uncracked), but with a smaller length (l_p). At increasing loads a second generation of cracks will occur. Each of the uncracked remaining parts will act as a short member and cracking may only occur in the symmetry section of each p part, thus at a $l_p/2$ distance from the crack.

The previous considerations lead to the conclusion that under monotonically increasing loads, after first generation of primary cracks, further cracks can occur only by cracking each single part at mid-span [3]. This statement is valid on the condition that the material is homogeneous, which is not the case for concrete, and therefore, should be taken as a theoretical approach.

6.1.1.4 Stabilizing phase

A stabilized phase is the one corresponding to the situation in which the length of a single part is no longer large enough to allow the concrete strain to reach the failure value in tension at mid-span, whatever the increase of the load is. At increasing loads, no more cracks will normally appear, and the already existing ones will expand due to the increasing steel strains.

6.1.2 Tension stiffening phenomena

As stated before, in a reinforced concrete member loaded in tension the tensile forces are resisted by the combined action between steel and concrete because of the bond interaction between the two materials. Only across a crack is the load only carried entirely by the reinforcement (see Figure 3-33). Consequently, the mean strains in the reinforcement embedded in concrete are smaller than those in a naked bar: this bond-related phenomenon is called "tension stiffening" [3].

The stiffening effect of the concrete can be explained by considering the relationship between the stress and the mean strain in both uncracked and cracked states. A typical stress-strain diagram is shown in Figure 3-38. The behaviour of the embedded bar (continuous line) can be compared to the tensile behaviour of the naked bar (dashed line), being the difference between both of them the contribution of the concrete to the stiffening effect.

In the same diagram, Figure 3-38, the cracking phases previously described are plotted: the first stiffer phase (a), is the uncracked phase, in which an elongation of the test specimen occurs without any crack appearance. This phase ends when the first crack appears at a stress level equal to σ_{cr} (R). The second stage corresponds to the crack formation phase (b), in which more cracks appear with increasing load. The third phase goes from the last crack formation (S) until the yielding (Y) of the bar starts at σ_y (c). During this phase, the so-called stabilized cracking phase, normally no more cracks appear, and the already existing cracks expand. The last phase (d), corresponds to the yielding of the reinforcement until the failure of the reinforcement.

For the characterization of the tension stiffening and to allow for the mean strain calculation, Eurocode 2 [54] defines a distribution or tension stiffening coefficient defined as given by Equations 3-19 and 3-20, depending on the cracking phase:

$$\zeta = 0 \qquad \text{for uncracked sections, } \sigma < \sigma_{cr} \qquad (3\text{-}19)$$

$$\zeta = 1-\beta_1\beta_2(\sigma_{cr}/\sigma)^2 \qquad \text{for cracked section, } \sigma > \sigma_{cr} \qquad (3\text{-}20)$$

where, σ_{cr} is the tensile stress at first cracking, σ the actual stress of the reinforcement, β_1 is a coefficient taking into account the bond characteristics of the reinforcement (β_1 = 1 for ribbed bars, and β_1 = 0,5 for smooth bars) and β_2 is a coefficient taking into account the influence of the duration of the loading or of repeated loading (β_2 = 1 for a single short-term loading, and β_2 = 0,5 for sustained loads or many cycles of repeated loads).

The average strain is calculated according to Equation 3-21, where ε_I and ε_{II}, represent the strain at uncracked and fully cracked phases, respectively.

$$\varepsilon_m = (1-\zeta)\,\varepsilon_I + \zeta\,\varepsilon_{II} \qquad (3\text{-}21)$$

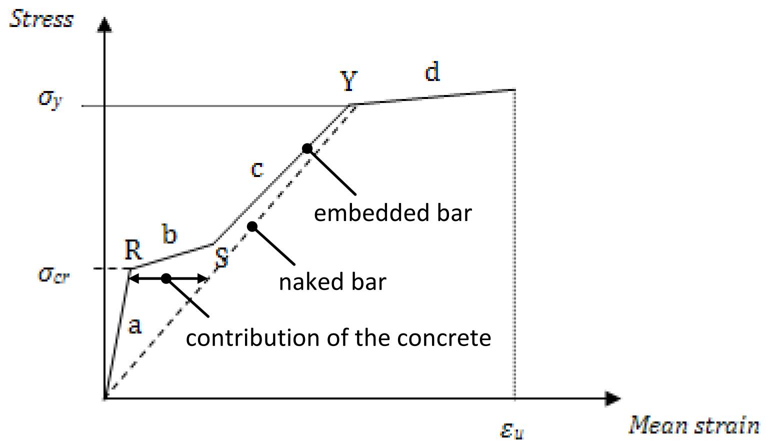

Figure 3-38 Tension stiffening: tensile stress vs. mean tensile strain

6.2 Serviceability limit state of cracking

For a reinforced concrete structure it should be ensured that, with adequate probability, cracks will not impair the serviceability and durability of the structure. Cracks do not necessarily indicate a lack of serviceability or durability: in reinforced concrete structures, cracking may be inevitable due to tension, bending, shear and torsion, or plastic shrinkage and chemical reactions, without necessarily impairing serviceability or durability.

Thus, design crack widths can be specified to satisfy requirements with regard to functionality (the function of the structure should not be harmed by the cracks formed), durability (intended lifetime of the structure should not be harmed) or appearance (the aesthetic aspect of the structure should be acceptable). The design crack width (w_d) should meet the requirement of being less (or equal) to a limited crack width value ($w_d \leq w_{lim}$); the latter considered at the concrete surface which is specified for cases of expected functional consequences of cracking, or for some particular cases related to durability problems and appearance of the structure [10]. The specific requirements for each situation may be met by an appropriate limitation of crack widths, which can be achieved by analytical procedures or by appropriate practical rules.

Several predicting equations have been formulated for crack width (maximum or average) calculation [55][56][57][58][59]. All the investigators agree that the crack width increases with the steel stress at the cracked section; however, variables such as bar diameter, reinforcement ratio and concrete cover are embedded in the prediction formulas differently. As a general trend, it can be concluded that if other parameters are kept constant, an increase in the bar diameter and concrete cover, as well as a decrease in the reinforcement ratio will increase the crack width [53].

Existing standards and design guides, as the Model Code 1990 by fib [8] as well as the Draft version of the next Model Code 2010 [10], or the Eurocode 2 [54], give guidelines on the analytical procedure to be followed for the predictive calculation of the crack width for a given structure. Furthermore, maximum crack widths limitations depending on the exposure class and/or proposed function are also provided by these documents. As an example, Table 3-14 gives the recommended values for maximum crack width as given by Eurocode 2 [54], in mm.

Table 3-14 Recommended values of maximum crack width according to Eurocode 2 [54]in mm. Exposure classes according to Table 4.1 in [54]

Exposure class	***Reinforced members and prestressed members with unbounded tendons***	***Prestressed members with bonded tendons***
	Quasi-permanenet load combination	*Frequent load combination*
X0, X1	0,4*	0,2
XC2, XC3, XC4	0,3	0,2**
XD1, XD2, XS1, XS2, XS3		Decompression

* For X0 and XC1 exposure classes, crack width has no influence on durability and this limit is set to guarantee acceptable appearance. In the absence of appearance conditions this limit may be relaxed

** For these exposure classes, in addition, decompression should be checked under the quasi-permanent combination of loads

Chapter 6 of this work compiles tension stiffening tests performed to stainless steel flat rebars (with and without rib alternate patterns). The tension stiffening and the observed cracking behaviour are analyzed and existing maximum crack width prediction formulas are applied for comparison of the test results. According to the literature available to the author, no tension stiffening tests have been conducted so far with respect to stainless steel flat rebars.

7 Conclusions

The bond interaction between the reinforcement and the steel is the mechanism by which the necessary forces are transferred in a reinforced concrete member. In this way the combined action of the two materials is guaranteed. It is therefore of great importance that the bond behaviour of a given type of reinforcement when embedded in concrete is understood and characterized for guaranteeing an appropriate structural behaviour of a reinforced concrete structure reinforced with such reinforcement.

The bond behaviour of reinforcement embedded in concrete is characterized by its bond stress-slip behaviour, which will first of all depend on the surface configuration of the bar: for smooth bars, the main adhesion mechanism is chemical and it is followed by friction forces acting on the contact surface between the two materials once the chemical forces are broken. In this way, the bond stress-slip relationship of a smooth rebar, substantially differs from the one corresponding to ribbed reinforcement, for which the predominating bond interaction is due to the mechanical forces developed (bearing effect) at the ribs of the rebar. Due to the bearing forces, a radial component of stresses will develop around the reinforcement, which might lead to radial cracks spreading towards the surface of the concrete member. When these cracks reach the surface of the concrete a splitting type of failure occurs if the tensile stress hoop that resists the radial forces reaches the tensile capacity of concrete. On the other hand, if the confinement of the reinforcement is sufficient, the radial cracks will not spread and a pull out type of failure will occur. Depending on the type of bond failure present on a reinforced concrete member, the bond stress-slip relationship describing the bond behaviour of the reinforcement will vary.

The bond strength that a reinforcing bar can develop when embedded in concrete, as well as the bond stress-relationship governing its behaviour, are dependent on several factors: the concrete strength, the provided confinement, bar geometry, surface configuration of the rebar, and environmental factors as reinforcement corrosion are some of the parameters that are relevant to take into account in this research. Furthermore, the influence of reinforcement material has been analyzed regarding bond capacity of SS rebars in comparison to CS rebars. Results show that the performance of SS rebars is better than for carbon steel when talking about small diameters (~Ø13 mm) and when limiting test data to those with an optimal relative rib area (relative rib area values ranging from 0,05 to 0,01). For higher diameters (~Ø19 and Ø20 mm) and/or considering data for rebars with a no-optimal relative rib area, bond capacity of the SS reinforcement varies compared to the performance of carbon steel. In any case, obtained values were always higher than the predicted ones and therefore, no modifications were suggested when proposing SS reinforcements as a one-to-one replacement for the corresponding carbon steel.

For bond capacity characterization the beam test and the pull out test are the most widely used test methods. For this research, pull out test are conducted: although for this type of test the concrete surrounding the bar is in compression (which is not realistic regarding flexural members situation), it allows for an effective characterization of the bond behaviour and an effective comparison of the influence of different parameters on the bond behaviour of the reinforcement.

Finally, in this chapter, an introduction on the role of the bond in serviceability limit state has been presented. The cracking behaviour of an axially loaded reinforced concrete member in tension has been analyzed, and the tension stiffening phenomenon has been defined: the bond interaction between the steel and the concrete allows for a stiffer tensile behaviour developed by the reinforcement, in comparison to the tensile behaviour of the naked bar.

For a transversally cracked reinforced concrete member, it is of great importance that the cracking is controlled and that a maximum allowable crack width is established, for functional, durability and appearance requirements to be fulfilled. Existing experimental investigations, as well as standards and design guides allow for the predictive calculation of the maximum crack width.

8 References

[1] Lowes L.N. (1999) *Finite element modeling of reinforced concrete beam-column bridge connections*. PhD Dissertation, University of California, Berkeley

[2] Lutz L.A., Gergely P. (1967) *Mechanics of bond and slip of deformed bars in concrete.* ACI Journal 64 (11): 711-72

[3] fib (2000) *Bond of reinforcement in concrete. State of the art report.* fib Bulletin 10. International Federation for Structural Concrete, Switzerland

[4] Luccioni B.M., Lopez D.E., Danesi R.F. (2005) *Bond-slip in reinforced concrete elements.* Journal of Structural Engineering, 131 (11): 1690-1698

[5] Fernandez Ruiz M., Muttoni A., Gambarova P.G. (2007) *Analytical Modeling of the pre-and postyielding behavior of bond in reinforced concrete*. ASCE Journal of Structural Engineering, Vol 133 (10): 1364-1372

[6] Desnerck P. (2011) *Compressive, bond and shear behaviour of powder-type self-compacting concrete*. PhD Dissertation, Ghent University, Ghent

[7] Johnson J.B. (2010) *Bond strength of corrosion resistant steel reinforcement in concrete*. Master Thesis, Virginia Polytechnic and State University, Blacksburg, Virginia

[8] CEB-FIP (1993) *Model Code 1990 – Design Code.* International Federation for Structural Concrete, Switzerland

[9] Darwin D., Zuo J., Tholen M.L., Idun E.K. (1996) *Development length criteria for conventional and high rib area reinforcing bars*. ACI Structural Journal, Vol 93 (3): 347-359

[10] fib (2010) *Model Code 2010 – First complete draft*. fib Bulletin 55. International Federation for Structural Concrete, Switzerland

[11] Eligehausen R., Popov E. P., Bertero V. V. (1983) *Local bond stress-slip relationship of deformed bars under generalized excitations*. Report UCB/EERC-83/23, University of California, Berkeley

[12] Huang Z., Engstrom B., Magnusson J. (1996) *Experimental and analytical studies of the bond behavior of deformed bars in high strength concrete*. 4th International Symposium on Utilization of High-Strength/High-Performance Concrete, Paris: 1115-1124

[13] Soroushian P., Choi K.B., Park G.H., Aslani F. (1991) *Bond of deformed bars to concrete: effects of confinement and strength of concrete*. ACI Materials Journal, Vol 88 (3): 227-232

[14] Harajli M.H., Hout M., Jalkh W. (1995) *Local bond stress-slip behaviour of reinforcing bars embedded in plain and fiber concrete*. ACI Materials Journal, Vol 92 (4): 343-354

[15] Gomes Barbosa M.T., Sanchez Filho E. S., Mayra de Oliveira T., Dos Santos W.J. (2008) *Analysis of the relative rib area of reinforcing bars pull out tests*. Materials Research, Vol 11 (4), pp 453-457

[16] Kankam C.K. (1997) *Relationship of bond stress, steel stress and slip in reinforced concrete*. Journal of Structural Engineering, Vol 123 (1): 79-85

[17] Zuo J., Darwin D. (2000). *Splice strength of conventional and high relative rib area bars in normal and high-strength concrete*. ACI Structural Journal, Vol 97(4): 630-641

[18] Al-Jahdali F.A., Wafa F.F., Shihata S.A. (1994) *Development length for strainght deformed bars in high-strength concrete*. ACI Special Publication, 149: 507-522

[19] Wight J.K., MacGregor J.G. (2009) *Reinforced Concrete. Mechanics and Design*. Pearson International Edition (5th edition)

[20] Hadje-Ghaffari H., Choi O.C., Darwin D., McCabe S.L. (1994) *Bond of epoxy-coated reinforcement: cover, casting position, slump and consolidation*. ACI Structural Journal Vol 91 (1): 59-68

[21] Feldman L. R., Bartlett F. M. (2005) *Bond strength variability in pullout specimens with plain reinforcement*. ACI Structural Journal, Vol 102 (6): 860-867

[22] Giuriani E., Plizzari G.A., Schumm C. (1991) *Role of stirrups and residual tensile strength of cracked concrete on bond*. ASCE Journal of Structural Engineering, Vol 117 (1): 1-18

[23] Darwin D. (2005) *Tension development length and lap splice design for reinforced concrete members*. Progress in Structural Engineering and Materials, Vol 7(4): 210-225

[24] CEN (2010) EN ISO 15630 *Steel for the reinforcement and prestressing of concrete-Test methods-Part 1: Reinforcing bars, wire rod and wire*. European Committee for Standardization, Brussels

[25] Darwin D., Graham K.E. (1993) *Effect of deformation height and spacing on bond strength of reinforcing bars*. ACI Structural Journal, Vol 90 (6): 646-657

[26] El-Hacha R., El-Agroudy H., Rizkalla S.H. (2006) *Bond characteristics of high-strength steel reinforcement*. ACI Structural Journal, Vol 103 (6): 771-782

[27] Cairns J., Abdullah R.B. (1995) *Influence of rib geometry on strength of epoxy-coated reinforcement*. ACI Structural Journal, Vol 92 (1): 23-27

[28] Tepfers R. (1979) *Cracking of concrete cover along anchored deformed reinforcing bars.* Magazine of Concrete Research, Vol 31 (106): 3-12

[29] Hamad B.S. (1995) *Bond strength improvement of reinforcing bars with specially designed rib geometries*. ACI Structural Journal, Vol 92 (1): 3-13

[30] Mo Y.L., Chan J. (1996) *Bond and slip of plain rebars in concrete*. Journal of Materials in Civil Engineering, Vol 8 (4): 208-211

[31] Abrams D. A. (1913) *Tests of bond between concrete and steel*. Bulletin 71, University of Illinois, Illinois

[32] Fang C., Lundgren K., Chen L., Zhu C. (2004) *Corrosion influence on bond in reinforced concrete*. Cement and Concrete Research, Vol 34: 2159-2167

[33] Lee H.S., Noguchi T., Tomosawa F. (2002) *Evaluation of the bond properties between concrete and reinforcement as a function of the degree of reinforcement corrosion*. Cement and Concrete Research, Vol 32: 1313-1318

[34] Fu X., Chung D.D.L. (1997) *Effect of corrosion on the bond between concrete and steel rebar*. Cement and Concrete Research, Vol 27 (12): 1811-1815

[35] Cabrera J.G. (1996) *Deterioration of concrete due to reinforcement steel corrosion*. Cement & Concrete Composites, Vol 18: 47-59

[36] Almudallam A.A., Al-Gahtani A.S., Aziz A.R. et al. (1996) *Effect of reinforcement corrosion on bond strength*. Construction and Building Materials, Vol 10 (2): 123-129

[37] Alhborn T.M., DenHartigh T.C. (2003) *Comparative Bond Study of Stainless and High-Chromium Reinforcing Bars in Concrete*. Transportation Research Record 1845: 88-95

[38] ASTM (2009) A 615/A 615M – 09 *Specification for deformed and plain carbon steel bars for concrete reinforcement.* American Society for Testing and Materials, USA

[39] ACI (2009) 408.3R-09 *Guide for Lap Splice and Development Length of High Relative Rib Area Reinforcing Bars in Tension and Commentary*. American Concrete Institute, USA

[40] ASTM (2010) A 944-10 *Standard test method for comparing bond strength of steel reinforcing bars to concrete using beam-end specimens*. American Society for Testing and Materials, USA

[41] Orangun C.O., Jirsa J.O., Breen J.E. (1977) A reevaluation of test data on development length and splices. ACI Journal 74-11: 114-122

[42] Johnson J.B. (2010) Bond *strength of corrosion resistant steel reinforcement in concrete*. Master Thesis, Virginia Polytechnic and State University, Blacksburg, Virginia

[43] ACI (2004) ACI 318-05 *Building code requirements for structural concrete*. American Concrete Institute, USA

[44] Aal Hassan A.A.A. (2003) *Bond of reinforcement in concrete with different types of corroded bars*. Master Thesis, Theses and dissertations -Paper 133, Reyerson University, Toronto

[45] Jayasankar K.R. (2006) *Nuovinox–a rebar with a difference*. National Conference on Advances in Bridge Engineering. India

[46] British Standards (2001) BS 6744:2001 *Stainless steel bars for the reinforcement of and use in concrete – Requirements and test methods*. British Standards, UK

[47] ASTM (2005) A 955/A 955M – 05 *Specification for deformed and plain stainless steel bars for concrete reinforcement*. American Society for Testing and Materials, USA

[48] AFNOR (2003) XP A35-014 *Reinforcing steels – Plain, indented or ribbed stainless steel bars and coils.* Association Française de Normalisation, France

[49] RILEM (1970) *Technical Recommendations for the Testing and Use of Construction Materials: RC6, Bond Test for reinforcing Steel. 2. Pull-out test*. International union of laboratories and experts in construction material, systems and structures

[50] RILEM (1970) *Technical Recommendations for the Testing and Use of Construction Materials: RC6, Bond Test for reinforcing Steel. 1. Beam test*. International union of laboratories and experts in construction material, systems and structures

[51] Soretz S. (1972) *A comparison of beam tests and pull-out tests*. Materiaux et Constructions, Vol 5 (28): 261-264

[52] De Almeida F.M., El Debs M.K., El Debs A.L. (2008) *Bond-slip behaviour of self-compacting concrete and vibrated concrete using pull-out and beam tests*. Materials and Structures, 41: 1073-1089

[53] Piyasena R. (2002) *Crack spacing, crack width and tension stiffening effect in reinforced concrete beams and one-way slabs*. PhD Dissertation, Griffith University, Gold Coast Campus, Australia

[54] CEN (2004) Eurocode 2: EN 1992-1-1 *Design of concrete structures - Part 1-1: General rules and rules for buildings*. European Committee for Standardization, Brussels

[55] Watstein D., Parson D.E. (1943) *Width and spacing of tensile cracks in axially reinforced concrete cylinders*. Journal of Research of the National Bureau of Standards, Vol 31, No. RP545: 1–24

[56] Kaar P.H., Muttock A.H. (1963) *High strength bars as concrete reinforcement – Part 4 Control of cracking*. Journal of Portland Cement Association Research and Development Laboratories, Vol 7 (1): 42-53

[57] Gergely P., Lutz L.A. (1968) *Maximum crack width in reinforced concrete flexural members*. Causes, Mechanism and Control of Cracking in Concrete, SP-20, ACI: 87-117

[58] Lan Z., Ding D. (1992) *Crack width in reinforced concrete members*. International Journal of Structures, Vol 12 (2): 137-163

[59] Chowdhury S.H., Loo Y.C. (2001) *A new formula for prediction of crack widths in reinforced and partially prestressed concrete beams*. Advances in Structural Engineering, Vol 4 (2): 101-109

Chapter 4 Bond Behaviour of Flat Stainless Steel Rebars in Concrete

1 Introduction

An interest on applying flat rebars as reinforcement elements for reinforced concrete structures has emerged. This allows, for a given rebar cross section, to increase the bond transfer contact area between the steel and the concrete. Flat rebars are also of interest for an optimization of shallow slabs, where the thickness of concrete plays a key role on the characterization of design parameters (see Chapter 1). Indeed, the use of flat rebars allows for a reduction of the slab thickness without decreasing the required minimum concrete cover. Furthermore, if SS reinforcement is used for reinforcing of the concrete slab, a concrete cover reduction is possible according to Eurocode2 [1] when defining the minimum concrete cover needed for durability aspects (see Chapter 2, Section 4.3.2 and Equation 2-3). Several existing design codes (see Chapter 2) give values of the concrete cover reduction if SS is applied instead of carbon steel for concrete reinforcing.

The good performance of reinforced concrete depends on the appropriate transfer of forces between reinforcing bars and concrete, which relies on the bond interaction between the two materials. Thus, for SS flat reinforcement to be able to replace traditional CS round reinforcing bars, sufficient transfer of forces between SS flat reinforcement and concrete should be available. To assess the bond behaviour of SS flat reinforcement when embedded in concrete, and to compare the behaviour with standard round CS reinforcement, 72 bond tests were conducted at the Magnel Laboratory for Concrete Research. These consisted of pull out tests on centrally embedded reinforcing elements. Steel rebar geometry (shape and aspect ratio), reinforcement material, surface roughness (micro and macro roughness) and concrete type (traditional concrete TC and self compacting concrete SCC) are the studied parameters. Test results are presented in terms of bond strength and force transfer stiffness, as well as in terms of bond stress-slip relationship.

According to the literature available to the author, bond tests with respect to SS flat reinforcement have not been reported. For a discussion on literature available for bond behaviour of flat CS rebars and round SS rebars, reference is made to Chapter 3.

2 Test programme

An overview of the test programme, in terms of materials used and corresponding bond length is given in Table 4-1. Besides flat SS rebars, standard round CS bars are tested as reference elements. Two different diameters (Ø10 mm and Ø12 mm; comparable to the different cross sectional areas of the flat elements) and two bond lengths (30 mm and 50 mm) are tested. CS round smooth bars (Ø10 mm), CS smooth strips (4x20 mm^2) and CS ribbed strips (3,5x25 mm^2) are also tested for a more accurate comparison between CS and SS. Among the SS material, two different types, austenitic 304L (1.4307 according to European standard designation EN 10088 [2]) and ferritic K31 (1.4017); three different types of roughness (type 2B and 1D which are smooth microrough finishes, and one ribbed); and Ø10 mm and Ø12 mm equivalent cross sectional dimensions are tested. For the concrete both traditional concrete (TC) and self compacting concrete (SCC) are investigated. The numbers from 1 to 17 between brackets in Table 4-1 represent the concrete batch in which the specimens were casted. For each parameter combination 3 specimens were tested.

Specimen designation is done by referring to the rebar properties as follows: material (CS or SS), SS type (304L or K31), geometry of the rebar in terms of dimension of the cross section, roughness (smooth, S, or ribbed, R) and smooth rebar finish (2B or 1D).

Table 4-1 Overview of the test program

Material	***Geom. (mm)***	***Roughness***		***Rebar designation***	***Bond length***	***TC***	***SCC***
CS	Ø10	Ribbed	f_R = 0,078	CS-Ø10-R	50 mm	(1)	(11)
					30 mm	(2)	(11)
		Smooth	R_a = 13,2 µm	CS-Ø10-S	50 mm	(3)	-
	Ø12	Ribbed	f_R = 0,070	CS-Ø12-R	50 mm	(2)	-
					30 mm	(2)	(11)
	4x20	Smooth	R_a = 5,3 µm	CS-4x20-S	50 mm	(4)	(12)
	3,5x25	Ribbed	f_R = 0,023	CS-3,5x25-R	50 mm	(5)	-
					30 mm	(6)	(13)
SS-304L	4x20	Smooth-2B	R_a = 0,4 µm	SS-304L-4x20-S-2B	50 mm	(7)	(14)
		Smooth-1D	R_a = 3,0 µm	SS-304L-4x20-S-1D	50 mm	(7)	(14)
	5x16	Smooth-1D	R_a = 3,4 µm	SS-304L-5x16-S-1D	50 mm	(8)	(15)
SS-K31	5x16	Smooth-1D	R_a = 4,5 µm	SS-K31-5x16-S-1D	50 mm	(9)	(16)
	5x23	Ribbed	f_R = 0,022	SS-K31-5x23-R	50 mm	(5)	-
					30 mm	(10)	(17)

2.1 Test materials

2.1.1 Concrete

To cast the specimens for the different test series, 17 concrete batches have been applied. Table 4-2 gives the concrete composition for the traditional and self compacting concrete, respectively. A concrete class of C50/60 has been applied. Mixing time has been taken equal to 3 minutes. The fresh concrete is placed in the form in which the bar is kept horizontal in the axis of the mould, resulting in a vertical casting direction, perpendicular to the bar axis. Concrete compaction is executed by means of a vibrating needle in the case of TC. Both mixing and casting have been performed at ambient laboratory conditions. Demoulding of the test specimens is done 24 hours after casting. Curing of the casted specimens takes place in a wet room (20 ± 2 °C and 95 ± 3 % of relative humidity) for the first seven days, after which the specimens are stored at ambient laboratory conditions until the age of testing (28 days).

Properties of the fresh concrete are tested according to EN 12350 [3] and are given in Table 4-3. Average values and the corresponding standard deviation of the tested properties are also presented in the table. Due to the difference between the fluidity of TC and SCC, different tests are used to assess those parameters for each concrete type. Slump test (by Abraham's cone) and flow test (by shaking table) are performed for TC. On the other hand, both the Abraham's cone slump flow and a V-shape funnel are used for measuring the flow properties of SCC. Density of each mixture is also measured.

Table 4-2 Concrete composition

Material	***TC (kg/m³)***	***SCC (kg/m³)***
Sand 0/4	640	853
Gravel 2/8	462	263
Gravel 8/16	762	434
Limestone filler	-	300
Cement CEM I 52.5 N	360	300
Superplastifier	-	2,4
Water	165	165

Table 4-3 Fresh concrete properties

Batch	*Type of concrete*	*Slump (mm)*	*Flow (-)*	*Slump flow (mm)*	*V-tunnel (s)*	*Density (kg/m³)*
1	TC	37	1,74	-	-	2400
2	TC	50	1,84	-	-	2400
3	TC	25	1,72	-	-	2400
4	TC	55	1,74	-	-	2400
5	TC	10	1,69	-	-	2400
6	TC	20	1,67	-	-	2400
7	TC	27	1,71	-	-	2400
8	TC	38	1,69	-	-	2400
9	TC	30	1,74	-	-	2400
10	TC	30	1,64	-	-	2350
11	SCC	-	-	933	6,9	2350
12	SCC	-	-	810	12,3	2350
13	SCC	-	-	805	15,3	2350
14	SCC	-	-	780	10,9	2350
15	SCC	-	-	830	9,9	2400
16	SCC	-	-	697	14,1	2350
17	SCC	-	-	760	18,1	2350
Average	TC	32	1,72	-	-	2395
St. dev.		13,4	0,05	-	-	16
Average	SCC	-	-	802	12,5	2357
St. dev.		-	-	72,2	3,71	19

Properties of the hardened concrete at 28 days are given in Table 4-4, determined following EN 12390 [4]. Per batch, 3 cylinders (Ø150 mm x 300 mm) and 3 cubes (150 x 150 x 150 mm³) have been casted for determination of the compressive strength, f_c and $f_{c,cub150}$ respectively. The tensile strength is determined by performing bending tests on 3 prisms (150 x 150 x 600 mm³) ($f_{ct,fl}$) and by splitting tests on the remaining halves of the previous prisms ($f_{ct,sp}$). The secant modulus of elasticity E_c is derived from a compressive test on 1 cylinder (Ø150 mm x 300 mm). Average values and the corresponding standard deviation of the tested properties are presented in the table for TC and SCC separately. Furthermore, overall average values are also given.

Table 4-4 Hardened concrete properties at 28 days

Batch	Type of concrete	$f_{c,cub150}$ (N/mm²)	f_c (N/mm²)	$f_{ct,fl}$ (N/mm²)	$f_{ct,sp}$ (N/mm²)	E_c (N/mm²)
1	TC	59,6	51,3	5,7	3,7	37000
2	TC	64,6	54,4	4,6	3,8	37000
3	TC	61,7	54,3	6,3	3,9	37000
4	TC	58,8	52,2	6,6	3,3	37000
5	TC	67,1	58,0	5,6	4,3	36200
6	TC	62,5	55,0	4,9	4,2	35900
7	TC	59,8	54,0	4,8	3,8	36500
8	TC	61,0	55,3	6,5	3,9	36400
9	TC	64,6	54,9	6,3	3,7	37400
10	TC	62,9	54,9	5,0	4,3	36400
11	SCC	68,7	60,7	5,6	4,5	39000
12	SCC	63,6	57,3	5,5	3,9	38000
13	SCC	70,3	62,0	5,9	3,9	38000
14	SCC	67,3	59,4	5,3	3,9	39000
15	SCC	62,4	58,0	4,8	4,0	38300
16	SCC	65,3	58,4	5,1	3,8	38700
17	SCC	67,7	61,9	5,2	4,0	38500
Average	TC	62,3	54,4	5,6	3,9	36680
St. dev.		2,62	1,80	0,77	0,31	466
Average	SCC	66,5	59,7	5,3	4,0	38500
St. dev.		2,83	1,90	0,36	0,23	424
Average	Total	63,9	58,0	5,5	3,9	37429
St. dev.		3,38	3,20	0,63	0,28	1021

2.1.2 Steel

Yield strength, ultimate strength and ultimate strain are obtained by performing tensile tests to each steel rebar (3 tests per type) following EN ISO 15630 [5]. The modulus of elasticity of the rebars has been also calculated out of the performed tensile tests. For SS rebars tested in this work, yielding strength is given as the proof strength at an elongation of 0,2%. Average values for each reinforcement type, together with the values of nominal cross sectional area (A) and nominal perimeter (u), are presented in Table 4-5. For flat rebars the aspect ratio (A_r) is also given, defined as the ratio between the wider and the narrower side of the cross section. The tensile stress-strain relationship of the tested rebars (individual results) are given in Figure 4-1 and Figure 4-2, for smooth rebars and ribbed rebars, respectively. Note that the different rebars have similar stiffness though yield load, hardening and ultimate strain may differ. As pull out type of failure is expected in the bond tests, and steel is not expected to yield, possible differences in yielding properties of the rebars are not regarded of influence in this context.

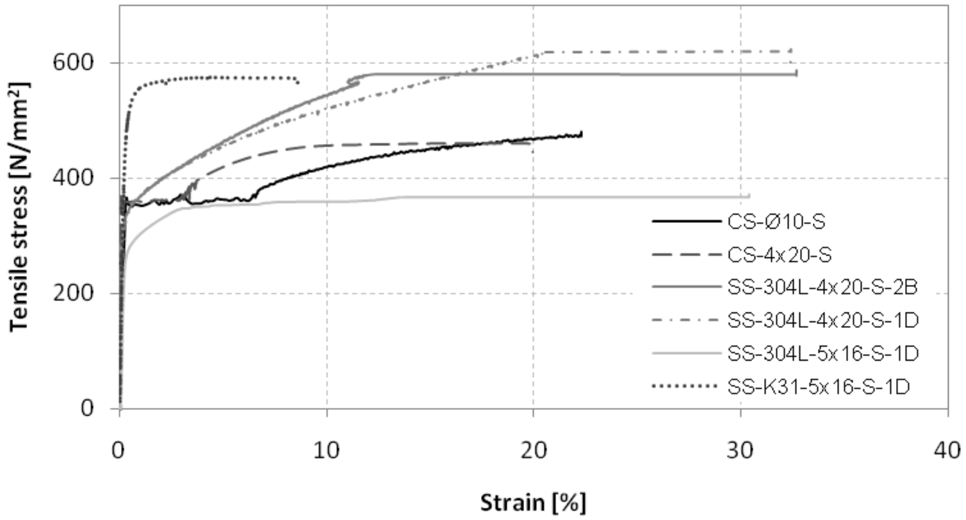

Figure 4-1 Tensile stress-strain relationship for smooth rebars tested

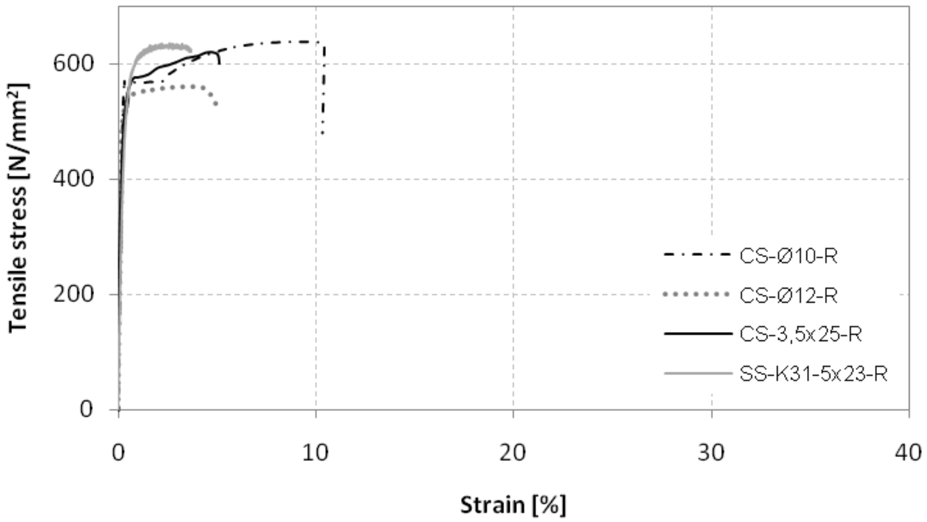

Figure 4-2 Tensile stress-strain relationship for ribbed rebars tested

In order to assess the influence of the roughness (micro and macro) on the bond behaviour of the rebars, two types of measurements are performed:

1) To smooth samples, 2D linear roughness measurements (5 measurements per smooth rebar type) and 3D mappings (1 per type) are conducted at Aperam Isbergues R&D following ISO 4287 [6] and ISO 25178 [7] for 2D and 3D, respectively. In Table 4-1, values of obtained R_a (arithmetic average of absolute

roughness values) are given for the smooth samples. Other roughness parameters as well as mapping images can be found in Appendix A of this work;

2) For ribbed elements, the relative rib area (f_R) is calculated according to the so-called parabola formula described in EN ISO 15630 [5]: Equation 4-1 gives the general definition for relative rib area, while Equation 4-2 is a simplified formula of the definition based on the so-called parabola formula. The different parameters involved are: u, nominal bar perimeter; a_m, rib height at the mid-point; c, transverse rib spacing; e_i, average gap between two adjacent rib rows; and f_R, relative rib area. The parabola formula considers the projected rib area normal to the bar axis as the area comprised for an average rib height of 2/3 times the rib height at the mid-point ($2a_m/3$) along a distance equal to the nominal bar diameter minus the average gap between adjacent rib rows (u-Σe_i). f_R values for the ribbed samples are given under the roughness column of Table 4-1. The measurements of the rib geometry have been conducted assisted by an Automatic Laser Measurement (ALM) system, which consists of a laser-optical displacement sensor (with a wavelength of 670 nm (visible-red) and a resolution of 10 µm). Measurement steps of 0,075 mm have been applied. Given the available machinery for a laboratory scale manufacturing of the flat ribbed rebars (by Aperam and Matière), the relative rib area of the flat rebars is lower (~70% lower values) than the one of round ribbed rebars.

Regarding smooth roughness finishes, the 1D corresponds to a hot-rolled, annealed and pickled surface finish, whereas the 2B is the designation for a cold-rolled, annealed, pickled and skinpassed surface condition. Pictures of different roughness types applied are presented in Figure 4-3.

$$f_R = \frac{projected\ rib\ area\ normal\ to\ the\ axis}{nominal\ bar\ perimeter \times centre\ to\ centre\ rib\ spacing} \tag{4-1}$$

$$f_R = (2a_m/3uc).(u\text{-}\Sigma e_i) \tag{4-2}$$

Table 4-5 Rebar geometrical and tensile properties

Material	*A (mm²)*	*u (mm)*	*A_r (-)*	*Yield strength (N/mm²)*	*Tensile strength (N/mm²)*	*Ultimate strain (%)*	*E-modulus (GPa)*
CS-Ø10-R	78,5	31,4	-	574	642	9,87	205
CS-Ø10-S	78,5	31,4	-	354	488	21,14	200
CS-Ø12-R	113,1	37,7	-	526	566	3,64	206
CS-4x20-S	80,0	48,0	5,0	356	455	19,62	214
CS-3,5x25-R	87,5	57,0	7,1	460	630	8,75	213
SS-304L-4x20-S-2B	80,0	48,0	5,0	326	591	35,67	195
SS-304L-4x20-S-1D	80,0	48,0	5,0	338	579	36,67	201
SS-304L-5x16-S-1D	80,0	42,0	3,2	304	608	49,25	205
SS-K31-5x16-S-1D	80,0	42,0	3,2	420	574	9,16	220
SS-K31-5x23-R	115,0	56,0	4,6	490	630	3,83	212

Round ribbed

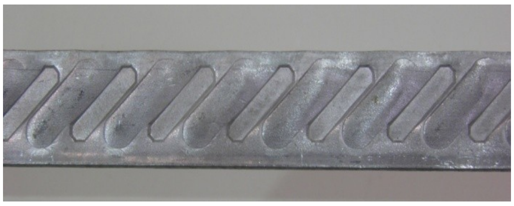

Flat ribbed

1D finish (picture from [8])

2B finish (picture from [8])

Figure 4-3 Pictures of surface roughness applied in the test programme

2.2 Test set-up and testing conditions

The test specimen (Figure 4-4) is a cube of concrete and the steel bar is embedded in its axis. The bar to be tested extends beyond the two sides of the specimen; the tension is applied to the longer end. According to RILEM recommendations for bond testing of reinforcing steel [9], the side length of the concrete specimens is at least 10 times the steel bar diameter. For this test program the side length is taken as 200 mm. The effective embedment length of the bar corresponds to 5 times the bar diameter (5Ø). The other part of the bar does not adhere as it is covered by a plastic tube. The unbonded length is located near the bearing plate, so to avoid its influence. The bond length is limited to obtain pull out failure before yielding of the steel. For this test program, the bond length has been firstly fixed at 50 mm, which corresponds to 5Ø for an equivalent diameter of 10 mm. However, because of the higher splitting tendency of the flat ribbed bars when embedded in concrete, the bond length is later reduced to 30 mm. As required by the measuring devices, the part of the rebar extending from the concrete at the passive end is 100 mm long and 800 mm long at the active end.

For the pulling out of the bar a tensile machine (with load capacity up to 1000 kN, class 1 according to ISO 7500-1 [10], and a relative error of the accuracy of 0,8%) has been used. The specimen is placed vertically on the bearing plate and the tension force is applied at the lower extremity (see Figure 4-4 and Figure 4-5-a). To register the displacement between the steel bar and the concrete, a single Linear Variable Data Transducer (LVDT) is used for the passive end (Figure 4-5-b) while 3 LVDT's (2 LVDT's for flat rebars) are placed at the active end (Figure 4-5-c). For measuring of the bar deformation, 2 extra LVDT's are set at the longer extremity of the bar, underneath the active-end slip measuring system (Figure 4-5-d). The applied LVDT's have a measuring range of 20 mm with an accuracy of 0,001 mm. The LVDT´s for slip measurements have been fixed to the specimen with a gauge length of 100 mm. For the bar deformation a 200 mm gauge length was applied.

Tests are carried out at ambient laboratory conditions of humidity and temperature (~60% of relative humidity and ~20 °C of temperature). The load is applied in a controlled way as follows. At a first stage, load control is applied at a rate of 0,03 kN/s until a small pre-load of 2 kN is reached. The second loading stage applies a displacement control rate of 0,006 mm/s until the end of the test. The test is stopped once the active-end slip is at least 2,5 mm.

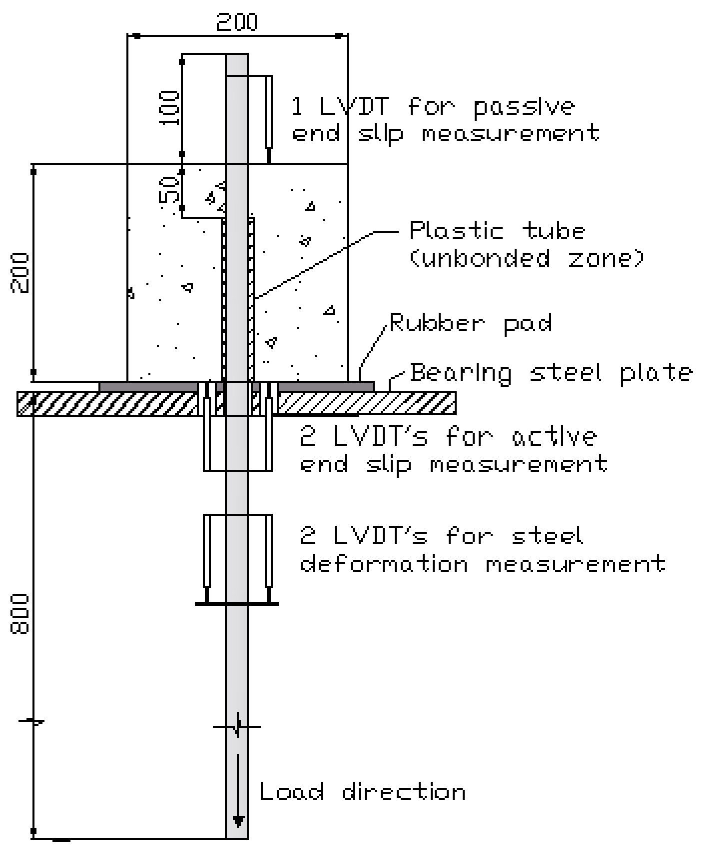

Figure 4-4 Test specimen and measurement devices

3 Test results

3.1 General considerations

Due to the behaviour difference observed between smooth and ribbed samples (the bond strength of smooth samples is significantly lower -up to 95% in this test programme- compared to corresponding ribbed samples), the author believes that results are better understood if they are separately analyzed based on the surface roughness. Thus, in this section smooth samples will be firstly discussed and will be followed by an analysis of the ribbed elements' results. In any case, both for smooth and ribbed samples, the same procedure is applied for the calculation of the desired parameters.

Note that in this section individual test results that are representative for the observed behaviour are given. Appendix B compiles all the individual test results of the flat rebars as well as an average curve for each testing condition.

Figure 4-5 a) General view of the testing machine with the specimen; b) measuring device at the passive end; c) measuring system at the active end; d) bar deformation measurement

Equation 4-3 is used for the calculation of the mean bond stress along the bond length, τ_b (in N/mm^2), where F is the measured force (in N), u stands for perimeter of the rebar (in mm) and l_b refers to the bond length (in mm). For determining the bond strength f_b (in N/mm^2), Equation 4-4 is used, where F_{max} represents the maximum measured force (in N). Equation 4-5 gives the value of the bar slip at the active end (s_a, in mm), being s_a' the measured slip at the active end, including the bar deformation Δl_s, which is the deformation of the bar along the gauge length of the slip measurement device (both in mm). The value of Δl_s has been calculated from the measured strain of the bar deformation device, for a gauge length of 200 mm, and considering uniform deformation of the rebar, applied to the gauge length of the slip measuring device (100 mm).

$$\tau_b = F/(u.l_b) \tag{4-3}$$

$$f_b = F_{max}/(u.l_b) \tag{4-4}$$

$$s_a = s_a' - \Delta l_s \tag{4-5}$$

Table 4-6 to 4-9 give the average (out of 3) test results for each tested bar type and condition that failed by pulling out of the bar. The maximum measured load (F_{max}), the corresponding bond strength (f_b) and the standard deviation of the bond strength are presented in these tables. Furthermore, a bond strength ratio ($f_b/f_{b,ref}$) is calculated taking as reference the bond strength calculated for Ø10 mm CS ribbed bar, which has a cross sectional area equivalent to 4x20 mm^2, to 5x16 mm^2 and to 3,5x25 mm^2 flat bars. In the case of 5x23 mm^2 flat strips, the ratio is calculated taking as reference Ø12 mm CS ribbed bar. Finally, a second ratio ($f_b/s_{a,fb}$) is calculated in terms of developed bond strength divided by the active end slip at the moment of maximum strength. This parameter gives an indication of the bond stiffness in the ascending part of the bond stress-slip relationship. Table 4-6 gives the test results for smooth samples tested with TC and an effective embedding length of 50 mm, Table 4-7 summarizes results for smooth reinforcements embedded in SCC and bond length of 50 mm, Table 4-8 and Table 4-9 give results of ribbed elements, with a bond length of 30 mm and embedded in TC and SCC, respectively.

For a more comprehensive analysis of the test results, a two-tailed t-test [11] with a significance level, α, equal to 0,05 has been used in this work for comparison of the obtained bond strength results. According to [11], typical values of α range from 0,01 to 0,10; for the comparison performed in this work, α has been taken equal to 0,05 as done by [12]. The t-test assesses whether the means of two considered groups are statistically different from each other, hence if the difference between the mean values of the two considered groups is significant or not, taken into account the variability of the test results. The calculation procedure is as follows: 1) the t-value (t) is calculated according to Equation 4-6, where $\bar{X}_T$ and $\bar{X}_C$ are the mean values of the two considered data groups, σ_T and σ_C are their standard deviation, and n_T and n_C are the number of samples considered for each group; 2) the t-value is compared to the table of significance existing for this test [11]: values of t are given in this table dependant on the degree of freedom (n_T + n_C -2) and the adopted significance level, α; 3) if the calculated t-value is higher than the one given by the significance table, the difference between the two mean values is significant, and therefore, they are statistically different. On the other hand, if the calculated t-value is lower than the one given by the significance table, the difference between the two mean values is not significant, and therefore, they can be considered statistically equals.

$$t = (\bar{X}_T - \bar{X}_C) \;/\; \sqrt{(\sigma_T^2 \;/\; n_T) \;+\; (\sigma_C^2 \;/\; n_C)} \tag{4-6}$$

The bond stress-slip relationship for each tested bar is calculated based on the derived measurements, whereas a continuous representation of the behaviour is possible due to the used continuous measurement system. When results are divided into smooth samples and ribbed ones, the bond stress-slip behaviour of used reinforcement elements is similar within each group.

Table 4-6 Smooth samples embedded in TC, bond length 50 mm

Bar/Strip	***Concrete type***	F_{max} ***(kN)***	f_b ***(N/mm²)***	***Sdev (N/mm²)***	$f_b/f_{b,ref}$ ***(-)***	$f_b/s_{a,fb}$ ***(N/mm³)***
CS-Ø10-R	TC (1)	39,75	25,31	3,18	1,00	16,14
CS-Ø10-S	TC (3)	8,27	5,26	0,34	0,21	11,84
CS-4x20-S	TC (4)	8,82	3,67	0,11	0,15	17,90
SS-304L-4x20-S-2B	TC (7)	3,58	1,49	0,15	0,06	30,40
SS-304L-4x20-S-1D	TC (7)	4,30	1,79	0,38	0,07	43,65
SS-304L-5x16-S-1D	TC (8)	10,00	4,76	1,37	0,19	23,91
SS-K31-5x16-S-1D	TC (9)	4,92	2,34	1,31	0,09	4,14

Table 4-7 Smooth samples embedded in SCC, bond length 50 mm

Bar/Strip	***Concrete type***	F_{max} ***(kN)***	f_b ***(N/mm²)***	***Sdev (N/mm²)***	$f_b/f_{b,ref}$ ***(-)***	$f_b/s_{a,fb}$ ***(N/mm³)***
CS-Ø10-R	SCC (11)	46,72	29,74	0,39	1,00	9,95*
CS-4x20-S	SCC (12)	13,68	5,70	0,84	0,19	18,32
SS-304L-4x20-S-2B	SCC (14)	4,12	1,72	0,26	0,06	18,10
SS-304L-4x20-S-1D	SCC (14)	7,97	3,32	0,71	0,11	23,38
SS-304L-5x16-S-1D	SCC (15)	15,20	7,24	0,23	0,24	16,87
SS-K31-5x16-S-1D	SCC (16)	7,43	3,53	1,27	0,12	3,99

* The bars started yielding before the bond strength was reached

Table 4-8 Ribbed samples embedded in TC, bond length 30 mm

Bar/Strip	***Concrete type***	F_{max} ***(kN)***	f_b ***(N/mm²)***	***Sdev (N/mm²)***	$f_b/f_{b,ref}$ ***(-)***	$f_b/s_{a,fb}$ ***(N/mm³)***
CS-Ø10-R	TC (2)	24,16	25,64	2,62	1,00*	23,56
CS-Ø12-R	TC (2)	23,91	21,14	4,38	1,00**	30,81
CS-3,5x25-R	TC (6)	31,45	18,40	3,34	0,72*	10,37
SS-K31-5x23-R	TC (10)	34,99	20,83	1,51	0,99**	8,44

* $f_{b,ref}$: corresponding with CS-Ø10-R

** $f_{b,ref}$: corresponding with CS-Ø12-R

Table 4-9 Ribbed samples embedded in SCC, bond length 30 mm

Bar/Strip	*Concrete type*	F_{max} *(kN)*	f_b *(N/mm²)*	*Sdev (N/mm²)*	$f_b/f_{b,ref}$ *(-)*	$f_b/s_{a,fb}$ *(N/mm³)*
CS-Ø10-R	SCC (11)	32,21	34,18	2,71	1,00*	27,83
CS-Ø12-R	SCC (11)	35,16	31,09	0,57	1,00**	38,38
CS-3,5x25-R	SCC (13)	33,36	19,51	1,33	0,57*	8,37
SS-K31-5x23-R	SCC (17)	31,41	18,80	1,42	0,60**	17,35

* $f_{b,ref}$: corresponding with CS-Ø10-R

** $f_{b,ref}$: corresponding with CS-Ø12-R

3.2 Smooth samples

3.2.1 Influence of reinforcement material

From the test results it can be observed that, for flat smooth elements, where chemical adhesion is the main developed bond mechanism [13], the material type has more influence than for ribbed samples, where mechanical bond mechanism due to the ribs governs the bond behaviour [13]. The test results for smooth CS show higher bond strength than austenitic 304L SS (85% higher values). This is in line with the micro roughness (R_a) of the CS smooth versus 304L-1D rebar, which is 75% higher. The higher bond strength may be explained both by difference in material type and micro roughness. On the other hand, 304L SS develops better bond capacity than the ferritic K31 SS (up to 100% higher bond strength values, being the R_a of K31 SS 25% higher). In this case, the difference in bond strength is mainly explained by the difference in material type. When looking to the bond strength/slip at maximum bond stress ratios, SS 304L has stiffer chemical bond behaviour than CS and SS K31, when tested in TC. However when SCC is used the chemical adhesion stiffness is similar for CS and for SS 304L, while the stiffness of the ferritic SS K31 is still lower.

3.2.2 Influence of reinforcement geometry

The bond strength developed by round bars (both smooth and ribbed samples) is higher than for flat elements. This difference is more pronounced when the rebars are embedded in SCC. However, the bigger perimeter corresponding to a flat rebar, for a comparable cross section and the same bond length, makes the reached maximum force to be higher for flat rebars. Nevertheless, for smooth samples comparison (CS-Ø10-S vs. CS-4x20-S), the difference in micro roughness (150% higher for the round element), might have influenced in developing higher bond capacity for the round specimen (*see 3.2.3 Influence of reinforcement roughness*).

When comparing samples of the same material, roughness, cross section area, but with different aspect ratio (5,0 for SS-304L-4x20-S-1D and 3,2 for SS-304L-5x16-S-1D), the smaller aspect ratio (36% smaller aspect ratio for 5x16 mm² geometry compared to 4x20 mm²) develops up to 140% higher bond strength value (both for TC and SCC). Based on the t-test, this dissimilarity is significant enough to conclude that the investigated aspect ratios develop different bond capacity.

Although there is almost no literature available regarding bond behaviour of flat smooth rebars, for the few tests results reported by Abrams 1913 [19] concerning bond capacity of flat smooth samples, the same influence of aspect ratio was observed. Abrams tested two different aspect ratios: 2 and 8, for strip sizes of 25,4 x 12,7 mm^2 and 50,8 x 6,35 mm^2, respectively. The results, given as maximum bond resistance, were 3,16 N/mm^2 for the lowest aspect ratio vs. 2,02 N/mm^2 for the largest one. In other words, a 4 times smaller aspect ratio, developed 156% higher bond capacity.

3.2.3 Influence of reinforcement roughness

According to [13], the initial chemical adhesion is accompanied by the micromechanical interaction associated with the microscopically rough steel surface. Thus, keeping other properties constant, 1D roughness (R_a = 3,0 µm) bond strength is better (20 to 50% higher for TC and SCC, respectively) than for 2B roughness (R_a = 0,4 µm). However, according to the test results, for similar micro roughness conditions, other parameters like geometry or material type have more pronounced influence on bond behaviour than differences related to micro roughness. Hence, it can be concluded that the micro roughness has a secondary influence on the adhesion forces developed by the reinforcement.

3.2.4 Influence of concrete type

From the test results it can be observed that for the majority of the tested bars a better bond capacity is obtained when working with SCC (ranging from 15 to 85% higher bond strength). Specimens made of SCC have a moderately higher compression strength (up to 9 N/mm^2 or 18% difference in comparison to their equivalent in TC) which should derivate in a higher bond capacity. However, the difference in the experimentally developed bond strength is higher than the one corresponding to the mentioned difference in compression strength (according to the fib Model Codes [14][15], the difference in bond strength, for a 18% difference on compression strength, is around 8%).

3.2.5 Bond stress-slip relationship

Figure 4-6 to 4-10 allow for a comparative analysis of the bond stress-slip behaviour between the studied different parameters within the smooth samples. Note that Figure 4-6 to 4-10 illustrate individual test results for the case of TC (similar curves were obtained for the case of SCC). Although differences in bond stress values dependant on the analyzed parameters are noticeable, the same bond stress-slip curve shape is repeatedly observed: a first ascending stiff branch, followed by an immediately descending second stage until the frictional forces are reached, and a third final plateau corresponding to the friction forces acting during the pulling out of the bar.

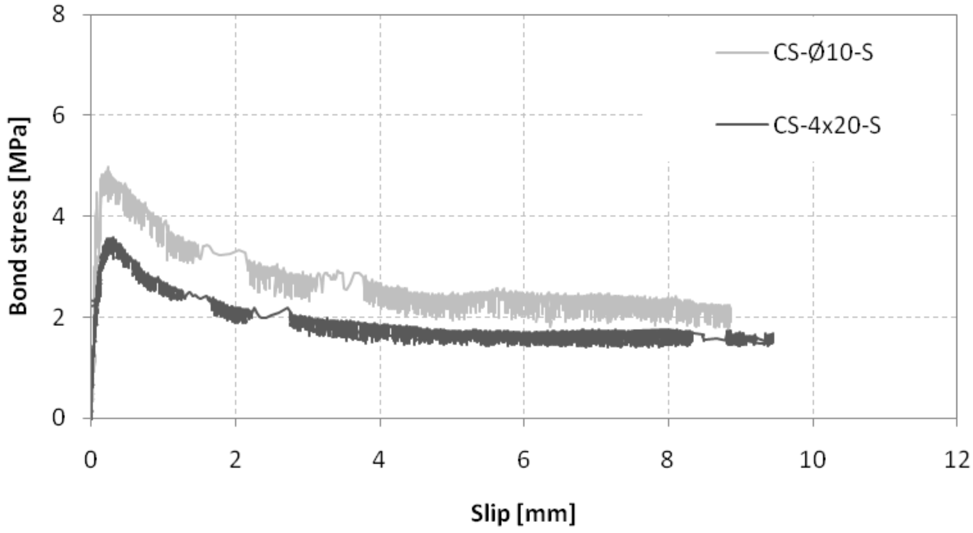

Figure 4-6 Bond stress-slip relationship. Round vs. flat (smooth)

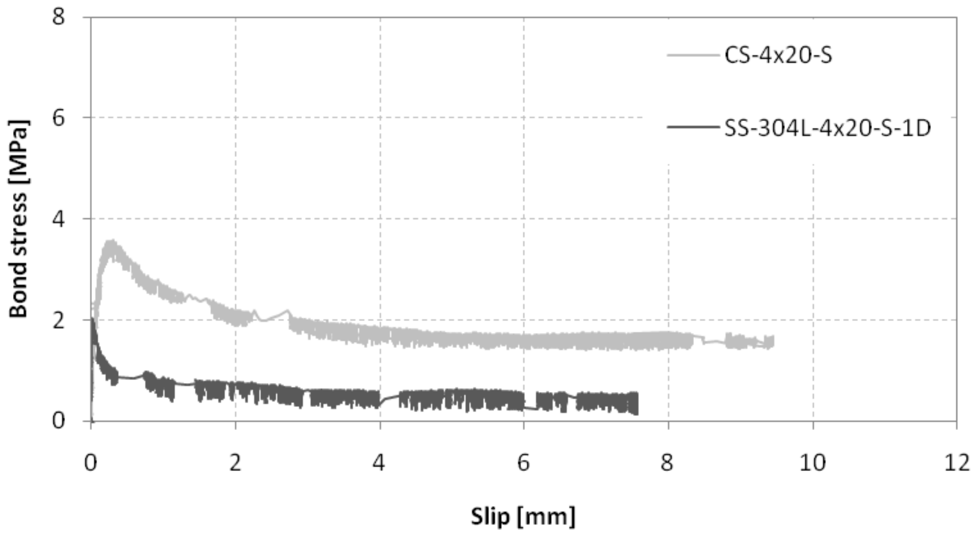

Figure 4-7 Bond stress-slip relationship. CS vs. SS (smooth)

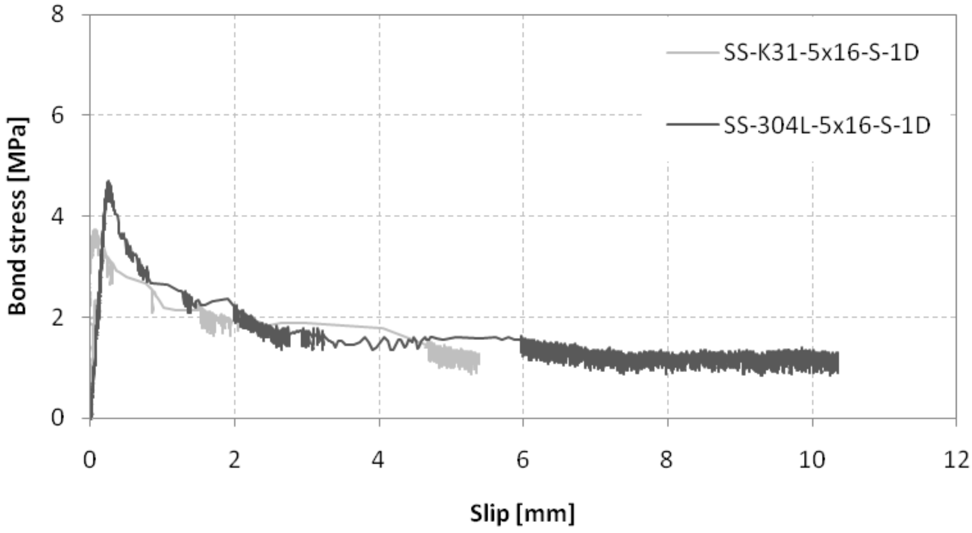

Figure 4-8 Bond stress-slip relationship. K31 vs. 304L (smooth)

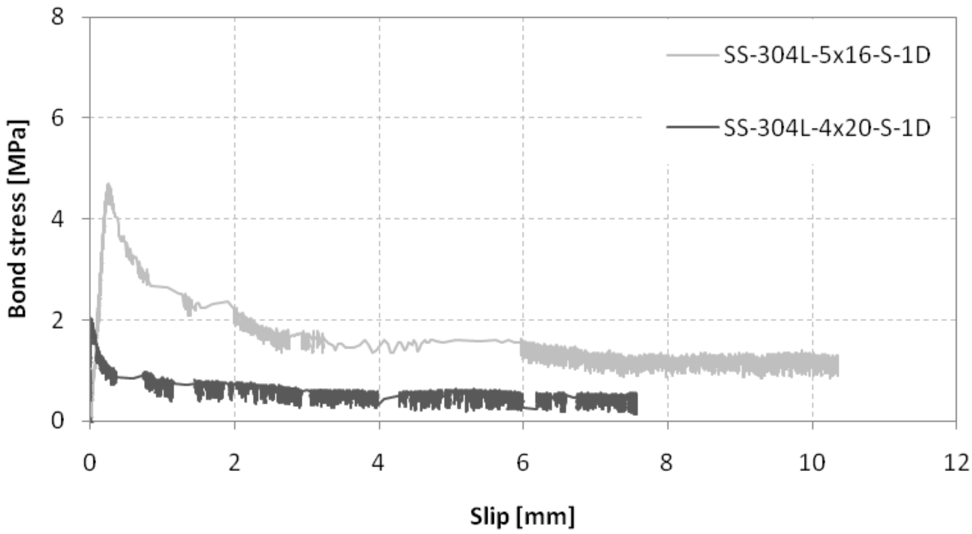

Figure 4-9 Bond stress-slip relationship. 5x16 vs. 4x20 (smooth)

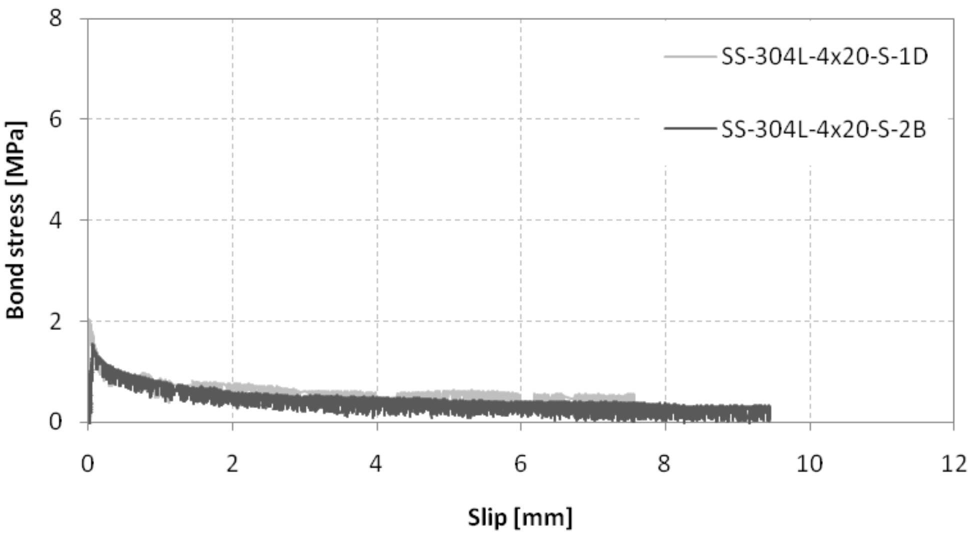

Figure 4-10 Bond stress-slip relationship. 1D vs. 2B (smooth)

3.3 Ribbed samples

In the first part of the test program the bond length was equal to 50 mm (equivalent to 5Ø recommended by RILEM [9]). It was observed that the flat ribbed elements (both CS and SS) did not fail by pull out, but rather by yielding of the steel (followed by rebar rupture) or by a splitting type of bond failure. As a result, it was decided to reduce the bond length from 50 to 30 mm for additional testing of flat ribbed elements. Consequently, the reference CS round bars (Ø10 mm and Ø12 mm) were also tested with a bond length of 30 mm for comparison.

3.3.1 Influence of reinforcement material

For ribbed samples, taking strips with a comparable perimeter and same rib geometry, and according to the mean bond strength values, SS behaves better (~10% higher bond strength) than CS when embedded in traditional concrete. On the other hand, when testing them with self compacting concrete CS develops 4% higher bond strength than the one developed by SS. However, if mean values are analyzed together with their standard deviation, the t-test statistical analysis confirms that the differences on bond strength developed by CS and SS are not significant. In other words, for geometrically comparable flat ribbed samples, no significant difference is observed between the bond strength of CS and SS.

3.3.2 Influence of reinforcement geometry

For most of the analyzed cases, the bond strength developed by round bars is higher than for flat elements. This difference is more pronounced when the rebars are embedded in SCC. However, the bigger perimeter corresponding to a flat rebar, for a comparable cross section and the same bond length, makes the reached maximum force to be higher for flat rebars. According to the t-test, only for the Ø12 equivalent ribbed samples when tested in TC, the significance of the difference between the bond strength developed by round and flat samples is low enough to consider the results comparable.

In the case of ribbed samples, the more optimal values of relative rib areas of round elements, versus low values for the strips, have also contributed to develop higher bond strength values for round bars (*see 3.3.3 Influence of reinforcement roughness*). Furthermore, according to the bond stress-slip relationship, it can be also concluded that the behaviour of the CS-Ø10-R and CS-Ø12-R is stiffer compared to the one of CS-3,5x25-R and SS-K31-5x23-R, respectively: the bond strength values related to the standard round ribbed bars are always reached at a lower slip values than for the strips, in all the cases, and for both TC and SCC.

3.3.3 Influence of reinforcement roughness

For ribbed samples, the roughness can be expressed in terms of relative rib area f_R. The generally accepted values for round rebars range from 0,05 to 0,10 and represent a good compromise for f_R in terms of bond strength, splitting tendency, industrial requirements and good service-load performances (limited crack opening and cover splitting) [13]. Regarding the flat ribbed elements (CS and SS) studied in this paper, the lower f_R values (~0,022) of their rib pattern might have contributed to the development of lower bond strength compared to the CS round ribbed bars ($f_R \approx 0{,}078$).

3.3.4 Influence of concrete type

Focusing on ribbed samples, the effect of the SCC is much more pronounced for round bars than for flat strips. The only material that shows better results in TC than when embedded in SCC is SS-K31-5x23-R (SS flat ribbed specimens): 10% higher bond strength values are reached when embedded in TC than for SCC. If the statistical analysis is applied (two-tailed t-test), however, both for CS and SS flat ribbed samples, it is derived that the dissimilarities on the bond strength between the two concrete types is not significant enough to consider the results different. In other words, flat ribbed specimens analyzed in this paper develop similar bond strength when they are embedded in TC or in SCC.

On the other hand, if the ratio $f_b/s_{a,fb}$ is considered and absolute values are analyzed, round bars develop stiffer behaviour in SCC than in TC. The same tendency is observed for SS flat strips. For CS flat members, however, lower slip values are reached at maximum bond stress situation when tested with TC. If the statistical analysis is applied in terms of the $f_b/s_{a,fb}$ ratio, only the differences developed by SS flat strips are significant. Thus, it can be concluded, that only for SS flat members significantly stiffer behaviour is developed when embedded in SCC (compared to TC). For CS, the stiffness of the bond forces is comparable when tested in TC and SCC.

3.3.5 Bond stress-slip relationship

For ribbed samples analyzed in this paper, τ-s relationships are given in Figure 4-11 and Figure 4-12 (individual specimen test results are shown, for the use of TC). The reference CS-Ø10-R specimen is compared to a CS flat ribbed sample in Figure 4-11, allowing for a bond-slip behaviour comparison between round and flat elements. Besides the already discussed higher maximum bond stress values reached by the round specimen, the stiffer ascending branch is also observed. Both elements show some degree of plateau at their corresponding maximum bond stress. The round element has a steeper descending branch, reaching the frictional forces at lower slips (~ 7 mm) comparing to the flat ribbed element, which shows a smoother descending stage and reaches the frictional forces at higher slip values (on average ~18 mm). Figure 4-12 compiles results obtained for CS and SS flat ribbed reinforcement: similar bond stress-slip relationship is observed both in terms of values and in terms of graph shape, which agrees with the non significant differences discussed before for material type of ribbed samples.

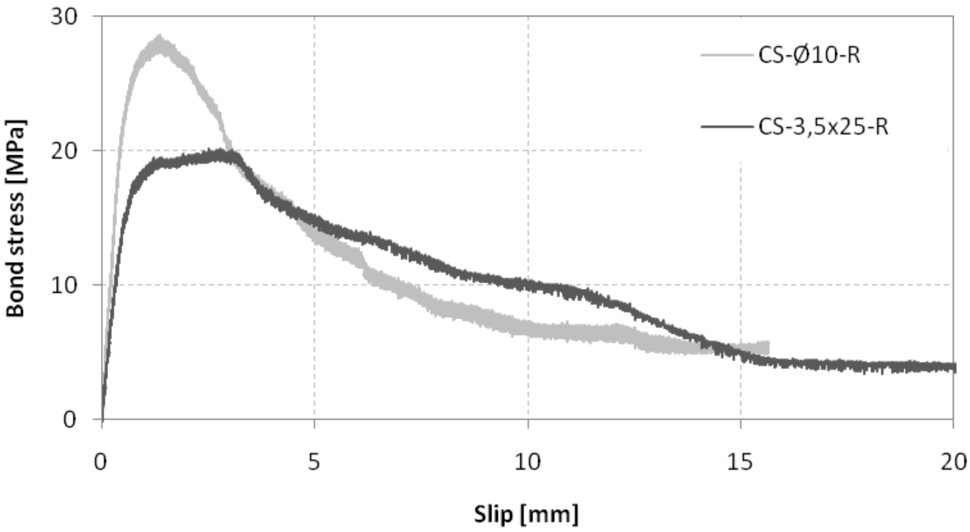

Figure 4-11 Bond stress-slip relationship. Round vs. flat (ribbed)

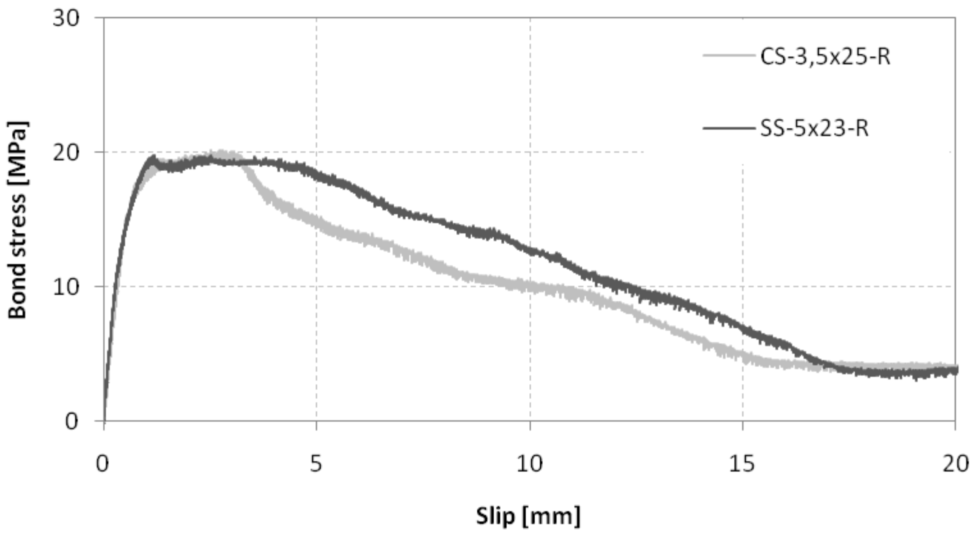

Figure 4-12 Bond stress-slip relationship. CS vs. SS (ribbed)

4 Analysis of the failure aspect

4.1 Epoxy injection procedure

To inspect the bond zone after extensive slip, the specimens are saw cut parallel to the rebar axis direction, and cutting the rebar in half, after injecting fluorescent epoxy for a better visualization. The procedure is as follows: the specimen (200x200x200 mm^3) is cut where the plastic tube begins and perpendicular to the bar axis. A plastic cylinder (inner diameter of 65 mm) is glued on top to limit the surface active in the epoxy injection (see Figure 4-13a). A sealant is used to avoid leaking of the epoxy outside the cylinder. Fluorescent epoxy injection is executed in a vacuum chamber (see Figure 4-13b). Due to the vacuum (applied for a minimum of 2 hours), the epoxy is able to fill all the pores, cracks and gaps that are present at the specimen. When the epoxy is hardened (minimum 24 hours), the specimen is saw cut parallel to the rebar axis direction (see Figure 4-13c). The specimen is then ready for inspection.

4.2 Visual and microscope analysis

Both visual and microscopic inspections are performed. To aid the visual inspection, UV light is used so that cracks or imperfections filled with fluorescent epoxy illuminate. An optical microscope (type Leica S8APO) has been used for microscopic failure aspect analysis.

Vertical cracks (parallel to the reinforcement longitudinal axis) are clearly observed in the rib area of the deformed standard CS round bars: these longitudinal cracks are seen extending at both sides of a rebar rib (see Figure 4-14a and Figure 4-15a), and crack propagation between two ribs of the rebar is also clearly observed. These vertical cracks are typical for a pull out failure [13]. For flat smooth strips, interface cracking can be noted which agrees with the dominating chemical bond behaviour of plain bars (Figure 4-14b and Figure 4-15b). For flat ribbed samples, vertical main cracks are clearly observed (Figure 4-14c and Figure 4-15c). Furthermore, radial cracks are also detected by microscope inspection: they are extending from the main vertical crack into the concrete matrix (yellowish lines in Figure 4-15d). Similar behaviour is observed for all the flat ribbed rebars, independently of steel or concrete type. For flat ribbed rebars tested in this project, the peak of a rib at one side is the valley of a rib at the other side of the bar and the rib spacing is larger than for standard round ribbed bars. These two properties lead to larger concrete volumes of concrete being dragged while slipping of the rebar (interpreted from large continuous areas of fluorescent epoxy observed both by visual and microscopic inspection, see Figure 4-14-c and Figure 4-15-c). This effect, together with the observed radial cracks, agrees with the observed splitting tendency of the strips when embedded in concrete (see *Chapter 2, section 2.2 Modes of bond* failure).

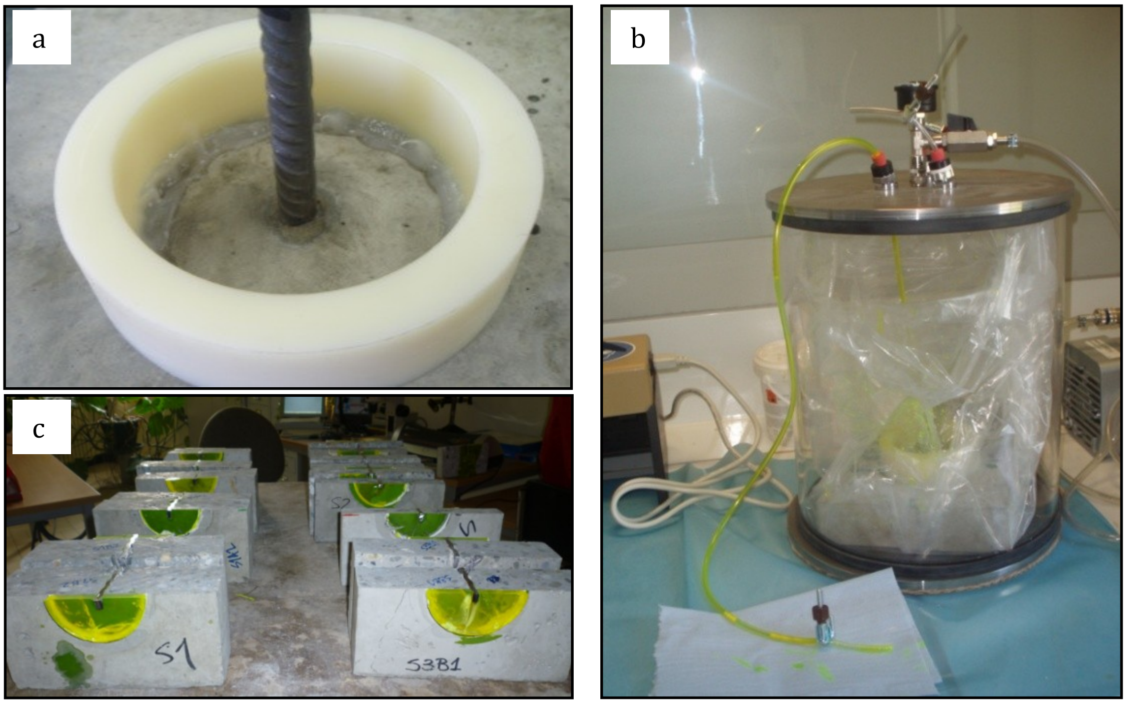

Figure 4-13 Epoxy injection procedure; a. Glued and sealed plastic cylinder for limiting the epoxy injection area; b. Vacuum chamber with the specimen in it; c. Specimens ready for inspection

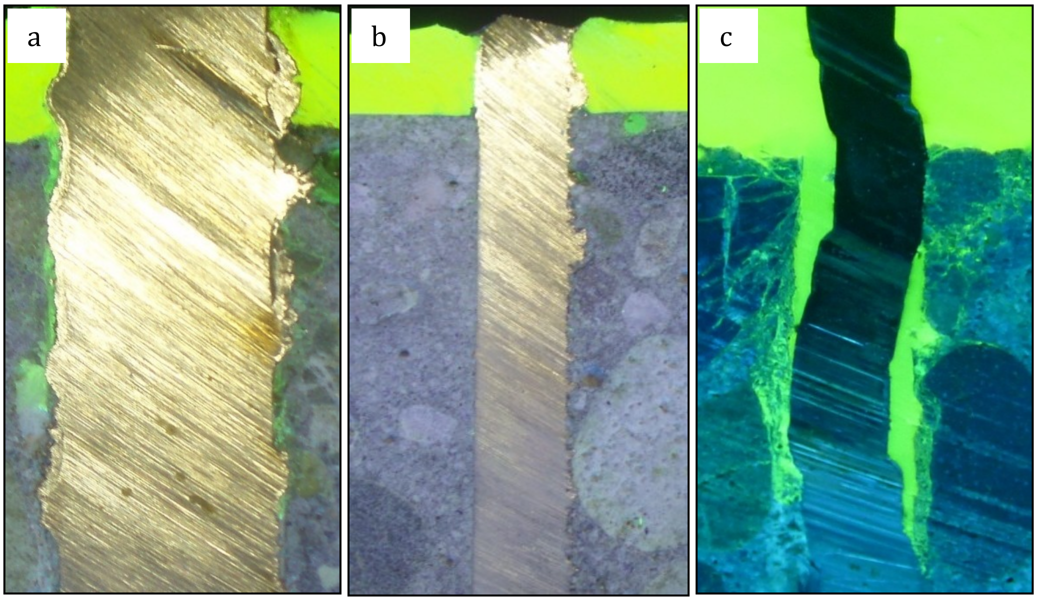

Figure 4-14 Visual inspection aided by UV light; a. CS-Ø10-R; b. SS-304L-5x16-S-1D; c. SS-K31-5x23-R

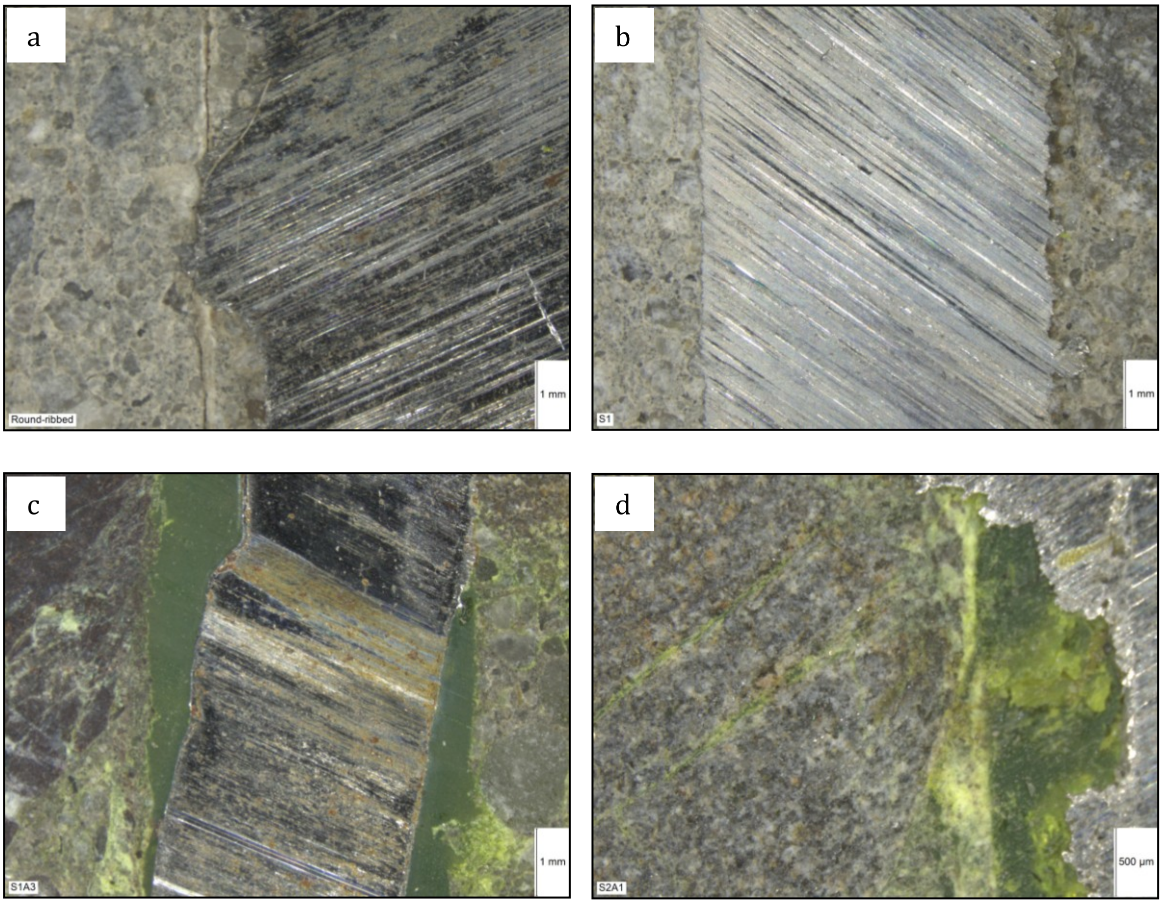

Figure 4-15 Microscopic inspection; a. CS-Ø10-R; b. SS-304L-5x16-S-1D; c. SS-K31-5x23-R
d. SS-K31-5x23-R

5 Analytical verification: comparison to existing bond models

Due to the differences in the bond-governing principles existing for smooth and for ribbed bars, an unique bond model that predicts the behaviour of both reinforcement types is unreal. Thus, in this section, bond stress-slip relationship for both surfaces are separately studied as it has been done with the test results.

5.1 Smooth samples

According to the literature available to the author no research has been conducted on developing a bond model for flat smooth reinforcing elements. It is the intention of this section to analyze how accurately the existing bond models (for round smooth bars) can predict the behaviour observed for the flat smooth elements tested in this work. Furthermore, an adaptation of the existing bond models will be proposed for a more accurate prediction of the bond behaviour of flat smooth reinforcements.

5.1.1 Model Codes: MC90 and MC2010

The draft version of the fib Model Code 2010 [15] (MC2010) does not apply any modification to the bond model proposed by the Model Code 90 [14] (MC90) for smooth round bars, and therefore both are analyzed together. Both models are based on the bond stress-slip behaviour given by Eligehausen et al. [16]. The model describes the bond behaviour of smooth round bars as two-stage behaviour, where a first ascending branch is suggested until the maximum bond stress is reached at a certain slip of the bar. The second branch is a horizontal line, which indicates that after the maximum bond stress is reached the bond stress is constant at increasing slips, and therefore the bond strength equals the residual frictional stress developed by the contact between the steel and the concrete. The model is defined by Equations 4-7 and 4-8 with the values of the different parameters given in Table 4-10 for different production methods and bond conditions. The model is represented in Figure 4-16. The MC90/MC2010 define the maximum bond stress and the frictional remaining bond stress only dependant on the characteristic compression strength of the concrete. However, according to the commentary of the Model Codes, the bond stress-slip relationship depends on a considerable number of influencing factors, and therefore the bond stress-slip relationships presented in these documents should be considered as statistical mean curves, applicable as an average formulation for a broad range of cases.

$$\tau(s) = \tau_{max} (s/s_1)^{\alpha} \qquad 0 \le s \le s_1 \tag{4-7}$$

$$\tau(s) = \tau_{max} \qquad s \ge s_1 \tag{4-8}$$

Table 4-10 Parameters for defining the bond stress –slip relationship of smooth bars

Parameters	***Cold drawn wire***		***Hot rolled bars***	
	Good bond conditions	*All other bond conditions*	*Good bond conditions*	*All other bond conditions*
s_1	0,01 mm	0,01 mm	0,1 mm	0,1 mm
α	0,5	0,5	0,5	0,5
$\tau_{max} = \tau_f$	$0{,}1\sqrt{f_{ck}}$	$0{,}05\sqrt{f_{ck}}$	$0{,}3\sqrt{f_{ck}}$	$0{,}15\sqrt{f_{ck}}$

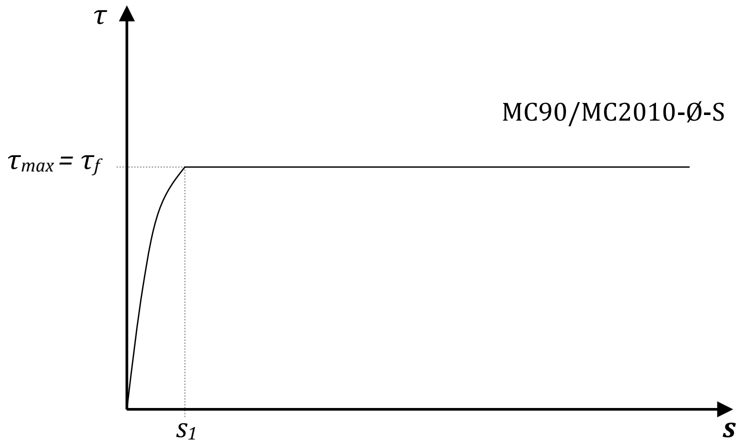

Figure 4-16 Bond stress-slip relationship for round smooth bars according to MC90 and MC2010

If we now represent the test results obtained for smooth rebars (both flat elements as well as round smooth CS) together with the predicting graph given by the MC90/MC2010 for an average characteristic compressive strength of concrete, f_{ck} (calculated and taken in this work as $f_{ck} = f_c - 8 = 50$ N/mm² [1], where f_c is the round number of the average compressive strength of the casted batches and equals to 58 N/mm²), the high variability of results obtained for flat smooth samples dependant on aspect ratio, steel type, and concrete type are exposed as plotted in Figure 4-17 and Figure 4-18. The author considers that the shape of the first ascending branch, quite acceptably agrees with the behaviour observed at low slip values of experimental results. However, after the maximum bond stress is reached, the model keeps the bond stress at that level for the remaining slip values. The observed behaviour has a completely different trend: after the maximum bond stress is reached, the bond forces decreases immediately, in a gradual way, until residual friction forces are reached. This last phenomena occurs at an average slip value of 10 mm.

It is believed that given the shape of the bond-slip relationship obtained repeatedly for flat smooth samples (as well as for CS-Ø10-S), the bond behaviour is more accurately defined if 3 stages are considered: an ascending first stiff part (related to the chemical and micromechanical adhesion) until the bond strength is reached, followed by a stage of gradual loss of bond at increasing slip until the residual friction adhesion and finally, a plateau related to the friction bond stresses follows.

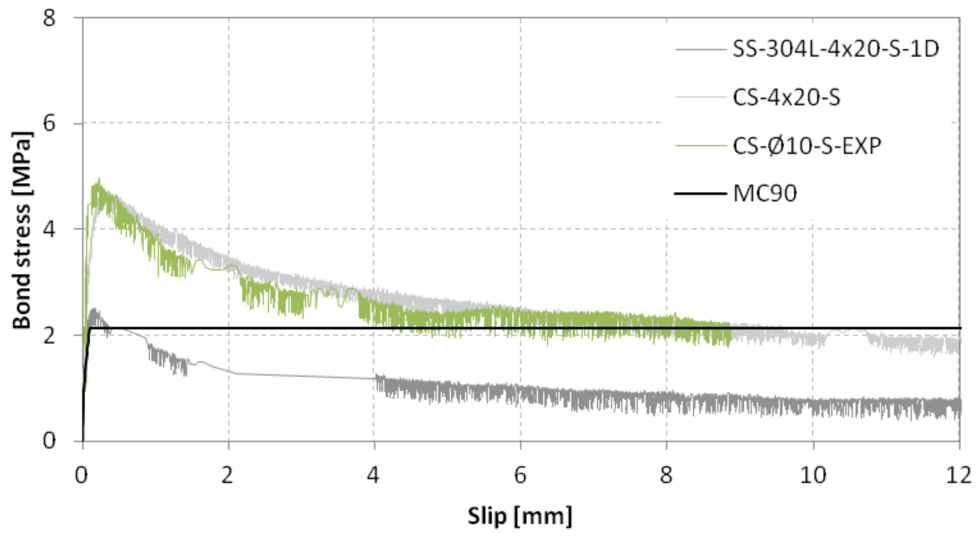

Figure 4-17 Bond stress-slip behaviour for flat smooth samples. Model given by MC90 vs. test results, for slip values until 12 mm

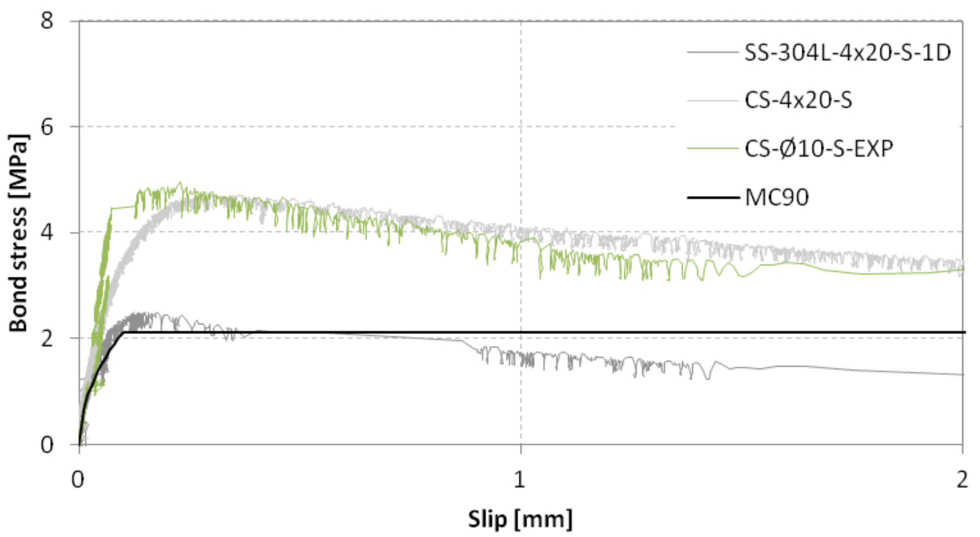

Figure 4-18 Bond stress-slip behaviour for flat smooth samples. Model given by MC90 vs. test results, for slip values until 2 mm

5.1.2 Feldman et al.

An experimentally calibrated bond model is proposed by Fedman et al. [17] (2005)based on the observed bond behaviour of smooth round and square samples, by means of 252 cylindrical pullout specimens performed at University of Western Ontario, Canada. Different development lengths, two different bar sizes, round and square shapes, several concrete covers and 3 different surface treatments were investigated. The load-slip behaviour observed is described as a maximum load reached at a negligible slip, followed by an asymptotical drop of load at increasing slips towards a limiting residual load at a slip of approximately 10 mm (see Figure 4-19). Feldman applied a regression analysis of 237 specimens considering all the influencing parameters to obtain the formulas for calculating the maximum and the residual bond stress as given by Equations 4-9 and 4-10. The bond stress is defined dependant on bar size (k_{sz} = 0 for bars of 16 mm and k_{sz} = 1 for bars of 32 mm of diameter (or side length for square reinforcements); bar shape (k_{sh} = 0 for round bars and k_{sh} = 1 for square bars); R_y is the surface roughness in µm and l_d is the development length in mm; f_c corresponds to the compressive cylinder strength of the concrete at 28 days. Furthermore, Feldman defines the asymptotical descending curve as a logarithmic branch (see Equation 4-11), starting from point (s_1, τ_{max}) to point (10 mm, τ_f). For the definition of coefficients β_0 and β_1, the slip at maximum bond stress, s_1, is taken as 0,01 mm. After a slip of 10 mm a constant bond stress of τ_f is assumed. However, no definition is given for describing the first ascending branch for slips lower than 0,01 mm, until the maximum bond stress is reached.

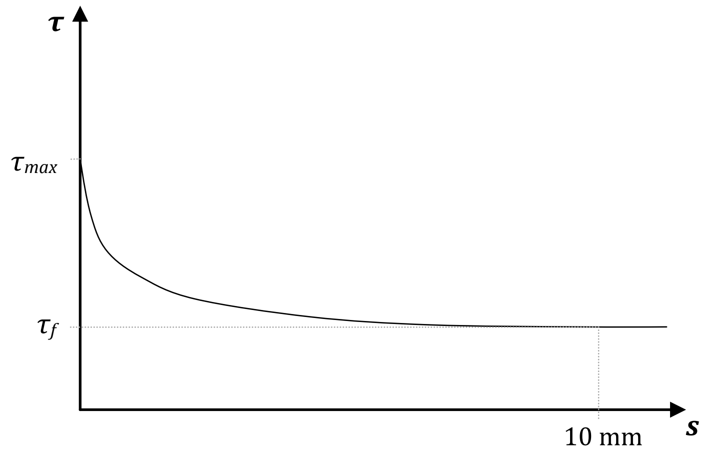

Figure 4-19 Bond stress-slip relationship for round smooth bars according to Feldman et al.

$$\tau_{max}/\sqrt{f_c} = (0{,}19-0{,}07k_{sz}+0{,}05k_{sh})\sqrt{R_y} + (-2{,}7\ 10^{-5} + 4{,}0\ 10^{-5}k_{sz} - 3{,}0\ 10^{-5}k_{sh})R_y l_d \quad (4\text{-}9)$$

$$\tau_f/\sqrt{f_c} = (0{,}042+0{,}009k_{sz}-0{,}007k_{sh})\sqrt{R_y} + (-1{,}65\ 10^{-5} + 1{,}41\ 10^{-5}k_{sh})R_y l_d \quad (4\text{-}10)$$

$$\tau(s)/\sqrt{f_c} = \beta_0 + \beta_1 \log s \quad (4\text{-}11)$$

The definition given by Feldman is limited to bars of certain size and shape, and is therefore not applicable to the flat rebars used in this research work. However, the logarithmic descending branch could be representative for the behaviour observed during testing, and therefore might be applicable to describe the behaviour of flat smooth rebars.

5.1.3 Proposed bond model for flat smooth reinforcing elements

The proposed model modifies the model given by the fib Model Codes for round smooth bars, and adapts it for using it to predict the bond behaviour of flat smooth rebars tested in this work. Note that individual test results which are representative of the observed behaviour are given in this section, while all test results and the corresponding comparison to the proposed model curves are given in Appendix B of this work. The main difference remains on the new 3 branches approach, in which a bond stress decreasing stage is considered at increasing slip after the maximum bond stress is reached. This behaviour is also observed in test results obtained by other authors when testing the bond capacity of smooth bars in concrete (Feldam 2005 [17], Mylrea 1948 [18], Abrams 1913 [19], Pul 2010 [20], Khandaker 2008 [21]). The descending branch is considered to happen immediately after the maximum bond stress and it lasts until the residual friction stress is reached. The 3-branch curve is defined by Equations 4-12 to 4-14.

$$\tau(s) = \tau_{max}\,(s/s_1)^{\alpha} \qquad 0 \le s \le s_1 \tag{4-12}$$

$$\tau(s) = a + b\log s \qquad s_1 \le s \le s_2 \tag{4-13}$$

$$\tau(s) = \tau_f \qquad s \ge s_2 \tag{4-14}$$

Values for s_1 and s_2 are taken according to the test results and α is taken as it is given in the fib Model Codes as the test results follow the shape given by the ascending branch defined in fib Model Codes (α = 0,5). Thus, considering that τ_{max} occurs at an average slip of 0,1 mm (s_1) and that the τ_f is reached at an average slip of 10 mm (s_2), this yields to:

$$a = (\tau_f + \tau_{max})/2 \tag{4-15}$$

$$b = (\tau_f - \tau_{max})/2 \tag{4-16}$$

For the definition of τ_{max} and τ_f two different approaches have been considered: (1) the one based on regression analysis and considering conditioning parameters according to test results; and (2) the one based on the same definition given as in the fib Model Codes, where the maximum bond stress and the frictional one are calculated as average values of several experiments and are expressed dependant only on the characteristic compression strength of the concrete.

5.1.3.1 Calculation of τ_{max} and τ_f by regression analysis of the test results

As discussed previously during the analysis of the test results for flat smooth reinforcement elements, it has been concluded that the most affecting parameters in the development of the bond capacity of the rebar are the material type, the geometry (the aspect ratio) and the concrete type.

Keeping these conclusions in mind, a regression analysis of the experimental data has been conducted in order to obtain equations that are able to predict the maximum bond stress and the residual friction stress for each bar type in a more accurate way. The concrete type influence has been considered to be only related to the higher compression strength of the SCC specimens. This influence on the maximum and residual bond stresses has been defined as directly proportional to the square root of the characteristic compression strength of the concrete as it is done by the fib Model Codes. On the other hand, two more variables have been defined for considering influence of material type and the aspect ratio of the flat geometry. Thus, k_{m} is an indicator of material type, and equals to 0 for the ferritic SS type used in this work (K31 or 1.4017 according to the European standard for SS designation EN 10088 [2]), equals to 1 for the austenitic SS used for the research (304L or 1.4307 according to EN 10088 [2]) and equals to 2 for the standard carbon steel. The aspect ratio is considered directly, not as an indicator, and it is referred as $A_r = w/h$, where w and h stand for the 2 sides of the cross section of the rebar taken as the perpendicular section to the longitudinal axis of the reinforcement, and being $w \geq h$. Figure 4-20 helps for a better understanding of the definition of w and h.

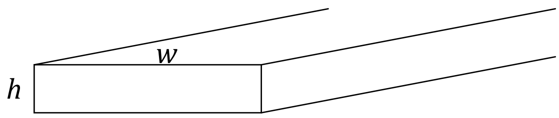

Figure 4-20 Cross section of a flat smooth sample. Definition of w and h

The equations obtained by regression analysis of the experimental data are:

$$\tau_{max} = (1{,}42 - 0{,}30A_r + 0{,}41k_m)\sqrt{f_{ck}} \tag{4-17}$$

$$\tau_f = (1{,}68 - 0{,}14A_r + 0{,}15k_m)\sqrt{f_{ck}} \tag{4-18}$$

For comparing the applicability of the obtained equations to the tests performed by Feldman et al., A_r is taken equal to 1 (square rebars) and k_m equals 2 (carbon steel). In this way, proposed equations yield to $\tau_{max}/\sqrt{f_{ck}}$ = 1,94 and $\tau_f/\sqrt{f_{ck}}$ = 1,84. The experimental results derived from Feldman´s research show an average value of $\tau_{max}/\sqrt{f_c}$ = 0,35 and $\tau_f/\sqrt{f_c}$ = 0,07 for square rebars. Although Feldaman´s values are given dependant on the mean compressive strength (by definition higher than the characteristic compressive strength), the values of τ_{max} and τ_f obtained by Feldman are overestimated by the Equations 4-17 and 4-18.

In Figure 4-21 to 4-24 individual test results that are representative for the observed bond behaviour are plotted together with their corresponding predicted curve. The maximum and the frictional bond stress are calculated for each testing condition based on Equations 4-17 and 4-18 obtained by regression analysis. "EXP" is used to identify the experimental curve, and "REGR" for the curve corresponding to the proposed model. Appendix B of this work compiles all the individual test results together with the proposed model curves. A good agreement between the two curves is observed for each testing condition. Figure 4-25 gives the correlation between the experimental and predicted maximum bond stress to square root of characteristic compression strength ratio, $\tau_{max}/\sqrt{f_{ck}}$, for each performed test (for flat smooth samples). The correlation is given for individual test results, as well as for average values out of 3 specimens tested for each testing condition. In the same way, Figure 4-26 represents the correlation for the residual bond stress to square root of characteristic compression strength ratio, $\tau_f/\sqrt{f_{ck}}$. A good agreement between the experimental values and the values calculated by regression analysis is observed with an average ratio of 1,05 for maximum bond stress values and 1,15 for the frictional bond stress values.

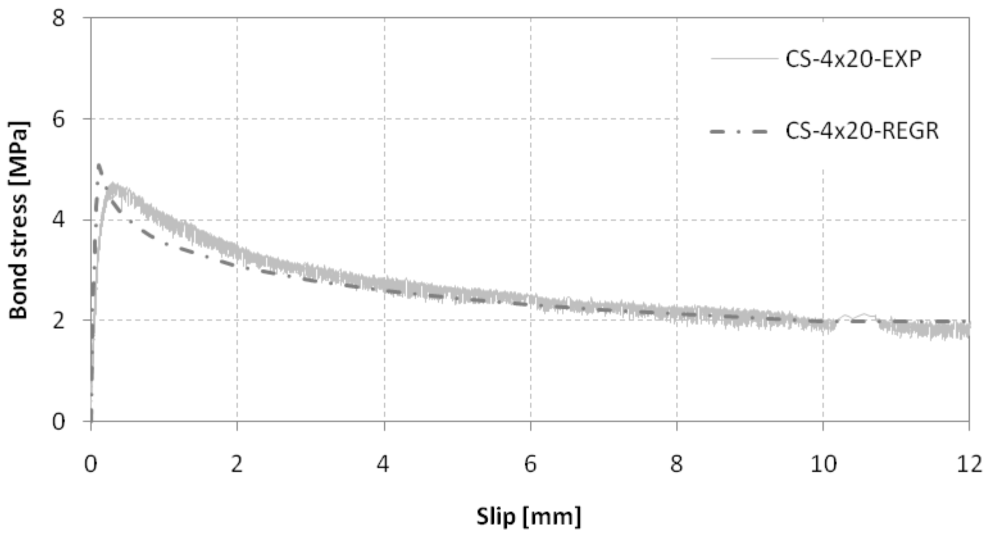

Figure 4-21 Bond stress-slip behaviour for smooth CS-4x20 sample. Experimental results vs. proposed model using regression analysis for defining τ_{max} and τ_f

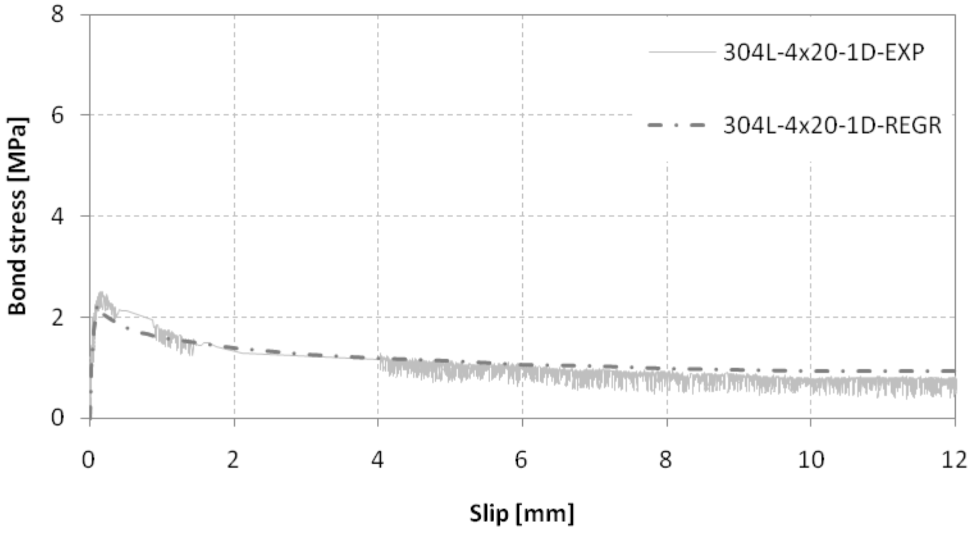

Figure 4-22 Bond stress-slip behaviour for smooth 304L-4x20-1D sample. Experimental results vs. proposed model using regression analysis for defining τ_{max} and τ_f

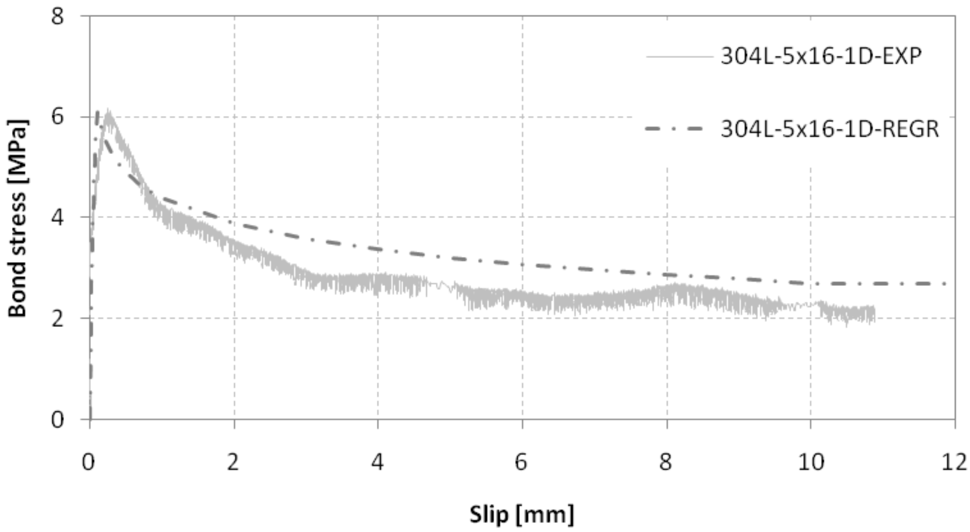

Figure 4-23 Bond stress-slip behaviour for smooth 304L-5x16-1D sample. Experimental results vs. proposed model using regression analysis for defining τ_{max} and τ_f

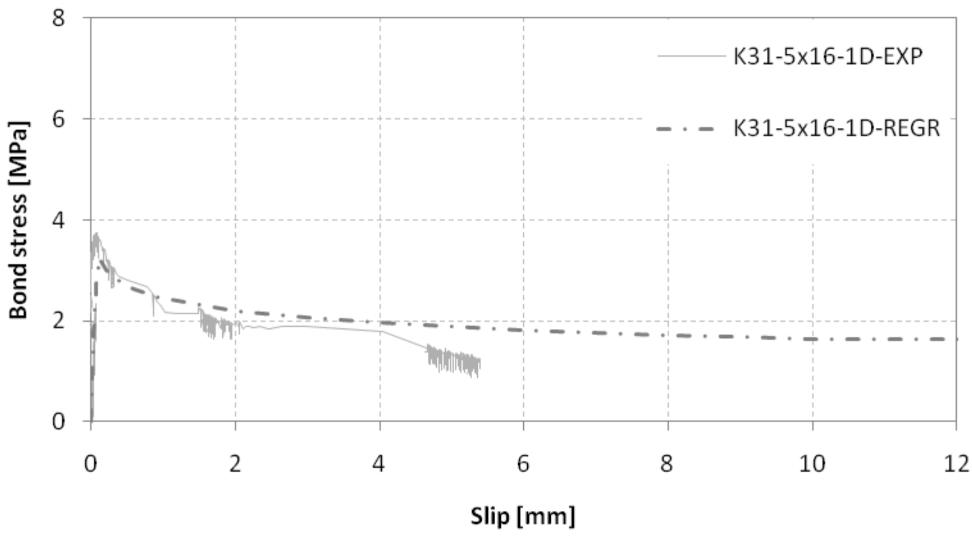

Figure 4-24 Bond stress-slip behaviour for smooth K31-5x16-1D sample. Experimental results vs. proposed model using regression analysis for defining τ_{max} and τ_f

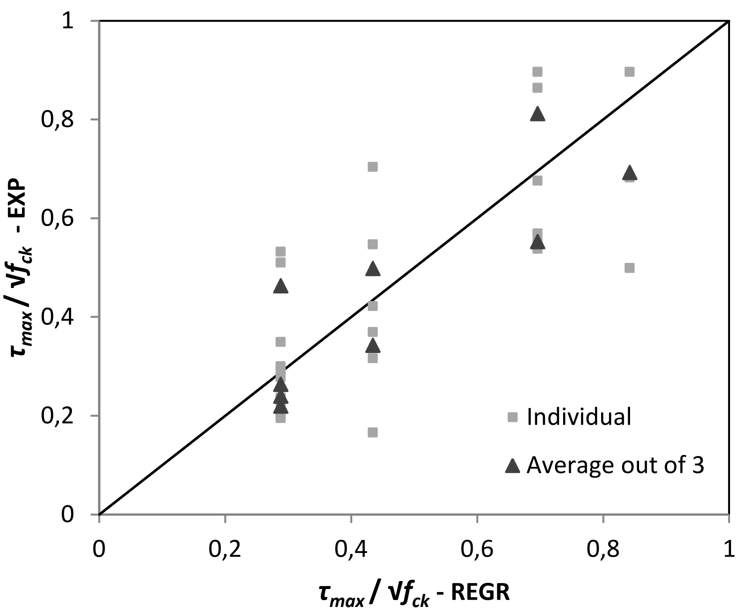

Figure 4-25 Correlation between experimental and proposed model using regression analysis for defining τ_{max} and τ_f, for $\tau_{max}/\sqrt{f_{ck}}$

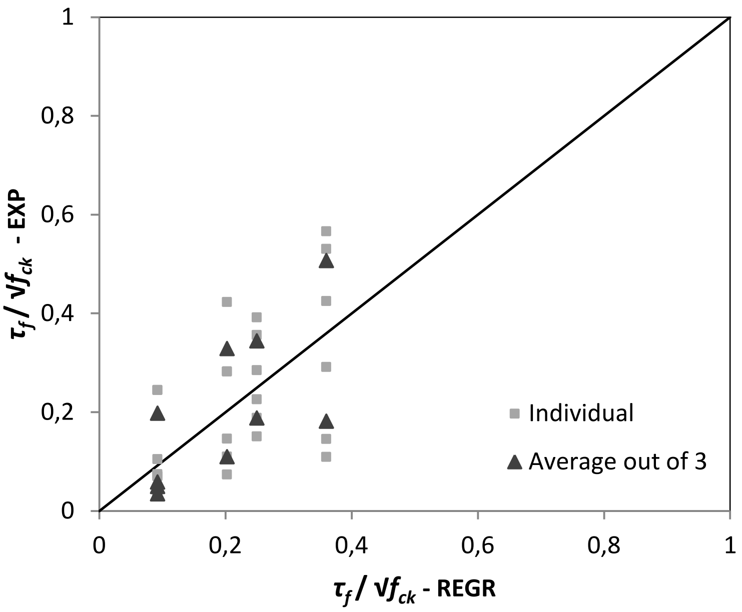

Figure 4-26 Correlation between experimental and proposed model using regression analysis for defining τ_{max} and τ_f , for $\tau_f/\sqrt{f_{ck}}$

5.1.3.2 Calculation of τ_{max} and τ_f by average values of the test results

The second considered approach for estimating the definition of the maximum and the friction bond stress for flat smooth samples tested in this work, is defining both values only dependant on the compression strength of the concrete. For that, a similar approach as the one used in the fib Model Codes has been used: all the tested samples are considered together and an average calculation of the $\tau_{max}/\sqrt{f_{ck}}$ ratio is performed. The same procedure is used for the estimation of the $\tau_f/\sqrt{f_{ck}}$ ratio. Equation 4-19 and 4-20 give the mean values obtained for the tested specimens. Note that for a given concrete characteristic compressive strength, the proposed model gives a value of maximum bond stress 70% higher than the value given by MC90/MC2010, and 33% lower for the residual friction stress.

$$\tau_{max,av} = 0{,}5103\ \sqrt{f_{ck}} \tag{4-19}$$

$$\tau_{f,av} = 0{,}1998\ \sqrt{f_{ck}} = 0{,}3915\ \tau_{max} \tag{4-20}$$

If we now plot the mean bond stress-slip curve obtained by combining Equations 4-12 to 4-16 together with Equations 4-19 and 4-20, for a mean characteristic compressive strength of concrete of 50 N/mm^2, with individual curves that are representative of the observed experimental results, see Figure 4-27, it can be concluded that the mean bond stress-slip curve's shape agrees with the behaviour observed experimentally. However, the dispersed values obtained for the different testing parameters are not well predicted by the mean curve. In Appendix B a compilation of all the test results with their corresponding modelled curve are given. Note that although for plotting of Figure 4-27 an average value of the characteristic compressive strength has been considered, in Appendix B the proposed model curves are plotted according to the f_{ck} value of each concrete batch.

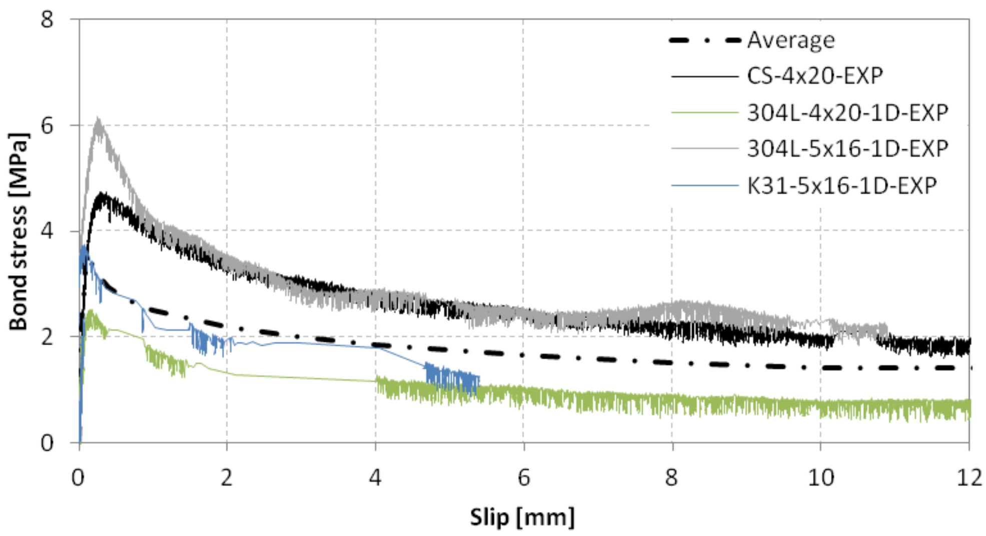

Figure 4-27 Bond stress-slip behaviour for flat smooth samples. Experimental results vs. proposed model using average values for defining τ_{max} and τ_f

If a comparison is made between the approach consisting of the regression analysis and the approach based on the average values of the test results for the calculation of the maximum bond stress and the frictional remaining bond stress, it is observed that the regression analysis approach allows for a more accurate prediction of the bond stress-slip relationship of the tested flat smooth rebars as more parameters are involved. However, the available data set is too limited and consequently the proposed model is specific for the tested rebars´ parameters. On the other hand, the approach based on the average values, allows for a more generalized prediction of the bond stress-slip behaviour of flat smooth rebars and follows the criteria given by MC90/MC2010. Moreover, as plotted in Figure 4-28, the average values approach is applicable for predicting the bond stress-slip behaviour of round smooth samples. Consequently, the approach based on the calculation of τ_{max} and τ_f by average values of the test results is further considered for modelling the bond stress-slip relationship of flat smooth rebars tested in this work.

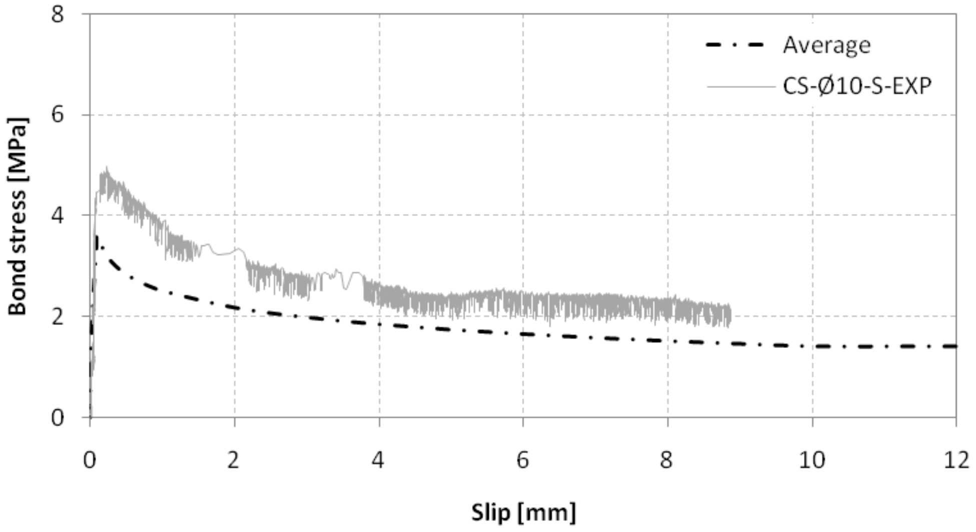

Figure 4-28 Bond stress-slip relationship. Proposed model vs. experimental results for round smooth rebar

5.1.3.3 Characteristic values of τ_{max} and τ_f

Further development of the proposed model is conducted for a more conservative approach consisting on the calculation of estimated characteristic values given the mean values and the variability of the test results. Assuming normal distribution of the bond strength and the residual bond stress values and a fractile of 0,05, the so-called "Bayesian prediction method with vague prior distributions" is used for calculation of the characteristic values [22][23][24]. This method allows for estimating the α-fractile value of a given parameter, with the probability of the estimated fractile being lower than the exact fractile of ~75% [22]. A major advantage of this method is that no arbitrary assumptions are needed. Instead all relevant information obtained by test results is used in order to update the vague prior information and based on this updated distribution, the characteristic value is determined [22]. Equations 4-21 and 4-22 allow for calculation of the estimated characteristic values, where $\hat{\tau}_{0,05}$ stands for the estimated characteristic value for a fractile of 5% (the probability of τ being less than $\hat{\tau}_{0,05}$ is 5%); $\bar{\tau}$ is the mean bond stress; d_τ is a ratio between the standard deviation (s_τ) and the mean value of the bond stress; λ is a statistical coefficient. Tabulated values of λ are given in [23] depending on the number of samples n and for a known or unknown exact coefficient of variation of the test results; a value of 1,73 is taken for this analysis (corresponding to n=30 and an unknown coefficient of variation).

The calculated characteristic maximum bond stress is limited to $\hat{\tau}_{max,0,05} = 0{,}035\sqrt{f_{ck}}$ (which means, for an average characteristic compression strength of the concrete of 50 N/mm², a maximum bond stress of ~0,25 N/mm²) and the residual bond stress drops to 0, independently of the compressive strength of the concrete. See Equation 4-23 and 4-24. Figure 4-29 compares: 1) the proposed model with average values of all tested data for determining τ_{max} and τ_f, 2) the proposed model with characteristic values calculated based on the average values of τ_{max} and τ_f, using the so-called "Bayesian prediction method with vague prior distribution".

$$\hat{\tau}_{0,05} = \bar{\tau}\,(1 - \lambda\, d_\tau) \tag{4-21}$$

$$d_\tau = s_\tau / \bar{\tau} \tag{4-22}$$

$$\hat{\tau}_{max,0,05} = 0{,}035\,\sqrt{f_{ck}} \tag{4-23}$$

$$\hat{\tau}_{f,0,05} = 0 \tag{4-24}$$

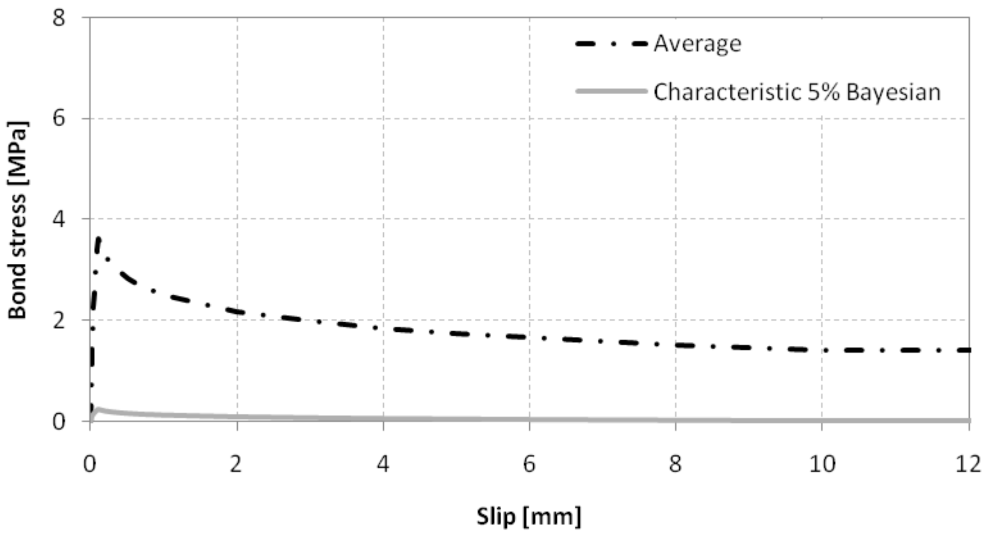

Figure 4-29 Bond stress-slip behaviour for flat smooth samples. Proposed model using average values for defining τ_{max} and τ_f vs. corresponding characteristic graph

Note that because of the high variability of the test results obtained for flat smooth samples tested in this work, dependant mostly on the material type, aspect ratio of the cross section and the concrete compression strength, the calculation of the characteristic values lead to a very conservative result.

5.2 Ribbed samples

In Chapter 3 several available bond models regarding round ribbed bars have been presented. However, according to the literature available to the author no research has been conducted on developing a bond model for flat ribbed reinforcing elements.

For the tested flat ribbed samples the observed variation of test results (related to material differences, CS vs. SS and TC vs. SCC) is relatively small and considered non significant following the performed t-test. This simplifies the use of the dataset and reduces the dependency on different parameters. The applicability of different bond models is presented in the following for the flat ribbed rebars studied in this work. Furthermore, adaptations to the bond model given by the Model Codes are proposed following the comparison made with the test results.

5.2.1 Model Code 1990: MC90

The MC90 model [14], based on Eligehausen et al. [16], describes the bond behaviour of ribbed round bars as a four-stage behaviour, where a first ascending branch is suggested until the maximum bond stress is reached at a certain slip of the bar. The second stage corresponds to a plateau at the maximum bond stress which finishes at slip s_2, and then the bond stress decreases linearly at increasing slips until the residual friction stress is reached. After the 3rd descending branch, the bond stress remains constant due to the friction between the steel bar and the concrete. The model is defined by Equations 4-25 to 4-28 with the values of the different parameters given in Table 4-11. The parameters are valid for ribbed reinforcing steel with a minimum relative rib area (not defined, but referred to relevant international standards), and are defined depending on the confinement, bond condition and concrete compression strength. Furthermore, the MC90 describes the unconfined concrete condition as the condition causing splitting type of concrete failure and the confined condition as causing shearing of the concrete between the ribs. The document comments on the bond stress-slip relationship as a behaviour dependant on many factors like: bar roughness, concrete strength, position and orientation of the bar during casting, state of stress, boundary conditions and concrete cover. However, the maximum bond stress and the frictional bond stress, are given only dependant on the characteristic compression strength of the concrete, and therefore, the MC90 remarks, that the bond stress-slip curve should be considered as a statistical mean curve, applicable as an average formulation for a broad range of cases. Figure 4-30 represents the bond stress-slip relationship defined by the MC90 for unconfined and confined concrete cases and for good bond conditions. Note that in case of splitting type of failure, the plateau at maximum bond stress disappears and the bond stress decreases immediately after reaching the maximum bond stress (dashed line in Figure 4-30, and defining parameters indicated as τ'_{max}, τ'_f, s'_1, s'_2 and s'_3).

$$\tau(s) = \tau_{max}\,(s/s_1)^{\alpha} \qquad 0 \leq s \leq s_1 \qquad (4\text{-}25)$$

$$\tau(s) = \tau_{max} \qquad s_1 \leq s \leq s_2 \qquad (4\text{-}26)$$

$$\tau(s) = \tau_{max} - (\tau_{max} - \tau_f)((s-s_2)/(s_3-s_2)) \qquad s_2 \leq s \leq s_3 \qquad (4\text{-}27)$$

$$\tau(s) = \tau_f \qquad s \geq s_3 \qquad (4\text{-}28)$$

Table 4-11 Parameters for defining the mean bond stress-slip relationship for round ribbed bars according to MC90

Parameters	***Unconfined concrete***		***Confined concrete***	
	Good bond conditions	*All other bond conditions*	*Good bond conditions*	*All other bond conditions*
s_1 *(mm)*	0,6	0,6	1,0	1,0
s_2 *(mm)*	0,6	0,6	3,0	3,0
s_3 *(mm)*	1,0	2,5	Clear rib spacing	Clear rib spacing
α	0,4	0,4	0,4	0,4
τ_{max} *(N/mm²)*	2,0 $\sqrt{f_{ck}}$	1,0 $\sqrt{f_{ck}}$	2,5 $\sqrt{f_{ck}}$	1,25 $\sqrt{f_{ck}}$
τ_f *(N/mm²)*	0,15 τ_{max}	0,15 τ_{max}	0,40 τ_{max}	0,40 τ_{max}

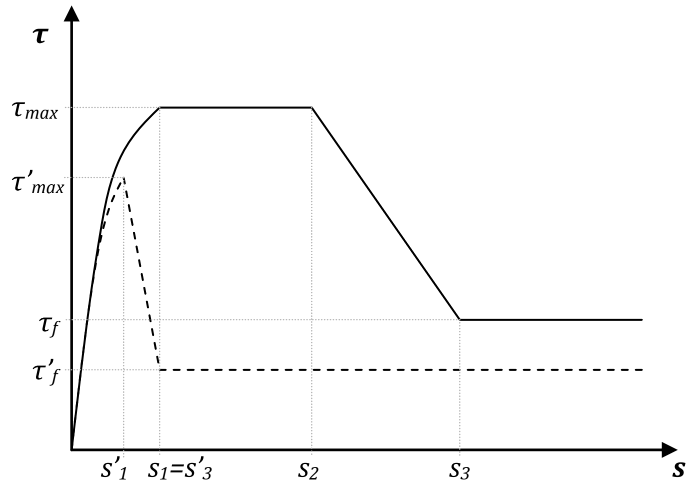

Figure 4-30 Bond stress-slip relationship for round ribbed bars according to MC90

The bond model proposed by MC90 has been plotted in Figure 4-31 and Figure 4-32 together with test results obtained for flat ribbed samples tested in this work. A characteristic compression strength of concrete of 50 N/mm² has been taken as average value of the tested specimens for plotting of the model curve, and parameters corresponding to confined concrete with good bond conditions in Table 4-11 have been considered. The clear rib spacing for the flat ribbed samples tested in this work equals, according to the performed measurements, to 18 mm.

An acceptably good agreement between the experimental results and the model for low slips (slips up to 3 mm), see Figure 4-32, is obtained. The model describes a stiffer beginning of the bond action, than the one observed for experimental results. However, at increasing slips, the stiffness decreases and gets closer to the ascending branch observed for the tested samples. The plateau at maximum bond stress is modelled in an accurate way. The residual bond stress related to frictional forces observed during testing are overestimated if this model is used for prediction, i.e. lower frictional forces are obtained for flat ribbed reinforcements than the value given by the model for a given characteristic compression strength of the concrete. Although the value of s_3, fixed at clear rib spacing of the reinforcement, agrees with the slip value at which frictional forces are reached experimentally, the difference in residual bond stress values makes the descending branch of the model to be softer than the one observed experimentally, see Figure 4-31.

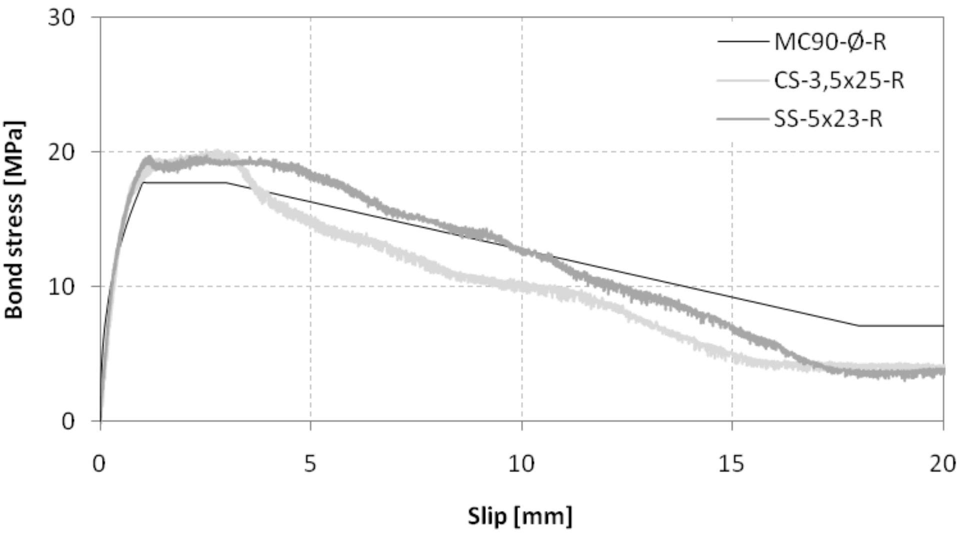

Figure 4-31 Bond stress-slip behaviour for flat ribbed samples. Model given by MC90 vs. test results, for slip values until 20 mm

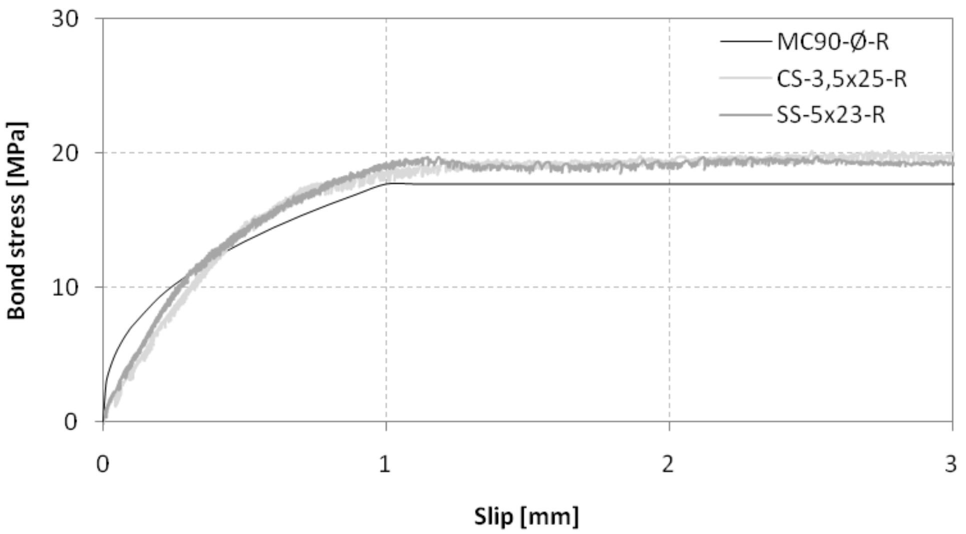

Figure 4-32 Bond stress-slip behaviour for flat ribbed samples. Model given by MC90 vs. test results, for slip values until 3 mm

5.2.2 Model Code 2010: MC2010

Similar to MC90, the draft version of the new fib Model Code 2010 [15], MC2010, describes the bond stress-slip relationship as a 4 branches curve given by Equations 4-25 to 4-28 and represented in Figure 4-30. It is again an implemented version of equations given by Eligehausen et al. [16]. Also, MC2010 states that the curve given in the model should be considered as a statistical mean curve, applicable as an average formulation for a broad range of cases. However, the values of the different parameters to be considered for applying the model differ from the ones given by the previous version of the model code, MC90. The parameters, see Table 4-12, are classified depending on the failure type, pull out or splitting, and depending on good or "other" bond conditions. Furthermore, for splitting type of failure, the model distinguishes between the use of stirrups or not, for giving (or not) more confinement to the specimen. As in the previous version of the Model Code, the maximum bond stress and the frictional bond stress, for each failure type and bond condition, are given only dependant on the characteristic compression strength of the concrete: for pull out type of failure, this dependency is related to the square root of the characteristic compressive strength, while for the splitting type of failure the dependency is related to the fourth root of f_{ck}. For splitting type of failure, an immediately descending branch is predicted after the maximum bond stress is reached (s_1 = s_2). According to MC2010, the remaining frictional bond stress equals 0,4 times the maximum bond stress, independently of the failure type (pull out or splitting (with stirrups)), unless for splitting unconfined. In the latter case, the residual frictional bond stress drops to 0.

Table 4-12 Parameters for defining the mean bond stress-slip relationship for round ribbed bars according to MC2010

Parameters	***Pull-out***		***Splitting***			
	Good bond conditions	*All other bond conditions*	*Good bond conditions*		*All other bond conditions*	
			Unconfined	*Stirrups*	*Unconfined*	*Stirrups*
s_1 *(mm)*	1,0	1,8	$s(\tau_{max})$	$s(\tau_{max})$	$s(\tau_{max})$	$s(\tau_{max})$
s_2 *(mm)*	2,0	3,6	s_1	s_1	s_1	s_1
s_3 *(mm)*	Clear rib spacing	Clear rib spacing	1,2 s_1	0,5 Clear rib spacing	1,2 s_1	0,5 Clear rib spacing
α	0,4	0,4	0,4	0,4	0,4	0,4
τ_{max} (N/mm^2)	2,5 $\sqrt{f_{ck}}$	1,25 $\sqrt{f_{ck}}$	7,0 $\sqrt[4]{(f_{ck}/20)}$	8,0 $\sqrt[4]{(f_{ck}/20)}$	5,0 $\sqrt[4]{(f_{ck}/20)}$	5,5 $\sqrt[4]{(f_{ck}/20)}$
τ_f (N/mm^2)	0,40 τ_{max}	0,40 τ_{max}	0	0,40 τ_{max}	0	0,40 τ_{max}

For comparing the relationship given by the MC2010 to the experimental results obtained in this work for flat ribbed samples, the first column of Table 4-12 is considered: pull-out type of failure and good bond conditions. Furthermore, a characteristic compression strength of concrete of 50 N/mm^2 is taken as it corresponds to the mean value obtained for the tested specimens, and a clear rib spacing of 18 mm is considered. Note that the only difference with the parameters given by the MC90 for the same testing conditions is that the MC2010 considers a lower value for s_2 (3 mm by MC90 vs. 2 mm by MC2010), which means that the plateau related to the maximum bond stress is 50% shorter according to the MC2010, and that the decrease of bond stress starts, therefore, at lower slip values.

Thus, the first ascending branch described by the MC2010 acceptably agrees with the behaviour observed for the flat ribbed bars tested, as commented for MC90. However, it can be clearly seen in Figure 4-33 and Figure 4-34 that at the moment that according to the model the bond stress starts to decrease at increasing slips (at 2 mm of slip), the experimentally tested samples still continue to sustain the maximum bond stress. At higher slip values, the observed behaviour is the same as the one described in the comparison made with MC90, see Figure 4-33.

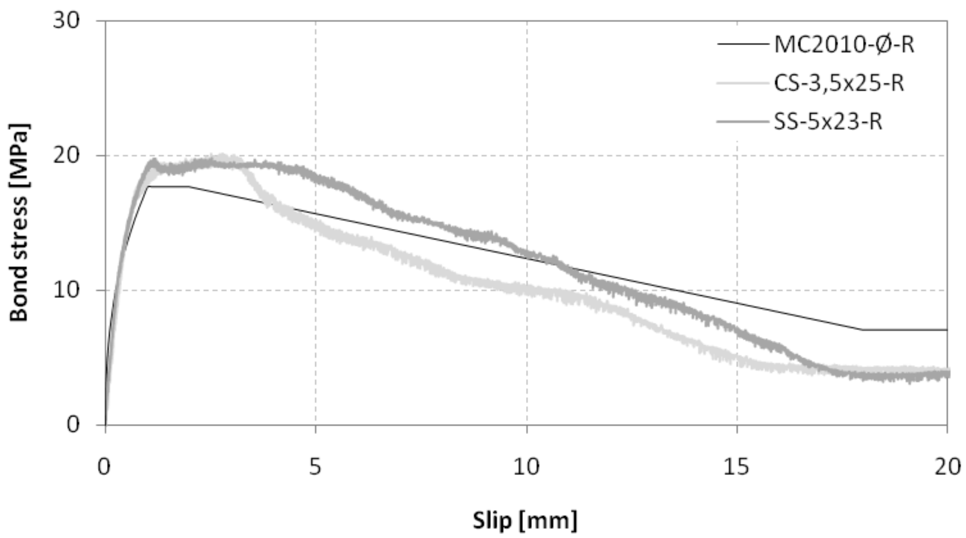

Figure 4-33 Bond stress-slip behaviour for flat ribbed samples. Model given by MC2010 vs. test results, for slip values until 20 mm

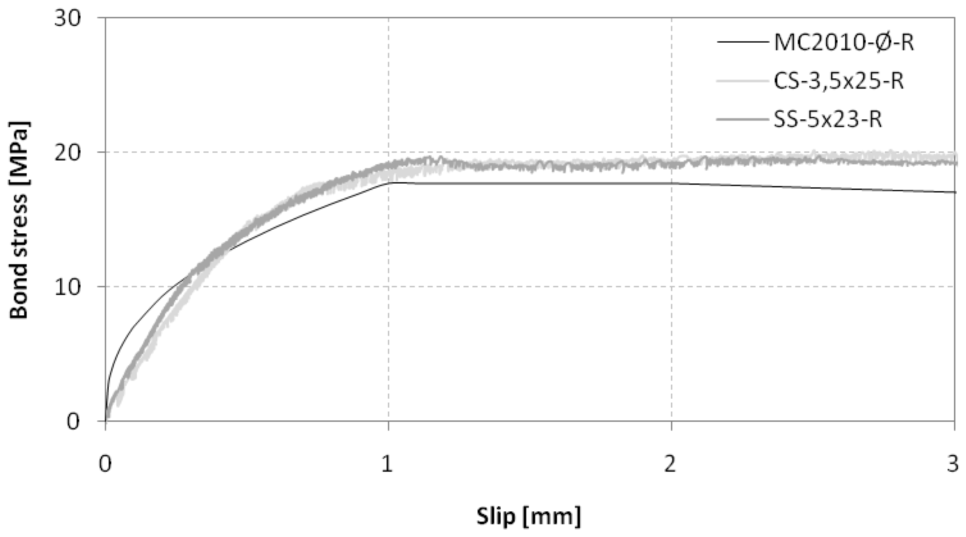

Figure 4-34 Bond stress-slip behaviour for flat ribbed samples. Model given by MC2010 vs. test results, for slip values until 3 mm

5.2.3 Soroushian et al.

This model [25] modifies the first ascending branch defined by Eligehausen et al. [16] and keeps the definition for the rest of the curve branches (Equations 4-26 to 4-28). The new definition of the ascending branch is given by Equation 4-29. As it has been discussed in Chapter 3, the definition of the first ascending branch given by Soroushian describes a less stiff initial behaviour of the ascending branch in comparison to the curve given by the Model Codes. Consequently and given the less stiff behaviour observed for the experimental results in comparison to the curves given by the Model Codes for low slip values (lower than 0,3 mm, see Figure 4-32 and Figure 4-34), the definition given by Sorohusian for the ascending branch has been adopted (with τ_{max} and s_1 as given by the Model Codes) compared to the test results.

$$\tau(s) = \tau_{max}\,(s/s_1)\;e^{(1-(s/s_1)^{\alpha})/\alpha} \qquad 0 \le s \le s_1 \qquad (4\text{-}29)$$

The curve obtained by applying the definition given by Soroushian's model for the ascending branch is plotted in Figure 4-35 together with the test results and the curve according to MC90. Although the stiffness of the ascending branch is still higher than the one observed experimentally, for low slip values (slips up to 0,3 mm) a less stiff behaviour is noticed compared to the one given by the Model Codes.

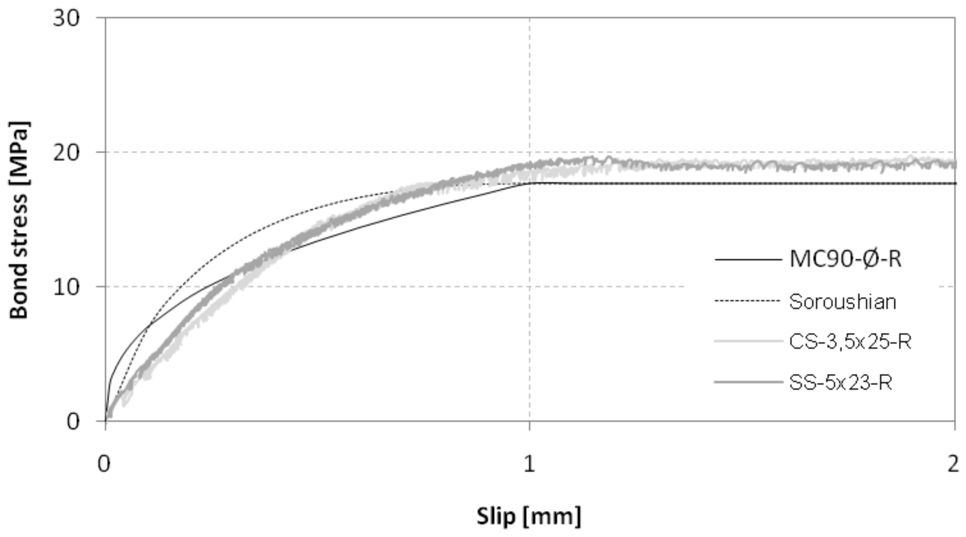

Figure 4-35 Bond stress-slip behaviour for flat ribbed samples. Model given by MC90 vs. Soroushian vs. test results, for slip values until 2 mm

5.2.4 Harajli et al.

Most of the analyzed bond models, give the curve defining slip values as fixed values based on experimental results, except for the value of s_3 which is taken equal to the clear rib spacing of the reinforcement. However, the model given by Harajli et al. (and Desnerck, see next section) defines also other slip values dependant on the clear rib spacing of the reinforcement.

The model proposed by Harajli et al. [26] is based again on the 4-branches definition given by Eligehausen et al. [16], Equations 4-25 to 4-28, but with modified defining parameters. The maximum bond stress and the frictional one are given dependant on the mean compressive strength of the concrete; and the slip values at which the bond behaviour changes (s_1, s_2 and s_3), are all considered to be dependent on the clear rib spacing of the bar. The parameters are given in Table 4-13. Note that the parameter α has been defined equal to 0,3, which allows for a stiffer initial bond behaviour approach.

Dashed lines in Figure 4-36 and Figure 4-37 represent the model given by Harajli et al. taken with the parameters regarding the tested specimens: clear rib spacing of 18 mm and mean compressive strength of 58 N/mm2. The initial stiffness of the bond behaviour is higher than the one observed during experiments. However, at increasing slip, and due to the definition given by the model for s_1 (0,15 times the clear rib spacing, which equals in this case 2,7 mm), the stiffness of the ascending branch later decreases and becomes lower than experimentally observed. According to the model, the plateau at maximum bond stress starts at higher slip values than occurred in the experiments. The frictional bond stresses are reached at a slip equal to 18 mm, which is the clear rib spacing. This value agrees with the experimental results as stated before; however, the value given by the model for the frictional bond stress overestimates the behaviour observed for flat ribbed samples.

Table 4-13 Parameters defining the bond stress –slip curve by Harajli et. al

Parameters	***Harajli et al.***
s_1 *(mm)*	0,15 x clear rib spacing
s_2 *(mm)*	0,35 x clear rib spacing
s_3 *(mm)*	Clear rib spacing
α	0,3
τ_{max} *(N/mm²)*	2,57 $\sqrt{f_{cm}}$
τ_f *(N/mm²)*	0,90 $\sqrt{f_{cm}}$

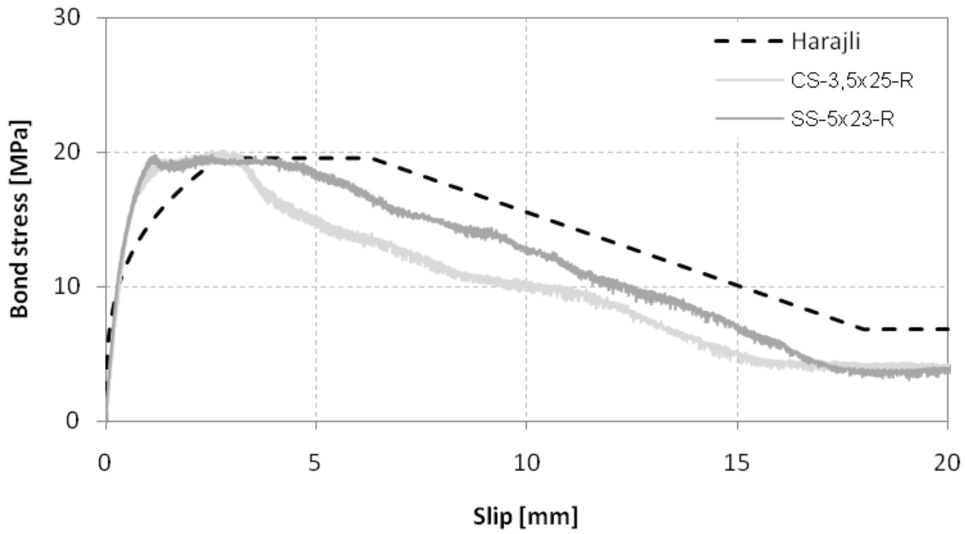

Figure 4-36 Bond stress-slip behaviour for flat ribbed samples. Model given by Harajli vs. test results, for slip values until 20 mm

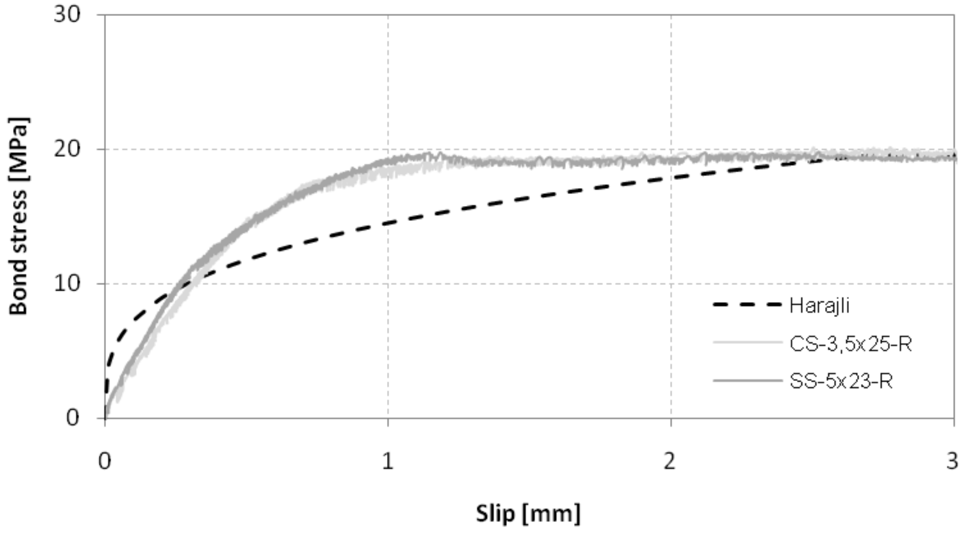

Figure 4-37 Bond stress-slip behaviour for flat ribbed samples. Model given Harajli vs. test results, for slip values until 3 mm

5.2.5 Desnerck

Desnerck [27] defines the bond stress-slip relationship based on the Eligehausen [16] model for the first ascending branch as done by the Model Codes. However, Desnerck provides a new approach for the definition of the slip corresponding to the maximum bond stress (s_1), which is defined related to the clear rib spacing c of the reinforcement, see Equation 4-30. For the flat ribbed reinforcements tested in this work, the clear rib spacing equals 18 mm, which corresponds, according to Desnerck, to a slip at maximum bond strength of 1,08 mm; this value agrees with the trend observed for the experimental results.

$$s_1 = 0{,}0032\ c^2 + 0{,}041 \qquad (4\text{-}30)$$

5.2.6 Proposed bond model for flat ribbed reinforcing elements

Based on the performed analysis on the applicability of existing bond models for predicting the bond behaviour of flat ribbed rebars tested in this work, several steps have been considered for the definition of an adapted model. Based on the often used fib Model Code, some modifications are proposed for the definition of the involved parameters and curve shape to better adapt the bond stress-slip relationship to the flat ribbed reinforcements analyzed. The shape of the first ascending branch is adapted by the definition given by Soroushian et al. as it better characterizes the bond stress-slip behaviour observed for flat ribbed rebars until the maximum bond stress is reached. Furthermore, the proposed equation for s_1 definition given by Desnerck is implemented for a more accurate approach: it allows for characterizing the slip at maximum bond stress dependant on the clear rib spacing of a given rebar, while the fib Model Codes give a fixed value (1 mm for pull out failure and good bond conditions) independently of the rebar considered. Note that individual test results graphs are given in this section which are representative for the observed behaviour. All test results are compiled in Appendix B, where a comparison to the proposed model is also provided. In this section an average characteristic compressive strength of 50 N/mm^2 is considered for plotting the proposed model curves because different test results are plotted together; however, individual f_{ck} values of each concrete batch are applied in Appendix B.

5.2.6.1 Based on the fib Model Codes

Following the same approach as in MC90 and MC2010, for flat ribbed reinforcement the main parameters are defined dependant on the characteristic compression strength of the concrete and are calculated as mean values of the experimental results. Thus, based on the mean test results, the maximum average bond stress developed by the flat ribbed rebars can be redefined as $2{,}54\sqrt{f_{ck}}$ and the average frictional bond stress as $0{,}17\tau_{max}$. Comparing these values with the ones given by the Model Codes for pull out failure and good bond conditions ($2{,}5\sqrt{f_{ck}}$ and $0{,}4\tau_{max}$, respectively), it is observed that the maximum bond stress value observed for the flat ribbed rebars is slightly (2%) underestimated by the Codes and the frictional bond stress is significantly (135%) overestimated. The MC90 and MC2010, for pull out type of failure and good bond conditions, give the same definition of the bond model, except for the value of s_2, which is reduced from 3 to 2 mm in the newer version of the model. However, as analyzed in the previous section, the value given by MC90 is more appropriate for simulating the trend observed for flat ribbed rebars.

In summary, an adapted version of the MC90/MC2010 bond model based on Equations 4-25 to 4-28 and with the parameters given in Table 4-14 is presented as a first step on the definition of the bond stress-slip relationship model for defining the bond behaviour observed for flat ribbed samples (designated as *Adapted-flat-R-I* in Table 4-14, Figure 4-38 and Figure 4-39). The corresponding curve is plotted in Figure 4-38 and Figure 4-39 together with individual test results. It is observed from Figure 4-39 that the initial bond stiffness of the first ascending branch (for slip values up to 0,4 mm) is overestimated by the equation given by the Model Codes. However, after the maximum bond stress is reached, a good agreement between the curves is observed (Figure 4-38).

Table 4-14 Parameters defining the bond stress –slip curve of flat ribbed samples for the approach based on MC90

Parameter	***Adapted-flat-R-I***
s_1 *(mm)*	1
s_2 *(mm)*	3
s_3 *(mm)*	Clear rib spacing (~18 mm)
α	0,4
τ_{max} *(N/mm²)*	$2{,}54\,\sqrt{f_{ck}}$
τ_f *(N/mm²)*	$0{,}17\,\tau_{max}$

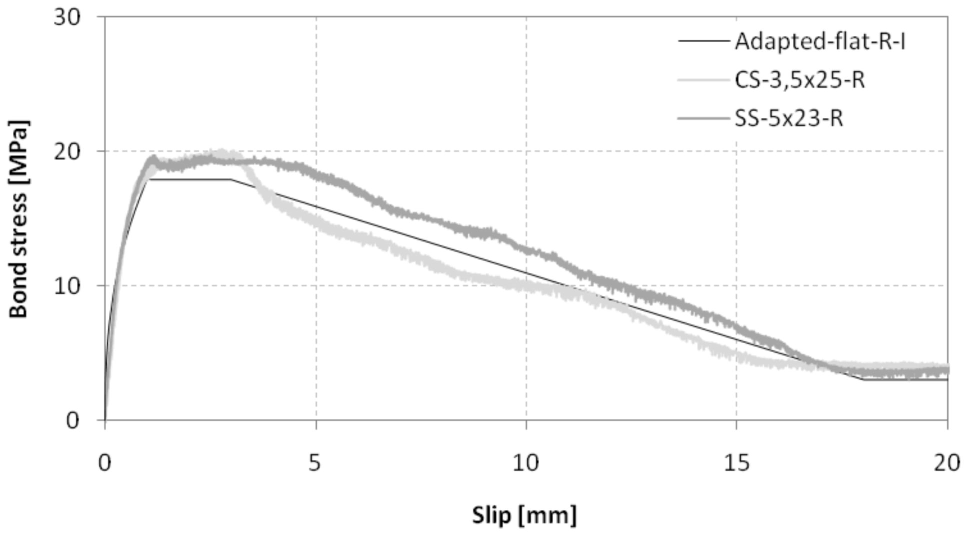

Figure 4-38 Bond stress-slip behaviour for flat ribbed samples. Adaptation based on MC90 with modified parameters, for slip values until 20 mm

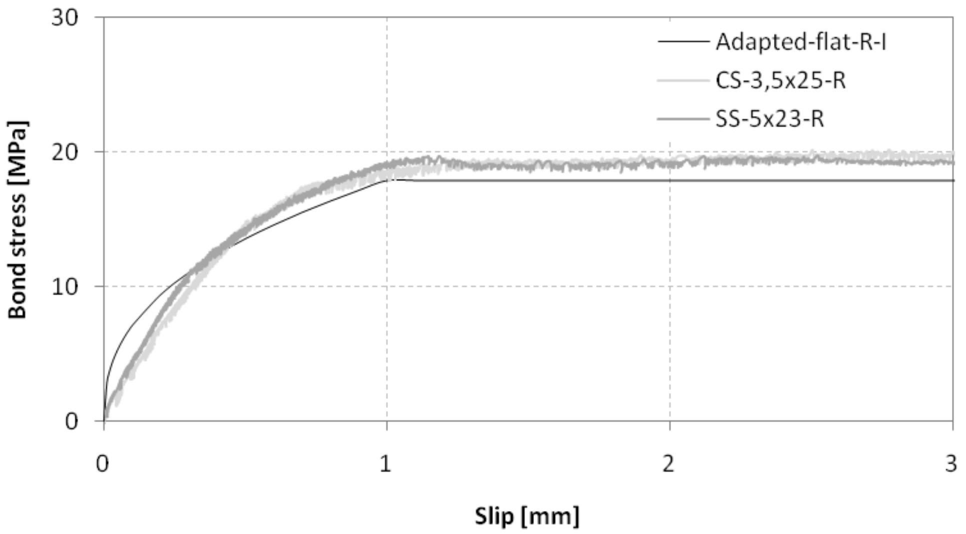

Figure 4-39 Bond stress-slip behaviour for flat ribbed samples. Adaptation based on MC90 with modified parameters, for slip values until 3 mm

5.2.6.2 Modified ascending branch definition by Soroushian et al.

Considering the MC90 based model (*Adapted-flat-R-I*) derived in Section 5.2.6.1, a further refinement is considered by replacing the first ascending branch by Equation 4-29 proposed by Soroushian et al. [25]. The value of the factor α has been modified (increased from 0,4 to 0,8) for a better curve fitting of the test results. The bond stress-slip curve resulting from this refinement (*Adapted-flat-R-II)* has been plotted in Figure 4-40 (only the curve for slip values until 3 mm is given as for higher slip values the model has not been modified). A good agreement is observed between the proposed improved bond model and the curves obtained by the experimental results.

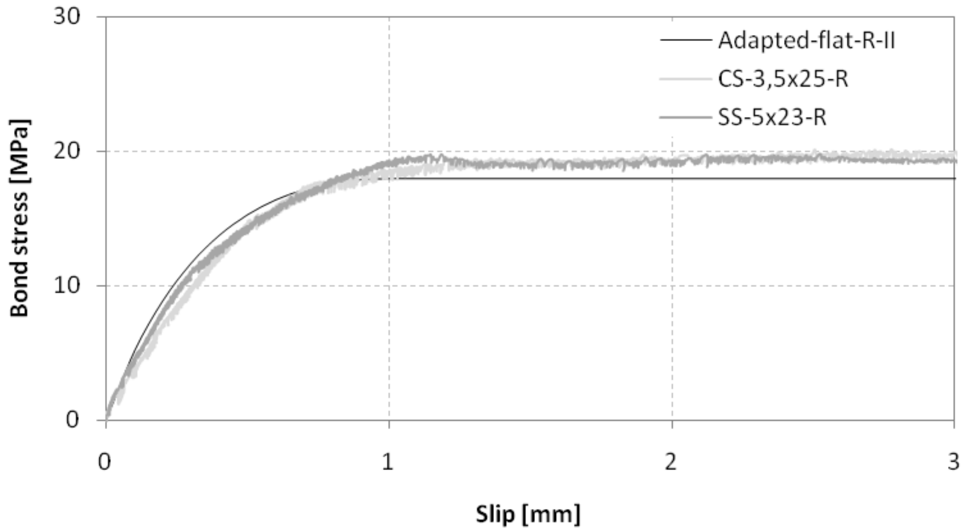

Figure 4-40 Bond stress-slip behaviour for flat ribbed samples. Adaptation implemented by the definition of first ascending branch given by Soroushian, for slip values until 3 mm

5.2.6.3 Modified s_1 definition by Desnerck

As described before, this approach [27] suggests a new way of predicting the slip corresponding to the maximum bond stress value, based on the clear rib spacing of the rebar. The previous *Adapted-flat-R-II* model has been improved by adding this new definition to the bond model as given in Table 4-15. For the set of reinforcements tested in this work, the clear rib spacing is 18 mm. This yields a value of s_1 equal to 1,08 mm, which is 8% higher than the original MC90 definition. Figure 4-41 gives the bond stress-slip relationship for slip values until 3 mm for the model implemented with the s_1 definition given by Desnerck (designated as *Adapted-flat-R-III*).

Table 4-15 Parameters defining the bond stress –slip curve for the approach implemented by the definition of s_1 given by Desnerck

Parameter	***Adapted-flat-R-III***
s_1 *(mm)*	0,0032 x (clear rib spacing)^2 + 0,041
s_2 *(mm)*	3
s_3 *(mm)*	Clear rib spacing (~18 mm)
α	0,8
τ_{max} *(N/mm²)*	2,54 $\sqrt{f_{ck}}$
τ_f *(N/mm²)*	0,17 τ_{max}

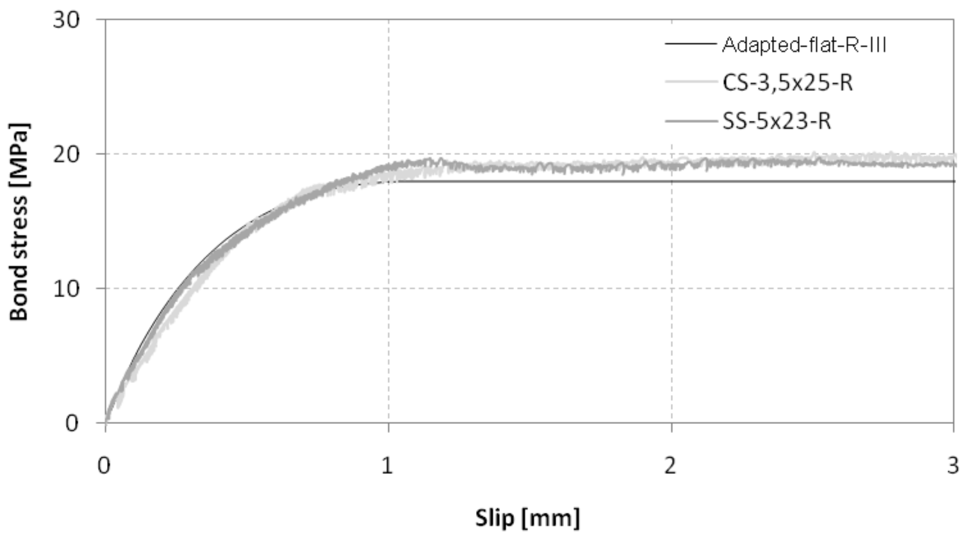

Figure 4-41 Bond stress-slip behaviour for flat ribbed samples. Adaptation implemented by the definition of s_1 given by Desnerck, for slip values until 3 mm

5.2.6.4 Applicability of proposed model for round rebars

For verifying the applicability of the proposed flat ribbed rebars model to standard round reinforcement, the test results of carbon steel round rebars of diameter 10 mm and 12 mm are compared to the proposed bond model. The bond stress-slip relationship given by MC90 is also plotted in Figure 4-42 and Figure 4-43, which give the comparison for slip values until 20 mm and until 3 mm, respectively. The clear rib spacing of the round reinforcements is around 7 mm (6,90 mm for Ø10 mm and 7,15 mm for Ø12 mm), which yields to an average s_1 value equal to 0,20 mm and a s_3 value equal to 7 mm. It is observed from the comparison, that the slip value at which the maximum bond stress is reached is significantly underestimated by the model (0,20 mm given by the model vs. ~1,20 mm observed experimentally for Ø10 mm and ~0,90 mm observed for Ø12 mm, which represent 83% and

78% lower slip values at maximum bond stress). The slip value at maximum bond stress given by MC90 (1 mm), represents better the experimentally observed behaviour for round ribbed rebars. The slip value at which only the friction bond stresses remain (s_3) is well predicted by both models.

Regarding maximum bond stress and frictional bond stress values, both are underestimated by the proposed model: the maximum average bond stress value is 25,31 N/mm^2 for Ø10 mm CS bars tested in TC and 21,14 N/mm^2 for Ø12 mm CS bars, while the model predicts a value of 17,94 N/mm^2. The MC90 underestimates in the same way the maximum bond stress observed experimentally. Furthermore, the frictional bond stress is set by the model at a value of 3,02 N/mm^2 and the experimental results show in average a value of around 5,61 N/mm^2 for Ø10 mm CS bars and 12,33 N/mm^2 for Ø12 mm (which means that the model underestimates the experimental behaviour in 46% and 75%, respectively). However, the frictional bond stress values given by MC90 are closer to the ones observed experimentally for round ribbed rebars: 7,07 N/mm^2 given by the MC90, which overestimates (26%) the average values obtained for diameter 10 mm bars, and underestimates (42%) the average values observed for diameter 12 mm round bars. Consequently, the application of the proposed bond model for round ribbed rebars is not recommended.

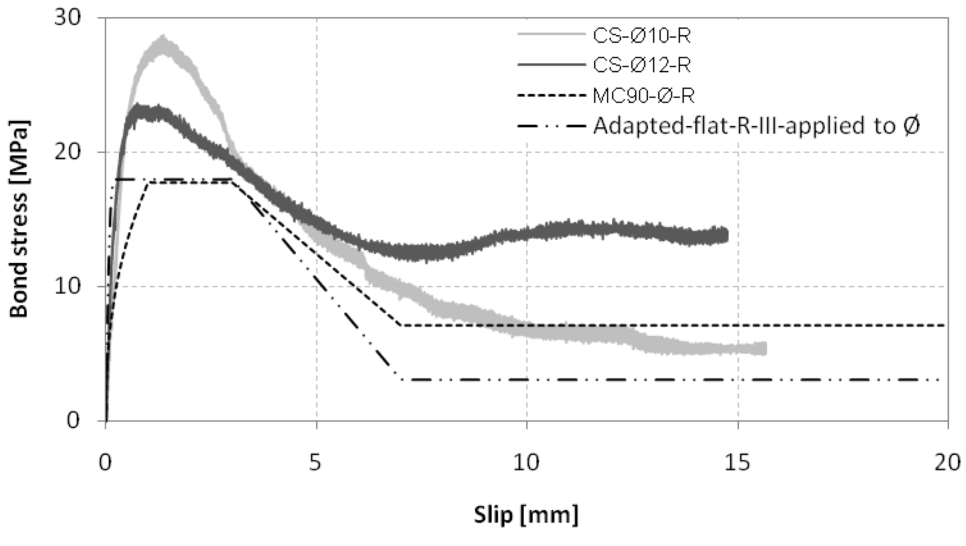

Figure 4-42 Applicability of the proposed bond model for round ribbed rebars. Slip values until 20 mm

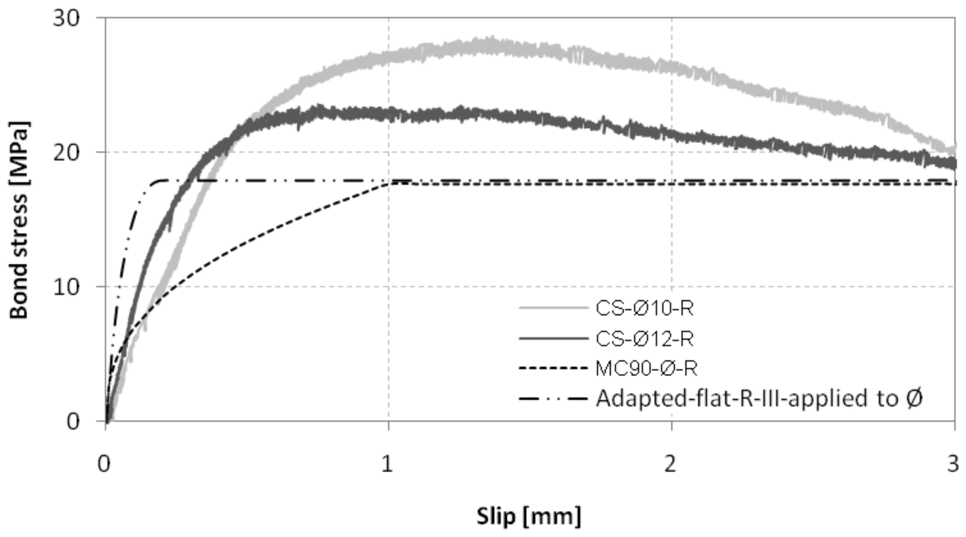

Figure 4-43 Applicability of the proposed bond model for round ribbed rebars. Slip values until 3 mm

5.2.6.5 Characteristic values of τ_{max} and τ_f

As performed for the smooth samples, a more conservative approach is applicable based on characteristic values calculated from the mean values and given the variability of the test results. The previously described "Bayesian prediction method with vague prior distributions" assumes normal distribution of the bond stress values and the characteristic value is defined as the 0,05 fractile. Equations 4-21 and 4-22 allow for calculation of the characteristic values, where $\hat{\tau}_{0,05}$ stands for the estimated characteristic value of the bond stress for a fractile of 5%. The factor λ is defined as a statistical factor dependant on the number of samples (n) and its definition varies depending on whether the coefficient of variation is known or not. According to λ values tabulated in [23] and [24], the Bayesian method is applied for this analysis with a value of λ equal to 1,89 (n = 12 and unknown coefficient of variation).

According to the calculated characteristic values and following the same approach as for the mean values, the maximum and frictional bond stresses are defined only dependant on the characteristic compression strength of the concrete. The following characteristic values are obtained: $\hat{\tau}_{max,0,05} = 1{,}98\sqrt{f_{ck}}$ and $\hat{\tau}_{f,0,05} = 0{,}05\tau_{max}$. Figure 4-44 and Figure 4-45 give the plotted version of the new proposed characteristic curves, together with the mean curve of the proposed model, for slip values until 20 mm and until 3 mm, respectively.

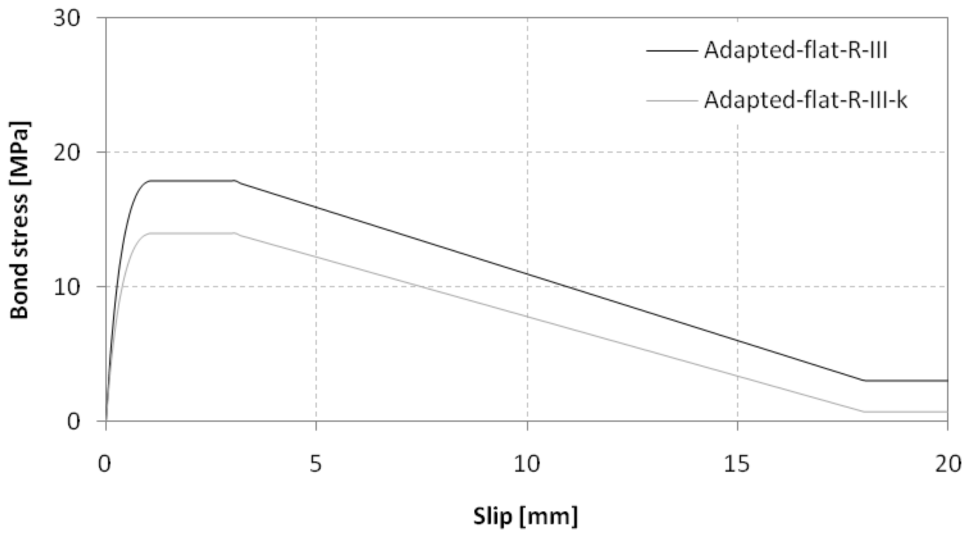

Figure 4-44 Bond stress-slip behaviour for flat ribbed samples. Mean and characteristic curves of the proposed model, for slip values until 20 mm

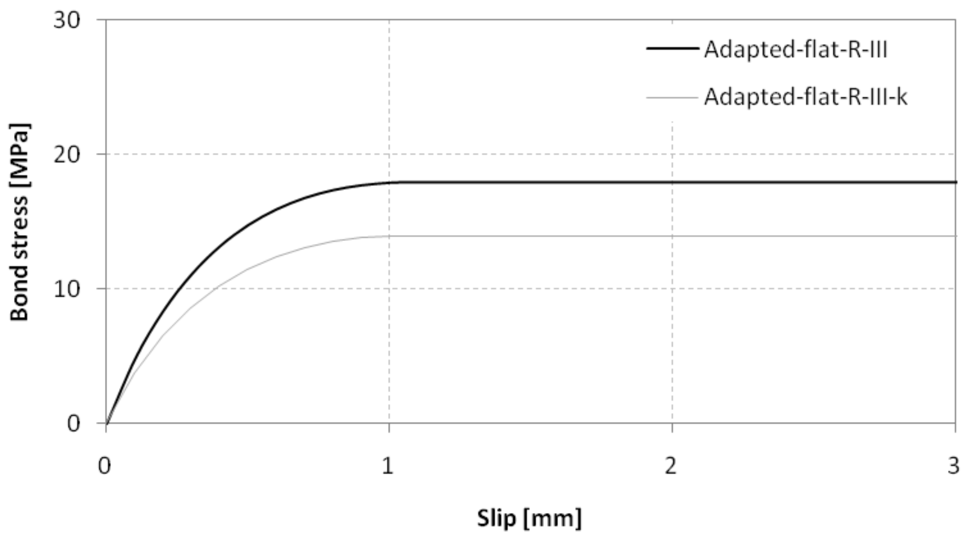

Figure 4-45 Bond stress-slip behaviour for flat ribbed samples. Mean and characteristic curves of the proposed model, for slip values until 3 mm

6 Conclusions

The bond behaviour of flat SS strips when embedded in concrete has been analyzed by performing a series of 72 pull out tests to assess the influence of different parameters in the developed bond capacity. Both smooth and ribbed samples have been tested, and both TC and SCC have been used for embedding. Standard CS round ribbed samples have also been tested for comparison. Based on the obtained test results, the following conclusions can be drawn:

1. The reinforcement material (CS or SS) influences the bond strength developed by smooth rebars: CS develops higher bond strength than austenitic 304L SS and the latter develops higher bond strength than the ferritic K31 SS. Regarding ribbed reinforcement, no differences are observed in terms of influence of material type on the developed bond capacity. The chemical adhesion mechanism governing smooth samples bond behaviour explains the difference on material influence between smooth and ribbed rebars.

2. Micro roughness has a secondary influence on the bond behaviour of smooth samples. Other parameters, as reinforcement material, geometry and concrete type, are more deterministic.

3. Regarding flat ribbed samples, where bond mechanisms are governed by the mechanical interaction between the concrete and the ribs of the reinforcement, roughness of the rebar (characterized by the relative rib area) influences the bond capacity of the specimen.

4. For comparable cross section areas, round bars develop higher bond strength values than flat elements: up to 43% higher bond strength values in the case of smooth rebars and up to 75% higher bond strength values in the case of ribbed rebars. Note that the latter comparison is made for ribbed rebars with relative rib area differences of factor 3. However, higher forces are reached with strips as larger contact areas are involved.

5. SCC allows for developing higher bond strength values compared to TC. This influence is more pronounced for round ribbed bars (up to 47% higher bond strength values when tested in SCC compared to TC) than for flat ribbed elements (maximum differences of 6%).

6. The flat ribbed elements analyzed in this paper show higher splitting tendency when embedded in concrete, compared to round ribbed bars with comparable cross section.

7. When test results are compared to the existing bond models,

   a. For flat smooth samples, a poor agreement is observed between the 2 branches definition given by MC90/MC2010 [14][15] and the 3-stages behaviour observed during testing. Thus, an adapted bond model is proposed which includes a first ascending branch based on the definition given by the fib Model Codes, and implements a second logarithmic and asymptotic descending branch after maximum bond stress and until the residual friction forces are reached. A final plateau is defined for predicting the residual friction bond stress. The proposed model is defined by Equations 4-31 to 4-35 with parameters given in Table 4-16 for mean curve and 0,05 fractile characteristic curve prediction.

      The proposed bond model allows for predicting the bond stress-slip behaviour observed for round and flat smooth rebars.

$$\tau(s) = \tau_{max}\,(s/s_1)^{\alpha} \qquad 0 \leq s \leq s_1 \qquad (4\text{-}31)$$

$$\tau(s) = a + b\log s \qquad s_1 \leq s \leq s_2 \qquad (4\text{-}32)$$

$$\tau(s) = \tau_f \qquad s \geq s_2 \qquad (4\text{-}33)$$

$$a = (\tau_f + \tau_{max})/2 \qquad (4\text{-}34)$$

$$b = (\tau_f - \tau_{max})/2 \qquad (4\text{-}35)$$

Table 4-16 Parameters of the proposed bond model for defining the bond stress-slip behaviour of flat smooth rebars

Parameter	***Mean curve***	***Characteristic curve***
s_1 *(mm)*	0,1	0,1
s_2 *(mm)*	10	10
α	0,5	0,5
τ_{max} *(N/mm²)*	$0{,}5103\ \sqrt{f_{ck}}$	$0{,}035\ \sqrt{f_{ck}}$
τ_f *(N/mm²)*	$0{,}3915\ \tau_{max}$	0

   b. For the analyzed flat ribbed samples, where reinforcement material and concrete type play a minor role on the developed bond behaviour, several steps have been considered for proposing an adapted bond model: the basis is taken from MC90 and an adaptation is done to the curve defining parameters, with refinement performed for the first ascending branch definition and for the slip at maximum bond stress definition. The model consist of 4-branches curve to define the bond stress-slip behaviour: a first stiff ascending branch, followed by a plateau at maximum bond stress, which continuous with a third descending stage until the friction forces are reached; the fourth branch corresponds to the residual friction bond stress plateau. The proposed model is defined by Equations 4-36 to 4-39, with curve defining parameter values as given in Table 4-17 for mean curve and 0,05 fractile characteristic curve prediction.

$$\tau(s) = \tau_{max}\,(s/s_1)\; e^{(1-(s/s_1)^{\alpha})/\alpha} \qquad 0 \le s \le s_1 \qquad (4\text{-}36)$$

$$\tau(s) = \tau_{max} \qquad s_1 \le s \le s_2 \qquad (4\text{-}37)$$

$$\tau(s) = \tau_{max} - (\tau_{max} - \tau_f)((s\text{-}s_2)/(s_3\text{-}s_2)) \qquad s_2 \le s \le s_3 \qquad (4\text{-}38)$$

$$\tau(s) = \tau_f \qquad s \ge s_3 \qquad (4\text{-}39)$$

The application of the proposed bond model for predicting the bond stress-slip behaviour of round ribbed rebars is not recommended. The slip at the maximum bond stress, the maximum bond stress and the frictional remaining stresses observed experimentally for round ribbed rebars are considerably underestimated by the proposed model.

Table 4-17 Parameters of the proposed bond model for defining the bond stress-slip behaviour of flat ribbed rebars

Parameter	***Mean curve***	***Characteristic curve***
s_1 *(mm)*	0,0032 (clear rib spacing)^2 + 0,041	0,0032 (clear rib spacing)^2 + 0,041
s_2 *(mm)*	3	3
s_3 *(mm)*	Clear rib spacing	Clear rib spacing
α	0,8	0,8
τ_{max} *(N/mm²)*	2,54 $\sqrt{f_{ck}}$	1,98 $\sqrt{f_{ck}}$
τ_f *(N/mm²)*	0,17 τ_{max}	0,05 τ_{max}

7 References

[1] CEN (2004) Eurocode 2: EN 1992-1-1: *Design of concrete structures - Part 1-1: General rules and rules for buildings.* European Committee for Standardization, Brussels

[2] CEN (2005) EN 10088:2005 *Stainless steels - Part 1: List of stainless steels.* European Committee for Standardization, Brussels

[3] CEN (2009) EN 12350 *Testing fresh concrete*. European Committee for Standardization, Brussels

[4] CEN (2009) EN 12390 *Testing hardened concrete.* European Committee for Standardization, Brussels

[5] CEN (2010) EN ISO 15630 *Steel for the reinforcement and prestressing of concrete-Test methods-Part 1: Reinforcing bars, wire rod and wire.* European Committee for Standardization, Brussels

[6] ISO (1997) ISO 4287 *Geometrical Product Specifications (GPS) - Surface texture: Profile method - Terms, definitions and surface texture parameters*. International Organization for Standarization, Geneva

[7] ISO (2010) ISO 25178 *Geometric Product Specifications (GPS) - Surface texture: areal.* International Organization for Standarization, Geneva

[8] Euroinox (2005) *Guide to stainless steel finishes.* The European Stainless Steel Development Association, Brussels

[9] RILEM (1970) *Technical Recommendations for the Testing and Use of Construction Materials: RC6, Bond Test for reinforcing Steel. 2. Pull-out test*. International union of laboratories and experts in construction material, systems and structures

[10] ISO (2004) ISO 7500-1 *Metallic materials - Verification of static uniaxial testing machines - Part 1: Tension/compression testing machines - Verification and calibration of the force-measuring system.* International Organization for Standarization, Geneva

[11] Freund J.E. (1984) *Modern elementary statistics.* Ed. Prentice-Hall, ISBN: 0-13-593525-3: 289

[12] Alhborn T.M., DenHartigh T.C. (2003) *Comparative Bond Study of Stainless and High-Chromium Reinforcing Bars in Concrete*. Transportation Research Record 1845: 88-95

[13] fib (2000) *Bond of reinforcement in concrete. State of the art report*. fib Bulletin 10. International Federation for Structural Concrete, Switzerland

[14] CEB-FIP (1993) *Model Code 1990 – Design Code.* International Federation for Structural Concrete, Switzerland

[15] fib (2010) *Model Code 2010 – First complete draft*. fib Bulletin 55. International Federation for Structural Concrete, Switzerland

[16] Eligehausen R., Popov E. P., Bertero V. V. (1983) *Local bond stress-slip relationship of deformed bars under generalized excitations*. Report UCB/EERC-83/23, University of California, Berkeley

[17] Feldman L. R., Bartlett F. M. (2005) *Bond strength variability in pullout specimens with plain reinforcement*. ACI Structural Journal, Vol 102 (6): 860-867

[18] Mylrea T.D. (1948) *Bond and anchorage*. ACI Journal, Proceedings, Vol 44: 521- 552

[19] Abrams D. A. (1913) *Tests of bond between concrete and steel*. Bulletin 71, University of Illinois, Illinois

[20] Pul S. (2010) *Loss of concrete-steel bond strength under monotonic and cyclic loading of lightweight and ordinary concrete*. Iranian Journal of Science & Technology, Vol 34 (B4): 397-406

[21] Khandaker M.A. H. (2008) *Bond characteristics of plain and deformed bars in lightweight pumice concrete*. Construction and Building Materials, Vol 22: 1491-1499

[22] Caspeele R (2010) *Probabilistic evaluation of conformity control and the use of Bayesian updating techniques in the framework of safety analysis of concrete structures*. PhD dissertation, Ghent University, Ghent

[23] CEN (2002) Eurocode 0: EN 1990: *Basis of the structural design.* European Committee for Standardization, Brussels

[24] ISO (1998) ISO 2394 *General principles on reliability for structures*. International Organization for Standarization, Geneva

[25] Soroushian P., Choi K.B., Park G.H., Aslani F. (1991) *Bond of deformed bars to concrete: effects of confinement and strength of concrete*. ACI Materials Journal, Vol 88 (3): 227-232

[26] Harajli M.H., Hout M., Jalkh W. (1995) *Local bond stress-slip behaviour of reinforcing bars embedded in plain and fiber concrete*. ACI Materials Journal, Vol 92 (4): 343-354

[27] Desnerck P. (2011) *Compressive, bond and shear behaviour of powder-type self-compacting concrete*. PhD Dissertation, Ghent University, Ghent

Chapter 5 Bond Behaviour of Flat Rebars with an Alternate Rib Pattern in Concrete

1 Introduction

An optimal surface configuration containing an alternate rib pattern combining ribbed and smooth areas within the same reinforcing element, may improve the cracking behaviour of a reinforced concrete structure that has been reinforced with this type of rebars [1].

In this chapter, this new idea is combined together with the idea of applying stainless steel as reinforcement material and together with using flat rebars instead of round bars for an optimization of the concrete thickness, and for an increase of the contact area between the reinforcement and the concrete. In this way, flat rebars made of SS or CS and containing different surface configurations are studied in this section. For studying the bond behaviour of these rebars, a total of 54 pull out tests have been carried out at the Magnel Laboratory for Concrete Research with both traditional concrete (TC) and self compacting concrete (SCC). Completely ribbed flat rebars have been tested as reference specimens, and alternate surface patterns combining ribbed and smooth zones have been further assessed by performing pull out tests to the centrally embedded strips. The influence of adding a smooth area and its position within the bond length have been analyzed. Test results are presented in terms of bond strength, force transfer stiffness and the bond stress-slip relationship. For a more comprehensive and accurate interpretation and discussion of the test results, the t-test statistical tool has been applied as discussed in Section 3 of this chapter.

According to the literature available to the author, bond tests regarding these type of alternate reinforcements have not been reported.

2 Test programme

Table 1 gives an overview of the test program in terms of materials used and bond length configuration. Both carbon steel and stainless steel flat rebars are tested; with 3,5x25mm^2 and 5x23 mm^2 cross sectional areas, respectively. Note that, although different cross section areas are involved, both have a comparable perimeter value which leads to a comparable contact surface between the reinforcement and the concrete. For both material types 3 surface rib patterns are tested, see Figure 5-1 and Figure 5-2: completely ribbed (CR) and 2 alternate patterns (combining ribbed and smooth areas): 50 mm of ribbed area followed by 10 mm of smooth area (50R_10S) and 50 mm of ribbed area followed by 20 mm of the smooth one (50R_20S). The embedded length of the reinforcement in the pull out specimens has been set at 30 mm of ribbed zone (plus the length of the smooth zone, if any) and accordingly different ribbed-smooth alternate combinations are used for the bond length configuration (see Table 5-1 and Figure 5-3). The total bond length involved for each configuration is also given in Table 5-1. For those flat elements with an alternate rib pattern, the smooth area has been positioned firstly at the middle of the embedded length, having the two following configurations of the bond length: 15 mm of ribbed area + 10 mm smooth + 15 mm ribbed (15R_10S_15R), and 15 mm ribbed + 20 mm of smooth area + 15 mm ribbed (15R_20S_15R). For a better understanding of the effect of the smooth area on the developed bond strength, extra tests have been performed with TC in which the position of the smooth area within the bond length has been changed. The total length of the ribbed area has been kept at 30 mm and the smooth surface has been moved from the middle to the edges of the embedded length:

- For CS-3,5x25-50R_10S: 10 mm of smooth area at the passive end, followed by 30 mm of ribbed surface (10S_30R);
- For CS-3,5x25-50R_10S: 30 mm of ribbed surface at the passive end followed by 10 mm of smooth area (30R_10S);
- For CS-3,5x25-50R_20S: 20 mm of smooth area at the passive end plus 30 mm of ribbed surface (20S_30R).

Both traditional concrete and self compacting concrete are investigated. Furthermore, given the high splitting tendency observed for these type of completely ribbed flat reinforcements (see Chapter 4), other 9 tests are conducted using extra reinforcement (in form of stirrups, see discussion in Section 2.2 and Figure 5-7) with TC. The numbers from 1 to 6 between brackets in Table 5-1 represent the concrete batch in which the specimens were casted. For each parameter combination 3 specimens have been tested.

Rebar designation (Table 5-1) is defined following the sequence: material (CS or SS), dimensions of the cross section and bond length configuration. Note that the SS grade used in the case of this investigation is the ferritic K31 (grade 1.4017 according to European standard designation EN 10088 [5]). However, as it is the only grade analyzed it is further referred in this Chapter as SS.

Table 5-1 Overview of the test program

Mat.	***Geom. (mm²)***	***Rib pattern****	***Config.*****	***Rebar designation***	***l_b (mm)***	***TC***	***SCC***	***TC+ stir.***
CS	3,5x25	CR	30R	CS-3,5x25-30R	30	(1)	(4)	(6)
		50R_10S	15R_10S_15R	CS-3,5x25-15R_10S_15R	40	(1)	(4)	(6)
			10S_30R	CS-3,5x25-10S_30R	40	(3)	-	-
			30R_10S	CS-3,5x25-30R_10S	40	(3)	-	-
		50R_20S	15R_20S_15R	CS-3,5x25-15R_20S_15R	50	(1)	(4)	(6)
			20S_30R	CS-3,5x25-20S_30R	50	(3)	-	-
SS	5x23	CR	30R	SS-5x23-30R	30	(2)	(5)	-
		50R_10S	15R_10S_15R	SS-5x23-15R_10S_15R	40	(2)	(5)	-
		50R_20S	15R_20S_15R	SS-5x23-15R_20S_15R	50	(2)	(5)	-

* CR: completely ribbed; 50R_10S: alternate pattern, 50 mm ribbed area followed by 10 mm smooth zone; 50R_20S: alternate pattern, 50 mm ribbed surface followed by 20 mm smooth area

** Surface configuration of the embedded length, starting from the passive end (mm) R: ribbed; S: smooth

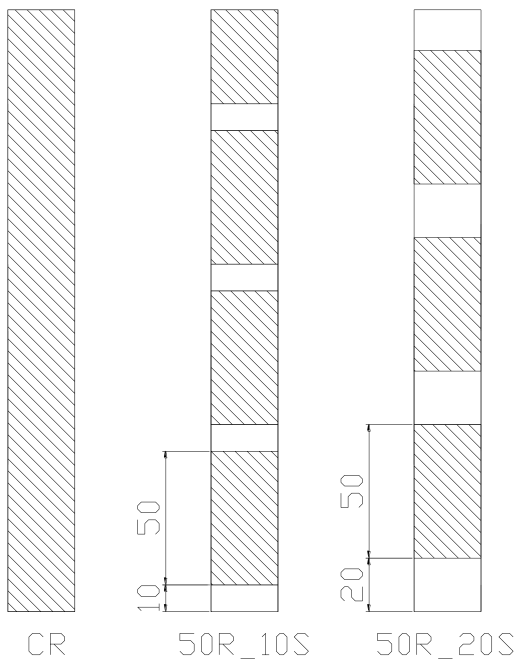

Figure 5-1 Schematic drawing of tested rib patterns: completely ribbed (CR); and two alternate patterns, 50 mm of ribbed area followed by 10 mm and 20 mm of smooth length (50R_10S and 50R_20S), respectively

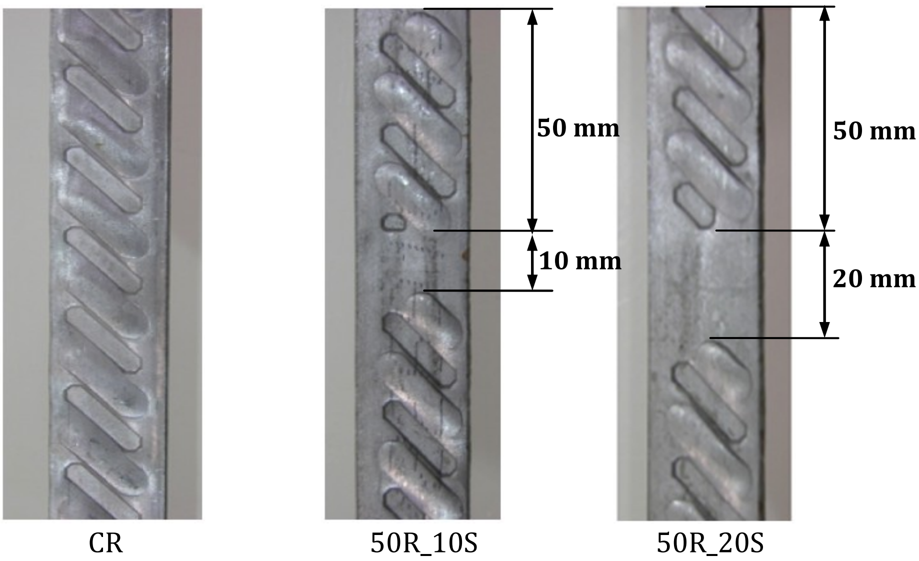

Figure 5-2 Pictures of tested rib patterns: completely ribbed one; and two alternate patterns, 50 mm of ribbed area followed by 10 mm and 20 mm of smooth length, respectively

2.1 Test materials

2.1.1 Concrete

As indicated in Table 5-1, 6 different concrete batches have been used for the casting of the specimens. As in the previous test program (Chapter 4), traditional concrete and self compacting concrete have been tested and the same concrete composition as in the previous test program has been used (see Table 4-2). Concrete mixing time has been set to 3 minutes and a vibrating needle has been used for compaction. The fresh concrete is placed in the form in which the bar is kept horizontal in the axis of the mould, resulting in a vertical casting direction, perpendicular to the bar axis. Note that the wider side of the flat rebars is placed perpendicular to the casting direction. Specimens are demoulded 24 hours after casting process. For the curing of the specimens, during the first 7 days the samples are kept in a wet room at 20 ± 2 °C and at 95 ± 3 % of relative humidity. For the rest of the curing time and until the age of testing, 28 days, the specimens are stored at ambient laboratory conditions.

For a better characterization of the applied concrete, properties of fresh and hardened concrete have been determined by means of standardized testing procedures (according to EN 12350 [2] for fresh concrete properties and according to EN 12390 [3] for hardened concrete properties). Obtained fresh properties' values for each casted concrete batch are given in Table 5-2, whereas properties of the hardened concrete at 28 days are given in Table 5-3.

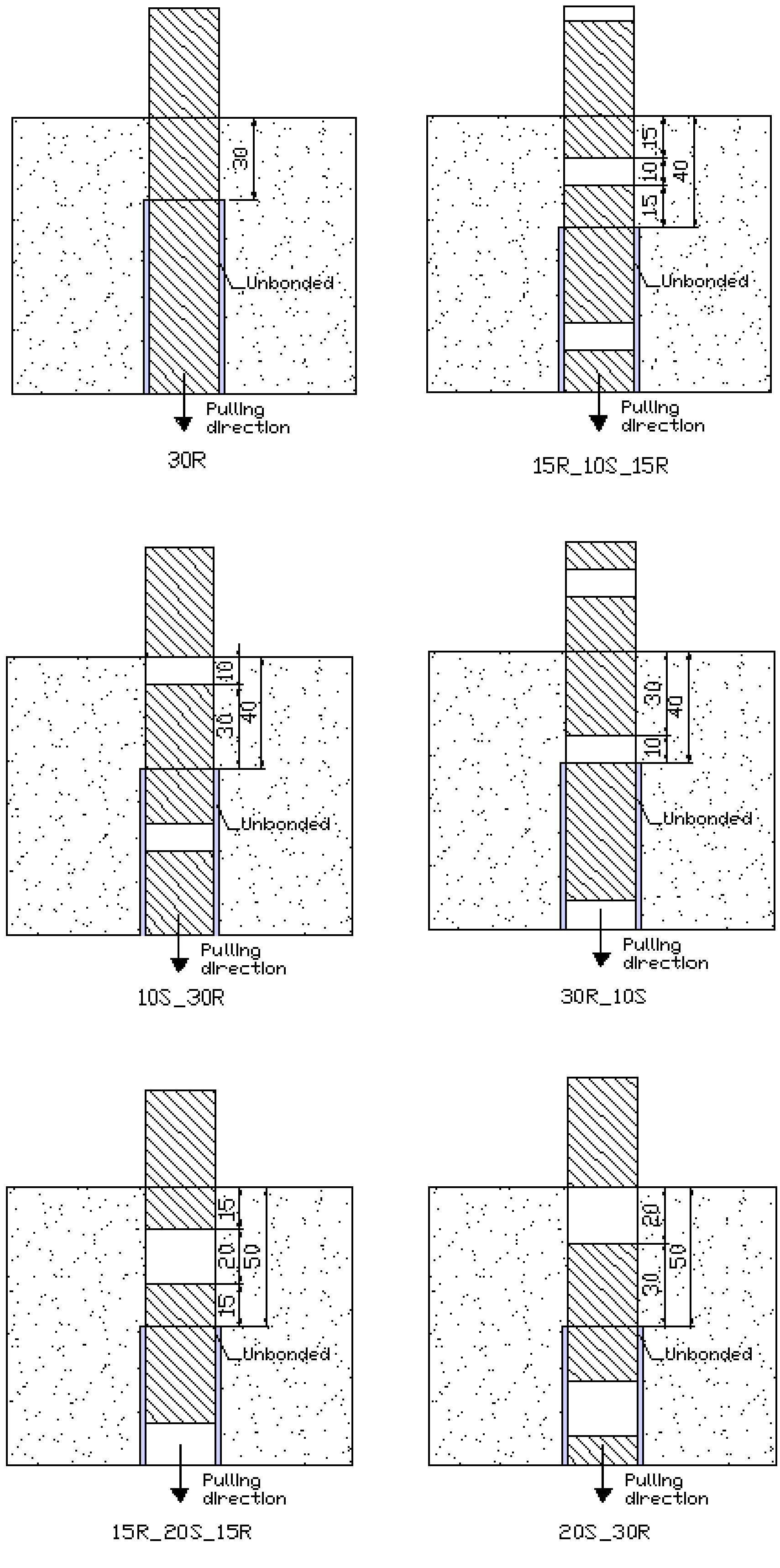

Figure 5-3 Schematic drawings of applied different bond length configurations (in mm)

Table 5-2 Fresh concrete properties

Batch	Type of concrete	Slump (mm)	Flow (-)	Slump flow (mm)	V-tunnel (s)	Density (kg/m3)
1	TC	20	1,67	-	-	2400
2	TC	30	1,64	-	-	2350
3	TC	50	1,51	-	-	2400
4	SCC	-	-	805	15,3	2350
5	SCC	-	-	760	18,0	2350
6	TC	30	1,61	-	-	2400
Average	TC	32	1,61	-	-	2388
St. dev.		12,6	0,07	-	-	25
Average	SCC	-	-	782	16,7	2350
St. dev.		-	-	31,8	1,92	0

Table 5-3 Hardened concrete properties at 28 days

Batch	Type of concrete	$f_{c,cub150}$ (N/mm^2)	f_c (N/mm^2)	$f_{ct,fl}$ (N/mm^2)	$f_{ct,sp}$ (N/mm^2)	E_c (N/mm^2)
1	TC	62,5	55,0	4,9	4,2	35900
2	TC	62,9	54,9	5,0	4,3	36400
3	TC	61,8	50,0	4,4	3,9	37500
4	SCC	70,3	62,0	5,9	3,9	38000
5	SCC	67,7	61,9	5,2	4,0	38500
6	TC	63,8	52,2	5,3	3,8	36400
Average	TC	62,8	53,0	4,9	4,1	36550
St. dev.		0,83	2,40	0,37	0,24	675,77
Average	SCC	69,0	62,0	5,6	4,0	38250
St. dev.		1,84	0,07	0,49	0,07	354
Average	Total	64,8	56,0	5,1	4,0	37117
St. dev.		3,39	4,97	0,50	0,19	1034

2.1.2 Steel

Steel properties are obtained by performing standardized tests according to EN ISO 15630 [4]. Tensile tests to each tested steel rebar (3 tests per type) are performed for determining the yield strength, the ultimate strength and the ultimate strain. For SS rebars, yielding strength is given as the proof strength at an elongation of 0,2%. Average values of the performed tensile tests, for each reinforcement type, together with the values of nominal cross sectional area and nominal perimeter, are presented in Table 5-5. Figure 5-4 and Figure 5-5 give the tensile stress-strain relationship for the CS rebars and SS rebars, respectively. Note that no differences are observed regarding tensile behaviour of completely ribbed pattern rebar compared to the tensile behaviour of alternate patterns, for both material types.

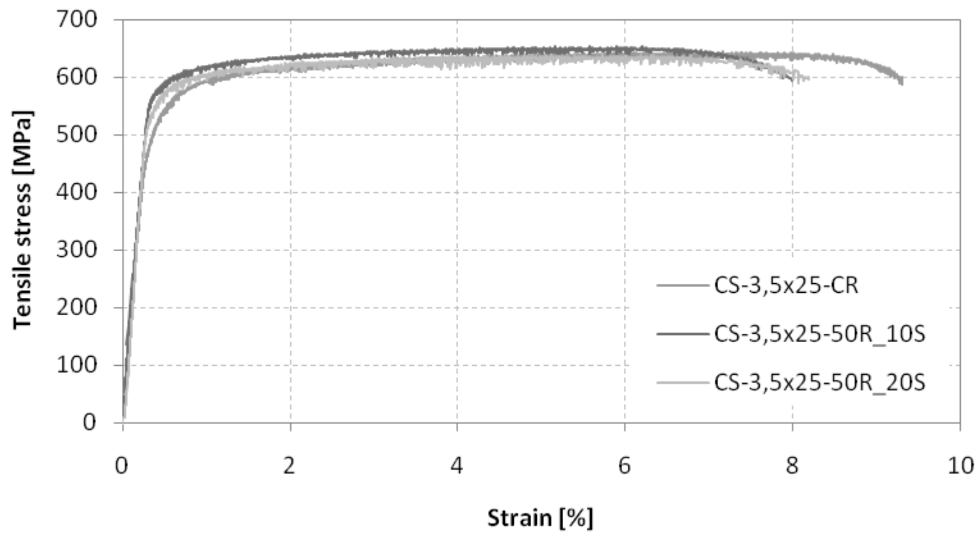

Figure 5-4 Tensile stress-strain curves for flat CS rebars

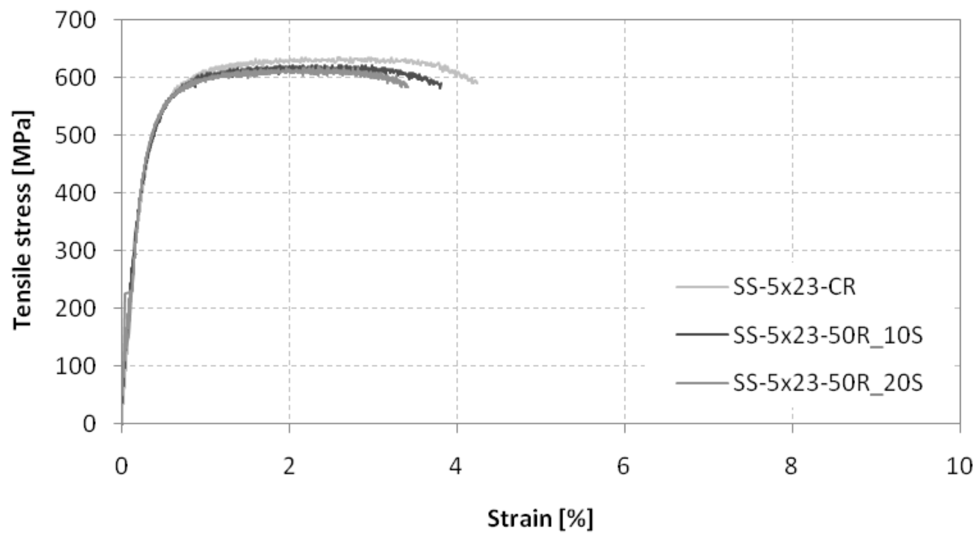

Figure 5-5 Tensile stress-strain curves for flat SS rebars

Given the importance of the rib geometry of the reinforcement in the developed bond strength (see Chapter 2, Section 3.3) and for a better understanding of the bond behaviour of the applied reinforcement elements, the rib pattern has been analyzed. Rib height, rib spacing and the corresponding relative rib area are the considered main parameters. According to ISO 15630 [4], Equation 5-1 gives the general definition for relative rib area, while Equation 5-2 is a simplified formula of the definition based on the so-called parabola formula (see Chapter 4). A description of the different parameters involved is given in Table 5-4 and Figure 5-6 allows for a better understanding of the e_i parameter, giving a schematic drawing of the bar along its perimeter. Results of the performed measurements and calculated (Equation 5-2) relative rib area per each used bar type are given in Table 5-6. The measurements of the rib geometry have been conducted assisted by an Automatic Laser Measurement (ALM) system as described in Chapter 4. Note that for the alternate patterns, the relative ribbed area is the one referred only to the ribbed zone of the rebar.

$$f_R = \frac{projected\ rib\ area\ normal\ to\ the\ bar\ axis}{nominal\ bar\ perimeter \times centre\ to\ centre\ rib\ spacing} \tag{5-1}$$

$$f_R = (2a_m/3uc).(u\text{-}\Sigma e_i) \tag{5-2}$$

Table 5-4 Definition and units of different parameters

Parameter	***Description***	***Unit***
f_R	Relative rib area	(-)
a_m	Rib height at mid-point	mm
c	Transverse rib spacing	mm
u	Nominal bar perimeter	mm
e_i	Average gap between two adjacent rib rows	mm

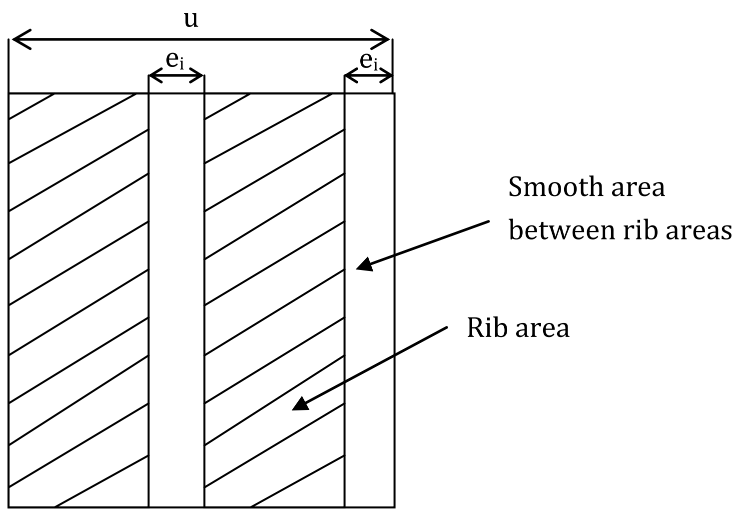

Figure 5-6 Schematic drawings of the surface geometry (surface fault open view)

Table 5-5 Embedded steel properties

Material		Area (mm^2)	Perimeter (mm)	Yield strength (N/mm^2)	Tensile strength (N/mm^2)	Ultimate strain (%)
CS-3,5x25-CR		87,5	57,0	460	630	8,75
CS-3,5x25-50R_10S		87,5	57,0	470	645	7,25
CS-3,5x25-50R_20S		87,5	57,0	470	640	7,75
SS-5x23-CR		115,0	56,0	490	630	3,83
SS-5x23-50R_10S		115,0	56,0	480	630	3,50
SS-5x23-50S_20S		115,0	56,0	480	615	3,50
Average	CS-3,5x25	87,5	57,0	578	638	7,92
St. dev.				10,4	7,6	0,76
Average	SS-5x23	115,0	56,0	483	625	3,61
St. dev.				5,8	8,7	0,19

Table 5-6 Rib pattern parameters' values for each reinforcing element

Material		u (mm)	a_m (mm)	c (mm)	f_R (-)
CS-3,5x25-CR		57,0	0,70	18,05	0,023
CS-3,5x25-50R_10S		57,0	0,71	18,01	0,023
CS-3,5x25-50R_20S		57,0	0,70	17,98	0,023
SS-5x23-CR		56,0	0,71	18,01	0,022
SS-5x23-50R_10S		56,0	0,73	18,08	0,022
SS-5x23-50S_20S		56,0	0,71	18,04	0,022
Average	CS-3,5x25	57,0	0,70	18,01	0,023
St. dev.			0,01	0,04	0,000
Average	SS-5x23	56,0	0,72	18,04	0,022
St. dev.			0,01	0,04	0,000

2.2 Test set-up and testing conditions

As explained in Chapter 4 of this work, the test specimen is a concrete cube (side length 200 mm) with a steel bar (1100 mm long) centrally embedded in and extending beyond the two sides of the cube. The sample is placed at the testing machine on top of the bearing plate keeping the steel bar axis vertical and the force is applied vertically at the lower extremity of the longer end (800 mm). The bar length at the passive end is 100 mm. The specimen has been designed following the minimum dimensions given by RILEM recommendations for bond testing of reinforcing steel [6]. However, the effective bond length recommendation (5Ø) is not appropriate for the flat reinforcements tested in this program due to their splitting tendency (as observed and reported in Chapter 4). Therefore, in order to obtain a pull out type failure, the effective bond length corresponding to the ribbed zone has been limited to 3 times the equivalent bar diameter (3Ø), which in this case corresponds to 30 mm. The other part of the bar does not adhere as it is covered by a plastic tube. A schematic drawing of the test set-up has been already provided in the previous Chapter, see Figure 4-4, (page 106).

For concrete batch number 6, extra reinforcement has been applied in the form of stirrups. Standard carbon steel Ø6 has been used for building the cage type reinforcement as shown in Figure 5-7. A full set of LVDT's (Linear Variable Data Transducer) has been used for displacement data registration: one at the passive end, 2 at the active end and another 2 underneath the active end slip measuring system for measuring of the bar deformation as detailed in Chapter 4. For the pulling out of the bar a tensile testing machine (with load capacity up to 1000 kN, class 1 according to ISO 7500-1 [7], and a relative error of the accuracy of 0,8%) has been used. The load is firstly applied in load control way at a rate of 0,03 kN/s until a small pre-load of 8kN is reached. Secondly, a displacement control rate of 0,006 mm/s is applied until the end of the test. The test is stopped once the active-end slip is at least 2,5 mm.

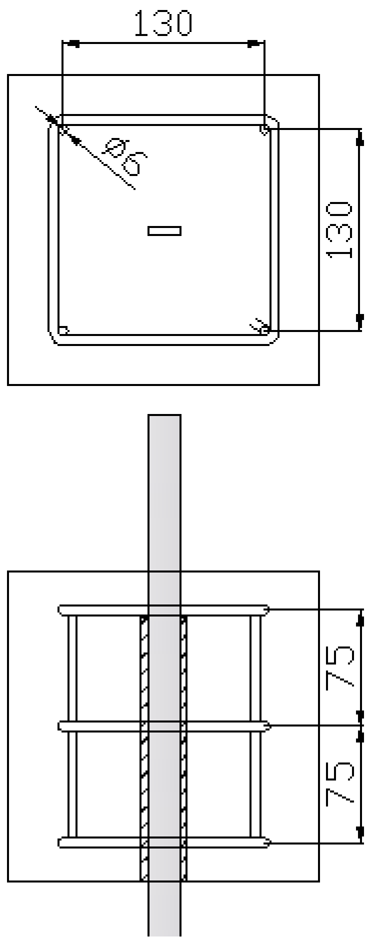

Figure 5-7 Test specimen with extra confinement (dimensions in mm)

3 Test results

3.1 General considerations

Recorded load and displacement measurements are further used for calculation of the main bond characteristics. As described in Chapter 4, the mean bond stress along the bond length, τ_b (in N/mm^2), is calculated based on the measured force, F (in N), and dividing it by the nominal perimeter of the rebar, u (in mm) and by the bond length (total bond length considering both ribbed and smooth areas), l_b (in mm), see Equation 4-3. For determining the mean bond strength f_b (in N/mm^2), Equation 4-4 is used, where F_{max} represents the maximum measured force (in N). The bar slip at the active end s_a (in mm), is calculated according to Equation 4-5 considering s_a' (the measured slip at the active end) and Δl_s, (deformation of the bar along the gauge length of the slip measurement device and along the unbounded plastic tube zone).

An overview of the test results is given in Table 5-7 till 5-10 , in terms of F_{max}, f_b, S_{dev} (derived standard deviation of the bond strength) and failure aspect. Results for specimens embedded in traditional and self compacting concrete are given in Table 5-7 and Table 5-8, respectively. The test set including confinement reinforcement is given in Table 5-9, while the test set considering the position of the smooth area is reported in Table 5-10.

For an easier comparison, a bond strength ratio ($f_b/f_{b,ref}$) which compares the bond strength of the tested reinforcement with alternate rib pattern to the bond strength of the completely ribbed configuration, has been calculated. Thus the ratio is calculated taking as reference the bond strength of CS-3,5x25-CR (30R), for comparison with CS-3,5x25 configurations 15R_10S_15R , 15R_20S_15R, 10S_30R, 30R_10S and 20S_30R. SS-5x23-CR (30R) is the reference for SS-5x23 with 15R_10S_15R and 15R_20S_15R configurations. In order to assess the stiffness of the bond stress-slip relationship until the maximum bond stress is reached a second ratio is calculated in terms of maximum measured force divided by the active end slip at the moment of maximum force, $F_{max}/s_{a,Fmax}$.

Regarding the failure aspect, PO stands for pull out type of failure, SC means that splitting of the concrete occurred and B corresponds to the failure of the bar (steel yielding followed by bar rupture). Note that when the 3 specimens of each testing condition failed in the same way, average numerical values are given independently of the failure type. On the contrary, if one of the specimens failed in a different way than the other two, test results are considered only for the two specimens that failed in the same way and the failure type which occurred only once is given between brackets. However, exceptionally if PO failure type occurred for only one of the 3 specimens, test results of that specimen are only considered (this is the case for SS-5x23 embedded in TC and CS-3,5x25 embedded in TC with stirrups, in both cases for the 15R_20S_15R bond length configuration).

In a similar way as for the bond tests described in Chapter 4, statistical tools are applied for a more comprehensive and appropriate analysis of the test results. In this way it can be established whether the mean values of two considered groups are statistically different from each other, considering the variability of the test results.

Due to the continuously measured force and displacement, a continuous representation of the bond stress-slip relationship is possible. Figure 5-8 to 5-12 give the τ_b-s_a relationship for comparison of the studied parameters. Note that plotted graphs illustrate individual test results (one out of the performed 3 test per testing condition) which are representative of the observed behaviour. However, all individual test results are included in Appendix B. Figure 5-8 allows for a comparison between the bond behaviour of CS and SS in the case of completely ribbed flat samples (30R). The influence of the concrete type is illustrated in Figure 5-9 for CS rebars with 15R_10S_15R alternate configuration when embedded in TC and in SCC. In order to assess the influence of adding extra confinement reinforcement in form of stirrups to the test specimen, Figure 5-10 is presented, where 2 individual test results of CS-3,5x25-CR are plotted, with and without stirrups. Finally, the alternate patterns are considered for study. Figure 5-13 and Figure 5-14 give the results of adding a smooth area in the middle of the bond length and are compared to the equivalent test condition with a completely ribbed bond zone (15R_10S_15R vs. 30R), for TC and SCC, respectively. The influence of increasing the smooth area in the middle of the bond length from 10 mm to 20 mm is characterized by Figure 5-17, where results of CS flat rebar are presented for the mentioned testing conditions. Changes in the position of the smooth area within the bond length result in changes on the bond behaviour of the tested bar. Figure 5-18 allows for a comparison between 30R, 15R_10S_15R, 10S_30R and 30R_10S bond length configurations, all of them tested for CS and embedded in TC.

Table 5-7 Test results TC

Material (Batch)	***Bond length configuration***	***F_{max} (kN)***	***f_b (N/mm²)***	***S_{dev} (N/mm²)***	***$f_b/f_{b,ref}$ (-)***	***$F_{max}/s_{a,Fmax}$ (kN/mm)***	***Failure type***
CS-3,5x25 (1)	30R	31,45	18,40	3,34	1,00*	17,73	PO
CS-3,5x25 (1)	15R_10S_15R	46,31	20,31	1,19	1,10*	6,67	PO (SC)
CS-3,5x25 (1)	15R_20S_15R	44,86	≥ 15,74	2,61	0,86*	9,10	SC
SS-5x23 (2)	30R	34,99	20,83	1,51	1,00**	14,19	PO (SC)
SS-5x23 (2)	15R_10S_15R	44,83	≥ 20,01	2,60	0,96**	8,93	SC
SS-5x23 (2)	15R_20S_15R	56,44	20,16	-	0,97**	3,51	SC (PO)

* $f_{b,ref}$: CS-3,5x25-CR in TC
** $f_{b,ref}$: SS-5x23-CR in TC

Table 5-8 Test results SCC

Material (Batch)	*Bond length configuration*	*F_{max} (kN)*	*f_b (N/mm²)*	*S_{dev} (N/mm²)*	*$f_b/f_{b,ref}$ (-)*	*$F_{max}/s_{a,Fmax}$ (kN/mm)*	*Failure type*
CS-3,5x25 (4)	30R	33,36	19,51	1,33	1,00*	14,32	PO
CS-3,5x25 (4)	15R_10S_15R	50,20	22,02	1,05	1,13*	7,57	PO (SC)
CS-3,5x25 (4)	15R_20S_15R	41,57	≥ 14,59	0,95	0,75*	11,81	SC
SS-5x23 (5)	30R	31,41	18,80	1,43	1,00**	29,00	PO
SS-5x23 (5)	15R_10S_15R	50,46	≥ 22,53	3,38	1,20**	10,14	SC
SS-5x23 (5)	15R_20S_15R	52,86	≥ 18,88	3,58	1,00**	8,40	SC

* $f_{b,ref}$: CS-3,5x25-CR in SCC
** $f_{b,ref}$: SS-5x23-CR in SCC

Table 5-9 Test results TC with stirrups

Material (Batch)	*Bond length configuration*	*F_{max} (kN)*	*f_b (N/mm²)*	*S_{dev} (N/mm²)*	*$f_b/f_{b,ref}$ (-)*	*$F_{max}/s_{a,Fmax}$ (kN/mm)*	*Failure type*
CS-3,5x25 (6)	30R	32,20	18,83	2,52	1,02*	7,29	PO
CS-3,5x25 (6)	15R_10S_15R	51,96	22,79	1,43	1,24*	6,29	PO
CS-3,5x25 (6)	15R_20S_15R	55,92	19,62	-	1,07*	2,73	B (PO)

* $f_{b,ref}$: CS-3,5x25-CR in TC

Table 5-10 Test results for different bond length configurations, TC

Material (Batch)	*Bond length configuration*	*F_{max} (kN)*	*f_b (N/mm²)*	*S_{dev} (N/mm²)*	*$f_b/f_{b,ref}$ (-)*	*$F_{max}/s_{a,Fmax}$ (kN/mm)*	*Failure type*
CS-3,5x25 (3)	10S_30R	26,69	11,69	0,43	0,64*	12,24	PO
CS-3,5x25 (3)	30R_10S	38,78	17,01	2,26	0,92*	21,43	PO (SC)
CS-3,5x25 (3)	20S_30R	24,63	10,81	0,56	0,59*	15,29	PO

* $f_{b,ref}$: CS-3,5x25-CR in TC

3.2 Influence of reinforcement material

Comparing CS to SS, and taking results of specimens that failed by pulling out of the rebar, if mean values are analyzed together with their standard deviation, the t-test statistical analysis confirms that the differences (up to 11%) on bond strength developed by CS and SS are not significant. In other words, for geometrically comparable flat ribbed samples, no significant difference is observed between the bond strength of CS and SS. The same conclusion is derived from Figure 5-8, where bond stress-slip relationships of CS vs. SS are given. The same tendency has been also observed in Chapter 4, where no steel material influences have been reported for ribbed flat reinforcements.

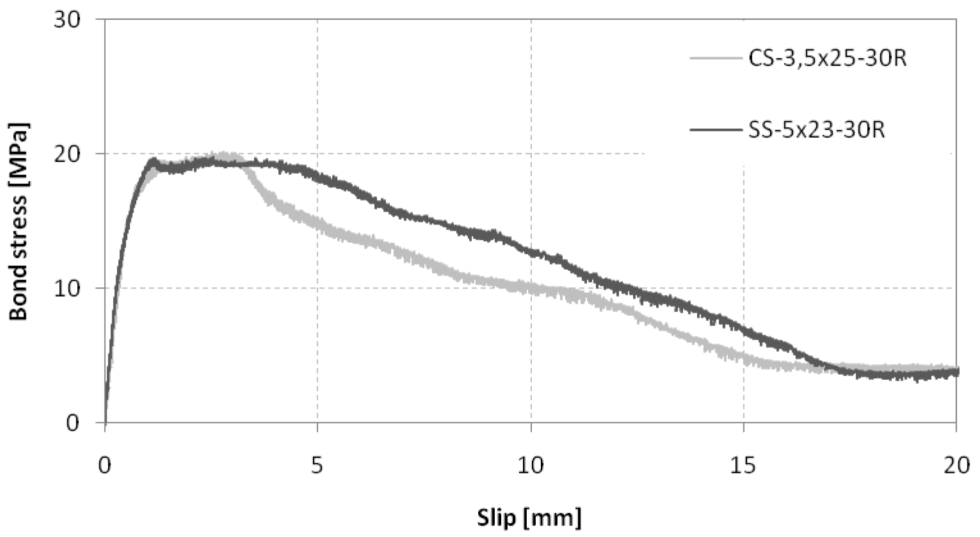

Figure 5-8 Bond stress-slip relationship. CS vs. SS

3.3 Influence of concrete type

According to the mean test results and bond-stress slip relationships, higher bond strength and therefore, higher maximum forces are reached with SCC than for TC, when testing CS. The difference on the developed bond strength is around 7-8% higher when embedded in SCC. For stainless steel specimens that failed by pulling out of the strip (SS-5x23-CR), 10% higher bond strength values are reached when embedded in TC than for SCC. If the statistical test is applied to both CS and SS flat samples, however, it is derived that the dissimilarities on the bond strength between the two concrete types is not significant enough to consider the results different. In other words, the analyzed flat ribbed rebars develop comparable bond strength when they are embedded in TC or in SCC. This observation agrees with the conclusions drawn in Chapter 4, where opposite to the round rebars, no concrete type influence has been observed regarding completely ribbed flat rebars.

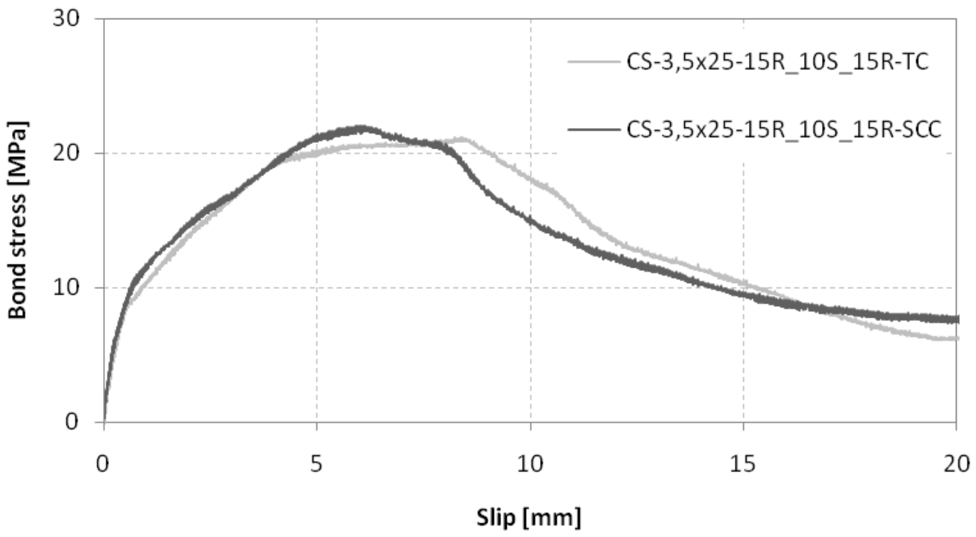

Figure 5-9 Bond stress-slip relationship. TC vs. SCC (for CS-3,5x25-15R_10S_15R)

3.4 Influence of adding confinement reinforcement to the concrete

The influence of providing extra stirrups differs depending on the strip type:

1) For CS-3,5x25-CR (30R bond length configuration), the influence is negligible (see Figure 5-10): mean values show slightly higher developed bond strength (~2% higher) when stirrups are used; however, if standard deviation is considered the difference is insignificant, as it is confirmed by the t-test.

2) For CS-3,5x25-50R_10S (15R_10S_15R configuration), the extra confinement given by the stirrups allows developing higher average bond strength (~12% higher) and avoids splitting of the concrete, which occurred for one specimen without stirrups. If statistical t-test results are considered, where the mean bond strength values are evaluated together with their standard deviation, it can be concluded that differences between the mean values are not significant to consider them different.

3) For CS-flat-50R_20S, the added stirrups avoids splitting of the concrete, which occurred when no stirrups are used, but yielding of the bar is then reached, and the specimens fail because ultimate tensile values of the bar are reached.

Although conclusions with respect to the extra confinement stirrups are specific for the tested stirrup configuration, the observed behaviour regarding effect of the confinement reinforcement on the failure aspect, agrees with the behaviour observed by Darwin et al. [8]. They stated that once the point where a pull out failure governs over a splitting failure is past, increasing the confinement has little to no effect on the bond capacity developed by the rebar. This is the case for the completely ribbed (30R) and the 15R_10R_15R bond length configurations, for which no significant influence of adding confinement reinforcement has been observed. However, if the splitting behaviour governs for an unconfined specimen, implementing of enough confinement will allow for avoiding the splitting type of failure.

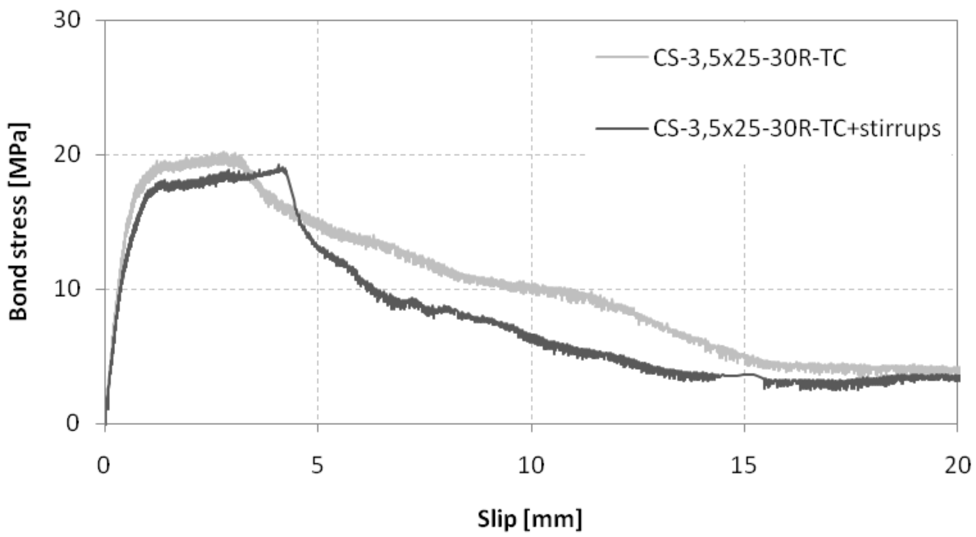

Figure 5-10 Bond stress-slip relationship. TC vs. TC+stirrups

3.5 Influence of the bond length configuration

For a better understanding of the influence of the alternate pattern on the bond behaviour of the rebar, an analysis of the stiffness of the bond capacity has been performed based on the recorded data. This analysis has been done for CS specimens casted in TC (without stirrups) with all tested bond length configurations. Figure 5-11 gives, in a schematic way the procedure used for the slope or stiffness calculation, together with Equations 5-3 and 5-4. For a more reliable analysis force values have been considered instead of bond stress values in order to avoid differences coming from applied different total bond lengths. Based on the slope change observed for 15R_10S_15R and 15R_20S_15R configurations, an initial stiffness ratio has been calculated (F'/s'_a, Equation 5-3) based on a slip value fixed at point A (see Figure 5-11), and with the corresponding force value (F_A). Furthermore, for those specimens for which a change in the slope of the ascending branch has been observed, a second stiffness ratio has been further calculated (F''/s''_a, Equation 5-4), based on a fixed slip of 2 mm (B) and on the corresponding F_B force value. The slip corresponding to the second ascending branch has been fixed at 2 mm due to a lack of graph continuation for most of the 15R_20S_15R samples (because splitting of concrete occurred before pulling out of the bar). Table 5-11 summarizes the obtained values and Figure 5-12 allows for a comparison of the initial stiffness with respect to the completely ribbed configuration (30R). From these test results various observations can be made as discussed in the following sections.

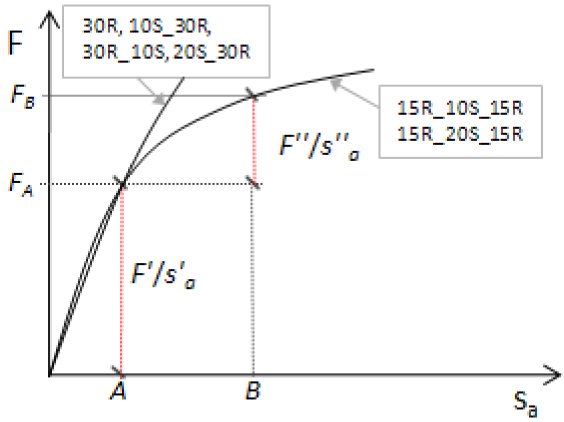

Figure 5-11 Schematic drawing of slope/stiffness calculation procedure

$$F'/s'_a = F_A/A \tag{5-3}$$

$$F''/s''_a = (F_B - F_A)/(B - A) \tag{5-4}$$

Table 5-11 Numerical slip and force values for slope/stiffness calculation

Configuration	***A (mm)***	***F_A (kN)***	***B (mm)***	***F_B (kN)***	***F'/s'$_a$ (kN/mm)***	***F''/s''$_a$ (kN/mm)***
30R	0,75	26,44	NA	NA	35,25	NA
15R_10S_15R	0,75	26,64	2	35,44	35,68	7,08
10S_30R	0,75	18,29	NA	NA	24,39	NA
30R_10S	0,75	27,84	NA	NA	37,11	NA
15R_20S_15R	0,93	32,07	2	36,92	35,29	4,54
20S_30R	0,93	22,07	NA	NA	23,73	NA

NA: not applicable

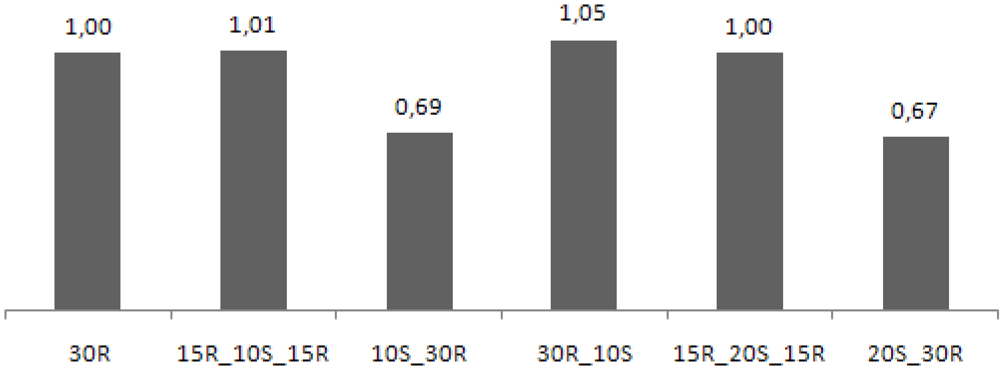

Figure 5-12 Comparative initial stiffness ratio at slip of 0,75 mm for 30R, 15R_10S_15R, 10S_30R and 30R_10S configurations and at 0,93 mm for 15R_20S_15R and 20S_30R configurations, taking 30R as reference.

3.5.1 Influence of adding a smooth area in the middle of the bond length

The main difference and characteristic of the bond behaviour of alternate pattern rebars comparing them to the completely ribbed samples is that when a smooth area (10 mm long) is positioned in the middle of the bond length (15R_10S_15R configuration), it can be observed that the first stage of the graph corresponding to the situation in which the bond stress is increasing, is divided into two different branches (whereas for completely ribbed strips only one ascending branch is observed): see Figure 5-13 for TC and Figure 5-14 for SCC. The first ascending stiffer branch extends on average up till a bond stress value of ~11,77 N/mm^2 at an average active end slip value of ~0,75 mm. If absolute values in terms of measured force are considered (to avoid differences related to different bond lengths) the stiffness of the first ascending branch can be expressed as F'/s'_a initial ratio and has a value of 35,68 kN/mm for the 15R_10S_15R configuration (see Table 5-11). If we then look at the completely ribbed samples (30R), at the same slip of 0,75 mm, the average force is ~26,44 kN, which implies an initial F'/s'_a ratio of 35,25 kN/mm. Thus, it can be concluded that both configurations develop comparable stiffness at first stage (slips up to 0,75 mm); see Figure 5-12 and Table 5-11. This conclusion is confirmed by the statistical t-test.

However, for the alternate pattern, a second ascending branch with a lower slope than the first one is further developed until the maximum bond stress is reached. The behaviour of this second branch is therefore less stiff than the first one (F''/s''_a= 7,08 kN/mm vs. F'/s'_a = 35,68 kN/mm) and makes the total (considering both ascending branches) $F_{max}/s_{a,Fmax}$ ratio to be up to 2,9 times smaller for the alternate pattern with 10 mm of smooth area in the middle of the bond length than for a completely ribbed bond length configuration. These slope differences are well observed in Figure 5-13 and Figure 5-14. Regarding bond strength values, only specimens that failed by pulling out of the bar are considered to make the comparison. Taking specimens tested under the same conditions of reinforcement and concrete type (also considering the samples with or without stirrups), with the only dissimilarity of bond length configuration (30R vs. 15R_10S_15R) and considering mean values together with their corresponding standard deviation, the statistical t-test results show that the differences between mean values are not significant to consider the bond strength values different, for any of the testing conditions (TC, SCC or TC with stirrups). In other words, comparable bond strength values are obtained for completely ribbed (30R) and for the alternate pattern (15R_10S_15R) configurations, although the values are reached at higher slip values for the alternate pattern. Note that for the calculation of the bond stress the bond length of the alternate pattern has been taken as 40 mm (sum of ribbed and smooth zones length), while for the completely ribbed configuration the bond length is 30 mm; consequently, the reached comparable bond strength shows that the smooth area is actively contributing to the developing of the bond forces.

These observations lead to the following statement. The smooth area between the two ribbed areas has an influence on the bond behaviour developed by the strip: it actively contributes to the development of the bond strength but the latter is reached at higher slip values. This phenomenon can be understood by looking to the failure aspect observed for the tested specimens, where shearing off of the concrete occurred following the axial direction of the steel reinforcement at the outer part of the rib level (as it is the case for a pull out type of failure according to [9]). From the failure aspect it becomes clear that the smooth area between the two ribbed parts acts as a large "rib" (see Figure 5-15 left, dashed zone). The stiffness of the concrete part to be sheared off by the ribbed area is higher (larger concrete volume) than the one at the surroundings of the smooth zone (see coloured zones vs. dashed ones in Figure 5-15 left). The different concrete volumes to be sheared off that are involved at the surroundings of ribbed or smooth zones are clearly visible by the microscopic inspection performed to the specimens for failure aspect analysis. The specimens have been submitted to epoxy injection procedure (as explained in Chapter 4) and were inspected both visually and by microscope. Figure 5-16 shows the different concrete volumes that have been sheared off (the fluorescent epoxy has filled the gap) at the surrounding of a ribbed area (Figure 5-16-a) and at the surrounding of a smooth area (Figure 5-16-b), observed by microscope inspection. Thus, when pulling forces are applied, the initial bond stiffness is higher than the one later developed until the maximum force is reached as larger concrete volume need to be sheared off at a first stage (corresponding to the coloured areas closer to the active end in Figure 5-15 left). This phenomenon explains the change in the slope observed in the first stage of the bond stress-slip relationship for alternate samples.

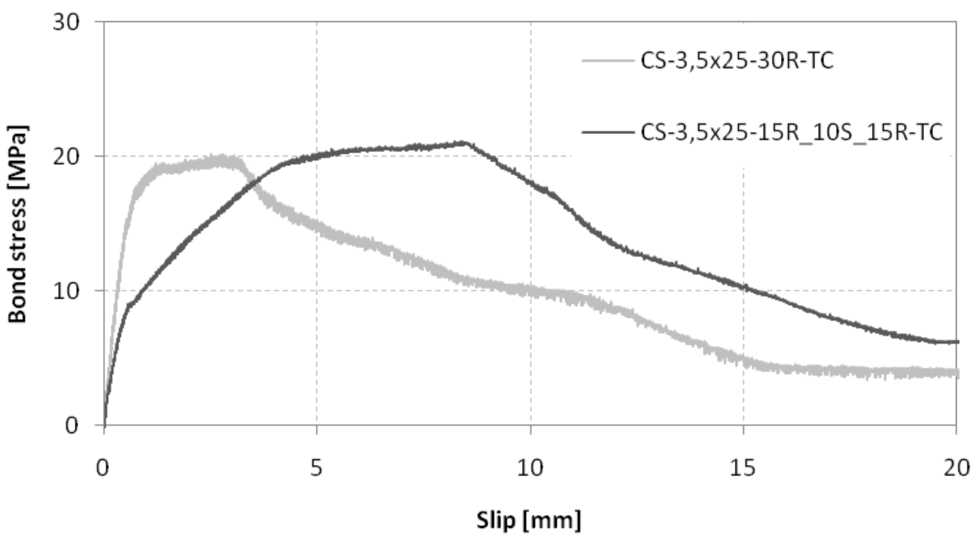

Figure 5-13 Bond stress-slip relationship. 30R vs. 15R_10S_15R (for TC)

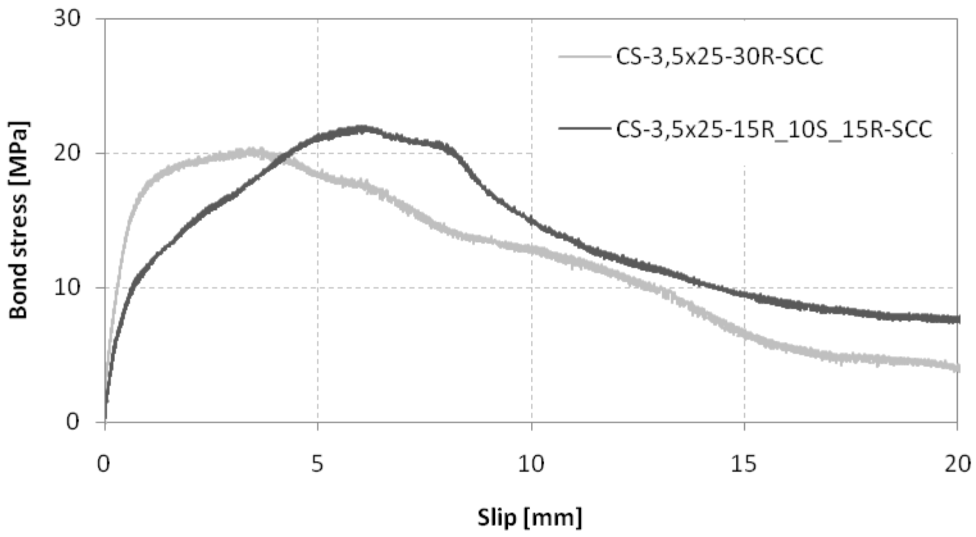

Figure 5-14 Bond stress-slip relationship. 30R vs. 15R_10S_15R (for SCC)

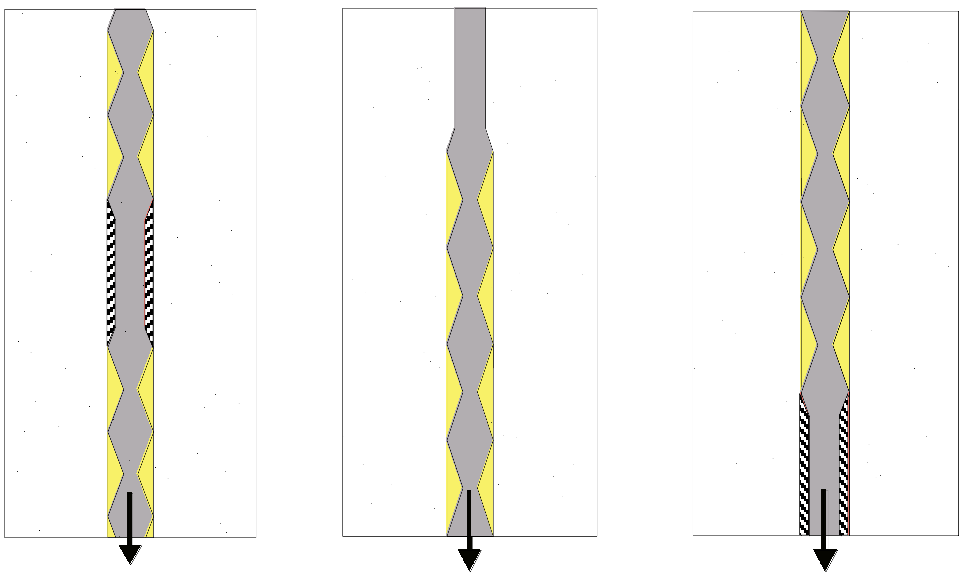

Figure 5-15 Schematic drawing of the shearing off of the concrete when pull out forces are applied to the alternate pattern with smooth area in the middle of the bond length (left), with the smooth area at the passive end (middle) and with smooth zone close to the plastic tube (right)

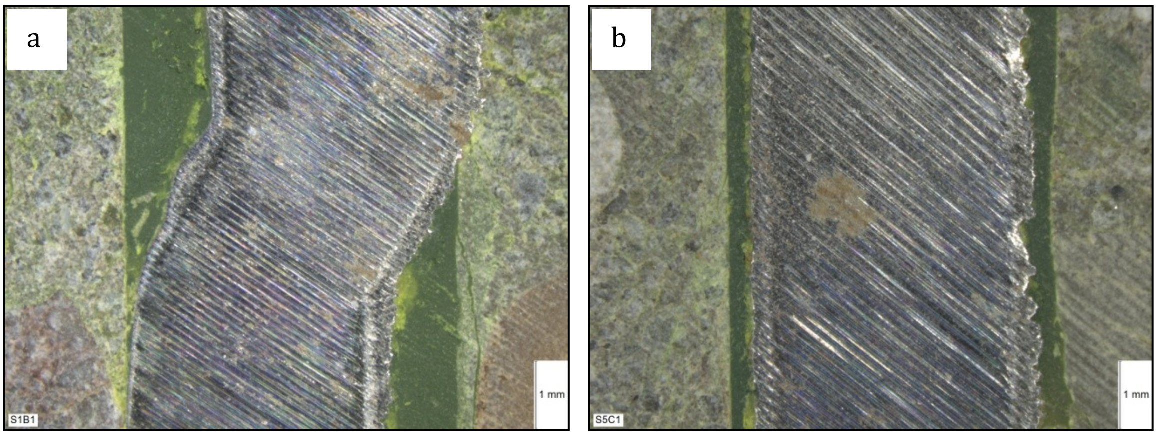

Figure 5-16 Failure aspect observed by microscopic inspection after epoxy injection procedure: a) at the surroundings of a ribbed area, b) at the surrounding of a smooth area

3.5.2 Influence of increasing the smooth area in the middle of the bond length

An interpretation of the influence of increasing the smooth area in the middle of the bond length from 10 mm to 20 mm is difficult due to a lack of pull out failure for the 15R_20S_15R configuration. However, the splitting behaviour observed together with the recorded higher force values reaffirms the active role of the smooth zone in developing bond stresses. Furthermore, the two ascending branches are again observed for this bond length configuration. The change in the slope for the 15R_20S_15R configuration occurs in average at higher slip and similar bond stress values (at 0,93 mm of slip at the active end and for 11,34 N/mm^2) compared to the 15R_10S_15R configuration. If the absolute measured force values are considered and a F'/s'_a ratio is calculated for the initial stage of each configuration (see Table 5-11), comparable values are obtained between 20 mm of smooth zone added in the middle of the bond length and 10 mm (35,29 kN/mm vs. 35,68 kN/mm, respectively, see Figure 5-12). These differences in the mean initial force/slip ratios are not significant according to the t-test, and therefore, it can be concluded that similar stiffness is developed at the initial stage of the bond behaviour for 15R_20S_15R and for 15R_10S_15R configurations. From the bond stress-slip curves (Figure 5-17) it can be observed that the tendency of the second ascending branch for alternate samples with 20 mm of smooth zone in the middle of the bond length is less stiff than for the 15R_10S_15R configuration. This tendency is verified by the stiffness calculation (Table 5-11), where a F''/s''_a ratio of 4,54 kN/mm is obtained for the second ascending branch for the 15R_20S_15R configuration (vs. F''/s''_a= 7,08 kN/mm obtained when a 10 mm long smooth area is placed in the middle of the bond length). If the same reasoning as before is used for explaining the two ascending branches tendency, the less stiff second ascending stage is obtained due to a larger smooth zone involved in this case.

Further observations in terms of developed bond strength values are difficult to make, due to the lack of pull out failure. However, it should be noted that in case of premature failure due to splitting instead of pull out, calculated f_b values refer to the registered maximum forces at splitting which are equal or smaller than the forces needed for a pull out type of failure to occur. From this observation it can be concluded that bond strength values related to the 15R_20S_15R configuration will be in the range (or higher) than for the 15R_10S_15R configuration.

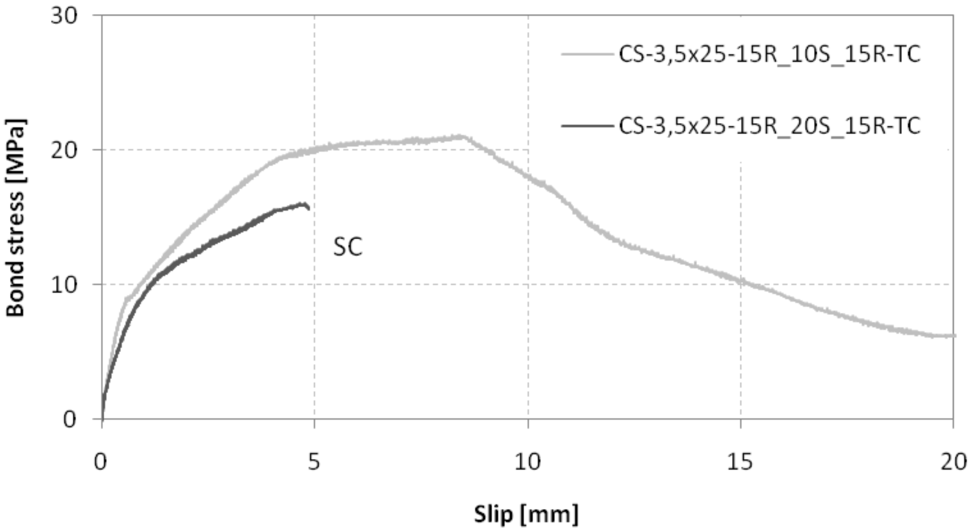

Figure 5-17 Bond stress-slip relationship. 15R_10S_15R vs. 15R_20S_15R

3.5.3 Influence of the smooth area position within the bond length

Influence of the position of the smooth area within the bond length is analyzed by moving it from the centre to the edges of the bond length: 10S_30R, 20S_30R and 30R_10S configurations, tested for CS embedded in TC. The most evident difference is that the two ascending branches tendency observed for the alternate pattern when the smooth area is positioned in the middle of the bond length, has now disappeared for the studied cases (Figure 5-18).

For specimens for which the smooth area has been positioned close to the passive end of the specimen (10S_30R and 20S_30R) the developed bond strength is considerably lower than for their equivalent configuration with smooth area in the middle of the bond length (up to 40% lower bond strength values). Furthermore, the initial stiffness of the ascending branch of the curves (F'/s'_a) for 10S_30R and 20S_30R configurations are respectively 31% and 33% lower than that of the 30R configuration (see Figure 5-12 and Table 5-11). For the calculation of the initial stiffness of the 10S_30R, force values at a slip of 0,75 mm have been considered as done for the 30R and 15R_10S_15R configurations.

On the other hand, force values at a slip of 0,93 mm has been used for 20S_30R as also done for the 15R_20S_15R configuration. It is therefore concluded that in case of having the smooth area close to the passive end, the smooth area does not contribute to the development of the bond strength, and decreases the stiffness of the bond capacity of the rebar. Furthermore, if it is assumed that the smooth area is not contributing to the development of the bond stress and therefore, only the ribbed zone is considered as bond length (l_b = 30 mm) for the calculation of the bond strength (see Equation 4-4), the calculated new bond strength , f_b, (15,58 N/mm^2) is still lower than to the one obtained for 30R (18,40 N/mm^2) and for 15R_10S_15R (20,31 N/mm^2).

Thus, the position of the smooth zone close to the passive end, not only does not contribute to the development of the bond stress but it also makes the total bond length to be less efficient on the development of the bond capacity of the rebar by decreasing both the bond strength and the bond stiffness developed by the rebar. This observation can be explained following the same criteria as for the case where the smooth zone is placed in the middle of the bond length. Looking to the shearing off of the concrete schematically drawn in Figure 5-15 (middle) for this configuration, it is clearly observed that no concrete need to be crushed at the surroundings of the smooth zone to activate the pull out type of failure. Thus, the smooth zone does not contribute to the development of any mechanical adhesion at early slips reducing the force needed for the pulling out of the rebar.

For the case in which the smooth area is placed close to the plastic tube (towards the active end), 30R_10S, both the developed bond strength (see Figure 5-18 and Table 5-10) as well as the stiffness of the ascending branch (Figure 5-12) are comparable to the ones of 30R configuration. If mean values are considered together with their corresponding standard deviation, and the statistical t-test tool is applied, the latter similarity is reaffirmed. In this case, the smooth area actively contributes to the development of the bond strength and the latter is reached at the same slip levels as for the completely ribbed configuration. The dashed area in Figure 5-15 right demonstrates that for activating the pulling out of the reinforcement, firstly the concrete around the smooth zone has to be sheared off, which explains the active role of the smooth area in the development of the bond capacity of the rebar. Furthermore, the position of the smooth zone close to the active end, followed by a continuous ribbed area, makes the total developed stiffness to be comparable to the one of 30R configuration.

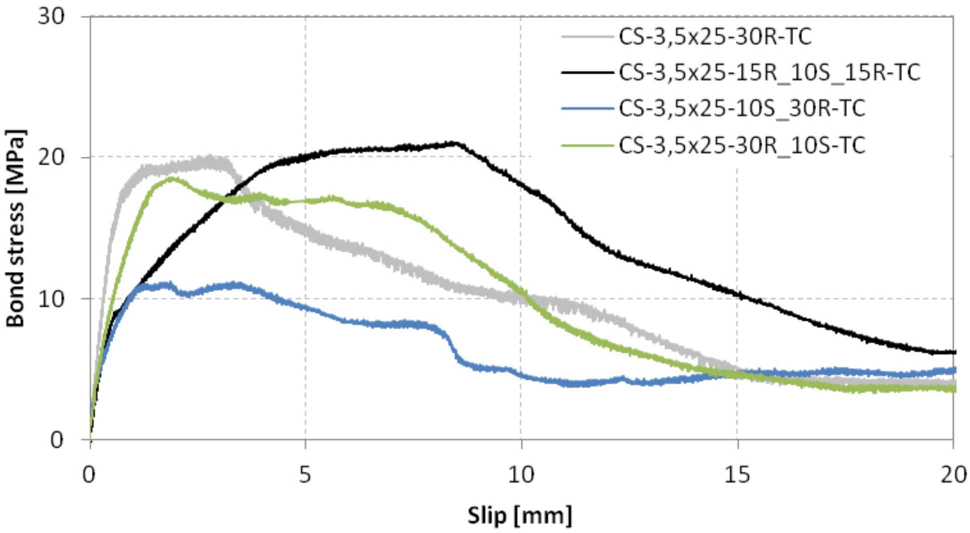

Figure 5-18 Bond stress-slip relationship. 30R vs. 15R_10S_15R vs. 10S_30R vs. 30R_10S

4 Analytical verification

4.1 General considerations

According to the available literature [4][10][11][12][13] the relative ribbed area, which is considered as a bond index, is directly proportional to the rib height, and inversely proportional to the clear rib spacing. However, as already mentioned in this work, optimum values of the relative rib area exist (f_R values between 0,05 and 0,10) which ensure the acceptable combination of the bond strength together with limiting deflections and crack openings of concrete structures [9].

On the other hand, regarding stiffness of the bond capacity (bond stress to slip ratio), it has been demonstrated that for smaller relative ribbed area values, the same bond stress levels are reached at higher slip values, i.e. the bond stiffness decreases with decreasing the relative ribbed area [12][14][15]. The latter has been experimentally tested by performing bond tests to reinforcements with a constant rib height and with increasing the clear rib spacing. Although not a clear trend is observed for the developed bond strength with decreasing the relative ribbed area, the trend in the slip at which the maximum bond stress is reached is clear: it increases with increasing of the clear rib spacing. Consequently, some authors [16][17] develop equations to predict the slip at which the maximum bond stress of a given reinforcement is reached. The one developed by Desnerck [17] (see Equation 5-5), has been already applied in Chapter 4 for characterizing the slip at maximum bond stress of the completely ribbed flat reinforcements tested in this study.

$$s_1 = 0{,}0032\ c^2 + 0{,}041 \qquad (5\text{-}5)$$

For the analytical study, the surface configuration of the rebars with an alternate rib pattern is considered at two different levels: a first rib level corresponding to the ribbed area with the rib parameters defined by the clear rib spacing c_1 and the rib height h_1 (see Figure 5-19); and the second level considering both the ribbed and the smooth zones, where the valley of the rib pattern corresponds to the smooth zone, as described in the discussion of the test results. The second rib level is defined by c_2 and h_2, as given by Figure 5-19. The average values of the rib defining parameters for the tested flat reinforcements with an alternate rib pattern are given in Table 5-12.

Table 5-12 Rib pattern defining parameters for the considered two surface configuration levels

Surface configuration	*Rib pattern*	*Clear rib spacing*	*Rib height*
Level 1	50R_10S	18 mm	1,4 mm
	50R_20S	18 mm	1,4 mm
Level 2	50R_10S	60 mm	0,7 mm
	50R_20S	70 mm	0,7 mm

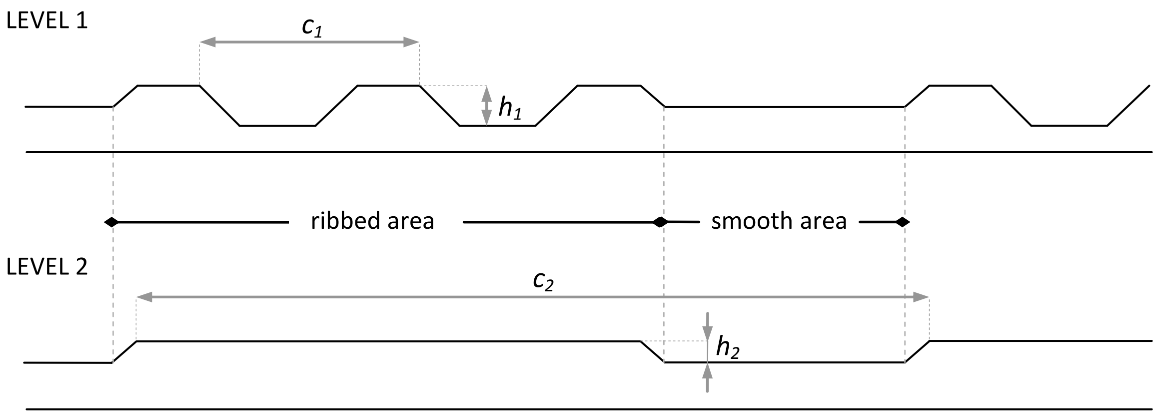

Figure 5-19 Schematic drawing of the surface configuration considered at two different levels

The analysis and understanding of the change in the slope in the ascending branch observed from the test results becomes more clear if these two levels of surface configuration are considered. When the smooth area is positioned in the middle of the bond length, between two ribbed zones, and considering the pulling direction, only the ribbed zone will be actively contributing to the bond stress development at the beginning of the test. Thus, it can be considered that only the surface configuration corresponding to the ribbed zone is active. At increasing loads, however, the second level of surface configuration (the one considering the ribbed and the smooth areas) will be activated by crushing of the concrete key developed at the surroundings of the smooth zone. Given the rib spacing differences involved for each considered surface configuration level, the stiffness of the bond capacity varies. Thus, at low loads, where only the ribbed zone is active, a smaller rib spacing is involved, which leads to a stiffer bond behaviour. On the other hand, when the smooth zone becomes active in the bond behaviour development, a higher rib spacing is involved, leading to a less stiff behaviour. Although the rib heights involved are not the same for the considered 2 surface configuration levels, note that $c_1 < c_2$, being $h_1/c_1 > h_2/c_2$, which means a smaller relative ribbed area involved for the situation in which the smooth zone is active, corresponding to less stiff bond behaviour.

For the bond length configurations applied in this work, 15R_10S_15R and 15R_20S_15R, the effective length of the ribbed zone positioned at the active end (15 mm) is smaller than the existing rib spacing corresponding to level 1 of the surface configuration (c_1 = 18 mm). Thus, for the analysis an effective rib spacing at level 1 of the surface configuration is defined: $c_{1,ef}$ = 15 mm. At increasing loads, the second level of surface configuration will be activated. The existing clear rib spacing for this rib level 2 is 60 mm for the 15R_10S_15R and 70 mm for the 15R_20S_15R bond length configuration (see Table 5-12). However, the effective length active on developing the bond forces are 40 mm and 50 mm, respectively (corresponding to the bond length for each configuration). Consequently, an effective rib spacing at level 2 of surface configuration is defined: $c_{2,ef}$ = 40 mm for 15R_10S_15R and $c_{2,ef}$ = 50 mm for 15R_20S_15R.

4.2 Proposed bond model for flat reinforcing elements with an alternate rib pattern

4.2.1 Based on the bond model given by the fib Model Codes

As previously done for the completely ribbed flat reinforcing elements tested in this work, the bond slip relationship given by the fib Model Codes [19][20], which is based on the work performed by Eligehausen et al. [21], is taken as reference. This model defines the bond behaviour of the reinforcement when embedded in concrete as a four different branches approach: a first ascending branch until the maximum bond stress is reached at a certain slip value (s_1), followed by a second phase of constant bond stress until a slip s_2. The third branch is a descending branch until a slip s_3 is reached at a bond stress level corresponding to the friction forces. The fourth and last branch is related to the frictional forces which are constant with increasing slip. This approach has been adopted for the completely ribbed flat rebars that have been tested in this work as given in Chapter 4: the first ascending branch has been modified according to the definition given by Soroushian [18] and the slip at maximum bond stress has been defined as given by Desnerck [17].

For the rebars with an alternate rib pattern, positioning the smooth area in between two ribbed zones within the bond length, the concept of a single ascending phase of the bond stress-slip curve is not suitable as two different branches are clearly observed from the test results as discussed previously. Figure 5-20 gives the comparison between the adapted curve proposed for completely ribbed bars (adaptation of the bond stress-slip relationship of fib Model Codes, see Chapter 4, Equations 4-36 to 4-39 and Table 4-17) versus the test result obtained for the alternate 15R_10S_15R configuration, tested for CS and embedded in TC. For applying the bond model curve, a characteristic compressive strength of 48 N/mm² (related to the hardened concrete properties registered) and a clear rib spacing of 18 mm have been assumed. Applying the curve for predicting the behaviour of the completely ribbed bars in case of an alternate pattern with the smooth area positioned in between two ribbed zones within the bond length appears not suitable.

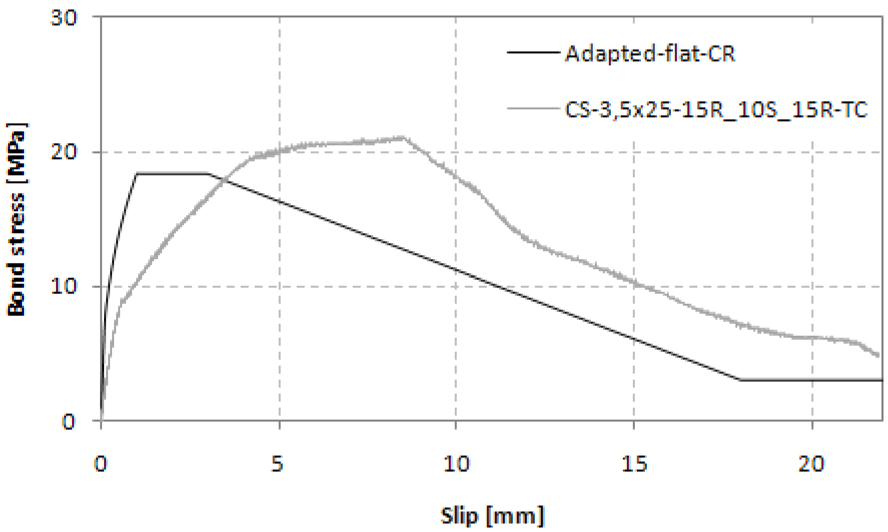

Figure 5-20 Comparison between the adapted curve for completely ribbed flat reinforcements and experimental result obtained for the alternate pattern, represented by the CS-15R_10S_15R specimen when tested in TC

Given the shape of the bond stress-slip curve observed for the flat rebars with an alternate rib pattern, the behaviour can be defined by 5 different phases (see Figure 5-21):

i. A first ascending branch which corresponds to the activation of the ribbed zone close to the active end. The surface configuration is at level 1 (see Figure 5-19) and the effective rib spacing is $c_{1,ef}$ = 15 mm for the tested specimens. The relation between the bond stress and the slip is given by Equation 5-6, based on the definition given by Soroushian [18] for the first ascending branch. The curve defining parameters are: τ_1 and s_1. τ_1 corresponds to the bond stress at the point where the change of the bond stiffness occurs and s_1 is the slip of the rebar related to the concrete at the same point (both related to level 1 of surface configuration).

$$\tau(s) = \tau_1 \, (s/s_1) \, e^{(1-(s/s_1)^{\alpha})/\alpha} \qquad 0 \le s \le s_1 \qquad (5\text{-}6)$$

ii. The second phase is also an ascending branch which extends from (s_1, τ_1) to (s_2, τ_{max}) and corresponds to the activation of the second level of surface configuration (see Figure 5-19). As explained previously, the effective rib spacing is considered to be $c_{2,ef}$ = 40 mm for the 15R_10S_15R bond length configuration and $c_{2,ef}$ = 50 mm for the 15R_20S_15R one, for the tested elements. The relation between the bond stress and the slip for this branch is given by Equation 5-7 and is taken as linear.

$$\tau(s) = \tau_{max} - (\tau_{max} - \tau_1)((s_2 - s)/(s_2 - s_1)) \qquad s_1 \leq s \leq s_2 \qquad (5\text{-}7)$$

iii. The third branch is the plateau at maximum bond stress and extends from s_2 to s_3. Equation 5-8 gives the analytical definition.

$$\tau(s) = \tau_{max} \qquad s_2 \leq s \leq s_3 \qquad (5\text{-}8)$$

iv. The fourth phase is represented as a linear descending branch going from the maximum bond stress value until the frictional stress (τ_f) is reached at a slip value s_4. Equation 5-9 gives the definition of this phase.

$$\tau(s) = \tau_{max} - (\tau_{max} - \tau_f)((s - s_3)/(s_4 - s_3)) \qquad s_3 \leq s \leq s_4 \qquad (5\text{-}9)$$

v. The last phase corresponds to the remaining frictional forces present at increasing slip due to the contact between the reinforcement and the concrete. It is given by Equation 5-10.

$$\tau(s) = \tau_f \qquad s \geq s_4 \qquad (5\text{-}10)$$

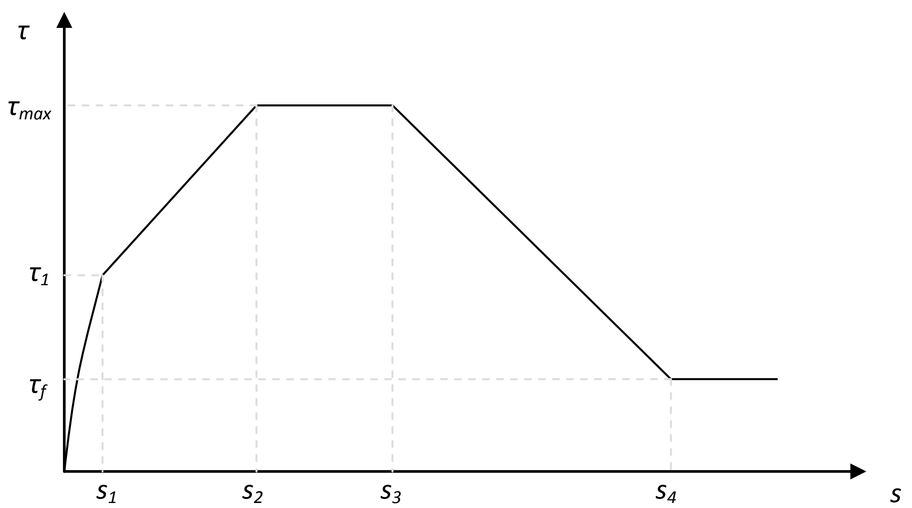

Figure 5-21 Proposed bond stress-slip relationship for flat rebars with an alternate rib pattern, when the smooth zone is positioned between two ribbed zones within the bond length

The parameters involved in the bond stress-slip relationship given by Equations 5-6 to 5-10, and plotted in Figure 5-21, have been defined as follows: the values of τ_1, τ_{max} and τ_f are defined only dependant on the square root of the characteristic compressive strength of the applied concrete, and the mean value of the experimental results is used for calculating the relating factor. For the calculation, experimental results are considered independent of the reinforcement material and concrete type, and independent of the use of confinement reinforcement (as it has been concluded from the discussion of the test results), and a characteristic compressive strength of the concrete of 48 N/mm² (applying $f_{ck} = f_c$ - 8 N/mm² [22] on the tested concrete properties, see Table 5-3) has been considered. The obtained parameters are given in Table 5-13 and are derived as follows. Based on the test results obtained for both 15R_10S_15R and 15R_20S_15R configurations, τ_1 equals 1,69$\sqrt{f_{ck}}$. For definition of τ_{max} and τ_f, only experimental results regarding the 15R_10S_15R are analyzed due to the lack of pull out type of failure for the configuration with 20 mm of smooth zone. Calculated values give τ_{max} = 2,85 $\sqrt{f_{ck}}$ and τ_f = 0,27 τ_{max}. The value of α has been taken equal 0,8 as done for the bond model proposed for completely ribeed flat rebars in Chapter 4.

The values of s_1 and s_2 can be calculated if they are considered as the slip values at which the maximum bond stress are reached for the surface configuration levels 1 and 2, respectively, and applying the formula given by Desnerck [17], see Equation 5-5. The value of s_3 (the slip at which the bond stress starts decreasing) is given by the fib Model Codes as a value coming from a large number of experimental results, and not dependant on any other parameter. On the other hand, s_4 is defined equal to the clear rib spacing of the reinforcement. However, given the involved alternate pattern and the concept of two levels of surface configuration, it is difficult to establish a single value for the clear rib spacing. Furthermore, given the lack of pull out failure present during the testing program carried out for the 15R_20S_15R configuration, experimental values of s_2, s_3 and s_4 are only available for the 15R_10S_15R configuration, which makes the analytical verification of the test data difficult.

Appendix B compiles individual bond test results and compares them with the predicted behaviour, based on the proposed bond model. This is further elaborated in the following.

For the analytical verification of the 15R_10S_15R configuration, experimental results of the specimens that failed by pulling out of the reinforcement have been considered and s_3 has been defined equal to 8 mm and s_4 equal to 20 mm. On the other hand, as explained before, the effective rib spacing related to the level 1 of surface configuration is considered for c_1 (15 mm) and the one related to the level 2 of surface configuration for c_2 (40 mm). Figure 5-22 compares the adapted bond stress-slip relationship to the experimental results obtained for CS when embedded in TC and SCC, for the 15R_10S_15R configuration. A good agreement is observed between the curves.

The analytical verification of the 15R_20S_15R configuration has been limited until the maximum bond stress is reached as the experimental values of s_3 and s_4 are not available. The experimental maximum bond stress values are neither available for this configuration.

However, as τ_{max} is taken only dependant on the characteristic compressive strength of the concrete in this analysis, the same value as for the 15R_10S_15R configuration is considered. Regarding rib spacing values involved in this case, the effective rib spacing used for the calculation of s_1 is taken equal to 15 mm (level 1), while 50 mm is considered for the calculation of s_2 (level 2). Figure 5-23 gives the comparison between the analytical curve for flat reinforcement with an alternate rib pattern and the experimental curves obtained for SS when embedded in both TC and SCC, for the 15R_20S_15R configuration. Although the entire curve cannot be plotted due to the lack of pull out type of failure, the two ascending branches defined by the adapted bond stress-slip relationship are in good agreement with the experimental results.

For comparing the two bond length configurations analyzed in this work, Figure 5-24 gives the adapted curves for the two tested configurations: 15R_10S_15R and 15R_20S_15R. The influence of the length of the smooth area between the two ribbed zones within the bond length is clearly observed: the slip at which the maximum bond stress is reached increases with increasing the length of the smooth zone, leading to a less stiff bond behaviour.

Table 5-13 Parameters defining the bond stress –slip curve of the proposed model for flat rebars with an alternate rib pattern

Parameter	***Adapted-flat-R_S_R***
s_1 *(mm)*	$0{,}0032\ c_1^2 + 0{,}041$
s_2 *(mm)*	$0{,}0032\ c_2^2 + 0{,}041$
s_3 *(mm)*	8 *
s_4 *(mm)*	20 *
α	0,8
τ_1 *(N/mm²)*	$1{,}69\sqrt{f_{ck}}$
τ_{max} *(N/mm²)*	$2{,}85\sqrt{f_{ck}}$
τ_f *(N/mm²)*	$0{,}27\ \tau_{max}$

* For 15R_10S_15R specific bond length configuration

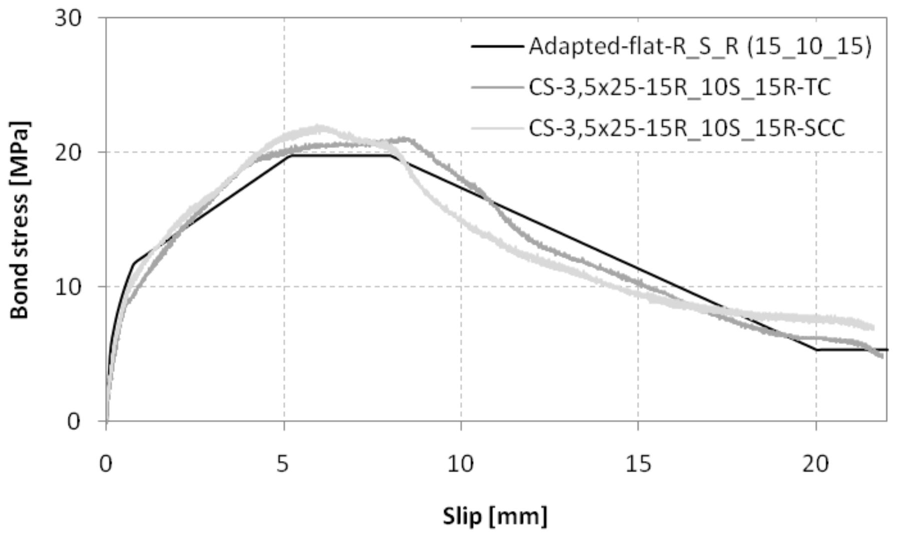

Figure 5-22 Bond stress-slip behaviour for flat rebars with an alternate rib pattern. Proposed model for the 15R_10S_15R bond length configuration

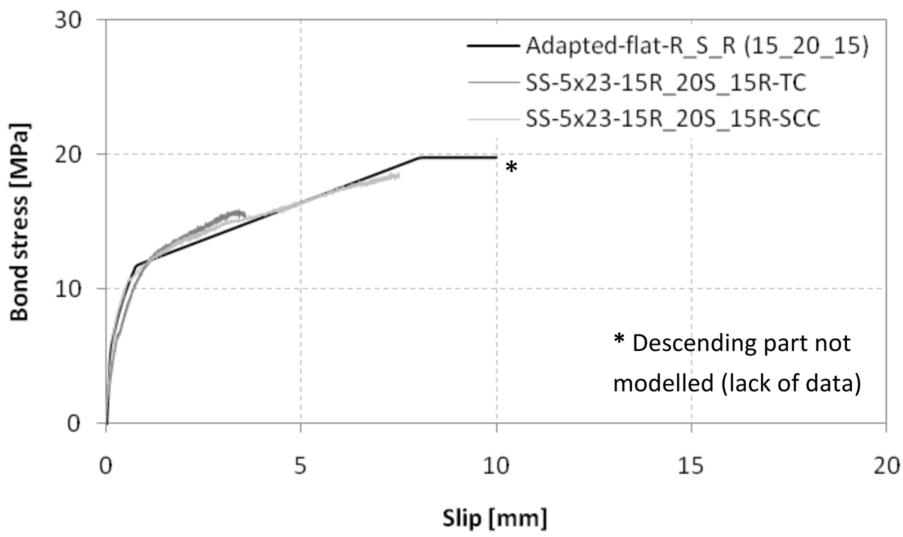

Figure 5-23 Bond stress-slip behaviour for flat rebars with an alternate rib pattern. Proposed model for the 15R_20S_15R bond length configuration

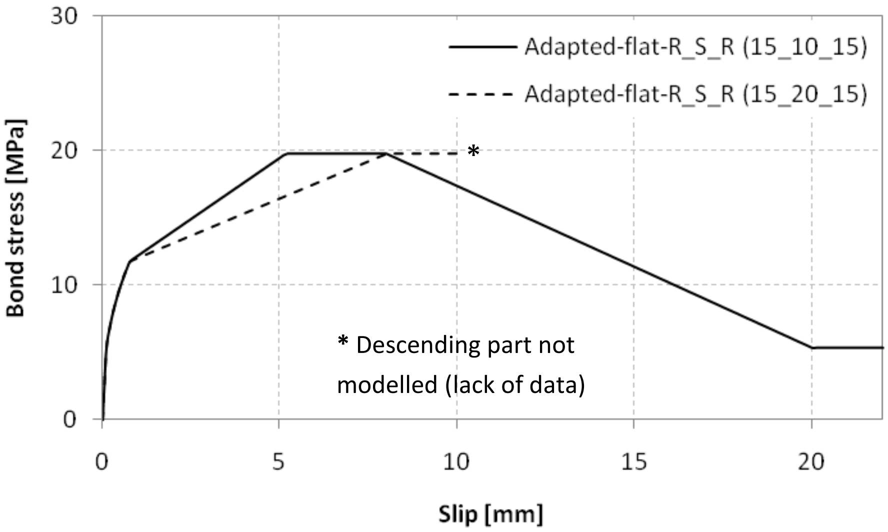

Figure 5-24 Analytical bond stress-slip behaviour for flat rebars with an alternate rib pattern.. 15R_10S_15R vs. 15R_20S_15R

4.2.2 Characteristic values of τ_1, τ_{max} and τ_f

As performed for the completely ribbed flat reinforcements, a more conservative approach is applicable based on characteristic values calculated from the mean values and given the variability of the test results. The "Bayesian prediction method with vague prior distributions" has been applied for the calculation of characteristic values of the bond stress for a fractile of 5%, following the description given in Chapter 4. According to λ values tabulated in [23] and [24], the Bayesian method is applied for this analysis with a value of λ equal to 2,00.

According to the estimated characteristic values the bond stress corresponding to the end of the first ascending branch (τ_1), the maximum bond stress (τ_{max}) and the frictional one (τ_f) are defined as follows: $\hat{\tau}_{1,0,05}$ = 1,18$\sqrt{f_{ck}}$, $\hat{\tau}_{max,0,05}$ = 2,48$\sqrt{f_{ck}}$ and $\hat{\tau}_{f,0,05}$ = 0,17τ_{max}. Figure 5-25 and Figure 5-26 give the mean proposed model curve together with the characteristic (k) curve obtained considering the Bayesian method, for the case of 15R_10S_15R and 15R_20S_15R, respectively.

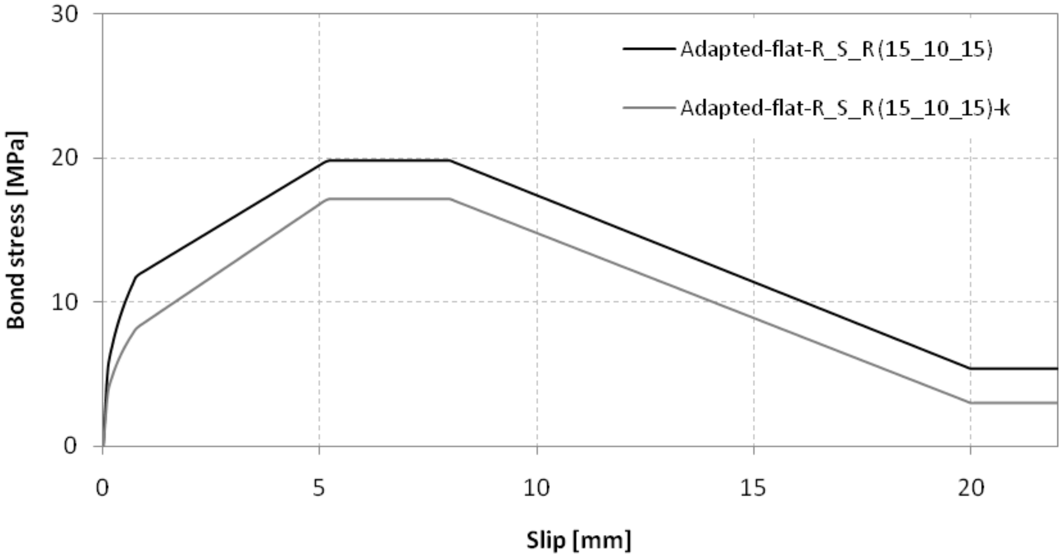

Figure 5-25 Bond stress-slip behaviour for flat rebars with an alternate rib pattern. Mean and characteristic (k) curves of the proposed model. For 15R_10S_15R configuration

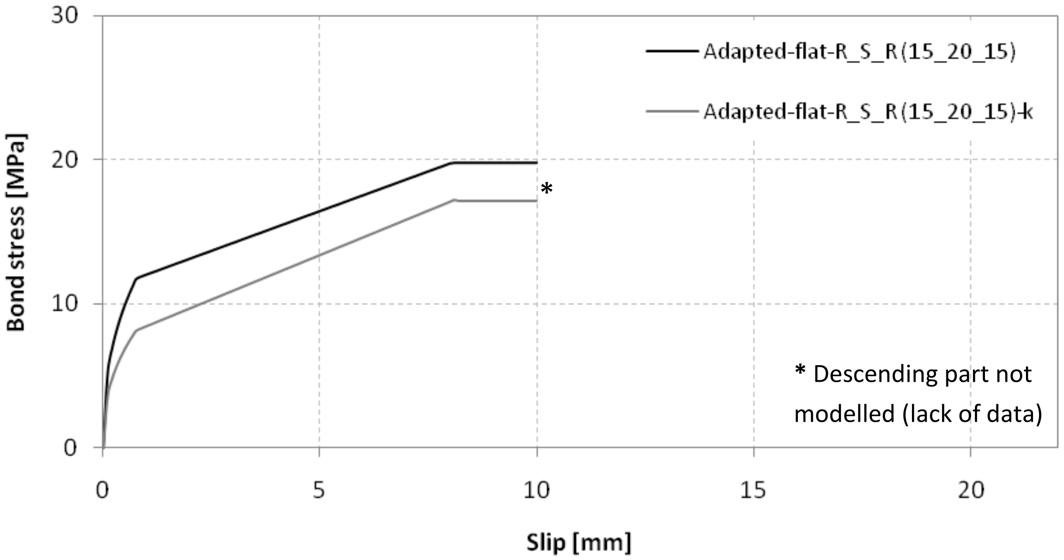

Figure 5-26 Bond stress-slip behaviour for flat rebars with an alternate rib pattern. Mean and characteristic (k) curves of the proposed model. For 15R_20S_15R configuration

5 Conclusions

The bond behaviour of flat rebars with an alternate rib pattern, combing smooth and ribbed areas, is generally characterized by a high, yet less stiff, bond strength development. This has been observed from 54 pull out tests. Both CS and SS have been used for reinforcement and both TC and SCC for embedding. Extra samples containing extra confinement reinforcement in form of stirrups have been also tested to avoid the splitting tendency observed during first tests. Different bond length configurations have been defined and tested depending on the smooth area length and its position within the bond length.

1. Regarding the influence of material type (steel and concrete) on the bond capacity of flat ribbed rebars with comparable perimeter (same contact area between steel and concrete for the same bond length), it is concluded that comparable bond behaviour is developed by CS and SS flat rebars, independently of being embedded in TC or in SCC. Indeed, though limited differences (up to ~10%) were found, they proved not significant when considering variability of the test results. These results are in line with the conclusions coming from Chapter 4 where no significant influence of steel and concrete material was observed for completely ribbed flat rebars.

2. Providing extra stirrups avoids the splitting tendency observed during testing. However, for specimens that failed by pull out of the rebar, no influence is observed on the developed bond capacity when confinement reinforcement is added to the specimens.

3. The use of alternate rib patterns combining smooth and ribbed areas does influence the bond capacity of the steel rebar, both in terms of bond strength and stiffness of the bond action:

    a. If a smooth area of 10 mm is positioned in the middle of the bond length, in between 2 ribbed zones of 15 mm each, the bond strength is comparable to the one developed by 30 mm of continuous ribbed zone bond length. However, the bond strength development occurs at up to 5 times larger slips (less stiff bond behaviour).

    b. The larger slip is caused, although initially comparable stiffness, by a second less stiff ascending stage for the samples with smooth area in the middle of the bond length.

    c. It is believed that the second less stiff ascending branch results from a secondary effect caused by the smooth zone, due to the concrete key formed at its surroundings. This creates a second level of rib spacing.

d. According to the tested parameters, the larger the smooth zone in the middle of the bond length, the less stiff is the second ascending branch.

e. If the smooth zone is positioned at the passive end of the bond length, the bond capacity of the rebar is negatively affected decreasing both the bond strength and the stiffness of the bond action.

f. When the smooth area (10 mm) is positioned close to the plastic tube, towards the active end of the bond length, the smooth zone does actively contribute to the development of the bond strength reaching comparable values as for the completely ribbed configuration, and at comparable slip values.

4. The fib Model Codes [19][20] based bond model adaptation proposed in Chapter 4 for completely ribbed flat rebars does not represent the behaviour observed for flat rebars with an alternate rib pattern, when the smooth zone is positioned between two ribbed zones within the bond length.

5. For the bond modelling, the surface configuration of the rebars with an alternate rib pattern is considered at two different levels: a first rib level corresponding to the ribbed area and a second level considering both the ribbed and the smooth zone.

6. A new bond stress-slip relationship has been defined for flat rebars with an alternate rib pattern, when the smooth zone is positioned between two ribbed zones within the bond length. The curve is defined by 5 different branches (Equations 5-13 to 5-17), and comprises two differentiated ascending branches depending on the surface configuration level active at the moment. The curve defining parameters are given in Table 5-14, where the slips of the two ascending branches are calculated dependant on the rib spacing involved for each surface configuration level (c_1 and c_2). The values of s_3 and s_4 have been set at 8 mm and 20 mm, respectively for the 15R_10S_15R bond length configuration. However, regarding the the 15R_20S_15R configuration, the descending part of the curve has not been modelled due to lack of data.

   Values for the bond stress at which the change of the slope of the ascending branch occurs (τ_1), the maximum bond stress (τ_{max}) and the remaining frictional bond stress (τ_f) have been defined both in terms of mean and characteristic bond behaviour. For the latter, the "Bayesian prediction method with vague prior information" method has been used to assess the 5% fractile. The obtained bond model parameters are given in Table 5-14.

$$\tau(s) = \tau_1\ (s/s_1)\ e^{(1-(s/s_1)^{\alpha})/\alpha} \qquad 0 \le s \le s_1 \qquad (5\text{-}11)$$

$$\tau(s) = \tau_{max} - (\tau_{max} - \tau_1)((s_2 - s)/(s_2 - s_1)) \qquad s_1 \le s \le s_2 \qquad (5\text{-}12)$$

$$\tau(s) = \tau_{max} \qquad s_2 \le s \le s_3 \qquad (5\text{-}13)$$

$$\tau(s) = \tau_{max} - (\tau_{max} - \tau_f)((s - s_3)/(s_4 - s_3)) \qquad s_3 \le s \le s_4 \qquad (5\text{-}14)$$

$$\tau(s) = \tau_f \qquad s \ge s_4 \qquad (5\text{-}15)$$

Table 5-14 Parameters defining the bond stress –slip curve of flat rebars with and alternate rib pattern

Parameter	***Mean curve***	***Characteristic curve***
s_1 *(mm)*	0,0032 c_1^2 + 0,041	0,0032 c_1^2 + 0,041
s_2 *(mm)*	0,0032 c_2^2 + 0,041	0,0032 c_2^2 + 0,041
s_3 *(mm)*	8 *	8 *
s_4 *(mm)*	20 *	20 *
α	0,8	0,8
τ_1 *(N/mm²)*	1,69 $\sqrt{f_{ck}}$	1,18 $\sqrt{f_{ck}}$
τ_{max} *(N/mm²)*	2,85 $\sqrt{f_{ck}}$	2,48 $\sqrt{f_{ck}}$
τ_f *(N/mm²)*	0,27 τ_{max}	0,17 τ_{max}

* For 15R_10S_15R specific bond length configuration

6 References

[1] Matière M. (2010) *Method for producing a reinforced concrete part, and thus-produced part*. International Patent application: WO 2010/067023 A1

[2] CEN (2009) EN 12350 *Testing fresh concrete.* European Committee for Standardization, Brussels

[3] CEN (2009) EN 12390 *Testing hardened concrete*. European Committee for Standardization, Brussels

[4] CEN (2010) EN ISO 15630 *Steel for the reinforcement and prestressing of concrete-Test methods-Part 1: Reinforcing bars, wire rod and wire.* European Committee for Standardization, Brussels

[5] CEN (2005) EN 10088:2005 *Stainless steels - Part 1: List of stainless steels*. European Committee for Standardization, Brussels

[6] RILEM (1970) *Technical Recommendations for the Testing and Use of Construction Materials: RC6, Bond Test for reinforcing Steel. 2. Pull-out test*. International union of laboratories and experts in construction material, systems and structures

[7] ISO (2004) ISO 7500-1 *Metallic materials - Verification of static uniaxial testing machines - Part 1: Tension/compression testing machines - Verification and calibration of the force-measuring system.* International Organization for Standarization, Geneva

[8] Darwin D. (2005) *Tension development length and lap splice design for reinforced concrete members*. Progress in Structural Engineering and Materials, Vol 7(4): 210-225

[9] fib (2000) *Bond of reinforcement in concrete. State of the art report*. fib Bulletin 10. International Federation for Structural Concrete, Switzerland

[10] Hamad B.S. (1995) *Comparative bond strength of coated and uncoated bars with different rib geometries*. ACI Materials Journal, Vol 92 (6), pp 579-590

[11] Gomes Barbosa M.T., Sanchez Filho E. S., Mayra de Oliveira T., Dos Santos W.J. (2008) *Analysis of the relative rib area of reinforcing bars pull out tests*. Materials Research, Vol 11 (4), pp 453-457

[12] Hamad B.S. (1995) *Bond strength improvement of reinforcing bars with specially designed rib geometries*. ACI Structural Journal, Vol 92 (1), pp 3-13

[13] Semchenkov A., Meshkov V., Kvasnikov A. (2009) *Bond to concrete action of reinforcing bars with different deformation patterns*. Structural Concrete, Vol 10 (4), pp 203-209

[14] Darwin D., Graham K.E. (1993) *Effect of deformation height and spacing on bond strength of reinforcing bars*. ACI Structural Journal, Vol 90 (6): 646-657

[15] Hao Q., Wang Y., He Z., Ou J. (2009) *Bond strength of glass fiber reinforced polymer ribbed rebars in normal strength concrete*. Construction and Building materials, Vol 23: 865-871

[16] Harajli M.H., Hout M., Jalkh W. (1995) *Local bond stress-slip behaviour of reinforcing bars embedded in plain and fiber concrete*. ACI Materials Journal, Vol 92 (4), pp 343-354

[17] Desnerck P. (2011) *Compressive, bond and shear behaviour of powder-type self-compacting concrete*. PhD Dissertation, Ghent University, Ghent

[18] Soroushian P., Choi K.B., Park G.H., Aslani F. (1991) *Bond of deformed bars to concrete: effects of confinement and strength of concrete*. ACI Materials Journal, Vol 88 (3): 227-232

[19] CEB-FIP (1993) *Model Code 1990 – Design Code.* International Federation for Structural Concrete, Switzerland

[20] fib (2010) *Model Code 2010 – First complete draft*. fib Bulletin 55. International Federation for Structural Concrete, Switzerland

[21] Eligehausen R., Popov E. P., Bertero V. V. (1983) *Local bond stress-slip relationship of deformed bars under generalized excitations*. Report UCB/EERC-83/23, University of California, Berkeley

[22] CEN (2004) Eurocode 2: EN 1992-1-1: *Design of concrete structures - Part 1-1: General rules and rules for buildings*. European Committee for Standardization, Brussels

[23] CEN (2002) Eurocode 0: EN 1990: *Basis of the structural design.* European Committee for Standardization, Brussels

[24] ISO (1998) ISO 2394 *General principles on reliability for structures.* International Organization for Standarization, Geneva

Chapter 6 Tension Stiffening and Cracking Behaviour of Flat Rebars with Continuous or Alternate Rib Pattern

1 Introduction

The idea of combining alternately ribbed and smooth areas within the same reinforcement deals with the expected improvement of the cracking behaviour of tensile members reinforced with this type of alternate rib pattern rebars. The cracking behaviour and more general the serviceability behaviour is a crucial aspect for the use of a structure. To understand and predict the effect of the alternate rib pattern on the serviceability behaviour, tests on reinforced tensile members are conducted. These so-called “tension stiffening” tests typically consist of a tensile test on a reinforcing bar embedded in a concrete prism. A total of 16 tension stiffening tests have been performed at the Magnel Laboratory for Concrete Research. Studied parameters comprise reinforcement geometry (comparing flat rebars to standard round ones), reinforcement material (standard carbon steel compared to ferritic stainless steel), concrete type (conventionally vibrated concrete vs. self compacting concrete), the effect of the alternate pattern (completely ribbed samples compared to strips containing both ribbed and smooth areas) and the effect of the length of both the ribbed and/or the smooth zone (different ribbed-smooth configurations).

Results of the tension stiffening tests are presented and discussed in this chapter. Stress of the steel at first cracking is analyzed together with the mean crack opening and mean crack spacing at 50% of the yielding stress of each rebar. Stress-strain curves are also provided, which compared to the tensile behaviour of the naked rebar, allow for a visualization of the tension stiffening effect. Other cracking parameters like mean crack width, total crack opening, maximum crack width and mean crack spacing are also given in function of the tensile stress of the reinforcement. Comparison of the test results to existing standards and design models is also provided. Furthermore, new equations are proposed for prediction of the mean crack width for completely ribbed flat rebars, and for rebars with an alternate rib pattern.

Although the tension stiffening effect and cracking behaviour at serviceability state have been extensively studied for standard carbon steel round bars, no literature has been found regarding the tension stiffening and cracking behaviour of flat stainless steel rebars with or without alternate rib pattern.

2 Test program

Table 6-1 gives an overview of the test program in terms of materials used and reinforcement rib configuration (the number between brackets gives the concrete casting batch number). Both standard carbon steel (CS) and stainless steel (SS) flat rebars are tested, with 3,5x25 mm^2 and 5x23 mm^2 cross sectional areas, respectively. The stainless steel grade used for these tests is as mentioned in the previous chapter a ferritic SS, grade 1.4017 according to the European Standard EN 10088 [1]. For the surface pattern analysis, both material types are tested with completely ribbed (CR) and with 50 mm ribbed area followed by 10 mm of smooth area (50R_10S) configurations. However, only stainless steel strips are further investigated for other alternate pattern configurations: 100 mm of ribbed area followed by 10 mm or 20 mm of smooth length and 150 mm of ribbed area with 10 or 20 mm of smooth length (100R_10S, 100R_20S, 150R_10S and 150R_20S, respectively).

Besides flat elements, standard carbon steel ribbed reinforcing bars are used for comparison (Table 6-1). Two different diameters, Ø10 mm and Ø12 mm (comparable to the two different cross sectional areas of the flat elements), are tested. Both traditional concrete (TC, batch 1 and 2) and self compacting concrete (SCC, batch 3) are investigated. Besides reference bars and completely ribbed flat strips, only 100R_10S and 100R_20S alternate pattern configurations are tested using SCC, while TC is applied for all test configurations (Table 6-1).

Designation of each material (Table 6-1) is done based on the following sequence: steel material type (CS or SS), dimensions of the cross sectional area and surface rib configuration (CR, 50R_10S, 100R_10S, 100R_20S, 150R_10S or 150R_20S).

Table 6-1 Tension stiffening tests (1 specimen per type)

Material	*Geometry*	*Rib pattern**	*Rebar designation*	*TC*	*SCC*
CS	Ø10 mm	CR	CS-Ø10-CR	(1)	(3)
	Ø12 mm	CR	CS-Ø12-CR	(2)	(3)
	$3,5x25\ mm^2$	CR	CS-3,5x25-CR	(1)	(3)
		50R_10S	CS-3,5x25-50R_10S	(1)	-
SS	$5x23\ mm^2$	CR	SS-5x23-CR	(1)	(3)
		50R_10S	SS-5x23-50R_10S	(2)	-
		100R_10S	SS-5x23-100R_10S	(2)	(3)
		100R_20S	SS-5x23-100R_20S	(2)	(3)
		150R_10S	SS-5x23-150R_10S	(2)	-
		150R_20S	SS-5x23-150R_20S	(2)	-

* CR: completely ribbed; 50R_10S: alternate pattern 50 mm ribbed followed by 10mm smooth; 100R_10S: alternate pattern 100 mm ribbed followed by 10 mm smooth; etc.

2.1 Materials

2.1.1 Concrete

To cast the specimens for the different test series, 3 concrete batches have been applied. The same concrete composition as applied before has been used for the tension stiffening specimens. The details about the composition are provided in Chapter 4 (Table 4-2, page 99). Mixing time has been taken equal to 3 minutes. Concrete compaction (for TC) is executed by means of a vibrating needle. Both mixing and casting have been performed at ambient laboratory conditions. The fresh concrete is placed in the formwork, in which the bar is kept horizontal in the axis of the mould. Demoulding of the test specimens is done 24 hours after casting. Curing of the casted specimens takes place in a wet room (20 ± 2 °C and 95 ± 3 % of relative humidity) for the first seven days, after which the specimens are stored at ambient laboratory conditions until the age of testing (28 days).

Properties of the fresh concrete are given in Table 6-2. Due to the difference between the fluidity of TC and SCC, different tests are used to assess those parameters for each concrete type. Slump test (by Abraham's cone) and flow test (by shaking table) are performed for TC. On the other hand, both the Abraham's cone slump flow and a "v"-shape funnel are used for measuring the flow properties of SCC. The density of each mixture is also measured. Tests are performed according to EN 12350 [2].

Properties of the hardened concrete at 28 days are given in Table 6-3. Per batch, 3 cylinders (Ø150 mm x 300 mm) and 3 cubes (150 x 150 x 150 mm^3) have been casted for determination of the compressive strengths, f_c and $f_{c,cub150}$ respectively. The tensile strength is determined by performing bending tests on 3 prisms (150 x 150 x 600 mm^3) ($f_{ct,fl}$) and by splitting tests on the remaining halves of the tested prisms ($f_{ct,sp}$). The secant modulus of elasticity E_c is derived from a compressive test on 1 cylinder (Ø150 mm x 300 mm). Tests are performed following EN 12390 [3]. Furthermore, direct tensile tests are performed to 3 cylindrical cores (Ø113 mm x 120 mm) extracted from 3 cubes (150 x 150 x 150 mm^3) in order to obtain the tensile strength of the concrete (f_{ct}), following NBN B15-211[4].

Table 6-2 Fresh concrete properties

Batch	*Type of concrete*	*Slump (mm)*	*Flow (-)*	*Slump flow (mm)*	*V-tunnel (s)*	*Density (kg/m³)*
1	TC	75	1,52	-	-	2400
2	TC	110	1,60	-	-	2400
3	SCC	-	-	800	7,74	2350

Table 6-3 Hardened concrete properties at 28 days

Batch	*Type of concrete*	$f_{c,cub150}$ *(N/mm²)*	f_c *(N/mm²)*	f_{ct} *(N/mm²)*	$f_{ct,fl}$ *(N/mm²)*	$f_{ct,sp}$ *(N/mm²)*	E_c *(N/mm²)*
1	TC	65,6	55,9	3,3	4,4	4,2	39000
2	TC	60,1	52,3	3,6	4,1	3,7	38000
3	SCC	64,2	55,4	3,3	5,0	4,4	38500
Average	Total	63,3	54,5	3,4	4,5	4,1	38500
St. dev.		2,86	1,95	0,17	0,46	0,36	500

2.1.2 Steel

Yield strength, ultimate strength and ultimate strain are obtained by performing tensile tests to each steel rebar (3 tests per type), following EN ISO 15630 [5]. Average values for each reinforcement type, together with the values of nominal cross sectional area and nominal perimeter, are presented in Table 6-4. Note, that for flat rebars the yield strength is taken as the proof strength at 0,2% of strain.

Given the limited availability of the test material, tensile tests on flat reinforcements have been performed only for CR, 50R_10S and 50R_20S configurations, both for CS and for SS. However, given the highly similar tensile behaviour observed for CR, 50R_10S and 50R_20S configurations (see tensile tests results in Figure 6-1 for CS and Figure 6-2 for SS), and being these alternate patterns the most different patterns in comparison to the CR configuration, similar tensile behaviour is also assumed for 100R_10S, 100R_20S, 150R_10S and 150R_20S configurations. Figure 6-3 compares the tensile stress-strain behaviour of the applied strips with the tensile behaviour of round reference bars.

Table 6-4 Embedded steel properties

Bar/Strip	*Area (mm^2)*	*Perimeter (mm)*	*Yield strength (N/mm^2)*	*Tensile strength (N/mm^2)*	*Ultimate strain (%)*
CS-Ø10-CR	78,5	31,4	574	642	9,87
CS-Ø12-CR	113,1	37,7	526	566	3,64
CS-3,5x25-CR	87,5	57,0	450	630	8,75
CS-3,5x25-50R_10S	87,5	57,0	470	645	7,25
SS-5x23-CR	115,0	56,0	490	630	3,83
SS-5x23-50R_10S	115,0	56,0	480	630	3,50
SS-5x23-100R_10S	115,0	56,0	*nda*	*nda*	*nda*
SS-5x23-100R_20S	115,0	56,0	*nda*	*nda*	*nda*
SS-5x23-150R_10S	115,0	56,0	*nda*	*nda*	*nda*
SS-5x23-150R_20S	115,0	56,0	*nda*	*nda*	*nda*

* nda: no data available

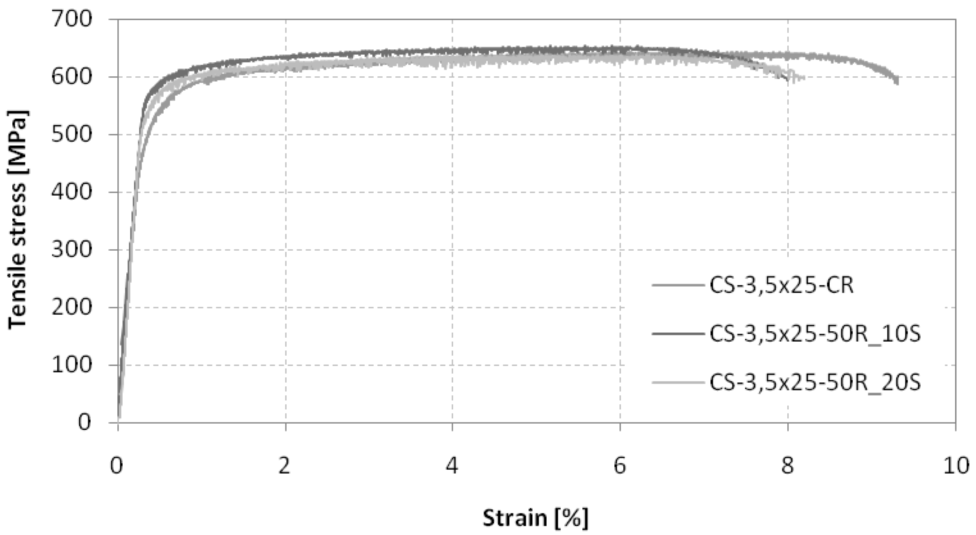

Figure 6-1 Tensile test on CS flat ribbed reinforcement

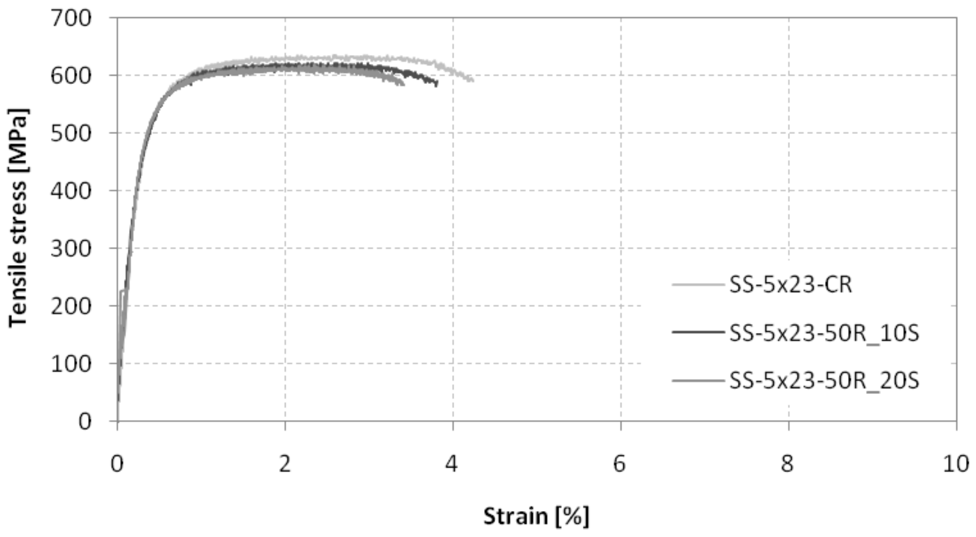

Figure 6-2 Tensile test on SS flat ribbed reinforcement

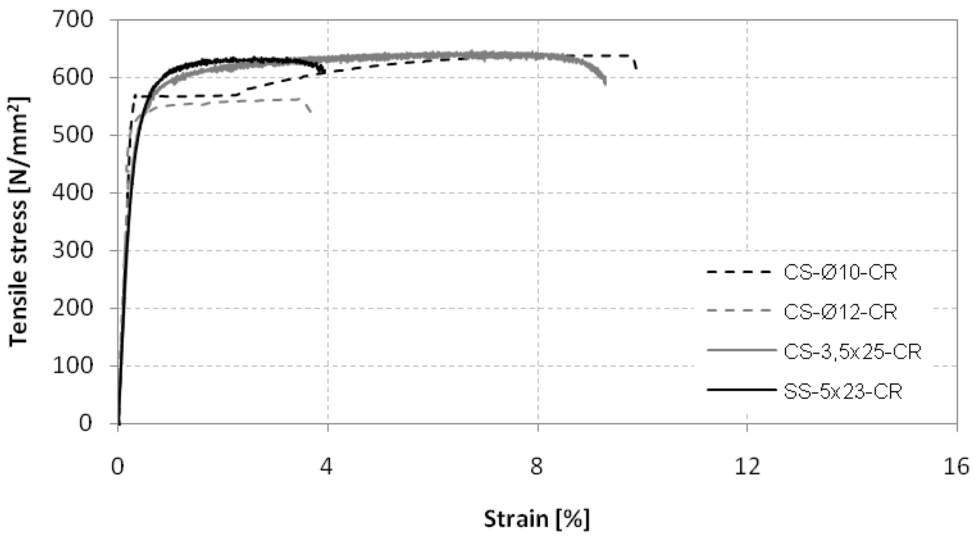

Figure 6-3 Tensile stress-strain curve comparison for completely ribbed samples

2.2 Test set-up and testing conditions

The performed tension stiffening tests consist of a tensile test on a reinforcing bar embedded in a concrete prism (see Figure 6-4). The test specimen is therefore a concrete prism (85 mm x 85 mm x 1000 mm) with a steel bar centrally embedded in its longitudinal axis. The cross section of the reinforcement varies depending on the reinforcement type used for each test (see Table 6-1 and Table 6-4), but in any case the length of the bar is 1600 mm. The bar to be tested extends, beyond the two sides of the prism (300 mm each side) for gripping in the test machine. As such the axial tension is applied to both ends.

The prisms are tested in a tensile testing machine with a capacity of 1000 kN (class 1 according to ISO 7500-1 [6], and a relative error of the accuracy of 0,8%). The specimen is placed vertically in the machine and the tensile force is applied by gripping of the steel reinforcement. To account for local stresses at the prism ends, extra confinement reinforcement has been provided over a distance of 135 mm (see Figure 6-5). Tests are carried out at laboratory ambient conditions. The load is applied in a controlled way as follows. At a first stage, load control is applied at a rate of 0,03 kN/s until a total force of 8kN is reached. The second stage applies a displacement control rate of 0,0017 mm/s until the steel starts yielding. The third stage corresponds to a 0,017 mm/s displacement controlled final yielding phase. The tests are stopped when an advanced yielding stage has been reached (at a strain lower than the ultimate strain of the reinforcement).

Concrete strain, crack development and crack width are recorded during testing as a function of the applied load. Strains are measured by means of 8 strain stirrups (gauge length 200 mm, electronic measurement) located at two adjacent faces of the prism. On the remaining 2 faces measuring points are glued for measurement of concrete strains by means of mechanical deformeters (type DEMEC – gauge length 200 mm, manual measurement). See Figure 6-4 and Figure 6-6 for an overview of the strain measurements. At load intervals of 5 kN starting from the cracking load, crack development is recorded on all sides and also crack widths are measured by means of a small microscope. This is done until the steel starts yielding and at the end of the test after unloading. Due to the presence of the strain stirrups, crack widths are only recorded on 2 sides (free of stirrups).

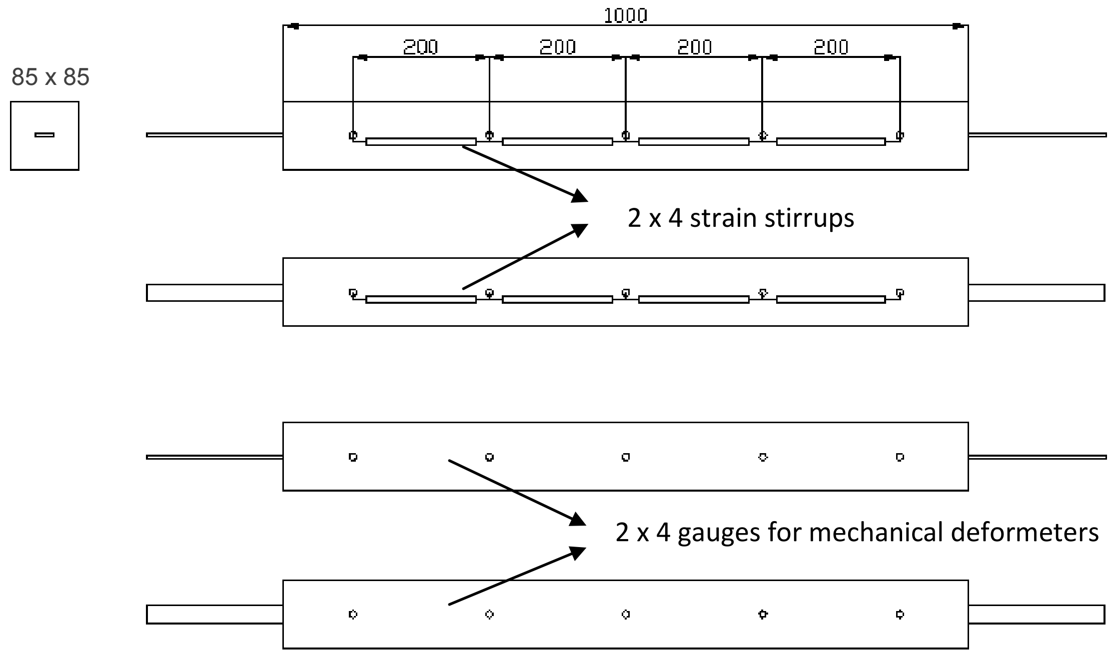

Figure 6-4 Test specimen and measuring devices/points in 4 sides of the prism (in mm)

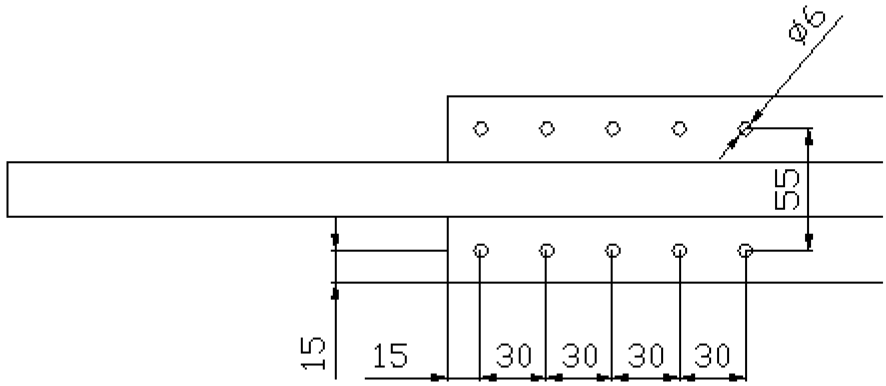

Figure 6-5 Detailed view of the internal extra reinforcement applied for avoiding local stresses at the ends of the prism (in mm)

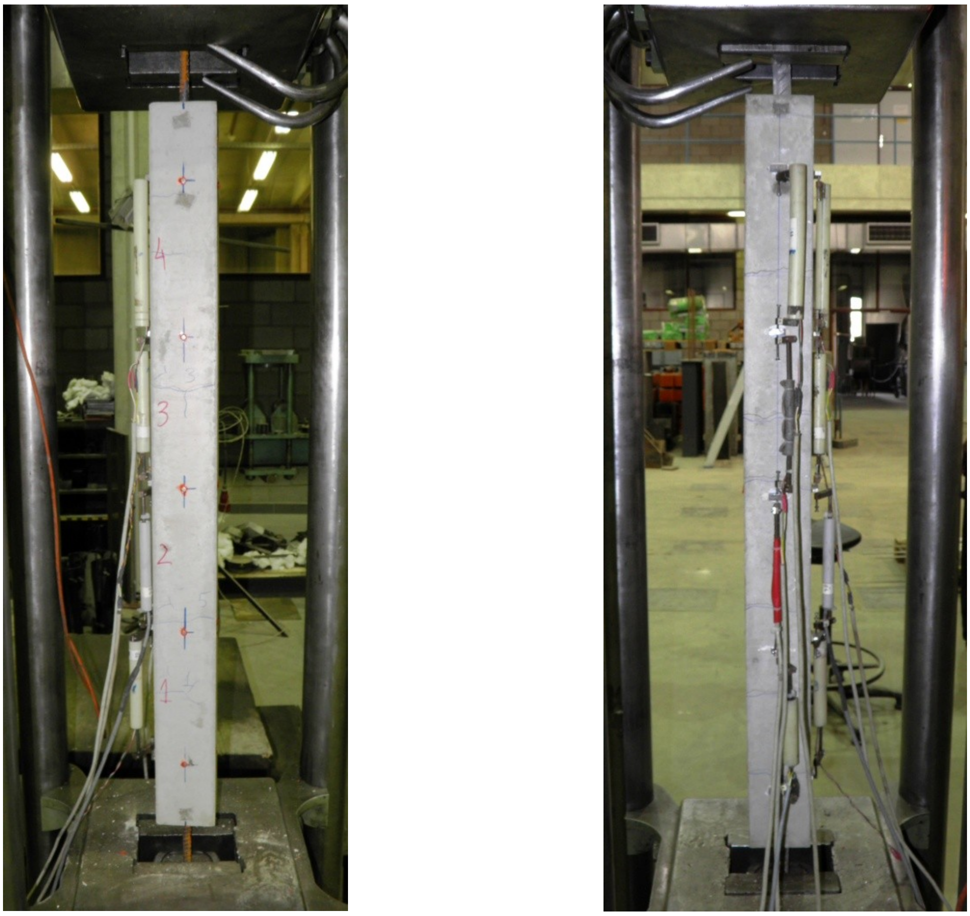

Figure 6-6 Test set up: specimen placed in the testing machine. Manual measurement points (left) and strain stirrups for continuous measurements (right)

3 Test results

3.1 General considerations

Concrete strain, crack development and crack width are recorded as a function of the applied load. The strain values are calculated by taking the average value of the gauge measurements. Form the crack development recording, calculation of the mean crack spacing is possible by taking the average of the observed crack spacing.

Table 6-5 summarizes the main values obtained from the performed tests. The first cracking load ($F_{cr,exp}$) together with the corresponding cracking stress ($\sigma_{cr,exp}$) are given. The latter is calculated dividing the experimental cracking load by the nominal cross sectional area of the reinforcement, and represents the tensile stress level of the reinforcement when the first crack occurs. Furthermore, mean cracking spacing and mean crack width at 50% of the yielding stress are also provided ($s_{rm,50\%y,exp}$ and $w_{rm,50\%y,exp}$, respectively).

Table 6-5 Main test results

Bar/Strip	***Concrete type (batch)***	***f_c (N/mm²)***	***f_{ct} (N/mm²)***	***$F_{cr,exp}$ (kN)***	***$\sigma_{cr,exp}$ (N/mm²)***	***$s_{rm,50\%y,exp}$ (mm)***	***$w_{rm,50\%y,exp}$ (mm)***
CS-Ø10-CR	TC (1)	55,9	3,3	14,13	179,89	144,00	0,20
CS-Ø12-CR	TC (2)	52,3	3,6	19,32	170,81	134,00	0,24
CS-3,5x25-CR	TC (1)	55,9	3,3	14,89	170,20	223,33	0,55
CR-3,5x25-50R_10S	TC (1)	55,9	3,3	18,95	216,59	147,50	0,45
SS-5x23-CR	TC (1)	55,9	3,3	12,51	108,79	165,00	0,78
SS-5x23-50R_10S	TC (2)	52,3	3,6	12,87	111,18	134,00	0,49
SS-5x23-100R_10S	TC (2)	52,3	3,6	17,24	149,93	170,00	0,58
SS-5x23-100R_20S	TC (2)	52,3	3,6	17,01	147,93	175,00	0,46
SS-5x23-150R_10S	TC (2)	52,3	3,6	16,20	140,91	187,50	0,25
SS-5x23-150R_20S	TC (2)	52,3	3,6	15,10	131,35	160,00	0,39
CS-Ø10-CR	SCC (3)	55,4	3,3	16,05	204,05	126,67	0,15
CS-Ø12-CR	SCC (3)	55,4	3,3	19,35	173,78	134,00	0,22
CS-3,5x25-CR	SCC (3)	55,4	3,3	18,09	206,83	192,50	0,50
SS-5x23-CR	SCC (3)	55,4	3,3	16,78	145,95	132,00	0,53
SS-5x23-100R_10S	SCC (3)	55,4	3,3	18,46	160,55	165,00	0,34
SS-5x23-100R_20S	SCC (3)	55,4	3,3	17,85	155,24	157,50	0,35

For all tested specimens similar axial stress-strain behaviour is observed, which is schematically plotted in Figure 6-7. Four stages are clearly differentiated, which are typically observed for this type of test. The first stiffer phase (a), is the uncracked phase, in which an elongation of the test specimen occurs without any crack appearance. This phase ends when the first crack appears (R). The second stage corresponds to the crack formation phase (b), in which more cracks appear with increasing load. The third phase goes from the last crack formation (S) until yielding (Y) of the bar starts (c). During this phase, the so-called stabilized cracking phase, normally no more cracks appear, and the already existing cracks expand. However, at high loading at the end of this phase, new transverse and longitudinal splitting cracks appeared for some of the performed tests (this is further explained in section *3.2 Influence of reinforcement geometry*). The last phase (d), corresponds to the yielding of the reinforcement and it ends at a certain strain value below the ultimate strain of the reinforcement (when the test has been stopped). Stress-strain measurements of the prisms are plotted together with the stress-strain relationship of the naked bar (obtained from the individual tensile tests) for stiffening effect evaluation (tensile test curves are referred as “tt” and plotted as dashed lines in Figure 6-8, 6-10, 6-12, 6-14, 6-16, 6-18, 6-20, 6-22, 6-24, 6-26 and 6-28).

Crack development behaviour is presented by plotting mean crack width values, observed maximum crack widths, total crack opening (calculated as the mean crack width times the number of cracks) and the mean crack spacing as a function of the tensile stress of the reinforcement (Figure 6-9, 6-11, 6-13, 6-15, 6-19, 6-21, 6-23, 6-25, 6-27 and 6-29).

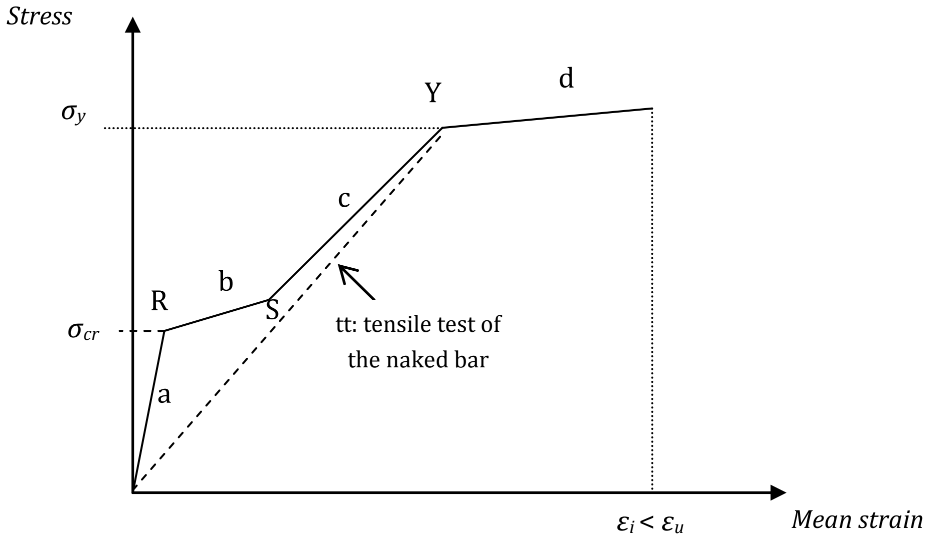

Figure 6-7 Schematic drawing of the stress-strain behaviour obseverd for the tension stiffening tests

In the following, the obtained test results are discussed further, considering the influence of the different parameters studied. Reinforcement geometry, reinforcement material type, concrete type and the influence of adding smooth areas within the rib pattern are the considered parameters. Furthermore, individual test results in terms of stress-strain relationship and cracking behaviour can be found in Appendix C of this work. Schematic drawings of developed cracks at the end of the each performed test are also provided in the mentioned appendix.

3.2 Influence of reinforcement geometry

To analyze the difference between results obtained with standard round bars and results for flat rebars, elements with comparable cross sectional area are considered. Thus, CS-Ø10-CR is compared to CS-3,5x25-CR. Furthermore, CS-Ø12-CR elements are comparable in cross sectional area to SS-5x23-CR. However, the steel type varies in this case, and therefore conclusions cannot be drawn directly. Comparison between the specimens is carried out for TC and for SCC.

Test results show that when embedded in traditional concrete, first cracking occurs at a higher steel stress level for round bars. The difference is more evident for Ø12 mm equivalent specimens (~57% higher σ_{cr} for round bar) than for Ø10 mm (~6% in favour of round bars). First cracking stress, when embedded in SCC, is similar for flat and round bars with an equivalent diameter of 10 mm. For diameter 12 mm equivalent specimens tested with SCC, round bars have a higher (~19%) cracking stress than flat ones. The obtained difference between diameter 10 mm equivalent and diameter 12 mm equivalent specimens might be explained by assuming that CS behaves better than SS (in case of diameter 12 mm equivalent, round bars are made of CS, whereas flat members are made of SS). This will be further confirmed in Section 3.3.

When looking to the tensile stress-mean strain relationships, flat members behave stiffer or with similar stiffness compared to round bars having the same cross sectional area. The stiffening curve of the round bars tends to get closer to the corresponding σ-ε curve of the naked bar, compared to the tendency of the flat rebars' curve. In other words, it can be concluded that the round bars develop less "tension stiffening effect" than the flat elements do (see Figure 6-8 and Figure 6-10). This observation might be related to the different perimeters of round and flat rebars: a higher perimeter related to the flat rebars is involved in the bond transfer, compared to equivalent round bars.

When analyzing data regarding cracking behaviour of the specimens (Figure 6-9 and Figure 6-11), in general flat members develop bigger crack spacing and higher crack width (up to 230% higher when comparing values at 50% of the yielding stress) than round bars. In other words, round bars develop better crack behaviour than flat members as they have smaller crack widths, smaller total crack opening values and lower maximum crack width values than flat bars, and less crack spacing (more cracks but thinner cracks). This difference becomes more pronounced with increasing loads.

During carrying out of the tests, another phenomenon has been observed related to the geometry of the reinforcement: longitudinal splitting cracks are detected for flat reinforcements. Some minor longitudinal cracks are also developed for round bars at high loads, when yielding of the reinforcement started and large deformations are happening in the steel. However, for flat elements, longitudinal cracks are observed already at the beginning of the stabilizing phase (at tensile stress of around 300 N/mm^2), which become more important and pronounced with increasing loads. Some of the longitudinal cracks are long enough to extend from one to two or more transverse cracks. The longitudinal splitting cracks occurred almost independent of the tested parameters. The higher splitting tendency of flat members has been previously observed and described in Chapter 4 and Chapter 5. The drawings of the crack distribution of each tested specimen are given in Appendix C, which allow to visually understand the described phenomena. As an example, the crack distribution at the end of the test is given for CS-Ø10-CR and CS-3,5x25-CR both embedded in TC in Figure 6-12 and Figure 6-13, respectively.

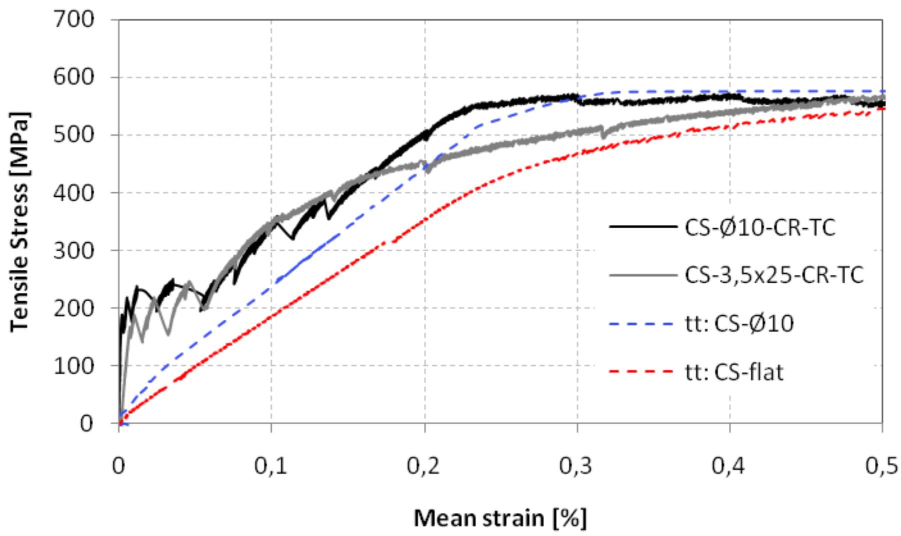

Figure 6-8 Stress-strain relationship. Round vs. Flat (Equiv. Ø10 - TC)

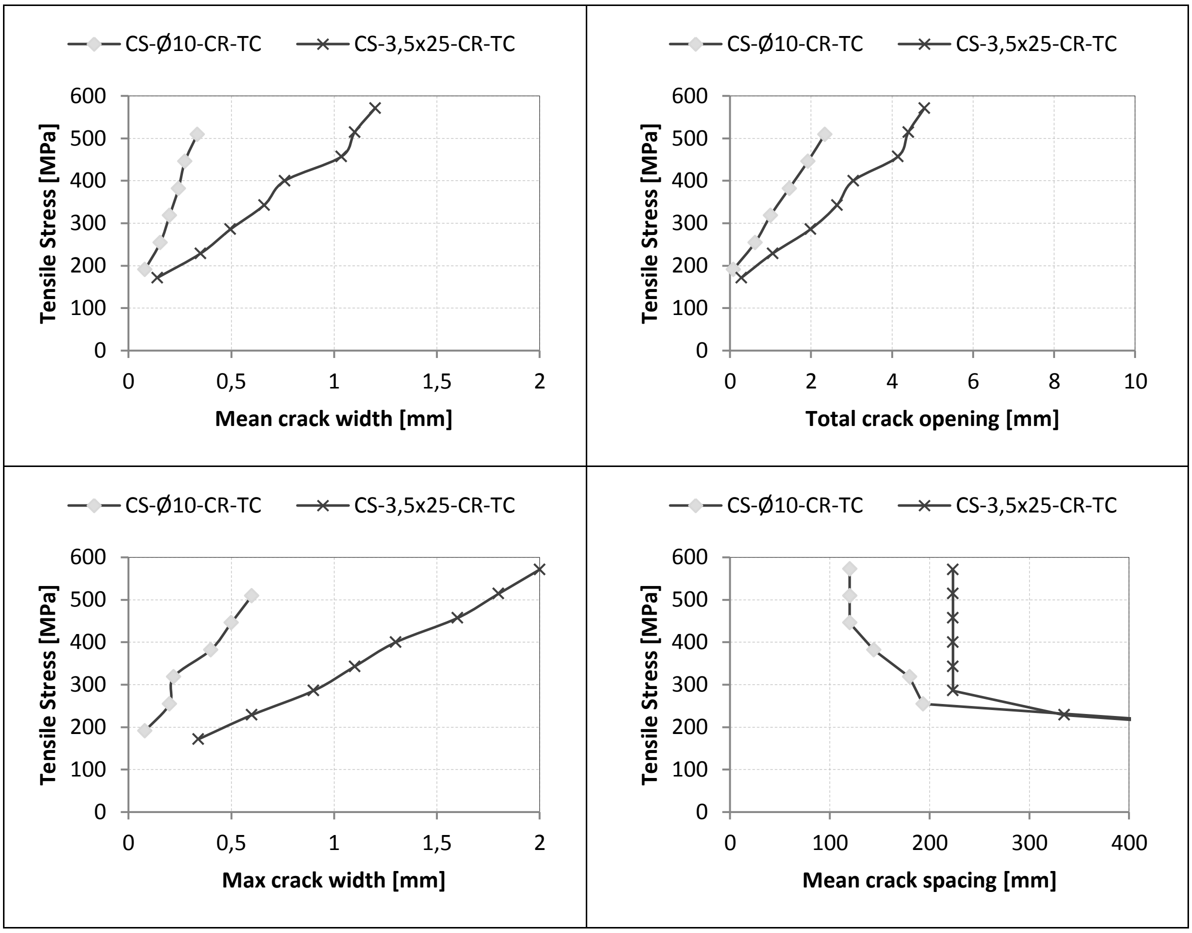

Figure 6-9 Cracking behaviour. Round vs. Flat (Equiv. Ø10 - TC)

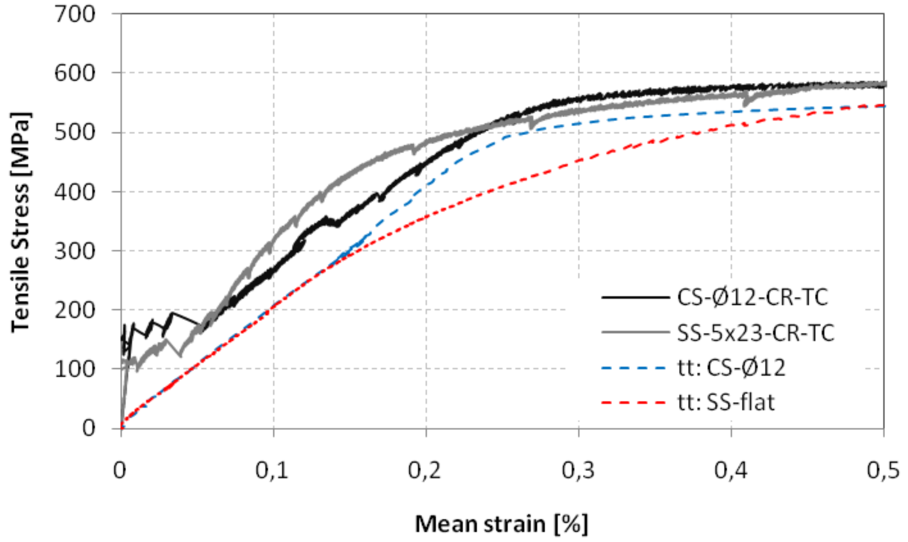

Figure 6-10 Stress-strain relationship. Round vs. Flat (Equiv. Ø12 - TC)

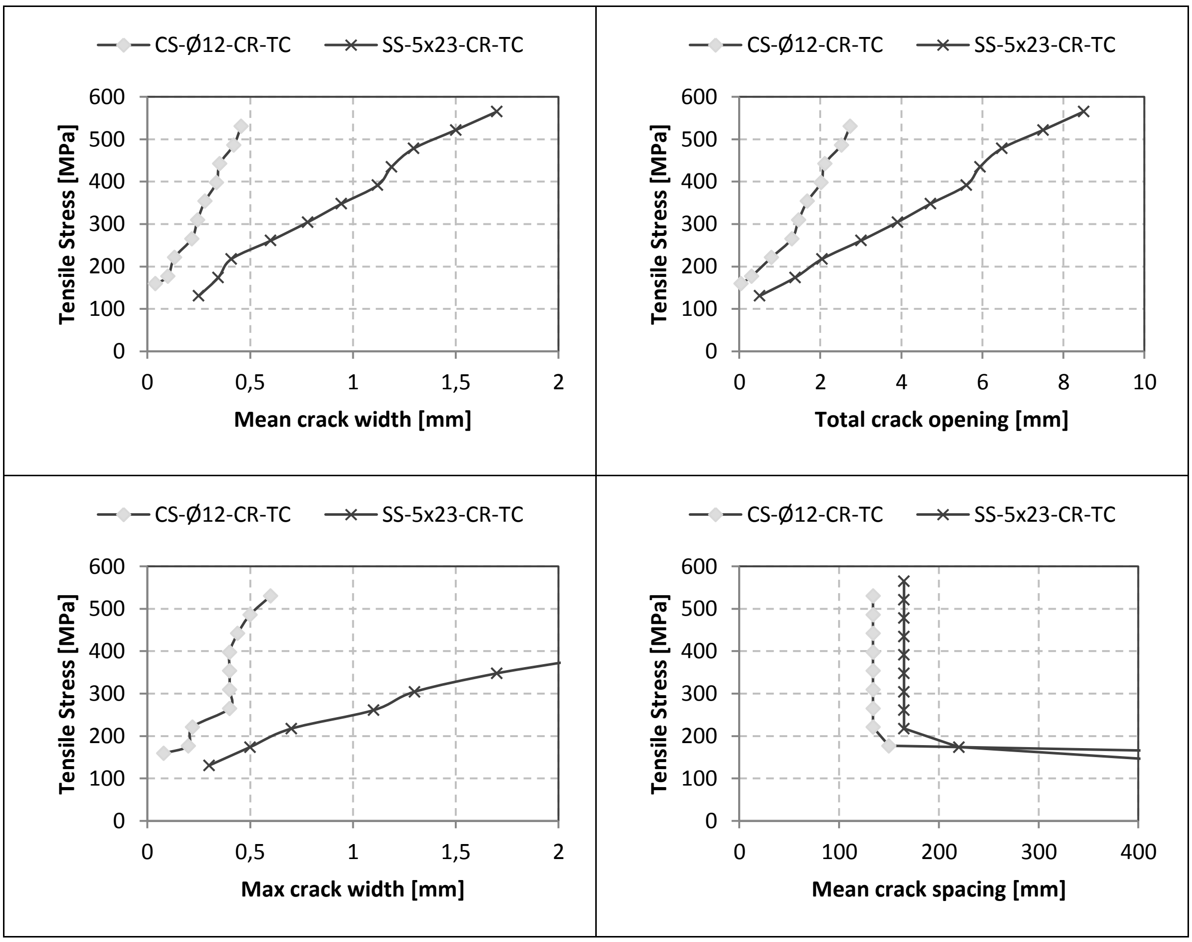

Figure 6-11 Cracking behaviour. Round vs. Flat (Equiv. Ø12 - TC)

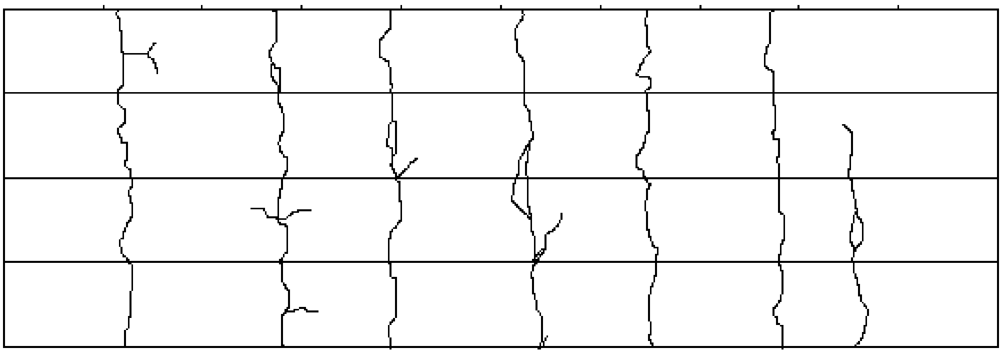

Figure 6-12 Schematic drawing of the crack dsitribution at the end of the test. CS-Ø10-CR in TC

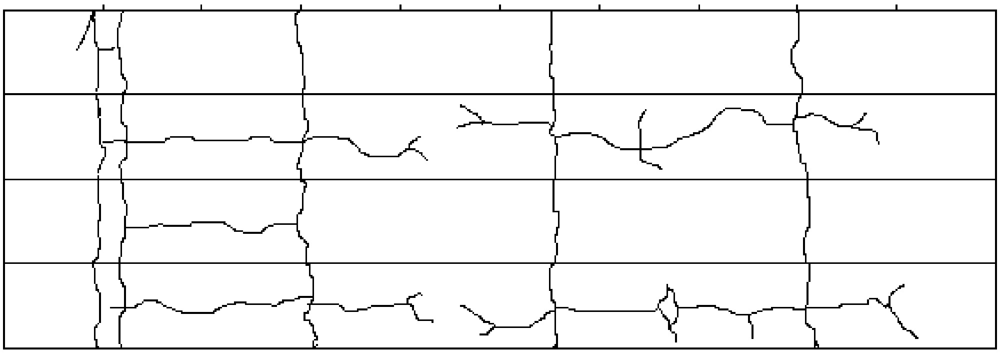

Figure 6-13 Schematic drawing of the crack dsitribution at the end of the test. CS-3,5x25-CR in TC

3.3 Influence of reinforcement material

Both carbon steel and stainless steel are tested for flat members. Cross sectional areas differ from each other (~30% higher cross sectional area for SS), but both elements have comparable perimeter. The same rib pattern is used for both material types and they are both tested with traditional concrete and for self compacting concrete. Thus, given the test matrix (Table 6-1) the CR and 50R_10S configurations are compared for TC and the CR configuration for SCC.

Regarding cracking stress, higher values are always obtained for CS, which is related to the lower reinforcement ratio provided when using this material (due to the lower cross sectional area). Theoretically, the stress at first cracking is the one calculated by dividing the cracking load by the steel section, ($\sigma_{cr} = F_{cr} / A_s$, being $F_{cr} = f_{ct} A_c(1+\rho_s \alpha_s)$, then $\sigma_{cr} = f_{ct} (A_c/A_s + \alpha_s)$ see section *4.1 Cracking load*). It is clearly derived that an increase of steel area (A_s) will decrease the stress if other parameters are kept constant. Thus, if we calculate the theoretical cracking stress corresponding to the two cross sectional areas studied, we get that the ratio between them is $\sigma_{cr,A1}/\sigma_{cr,A2}$ = 1,30. However the ratios derived from the test results ($\sigma_{cr,exp,A1}/\sigma_{cr,exp,A2}$) are higher than the theoretical one (1,56 for CR-TC, 1,95 for 50R_10S-TC and 1,42 for CR-SCC). The difference between the theoretical and the experimental ratios, indicates that CS specimens have a higher cracking stress than SS elements. The same observation has been made in section *3.2. Influence of reinforcement geometry* to explain the bigger differences observed for diameter 12 mm equivalent reinforcements.

The graphs describing the stress-strain relationship of the test specimens are not consistently in favour of one material or another: the first loading phase is always better for CS elements as concluded from cracking stress values; however, the cracking phase of SS elements is stiffer (with TC) or similar (with SCC) comparing to CS strips. The third phase (crack stabilizing stage) is similarly stiff for both material types for CR in TC, stiffer for SS when working with 50R_10S configuration in TC and stiffer for CS when having CR embedded in SCC. As an example, Figure 6-14 compares the strips with CR configuration and embedded in TC.

When analysing the cracking behaviour, for SS elements the distance between cracks is smaller than for CS in all the studied cases: more cracks are developed with SS elements. Furthermore, if mean crack width, maximum crack width and total crack opening are analyzed, better behaviour is observed for CS elements, which develop less and thinner (or similar in width) cracks than the ones formed when SS elements are used, for any of the tested configuration and for both TC and SCC. See Figure 6-15, which allows for a comparison of the cracking behaviour between CS and SS, for the completely ribbed configuration and when embedded in TC.

Nevertheless, given the area difference between the two materials and having only performed one test for each specimen type the magnitude of the influence of the reinforcement material type on the tension stiffening test is difficult to assess. Neither can the observed behaviour be generalized without further experimental evidence. However, on overall and focusing on serviceability limit state stress levels, the observed differences in behaviour between flat CS and SS rebars remains limited.

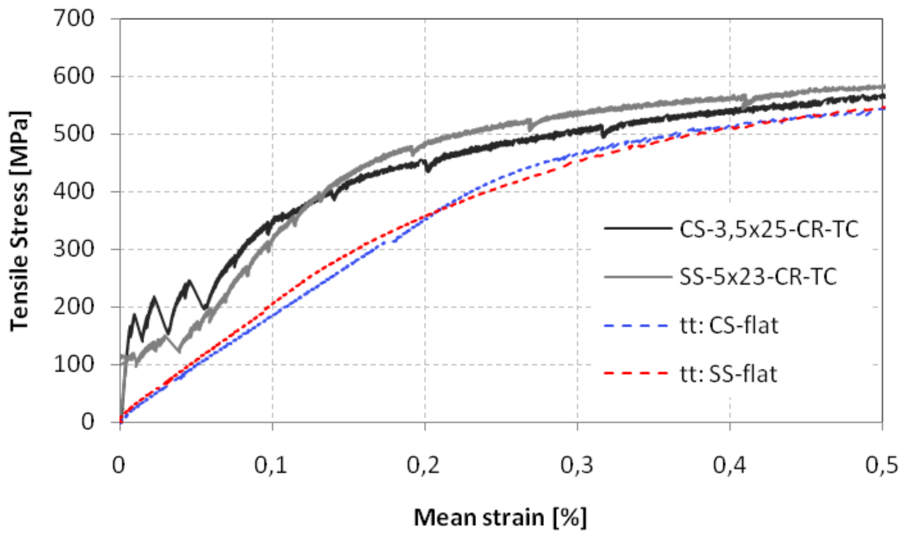

Figure 6-14 Stress-strain relationship. CS vs. SS (CR-TC)

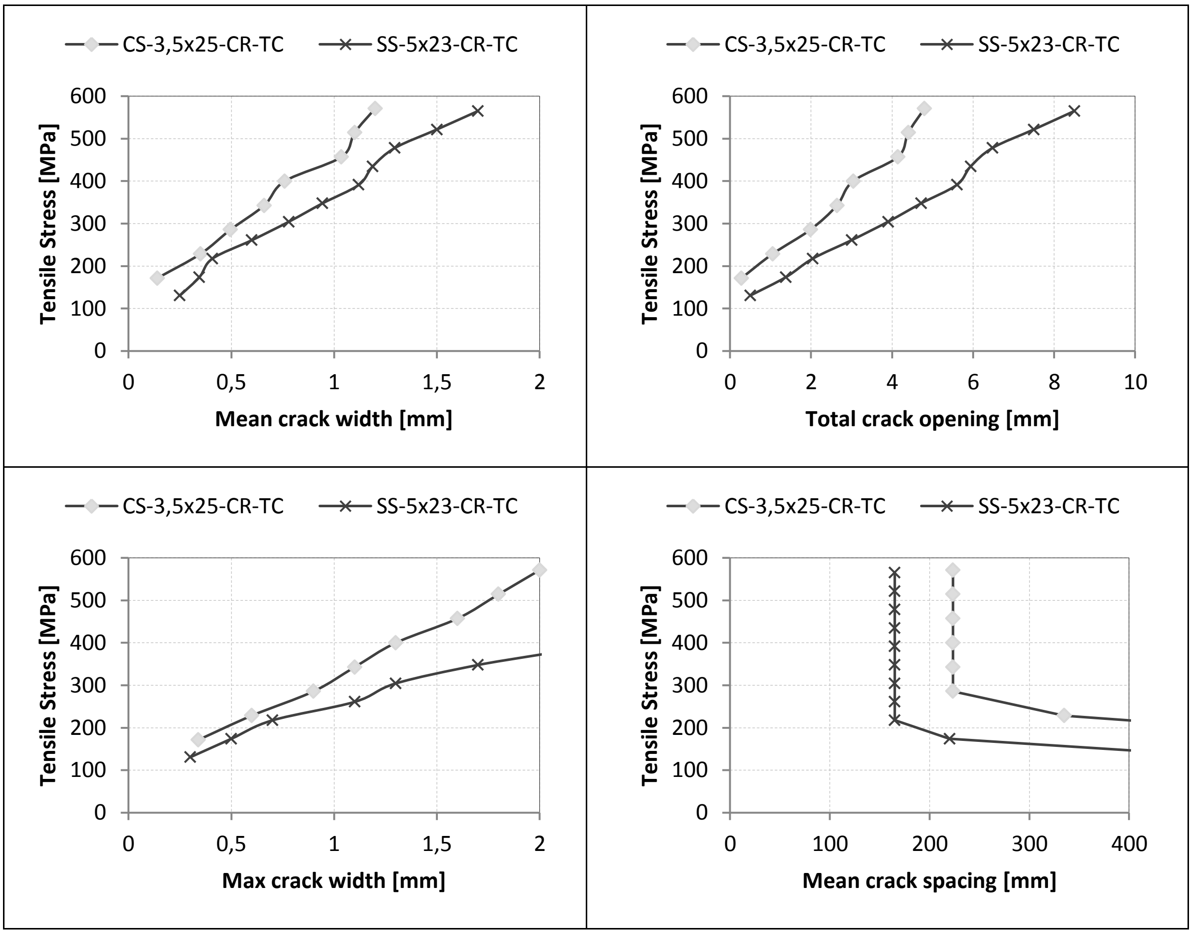

Figure 6-15 Cracking behaviour. CS vs. SS (CR-TC)

3.4 Influence of concrete type

Traditional concrete and self compacting concrete have been used to embed the reinforcing elements. Different reinforcement types (different in material, in geometry, in rib pattern) have been embedded in both TC and SCC; this allows for a comparison between the two concrete types.

For all the studied cases, first cracking stress values are higher (from 1,7% to up to 34% higher) when the reinforcement is embedded in SCC in comparison to TC. However, the biggest differences are observed for the CR configuration, for both carbon steel and stainless steel: 21% and 34%, respectively.

For round reinforcements, the stress-strain relationship is very similar when comparing results of the bars embedded in TC vs. SCC. For example, Figure 6-16 allows for comparing the behaviour of the CS-Ø10-CR reinforcement when embedded in TC to the one developed when embedded in SCC. However, for flat elements the influence of the concrete type on the stress-strain behaviour is not consistent. CS-3,5x25-CR specimens, when embedded in SCC behave in a stiffer way than with TC. For SS-5x23-CR and for SS-5x23-100R_10S configurations, the first two phases of the σ-ε curve are similar for both concrete types, but the 3rd stabilizing phase is stiffer at the beginning for TC but loses its stiffness faster so that SCC behaves stiffer at the end of the 3rd phase. Finally, for the SS-5x23-100R_20S configuration, the behaviour is similar for both concrete types along the 4 stages. As an example, Figure 6-18 gives the stress-strain curves obtained for SS-5x23-CR specimens when embedded in TC and SCC. On overall and focusing on serviceability limit state stress levels, the behaviour is similar for most of the specimens.

When looking to the cracking behaviour of the two concrete types, SCC develops more (lower crack spacing) and thinner cracks (up to 42% lower mean crack width values at 50% of the yielding stress). Although the total crack opening is similar for both concrete types, when using TC less but wider cracks are developed, which is considered to be a less favourable crack distribution. This trend can be observed from the test results given in Figure 6-17 and Figure 6-19, for CS-Ø10-CR and SS-5x23-CR, respectively.

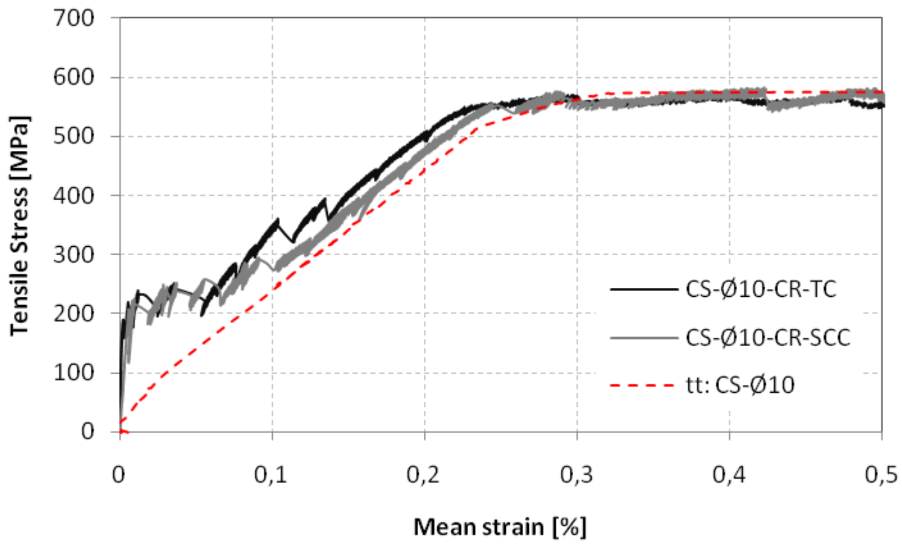

Figure 6-16 Stress-strain relationship. TC vs. SCC (CS-Ø10)

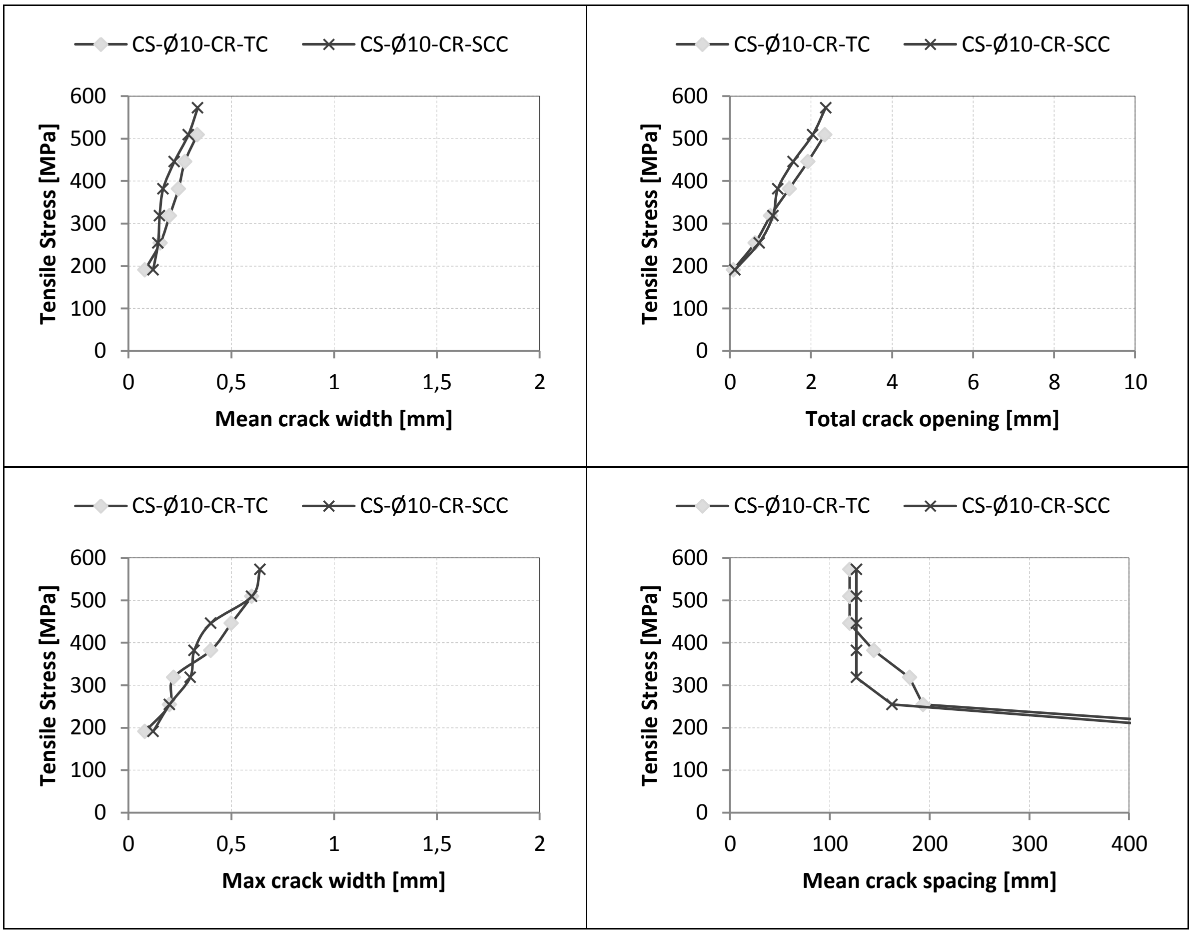

Figure 6-17 Cracking behaviour. TC vs. SCC (CS-Ø10)

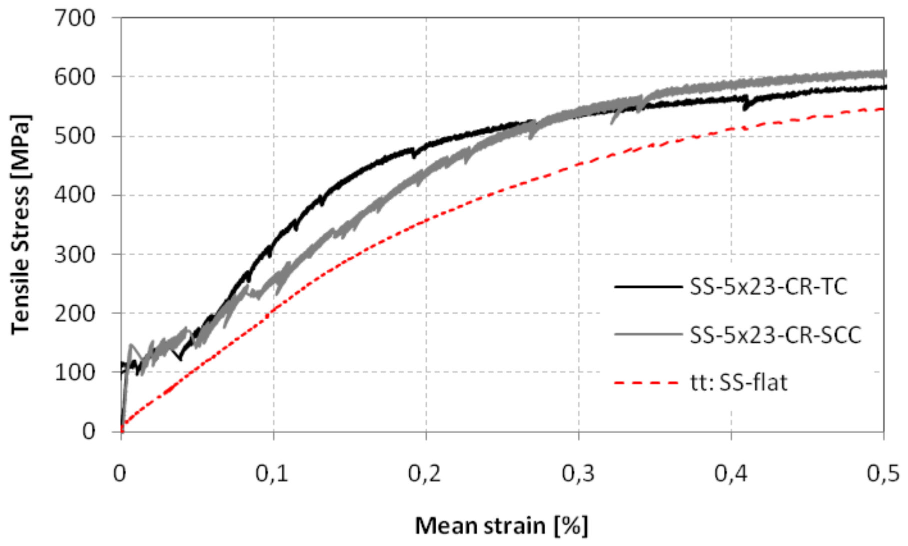

Figure 6-18 Stress-strain relationship. TC vs. SCC (SS-CR)

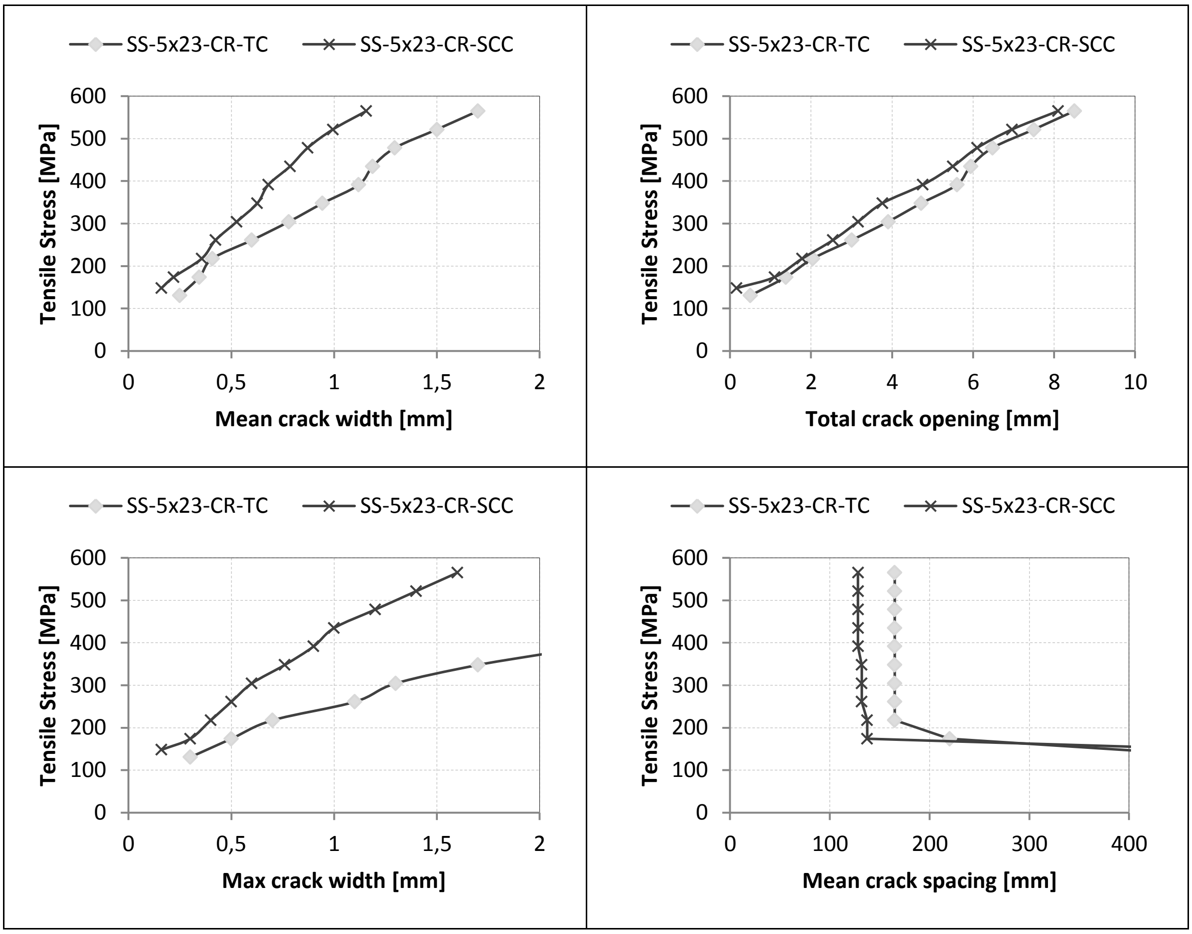

Figure 6-19 Cracking behaviour. TC vs. SCC (SS-CR)

3.5 Influence of adding smooth areas to the rib pattern

In this section the influence of working with an alternate pattern is studied. The continuity of the ribbed area is interrupted by adding smooth areas every certain length: for example, 50R_10S configuration stands for a rib pattern combining 50 mm of ribbed area followed by 10 mm of smooth zone. Thus, the alternate 50R_10S, 100R_10S and 150R_10S configurations are compared to the completely ribbed (CR) configuration. Following material availability and test matrix, the comparison is possible for both CS and SS and for both TC and SCC: SS-5x23-CR is compared to SS-5x23-50R_10S, SS-5x23-100R_10S and SS-5x23-150R_10S, all of them embedded in TC; and finally, SS-5x23-CR is compared to SS-5x23-100R_10S, when embedded in SCC. Note that for the SS-5x23-150R_10S specimen, electronic continuous measurements are only available for stress values up to 350 N/mm^2 due to a measuring error occurring during testing. For higher stress values, the curve derived from the manual measurements has been implemented in Figure 6-20.

Looking to the values of the first cracking stress, higher values are always obtained when smooth areas have been added to the rib pattern. These higher values range from 2% higher values in case of SS-5x23-50R_10S compared to SS-5x23-CR, up to 37% higher cracking stress values for SS-5x23-100R_10S compared to the corresponding CR configuration (embedded in TC). Furthermore, it can be observed for SS elements embedded in TC, that there is no proportional relationship between the cracking stress and the length of the rib surface: the cracking strain value increases (34%) when increasing the ribbed length from 50 mm to 100 mm, but on the other hand decreases (7%) when increasing the length from 100 mm to 150 mm.

Regarding the tension stiffening behaviour at stress levels corresponding to service load, alternate patterns show stiffer (or similar) behaviour than the completely ribbed configuration as it can be observed from the crack formation phase and the first part of the stabilized cracking stage of Figure 6-20 and Figure 6-22. The stiffest behaviour is observed for the 150R_10S and 100R_10S configurations (Figure 6-20).

The cracking behaviour improves in all the cases when adding smooth areas within the rib pattern. For SS and TC best results are obtained for the 150R_10S configuration for which less cracks are developed and they are thinner than for the other configurations. As a result, the total crack opening curve for this configuration differs substantially (up to 70% less total crack opening at 50% of the yielding stress of each bar) from the other alternate patterns (see Figure 6-21) However, there is no concluding relationship when changing from 150R_10S to 100R_10S or to 50R_10S. For SS and SCC, similar crack distribution is obtained for the continuous and for the alternate pattern. However, cracks are thinner when adding a smooth area within the pattern and the total crack opening is therefore smaller for the alternate configuration (see Figure 6-23).

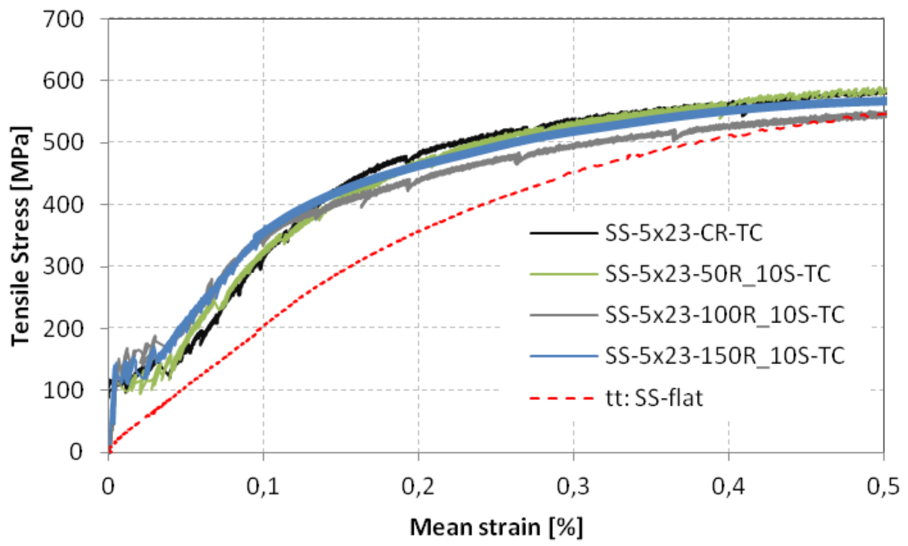

Figure 6-20 Stress-strain relationship. CR vs. 50R_10S vs. 100R_10S vs. 150R_10S (SS-TC)

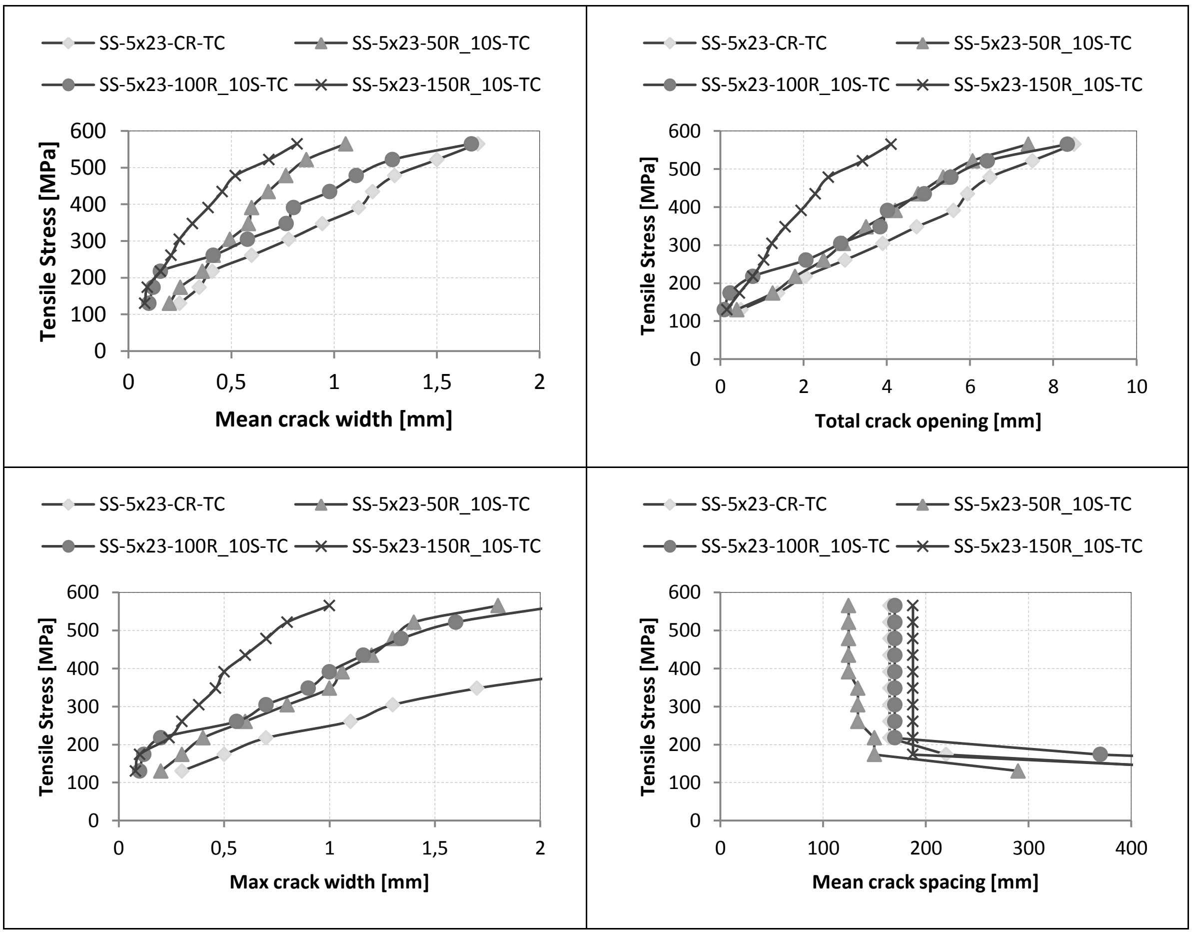

Figure 6-21 Cracking behaviour. CR vs. 50R_10S vs. 100R_10S vs. 150R_10S (SS-TC)

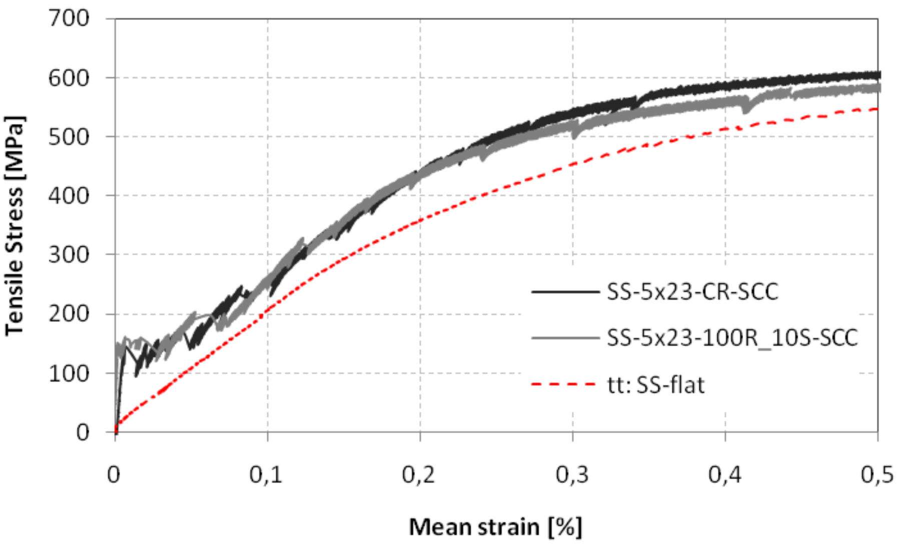

Figure 6-22 Stress-strain relationship. CR vs. 100R_10S (SS-SCC)

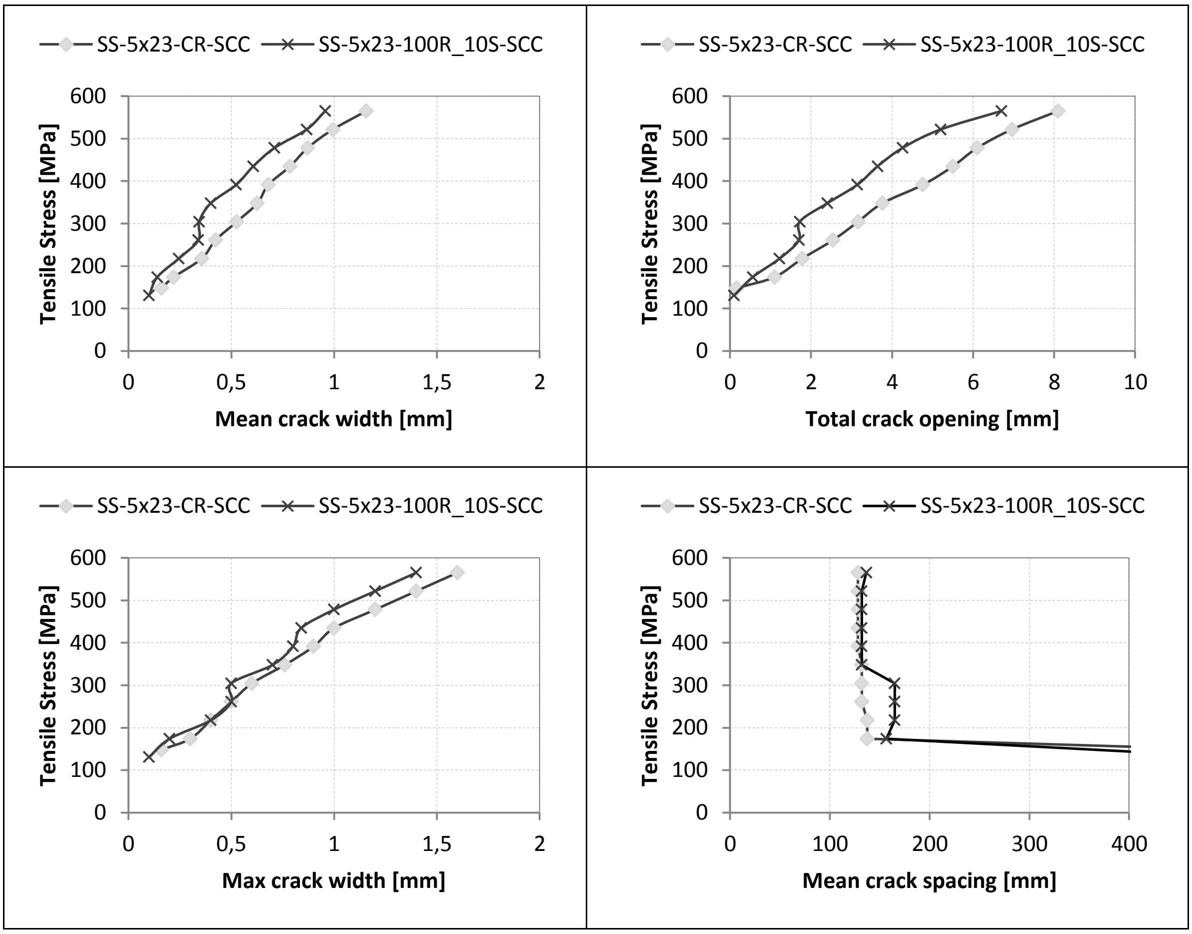

Figure 6-23 Cracking behaviour. CR vs. 100R_10S (SS-SCC)

In order to compare the tension stiffening and cracking behaviour between flat rebars with an alternate pattern and standard round ribbed rebars, comparison is done between CS-Ø12-CR and SS-3x25-150R_10S, for which best results are obtained among the alternate patterns. It is observed from Figure 6-24, that higher tension stiffening effect is developed by the flat rebar with an alternate pattern in comparison to a round ribbed rebar with a comparable cross section area. Furthermore, the cracking behaviour developed by the rebars is very similar as it is observed from Figure 6-25. Although the mean crack spacing is higher for the alternate pattern, the mean crack width and the total crack opening values are comparable, especially if focus is put at stress levels corresponding to service loads.

3.6 Influence of increasing the smooth area within the rib pattern

Next step in analyzing the effect of adding a smooth area within the bond length is to assess the influence of extending the smooth area from 10 mm to 20 mm (from 100R_10S configuration to 100R_20S and from 150R_10S to 150R_20S), without changing any other parameter. Comparison is done for SS and for both TC and SCC.

For all the studied specimens in this section, slightly higher values of σ_{cr} are obtained when smaller smooth areas are used (from 1,3% to 7,2% higher values). In other words, increasing the smooth area from 10 to 20 mm leads to a slightly earlier cracking of the concrete prism.

The σ-ε curves are stiffer when 10 mm of smooth area length is used for both TC and SCC when 100R_10S and 100R_20S configurations are evaluated (see Figure 6-28 in the case of SS embedded in SCC). Similarly, in the case of SS-3x25-150R_10S and SS-3x25-150R_20S when embedded in TC, stiffer behaviour is developed by SS-3x25-150R_10S (see Figure 6-26). It is therefore observed that increasing the smooth area of the alternate pattern from 10 mm to 20 mm, lowers the tension stiffening effect developed.

The influence of increasing the smooth are within the rib pattern on the cracking behaviour is not clearly visible when looking to the corresponding test results. When shifting from 100R_10S to 100R_20S and for TC, increasing the smooth length has a positive effect making the cracks thinner but keeping the number of cracks constant. However, for SCC, no clear influence of the 10S to 20S shift is observed (see Figure 6-29). On the other hand, for 150R_10S and 150R_20S embedded in TC, increasing the smooth area from 10 mm to 20 mm leads to a negative effect on the cracking behaviour of the specimen developing more and wider cracks (see Figure 6-27). In general cracking behaviour is very similar and no pronounced influence is observed between 10 mm and 20 mm smooth area.

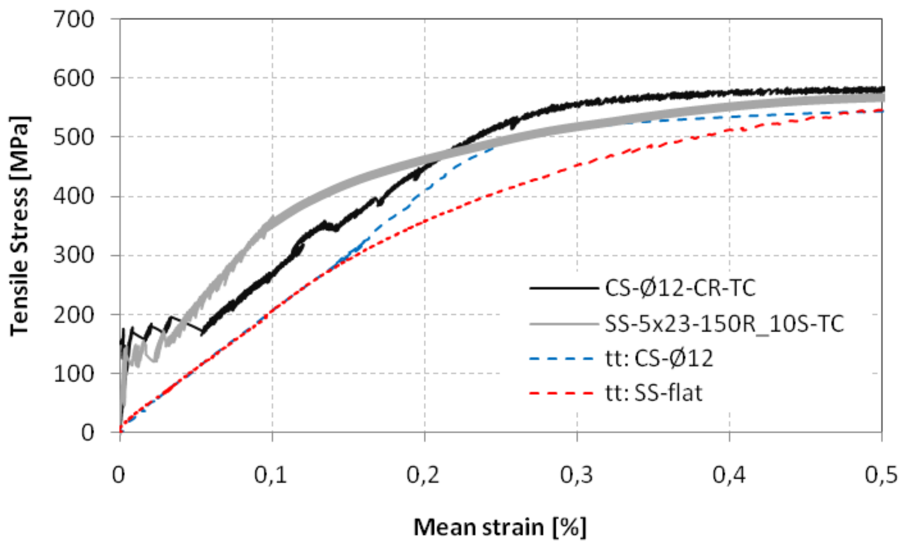

Figure 6-24 Stress-strain relationship. CS-Ø12-CR vs. SS-5x23-150R_10S (TC)

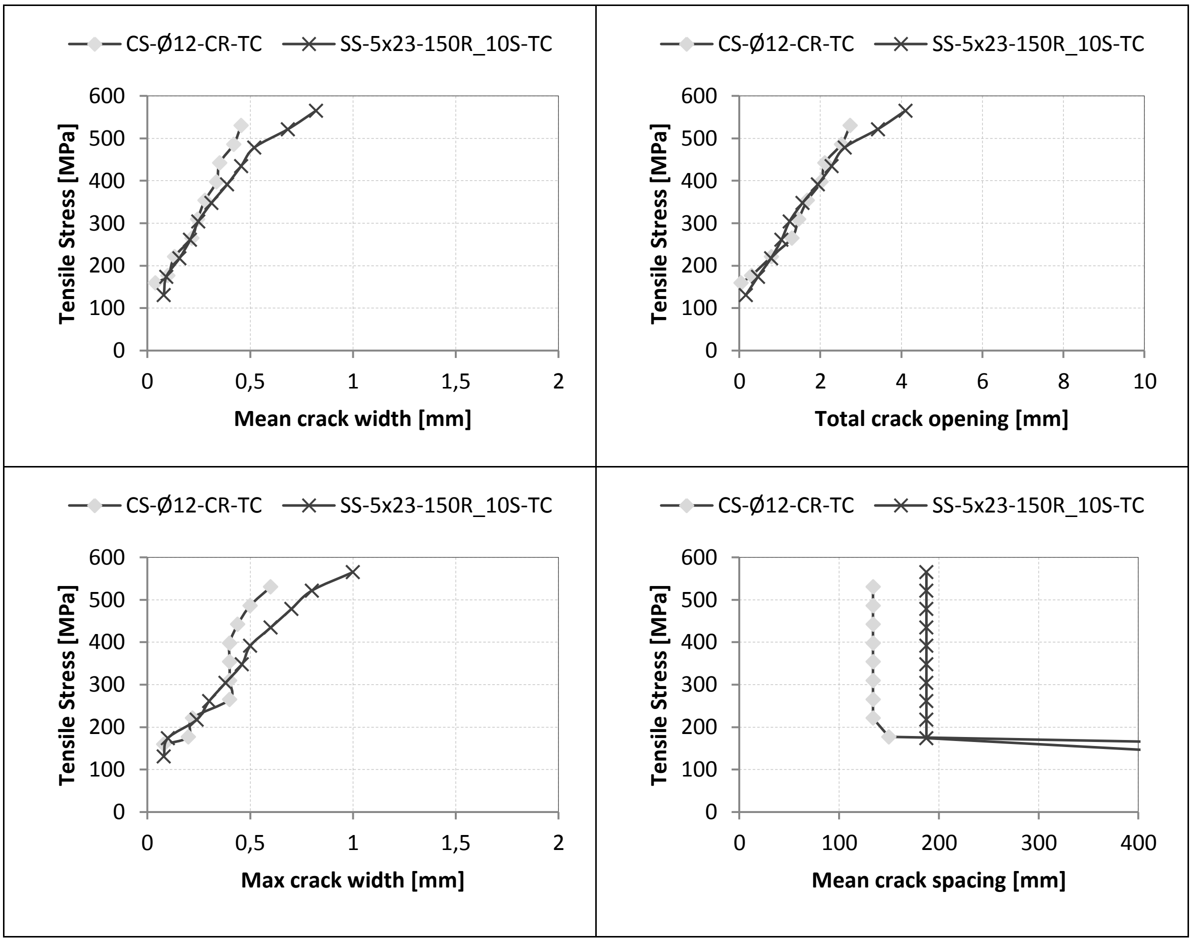

Figure 6-25 Cracking behaviour. CS-Ø12-CR vs. SS-5x23-150R_10S (TC)

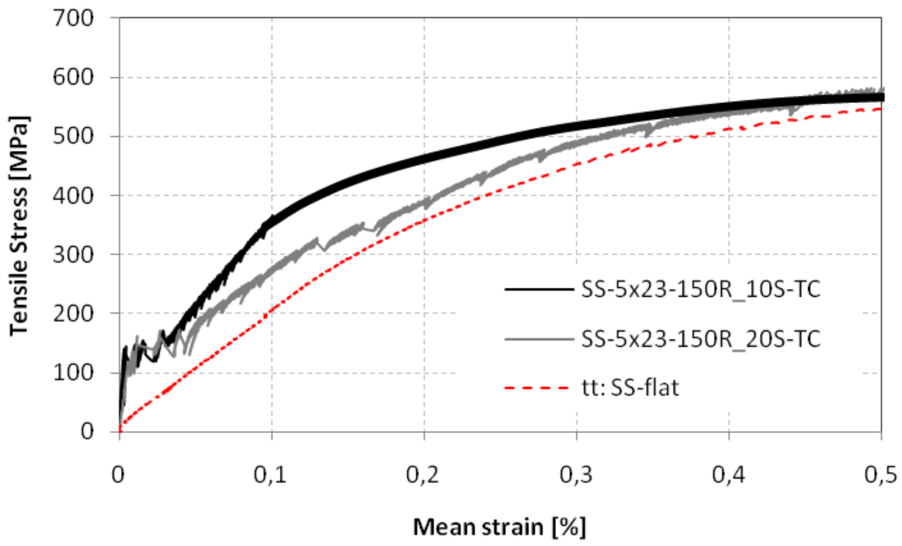

Figure 6-26 Stress-strain relationship. 150R_10S vs. 150R_20S (SS-TC)

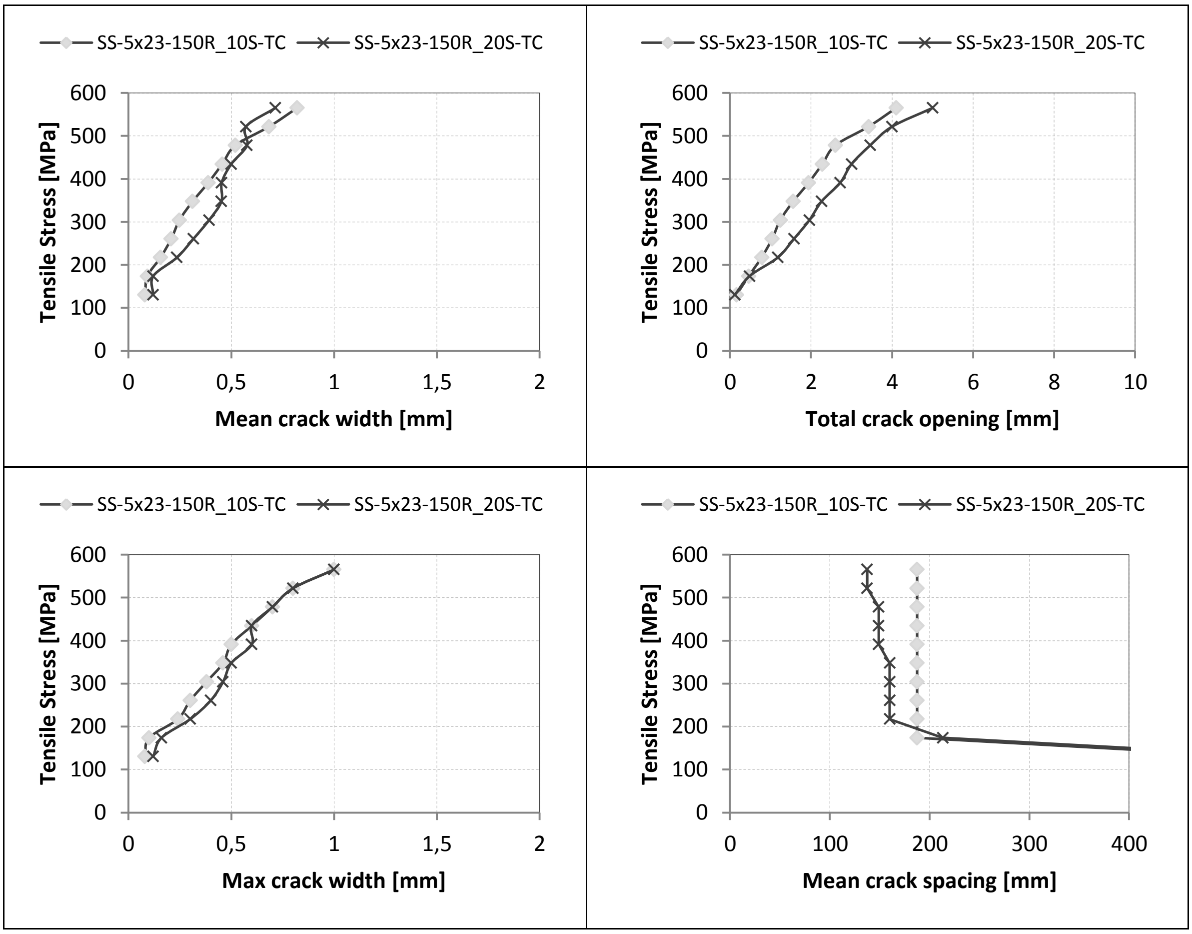

Figure 6-27 Cracking behaviour. 150R_10S vs. 150R_20S (SS-TC)

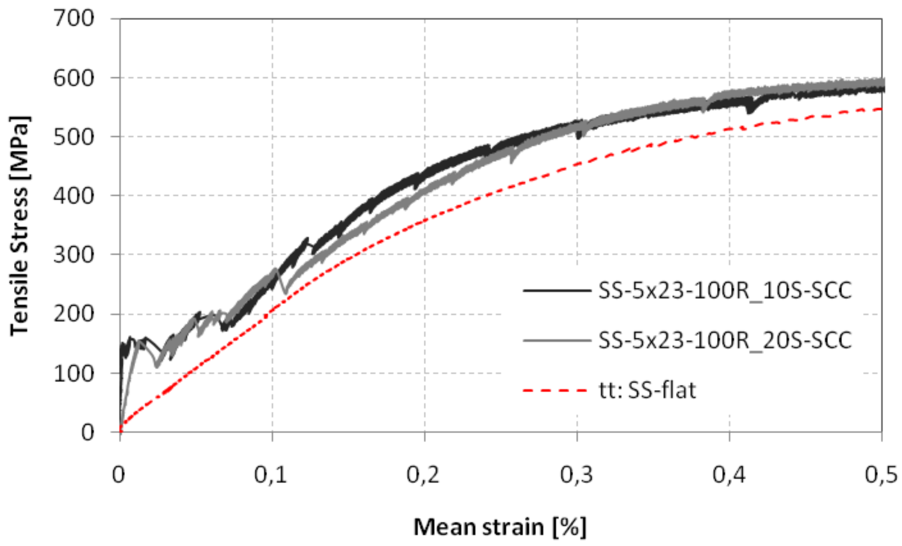

Figure 6-28 Stress-strain relationship. 100R_10S vs. 100R_20S (SS-SCC)

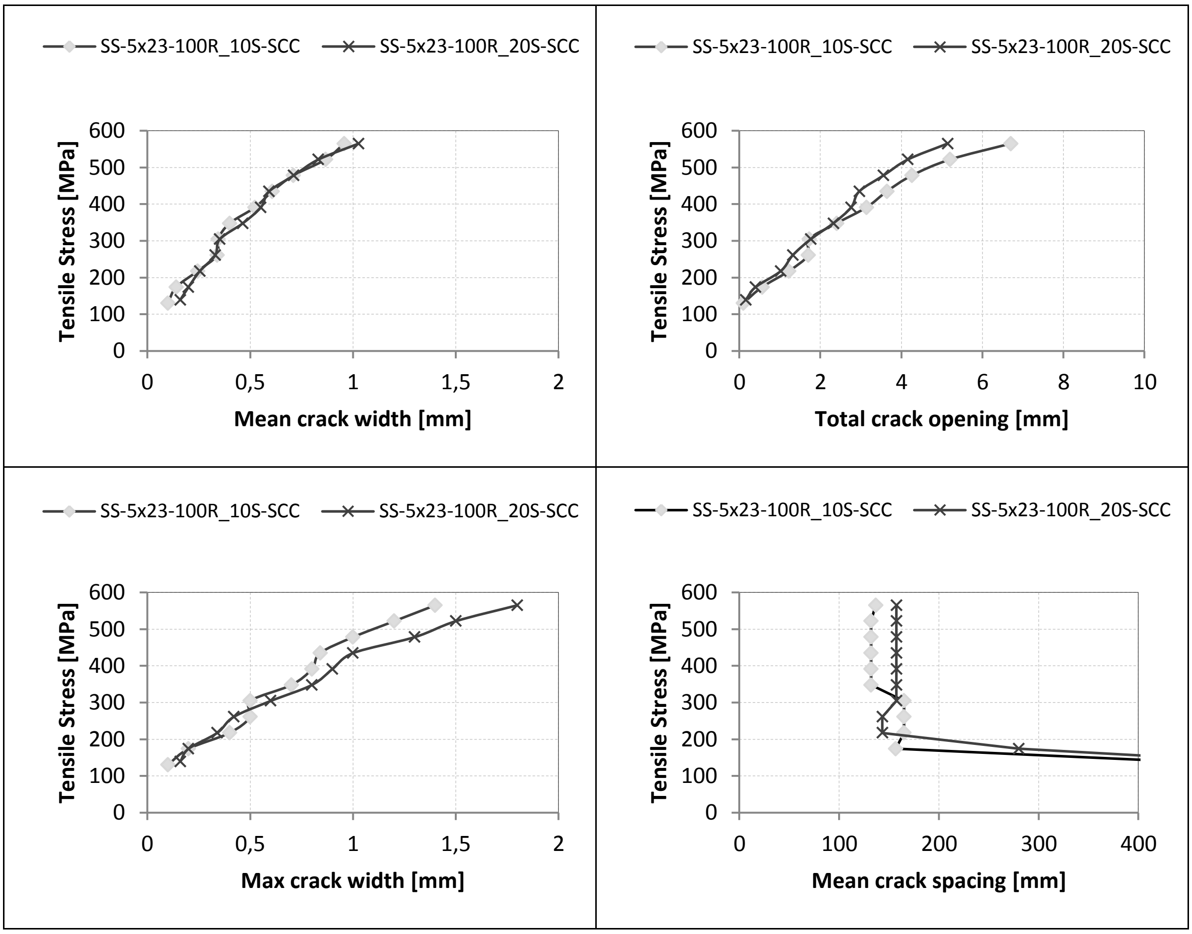

Figure 6-29 Cracking behaviour. 100R_10S vs. 100R_20S (SS-SCC)

4 Analytical verification: comparison to existing models

4.1 Cracking load

The stiffness of the reinforced prisms significantly decreases after first cracking, as it is observed from the stress-strain relationships given in the previous section (see Figure 6-8, 6-9, 6-13, 6-15, 6-17, 6-19, 6-21, 6-23 and 6-25). The load at which this first cracking occurs can be calculated as given by Equation 6-1, where f_{ctm} is the mean concrete tensile strength (determined by direct tensile tests on 3 cylindrical cores Ø113 mm x 120 mm, see Table 6-3), A_c the cross section of the concrete prism, α_s stands for the relation between the modulus of elasticity of the two materials ($\alpha_s = E_s/E_c$) and ρ_s is the reinforcement ratio calculated as the relation between the two cross section areas ($\rho_s = A_s/A_c$). The corresponding stress at first cracking is obtained dividing the cracking load by the cross section area of the reinforcement (see Equation 6-2).

$$F_{cr} = f_{ctm} A_c (1+\alpha_s \rho_s) \tag{6-1}$$

$$\sigma_{cr} = F_{cr} / A_s \tag{6-2}$$

Table 6-6 First cracking stress

Specimen	σ_{cr} [N/mm²]	$\sigma_{cr,exp}$ [N/mm²]	$\sigma_{cr}/\sigma_{cr,exp}$ [-]
CS-Ø10-CR-TC	317,62	179,89	1,77
CS-Ø12-CR-TC	245,89	170,81	1,44
CS-3,5x25-CR-TC	287,21	170,20	1,69
CR-3,5x25-50R_10S-TC	286,87	216,59	1,32
SS-5x23-CR-TC	221,96	108,79	2,04
SS-5x23-50R_10S-TC	242,94	111,18	2,17
SS-5x23-100R_10S-TC	242,75	149,93	1,62
SS-5x23-100R_20S-TC	242,75	147,93	1,64
SS-5x23-150R_10S-TC	242,75	140,91	1,72
SS-5x23-150R_20S-TC	242,75	131,35	1,85
CS-Ø10-CR-SCC	317,84	204,05	1,56
CS-Ø12-CR-SCC	225,17	173,78	1,32
CS-3,5x25-CR-SCC	287,44	206,83	1,39
SS-5x23-CR-SCC	222,20	145,95	1,52
SS-5x23-100R_10S-SCC	222,28	160,55	1,38
SS-5x23-100R_20S-SCC	222,28	155,24	1,43
Mean value			1,62
Standard deviation			0,25

As it is observed from Table 6-6, the experimental results show significantly lower cracking stress than the analytically calculated one. The difference is higher when traditional concrete is used than when self compacting concrete is applied (average ratio of 1,73 for TC and 1,43 for SCC); on the other hand, no influence of material type or reinforcement geometry is observed regarding first cracking stress.

4.2 Tension stiffening effect

4.2.1 According to Eurocode 2

For the characterization of the tension stiffening and to allow for the mean strain calculation, Eurocode 2 [7] (further referred to in this chapter as EC2) defines a distribution or tension stiffening coefficient as given by Equations 6-3 and 6-4, depending on the cracking phase:

$$\zeta = 0 \qquad \text{for uncracked sections, } \sigma < \sigma_{cr} \qquad (6\text{-}3)$$

$$\zeta = 1-\beta_1\beta_2(\sigma_{cr}/\sigma)^2 \qquad \text{for cracked section, } \sigma > \sigma_{cr} \qquad (6\text{-}4)$$

where, σ_{cr} is the tensile stress at first cracking, σ the actual stress of the reinforcement, β_1 is a coefficient taking into account the bond characteristics of the reinforcement (β_1 = 1 for ribbed bars, and β_1 = 0,5 for smooth bars) and β_2 is a coefficient taking into account the influence of the duration of the loading or of repeated loading (β_2 = 1 for a single short-term loading, and β_2 = 0,5 for sustained loads or many cycles of repeated loads).

The average strain is calculated according to Equation 6-5, where ε_I and ε_{II}, represent the strain at uncracked and fully cracked phases, respectively.

$$\varepsilon_m = (1-\zeta)\,\varepsilon_I + \zeta\,\varepsilon_{II} \qquad (6\text{-}5)$$

According to the EC2 therefore, the stress-strain relationship of an axially loaded reinforced prism can be defined by three different branches:

I. The first one corresponds to the uncracked situation (concrete tensile stress is smaller than the tensile strength of the concrete: $\sigma_{ct} < f_{ctm}$), and the strain can be calculated taking ε_I as given by Equation 6-6. The mean strain is calculated from the combination of Equations 6-3 (uncracked), 6-5 and 6-6.

$$\varepsilon_I = F/(E_c A_c + E_s A_s) \qquad (6\text{-}6)$$

II. The second branch starts after the first cracking occurs and extends until the yielding stress of the reinforcement is reached. The strain for the fully cracked phase, ε_{II} , can be expressed as given by Equation 6-7. Equations 6-4 to 6-7 are applied for the calculation of ε_m.

$$\varepsilon_{II} = F/\ E_s A_s \tag{6-7}$$

III. The third branch is the one corresponding to the yielding of the bar. This branch is considered horizontal: only the yielding of the bar occurs and the stress keeps constant with increasing strain until the ultimate strain value of the reinforcement is reached.

The tensile stress-mean strain curve considering the tension stiffening effect as described by EC2 is given in Figure 6-30 (for the reference case of a Ø10 mm bar). This figure allows for comparing the tension stiffening effect definitions given by different models.

4.2.2 According to Model Code 1990

The main difference between the prediction model given by the Model Code 1990 [8] (referred as MC90 further in this chapter) with respect to EC2 is that a cracking formation phase is foreseen in this case. Thus , the stress-strain relation is divided into four different branches:

I. The first branch is equal to the one defined by EC2: it corresponds to the uncracked phase, for concrete tensile stress values lower than the concrete tensile strength. In this case the mean strain equals the strain at the uncracked phase, $\varepsilon_m = \varepsilon_I$, which is defined as given by Equation 6-6.

II. The second branch deals with the crack formation phase, and it extends from the first cracking formation (at a stress level of σ_{cr}) until the last crack occurs (at a stress level of $\sigma_{cr,n}$). The mean stress is calculated as given by Equation 6-8, and considering Equation 6-7 for the calculation of the strain at fully cracked state. β_t is a coefficient dealing with the load duration and equals 0,40 for short term loading according to MC90. The value of the steel stress at which the last crack occurs is given as in Equation 6-9. $\varepsilon_{cr,I}$ deals with the steel strain at the point of zero slip (uncracked section) at the moment when the first crack occurs. $\varepsilon_{cr,II}$ represents the steel stress in the crack when first cracking occurs. The values of $\varepsilon_{cr,I}$ and $\varepsilon_{cr,II}$ are calculated according to Equations 6-10 and 6-11, respectively.

$$\varepsilon_m = \varepsilon_{II} - \frac{\beta_t(\sigma - \sigma_{cr}) + (\sigma_{cr,n} - \sigma)}{(\sigma_{cr,n} - \sigma_{cr})}\left(\varepsilon_{cr,II} - \varepsilon_{cr,I}\right) \tag{6-8}$$

$$\sigma_{cr,n} = 1{,}3\ \sigma_{cr} \tag{6-9}$$

$$\varepsilon_{cr,I} = F_{cr}/(E_c A_c + E_s A_s) \tag{6-10}$$

$$\varepsilon_{cr,II} = F_{cr}/E_s A_s \tag{6-11}$$

III. The third phase is the crack stabilizing phase. It covers the stress-strain relationship from last crack formation until the yielding stress is reached. The mean stress is calculated according to Equation 6-12 (and considering Equations 6-7, 6-10 and 6-11).

$$\varepsilon_m = \varepsilon_{II} - \beta_t \left(\varepsilon_{cr,II} - \varepsilon_{cr,I}\right) \tag{6-12}$$

IV. The fourth and last branch is the one corresponding to the yielding of the bar and is considered horizontal as is the case for the EC2 approach.

Figure 6-30 gives the tensile stress-mean strain curve considering the tension stiffening effect as described by MC90 (for the reference case of a Ø10 mm rebar).

4.2.3 According to Model Code 2010

The draft version of the new fib Model Code 2010 [9] (MC2010 further in this chapter) keeps the 4 stages defined by its predecessor (MC90). However, it simplifies the second phase related to the cracking stage by considering it happening instantaneously at the first cracking stress. Furthermore, it states that the cracking occurs until a certain value of the mean strain is reached; if the strain is larger than this value, the stabilized cracking stage applies. In the following the mentioned stages are given with the corresponding calculation equations:

I. The first branch is equal to the one defined by EC2 and MC90: the mean strain equals the strain at the uncracked phase, $\varepsilon_m = \varepsilon_I$, which is defined as given by Equation 6-6.

II. The second branch deals with the crack formation phase, and it extends from the first cracking formation (at a stress level of σ_{cr}) until a certain value of mean strain is reached. The tensile stress along this stage is considered to be constant and equal to σ_{cr}. The mean strain value until which this phase extends is given by Equation 6-13.

$$\varepsilon_m = f_{ctm} \left(0{,}6+\alpha_s \rho_s\right)/E_s \rho_s \tag{6-13}$$

III. The third phase is the stabilizing cracking phase and it extends from the mean strain value given by the previous Equation 6-13, until yielding stresses are reached. The mean stress is considered in this phase to be related to the naked bar (ε_{II}, as given by Equation 6-7) corrected by a constant value. The calculation is done as given by Equation 6-14.

$$\varepsilon_m = \varepsilon_{II} - 0{,}4\, f_{ctm} / E_s \rho_s \tag{6-14}$$

IV. The last branch which is the one corresponding to the bar yielding is again considered horizontal. The stress is kept constant at yielding stress value while increasing strain until the ultimate steel strain is reached.

Figure 6-30 gives the tensile stress-mean strain curve considering the tension stiffening effect as described by MC2010 (for the reference case of a Ø10 mm rebar).

4.2.4 Comparison between models

The tension stiffening effect as given by EC2, MC90 and MC2010 (for the reference case of a Ø10 mm rebar) are plotted together in Figure 6-30. The tensile stress-strain curve for the naked bar ($\varepsilon_m = \sigma_s/E_s$ for $0 \leq \sigma_s < \sigma_y$) is also given for visualization of the tension stiffening effect.

For the flat rebars tested in this work, due to the pronounced hardening of the rebars at increased stresses, the assumption of extending the stabilized cracking phase until the yielding forces are reached and then keeping the last branch horizontal (yielding branch) is not in good agreement with the real behaviour of the tested bars. Thus, the last branch has been modified and adapted to the tensile behaviour of the flat rebars tested in this work as follows. The stabilized cracking stage is extended until the stress values corresponding to the 0,2 % of strain (as it is done for characterizing the hardening behaviour of these type of bars, because of the difficulty of defining an unique yielding stress value). From that point on, the stress is assumed to increase linearly until the ultimate stress values are reached.

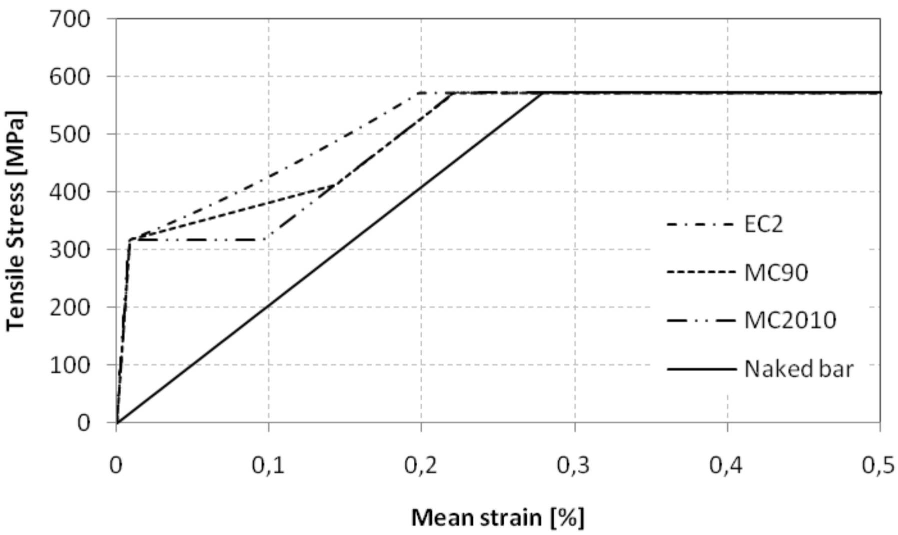

Figure 6-30 Tensile stress-mean strain curves considering the tension stiffening effect as given by EC2, MC90 and MC2010, for CS-Ø10-CR

4.2.5 Comparison of the test results to the existing models

In the following the described tension stiffening models are compared to the test results obtained. Due to the non negligible difference observed for the stress at the first cracking between the theoretical and experimental values (not only for the flat rebars but also for the standard round references), and to allow for a realistic comparison between the test results and the models, experimental values of σ_{cr} are considered in this section.

As observed from Figure 6-31 and 6-30, an acceptably good agreement is obtained between the models and the experimental results for reference reinforcements, CS-Ø10-CR and CS-Ø12-CR, respectively. In the case of the smaller diameter, the simplified curve given by the MC2010 is the one farther from the experimental results at cracking stage, while both EC2 and MC90 give a good approximation to the test results. In the case of diameter 12 mm bars, the test results show a closer behaviour to both MC90 and MC2010 curves, than to EC2, which slightly overestimated the tension stiffening effect observed experimentally.

For flat rebars, it is observed for CS-3,5x25-CR and SS-5x23-CR, in Figure 6-33 and Figure 6-34, respectively, that the uncracked and first cracking stage are well characterized by both EC2 and MC90 approaches, while the MC2010 slightly underestimates the stiffness of the flat bars at the first cracking stage. However, the models underestimate the tension stiffening effect experimentally observed for flat ribbed rebars at the stabilized cracking stage.

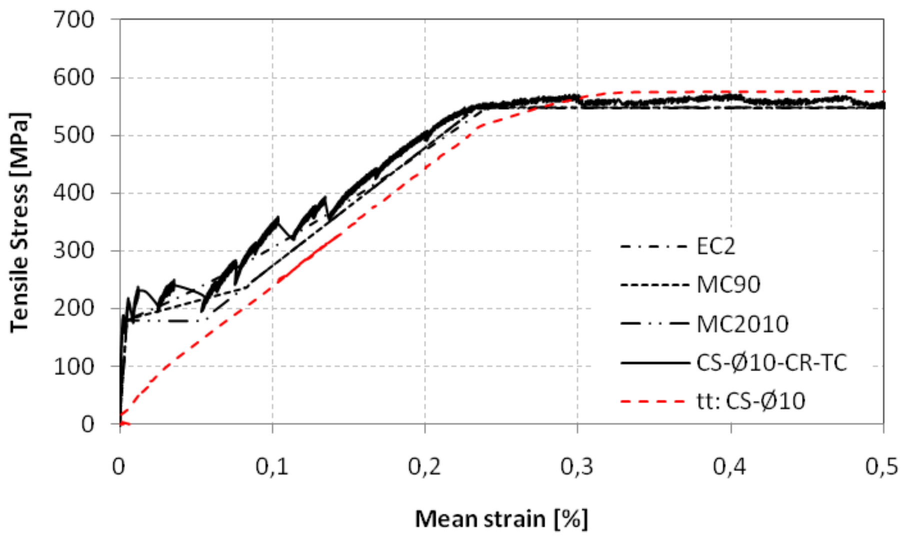

Figure 6-31 Comparison of tension stiffening tensile stress-mean strain curves for CS-Ø10-CR

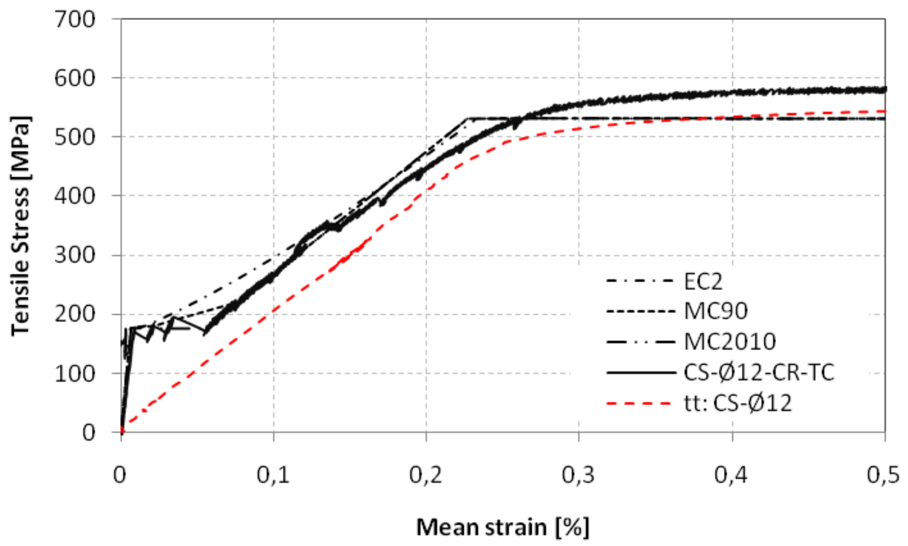

Figure 6-32 Comparison of tension stiffening tensile stress-mean strain curves for CS-Ø12-CR

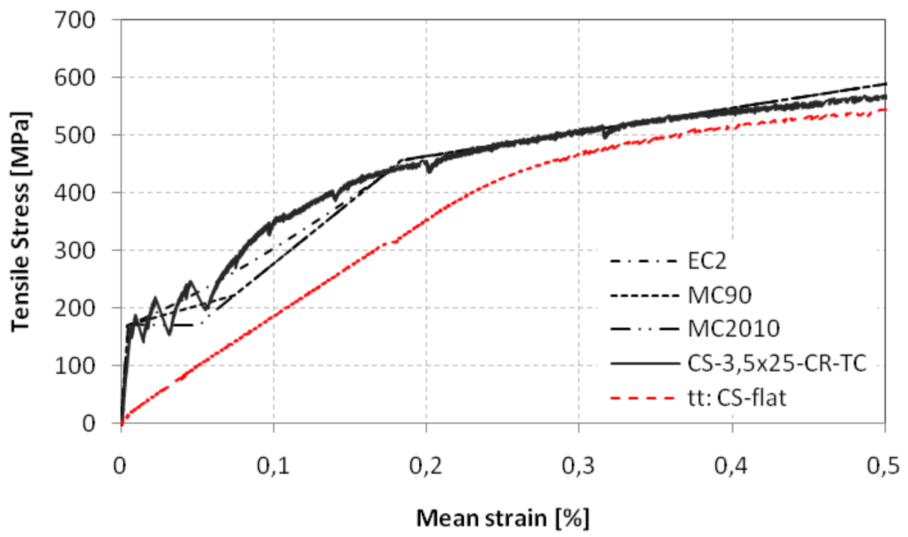

Figure 6-33 Comparison of tension stiffening tensile stress-mean strain curves for CS-3,5x25-CR

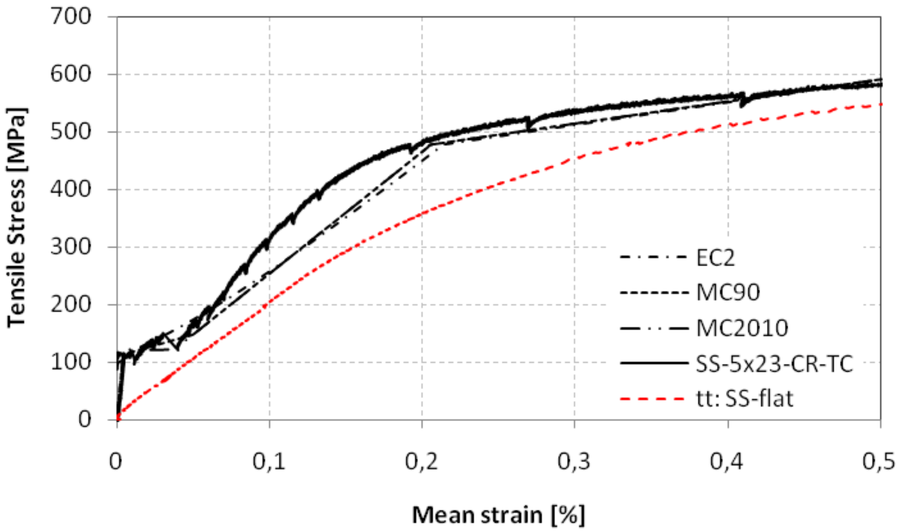

Figure 6-34 Comparison of tension stiffening tensile stress-mean strain curves for SS-5x23-CR

4.3 Crack spacing and crack width

As required by the serviceability limit state, the EC2, the MC90 and the MC2010 give the maximum acceptable crack widths depending on the exposure class and the applied load type. Furthermore, the guidelines also give a procedure to calculate the mean crack width for a given reinforced concrete member. For the stabilized cracking stage, the mean crack width is calculated based on the mean crack spacing and the mean concrete and steel strains, as given by Equation 6-15 [7][8][9]. According to [8], the mean crack spacing is related to the maximum crack spacing by a factor of 2/3 as given by Equation 6-16. The mean crack width can be therefore given in function of the maximum crack spacing (see Equation 6-17).

$$w_m = s_{r,m}\,(\varepsilon_{sm} - \varepsilon_{cm}) \tag{6-15}$$

$$s_{r,m} = 2/3\; s_{r,max} \tag{6-16}$$

$$w_m = 2/3\; s_{r,max}\,(\varepsilon_{sm} - \varepsilon_{cm}) \tag{6-17}$$

In the following different approaches will be considered and studied for the calculation of the mean crack width. Two approaches are considered for the calculation of the maximum crack spacing, $s_{r,max}$, and two for predicting the mean strain differences between the steel and the concrete ($\varepsilon_{sm} - \varepsilon_{cm}$).

4.3.1 First approach: EC2 definition for $s_{r,max}$

EC2 gives different definitions for estimating the maximum crack spacing depending on the actual situation of the reinforcements (bar spacing, angle between axes of principal stress and the direction of the reinforcement for orthogonal reinforcement, walls subjected to early thermal contraction, etc.). For the case studied here, the definition given by Equation 6-18 is adopted.

$$s_{r,max} = k_3\, c_c + k_1\, k_2\, k_4\, Ø/\rho_s \qquad (6\text{-}18)$$

where, c_c is the concrete cover; and k_1 to k_4 are defined as follows: k_1 considers the bond properties of the reinforcement, being 0,8 for high bond bars and 1,6 for bars with a plain surface; k_2 takes into account the distribution of strain being equal to 0,5 for bending and 1,0 for pure tension. The recommended values for k_3 and k_4 are 3,4 and 0,425, respectively.

For the reference carbon steel round bars tested in this work, it is feasible and easy to apply the former definition and $s_{r,max}$ values of 437 mm and 381 mm are obtained for diameter 10 and 12 mm, respectively. However, for the flat rebars tested in this work, an equivalent diameter needs to be calculated, and the concrete cover should be considered depending on the orientation of the rebar. Furthermore, the value of coefficient k_1 should be estimated given the lower relative rib area (f_R) of these flat reinforcements as studied in previous chapters. For a first approximation of this method to the flat rebars tested in this work, an equivalent diameter of 10 mm is taken for the CS-3,5x25-CR specimen and equivalent diameter of 12 mm for SS-5x23-CR. Note that these equivalent diameters have been calculated considering a round bar with a comparable cross section area with respect to the flat rebar. The concrete cover is taken as the one corresponding to the wider side of the rebar, and k_1 is taken equal to 1. The calculation is only performed for the completely ribbed specimens (both round and flat reinforcements).

The calculated mean crack spacing values are given in Table 6-7 (referred as first approach by using the suffix "(1)"), together with the experimentally obtained ones and the ratio between the calculated and the experimental values. For all the cases the experimentally obtained values are considerably smaller than the calculated ones, both for round reference reinforcements and for the flat ones. As results are not in good agreement with the experimentally obtained values, even for the reference bars, this approach is not longer considered for the analysis performed in this work.

Note that the equivalent diameter for flat rebars can also be calculated based on a comparable perimeter (instead of comparable cross section). However, the values obtained for the maximum crack spacing will be higher than when the equivalent diameter is calculated based on a comparable cross section area, making the difference between the experimental and analyitical results higher.

4.3.2 Second approach: considering the transfer length for defining $s_{r,max}$

Both the MC90 and the MC2010 give the maximum crack spacing related to the transfer length of the reinforcement embedded in concrete. According to the models, the maximum crack spacing is twice the transfer length (l_t), and the latter is defined as given by Equation 6-20, where u_s is the steel surface per unit length in contact with the concrete (the bond perimeter), and τ_m is the mean shear strength along the transfer length.

$$s_{r,max} = 2\, l_t \tag{6-19}$$

$$l_t = A_c\, f_{ctm} \,/ u_s\, \tau_m \tag{6-20}$$

For standard round reinforcement, stabilized cracking and short term loading, the MC90 and MC2010 define the mean bond strength τ_m equal to 1,8 times the mean tensile strength of the concrete (τ_m = 1,8 f_{ctm}).

If the mean crack spacing is calculated according to this approach, a clear difference is observed between the prediction given by this approach for round reference bars and for completely ribbed flat ones. While the approach slightly overestimates the mean crack spacing obtained experimentally for round reference bars (see Table 6-7, referred as second approach by suffix "(2)"), this approach significantly underestimates the mean crack spacing obtained for flat rebars. Given the involved parameters, and considering the differences observed in the bond behaviour between the reference samples and the flat samples (see previous Chapters 4 and 5 of this work), the definition of the mean bond strength (τ_m = 1,8 f_{ctm}) given by the model codes seem to be the only parameter that might have influenced on the differences of the prediction between round bars and flat samples tested in this work.

Table 6-7 Analytical verification of the mean crack spacing

Rebar	$s_{r,m,exp}$ *(mm)*	$s_{r,m\,(1)}$ *(mm)*	$s_{r,m\,(1)} / s_{r,m,exp}$ *(-)*	$s_{r,m\,(2)}$ *(mm)*	$s_{r,m\,(2)} / s_{r,m,exp}$ *(-)*
CS-Ø10-CR-TC	144,00	291,25	2,02	168,50	1,17
CS-Ø12-CR-TC	134,00	253,77	1,89	139,74	1,04
CS-3,5x25-CR-TC	223,33	323,48	1,44	92,75	0,41
SS-5x23-CR-TC	165,00	300,87	1,82	94,05	0,57
CS-Ø10-CR-SCC	126,67	291,25	2,30	168,50	1,33
CS-Ø12-CR-SCC	134,00	253,77	1,89	139,74	1,04
CS-3,5x25-CR-SCC	192,50	323,48	1,68	92,75	0,48
SS-5x23-CR-SCC	132,00	300,87	2,28	94,05	0,71
Mean value			1,92		0,85
Standard deviation			0,29		0,34

(1) Calculated as given by Equations 6-16 and 6-18

(2) Calculated as given by Equations 6-16, 6-19 and 6-20

4.3.3 Calculation of (ε_{sm} – ε_{cm}) considering the tension stiffening coefficient given by EC2

The second term for calculating the mean crack width as given by Equation 6-17, is related to the difference between the mean strains of steel and concrete. In other words, the mean crack width is dependent on the mean reinforcement strain with respect to the surrounding concrete. The latter can be expressed as the mean steel strain multiplied by a coefficient that takes into account the tension stiffening effect derived from the joint action between the steel and the concrete [10], as given by Equation 6-21. For the stabilized cracking stage, the mean steel strain can be calculated according to Equation 6-7 and the tension stiffening coefficient according to Equation 6-4, as given by EC2.

$$\varepsilon_{sm} - \varepsilon_{cm} = \varepsilon_{sm}\,\zeta \tag{6-21}$$

The mean crack value calculated for completely ribbed samples tested in this work (both round and flat reinforcements) is given in Table 6-8, for a stress level of the reinforcement fixed at 50% of the yielding stress. The calculation is performed considering the second approach, the transfer length approach, for the calculation of the mean crack spacing, where τ_m has been taken equal to 1,8 f_{ctm} as given by MC90 and MC2010. Note that experimental values of cracking loads have been considered for the calculation given the significant differences observed between the predicted and the experimental ones, as described before.

It is clearly observed from Table 6-8 that this approach gives underestimated values of the mean crack width for the flat rebars tested in this work, while the approximation to the experimentally observed behaviour for the reference round bars is acceptable. As discussed in the previous section, the transfer length definition taking τ_m equal to 1,8 f_{ctm} seems not to be appropriate for the flat rebars investigated. Furthermore, the definition of the coefficient β_1 in Equation 6-4 has been taken equal to 1 as it corresponds to ribbed bars. However, given the lower relative ribbed area involved for the flat rebars this value might be overestimated.

Table 6-8 Analytical verification of the mean crack width

Rebar	$w_{m,exp}$ *(mm)*	$w_{m\,(3)}$ *(mm)*	$w_{m\,(3)}$ / $w_{m,exp}$ *(-)*	$w_{m\,(4)}$ *(mm)*	$w_{m\,(4)}$ / $w_{m,exp}$ *(-)*
CS-Ø10-CR-TC	0,20	0,18	0,89	0,17	0,86
CS-Ø12-CR-TC	0,24	0,14	0,60	0.14	0,58
CS-3,5x25-CR-TC	0,55	0,10	0,16	0,09	0,16
SS-5x23-CR-TC	0,78	0,12	0,15	0,11	0,14
CS-Ø10-CR-SCC	0,15	0,15	1,01	0,16	1,06
CS-Ø12-CR-SCC	0,22	0,15	0,67	0,14	0,65
CS-3,5x25-CR-SCC	0,50	0,09	0,19	0,10	0,19
SS-5x23-CR-SCC	0,53	0,10	0,20	0,10	0,18
Mean value			0,48		0,47
Standard deviation			0,35		0,36

(3) Calculated as given by Equations 6-17, 6-19, 6-20 and 6-21

(4) Calculated as given by Equations 6-17, 6-19, 6-20 and 6-22

Figure 6-35 and Figure 6-36 compare the experimental crack width as a function of the tensile stress to the predicted crack width obtained by applying the transfer length approach (for maximum crack spacing calculation) combined with the approach of considering the tension stiffening coefficient given by EC2 for the calculation of the strain differences (referred as third approach by the suffix "(3)" and calculated with Equations 6-16, 6-19, 6-20 and 6-21). Figure 6-35 gives the comparison for the reference round ribbed bar with diameter 10 mm (CS-Ø10-CR) and for the CS-3,5x25-CR sample which have a comparable cross section area, tested with TC. Figure 6-36 gives the same comparison for CS-Ø12-CR and SS-5x23-CR, tested with TC. It is clearly observed from the graphs that while an acceptable approximation is achieved for the reference reinforcements, the experimental and the predicted values differ substantially from each other for the flat reinforcements.

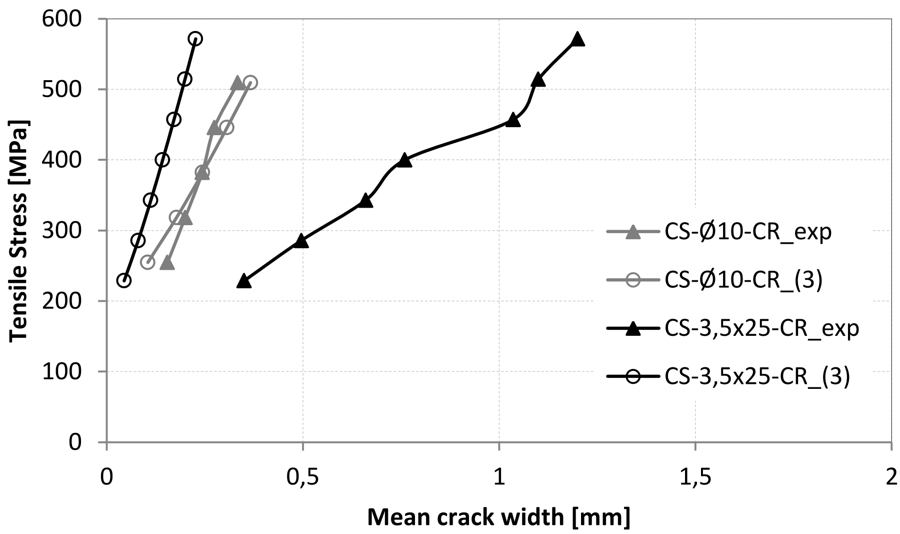

Figure 6-35 Mean crack width evolution obtained experimentally compared to the one calculated by applying the tension stiffening coefficient given by EC2. For CS-Ø10-CR and CS-3,5x25-CR tested in TC

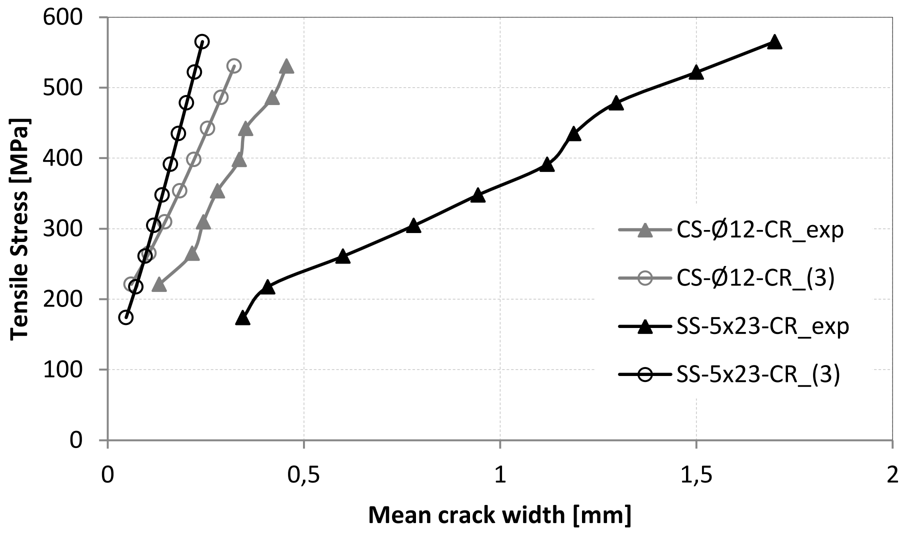

Figure 6-36 Mean crack width evolution obtained experimentally compared to the one calculated by applying the tension stiffening coefficient given by EC2. For CS-Ø12-CR and SS-5x23-CR tested in TC

4.3.4 Calculation of (ε_{sm} – ε_{cm}) according to MC90, MC2010 and EC2

As given by the three guidelines considered in this section, EC2, MC90 and MC2010, the difference between the mean strain of steel and concrete can be defined (see Equation 6-22) as the mean steel strain at the given situation minus the strain related to the cracking loads reduced by a factor k_t. The latter coefficient is an empirical factor to assess the mean strain over the transfer length, and equals to 0,6 for stabilized cracking stage and short term loading for round ribbed reinforcement [7][8][9]. The mean steel strain (ε_{sm}) is calculated according to Equation 6-7.

$$\varepsilon_{sm} - \varepsilon_{cm} = \varepsilon_{sm} - k_t\, \sigma_{cr}/E_s \qquad (6\text{-}22)$$

The mean crack width calculated by this fourth approach (suffix "(4)") for completely ribbed samples tested in this work (both round and flat reinforcements), for an stress level of the reinforcement fixed at 50% of the yielding stress is given in Table 6-8. As it has been done for the previous approach, the calculation is performed considering the second approach, the transfer length approach, for the calculation of the mean crack spacing, where τ_m has been taken equal to 1,8 f_{ctm} as given by MC90 and MC2010. The experimental values of the cracking stress are considered as it has been done previously.

Predicted values calculated according to this fourth approach are very close to the ones calculated by approach (3), as it can be deducted from Table 6-8 and comparing Figure 6-37 and Figure 6-38 to Figure 6-35 and Figure 6-36, respectively. For both approaches a quite acceptable approximation is obtained for the reference rebars, while results obtained experimentally for flat reinforcements differ substantially from the analytically calculated ones.

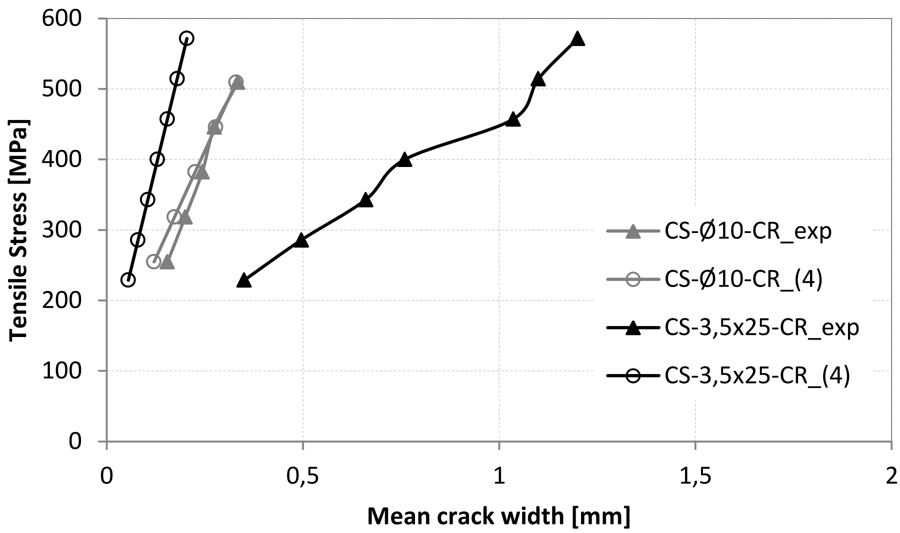

Figure 6-37 Mean crack width evolution obtained experimentally compared to the one calculated by applying the definition given by MC90, MC2010 and EC2 for strain difference calculation. For CS-Ø10-CR and CS-3,5x25-CR tested in TC

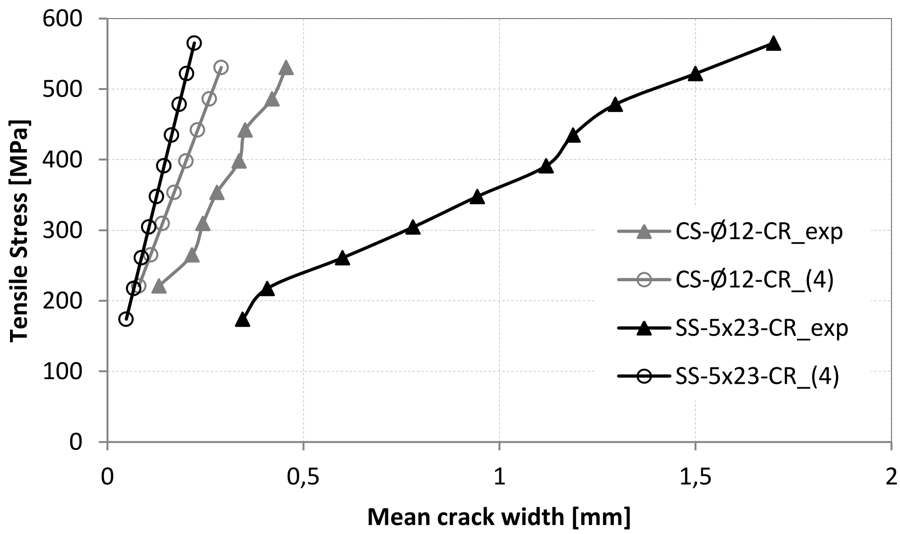

Figure 6-38 Mean crack width evolution obtained experimentally compared to the one calculated by applying the definition given by MC90, MC2010 and EC2 for strain difference calculation. For CS-Ø12-CR and SS-5x23-CR tested in TC

4.3.5 Proposed adaptation for the mean crack width calculation for completely ribbed flat reinforcing elements

Given the non accuracy observed for the analyzed models to predict the cracking behaviour observed experimentally for the flat reinforcements tested in this work with completely ribbed surface configuration, an adaptation is proposed in this section.

The first approach considered for calculation of the maximum crack spacing (based on the EC2 definition) is not being longer considered as no good prediction was obtained even for the reference round bars tested. Thus, the second approach dealing with the transfer length definition is further considered in this section.

Given the definition of the maximum crack spacing based on the second approach (see Equations 6-19 and 6-20), the only factor that might have influenced on the obtained inaccurate prediction is the definition given by MC90 and MC2010 for the mean bond strength along the transfer length. Due to the lower relative ribbed area involved in the flat rebars tested in this work (comparing to the corresponding values of the reference bars and considering optimum values of f_R between 0,05 and 0,10 [11]), the average bond strength developed by the bars along the transfer length might be smaller than 1,8 times the mean concrete tensile strength (which is the value given by MC90 and MC2010 for stabilized cracking stage and for short term loading).

Furthermore, the value of β_1 might have been overestimated when taking it equal to 1 for flat ribbed samples tested in this work. In a similar way, the empirical factor k_t has been assessed for round ribbed bars and this value might be different for the flat reinforcements. Thus, an analysis is performed in order to obtain an empirical coefficient λ, which modifies the definition given by the codes for the mean crack width calculation. The assessment of λ is based on the experimentally obtained test results for the mean crack width of completely ribbed flat reinforcements at several stress levels. λ should be considered as a factor modifying the parameters involving bond differences between the round and flat ribbed rebars tested in this work. The mean crack width for completely ribbed flat rebars should be considered as given by Equation 6-23, where $w_{m,Ø}$ stands for the mean crack width given by the model codes for round ribbed bars. The analysis is performed twice, considering both the third and the fourth approach studied previously for the mean strain difference definition, used for the calculation of $w_{m,Ø}$. As a result an average λ value is obtained for each considered approach, as given in Table 6-9.

$$w_{m,flat\_CR} = w_{m,Ø} / \lambda \tag{6-23}$$

Table 6-9 Analyticaly obtained mean λ values

Variable	$\boldsymbol{\lambda}_{(3)}$	$\boldsymbol{\lambda}_{(4)}$
Mean value	0,1636	0,1633
Standard deviation (%)	0,0465 (28,42)	0,0217 (13,31)

(3) Considering Equation 6-21

(4) Considering Equation 6-22

The obtained average λ values are applied to recalculate the mean crack spacing evolution for the completely ribbed flat reinforcements considering both third and fourth approaches. Some of the obtained results are plotted in Figure 6-39 and Figure 6-40, for the CS-3,5x25-CR tested in TC and SS-5x23-CR tested in SCC, respectively. Furthermore, Figure 6-41 compares the experimentally obtained mean crack width values to the ones calculated using Equation 6-23 and taking λ values as given by Table 6-9, for completely ribbed flat reinforcements tested with both TC and SCC and for all the recorded stress levels. As can be observed from the smaller standard deviation obtained in the calculation of λ by considering the fourth approach (Table 6-9 and the plotted graphs), both considered approaches are acceptably close to the experimental results, yet approach_(4) (based on Equation 6-22 for the calculation of the mean strain difference between steel and concrete) give less scattered prediction. The accuracy to the test results is higher for low mean crack width values, which is of main interest for serviceability limit state prediction.

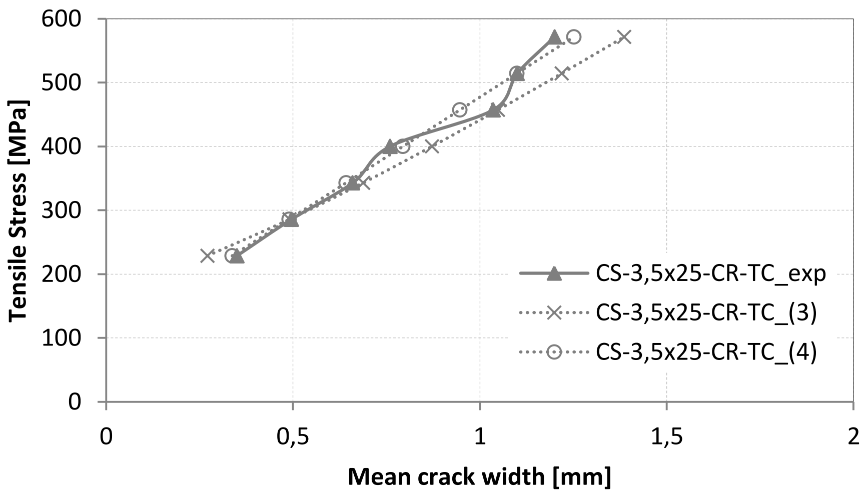

Figure 6-39 Mean crack width values. Comparison between experimental values and the proposed adaptation. For CS-3,5x25-CR tested in TC

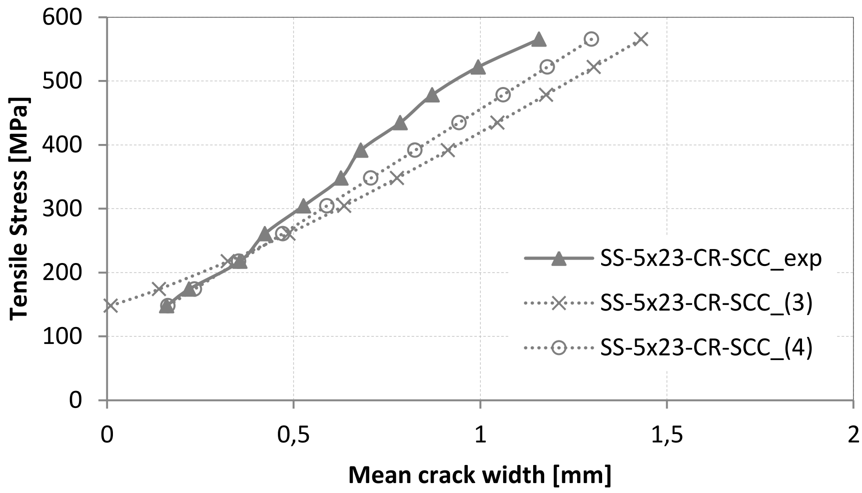

Figure 6-40 Mean crack width values. Comparison between experimental values and the proposed adaptation. For SS-5x23-CR tested in SCC

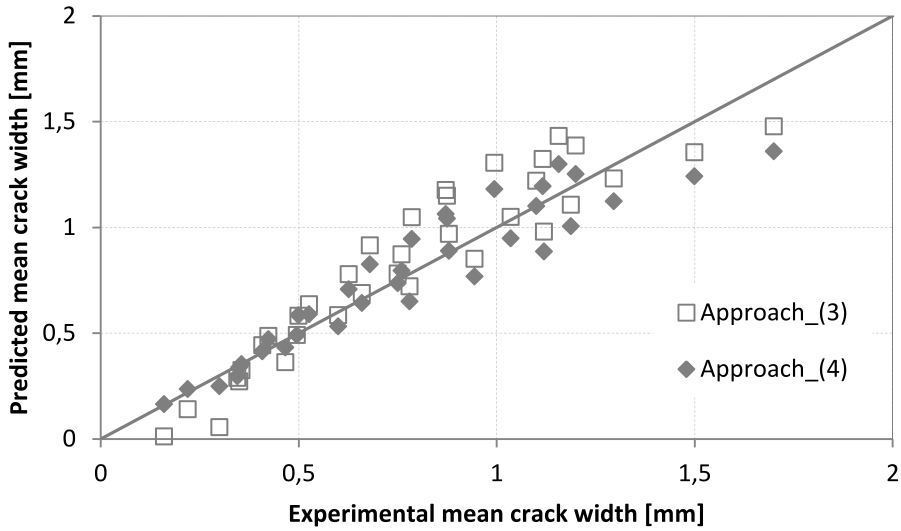

Figure 6-41 Comparison of experimental and predicted mean crack width values, for both considered approaches. Flat CR rebars

4.3.6 Proposed adaptation for the mean crack width calculation for flat reinforcing elements with an alternate rib pattern

From the analysis and discussion of the test results, it has been already observed that the flat reinforcements with an alternate pattern surface configuration which combines smooth and ribbed areas within the embedded length show different cracking behaviour than their corresponding (same material and same dimensions) completely ribbed sample. Although not for all the analyzed samples the number of cracks (and therefore, the mean crack spacing) differ in the same way from the one obtained for the completely ribbed sample, for all the cases the mean crack width is smaller when alternate patterns are used (see Table 6-5 for comparing values at 50% of the yielding stress of each rebar).

On the other hand, the theoretical hypothesis for applying the alternate surface patterns deals with the concept that if at the zones surrounding a crack, the steel is partially detached from the concrete, larger steel length is available to carry the existing tensile stresses, and therefore, the deformation will be more distributed leading to a smaller crack opening. The mentioned detachment is more likely to occur if a smooth zone is involved in the surrounding of the crack, as smaller stresses are necessary to break the bond between the steel and the concrete than in the case of a ribbed zone. However, it should be kept in mind that large areas of smooth zones and/or a large number of smooth zones might have a negative effect on the appropriate bond interaction between the steel and the concrete. As it has been already discussed in this work (Chapter 4 and 5) the smooth samples develop lower bond capacity than the ribbed samples and in the case of alternate patterns, it has been observed that introducing smooth zones within the bond length leads to larger slip values at increased bond stress values.

As a result, it is believed, that the number of smooth zones within the embedded length and the length of them with respect to the length of the ribbed zone might have influence on the cracking distribution. Based on this, two new parameters have been defined in order to analytically verify the cracking behaviour of the flat reinforcements with alternate rib pattern: (1) φ gives the number of single alternate patterns within the embedded length (equivalent to the number of smooth zones within the embedded length) relating the single alternate pattern (single smooth length l_S plus single ribbed length l_R) to the total embedded length $l_{b,TOT}$ (length of the concrete prism) and is defined as given by Equation 6-24. (2) ψ is defined by Equation 6-25 and gives the proportion of the smooth zone with respect to the single alternate pattern.

$$\varphi = (l_S + l_R) \,/\, l_{b,TOT} \tag{6-24}$$

$$\psi = l_S \,/\, (l_S + l_R) \tag{6-25}$$

Regression analysis of the test results has been performed in order to obtain an equation that relates the mean crack width of the alternate pattern with respect to its equivalent completely ribbed flat reinforcement. The analysis has been performed considering the mean crack width results obtained experimentally for all the tested alternate patterns, for all recorded stress levels. The regression analysis has been performed considering the parameters defined by Equations 6-24 and 6-25, and defining the relation between the mean crack width of the alternate pattern and the one of the completely ribbed sample as given by Equation 6-26.

The analysis has been performed twice by considering the previously discussed approach_(3) and approach_(4) for the calculation of $w_{m,flat\_CR}$, considering values of λ_(3) and λ_(4), given in Table 6-9, respectively.

$$w_{m,flat\_alternate} = (a + b\,\varphi + c\,\psi)\, w_{m,flat\_CR} \tag{6-26}$$

Table 6-10 Calculated parameters from regression analysis

Coefficient	*Approach_(3)*	*Approach_(4)*
a	0,856	0,915
b	-2,666	-2,785
c	0,453	0,343

Figure 6-42 to 6-44 give individual results of the regression analysis performed comparing experimentally obtained mean crack width results to the ones obtained by applying Equation 6-26 for both considered approaches. The figures show results for the tested different alternate patterns: SS-5x23-50R_10S, SS-5x23-100R_20S and SS-5x23-150R_20S tested in TC and for SS-5x23-100R_10S tested in SCC, respectively. As it is observed from the graphs, a good agreement is generally obtained between the experimental and the predicted values; in particular for low mean crack widths (corresponding to stress values under service load conditions). The accuracy of Equation 6-26 is also observed in Figure 6-46, where all the mean crack width test results of alternate rebars are plotted against their corresponding predicted value.

Although the difference between the predictions given by the different considered approaches is not substantial, and therefore not clearly concludible from the plotted graphs, if the mean ratio is calculated in terms of predicted/experimental mean crack width for samples with an alternate rib pattern obtained for each approach, the values given in Table 6-11 are obtained, which again verifies that the approach_(4) gives slightly more accurate values. The approximation of these mean ratios to 1 confirms the good accuracy obtained from the regression analysis performed.

Table 6-11 Average mean crack width ratios

	$w_{m,pred}/w_{m,exp\_}(3)$	$w_{m,pred}/w_{m,exp\_}(4)$
Mean values	1,0519	1,0403
Standard deviation (%)	0,2210 (21,01)	0,2129 (20,46)

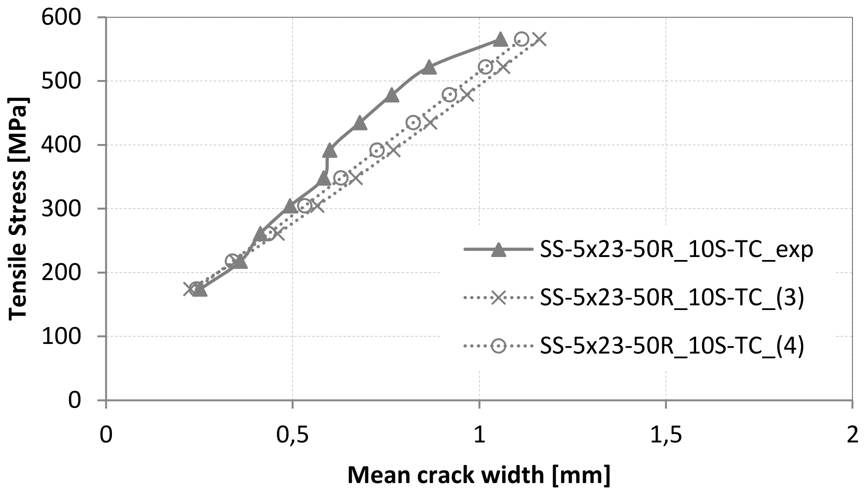

Figure 6-42 Mean crack width values. Comparison between experimental and predicted values. For SS-5x23-50R_10S tested in TC

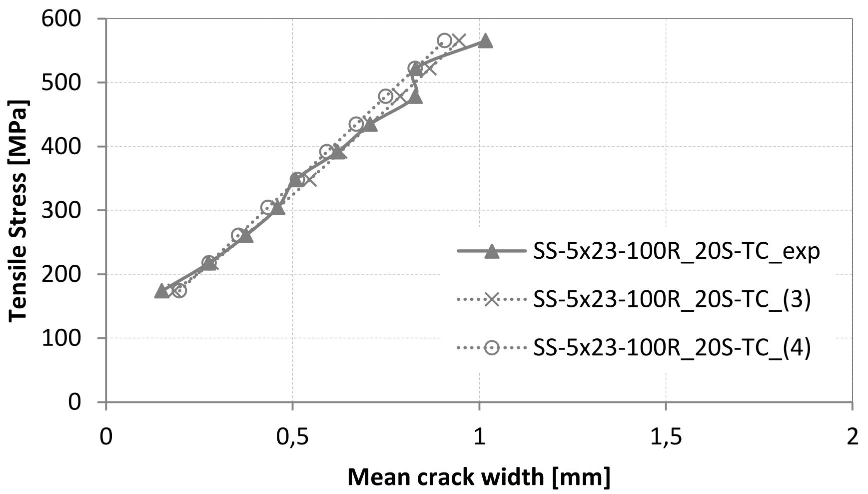

Figure 6-43 Mean crack width values. Comparison between experimental and predicted values. For SS-5x23-100R_20S tested in TC

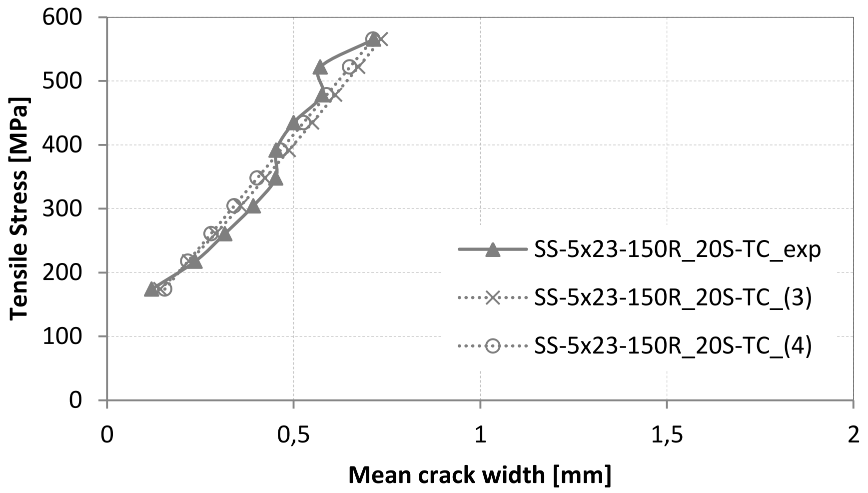

Figure 6-44 Mean crack width values. Comparison between experimental and predicted values. For SS-5x23-150R_20S tested in TC

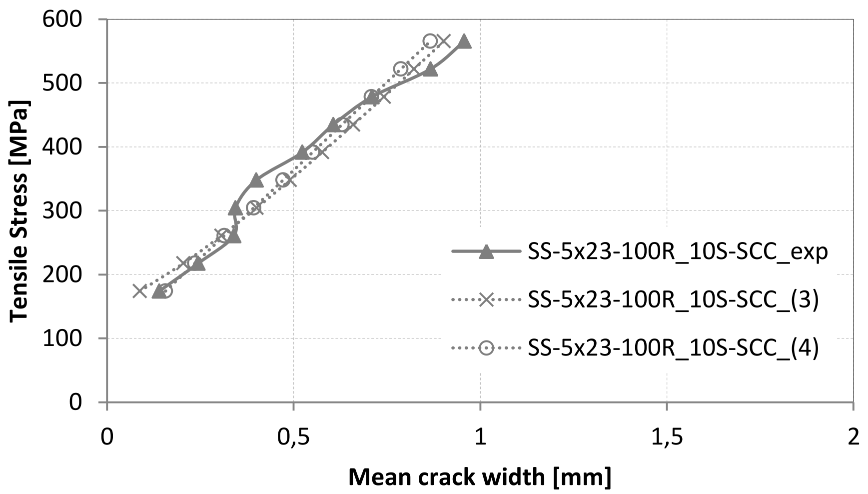

Figure 6-45 Mean crack width values. Comparison between experimental and predicted values. For SS-5x23-100R_10S tested in SCC

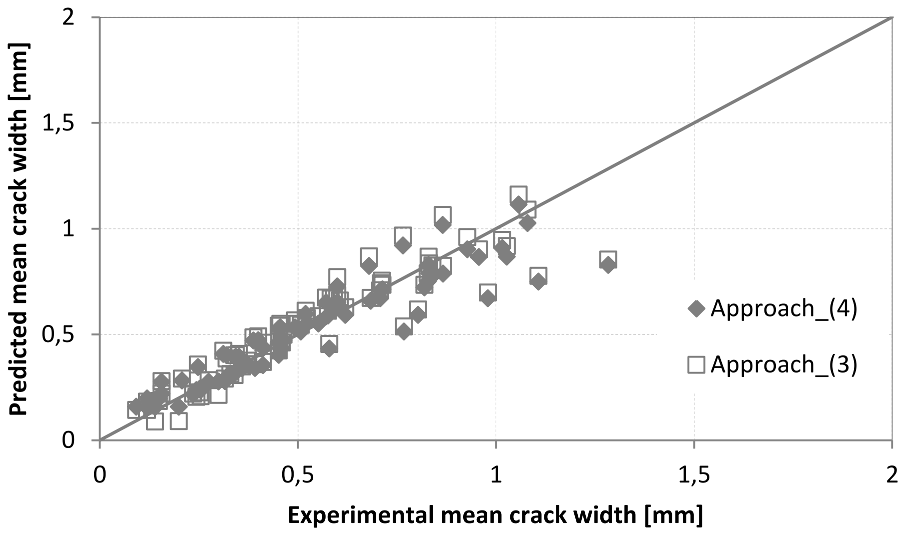

Figure 6-46 Comparison of experimental and predicted mean crack width values, for both considered approaches. Flat alternate rebars

The author would like to remark that the adaptations proposed in this chapter for predicting the cracking behaviour of the flat rebars (both for completely ribbed samples and for the alternate ones) are specific for the type of flat rebars tested and for the alternate patterns analyzed in this work.

5 Conclusions

The tension stiffening and the cracking behaviour of flat SS rebars when embedded in concrete have been analyzed by means of a series of tension stiffening tests. The influence of different parameters is characterized performing tests to both CS and SS flat rebars when embedded in TC or SCC. Several surface configurations have been studied: the behaviour of completely ribbed flat rebars has been compared to rebars with an alternate rib pattern; furthermore, different alternate patterns have been analyzed and compared. Standard CS round ribbed samples with a comparable cross section have also been used for comparison. Test results have been extensively discussed and compared to existing models. Adaptations of these models have been proposed for predicting the cracking behaviour of the flat rebars tested. Based on the obtained results, the following conclusions can be drawn out:

1. Regarding reinforcement geometry, it can be concluded that for comparable cross sectional areas, cracking occurs at lower steel stress levels for flat elements than for

round bars. On the other hand, regarding tensile stress-mean strain relationships, flat members behave stiffer or with similar stiffness compared to round bars with similar cross sectional area. In other words, it can be concluded that the round bars develop somewhat less “tension stiffening effect” than the flat elements do.

2. Round bars develop better crack behaviour than flat members do as they have smaller crack widths, smaller total crack opening, lower maximum crack width than flat bars, and less crack spacing (more cracks but thinner cracks). This difference becomes more pronounced with increasing loads.

3. Unlike for round bars, significant longitudinal splitting cracks are detected at early stages of the stabilized cracking phase for flat reinforcements during testing, which become more important and pronounced with increasing loads. The longitudinal splitting cracks occurred independently of the tested parameters (except for the reinforcement geometry). The observed higher splitting tendency of flat members agrees with conclusions derived from Chapter 4 and Chapter 5.

4. Given the different cross sectional areas involved, not a clear concluding trend is observed regarding the influence of reinforcement material (CS or SS) on the tension stiffening and/or cracking behaviour. On overall, and for stress levels corresponding to service load, the observed difference between CS and SS remains limited.

5. For all the studied cases, first cracking stress values are higher when the reinforcement is embedded in SCC in comparison to TC. However, the tensile stress-mean strain relationship is similar when round reinforcements are embedded in TC and in SCC. For flat reinforcements, the influence of the concrete type on the stress-strain behaviour is not consistent. On overall, and focusing on serviceability limit state stress levels, the behaviour is similar for most of the specimens.

6. Regarding the influence of applying an alternate surface configuration on the first cracking stress, it is concluded that higher values are always obtained when smooth areas have been added to the rib pattern. In other words, cracking occurs at higher stress levels for alternate rebars than for completely ribbed ones. Furthermore, stiffer behaviour is observed when smooth areas are added in comparison to the completely ribbed configuration.

7. The cracking behaviour improves in all the cases when adding smooth areas within the rib pattern leading to similar or higher number of cracks, which are always thinner than in the case of the completely ribbed configuration. Best results are obtained when less number of smooth areas are involved within the total embedded length (better results for the 150R_10S configuration than for the 100R_10S and for the 50R_10S). Furthermore, the best cracking results among the alternate patterns

are comparable to the cracking behaviour observed for round reinforcement with a comparable cross section, at service load stress levels.

8. For all the studied specimens, slightly higher values of σ_{cr} are obtained when smaller smooth areas are used. In other words, increasing the smooth area from 10 to 20 mm might lead to an earlier cracking of the concrete prism. The tensile stress-mean strain behaviour is stiffer when shorter smooth areas are applied. However, the influence of increasing the smooth are within the rib pattern on the cracking behaviour is not clearly visible when looking to the corresponding test results.

9. When test results are compared to the existing bond models, the following is observed.

    a. Predicted cracking stress values are always significantly higher than the ones observed experimentally, including values obtained for reference round ribbed bars.

    b. Regarding the tension stiffening effect, models given by EC2, MC90 and MC2010 give fairly good prediction compared to the test results, except for the hardening behaviour observed for flat elements at increased steel levels. At service load level (crack formation and lower part of crack stabilizing phase), the guidelines give a conservative prediction of the tension stiffening effect for the flat rebars tested.

    c. The existing equations for predicting the crack spacing and consequently the mean crack width are defined for round ribbed bars and show little accuracy to predict the cracking behaviour of the flat rebars tested in this work, for both completely ribbed and alternate surface configurations. As a consequence, adaptation of the exiting equations is proposed for predicting the behaviour of the flat rebars:

        i. For completely ribbed bars, an empirical factor which modifies the definition given for determining the mean crack width of round ribbed bars has been calculated. Thus, the predicted values of the mean crack width for completely ribbed flat rebars can be calculated according to Equations 6-27 to 6-31 with a λ value of 0,163 and k_t taken equal to 0,6, for the best approximation.

$$w_{m,flat\_CR} = w_{m,\varnothing} / \lambda \tag{6-27}$$

$$w_{m,\varnothing} = 2/3\, s_{r,max} \left(\varepsilon_{sm} - \varepsilon_{cm}\right) \tag{6-28}$$

$$s_{r,max} = 2\, A_c\, f_{ctm} / u_s\, \tau_m \tag{6-29}$$

$$\tau_m = 1{,}8\, f_{ctm} \tag{6-30}$$

$$\varepsilon_{sm} - \varepsilon_{cm} = (\sigma_s / E_s) - (k_t \, \sigma_{cr} / E_s) \tag{6-31}$$

ii. To predict the mean crack width of the rebars with an alternate pattern tested in this work, a regression analysis of the test results has been performed. Based on the mean crack width of the corresponding completely ribbed bar $w_{m,flat\_CR}$ (Equation 6-27) , the mean crack width of the alternate pattern has been defined dependant on the number of smooth zones within the total embedded length as well as on the ratio between the length of the smooth zone and the length of the single alternate pattern. Thus, the mean crack width of the flat rebars with an alternate rib pattern can be calculated according to Equations 6-32 to 6-34:

$$w_{m,flat\_alternate} = (a + b\,\varphi + c\,\psi)\, w_{m,flat\_CR} \tag{6-32}$$

$$\varphi = (l_S + l_R) / l_{b,TOT} \tag{6-33}$$

$$\psi = l_S / (l_S + l_R) \tag{6-34}$$

with, a=0,915; b=-2,785 and c=0,343, for the best approximation.

iii. The predicted values according to the adapted equations and calculated coefficients give an acceptably good approximation to the experimentally obtained mean crack values, for flat rebars analyzed in this work, for both completely ribbed and alternate surface configurations, when considering mean ratios (and standard deviation) between the model and individual results. Highest accuracy is obtained at service load levels.

6 References

[1] CEN (2005) EN 10088:2005 *Stainless steels - Part 1: List of stainless steels*. European Committee for Standardization, Brussels

[2] CEN (2009) EN 12350 *Testing fresh concrete*. European Committee for Standardization, Brussels

[3] CEN (2009) EN 12390 *Testing hardened concrete*. European Committee for Standardization, Brussels

[4] NBN (1974) NBN B 15-211 *Proeven op beton. Rechtstreekse trek*. Bureau voor Normalisatie, Brussels

[5] CEN (2010) EN ISO 15630 *Steel for the reinforcement and prestressing of concrete-Test methods- Part 1: Reinforcing bars, wire rod and wire*. European Committee for Standardization, Brussels

[6] ISO (2004) ISO 7500-1 *Metallic materials - Verification of static uniaxial testing machines - Part 1: Tension/compression testing machines - Verification and calibration of the force-measuring system.* International Organization for Standarization, Geneva

[7] CEN (2004) Eurocode 2: EN 1992-1-1: *Design of concrete structures - Part 1-1: General rules and rules for buildings.* European Committee for Standardization, Brussels

[8] CEB-FIP (1993) *Model Code 1990 – Design Code*. The International Federation for Structural Concrete, Switzerland

[9] fib (2010) *Model Code 2010 – First complete draft*. fib Bulletin 56. The International Federation for Structural Concrete, Switzerland

[10] Matthys S. (2000) *Structural behaviour and design of concrete members strengthened with externally bonded FRP reinforcement*. PhD Dissertation. Ghent University, Ghent, Belgium

[11] fib (2000) *Bond of reinforcement in concrete. State of the art report.* fib Bulletin 10. The International Federation for Structural Concrete, Switzerland

Chapter 7 Finite Element Modelling of Bond Behaviour and Tension Stiffening of Flat Rebars with Continuous and Alternate Rib Pattern

1 Introduction

Bond modelling by means of finite element (FE) discretization is generally used to investigate the bond behaviour at the local level in order to analyze the different resistant mechanisms involved at that scale, as well as to assess the efficiency of different proposed bond stress-slip relationships and to possibly improve the equations required for structural design. Within the context of the research work presented in this thesis, the FE analysis is performed in order to characterize the bond and tension stiffening behaviour observed experimentally for stainless steel flat rebars that are completely ribbed and rebars with an alternate rib pattern. The objective is to create a FE model that will allow for understanding and predicting the bond and tension stiffening behaviours of these new types of reinforcements.

The FE models that are available in the literature, deal with different basic concepts for developing the model [1]:

- *Layer models* consisting of defining a physical layer between the reinforcement and concrete to which specific properties are assigned.

- *Fracture mechanics models* consisting of the application of fracture mechanics for the modelling of the crack formation (nucleation), propagation and direction within the bond problem.

- *Dedicated finite elements models* which reduce the bond problem into a contact problem (reducing the bond layer to a negligible thickness) introducing specific contact elements (e.g. spring elements). The contact element may give a discontinuous or continuous connection between two adjacent elements, and the normal stress between the concrete and the reinforcement is taken into account.

- *Micromechanics-based models* based on a more or less simplified micromechanical representation of concrete. The failure occurs at the local level in the concrete and as a result, cracking can be described by means of cracked regions or bands.

- *Structural models* based on the modelling of full-size reinforced concrete specimens as bond strength (and bond behaviour) is a structural characteristic rather than a material property, controlled by both the geometry of the structure and the properties of the steel and the concrete.

2 Finite element modelling applied in this work

For the FE modelling work performed in this study, the DIANA (**Di**splacement **Ana**lyzer) software package has been used. DIANA is an extensive multi-purpose finite element software package that is dedicated, but not exclusively, to a wide range of problems arising in civil engineering including structural, geotechnical, tunnelling and earthquake disciplines and oil and gas engineering. For the pre- and post- processing of the analysis Midax FX+ has been used.

2.1 Considered approaches

For the FE analysis performed in this work different approaches have been considered for the characterization of the bond and cracking behaviour of flat stainless steel rebars when embedded in concrete. Both continuously ribbed elements and rebars with an alternate rib pattern have been modelled. In the following an overview of the applied approaches is given:

<u>Bond behaviour modelling:</u>

a) Phenomenological approach – 3D modelling
   i. Completely ribbed flat rebars
   ii. Flat rebars with an alternate rib pattern

b) Semi-detailed mixed approach – 3D modelling
   i. Flat rebars with an alternate rib pattern

c) Detailed geometry analysis – 2D modelling
   i. Completely ribbed flat rebars
   ii. Flat rebars with an alternate rib pattern

<u>Tension stiffening and cracking behaviour modelling:</u>

a) Phenomenological approach – 2D modelling

2.2 Phenomenological modelling vs. detailed analysis

The numerical modelling of the bond behaviour is principally performed in this work at two different levels: the first one deals with the phenomenological modelling, which is based on a discrete formulation of the bar-concrete interface; the second one is the detailed analysis in which the geometry of the reinforcement and the concrete is modelled by finite 2D elements.

In general, when a phenomenological modelling is performed, the link between the bar and the concrete is defined by discrete, zero-thickness elements whose behaviour is controlled by the stress-slip relationship [2]. The approach is able to realistically predict the bond behaviour for different geometries and different boundary conditions only if a realistic constitutive model for the surrounding concrete is used. However, this approach is not able to automatically predict the bond behaviour of a given rebar geometry: it is not possible to predict the influence of the geometry of the ribs as well as the influence of the rib spacing on the bond behaviour. Consequently the influence of these parameters must be stored in advance in the basic parameters of the bond stress-slip model if a phenomenological approach is applied [2].

On the other hand, if a detailed analysis is performed, the influence of the rib pattern geometry will be directly modelled. However, the FE mesh needs to be relatively fine which leads to a complex meshing configuration and, consequently, to an increase of the computing time.

2.3 Main characteristics of the applied models

2.3.1 Material properties

2.3.1.1 Linear concrete properties

In those areas of the modelled structure where cracking of the concrete is not expected, linear concrete properties have been considered for calculation time consumption reduction purposes. The parameters defining these linear properties are considered according to the concrete properties derived from the tests performed in the experimental program. An average modulus of elasticity and an average density are taken equal to 36.500 N/mm^2 and 2.400 kg/m^3, respectively. The Poisson coefficient is taken equal to 0,15.

2.3.1.2 Nonlinear concrete properties

When cracking of the concrete is likely to occur, nonlinear material properties have been considered. Thus, when modelling the bond behaviour of flat rebars, only the concrete area surrounding the steel reinforcement has been modelled as nonlinear. When characterizing the tension stiffening capacity and the cracking behaviour of the rebars when embedded in concrete, the entire concrete prism is modelled with nonlinear material properties. Depending on the considered approach different smeared cracking models have been taking into consideration for defining concrete properties: for the bond behaviour modelling a rotating total crack model has been chosen, which changes into a fixed type at a certain crack strain threshold value (this cracking model allows the rotation of the crack orientation). On the other hand, for characterizing the cracking behaviour of the rebars embedded in concrete when submitted to tensile forces, a fixed total crack model has been considered as cracks are expected to occur in one direction (perpendicular to the bar axis).

Furthermore, the tensile, shear and compressive behaviours of the nonlinear concrete have also been defined. For the tensile behaviour the so-called predefined HORDYK tensile stress-strain curve (see Figure 7-1-a) has been applied, as a function of the tensile strength of the concrete and the fracture energy value for the curve softening characterization.

For the compression behaviour characterization, different models have been considered depending on the modelled situation. For the bond behaviour characterization, where the concrete cube is basically in a compression situation the MULTLN (multilinear) compressive stress-strain curve (see Figure 7-1-b) has been defined (giving a set of stress-strain points) to more accurately model the concrete compressive behaviour. On the other hand, for the modelling of the axially loaded reinforced concrete prism (tension stiffening and cracking behaviour characterization), where the concrete prism is in a tensile situation, the compressive behaviour of the concrete has been represented by the predefined so-called CONSTA curve (Figure 7-1-c), which is defined only by implementing the compressive strength of the concrete.

For the fixed crack models considered, for which the shear stiffness is usually reduced after cracking, a shear retention factor BETA is provided.

2.3.1.3 Linear steel properties

In those situation where yielding of the bar is not expected to occur, and the failure is foreseen in the concrete or in the interface between the two materials, linear steel properties have been considered. The density of steel has been taken equal to 7.800 kg/m^3, a Poisson coefficient of 0,3 has been adopted and the modulus of elasticity has been taken equal to an average value of 210.000 N/mm^2.

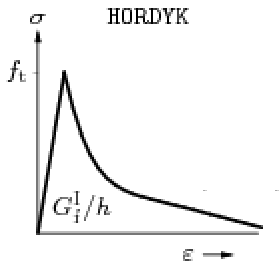

a)

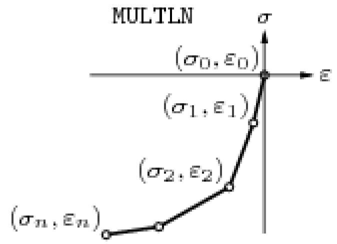

b)

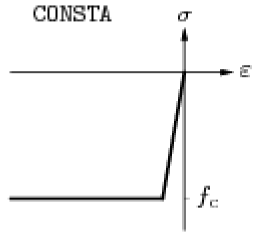

c)

Figure 7-1 Concrete behaviour defining curves predifined by DIANA: a) HORDYK tension softening behaviour, b) MULTLN compressive behaviour and c) CONSTA compressive behaviour

2.3.1.4 Non linear steel properties

For the modelling of the tension stiffening tests, where plastic deformation of the steel reinforcement occurred, nonlinear material properties are adopted. Besides basic parameters like density, Poisson coefficient and modulus of elasticity (values taken as for the linear steel properties), the hardening process corresponding to the plastic deformation is also implemented. For the modelled stainless steel reinforcement, the stress-strain values of the hardening plasticity are given according to the tests results obtained from the performed tensile tests (see Figure 6-2 in the previous chapter). The so-called VMISES (Von Mises) yielding criteria is adopted in this work with the HARDIA command to implement the hardening behaviour of the steel.

2.3.1.5 Interface properties

For the phenomenological analysis, interface elements with zero-thickness which describe the bond stress-slip relationship have been implemented. In reinforced concrete the interaction between the reinforcement and the concrete is governed by secondary transverse and longitudinal cracks in the vicinity of the reinforcement. This behaviour can be modelled with a bond-slip mechanism where the relative slip of the reinforcement and the concrete is described in a phenomenological sense. The mechanical behaviour of the slip zone is then described by the interface element with a zero thickness.

The constitutive laws for bond-slip are based on a total deformation theory, which expresses the stresses as a function of the total relative displacements. DIANA offers two predefined curves for the relationships between shear stress and slip: a cubic function according to Dörr (see Figure 7-2-a), and a power law relation proposed by Noakowski (see Figure 7-2-b). Moreover, a user-defined multilinear diagram is available

(Figure 7-2-c). The models set a nonlinear relation between the shear stress t_t and shear slip Δu_t. The relation between normal stress and normal relative displacement is kept linear, as defined by the first value of the stiffness matrix (DSTIF). The second value of the stiffness matrix gives the initial (linear) relationship between the shear stress and the relative displacement. For the multi-linear bond stress-slip relationship, if the initial shear modulus specified with DSTIF does not correspond to the initial slope of the implemented diagram, the modulus is replaced by the initial slope of the diagram during the initialization phase of the nonlinear analysis.

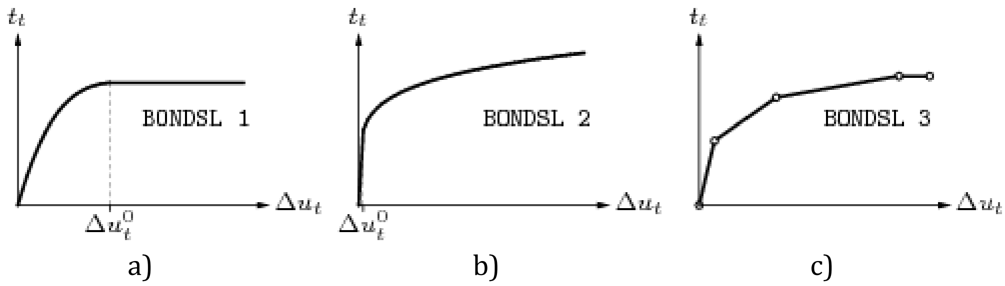

Figure 7-2 Bond shear stress-slip curves offered by DIANA software: a) cubic function, b) power law function and c) user defined multilinear function

For the performed FE analysis considering the phenomenological approach, the multilinear bond stress-slip relationship has been applied (Figure 7-2-c). The curve defining points have been introduced by the author, according to the bond-slip models proposed in the previous chapters of this work. Thus, interface elements corresponding to ribbed zones have been modelled using the curve obtained from the analytical verification performed in Chapter 4 of this work, considering mean values of τ_{max} and τ_f, as given by Equations 4-36 to 4-39 and plotted in Figure 7-3, calculated for a characteristic compression strength of concrete of 50 N/mm^2. On the other hand, smooth zones are characterised by the bond stress-slip relationship adaptation proposed for smooth samples as described in Chapter 4 of this work: Equations 4-31 to 4-35 and Figure 7-3. The values of the involved different parameters are presented in Table 7-1, for both completely ribbed and smooth flat rebars.

For the 15R_10S_15R alternate rib pattern an adaptation of the bond stress-slip relationship has been proposed in Chapter 5 of this work: see Equations 5-11 to 5-15, and Figure 7-3. The parameters defining the curve are given in Table 7-1.

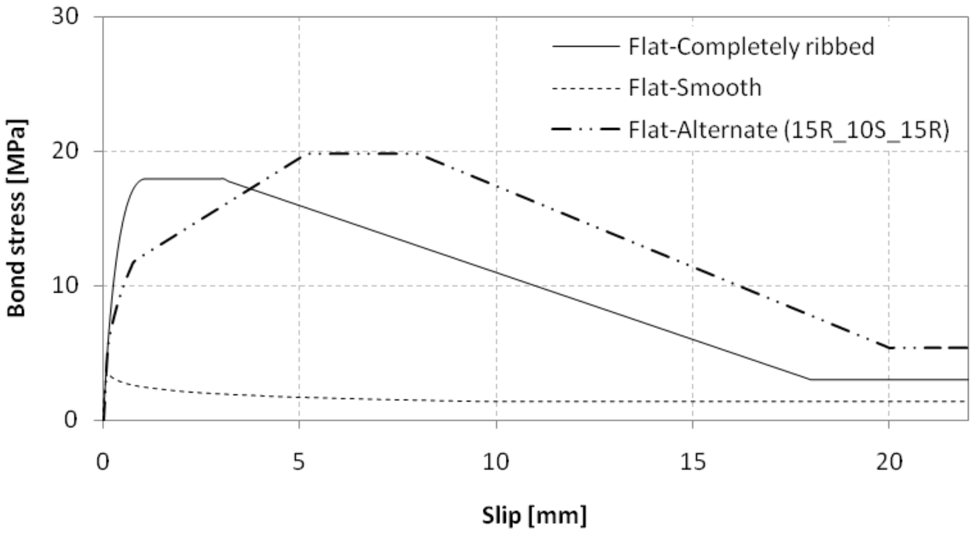

Figure 7-3 Bond stress-slip curve adopted for interface elements corresponding to ribbed zones

Table 7-1 Parameters of the proposed approach for defining the bond stress-slip behaviour of flat rebars tested in this work. For completely ribbed, smooth and alternate rebars

Parameter	***Flat ribbed***	***Flat smooth***	***Flat alternate (15R_10S_15R)***
s_1 *(mm)*	$0{,}0032\ c^2 + 0{,}041$	0,1	$0{,}0032\ c_1^2 + 0{,}041$
s_2 *(mm)*	3	10	$0{,}0032\ c_2^2 + 0{,}041$
s_3 *(mm)*	Clear rib spacing	-	8
s_4 *(mm)*	-	-	20
α	0,4	0,5	0,8
τ_1 *(N/mm²)*	-	-	$1{,}69\ \sqrt{f_{ck}}$
τ_{max} *(N/mm²)*	$2{,}54\ \sqrt{f_{ck}}$	$0{,}51\ \sqrt{f_{ck}}$	$2{,}85\ \sqrt{f_{ck}}$
τ_f *(N/mm²)*	$0{,}17\ \tau_{max}$	$0{,}39\ \tau_{max}$	$0{,}27\ \tau_{max}$

2.3.2 Used elements

The applied elements for the FE calculation (Figure 7-4) varies depending on the applied approach. For the phenomenological and semi-detailed approaches that have been used for the bond behaviour characterization, 3D elements are applied as follows: the concrete and the steel elements are type CHX60, which is a twenty-nodes isoparametric solid brick element that is based on quadratic interpolation and Gauss integration. In the contact zone between steel and concrete CQ48I elements are applied, which correspond to a plane quadrilateral eight+eight-nodes interface element between two planes in a three-dimensional configuration. The element is based in quadratic interpolation.

For the geometrically detailed analysis of the bond behaviour as well as for the tension stiffening modelling, which have been modelled in 2D, steel and concrete are modelled using CQ16M element: an eight-node quadrilateral isoparametric plane stress element. It is based on quadratic interpolation and Gauss integration. For the interface between the concrete and the steel of the tension stiffening modelling, the CL12I element has been applied: an interface element between two lines in a two-dimensional configuration. The element is based on quadratic interpolation.

3D	
Steel and concrete: CHX60	Interface: CQ48I
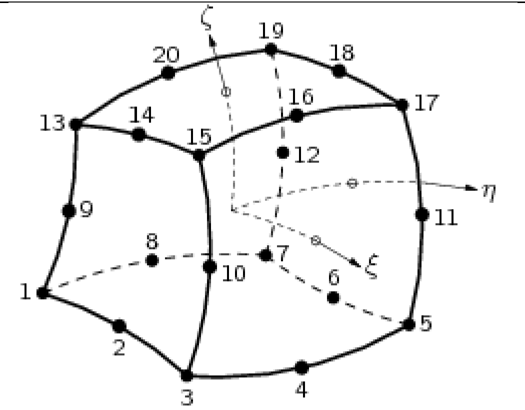	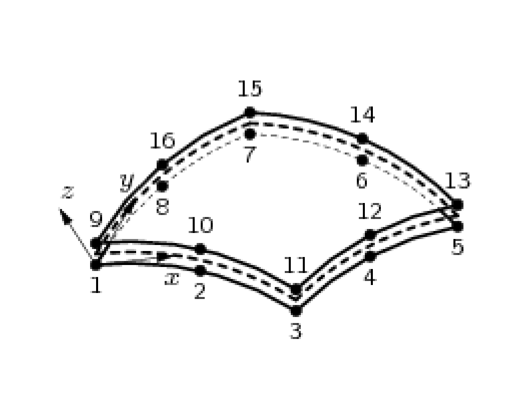
2D	
Steel and concrete: CQ16M	Interface: CL12I
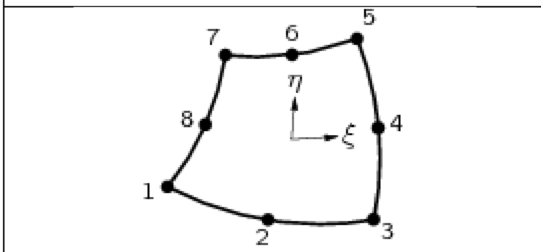	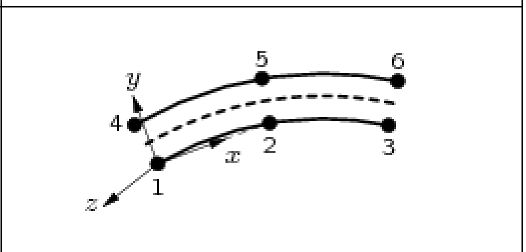

Figure 7-4 Applied element types

2.3.3 Symmetry

When allowed by symmetry properties of the modelled structures, half or a quarter of the structure has been modelled and symmetry boundary properties have been applied, reducing to half (or to one quarter) the number of elements, and as consequence reducing significantly the computing time.

2.3.4 Load application

As it has been done in the experimental program of this work, the load is applied in the models in a displacement controlled way: displacements are imposed to the reinforcement elements. The step size of these displacements varies from one model to another.

2.3.5 Calculation/analysis method

Nonlinear structural analysis is performed for all the considered models. By default, DIANA assumes that in a nonlinear analysis the model behaves geometrically linear. In this case, the equilibrium equations are based on the undeformed geometry and the strains are linear functions of the nodal displacements. However, as large displacements (deformations) are involved in the considered models, an analysis method including geometrical nonlinearities has been chosen. Furthermore, physical nonlinear analysis is performed in order to allow crack development in the model.

Regarding the solution procedure, the so-called Regular Newton Raphson incremental-iterative method is applied. In this method, the stiffness matrix is evaluated every iteration; this means that the prediction of the iterative increments is based on the last known or predicted situation. The Regular Newton Raphson method yields a quadratic convergence characteristic, which means that the method converges to the final solution within a relatively small amount of iterations. A disadvantage of the method is that the stiffness matrix has to be set up at every iteration and, if a direct solver is used to solve the linear set of equations, the time consuming decomposition of the matrix has to be performed every iteration.

3 Bond behaviour modelling

3.1 Phenomenological approach by 3D modelling

As a first step on the FE modelling of the bond behaviour of flat stainless steel rebars when embedded in concrete, a phenomenological 3D approach has been adopted. The concrete block is subdivided into two different parts comprising a concrete area with nonlinear material properties surrounding the reinforcement and a second linear concrete zone where cracks are not expected to occur. The reinforcement is modelled with linear material properties and only one quarter of the structure is modelled due to the symmetry properties: the test specimen is symmetric with respect to XZ and YZ planes (see Figure 7-5). Consequently, symmetry boundary properties have been adopted: along the XZ symmetry plane, the displacement in Y and the rotation in X and Z have been constrained; along the YZ symmetry plane, the degrees of freedom have been reduced by constraining the displacement in X and the rotation in Y and Z. Furthermore, to account for the supports applied experimentally, the vertical displacements (axis Z) have been constrained along the bottom part of the concrete. Interface elements are introduced in the contact area between the steel and the concrete. The contact area is modelled as a flat surface as the rib characteristics are included in the bond stress-slip relationship given to the interface element.

3.1.1 Completely ribbed flat rebars

For the modelling of the bond behaviour of completely ribbed flat rebars, the bond length has been taken equal to 30 mm as it has been done for the experimental program. Figure 7-5 gives the 3D model used for this analysis; Figure 7-6 shows the interface elements applied for the bond stress-slip relationship (Figure 7-3) between the reinforcement and the concrete.

For computing of the bond stress, the vertical forces at the bottom of the steel reinforcement (where the displacement load has been imposed) are considered. These forces are divided by the contact area (bond length times the perimeter of the reinforcement) between the steel and the concrete for calculating the bond stress (see Equation 4-3, in Chapter 4). As confirmed by the model, the bond stress is almost perfectly constant within the bond length (average error of 0,32%) and the calculated bond stress is assumed to be the average bond stress at the contact area. Obtained FE modelling (FEM) τ-s results are plotted together with the experimental (EXP) curve for SS completely ribbed flat rebars in Figure 7-7. It is clearly observed from the FEM curve that the model follows the bond-slip curve imposed by the interface elements.

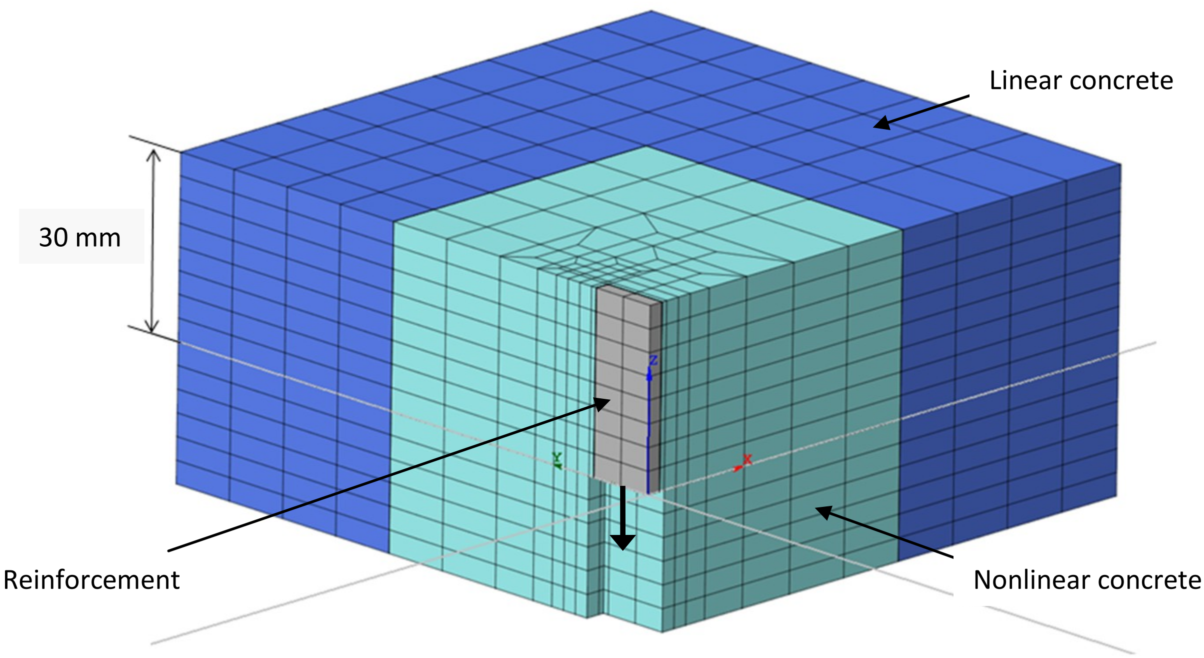

Figure 7-5 Phenomenological 3D model for completely ribbed flat rebars

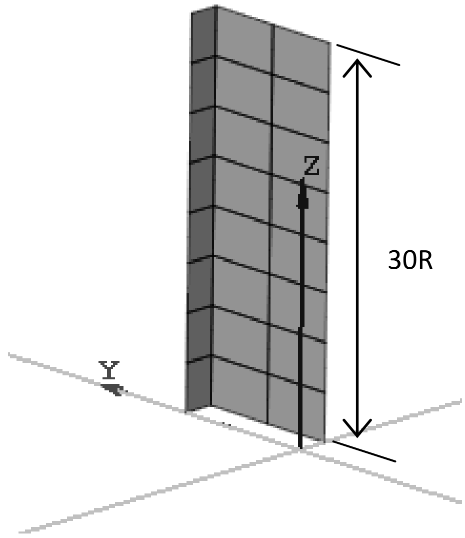

Figure 7-6 Interface elements applied in the phenomenological 3D model for completely ribbed flat rebars

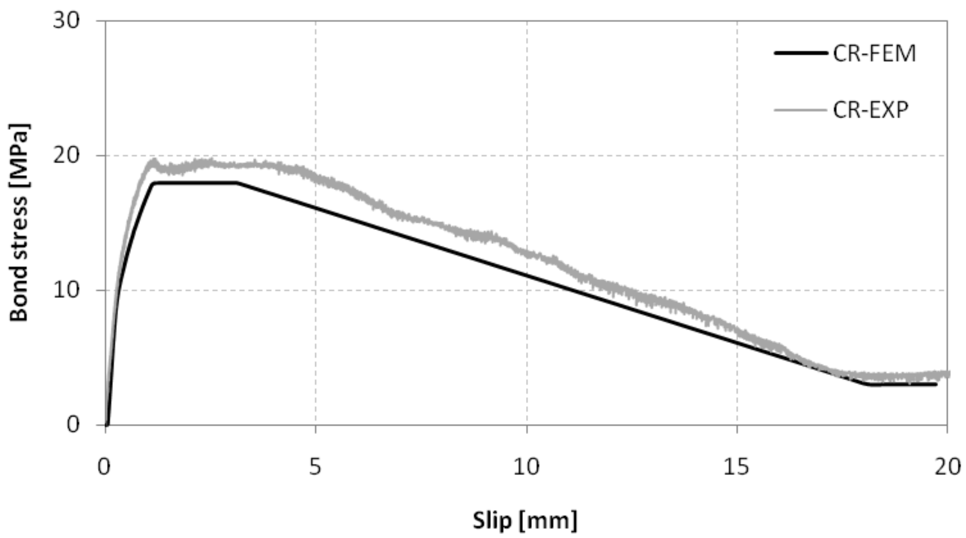

Figure 7-7 Bond stress-slip curve for completely ribbed flat reinforcement. Experimental vs. FE modelling results. Phenomenological approach

3.1.2 Flat rebars with an alternate rib pattern

3.1.2.1 Considering ribbed and smooth zones separately

Following the same strategy as done for the completely ribbed flat rebars, the 15R_10S_15R alternate rib pattern has been modelled by a phenomenological approach. The modelled structure is comparable to the one of the completely ribbed approach except for the bond length that has been now increased to 40 mm (15 mm of ribbed zone + 10 mm of smooth zone + 15 mm of ribbed zone). Accordingly, the interface elements have been also modified: flat ribbed bond stress-slip characteristics (Figure 7-3) have been imposed to the upper and lower 15 mm of the interface, whereas smooth flat reinforcement bond behaviour (Figure 7-3) has been imposed to the central 10 mm of the interface. The applied interface is shown in Figure 7-8.

As it has been done for the experimental program, the bond stress is considered to be constant within the entire bond length, and therefore, an average bond stress is calculated based on the vertical forces obtained by FEM at the bottom of the reinforcement. The obtained bond stress-slip relationship is plotted together with experimental results obtained for the 15R_10S_15R bond length configuration in Figure 7-9. It can be observed from the comparison that the obtained model curve does not represent the behaviour observed experimentally. The characteristic of two differentiated ascending branches observed for the alternate patterns when the smooth zone is positioned in between two ribbed zones within the bond length is not captured by this approach, and therefore, the maximum bond stress (significantly lower than the one obtained experimentally) is reached at slip values that do not correspond to the behaviour observed.

Moreover, if the bond stress-slip behaviour modelled by this approach for the 15R_10S_15R alternate pattern is compared to the behaviour modelled for the completely ribbed rebar, it can be observed that the same curve shape is obtained but the values of the bond stress are reduced due to the inserted smooth zone (see Figure 7-9).

It can be concluded that the modelling of the alternate pattern using the phenomenological approach and considering ribbed properties and smooth properties of the interface elements separately, does not represent the bond behaviour observed experimentally for the flat rebars with an alternate rib pattern.

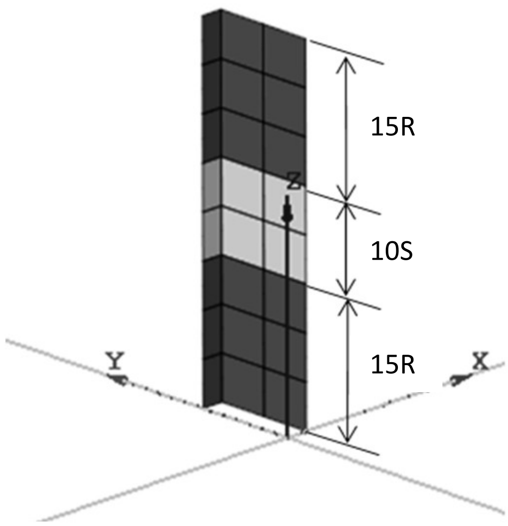

Figure 7-8 Interface elements applied in the phenomenological 3D model for flat rebars with 15R_10S_15R alternate pattern

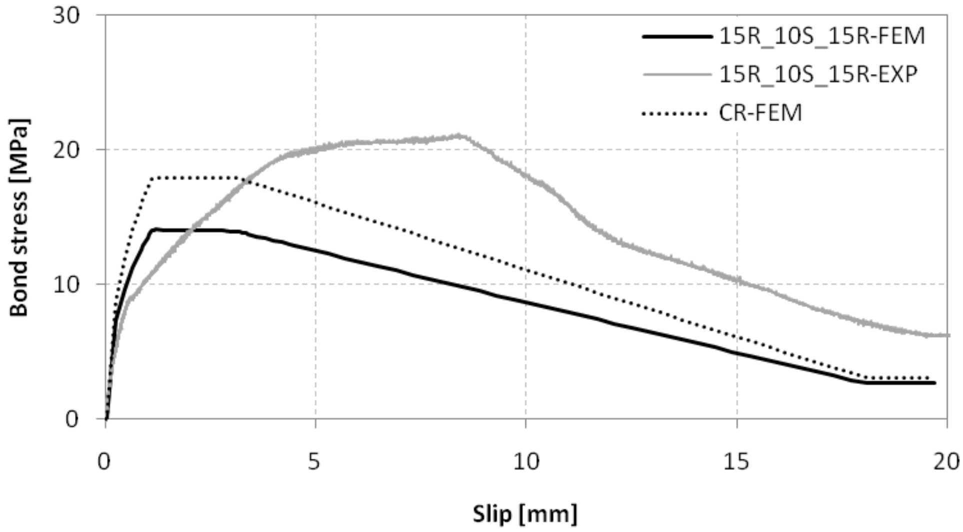

Figure 7-9 Bond stress-slip curve for flat reinforcement with 15R_10S_15R alternate pattern. Experimental vs. FE modelling results. Phenomenological approach, giving different bond stress-slip relationships to the ribbed and the smooth zone

3.1.2.2 Considering ribbed and smooth zones as one

For characterizing the alternate pattern, another solution might be to consider the ribbed and the smooth zones together, having an interface element between the reinforcement and the concrete which compiles the bond characteristics of the alternate pattern within a single bond stress-slip relationship. However, only the bond stress-slip relationship for the 15R_10S_15R alternate pattern has been developed as result of the analytical verification performed to the test results, which limits this approach to that specific alternate pattern. Thus, for the 15R_10S_15R configuration, the bond stress-slip relationship given in Figure 7-3 has been implemented to the entire interface which is 40 mm long as corresponds to the bond length of the analyzed alternate pattern, and a phenomenological FE modelling of the bond behaviour has been performed as done for the completely ribbed samples. The modelled bond stress-slip relationship is given in Figure 7-10 together with the obtained test results.

As concluded for the completely ribbed samples, when the bond behaviour of an specific reinforcement is entirely implemented into the interface properties, the real behaviour observed experimentally is well modelled. However, the disadvantage of this phenomenological approach is that the bond stress-slip relationship between a given reinforcement and concrete need to be known in advance, and therefore, it limits the analysis of the influence of the rib pattern of the reinforcement on its bond behaviour. On the other hand, the phenomenological approach can be useful for analyzing the structural behaviour of a reinforced concrete structure that has been reinforced with a rebar for which the bond stress-slip relationship is already known.

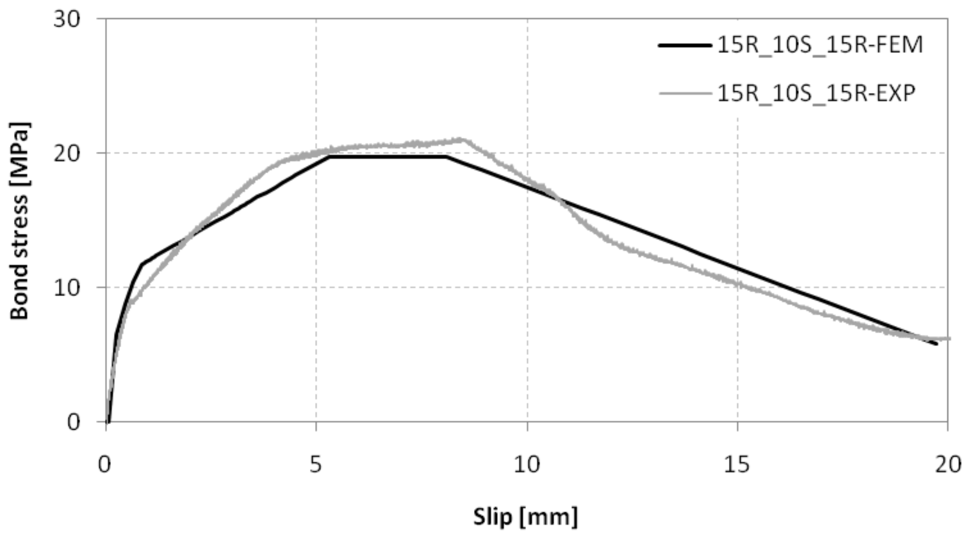

Figure 7-10 Bond stress-slip curve for flat reinforcement with 15R_10S_15R alternate pattern. Experimental vs. FE modelling results. Phenomenological approach, using a bond stress-slip relationship for the entire bond lenght

3.2 Semi-detailed mixed approach by 3D modelling

Considering the concept of two levels of surface configuration that has been described and adopted for understanding the bond behaviour of the alternate pattern when the smooth zone is positioned in between two ribbed zones within the bond length (see Chapter 5), a new mixed modelling approach has been considered for flat rebars with an alternate rib pattern: the ribbed zone has been modelled with the phenomenological approach described previously (flat interface with completely ribbed flat rebars bond stress-slip characteristics) and the second level of surface configuration (the one that considers the smooth zone as the valley of a larger rib pattern) has been modelled applying detailed geometry analysis approach.

The modelled structure is similar to the one used for the full phenomenological approach, except for the detailed geometry used for modelling the smooth zone of the reinforcement. For the 15R_10S_15R configuration, the applied reinforcement geometry and the corresponding interface are given in Figure 7-11. As done previously, flat ribbed bond stress-slip characteristics (given by Figure 7-3) have been imposed to the upper and lower 15 mm of the interface, whereas smooth flat reinforcement bond behaviour (see Figure 7-3) has been imposed to the central 10 mm of the interface. Following the geometry measurements performed to the flat rebars, the smooth zone has been modelled as a valley of 0,7 mm deep with respect to the ribbed zone area, and a rib face angle of 30° (see detailed view in Figure 7-11-a).

As it can be seen from the bond stress-slip relationship obtained with this FEM approach (Figure 7-12), the change in the slope of the ascending branch observed for the experimental results when an alternate rib pattern is used placing the smooth zone in between two ribbed zones within the bond length, is now captured. This observation confirms the concept of two levels of surface configuration involved in the alternate pattern that has been adopted for understanding the bond behaviour of this type of reinforcements. However, the model is only able to simulate the bond behaviour for slip values up to ~4 mm, and fails for larger displacements. The first ascending branch corresponding to the bond behaviour of the ribbed zone closest to the active end, is acceptably well modelled, whereas the stiffness of the second ascending branch (corresponding to the activation of the second level rib pattern) is fairly accurate, though slightly underestimated.

It is believed that the large displacements (deformations) involved in the analysis at increasing slips (due to the shearing off of the concrete at the level of the smooth zone and compared to the bond length being modelled) lead to the failure of the FE calculation process, premature to what is experimentally observed.

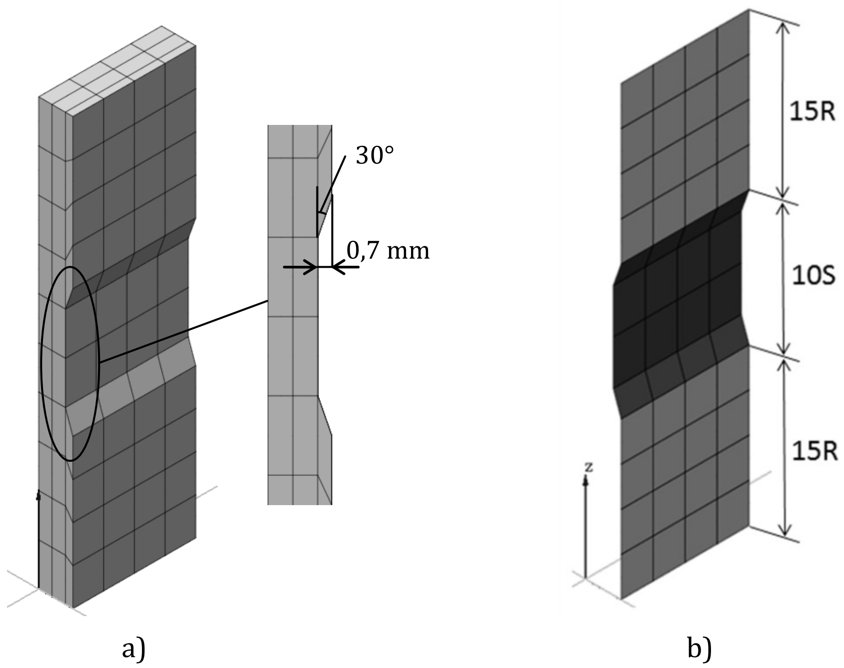

Figure 7-11 Semid-detailed mixed approach for the 15R_10S_15R alternate pattern: a) reinforcement b) interface

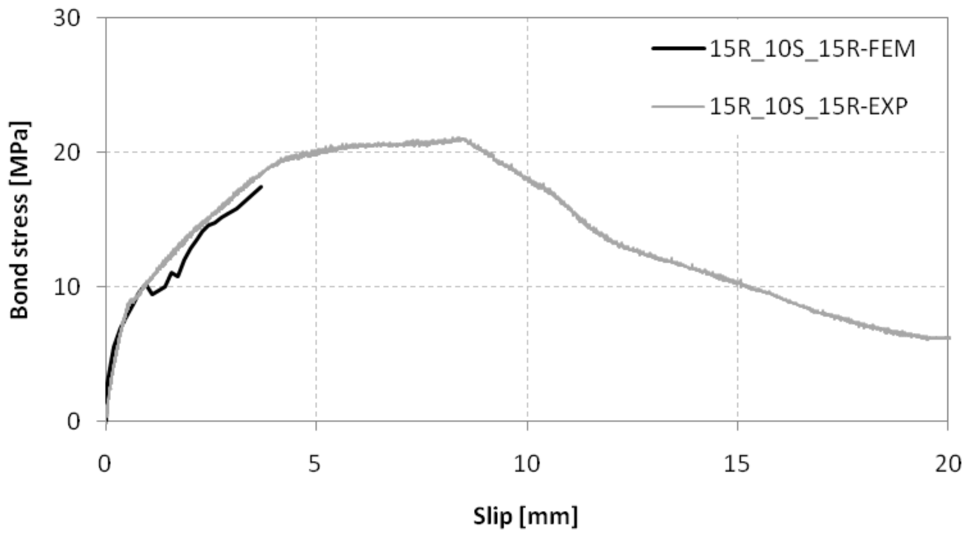

Figure 7-12 Bond stress-slip curve for flat reinforcement with 15R_10S_15R alternate pattern. Experimental vs. FE modelling results. Semi-detailed mixed approach

Similarly to the 15R_10S_15R alternate pattern, the semi-detailed mixed approach has been also applied to the 15R_20S_15R alternate configuration. In this case the bond length has been extended to 50 mm as the smooth zone is increased to 20 mm (see Figure 7-13). The obtained bond stress-slip relationship is given in Figure 7-14 together with the experimental results obtained for this bond length configuration. The two ascending branches are again observed. However, as occurred for the modelling 15R_10S_15R alternate pattern, the model is only able to simulate the bond behaviour for slip values under ~4 mm.

In Figure 7-15 the bond stress-slip curves obtained by FEM applying the semi-detailed mixed approach for the 15R_10S_15R and 15R_20S_15R alternate configurations are compared. The first ascending branch related to the ribbed area closest to the active end is similar for both curves. The slip value at which the change in the slope of the ascending branch occurs has been observed to be, in average, 0,75 mm and 0,93 mm for the experimental results of 15R_10S_15R and 15R_20S_15R alternate patterns, respectively. Regarding the analytical verification, this value has been set equal to 0,76 mm applying the formula developed by Desnerck [3] (see s_1 definition in the *Flat alternate* column of Table 7-1). According to the semi-detailed FEM analysis, the change in the stiffness is observed at slip values around 0,79 mm for both alternate configurations at a bond stress level of around 10,50 N/mm^2 .

On the other hand, as observed from the experimental results, and due to the larger rib spacing involved at the second level of rib configuration for the 15R_20S_15R pattern, a less stiff second ascending branch in comparison to the 15R_10S_15R configuration is observed.

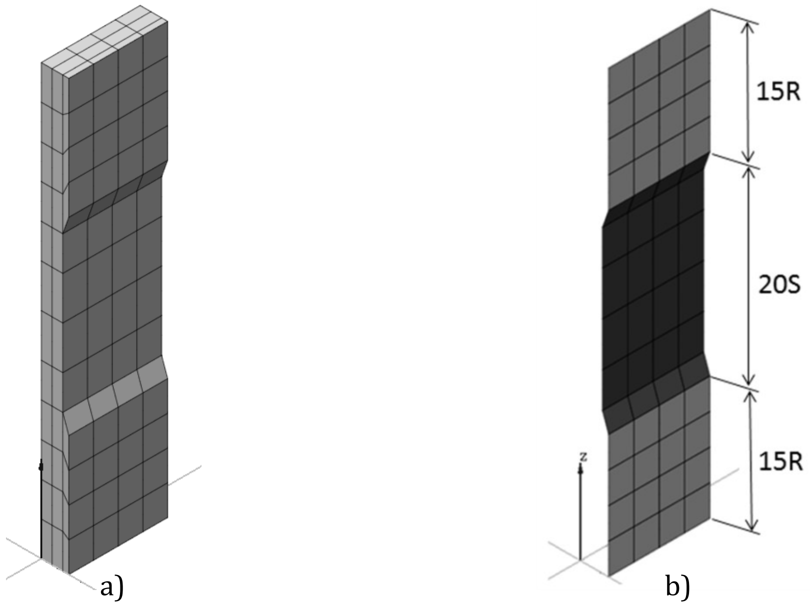

Figure 7-13 Semid-detailed mixed approach for the 15R_20S_15R alternate pattern: a) reinforcement b) interface

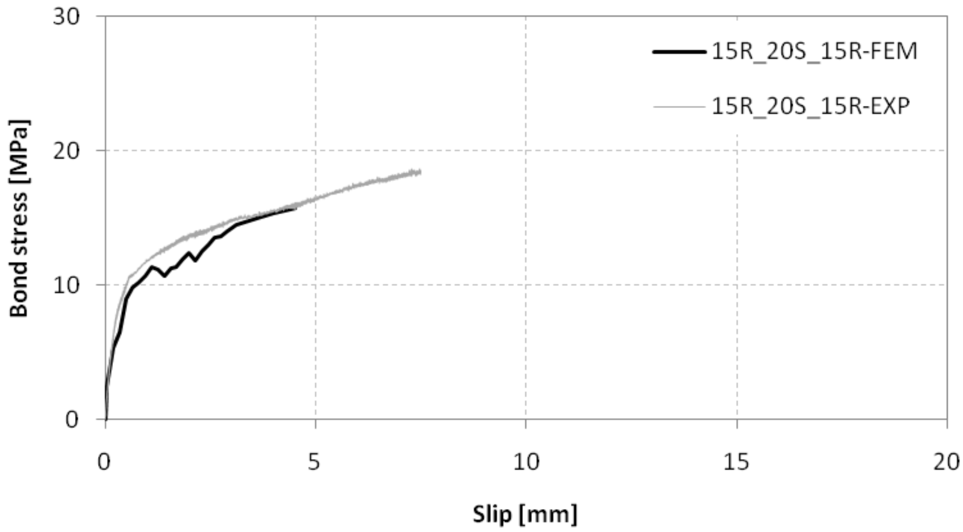

Figure 7-14 Bond stress-slip curve for flat reinforcement with 15R_20S_15R alternate pattern. Experimental vs. FE modelling results. Semi-detailed mixed approach

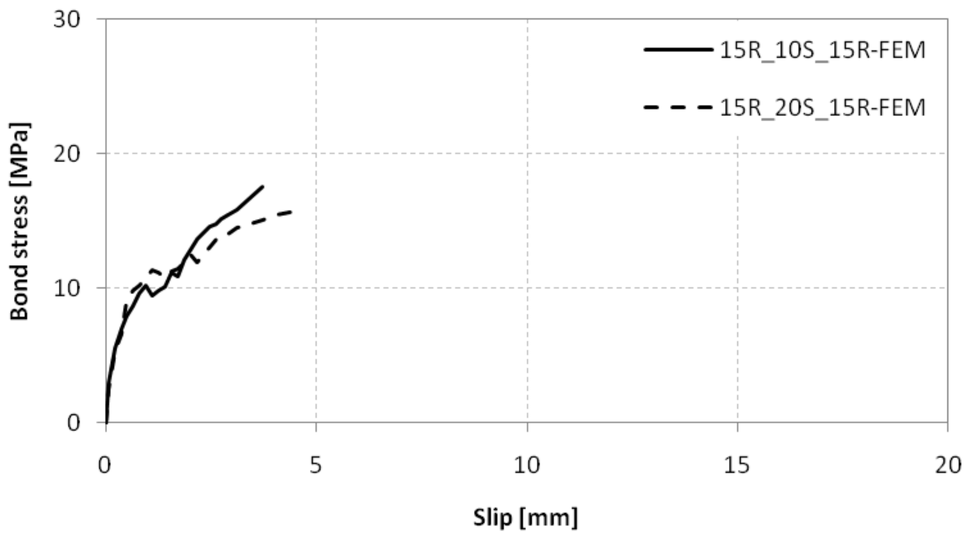

Figure 7-15 Bond stress-slip curve for flat reinforcement with 15R_10S_15R and 15R_20S_15R alternate pattern. FE modelling results. Semi-detailed mixed approach

3.3 Detailed geometry analysis by 2D modelling

As the third approach for modelling the bond behaviour of flat rebars tested in this work, both for completely ribbed surface configuration and for alternate rib patterns combining ribbed and smooth zones, the detailed geometry analysis has been adopted. Note that only the longitudinal profile of the rib pattern involved in the analyzed rebars has been considered and therefore only 2D analysis has been performed. The profile has been originally measured by an Automatic Laser Measurement (ALM) system, which consists of a laser-optical displacement sensor (with a wavelength of 670 nm (visible-red) and a resolution of 10 µm). Measurement steps of 0,075 mm have been applied, allowing for an accurate drawing of the profile. However, the meshing process needed for the FEM analysis of such an geometrically accurate profile is highly time consuming, and the small mesh size involved makes the calculation process to be very long. Consequently, a simplified (polygonal) profile derived from the original profile has been further considered for this approach (see Figure 7-16)

As for the previous approaches, the concrete at the surrounding of the steel has been modelled with nonlinear properties, whereas the one farther from the steel has been considered to be linear. The steel has been modelled as linear, as no failure of the steel is expected to occur. No interface elements have been included in this approach, and therefore, no bond stress-slip relationship has been imposed. The failure is expected to occur by shearing off of the concrete as observed from the microscopic investigation performed to the experimental results and due to the specific geometry of the surface configuration.

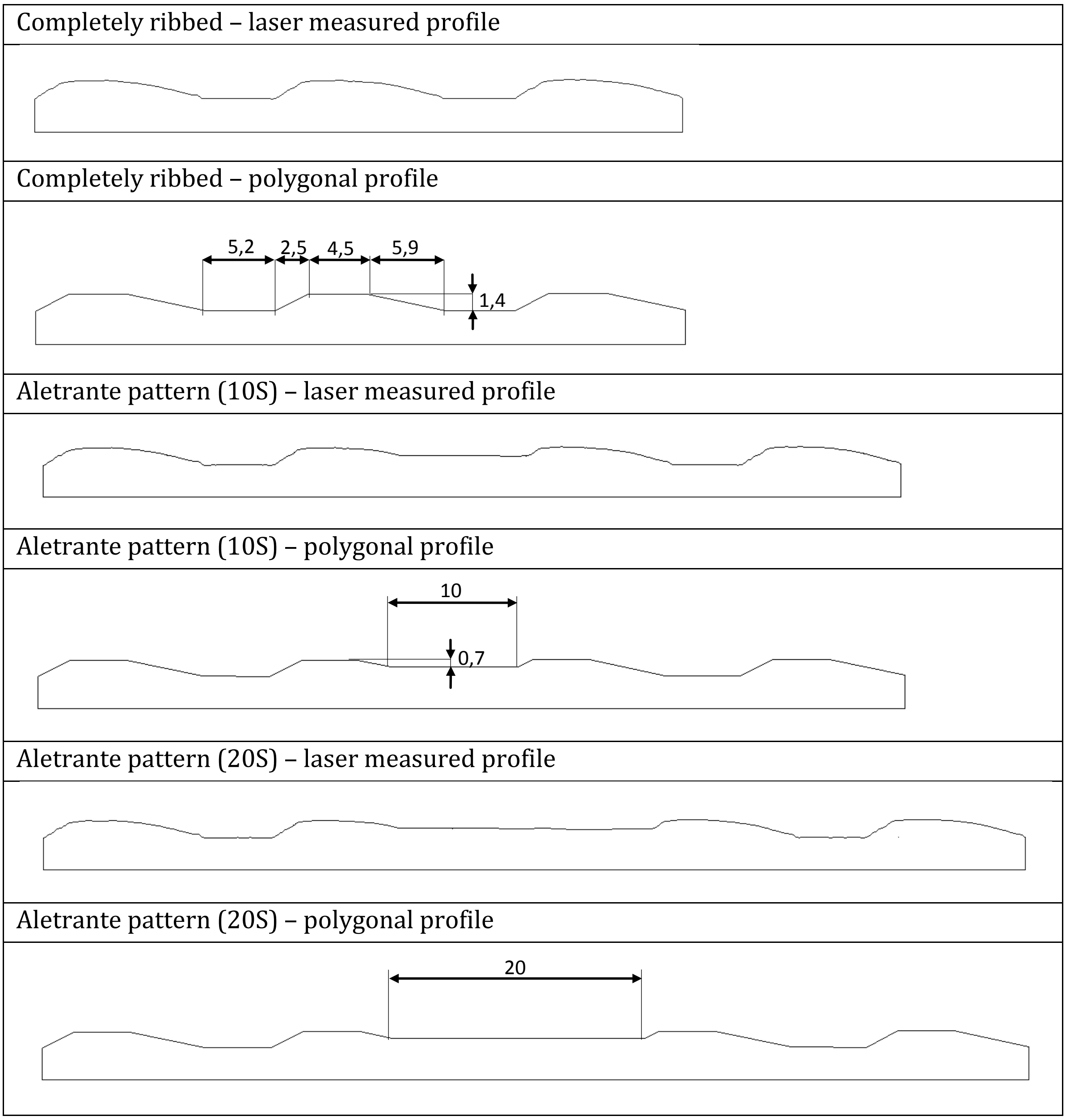

Figure 7-16 Rib pattern longitudinal profiles. Laser measured profile vs. poligonal profile (in mm)

3.3.1 Completely ribbed flat rebars

Firstly, the bond behaviour of completely ribbed flat rebars has been analyzed, applying the model given by Figure 7-17. As it can be seen from the figure, both the steel and the concrete have been modelled following the simplified ribbed geometry. A detailed view of the contact zone (30 mm of ribbed bond length) between the two materials is given in Figure 7-18-a. The load has been applied to the bottom part of the reinforcement in a displacement controlled way.

The obtained bond stress-slip relationship is compared to the one obtained experimentally in Figure 7-19. The model is able to predict in an accurate way the bond stress-slip behaviour of flat rebars that are completely ribbed up to a slip value of ~1,2 mm. However, for higher slip values, the FEM fails and therefore, the behaviour cannot be predicted. Note that for a better visualisation of the comparison, the figure is given only for low slip values (< 5 mm).

This approach, allows for a realistic visualization of the crack behaviour and the strain development in the contact zone between the two materials. As given by Figure 7-20, radial cracks start developing from the bottom part of the contact zone (active end) and they extend to the upper zones with increasing slips. Following the same behaviour as observed by visual and microscopic analysis of the failure aspect, at slip levels close to the ones related to maximum bond stress (~ 1mm), the cracks rotate and become parallel to the bar axis when shearing off of the concrete occurs following the outer profile of the reinforcement.

At increasing slips, the steel will drag the concrete parts that have been sheared off, resulting on relatively large displacements compared to the modelled bond length which might be the cause of divergences occurred during the calculation process.

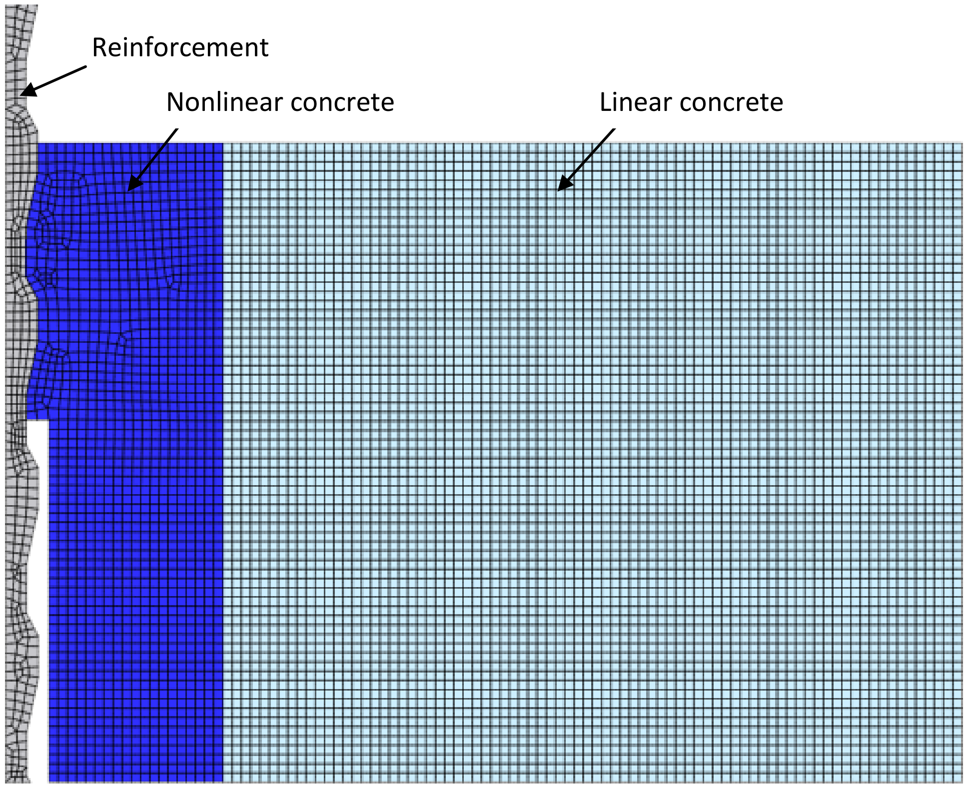

Figure 7-17 Detailed geometry analysis by 2D model for completely ribbed flat rebars

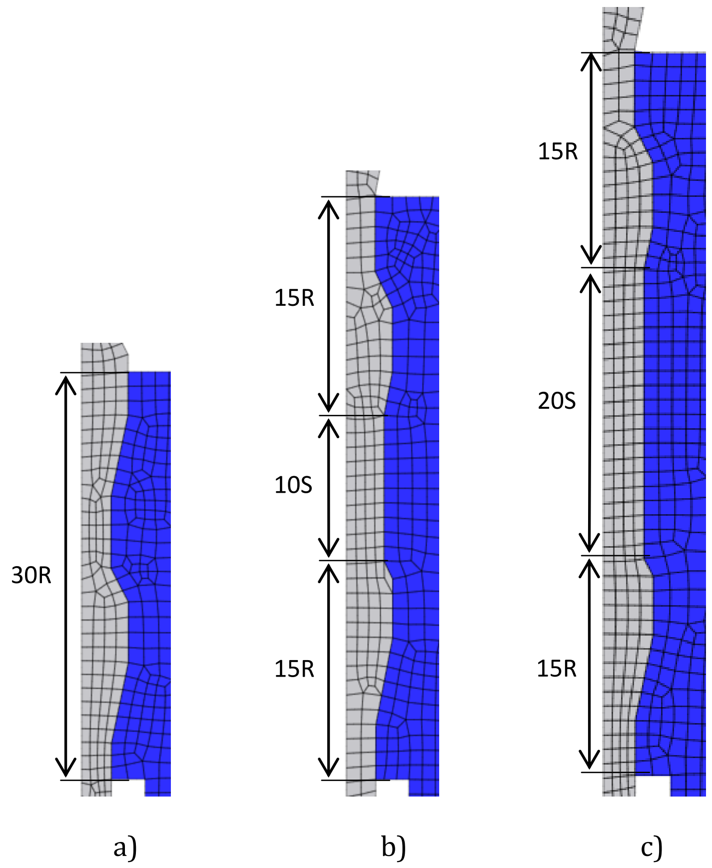

Figure 7-18 Deatiled view of the contact area between the reinforcement and the steel for: a) completely ribbed rebar b) 15R_10S_15R configuration and c) 15R_20S_15R configuration

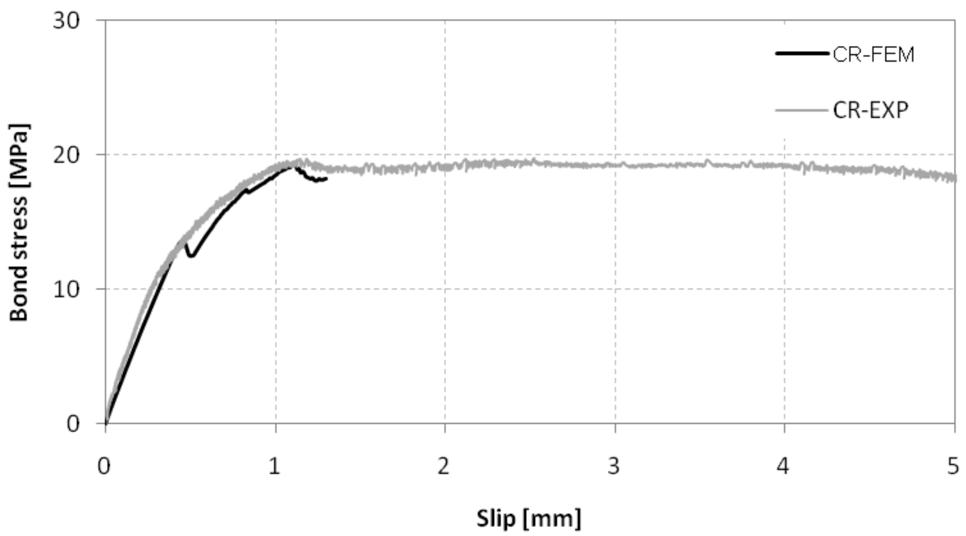

Figure 7-19 Bond stress-slip curve for completely ribbed flat reinforcement. Experimental vs. FE modelling results. Detailed geometry analysis approach

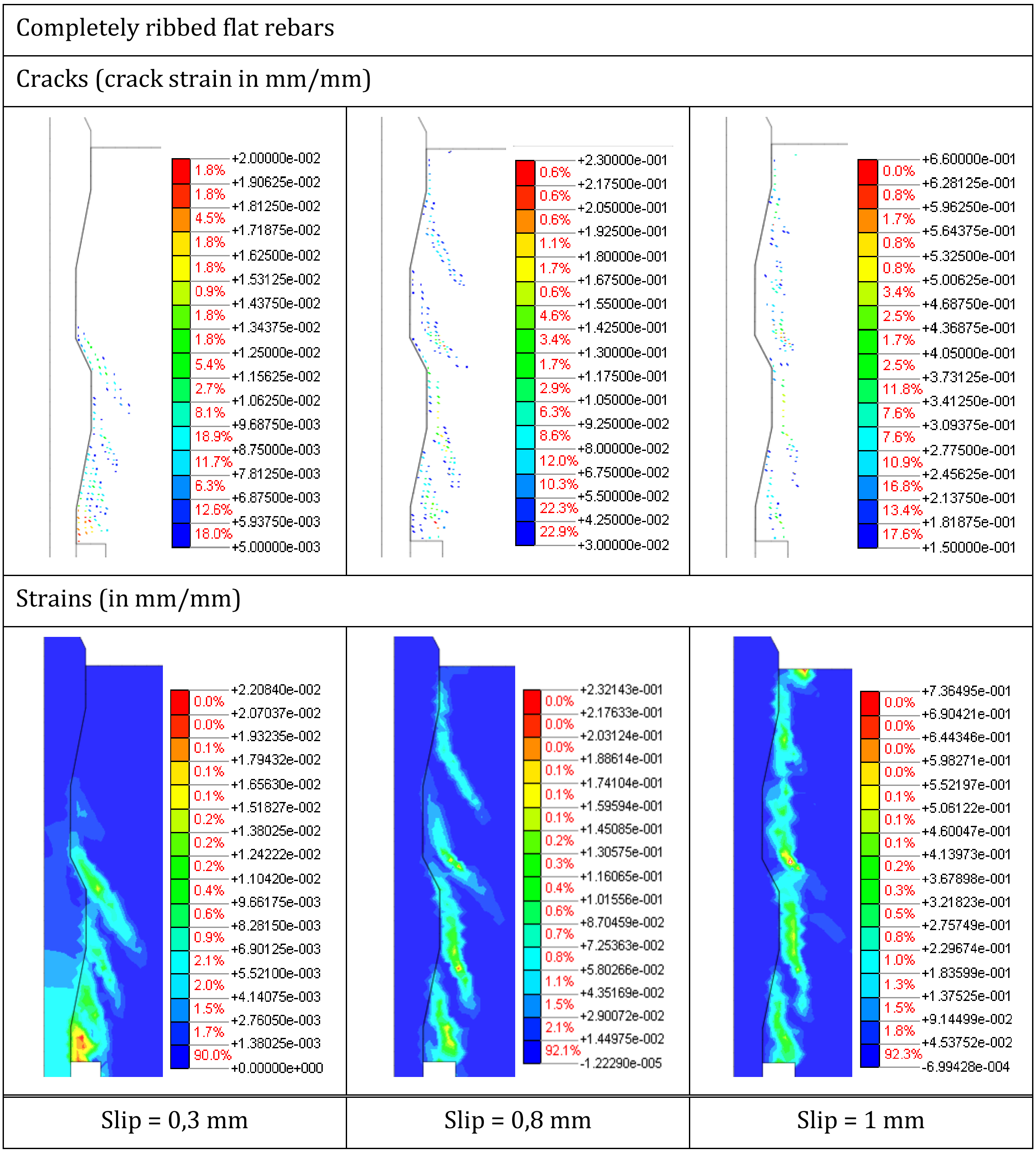

Figure 7-20 Crack and strain development for different slip values. Completely ribbed flat rebars. Detailed geometry analysis approach

3.3.2 Flat rebars with an alternate rib pattern

The same modelling procedure has been also followed for flat rebars with an alternate rib pattern: 15R_10S_15R and 15R_20S_10R bond length configurations. The detailed view of the contact zone between the steel and the concrete can be seen in Figure 7-18-b and Figure 7-18-c, respectively. Note that again a polygonal geometry has been adopted for simplifying the meshing process and to reduce the involved calculation time.

Similarly as done for completely ribbed flat rebars, the bond stress-slip relationship derived from the FEM analysis has been calculated and plotted together with the experimental results. See Figure 7-21 for the 15R_10S_15R configuration and Figure 7-22 for 15R_20S_15R. Furthermore, the cracking behaviour and the strain development in the concrete have been analyzed and are given in Figure 7-23 and Figure 7-24 for 15R_10S_15R and 15R_20S_15R, respectively.

It is observed from the plotted results, that the detailed geometry analysis based FEM gives an accurate prediction of the bond stress-slip behaviour of the alternate rebars for low slip values. As occurred for the completely ribbed bond length configuration, the FE analysis applied in this approach is only able to model the behaviour for slip values until ~1,2 mm and ~1,5 mm for 15R_10S_15R and 15R_20S_15R configurations, respectively. After these values are reached the model diverges, due to the relatively large deformations involved in comparison to the modelled bond length.

The typical change in the ascending slope related to the alternate patterns when the smooth part is positioned in between two ribbed zones, is observed for both bond length configurations modelled. For the 15R_10S_15R configuration, the change in the slope occurs at a slip value of ~0,70 mm with a bond stress value of 10,46 N/mm^2. When the smooth area in between the ribbed zones, is increased to 20 mm, the change in the slope occurs at a higher slip value: ~0,75 mm. The bond stress at that moment is 11,50 N/mm^2.

Regarding cracking behaviour, and strain development in concrete, it is observed that both configurations develop similar behaviour: radial cracks are initiated at the active end, and at increasing slips, more radial cracks develop further from the active end as a larger bond length zone is activated. At slip values of ~1 mm for the 15R_10S_15R configuration and ~1,25 mm for the 15R_20S_15R configuration, longitudinal cracks parallel to the bar axis develop. However, the shearing off of the concrete profile is not as evident as in the case of the completely ribbed configuration: at slip values of 1 mm the completely ribbed configuration has reached the maximum bond stress, whereas for the alternate pattern configurations at the same slip value the bond stress is at ~ 58% of its corresponding bond strength.

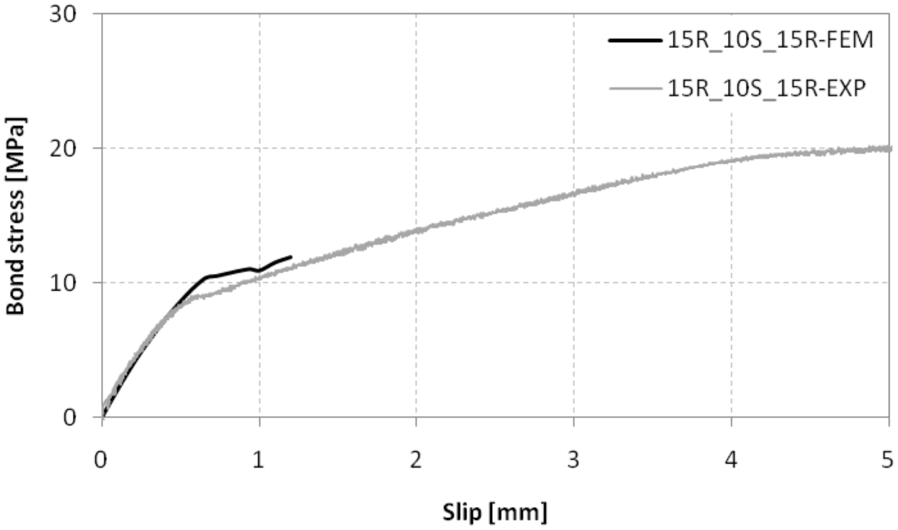

Figure 7-21 Bond stress-slip curve for flat reinforcement with 15R_10S_15R alternate pattern. Experimental vs. FE modelling results. Detailed geometry analysis approach

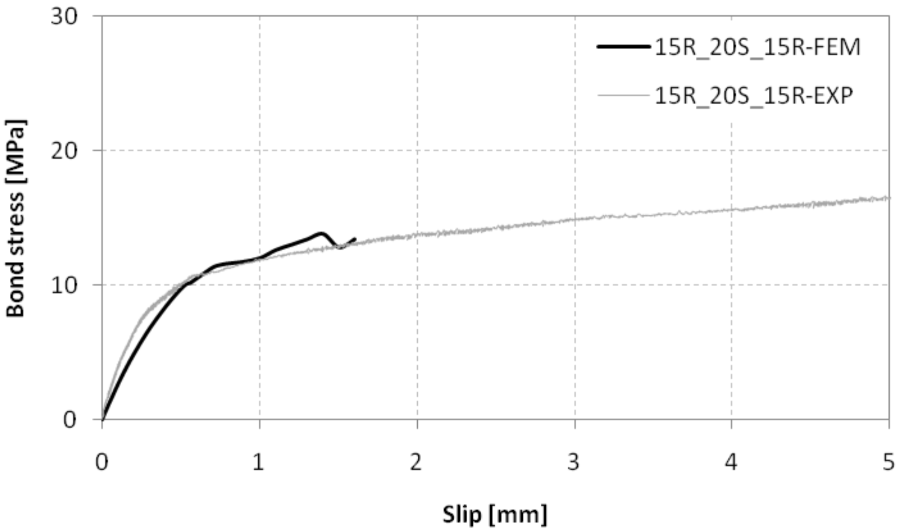

Figure 7-22 Bond stress-slip curve for flat reinforcement with 15R_20S_15R alternate pattern. Experimental vs. FE modelling results. Detailed geometry analysis approach

Flat rebars with an alternate rib pattern: 15R_10S_15R bond length configuration

Cracks (crack strain in mm/mm)

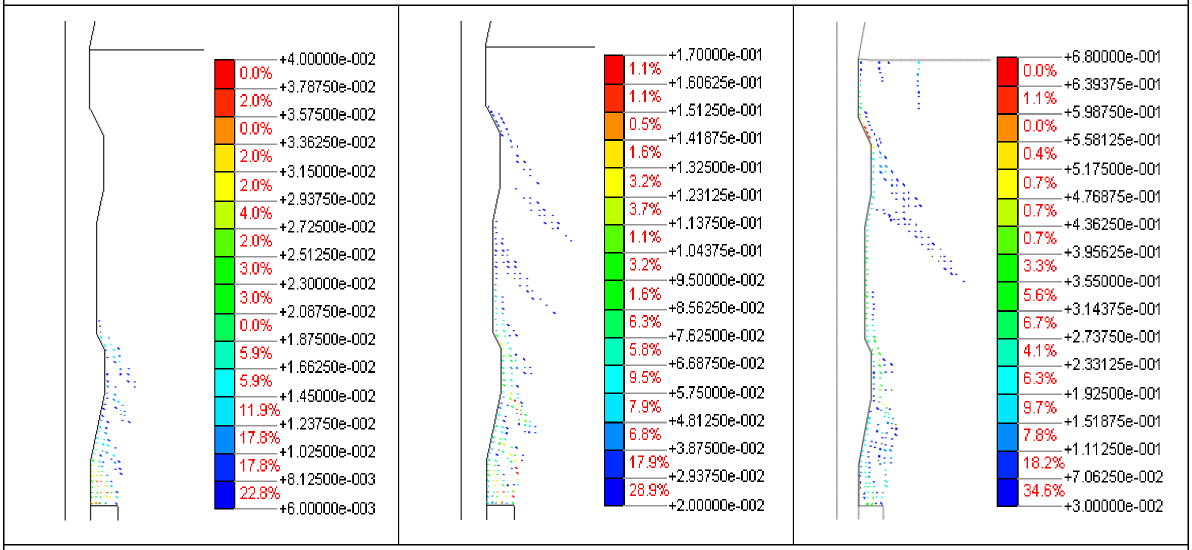

Strains (in mm/mm)

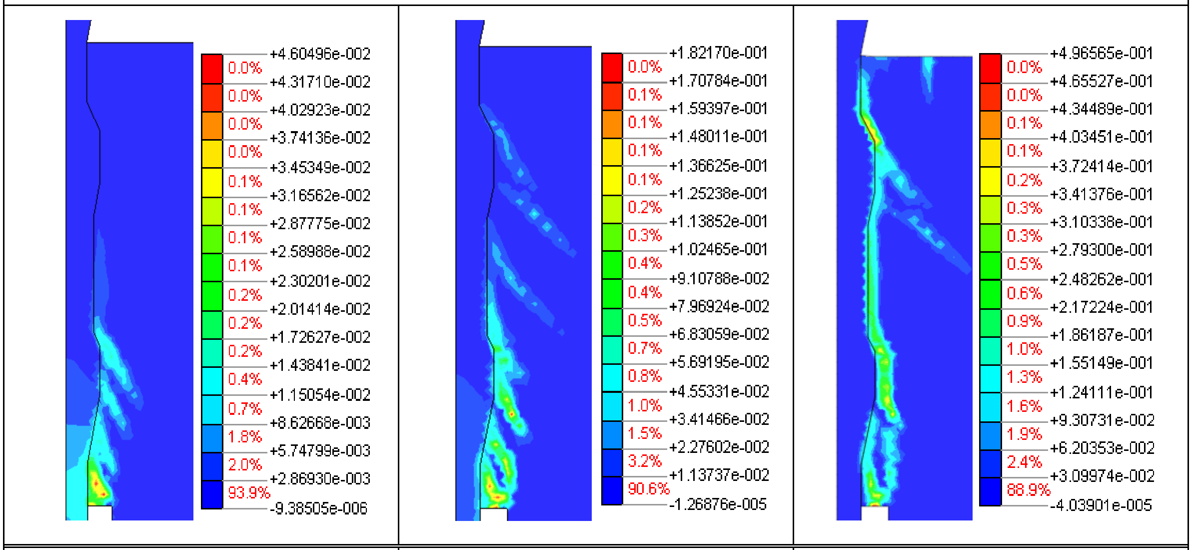

Slip = 0,3 mm	Slip = 0,8 mm	Slip = 1 mm

Figure 7-23 Crack and strain development for different slip values. 15R_10S_15R alternate pattern. Detailed geometry analysis approach

Flat rebars with an alternate rib pattern: 15R_20S_15R bond length configuration

Cracks (crack strain in mm/mm)

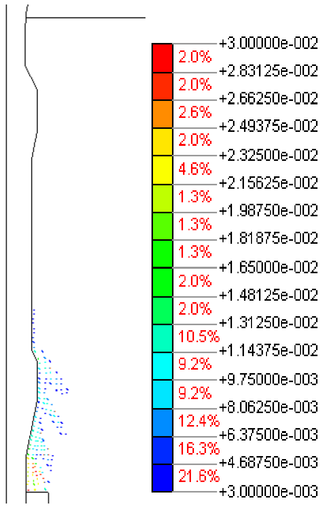

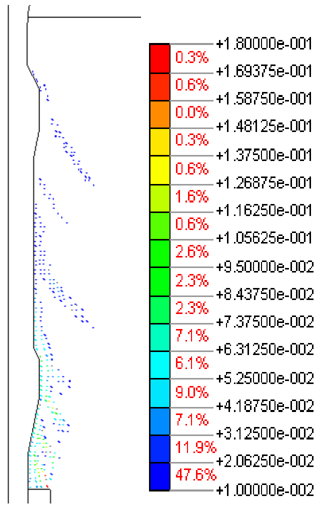

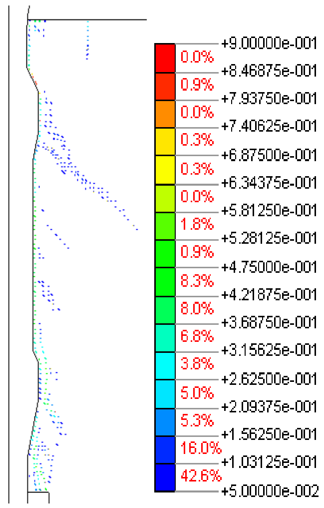

Strains (in mm/mm)

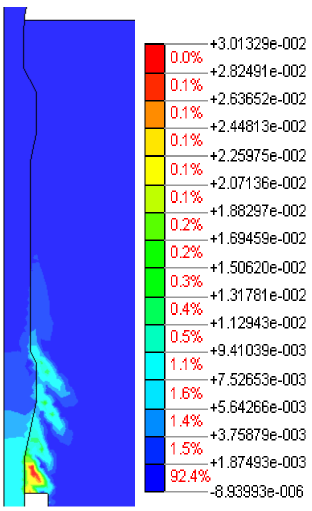

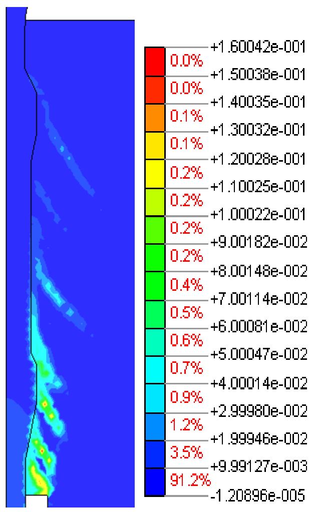

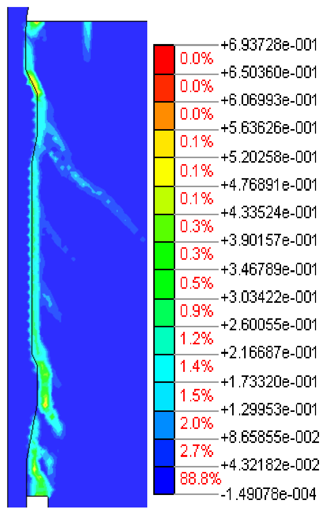

Slip = 0,3 mm	Slip = 0,8 mm	Slip = 1,25 mm

Figure 7-24 Crack and strain development for different slip values. 15R_20S_15R alternate pattern. Detailed geometry analysis approach

If comparison is made between the approaches considered for bond behaviour modelling for completely ribbed flat rebars, it can be concluded that the phenomenological approach (denominated by suffix (1) in Table 7-2 to Table 7-5) is able to predict the whole bond stress-slip relationship although it has the disadvantage that the bond stress-slip behaviour need to be known in advance. Both the maximum bond stress and the slip at which the latter is reached are slightly underestimated by the phenomenological approach in comparison to experimentally obtained mean results (see Table 7-2 and Table 7-3): the experimental values are 1,08 and 1,05 times the one obtained by phenomenological modelling for the maximum bond stress and the slip at maximum bond stress, respectively.

On the other hand, when the detailed geometry analysis is applied (denominated by suffix (3) in Table 7-2 to Table 7-5), only the first ascending branch is correctly modelled, and the model fails for larger slip values. However, the values of both the maximum bond stress and the slip at which this is reached are accurately predicted if comparison is made to experimentally obtained mean values: ratios of 0,99 and 1,01 for the maximum bond stress and the slip, respectively.

Regarding modelling of the bond behaviour of flat rebars with an alternate rib pattern, 3 different approaches have been applied. The phenomenological approach is able to predict the entire bond stress-slip behaviour if the overall relationship is known in advance and imposed to the interface elements. However, the semi-detailed mixed approach (denominated by suffix (2) in Table 7-4 and Table 7-5) and the detailed geometry analysis are only able to model the bond stress-slip behaviour until slip values of around 4 mm and 1,2 mm, respectively.

Regarding the typical change of slope of the ascending branch observed for the alternate bond length configurations, the applied 3 approaches are able to predict this behaviour. Table 7-4 and Table 7-5 give the comparison between the experimentally obtained results and the applied 3 modelling approaches for the values of the slip at which the change of the slope occurs and the bond stress at that moment.

For the 15R_10S_15R bond length configuration, the slip and the bond stress at the moment of change of slope of the ascending branch are best predicted (slightly overestimated) by the phenomenological approach compared to experimental results: ratio of 0,99 and 0,98, respectively. The s_1 value calculated by the semi-detailed approach is 1,05 times higher than the experimental one, and the s_1 given by the detailed geometry analysis underestimates in 7% the value obtained experimentally. Regarding τ_1, the experimental value is 12% and 13% higher than the one calculated by the semi-detailed and the detailed geometry analysis, respectively.

For the 15R_20S_15R configuration, the experimental s_1 values are always higher than the modelled values: 22%, 18% and 24% higher for the phenomenological, semi-detailed and detailed geometry approaches, respectively. The stress values at which the change of the ascending slope occurs is best modelled by the geometrical approach (ratio of 0,99 compared to experimental values). However, also the other two approaches give good approximation of the τ_1: the phenomenological approach overestimates the experimental value by 5% and the semi-detailed approach underestimates it by 8%.

The phenomenological approach is therefore recommended when the bond stress-slip relationship involved in the reinforced concrete is already known and if further analysis on this aspect is not needed. The approach is of great interest for structural models, where full scale reinforced concrete structures are modelled. However, if the bond behaviour of a given rib geometry needs to be investigated, the detailed geometrical approach should be considered. Furthermore, the detailed geometry approach allows for a realistic modelling of the strain and cracking phenomena occurring at the bond zone, which may be of interest if the bond mechanisms acting in the bond zone need to be analyzed and understood. In this sense an improvement of the applied FE model should be studied in the future for a better characterization of the entire bond stress-slip relationship.

Table 7-2 Comparison of slip values at maximum bond stress for CR flat rebars

Bond length configuration	$s_{1,EXP}$ ***[mm]***	$s_{1,FEM\,(1)}$ ***[mm]***	$s_{1,FEM\,(3)}$ ***[mm]***	$s_{1,EXP}/s_{1,FEM\,(1)}$ ***[-]***	$s_{1,EXP}/s_{1,FEM\,(3)}$ ***[-]***
CR	1,14	1,08	1,12	1,05	1,01

Table 7-3 Comparison of maximum bond stress values for CR flat rebars

Bond length configuration	$\tau_{max,EXP}$ ***[N/mm²]***	$\tau_{max,FEM\,(1)}$ ***[N/mm²]***	$\tau_{max,FEM\,(3)}$ ***[N/mm²]***	$\tau_{max,EXP}/\tau_{max,FEM\,(1)}$ ***[-]***	$\tau_{max,EXP}/\tau_{max,FEM\,(3)}$ ***[-]***
CR	19,38	17,96	19,42	1,08	0,99

Table 7-4 Comparison of slip values at which the change in the slope of the ascending branch occurs for flat rebars with an alternate rib pattern

Bond length configuration	$s_{1,EXP}$ ***[mm]***	$s_{1,FEM\,(1)}$ ***[mm]***	$s_{1,FEM\,(2)}$ ***[mm]***	$s_{1,FEM\,(3)}$ ***[mm]***	$s_{1,EXP}/s_{1,FEM\,(1)}$ ***[-]***	$s_{1,EXP}/s_{1,FEM\,(2)}$ ***[-]***	$s_{1,EXP}/s_{1,FEM\,(3)}$ ***[-]***
15R_10S_15R	0,75	0,76	0,79	0,70	0,99	0,95	1,07
15R_20S_15R	0,93	0,76	0,79	0,75	1,22	1,18	1,24

Table 7-5 Comparison of bond stress values at which the change in the slope of the ascending branch occurs for flat rebars with an alternate rib pattern

Bond length configuration	$\tau_{1,EXP}$ ***[N/mm²]***	$\tau_{1,FEM\,(1)}$ ***[N/mm²]***	$\tau_{1,FEM\,(2)}$ ***[N/mm²]***	$\tau_{1,FEM\,(3)}$ ***[N/mm²]***	$\tau_{1,EXP}/\tau_{1,FEM\,(1)}$ ***[-]***	$\tau_{1,EXP}/\tau_{1,FEM\,(2)}$ ***[-]***	$\tau_{1,EXP}/\tau_{1,FEM\,(3)}$ ***[-]***
15R_10S_15R	11,77	11,95	10,50	10,46	0,98	1,12	1,13
15R_20S_15R	11,34	11,95	10,50	11,50	0,95	1,08	0,99

4 Tension stiffening and cracking behaviour modelling

Based in the phenomenological approach explained for the bond behaviour modelling, the tension stiffening tests performed in the experimental program regarding flat stainless steel rebars have been modelled in 2D. In this way, both the tension stiffening effect and the cracking behaviour of the axially loaded concrete prism reinforced with flat rebars with continuous or alternate rib pattern have been assessed.

Figure 7-25 gives the model used for the analysis together with a detailed view of one of the prism ends where the involved elements can be identified:

- concrete prism: modelled with nonlinear material properties using a fixed cracking model,
- investigated rebar: modelled with nonlinear material properties as yielding of the bar is expected to occur at increasing loads,
- extra reinforcement for avoiding damage of concrete at the loading end: for a simplification of the model, the confinement applied experimentally over a length of 135 mm in form of stirrups (see Figure 6-5, Chapter 6), has been modelled as a 3 mm thick steel confinement plate (attached to the concrete at the outer sides of the prism over the same length). Linear material properties have been applied,
- interface: the contact zone between the concrete and steel has been modelled flat with interface elements to which a bond stress-slip relationship has been assigned.

A symmetry axis has been taken according to the longitudinal axis of the reinforcement, and the full length of the reinforced concrete specimen has been modelled because of the non symmetrical (with respect to the section at the half length of the prism) positioning of the bond length configuration due to the alternate rib pattern of the reinforcement.

The load has been applied as imposed displacement at both ends of the flat rebar with a step size of 0,01 mm. Symmetry boundary conditions have been adopted at the symmetry axis, YZ plane (see Figure 7-25), reducing the degrees of freedom of the specimen by constraining the displacement in X and the rotation in Y and Z.

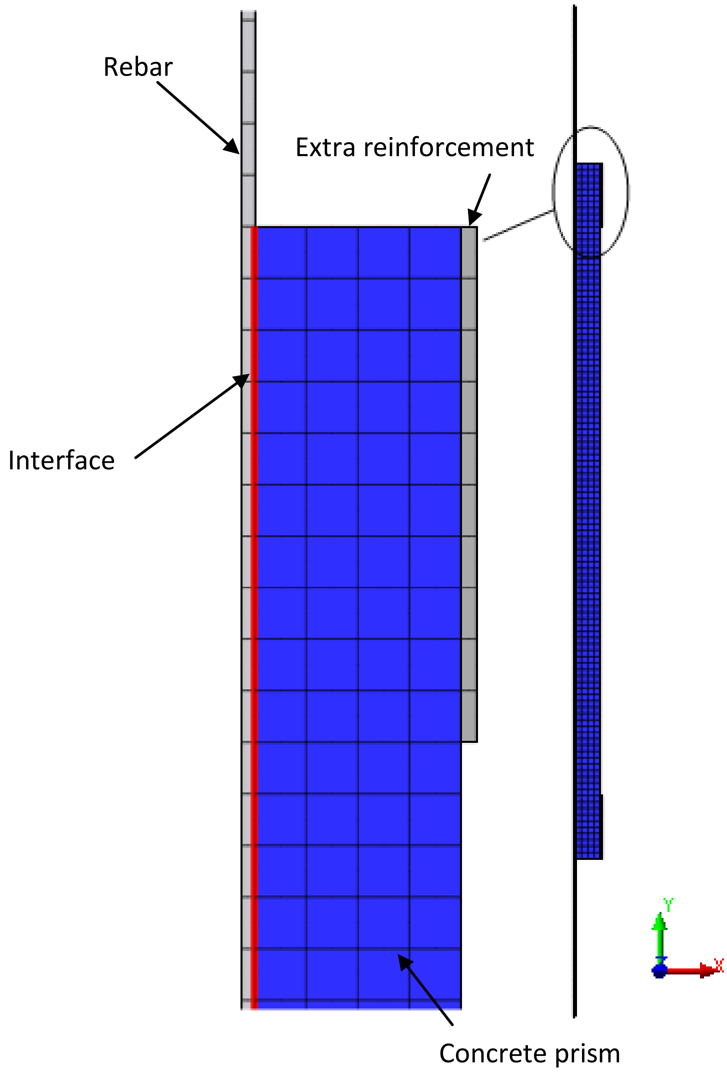

Figure 7-25 Full view of the modelled tension stiffening test specimen (right) and detialed view of the prism end (left).

For the completely ribbed sample the whole interface has been modelled as continuous and the bond stress-slip relationship for completely ribbed rebars has been imposed for the entire bond length. However, for other investigated alternate rib patterns, the interface between the steel and the concrete has been modelled as discontinuous, differentiating ribbed and smooth areas (lengths depending on the rebar pattern), and therefore, giving different bond stress-slip relationship accordingly, see Figure 7-3. The modelled rib patterns are: 50R_10S, 100R_10S, 150R_10S, 100R_20S and 150R_20S, as done experimentally. See Figure 7-26 where the discontinuous interface can be seen for the tested alternate patterns together with the completely continuous interface for the CR configuration (ribbed zones have been highlighted in red for a better visualization).

Note that the secondary rib effect observed experimentally for alternate rib patterns will be lost in this approach as concluded from the bond behaviour modelling. However, given the straightforward applicability of the phenomenological approach (and lack of divergences during the calculation process) the approach has been considered for a first approximation of the tension stiffening and cracking behaviour modelling.

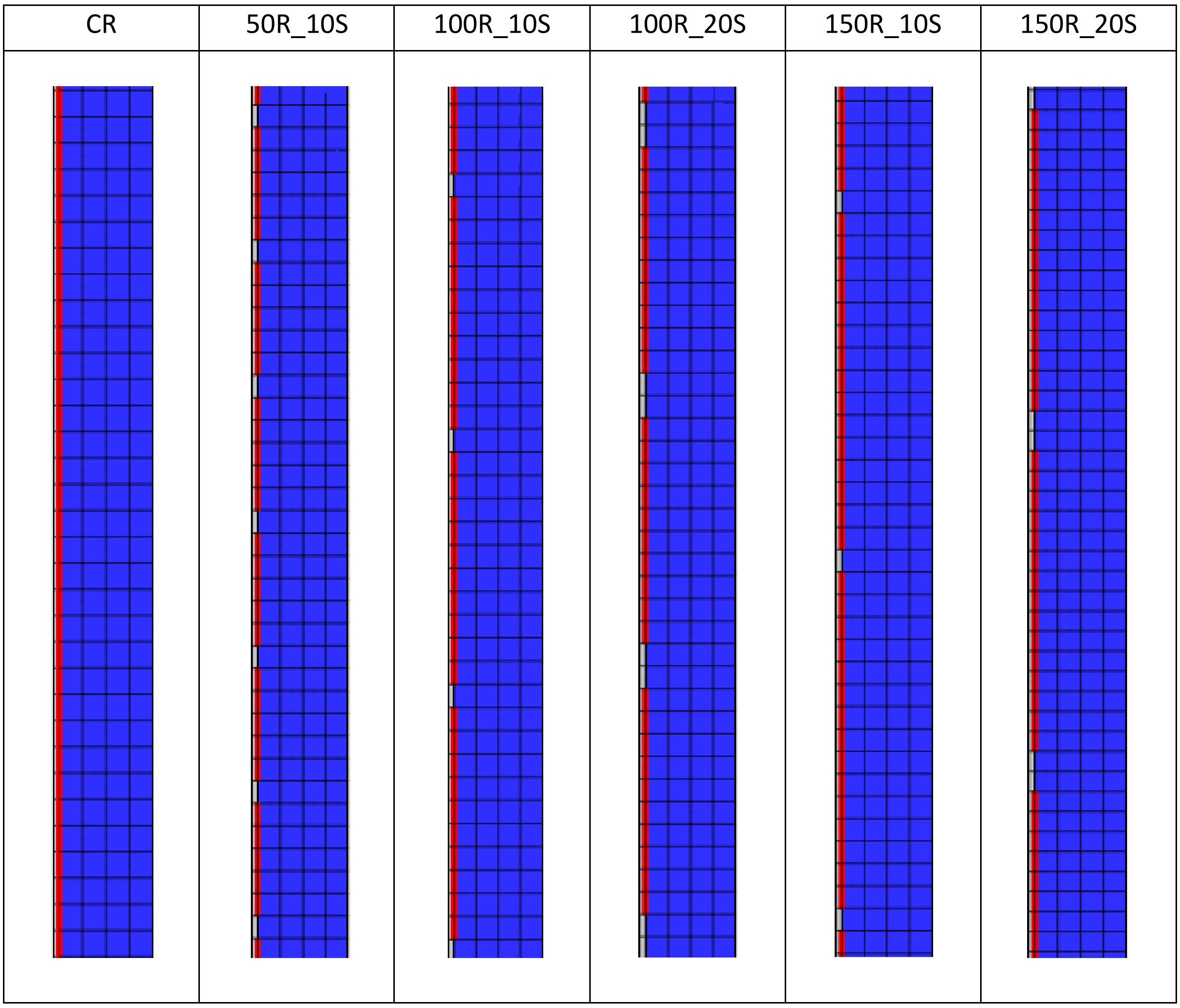

Figure 7-26 Detailed view of the interface for tested flat rebars

4.1 Tension stiffening modelling

Considering the forces at both ends of the rebars obtained from the model, the applied load and consequently the tensile stress at the rebar can be calculated. For plotting of the stress-strain diagram, the mean strain at the concrete interface has been computed as it has been done experimentally. The modelled stress-strain diagrams (FEM suffix), together with experimentally obtained ones (EXP suffix), are given in Figure 7-27 to Figure 7-32 for all the modelled samples. Note that the experimentally tested tensile behaviour of the naked rebar (dashed red line) is also given in the figures for an easy visualization of the tension stiffening effect. FEM results for different surface configurations are plotted together in Figure 7-33, which allows for a comparison of the tension stiffening effect developed by each configuration. Furthermore, Table 7-6 allows for a comparison between the stress values at first cracking calculated applying Equation 7-15 and 7-16 (σ_{cr}), obtained experimentally ($\sigma_{cr,EXP}$), and given by the FEM analysis ($\sigma_{cr,FEM}$). $\sigma_{cr,FEM}$ has been calculated from the load at which the first drop occurs and the initial linearly ascending branch is changing slope.

$$F_{cr} = f_{ctm} A_c (1+\alpha_s \rho_s) \tag{7-1}$$

$$\sigma_{cr} = F_{cr} / A_s \tag{7-2}$$

According to the FEM results the tensile behaviour of the axially loaded prisms are independent of the rib pattern of the tested flat rebars at the uncracked situation (see Figure 7-33). Furthermore, as it is also concluded from Table 7-6, the stress level at which the first crack appears is equal for all the analyzed rib patterns. The theoretically calculated first cracking stress (Equations 7-1 and 7-2) is in average 25% higher than the one obtained by FEM analysis (note that in both cases the experimental f_{ctm} values have been considered, see Table 6-3, Chapter 6). The first cracking stress levels given by the modelling results overestimate (in average 1,48 times higher values) the cracking values obtained experimentally.

Table 7-6 Comparison of the first cracking stress

Specimen	***σ_{cr} [N/mm²]***	***$\sigma_{cr,EXP}$ [N/mm²]***	***$\sigma_{cr,FEM}$ [N/mm²]***	***$\sigma_{cr}/\sigma_{cr,EXP}$ [-]***	***$\sigma_{cr}/\sigma_{cr,FEM}$ [-]***	***$\sigma_{cr,FEM}/\sigma_{cr,EXP}$ [-]***
SS-5x23-CR-TC	221,96	108,79	191,39	2,04	1,16	1,76
SS-5x23-50R_10S-TC	242,94	111,18	191,39	2,17	1,27	1,71
SS-5x23-100R_10S-TC	242,75	149,93	191,39	1,62	1,27	1,28
SS-5x23-100R_20S-TC	242,75	147,93	191,33	1,64	1,27	1,29
SS-5x23-150R_10S-TC	242,75	140,91	191,39	1,72	1,27	1,36
SS-5x23-150R_20S-TC	242,75	131,35	191,39	1,85	1,27	1,46
Mean value				1,84	1,25	1,48
Standard deviation				0,22	0,04	0,21

The initial stage of the crack formation phase is similar for all the modelled rib patterns (see Figure 7-33). The main differences between the analyzed rib patterns are observed from the end of the crack formation phase and during the crack stabilizing phase, which varies depending on the flat rebar surface configuration: the tensile stress-strain behaviour of the specimen reinforced with CR flat rebar develops the less tension stiffening effect, and the flat rebar with shorter rib zones (50R_10S alternate pattern) shows the stiffer behaviour. The trend is also respected by the other tested surface configurations, thus, the tension stiffening effect increases in the sequence: CR – 150R_10S – 100R_10S – 50R_10S at the stabilized cracking stage. The trend observed experimentally agrees with the FEM results in the sense that stiffer behaviour is developed by the alternate patterns in comparison to the completely ribbed rebar (see Figure 7-34).

If comparison is made between experimental and FEM results, the general observed trend is that the tension stiffening effect resulting from the FEM analysis is similar or more pronounced that the one obtained experimentally. The only case for which this effect is underestimated in comparison to the experimental results is for the completely ribbed flat rebar (see Figure 7-27). The mostly overestimated stiffness given by the models for the alternate patterns might be induced by the neglected secondary rib effect when applying the phenomenological approach. When applying the 50R_10S configuration, higher quantity of smooth zones are involved within the bond length compared to other tested alternate patterns (~17 smooth zones within the embedded length for the 50R_10S configuration compared to ~9 and ~6 for the 100R_10S and 150R_10S configurations, respectively). Therefore, the possible effect of neglecting the secondary rib level when applying the phenomenological approach might be more pronounced for the 50R_10S configuration in comparison to other alternate patterns. This may explain the higher differences observed for the tension stiffening effect between experimental and FEM analysis results for the 50R_10S configuration.

The effect of increasing the smooth zone length from 10 mm to 20 mm, keeping constant the length of the ribbed zone can be observed from Figure 7-35 and Figure 7-36, where the tensile stress-mean strain relationship for the 100R_10S vs. 100R_20S and 150R_10S vs. 150R_20S alternate patterns are given, respectively. It is observed from the figures that the increase on the smooth zone leads to a less stiff behaviour moving the curves towards the tensile curve of the naked bar. The same trend was observed from the experimental results.

An extra tension stiffening model has been developed by giving to the entire contact length between the steel and the concrete the bond stress-slip relationship given by the proposed model for alternate rib patterns (15R_10S_15R configuration, defined by Equations 5-11 to 5-15 with the parameters given in Table 7-1, see Figure 7-3). This bond stress-slip relationship includes the second rib level effect, however it is unclear how representative the short bond length configuration (15R_10S_15R) is for the applied configurations in the tension stiffening tests. The tensile stress-strain curve is plotted in Figure 7-37 (blue line) together with the results obtained for the different configurations by FE analysis. It is observed from the graph that the curve obtained by implementing the proposed model for alternate patterns within the entire length of the interface follow the stiffer trend observed for alternate patterns at the beginning of the stabilized cracking stage. However, its stiffness is later reduced and the curve gets close to the less stiff trend observed for the completely ribbed configuration.

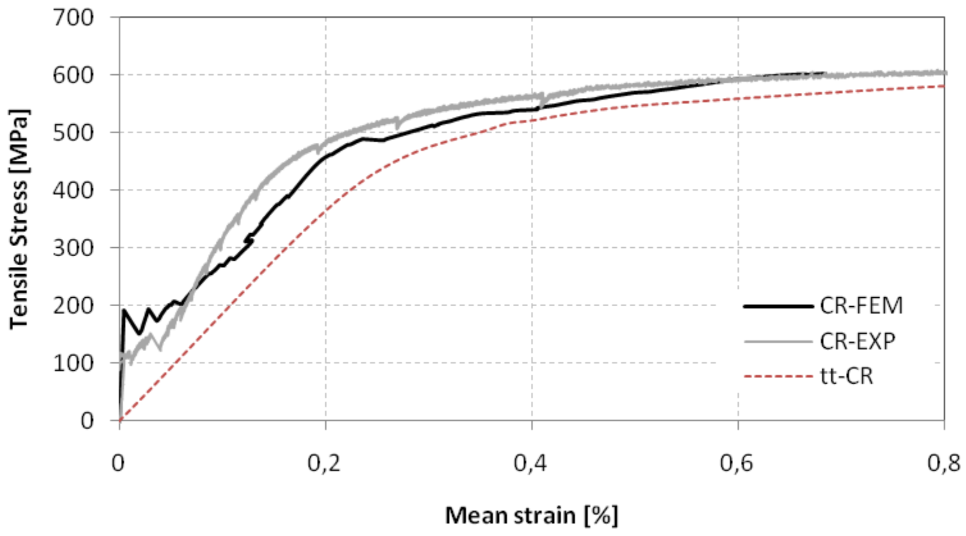

Figure 7-27 Tensile stress-mean strain curves for completely ribbed (CR) SS flat reinforcement. Experimental vs. FE modelling results. Phenomenological approach

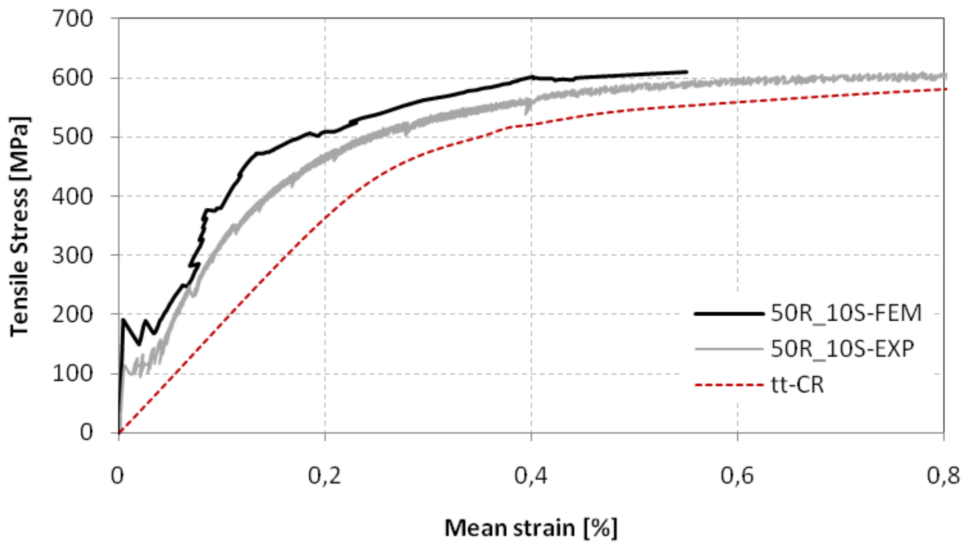

Figure 7-28 Tensile stress-mean strain curves for SS flat reinforcement with 50R_10S alternate pattern. Experimental vs. FE modelling results. Phenomenological approach

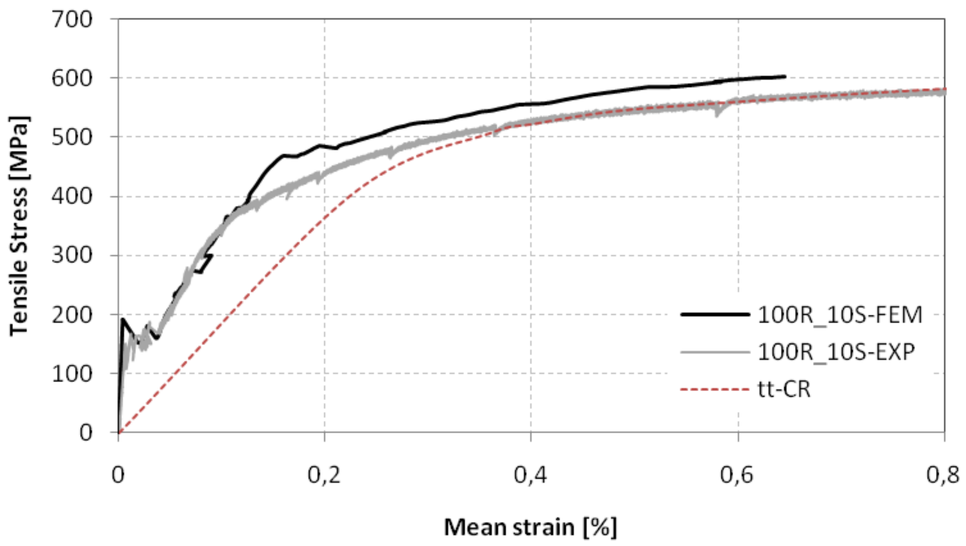

Figure 7-29 Tensile stress-mean strain curves for SS flat reinforcement with 100R_10S alternate pattern. Experimental vs. FE modelling results. Phenomenological approach

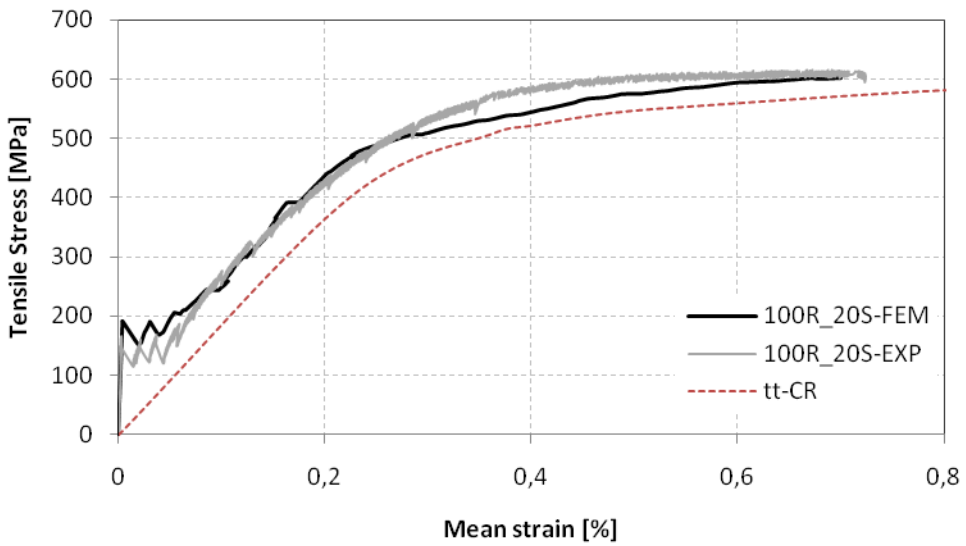

Figure 7-30 Tensile stress-mean strain curves for SS flat reinforcement with 100R_20S alternate pattern. Experimental vs. FE modelling results. Phenomenological approach

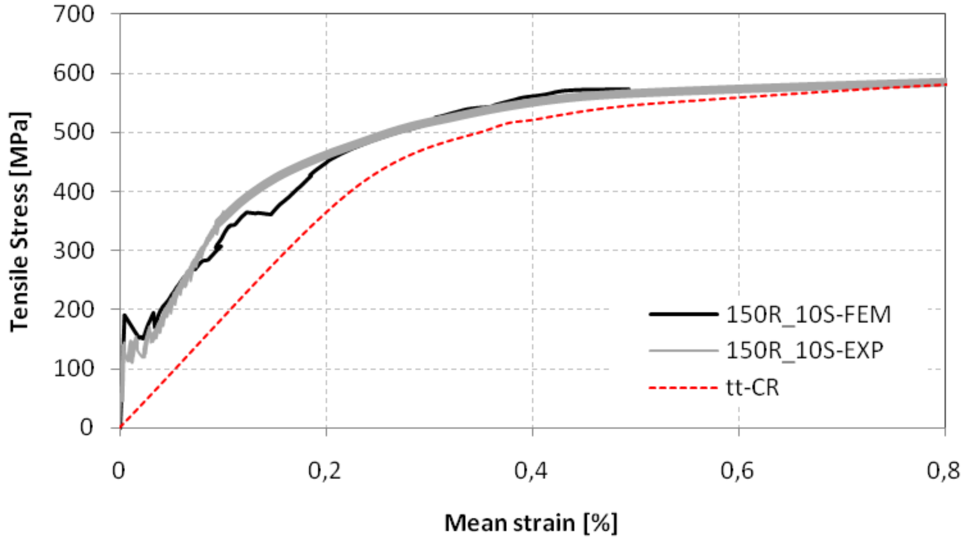

Figure 7-31 Tensile stress-mean strain curves for SS flat reinforcement with 150R_10S alternate pattern. Experimental vs. FE modelling results. Phenomenological approach

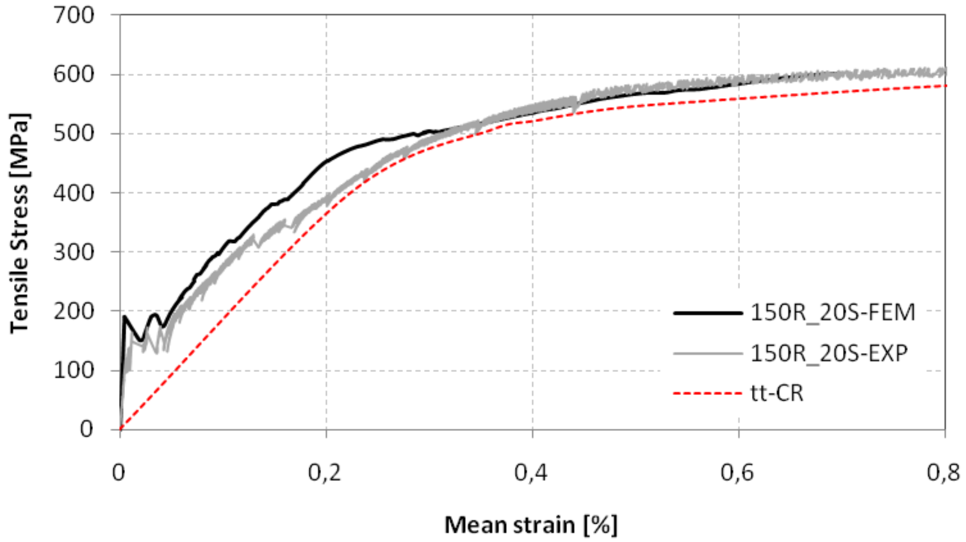

Figure 7-32 Tensile stress-mean strain curves for SS flat reinforcement with 150R_20S alternate pattern. Experimental vs. FE modelling results. Phenomenological approach

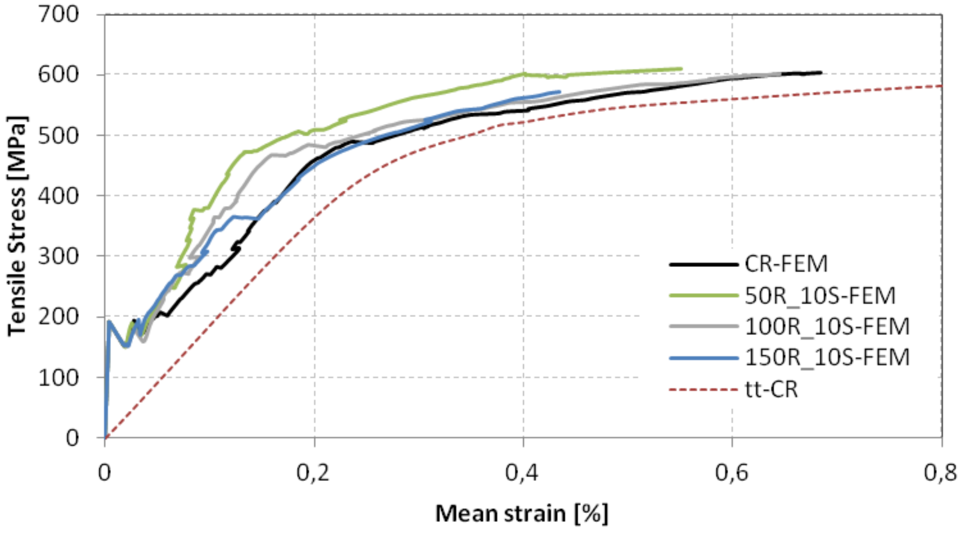

Figure 7-33 Tensile stress-mean strain curves for SS flat reinforcement. CR vs. 50R_10S vs. 100R_10S vs. 150R_10S. Phenomenological approach

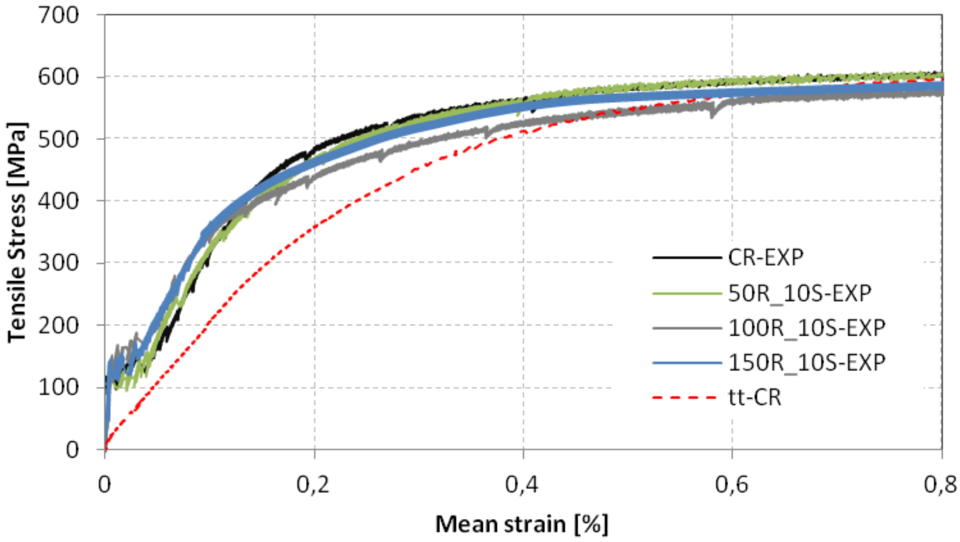

Figure 7-34 Tensile stress-mean strain curves for SS flat reinforcement. CR vs. 50R_10S vs. 100R_10S vs. 150R_10S. Experimental results

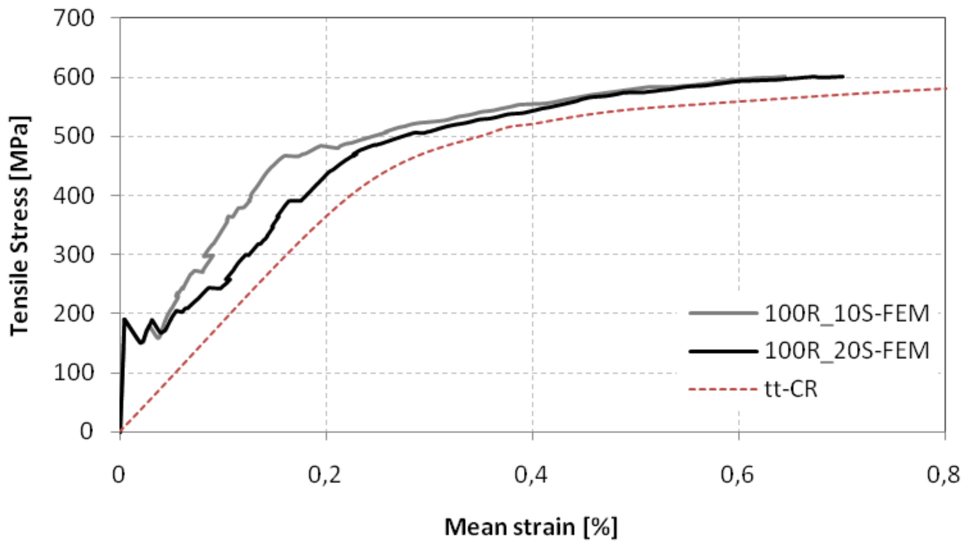

Figure 7-35 Tensile stress-mean strain curves for SS flat reinforcement with alternate rib pattern: 100R_10S vs. 100R_20S. Phenomenological approach

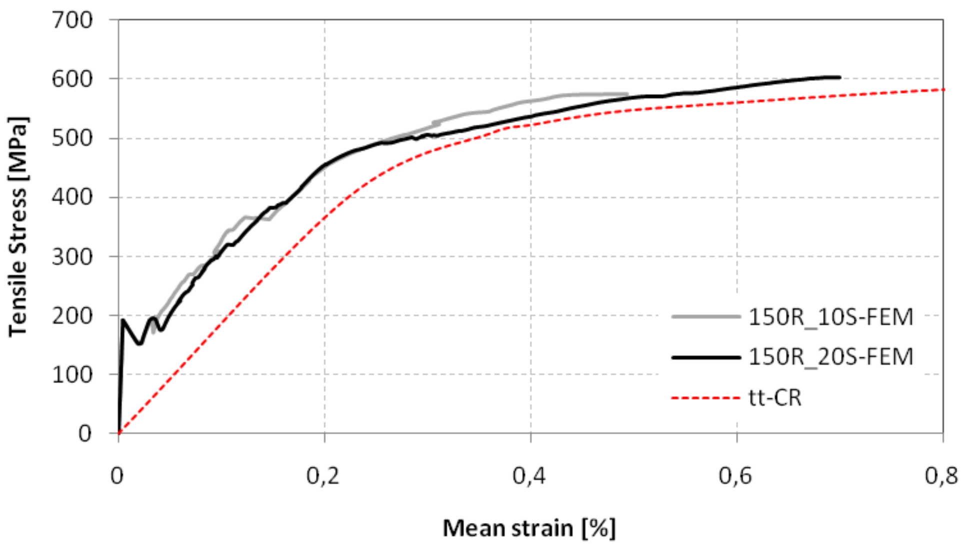

Figure 7-36 Tensile stress-mean strain curves for SS flat reinforcement with alternate rib pattern: 150R_10S vs. 150R_20S. Phenomenological approach

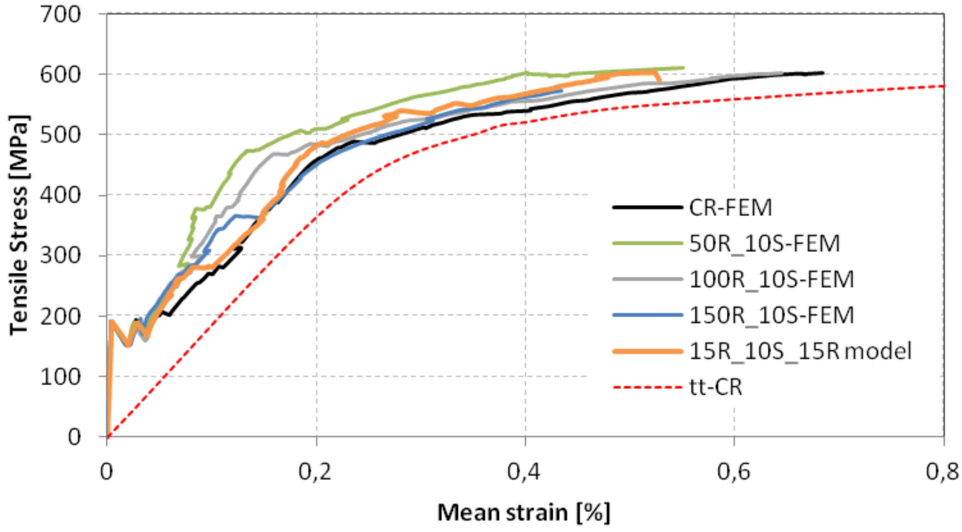

Figure 7-37 Comparison between tensile stress-mean strain curves for SS flat reinforcement with alternate rib pattern. Phenomenological approach

4.2 Cracking behaviour modelling

The cracking behaviour of the axially loaded reinforced concrete prisms has also been investigated using the same FEM analysis. The crack pattern and the corresponding mean crack spacing and mean crack opening at a stress level of 50% of the yield strength of the rebar have been assessed for all the investigated surface configurations. The obtained values are compared to those experimentally obtained in Table 7-7. Figure 7-38 to Figure 7-40 give a representation of the crack pattern observed for each of the tested surface configuration both experimentally and by FE analysis. Note that the FEM figures give the concrete strain as this allows for a better visualization of the crack pattern, than when crack vectors are represented.

Crack width values have been calculated by multiplying the normal crack strain of the integrating point by the corresponding crack band width of the model (the latter is equal, for a 2D analysis, to the square root of the area of the mesh element) taken at the surface of the concrete prism. Only crack widths above 0,01 mm have been considered as for the experimental investigation, corresponding to the accuracy of the applied measurement device (crack microscopy). From the crack pattern figures, the distances between consecutive cracks have been measured (see Figure 7-38), which allows for the calculation of the mean crack spacing.

When a comparison is made between the experimental and the modelled results, in average a good prediction of the mean crack spacing is obtained by the FEM analysis: ratio of 1,01 compared to the experimental values. However, mean crack width values observed experimentally are generally underestimated by the FEM analysis. The ratios between the experimentally observed mean crack width values and the values obtained by FEM analysis vary significantly depending on the tested surface configuration: for completely ribbed rebars, the FEM analysis gives mean crack values that are ~50% lower than the experimentally registered values. On the other hand, the modelled mean crack values corresponding to the 150R_10S and 150R_20S surface configurations are 97% and 93% of the experimental ones, respectively.

For both the experimental and the FEM approaches, best results are obtained with the 150R_10S alternate pattern: the mean crack width is up to 68% and 39% lower than for the completely ribbed pattern (experimental results and FEM results, respectively), and the number of cracks developed are equal or less than for the concrete prism reinforced with the completely ribbed rebar. However, the clear trend observed experimentally regarding significant decrease of the mean crack width if smooth areas are incorporated to the surface of the rebar regardless of the tested alternate pattern is not observed by the FEM analysis. The mean crack values of the modelling approach are equal for the CR, 50R_10S and 100R_20S configurations.

According to the FEM analysis, increasing the smooth area length from 10 mm to 20, the mean crack spacing decreases and the mean crack width increases, which corresponds to a less favourable cracking behaviour.

The mean crack spacing and the mean crack width calculated for the approach in which the entire embedded length has been modelled applying the proposed bond model for alternate patterns are close to the values obtained for the 100R_10S configuration: mean crack spacing of 162 mm and mean crack width of 0,33 mm, compared to 158 mm and 0,35 mm for the 100R_10S configuration. The obtained cracking pattern is also close to the one developed by the 100R_10S configuration (Figure 7-41).

It is finally concluded that the phenomenological approach applied for tension stiffening modelling is able to give a first approximation of the cracking behaviour observed experimentally for the flat rebars with an alternate rib pattern. However, the overall lower mean crack width values given by the FEM might have been influenced by the neglected secondary rib effect when the phenomenological approach is applied.

Table 7-7 Comparison of mean crack spacing and mean crack width at 50% of the yielding strength

Rebar	$s_{m,EXP}$ ***(mm)***	$w_{m,EXP}$ ***(mm)***	$s_{m,FEM}$ ***(mm)***	$w_{m,FEM}$ ***(mm)***	$s_{m,EXP}/s_{m,FEM}$ ***(-)***	$w_{m,EXP}/w_{m,FEM}$ ***(-)***
SS-5x23-CR-TC	165,00	0,78	165,00	0,39	1,00	1,98
SS-5x23-50R_10S-TC	134,00	0,49	158,00	0,40	0,85	1,24
SS-5x23-100R_10S-TC	170,00	0,58	158,00	0,35	1,08	1,65
SS-5x23-100R_20S-TC	175,00	0,46	157,00	0,39	1,11	1,18
SS-5x23-150R_10S-TC	187,50	0,25	174,00	0,24	1,08	1,03
SS-5x23-150R_20S-TC	160,00	0,39	168,00	0,36	0,95	1,08
Mean value					1,01	1,36
Standard deviation					0,10	0,38

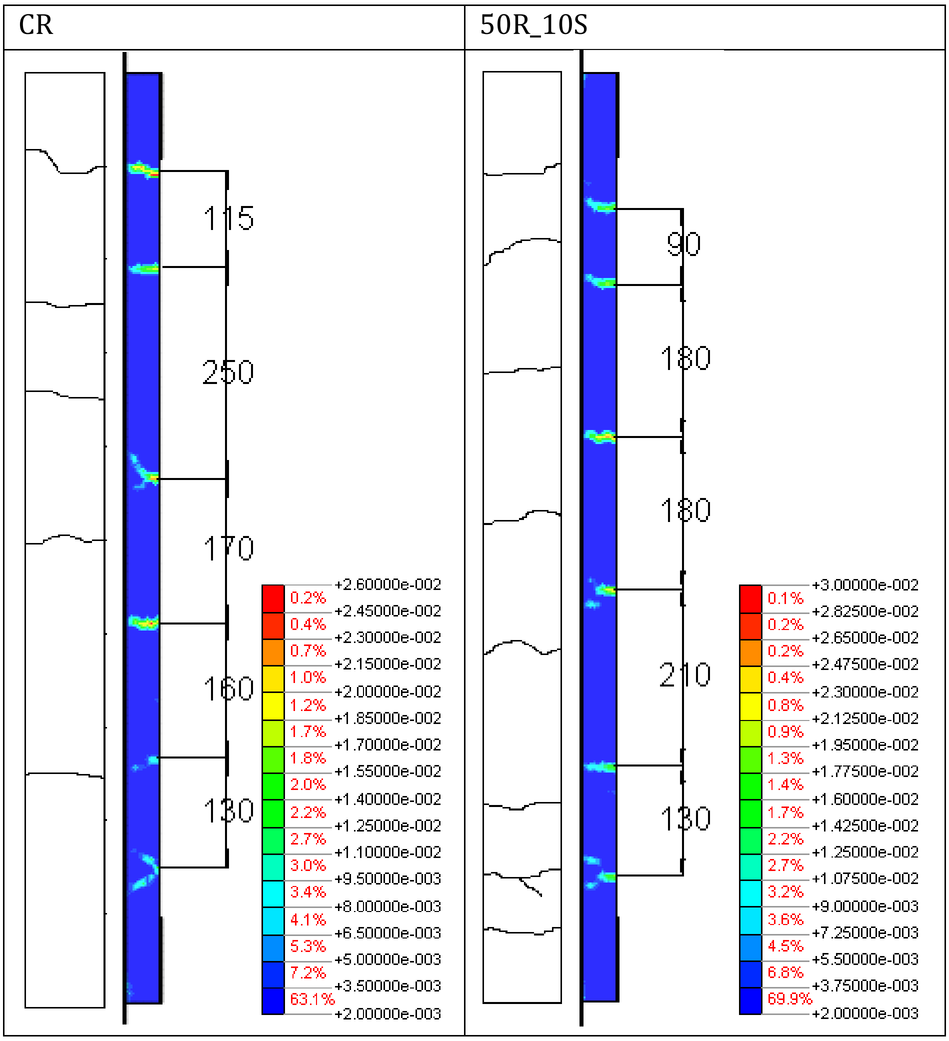

Figure 7-38 Crack patterns derived from the FEM analysis and experimentally. CR and 50R_10S. Crack spacing given in mm and strains in mm/mm

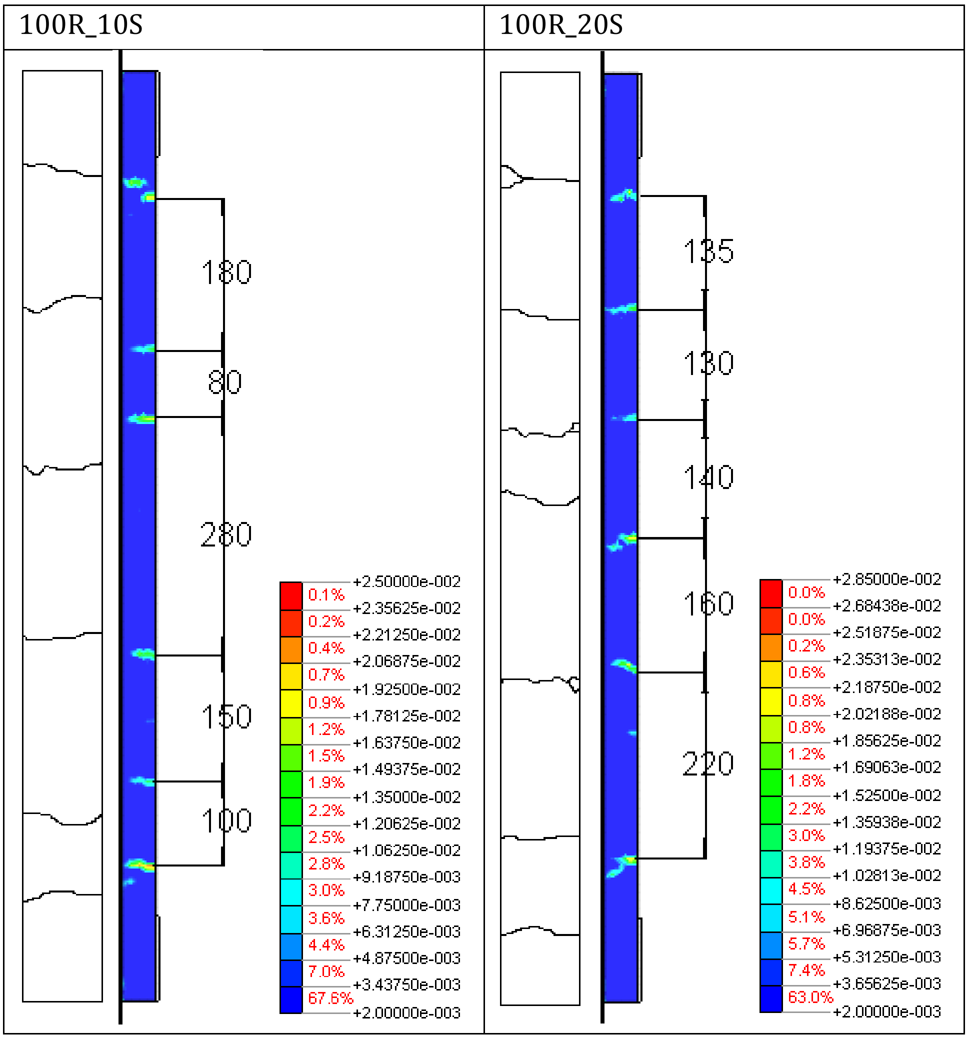

Figure 7-39 Crack patterns derived from the FEM analysis and experimentally. 100R_10S and 100R_20S. Crack spacing given in mm and strains in mm/mm

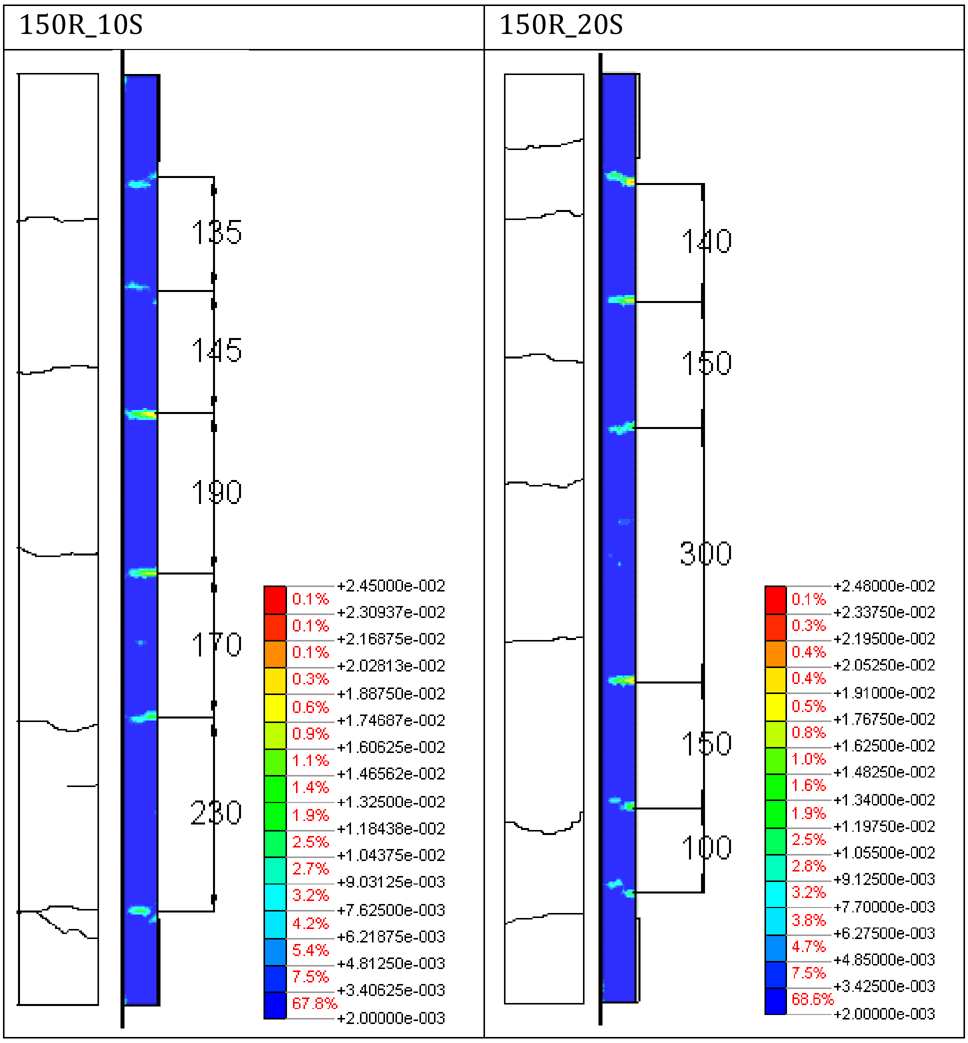

Figure 7-40 Crack patterns derived from the FEM analysis and experimentally. 150R_10S and 150R_20S. Crack spacing given in mm and strains in mm/mm

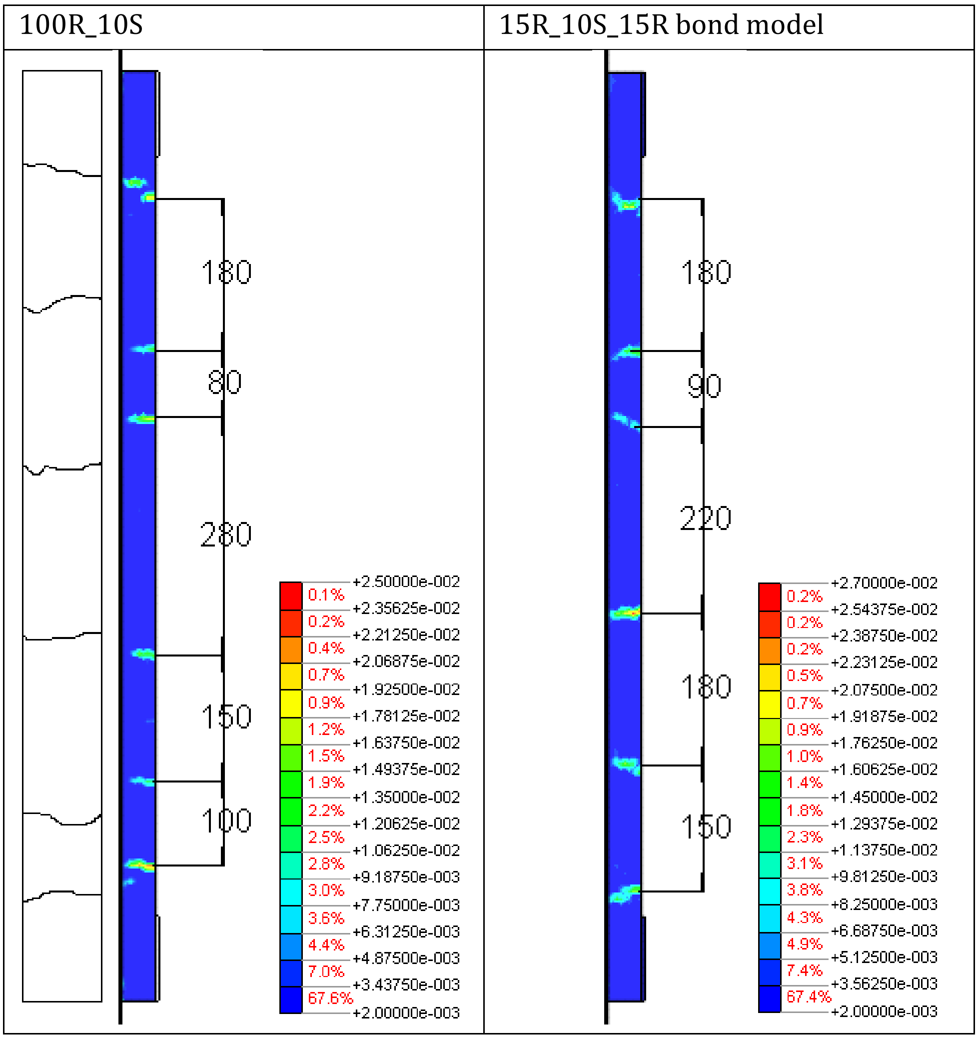

Figure 7-41 Crack patterns derived from the FEM analysis. 100R_10S configuration vs. Model based on the bond model for 15R_10S_15R configuration. Crack spacing given in mm and strains in mm/mm

5 Conclusions

Modelling of the bond behaviour and the tension stiffening effect and the cracking behaviour of concrete reinforced with stainless steel flat rebars continuously ribbed or with an alternate rib pattern has been conducted by FE analysis.

The bond behaviour has been modelled considering 3 different approaches:

i. A phenomenological approach by 3D modelling based on relating the concrete and the steel contact zone by means of flat interface elements to which a bond stress-slip relationship has been imposed. Modelling results show a good agreement between the experimental and the FEM results. However, this approach is limited to the knowledge of the bond stress-slip relationship between the reinforcement and the concrete. On the other hand, if this relationship is known for a given reinforcement, the approach is suitable for structural modelling of the full-size reinforced concrete structures.

ii. For the modelling of the bond behaviour of the alternate patterns tested in this work when the smooth zone is positioned between two ribbed zones within the bond length, a semi-detailed mixed approach has been considered combining the phenomenological approach at the ribbed zones, and introducing a detailed geometry of the transfer zone between the ribbed and the smooth zone. This approach is able to predict the concept of a second level of rib configuration introduced in Chapter 5: the model can predict the change in the slope of the ascending branch. However, the model is not able to predict the entire bond stress-slip relationship as the model failed for slip values larger than ~4 mm, due to the relatively large displacements (deformations) involved in comparison to the modelled bond length when shearing of concrete occurs.

iii. A detailed geometry analysis has been also conducted by means of FEM, for continuously ribbed flat rebars and for flat rebars with an alternate surface configuration, when the smooth zone is positioned between two ribbed zones within the bond length. This approach allows for a prediction of the bond stress-slip relationship for a given rib geometry at low slip values (lower than ~1,2 mm), and gives a realistic view of the cracking behaviour involved at the bond zone.

Comparison between experimental and FEM results of the maximum the bond stress and the slip at which the latter is reached, for completely ribbed rebars, shows a good prediction ability of the model with a maximum difference of 8%. For the alternate patterns, comparison between experimental and FEM results is executed for the bond stress and slip values at the point where the change of the ascending branch occurs: the slip values show a maximum difference of 24% when applying the third approach and for the 15R_20S_15R configuration; for the stress values a maximum difference of 13% is observed again for the third approach and for the 15R_10S_15R configuration.

If the bond behaviour of a given rib geometry needs to be investigated, the detailed geometrical approach should be considered. The detailed geometry approach allows for a realistic modelling of the strain and cracking phenomena occurring at the bond zone, which may be of interest if the bond mechanisms acting in the bond zone need to be analyzed and understood. In this sense an improvement of the developed FE model should be further studied in the future for a better characterization of the entire bond stress-slip relationship.

The tension stiffening tests performed experimentally have been modelled by the phenomenological approach. Although the secondary bond effect observed experimentally when applying alternate patterns is not captured, the approach has been applied for a first approximation of the tension stiffening and cracking behaviour modelling. As such, the contact zone between the reinforcement and the flat rebar has been modelled using interface elements which have been taken continuous or discontinuous depending on the surface configuration to be tested: continuous interface for the completely ribbed flat rebar and discontinuous interface for the alternate rib patterns. Bond stress-slip relationship have been imposed to the interface elements. Modelling results show the same trend as observed experimentally in terms of higher tension stiffening effect developed by the alternate patterns in comparison to the completely ribbed configuration. When comparing individual results, overall the FEM analysis overestimates the tension stiffening behaviour observed experimentally for the alternate patterns. This overestimation is more pronounced for the 50R_10S configuration, which is the configuration with larger amounts of smooth zones within the bond length. It is believed that neglecting the secondary bond effect related to the alternate patterns is the cause of this overestimation.

Regarding cracking behaviour, the crack pattern and the mean crack spacing are well predicted by the FEM analysis (average ratio of 1,01 compared to the experimental values). However, the modelling approach underestimates the mean crack opening obtained experimentally. Again, the neglecting of the secondary bond effect might have influenced these differences.

The best cracking behaviour has been observed for the 150R_10S configuration, as was concluded from the experimental results as well. It is also concluded from the FEM analysis that increasing the smooth area from 10 mm to 20 mm for a given ribbed zone length (100 mm or 150 mm), decreases the tension stiffening effect of the concrete prism, and worsens the cracking behaviour of the specimen.

Further work and analysis is necessary in order to introduce the second rib level effect within the tension stiffening and cracking behaviour modelling. A semi-detailed mixed approach might be of interest in this sense.

6 References

[1] fib (2000) *Bond of reinforcement in concrete. State of the art report.* fib Bulletin 10

[2] Lettow S., Ozbolt J., Eligehausen R., Mayer U. (2004) *Bond of RC members using nonlinear 3D FE analysis*. Fracture mechanics of concrete structures. IA-FraMCoS, pp 861–868

[3] Desnerck P. (2011) *Compressive, bond and shear behaviour of powder-type self-compacting concrete*. PhD Dissertation, Ghent University, Ghent

Chapter 8 Conclusions and future research

Recently an interest on applying flat stainless steel rebars for reinforcement of concrete structures has emerged. The use of stainless steel is motivated from a corrosion protection point of view, whereas the motivation of applying flat rebars deals with the larger contact surface between the steel and the concrete. However, the combination of the two concepts (flat and stainless steel) within the same reinforcement is of great interest in those cases where a minimum concrete thickness is required, as it is the case for shallow slabs. A third concept dealing with the use of alternate rib patterns has also been introduced: the principal motivation is the optimization of the crack pattern developed by a concrete structure reinforced with rebars combining alternately smooth and ribbed zones.

Existing research regarding stainless steel reinforcement suggests that, provided adequate rib geometry of the rebar is available, the bond interaction between the corrosion resistant reinforcement and the concrete is comparable to the behaviour developed by carbon steel reinforcement. The application of SS reinforcement, although increasing, is limited due to the higher price of the material compared to carbon steel. Nevertheless, life cycle cost analysis performed to existing reinforced concrete structures where stainless steel has been applied, has demonstrated that the initial incremented cost related to the SS can be balanced by the cost reduction due to the less amount of maintenance and repairing works needed. The selective use of the stainless steel within the structure and the choice of a not over-specified SS type, are key factors in the optimization of the cost aspects related to the use of SS reinforcement.

Provided the mechanical and physical properties of a material are adequate for reinforcement of concrete (ultimate strength and strain, yielding properties, thermal conductivity, density, coefficient of thermal expansion and magnetic properties, among others), the bond capacity of a reinforcement will mainly depend on the surface configuration. Consequently, tension stiffening and cracking of a reinforced concrete structure, which also relate to the constitutive bond behaviour, will be conditioned by the surface configuration of the reinforcement as well.

According to the literature available, no research has been conducted so far regarding flat stainless steel rebars with continuous or alternate surface configurations. Furthermore, no data was found regarding any scientific investigation on alternate surface configurations for standard round carbon steel rebars. Consequently, no design tools or guidelines exist for flat SS reinforcement with or without alternate surface configuration. In this sense, this PhD thesis has contributed to the understanding of the bond and tension stiffening behaviour, as well as to the knowledge of the cracking behaviour of axially loaded concrete prisms reinforced with flat stainless steel rebars with different surface configurations: completely smooth, completely ribbed and alternate rib configurations combining smooth and ribbed areas.

1 Bond behaviour

The bond behaviour of flat stainless steel rebars has been experimentally studied by means of 126 pullout test to centrally embedded specimens. Besides the surface configuration, other parameters like reinforcing material (carbon steel or stainless steel), geometry of the rebar (round or flat), applied concrete type (traditional or self compacting concrete) and influence of adding confinement reinforcement have been analyzed. Furthermore, for those rebars with an alternate surface configuration combining smooth and ribbed zones, the position and the length of the smooth zone within the bond length have also been studied.

Results show that for smooth flat rebars, where the bond mechanism is mostly governed by the chemical adhesion between the steel and the concrete, the reinforcement material influences the developed bond strength: higher values have been recorded for CS compared to SS. Among tested SS types, the austenitic 304L SS shows better bond behaviour than the ferritic K31: 2 times higher bond strength is developed with higher stiffness. Higher bond strength values (up to 85% higher) are also developed when the smooth rebars are embedded in SCC instead of TC. The geometry of the rebar has been studied in terms of round rebars vs. flat rebars, and different aspect ratios within the flat rebars. Round rebars develop 43% higher bond strength, but due to the larger involved perimeters for the flat rebars, higher loads were reached with the latter reinforcements. The rebars with lowest aspect ratios are the ones that developed higher bond strength values. Regarding influence of microroughness, this appeared of secondary importance compared to the influence of geometry, reinforcement material or concrete type. Regardless of the bar geometry, material, or surface roughness, the bond stress slip relationship showed the following trend: a first steep ascending branch until the maximum bond stress is reached at a slip of ~0,01 mm, followed by a descending branch until frictional bond forces are reached at a slip of ~ 10 mm. Afterwards, a constant bond stress value is kept at increasing slips.

The proposed analytical bond model for smooth flat rebars adopts the first ascending branch defined by the fib Model Codes. However, these documents equal the maximum bond stress to the remaining frictional stress, which disagrees with the observed behaviour. Consequently, the descending branch has been modelled as a logarithmic curve that asymptotically derives from the maximum bond stress till frictional forces are reached (see Equations 4-31 to 4-35 and Table 4-16, in Chapter 4). In this way the experimentally observed behaviour (both for flat smooth rebars and for round smooth rebars) is better represented.

Regarding flat ribbed rebars, the influence of the studied parameters differs compared to the smooth rebars. The governing bond mechanism is developed by mechanical bearing forces due to the ribs of the reinforcement. In this sense, the relative rib area of the reinforcement plays a key role on the developed bond behaviour. Consequently, and given the different relative rib areas involved for the round and flat tested rebars, conclusions regarding the influence of the bar geometry on the developed bond strength are difficult to make. Up to 40% higher loads were necessary for pulling out of the flat ribbed rebars, because of the larger perimeter involved. On the other hand, higher splitting tendency is observed for flat ribbed rebars tested in this work. Because of this, the bond length applied for pull out testing has been reduced from 5Ø (recommended by RILEM) to 3Ø, for pull out type of failure to occur.

Reinforcement material and concrete type show no significant influence on the bond behaviour developed by flat ribbed rebars. This conclusion regarding influence of concrete type differs from the tendency observed for round ribbed rebars. According to the test results as well as the literature available, up to 47% higher bond strength values have been reported when the reinforcements are embedded in SCC.

For characterizing the bond behaviour developed by the flat ribbed rebars tested in this work, an analytical bond model has been proposed based on the definition given for the bond stress-slip relationship of round ribbed rebars by the fib Model Codes for pull out type of failure. The definition of the first ascending branch given by the Model Codes describes a stiffer behaviour than the one observed experimentally. Consequently, the definition of the first ascending branch has been modified based on the work by Soroushian. Furthermore, the slip at which the maximum bond stress is reached has been defined, similar as proposed by Desnerck and related to the clear rib spacing of the reinforcement. In this way the proposed bond model (see Equations 4-36 to 4-39 and Table 4-17, in Chapter 4) showed a good ability to predict the bond response of the flat ribbed rebars tested in this work.

Although attention should be given to the splitting tendency observed for the flat ribbed rebars tested, the application of these bars in replacement of round ribbed rebars seem to be feasible given the bond behaviour developed by the strips. However, effort should be put in the improvement of the rib pattern of the rebars in order to increase the relative rib area involved, as at the moment this value is lower than the recommended value given by fib for an optimal bond behaviour development.

Besides completely ribbed flat rebars, strips with an alternate pattern combining smooth and ribbed areas have also been tested. The same non significant influence of reinforcement material and concrete type as observed for completely ribbed flat elements has been observed for the alternate patterns. When the smooth zone of the alternate pattern is positioned in between two ribbed zones within the bond length, it has been observed that the smooth zone actively contributes to the development of the bond strength: slightly higher (up to 12% for average values) or comparable bond strength values have been obtained for the alternate pattern compared to the completely ribbed reinforcement.

However, less stiff behaviour is developed by the alternate pattern: the maximum bond stress is reached at considerably higher slip values (in the range of 5 mm for the 15R_10S_15R bond length configuration, compared to ~1 mm for completely ribbed rebars). Furthermore, unlike for the completely ribbed samples, the alternate pattern developed a non-continuous ascending branch: a change to a less stiff behaviour is observed at slip values lower than the slip corresponding to the maximum bond stress. Furthermore, the larger the smooth zone in between two ribbed zones, the less stiff the second branch (similar bond strength but at higher slip values). This secondary effect developed by the alternate pattern is understood with the assumption that the smooth zone develops a second rib level with an increased clear rib spacing, which clarifies the less stiff second ascending branch.

Consequently, the analytical bond model proposed for the alternate pattern when the smooth zone is positioned in between two ribbed zones within the bond length, comprises two ascending branches corresponding to the two rib levels involved. Besides the two ascending branches definition, the bond model has been kept as defined for the completely ribbed flat rebars (see Equations 5-11 to 5-15 and Table 5-14, in Chapter 5).

The effect of providing confinement reinforcement to the test specimens has been concluded to be dependent on the failure aspect: for specimens that failed by pull out no influence was observed when confinement was added. However, splitting of the concrete was avoided and higher loads were registered when confinement was added to specimens that failed by splitting of the concrete (without confinement). However, given the higher loads involved, yielding of the bar occurred before forces to provoke pulling out of the rebar were reached.

Modelling of the bond behaviour of flat ribbed rebars with or without an alternate rib pattern has also been conducted by means of finite element analysis, in order to better understand the bond behaviour of flat rebars and to assess the efficiency of the proposed bond stress-slip relationships. Three different approaches have been considered for this study:

i. A phenomenological approach by 3D modelling based on relating the concrete and the steel contact zone by means of flat interface elements to which a bond stress-slip relationship is imposed.
ii. For the modelling of the bond behaviour of the alternate patterns tested in this work when the smooth zone is positioned between two ribbed zones within the bond length, a semi-detailed mixed approach has been considered combining the phenomenological approach at the ribbed zones, and introducing a detailed geometry of the transfer zone between the ribbed and the smooth zone.
iii. A detailed geometry analysis has also been conducted by means of FEM, for continuously ribbed flat rebars and for flat rebars with an alternate surface configuration.

Modelling results by the phenomenological approach show a good agreement between the experimental and the FEM results. However, this approach is limited to the knowledge of the bond stress-slip relationship between the reinforcement and the concrete. The second rib level concept involved in the alternate patterns has been confirmed by the modelling results coming from the semi-detailed mixed approach. The bond stress-slip curve derived from the FE analysis showed the two ascending branches observed experimentally. The geometrically detailed approach has the advantage of being able to predict the bond behaviour for a given rib geometry, in detail. Furthermore, it gives a realistic view of the cracking behaviour involved at the bond zone. However, due to the relatively large displacements (deformations) involved in comparison to the modelled bond length when shearing of concrete occurs, full bond stress-slip behaviour could not be modelled by the semi-detailed and detailed approaches.

If the bond behaviour of a given rib geometry needs to be investigated, the detailed geometrical approach should be considered. This approach allows for a realistic modelling of the strain and cracking phenomena occurring at the bond zone, which may be of interest if the bond mechanisms acting in the bond zone need to be analyzed in detail. In this sense an improvement of the developed FE model should be further studied in the future for a characterization of the entire bond stress-slip relationship.

2 Tension stiffening behaviour and developed cracking pattern

Tension stiffening behaviour has been studied by means of 16 tensile test applied to axially reinforced concrete prisms. The tension stiffening behaviour of flat SS rebars with an alternate rib pattern has been compared to the behaviour developed by completely ribbed SS rebars.

Conclusions related to the influence of the reinforcement material are not drawn from the conducted research, given the different reinforcement ratios involved. On the other hand, SCC showed a delayed first cracking behaviour in comparison to TC and overall cracking behaviour improved always when self compacting concrete was applied. With respect to the tension stiffening effect the test results are not conclusive on the influence of concrete type.

Regarding the influence of the bar geometry, compared to the behaviour of round ribbed rebars, the flat rebars showed an earlier cracking behaviour. However, flat rebars developed greater tension stiffening effect when embedded in concrete than the round rebars did. Regarding cracking pattern developed, the round rebars showed a considerably better behaviour than the flat rebars in terms of mean and maximum registered crack widths. Furthermore, following the splitting tendency observed during bond behaviour characterization for the flat rebars, unlike for the round rebars, longitudinal splitting cracks were observed for the concrete prisms reinforced with flat ribbed rebars, regardless of the alternate rib pattern.

Regarding influence of applying alternate rib patterns on the tension stiffening effect, a somewhat increased tension stiffening was observed from the test results. Also, first cracking occurred at higher stress values when smooth areas were incorporated to the bond length. The cracking behaviour of the concrete reinforced with rebars containing an alternate pattern, improved in comparison to the behaviour observed for completely ribbed rebar. The mean crack width decreased up to 69% when an alternate rib pattern was applied and the best cracking pattern was found for the alternate pattern with a limited amount of smooth areas within the entire bond length (alternate pattern: 150 mm of ribbed zone followed by 10 mm of smooth area). According to the experimental results, increasing the smooth area without modifying the length of the ribbed zone derived in an earlier cracking behaviour and slightly worse cracking pattern developed in the concrete.

Analytical equations have been verified and proposed for predicting the tension stiffening behaviour and the mean crack width of completely ribbed flat reinforcement as well as for the alternate rib patterns. Regarding tension stiffening effect, models given by EC2, MC90 and MC2010 give fairly good prediction compared to the test results, except for the hardening behaviour observed for flat elements at increased steel levels. Therefore, the yielding branch is taken as a linearly increasing branch until ultimate stress values are reached. At service load level the predicted tension stiffening is at the conservative side.

The equations existing in the literature for predicting the crack spacing and consequently the mean crack opening are defined for round ribbed bars. They show little accuracy to predict the cracking behaviour of the flat rebars tested in this work, for both completely ribbed and alternate surface configurations. As a consequence, adaptation of the exiting equations has been proposed for predicting the behaviour of the flat rebars:

i. For completely ribbed bars, a correlation factor λ –empirically derived- is introduced on the mean crack width formulation of round ribbed bars (see Equation 6-27, in Chapter 6).
ii. To predict the mean crack width of the rebars with an alternate pattern, the mean crack width of the corresponding completely ribbed rebar has been taken as reference and dependency on the number of smooth zones within the total embedded length as well as on the ratio between the length of the smooth zone and the length of the single alternate pattern length has been implemented (see Equations 6-32 to 6-34, in Chapter 6).

Modelling of the tension stiffening tests have been conducted by means of FE analysis as done for the bond behaviour characterization. A phenomenological approach has been adopted as a first approximation of the modelling given the straightforward applicability of the approach (and lack of divergences when bond behaviour of flat rebars was modelled). However, the secondary rib level effect is neglected by this approach, which resulted eg. in an overestimation of the tension stiffening effect. The FE analysis of the tension stiffening and cracking behaviour confirmed the conclusions obtained experimentally: the tension stiffening effect is more pronounced for flat rebars with an alternate rib pattern than for the completely ribbed configuration. Furthermore, the cracking behaviour is also improved and best results are obtained for the 150R_10S configuration (for a limited amount of smooth zones). Furthermore, increasing the smooth area of the alternate pattern reduces the tension stiffening effect and worsens the cracking behaviour of the concrete prism.

The theoretical motivation for applying an alternate rib pattern, meaning to improve the cracking behaviour of a concrete structure reinforced with this type of rebars, has been confirmed by the experimental and analytical study. A better cracking behaviour has been observed for flat rebars containing an alternate rib pattern, in comparison to the behaviour of completely ribbed flat rebars. Furthermore, the cracking behaviour of the flat rebars combining smooth and ribbed areas is (for the obtained best result) comparable to the one developed by standard round ribbed rebars for a comparable reinforcement ratio. An improvement of the relative rib area involved in the flat rebars together with an optimal ribbed-smooth zones combination might further improve the cracking behaviour observed.

A schematic representation of the trends observed from the experimental and analytical work performed in this thesis is given in Table 8-1. The table provides a summarized overview of the influence of the different analyzed parameters on the bond and tension stiffening behaviour as well as on the developed cracking pattern, as a function of the surface configuration of the flat rebar.

3 Future research

The research work performed within this thesis, gives detailed study regarding the bond and tension stiffening behaviour of stainless steel flat rebars with different surface configurations. Yet further fundamental research is needed to confirm the observations for a more wide interval of the studied parameters and for the assessment of other structural aspects (besides bond) of concrete structures reinforced with this type of reinforcement:

- Effort should be put on the optimization of the relative rib area involved in the flat rebars, based on fib recommended values. Bond behaviour of different relative rib areas should be studied.
- Extensive analysis should be conducted regarding aspect ratio influence on the developed bond behaviour for comparable contact areas.
- In this sense, and considering the aspect ratio as parameter, the multiaxial stress state should be studied. The orientation of the flat strip within the structure is also a parameter to be considered for further research.
- Given the geometry of a flat rebar, special attention should be put to the effect on the developed bond behaviour of the casting direction and the position of the bar within

the structure (top bar effect). In the same way, the so-called “good” and “bad” bond conditions derived from air trapped at the bottom of the rebar should be studied.

- The configuration of the lap splices with flat rebars and its influence in the splitting behaviour of the element should be assessed.
- The effect of the flat rebars on the postyielding behaviour (ductility) of the elements should be verified.
- As the bond and tension stiffening behaviour of round ribbed rebars have been already extensively studied by several authors and the involved bond mechanisms are well known, alternate rib configurations should be tested also with round rebars, for a better understanding of the influence of incorporating smooth zones within the bond length.
- In this sense, and given the short bond length involved in the pull out test recommended by RILEM, other test set-ups that allow for a longer embedded length should be considered for the characterization of the bond behaviour of different alternate rib patterns. The beam-end test might be of interest in this respect. Test set-ups involving heavy confinement might be of interest as well in order to be able to apply larger bond lengths.
- The effect of concrete cover in the bond capacity of the flat rebars should be studied given the splitting tendency observed.
- Repeatability of the obtained test results should be verified by performing additional tests per test condition (this is especially necessary for the tension stiffening tests conducted within this program, where only one specimen has been tested per testing condition).
- Effort should be put on research focused on a further optimization of the alternate rib pattern. In this sense, analytical equations allowing for defining an optimal ribbed-smooth combination for the alternate rib pattern should be developed. Further FEM based analysis may be helpful in the assessment of different ribbed-smooth combinations.
- The overall structural behaviour of concrete elements reinforced with flat rebars with an alternate rib pattern should be studied (eg. with large scale tests on shallow slabs).

To conclude, flat stainless steel rebars are of interest for replacing carbon steel round reinforcement in those situations where a concrete thickness reduction is required. Whereas this study focussed on the bond behaviour, further understanding of the involved structural behaviour is necessary and therefore, further research is recommended. The application of alternate rib patterns has been proven viable, and has been thoroughly studied for the first time with this work. This research line is to be continued in the future, to be able to generalize the obtained results, and to verify and possibly improve the proposed models.

Table 8-1 Summary of observed trends

Influence of	***Bond behaviour***			***Tension stiffening***		***Cracking pattern***	
	Flat-smooth	Flat-completely ribbed	Flat-alternate	Flat-completely ribbed	Flat-alternate	Flat-completely ribbed	Flat-alternate
Reinforcement material	CS > SS	CS ≈ SS	CS ≈ SS	nc	nc	nc	nc
Concrete type	SCC >TC	SCC ≈ TC	SCC ≈ TC	First cracking SCC >TC Tension stiffening nc	First cracking SCC >TC Tension stiffening nc	SCC > TC	SCC >TC
Reinforcement geometry	f_b: Ø > ▭ F_{max}: ▭ > Ø f_b: □ > ▭	f_b: Ø > ▭ F_{max}: ▭ > Ø	-	First cracking Ø > ▭ Tension stiffening ▭ > Ø	-	Ø > ▭	Ø ≈ ▭ R_S
Confinement	-	If PO: ≈ If SC: avoids splitting	If PO: ≈ If SC: avoids splitting	-	-	-	-
Application of alternate pattern			f_b : ↑ f_b/s : ↓		First cracking ↑ Tension stiffening ↑		↑
Increasing the length of the smooth zone			f_b: ≈ f_b/s: ↓		First cracking ↓ Tension stiffening ↓		↓
Legend	- : not tested nc: not conclusive Ø: round rebar ▭ : flat rebar	> : better (higher) ↑ : improved/ better ↓ : deteriorated/ worst	PO: pull out SC: concrete splitting CS: carbon steel SS: stainless steel	TC: traditional concrete SCC: self compacting concrete	f_b : bond strength f_b/s : stiffness F_{max} : maximum load		

Appendix A Micro Roughness Measurements

Roughness is a measure of the texture of a surface. It is quantified by the vertical deviations of the surface with respect to a perfectly flat form. If these deviations are large, the surface is rough; if they are small the surface is smooth. For the characterization of the roughness, 2D roughness parameters as defined in Table A1 are used. Figure A1 and A2 represent graphically the meaning of the 2D roughness parameters. The horizontal axis of the graphs (hence, y = 0) is defined as the line that makes the accumulated area above the line to be equal to the one under it.

The 2D measurement is taken by means of a Hommel WaveLine-60 roughness-meter (resolution of 0,01 μm) along the centre line of the smooth rebar and for a distance of 15 mm. Each time 5 measurements are taken and average values are considered.

In addition to establishing the roughness parameters R, a 3D scan of the smooth surface has been taken for visual representation of the roughness. The scanning has been performed by the same equipment, and the mapping is obtained from successive 2D line measurements with a distance of 10 μm between each measurement line. This 3D roughness dimensional scan is performed for a zone of about 1 mm^2.

In the following pages roughness measurements performed to the tested smooth rebars by Ugine & Alz Research Center are presented. Results are given for 2D measurements first. In addition the 3D roughness dimensional scan is given.

Table A 1 Mathematical definition of roughness parameters

Parameter	Definition
R_a	$R_a = \frac{1}{n}\sum_{i=1}^{n}\lvert y_i\rvert$
R_t	$R_t = R_p - R_v$
R_p	$R_p = max\lvert y_i\rvert$
R_v	$R_v = min\lvert y_i\rvert$
R_z	$R_z = \frac{1}{s}\sum_{i=1}^{s} R_{zi}$
R_{max}	$R_{max} = max\lvert R_{zi}\rvert$
R_{sk}	$R_{sk} = \frac{1}{n.R_q^3}\sum_{i=1}^{n} y_i^3$ *where, R_q (root mean squared):* $R_q = \sqrt{\frac{1}{n}\sum_{i=1}^{n} y_i^2}$

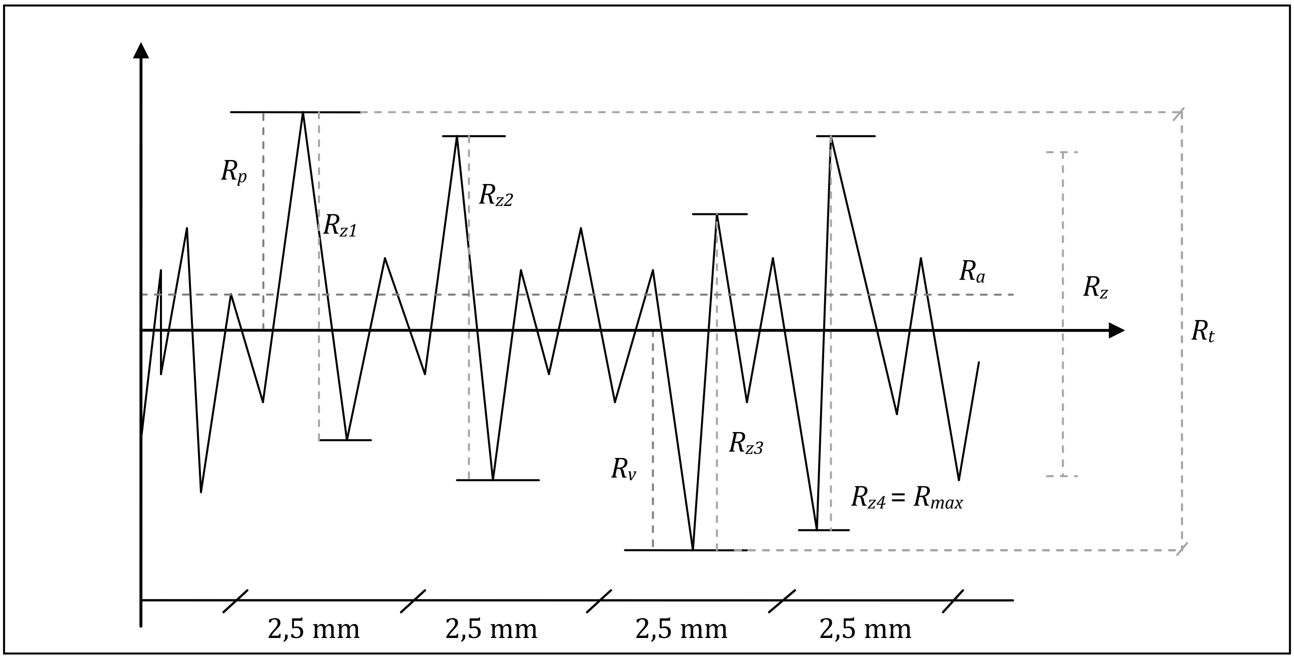

Figure A 1 Definition of roughness parameters

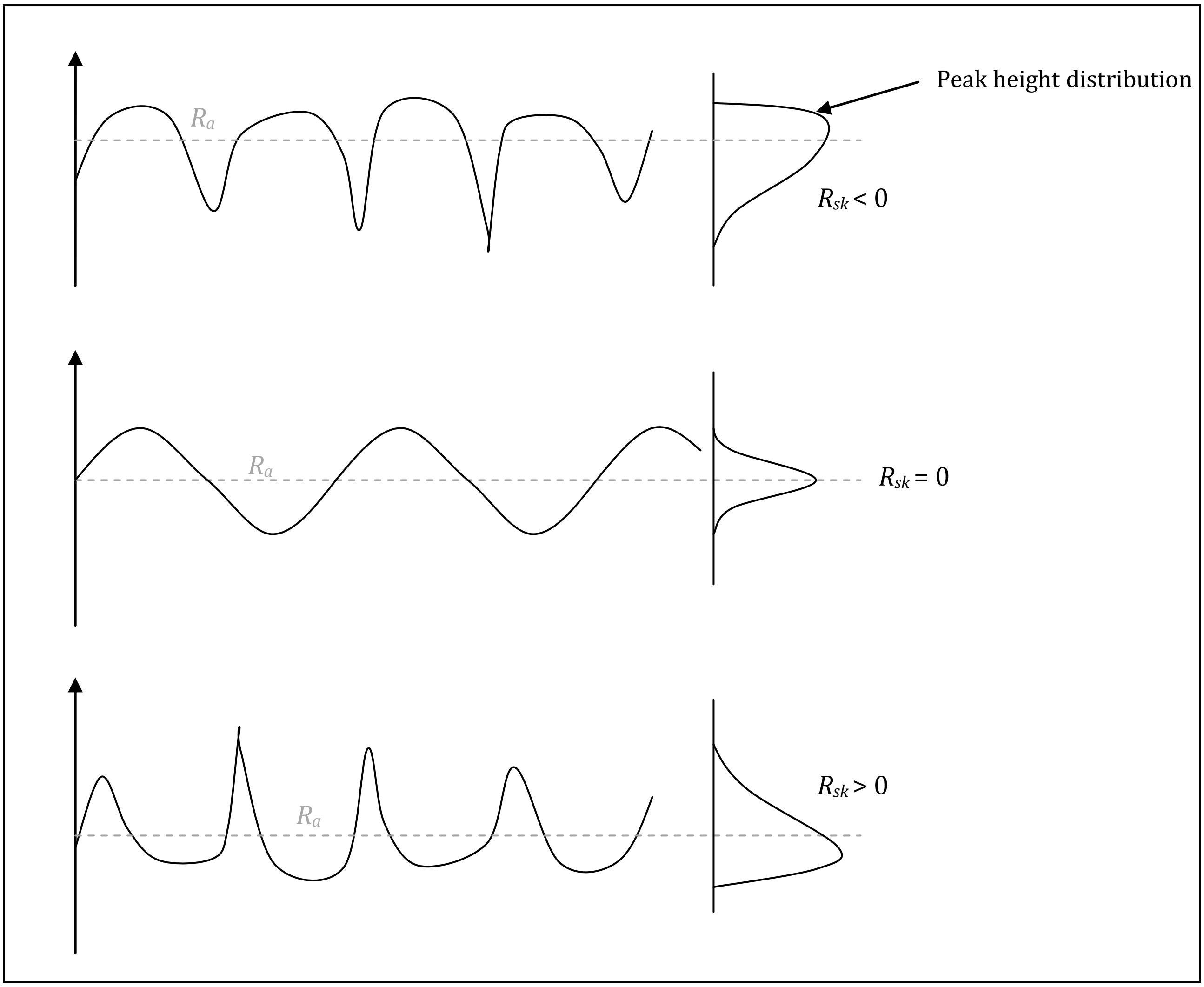

Figure A 2 Skewness (measure of asymmetry)

CS-Ø10-S	2D measurements

22.04.09
cut-off 2.5mm - gamme +/- 800µ

STATISTIQUE n = 5
Filtre=ISO 11562(M1) Lc/Ls =300 Lc =2.500 mm
Capteur=TK300 Lt =15.00 mm Vt =1.00 mm/s

N°	Paramètres	Xq	Echelle de mesure	S	Xmax	Xmin
1	Ra	13.2	9.2	3.3	18.8	9.6
2	Rt	74.8	38.2	14.3	97.1	58.9
3	Rp	39.0	20.7	8.3	48.1	27.4
4	Rz	60.5	33.2	12.0	82.9	49.7
5	Rmax	69.9	35.4	14.5	90.2	54.8
6	Rsk	0.088	0.497	0.199	0.340	-0.157

Bobine Round swooth dia. 10
face

Ra	18.8 µm
Rt	97.1 µm
Rp	46.0 µm
Rz	82.9 µm
Rmax	90.2 µm
Rsk	-0.157

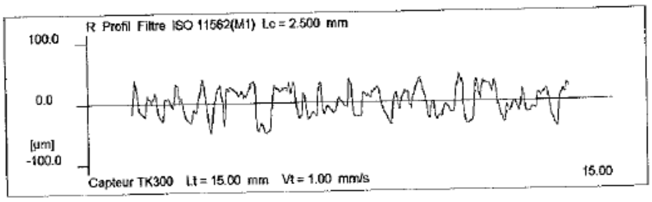

Ra	13.8 µm
Rt	74.5 µm
Rp	42.3 µm
Rz	59.2 µm
Rmax	66.7 µm
Rsk	0.340

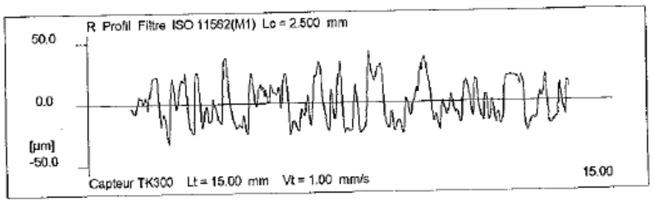

Ra	9.6 µm
Rt	60.4 µm
Rp	27.4 µm
Rz	50.3 µm
Rmax	54.9 µm
Rsk	-0.135

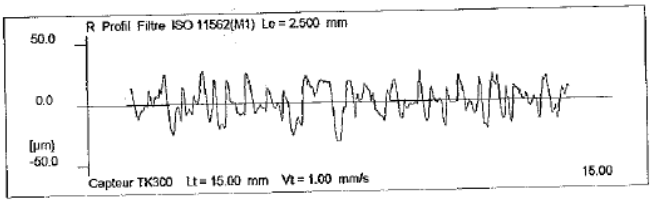

Ra	13.3 µm
Rt	82.9 µm
Rp	48.1 µm
Rz	60.5 µm
Rmax	82.9 µm
Rsk	0.203

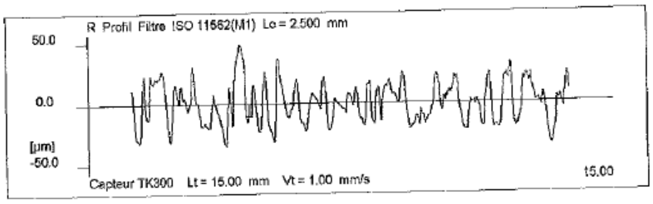

Ra	10.3 µm
Rt	58.9 µm
Rp	31.0 µm
Rz	49.7 µm
Rmax	54.8 µm
Rsk	0.191

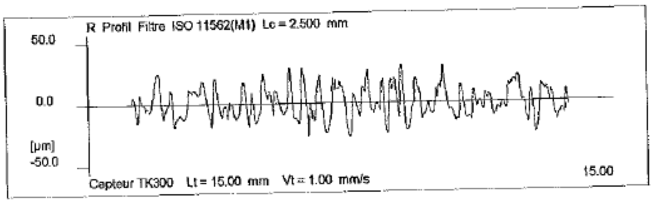

UGINE & ALZ
Groupe Arcelor

R & D

CS-Ø10-S	**3D mapping**

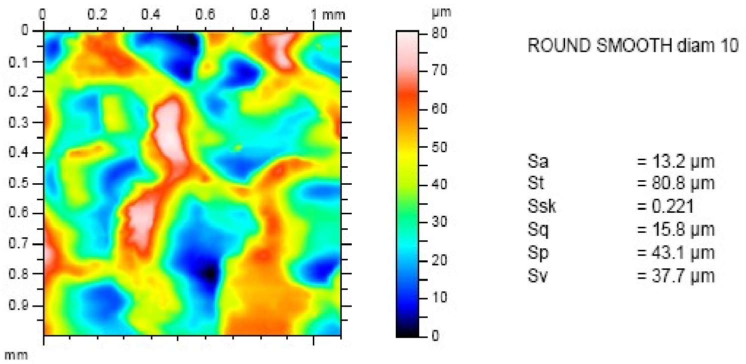

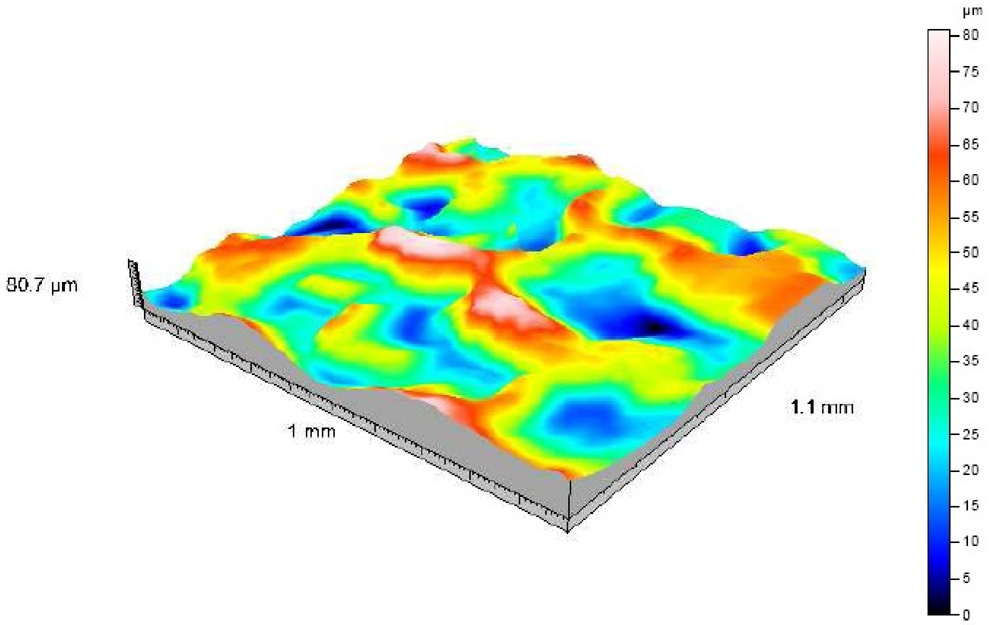

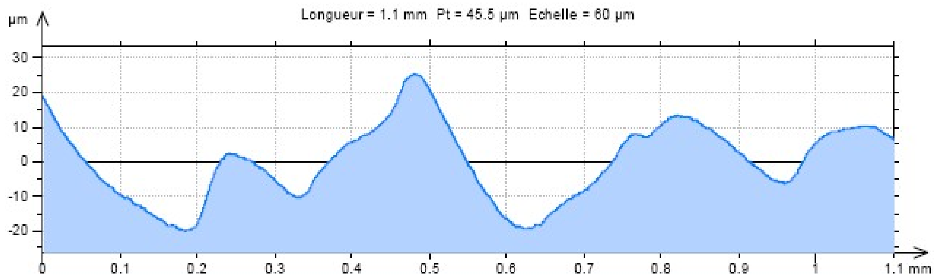

CS-Ø12-S	2D measurements

25.03.09
cut-off 2.5mm - gamme +/- 800µ

Bobine round smooth Ø 12
face

STATISTIQUE n = 5
Filtre=ISO 11562(M1) Lc/Ls =300 Lc =2.500 mm
Capteur=TK300 Lt =15.00 mm Vt =1.00 mm/s

N°	Paramètres	Xq	Echelle de mesure	S	Xmax	Xmin
1	Ra	3.0	1.5	0.5	3.6	2.1
2	Rt	24.3	22.3	7.8	39.6	17.3
3	Rp	12.5	2.3	0.9	13.9	11.6
4	Rz	16.6	8.2	2.7	20.5	12.3
5	Rmax	23.5	22.2	8.1	39.5	17.3
6	Rsk	0.407	1.849	0.684	0.897	-0.952

Ra	2.1 µm
Rt	17.3 µm
Rp	11.8 µm
Rz	12.3 µm
Rmax	17.3 µm
Rsk	0.897

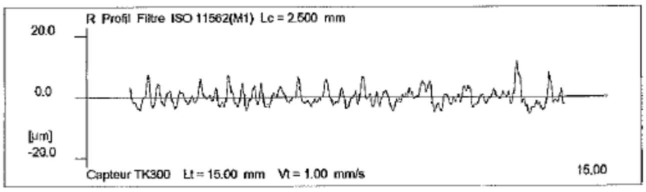

Ra	3.1 µm
Rt	20.7 µm
Rp	12.2 µm
Rz	16.5 µm
Rmax	20.1 µm
Rsk	0.680

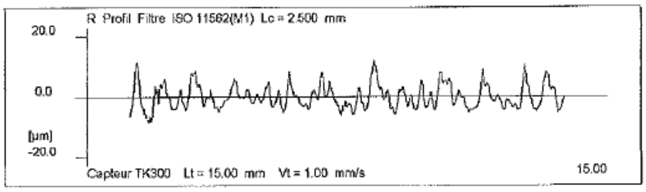

Ra	3.5 µm
Rt	39.6 µm
Rp	11.6 µm
Rz	20.5 µm
Rmax	39.5 µm
Rsk	-0.952

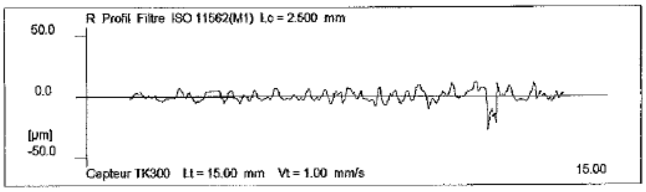

Ra	2.9 µm
Rt	21.7 µm
Rp	13.1 µm
Rz	15.8 µm
Rmax	19.6 µm
Rsk	0.663

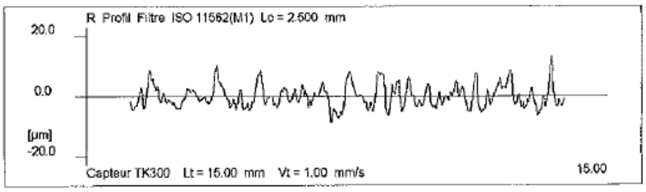

Ra	3.6 µm
Rt	22.3 µm
Rp	13.9 µm
Rz	17.7 µm
Rmax	21.2 µm
Rsk	0.746

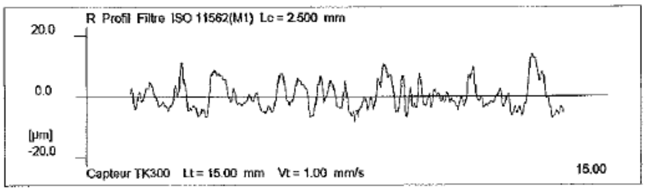

UGINE & ALZ
Groupe Arcelor

R & D

CS-Ø12-S	**3D mapping**

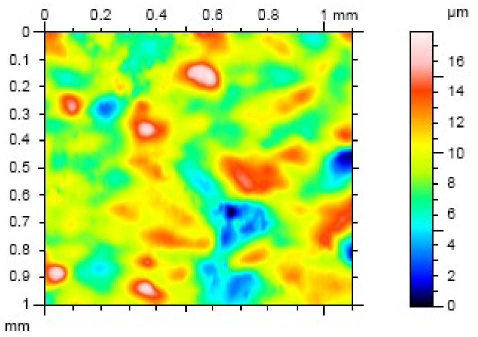

ROUND SMOOTH Ø12

Paramètres d'amplitude

Sa	= 1.85 µm
St	= 17.9 µm
Ssk	= 0.0175
Sq	= 2.38 µm
Sp	= 8.64 µm
Sv	= 9.23 µm

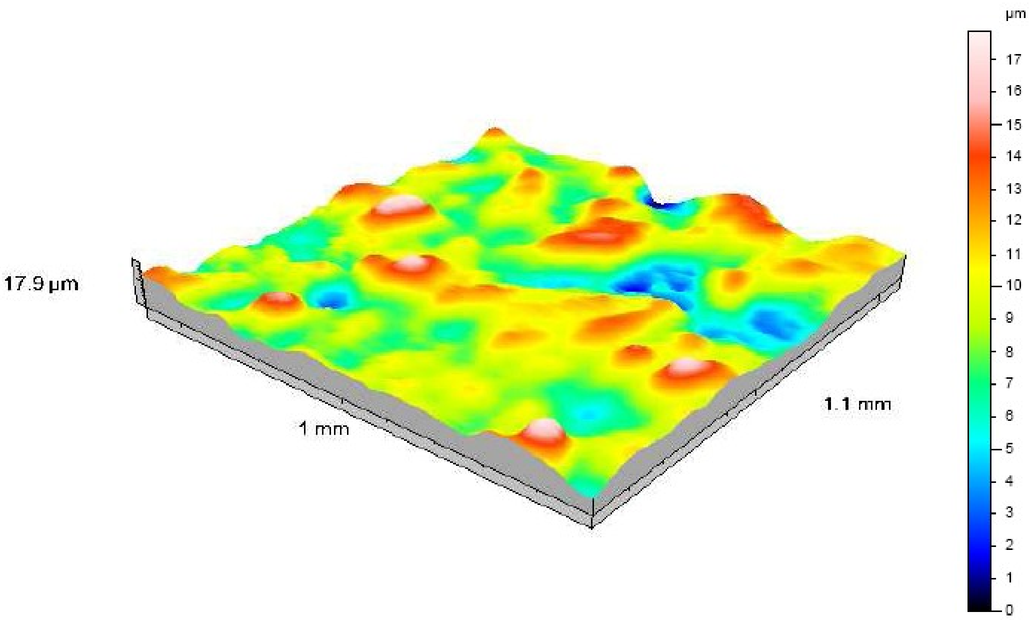

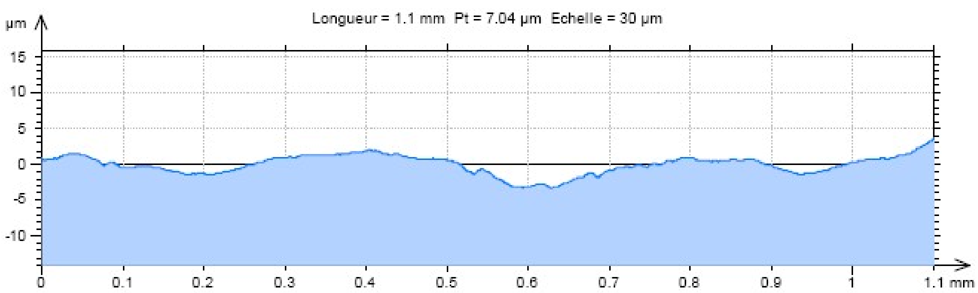

CS-4x20-S	2D measurements

23.03.09
cut-off 2.5mm - gamme +/- 800µ

Bobine	Black
face	marquée
.	4x20
.	
.	
.	
.	

STATISTIQUE n = 5
Filtre=ISO 11562(M1) Lc/Ls =300 Lc =2.500 mm
Capteur=TK300 Lt =15.00 mm Vt =1.00 mm/s

N°	Paramètres	Xq	Echelle de mesure	S	Xmax	Xmin
1	Ra	5.3	2.8	0.9	6.6	3.8
2	Rt	38.1	11.8	4.0	43.5	31.7
3	Rp	20.1	7.9	2.8	25.3	17.4
4	Rz	30.5	9.1	3.0	34.5	25.4
5	Rmax	35.9	11.6	4.0	40.8	29.2
6	Rsk	0.275	0.791	0.260	0.662	-0.129

Ra	5.3 µm
Rt	43.5 µm
Rp	25.3 µm
Rz	34.5 µm
Rmax	38.7 µm
Rsk	0.662

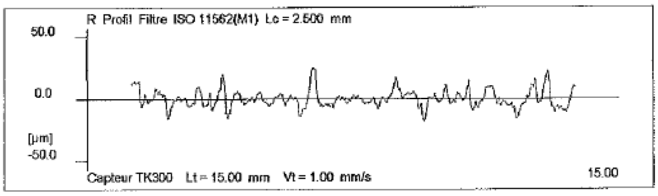

Ra	4.8 µm
Rt	40.8 µm
Rp	20.6 µm
Rz	30.8 µm
Rmax	40.8 µm
Rsk	0.239

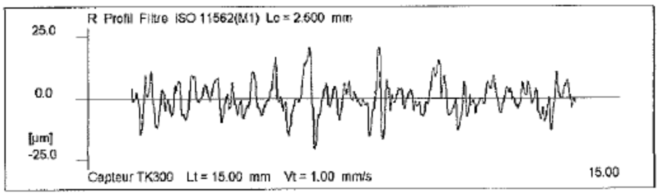

Ra	3.8 µm
Rt	31.7 µm
Rp	18.2 µm
Rz	25.4 µm
Rmax	29.2 µm
Rsk	0.409

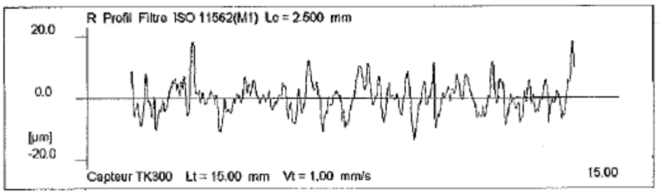

Ra	5.8 µm
Rt	37.5 µm
Rp	18.8 µm
Rz	29.7 µm
Rmax	36.4 µm
Rsk	0.193

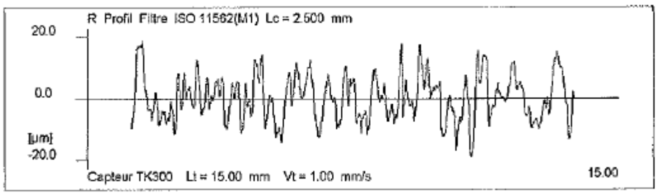

Ra	6.6 µm
Rt	36.8 µm
Rp	17.4 µm
Rz	32.0 µm
Rmax	34.2 µm
Rsk	-0.129

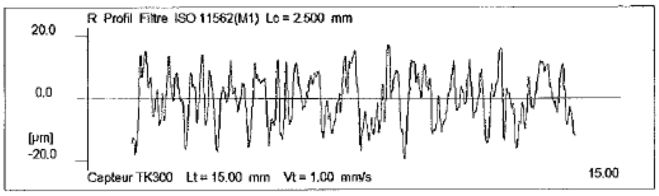

UGINE & ALZ
Groupe Arcelor

R & D

CS-4x20-S	**3D mapping**

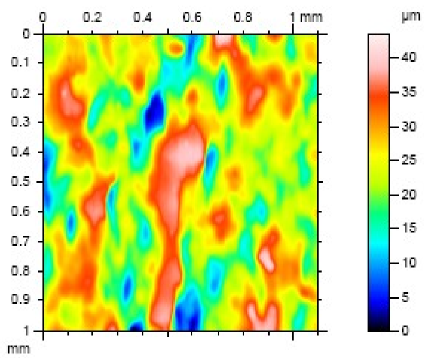

BLACK STEEL - 4x20

Paramètres d'amplitude

Sa	= 5.54 µm
St	= 43.5 µm
Ssk	= -0.129
Sq	= 6.94 µm
Sp	= 19.3 µm
Sv	= 24.2 µm

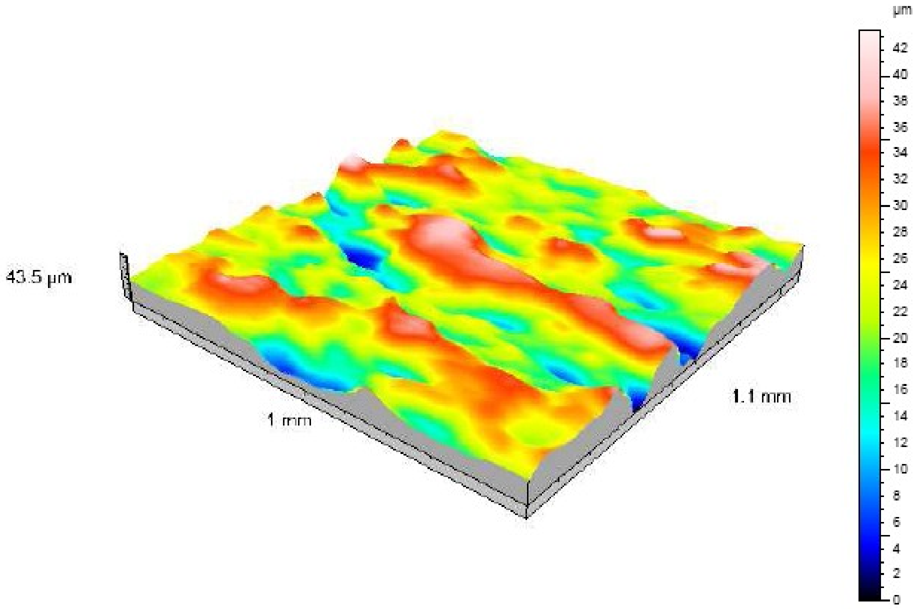

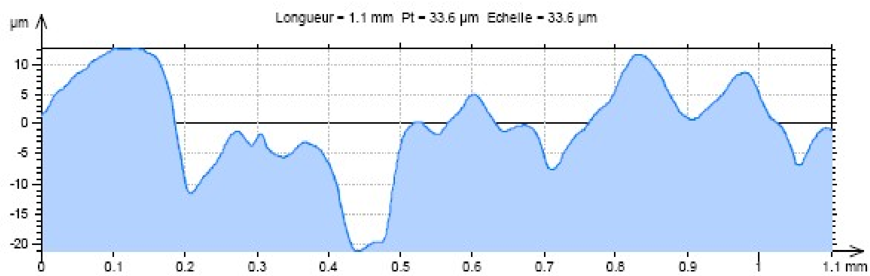

SS-K31-5x16-S-1D	2D measurements

23.03.09
cut-off 2.5mm - gamme +/- 800µ

Bobine	K31
face	marquée
.	1D 5x16

STATISTIQUE n = 5
Filtre=ISO 11562(M1) Lc/Ls =300 Lc =2.500 mm
Capteur=TK300 Lt =15.00 mm Vt =1.00 mm/s

N°	Paramètres	Xq	Echelle de mesure	S	Xmax	Xmin
1	Ra	4.5	0.3	0.1	4.6	4.3
2	Rt	29.3	5.2	1.9	31.9	26.7
3	Rp	10.9	2.7	0.9	12.4	9.7
4	Rz	25.4	4.7	1.7	27.3	22.6
5	Rmax	28.6	6.0	2.3	31.8	25.8
6	Rsk	-0.508	0.589	0.189	-0.199	-0.788

Ra	4.6 µm
Rt	31.9 µm
Rp	10.7 µm
Rz	27.3 µm
Rmax	31.8 µm
Rsk	-0.557

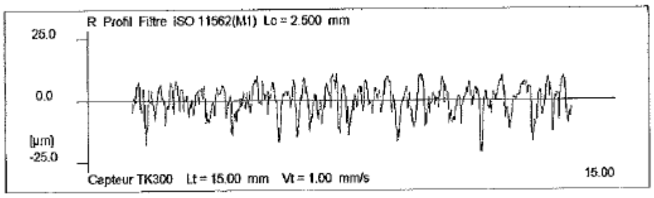

Ra	4.3 µm
Rt	27.8 µm
Rp	10.5 µm
Rz	25.3 µm
Rmax	26.4 µm
Rsk	-0.523

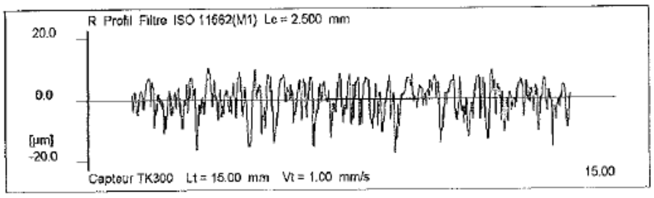

Ra	4.4 µm
Rt	30.2 µm
Rp	11.4 µm
Rz	24.8 µm
Rmax	29.0 µm
Rsk	-0.474

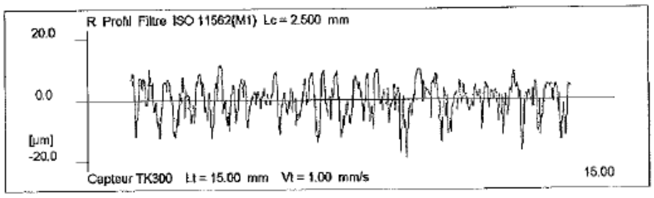

Ra	4.5 µm
Rt	26.7 µm
Rp	12.4 µm
Rz	22.6 µm
Rmax	25.8 µm
Rsk	-0.199

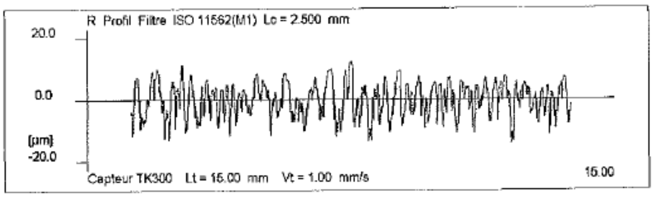

Ra	4.5 µm
Rt	30.1 µm
Rp	9.7 µm
Rz	27.0 µm
Rmax	30.1 µm
Rsk	-0.788

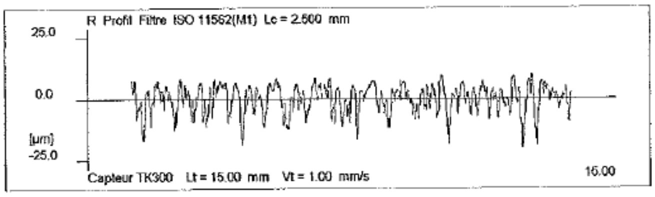

UGINE & ALZ
Groupe Arcelor

R & D

SS-K31-5x16-S-1D	3D mapping

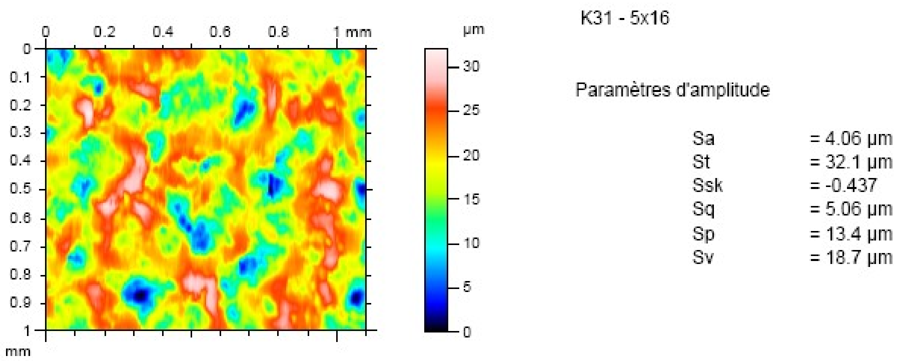

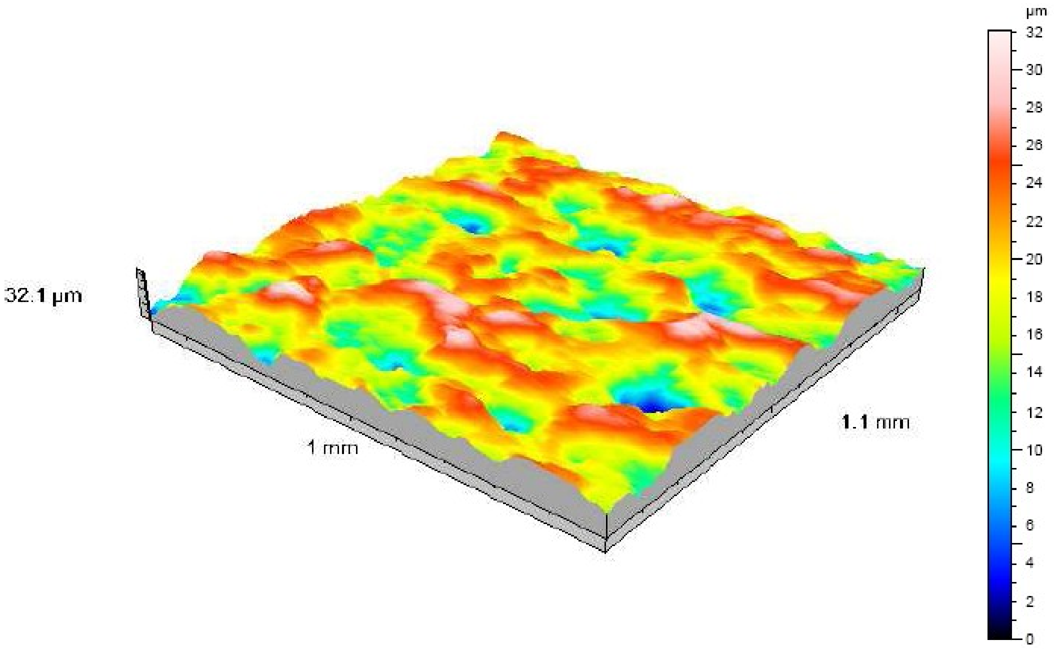

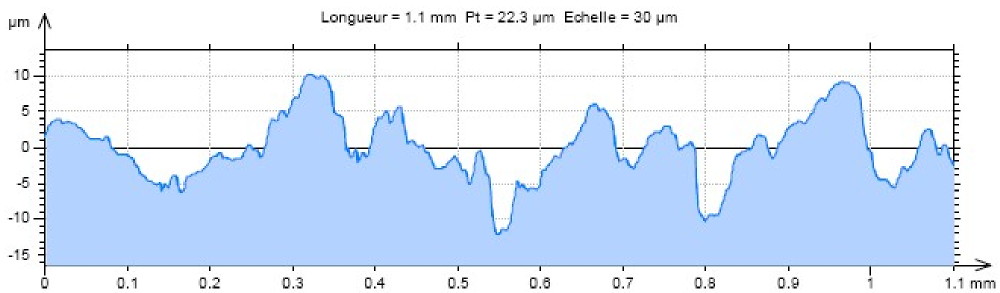

SS-304L-5x16-S-1D	2D measurements

23.03.09
cut-off 2.5mm - gamme +/- 800µ

Bobine	304L 1D
face	marquée
.	5x16

STATISTIQUE n = 5
Filtre=ISO 11562(M1) Lc/Ls =300 Lc =2.500 mm
Capteur=TK300 Lt =15.00 mm Vt =1.00 mm/s

N°	Paramètres	Xq	Echelle de mesure	S	Xmax	Xmin
1	Ra	3.4	0.5	0.2	3.7	3.2
2	Rt	25.3	3.6	1.2	27.4	23.8
3	Rp	9.1	3.1	1.0	10.5	7.4
4	Rz	19.5	1.6	0.6	20.3	18.7
5	Rmax	23.9	2.3	1.0	24.7	22.4
6	Rsk	-0.497	0.403	0.151	-0.372	-0.775

Ra	3.5 µm
Rt	24.7 µm
Rp	9.4 µm
Rz	19.2 µm
Rmax	24.7 µm
Rsk	-0.427

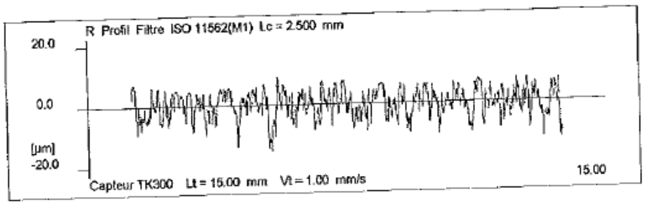

Ra	3.2 µm
Rt	24.6 µm
Rp	10.5 µm
Rz	19.3 µm
Rmax	23.0 µm
Rsk	-0.376

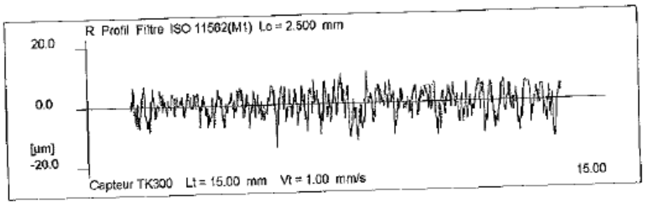

Ra	3.4 µm
Rt	23.8 µm
Rp	8.6 µm
Rz	18.7 µm
Rmax	22.4 µm
Rsk	-0.537

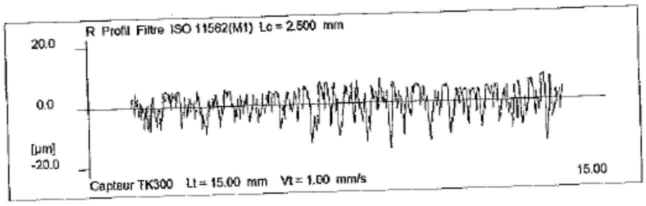

Ra	3.3 µm
Rt	27.4 µm
Rp	9.5 µm
Rz	20.3 µm
Rmax	24.7 µm
Rsk	-0.372

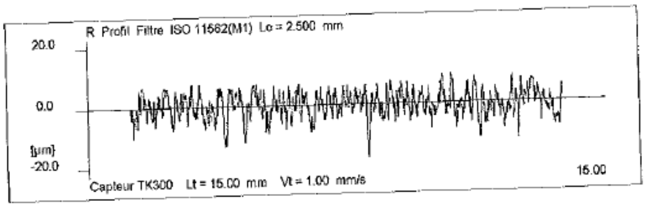

Ra	3.7 µm
Rt	25.8 µm
Rp	7.4 µm
Rz	19.9 µm
Rmax	24.7 µm
Rsk	-0.775

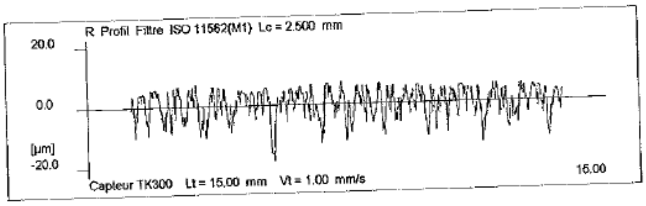

UGINE & ALZ
Groupe Arcelor

R & D

SS-304L-5x16-S-1D	3D mapping

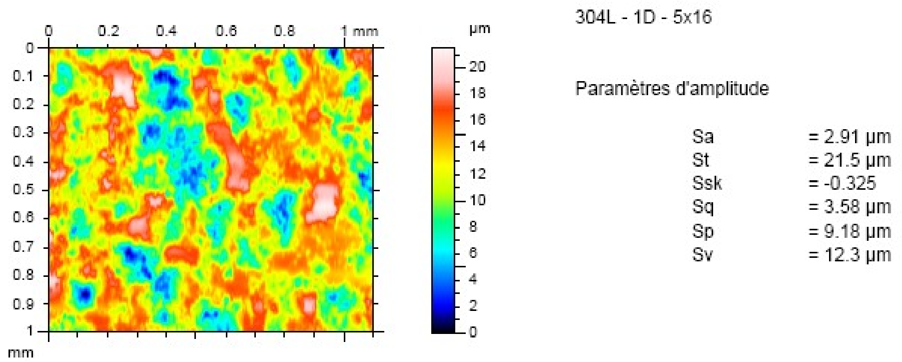

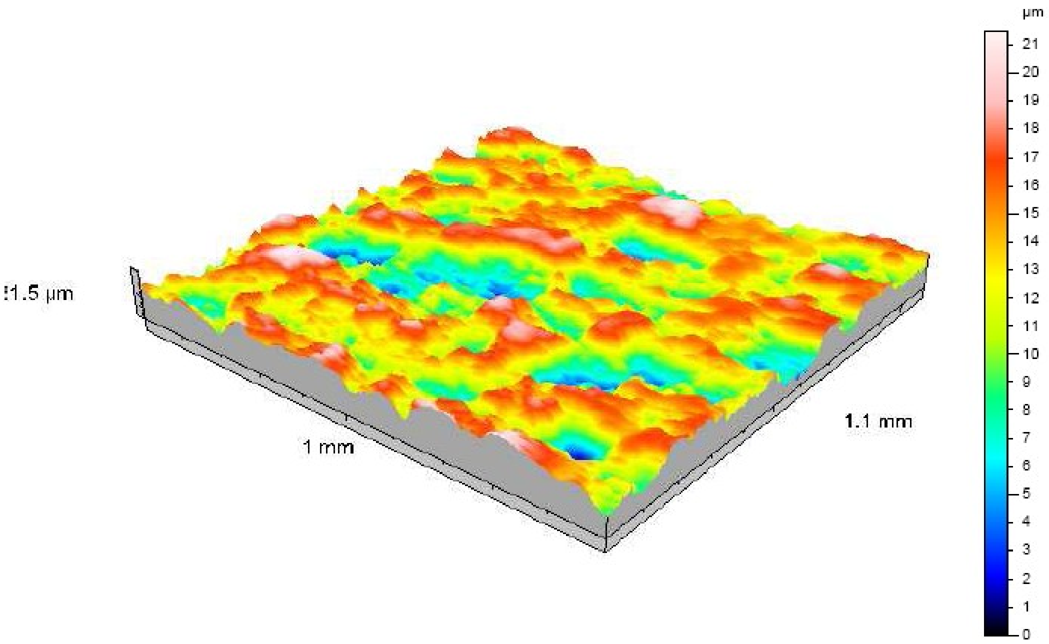

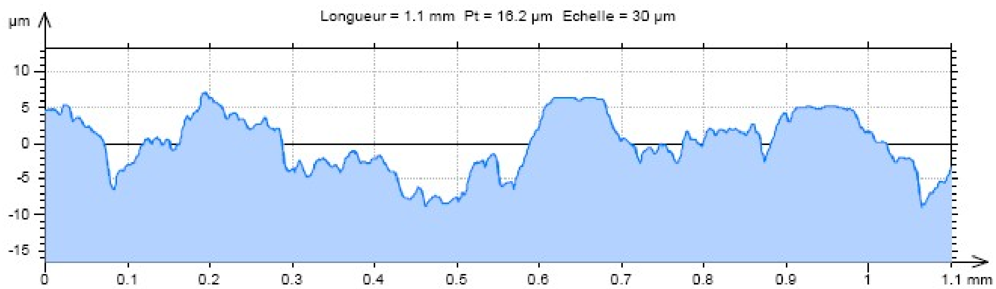

SS-304L-4x20-S-1D	2D measurements

23.03.09
cut-off 2.5mm - gamme +/- 800µ

Bobine	304 1D
face	marquée
.	4x20
.	
.	
.	
.	

STATISTIQUE n = 5
Filtre=ISO 11562(M1) Lc/Ls =300 Lc =2.500 mm
Capteur=TK300 Lt =15.00 mm Vt =1.00 mm/s

N°	Paramètres	Xq	Echelle de mesure	S	Xmax	Xmin
1	Ra	3.0	0.8	0.3	3.5	2.7
2	Rt	23.1	9.5	3.2	28.7	19.2
3	Rp	7.8	1.5	0.5	8.4	6.9
4	Rz	18.1	4.1	1.3	20.4	16.3
5	Rmax	22.6	7.3	2.6	26.5	19.2
6	Rsk	-0.645	0.504	0.178	-0.485	-0.989

Ra	2.9 µm
Rt	21.8 µm
Rp	8.4 µm
Rz	17.7 µm
Rmax	21.8 µm
Rsk	-0.603

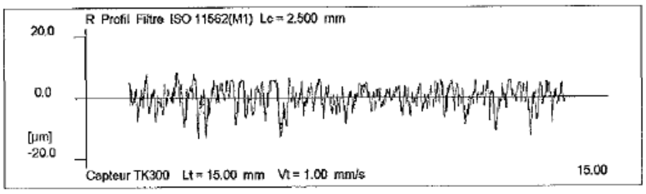

Ra	2.9 µm
Rt	21.7 µm
Rp	8.3 µm
Rz	18.1 µm
Rmax	21.1 µm
Rsk	-0.608

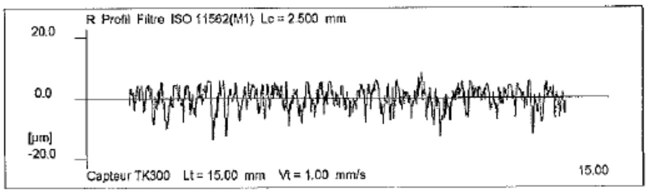

Ra	3.5 µm
Rt	28.7 µm
Rp	7.9 µm
Rz	20.4 µm
Rmax	26.5 µm
Rsk	-0.989

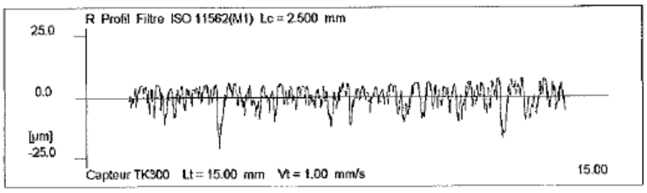

Ra	2.7 µm
Rt	19.2 µm
Rp	7.6 µm
Rz	16.3 µm
Rmax	19.2 µm
Rsk	-0.485

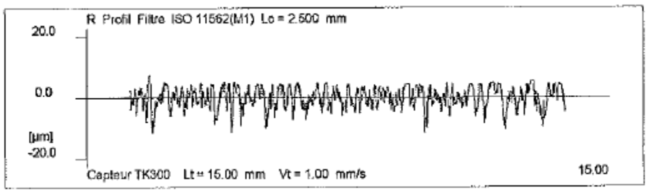

Ra	3.0 µm
Rt	24.3 µm
Rp	6.9 µm
Rz	17.9 µm
Rmax	24.3 µm
Rsk	-0.539

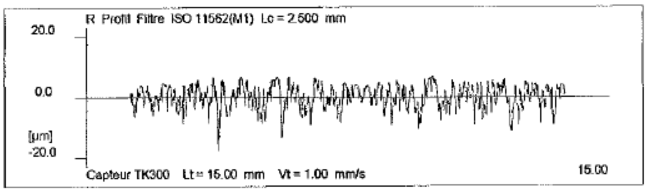

UGINE & ALZ
Groupe Arcelor

R & D

SS-304L-4x20-S-1D	3D mapping

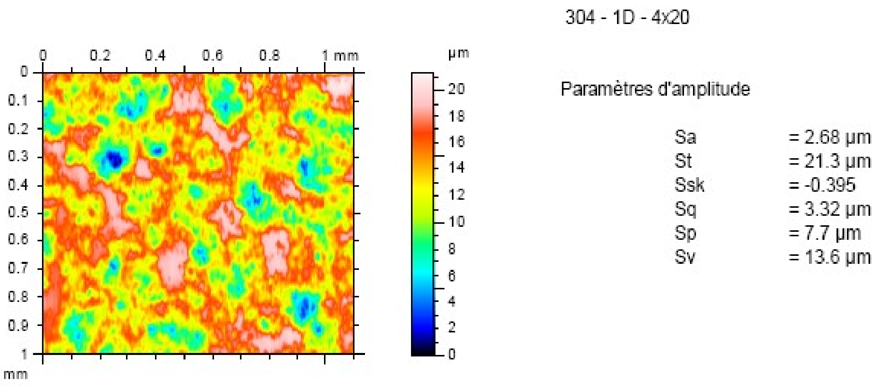

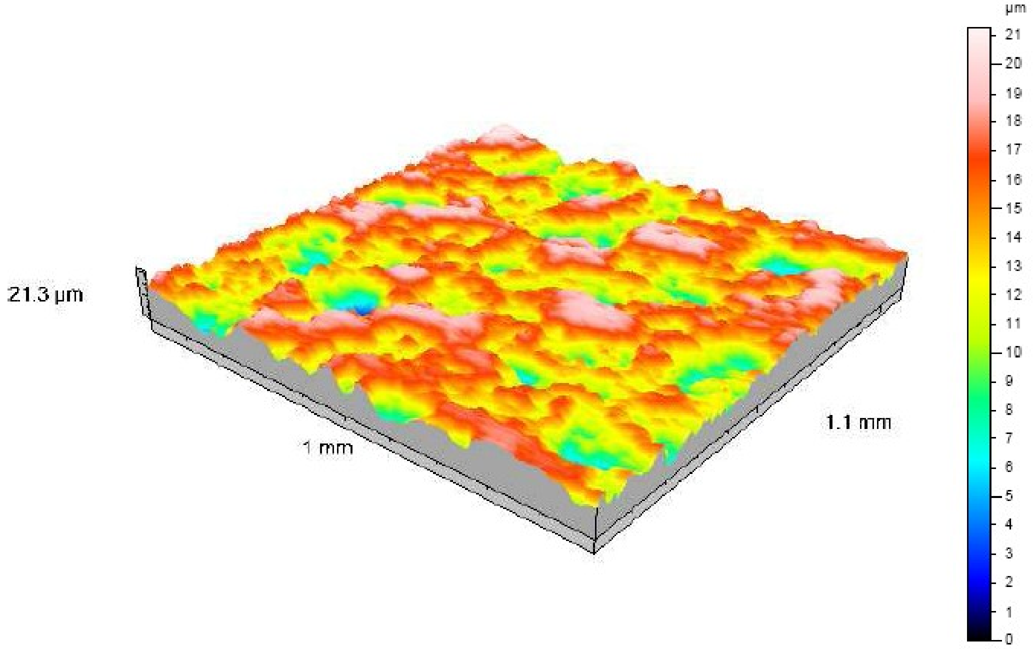

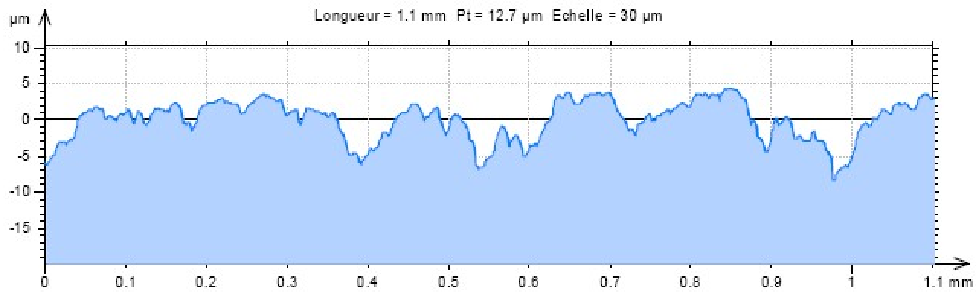

SS-304L-4x20-S-2B	2D measurements

23.03.09
Rugo cut-off 0.8mm

Bobine	304L 2 B
face	marquée
.	4x20
.	
.	
.	
.	

STATISTIQUE n = 5
Filtre=ISO 11562(M1) Lc/Ls =300 Lc =0.800 mm
Capteur=TK300 Lt =4.80 mm Vt =0.50 mm/s

N°	Paramètres	Xq	Echelle de mesure	S	Xmax
1	Ra	0.42	0.32	0.11	0.58
2	Rt	5.58	3.20	1.19	7.00
3	Rp	1.03	1.76	0.64	2.29
4	Rz	3.63	1.66	0.64	4.35
5	Rmax	5.45	3.20	1.10	7.00
6	Rsk	-2.767	0.771	0.263	-2.407

Ra	0.58 µm
Rt	5.81 µm
Rp	0.83 µm
Rz	4.28 µm
Rmax	5.81 µm
Rsk	-2.407

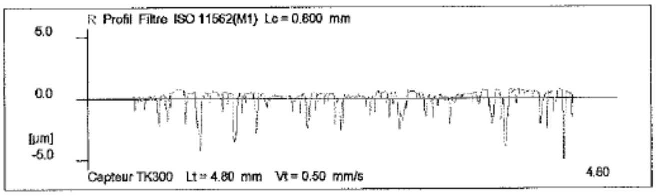

Ra	0.36 µm
Rt	4.69 µm
Rp	0.65 µm
Rz	3.19 µm
Rmax	4.69 µm
Rsk	-2.577

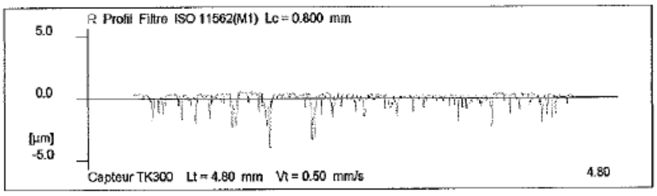

Ra	0.48 µm
Rt	7.00 µm
Rp	0.84 µm
Rz	4.35 µm
Rmax	7.00 µm
Rsk	-3.178

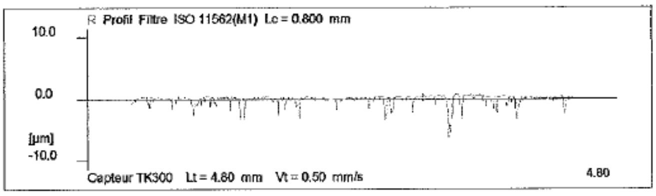

Ra	0.26 µm
Rt	3.80 µm
Rp	0.53 µm
Rz	2.69 µm
Rmax	3.80 µm
Rsk	-2.859

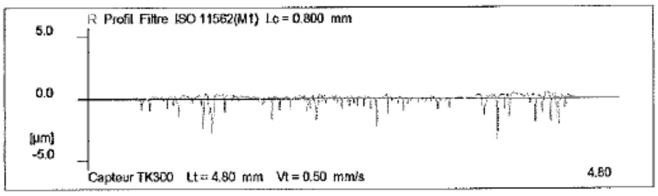

Ra	0.42 µm
Rt	6.62 µm
Rp	2.29 µm
Rz	3.62 µm
Rmax	5.94 µm
Rsk	-2.816

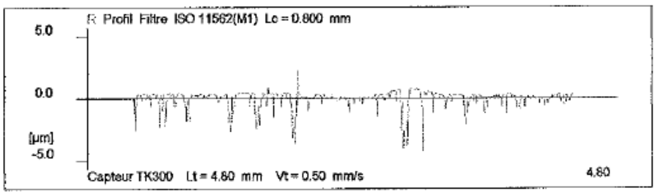

UGINE & ALZ
Groupe Arcelor

R & D

SS-304L-4x20-S-2B	3D mapping

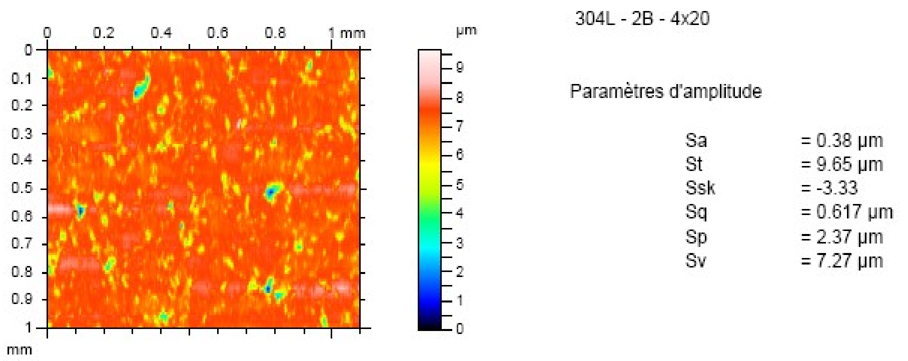

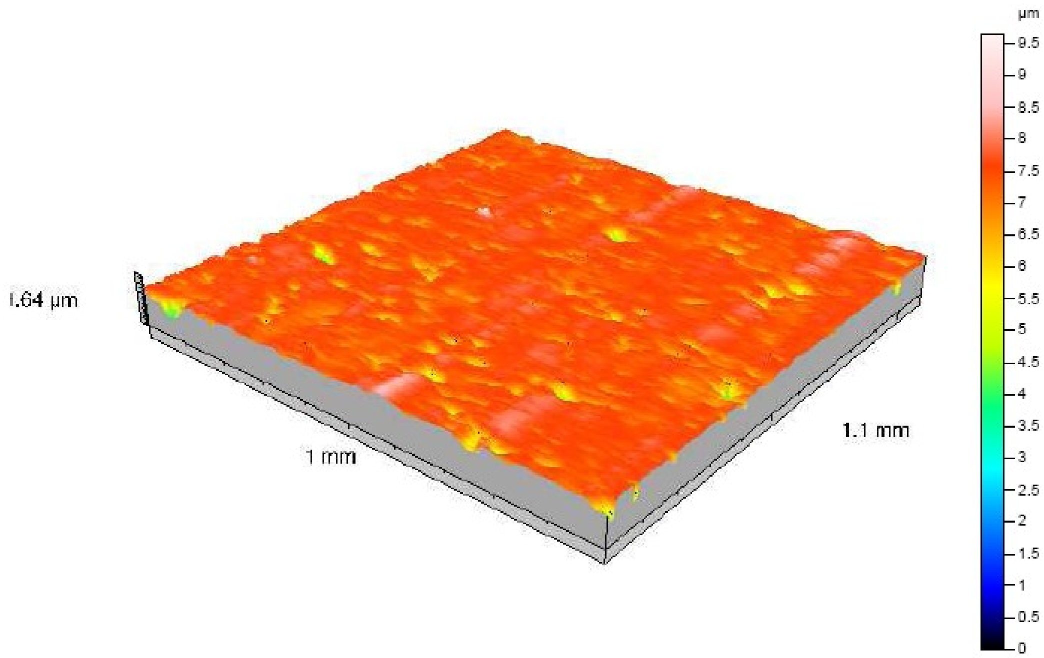

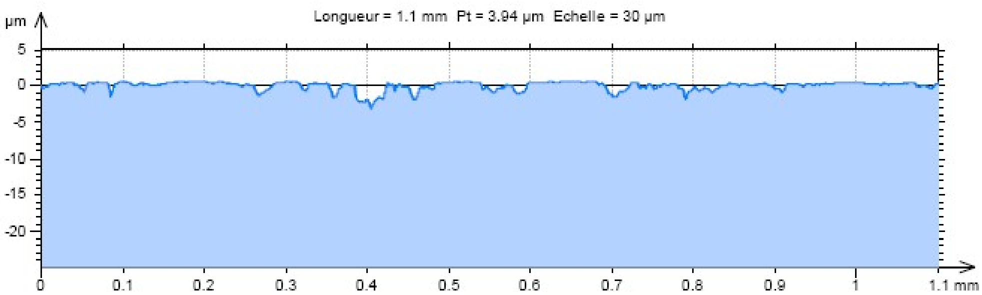

Appendix B Individual Bond Stress-Slip Experimental Curves and Proposed Bond Models

1 Smooth flat rebars

In Chapter 4 two bond models have been developed to predict the bond stress-slip relationship of flat stainless steel smooth rebars when embedded in concrete. Both of them are defined by Equations 4-31 to 4-35. The calculation of the maximum and frictional bond stress has been done in two ways: (1) by regression analysis of the obtained results (Equations 4-17 and 4-18) and (2) by considering average values of the test results (parameters given in Table 4-16). In the following individual test results are given for each testing condition. Furthermore, the mean curve of 3 tests per testing condition is compared to both developed bond models. In the following graphs, the curves are referred as: “Exp1”, “Exp2” and “Exp3” for the individual test results and “Exp AV” for the average curve. The developed models are referred as “Model RA” and “Model AV”, for the regression analysis and average values of maximum and frictional bond stress values calculation, respectively.

2 Continuously ribbed flat rebars

In a similar way, a bond model has been proposed for predicting the bond behaviour of completely ribbed flat rebars (Chapter 4). Equations 4-36 to 4-39 define the proposed bond model with curve defining parameters given in Table 4-17. The individual test results, “Exp1”, “Exp2” and “Exp3”, are plotted in the following graphs. The mean experimental curve, “Exp AV”, is compared to the proposed bond model, “Model”.

3 Flat rebars with an alternate rib pattern

The bond model proposed for predicting the bond stress-slip relationship of flat rebars with an alternate rib pattern has been defined by Equations 5-11 to 5-15, with parameters given in Table 5-14 (Chapter 5). The individual test results, “Exp1”, “Exp2” and “Exp3”, are plotted in the following graphs. The mean experimental curve, “Exp AV”, is compared to the proposed bond model, “Model”.

Smooth flat rebars
CS-4x20-S-TC
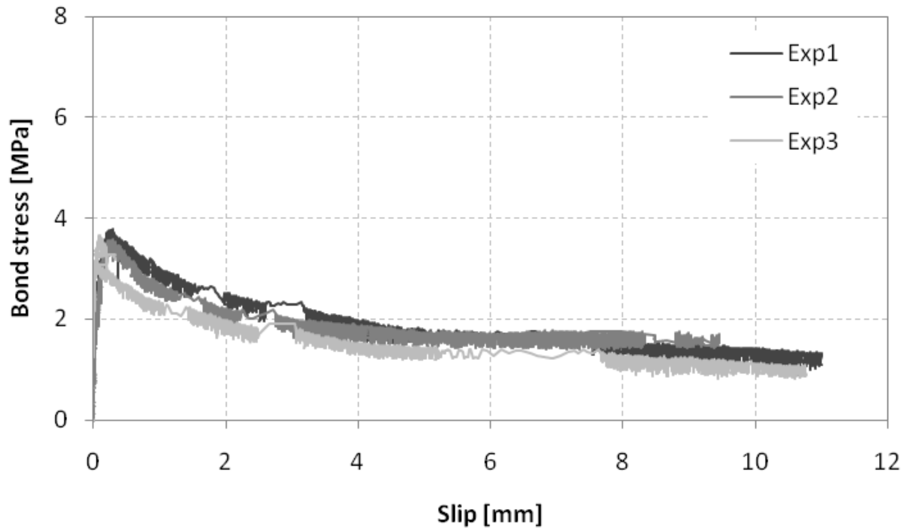
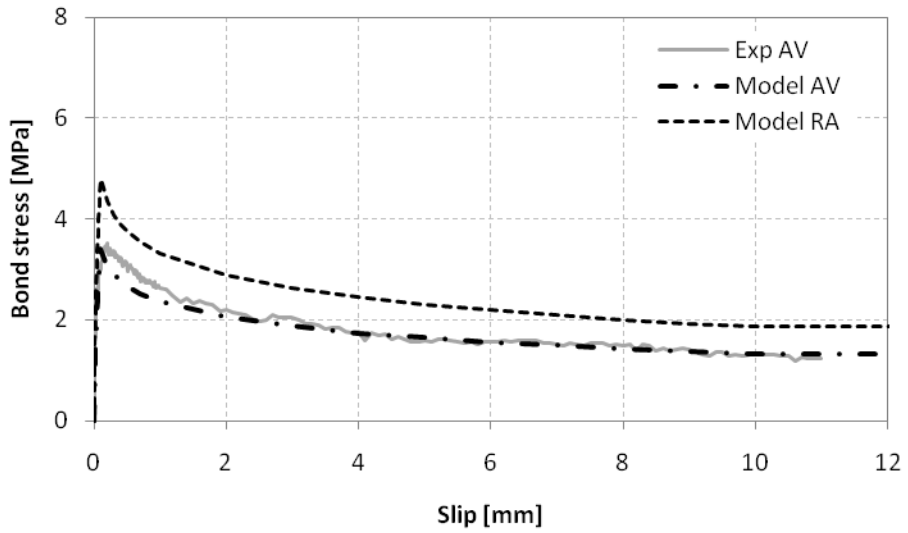

Smooth flat rebars
CS-4x20-S-SCC
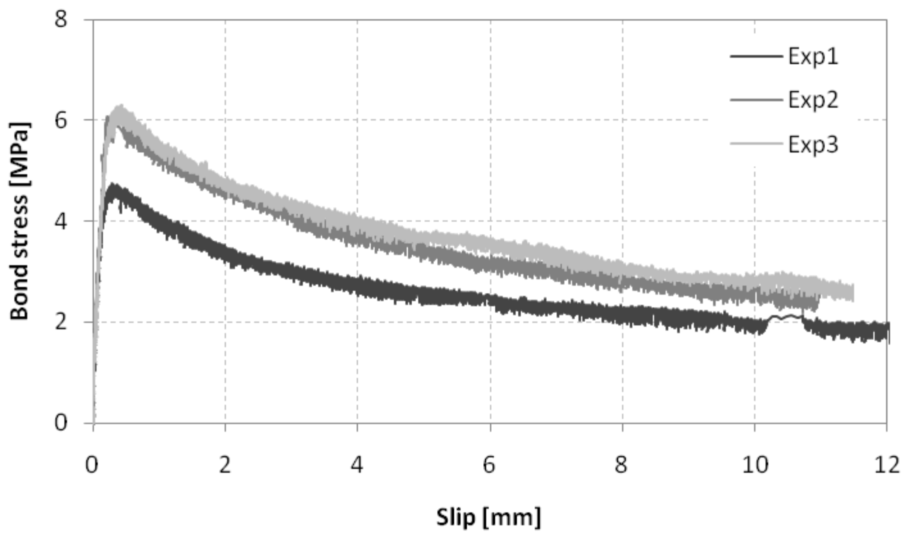
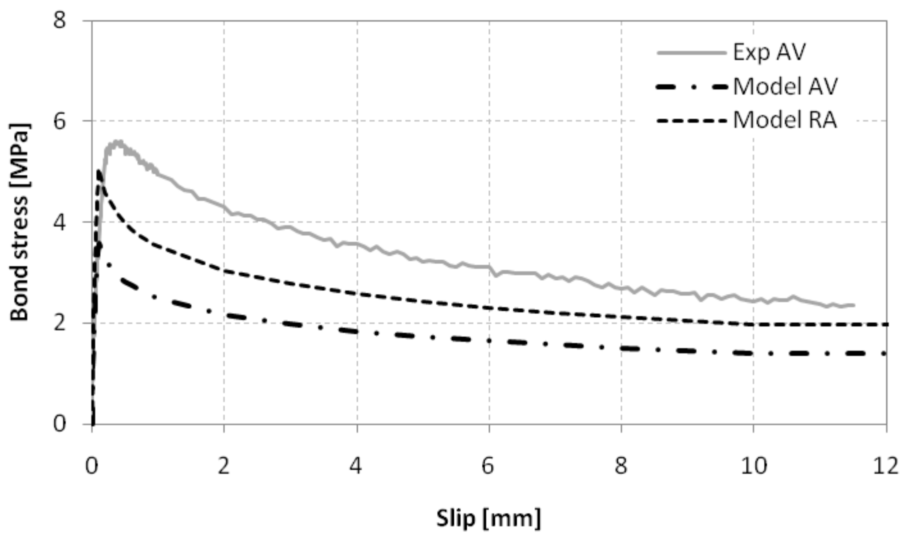

Smooth flat rebars
SS-304L-4x20-S-2B-TC
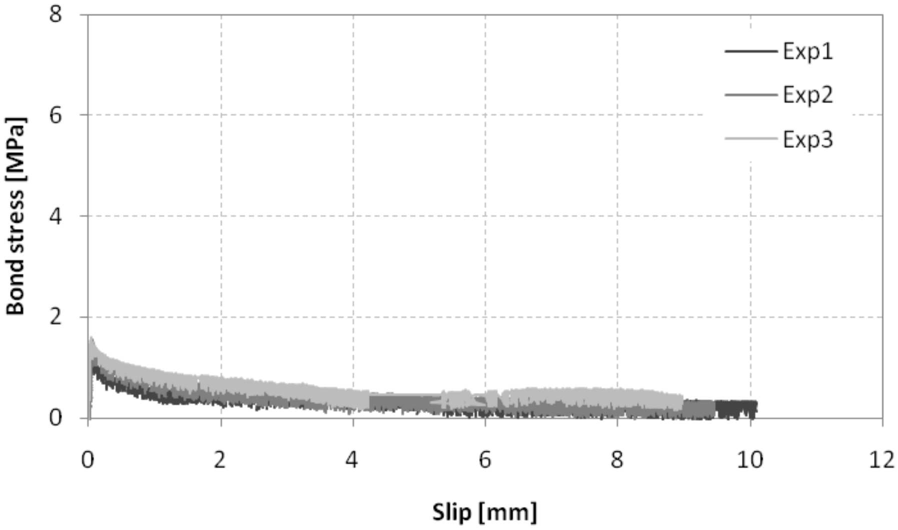
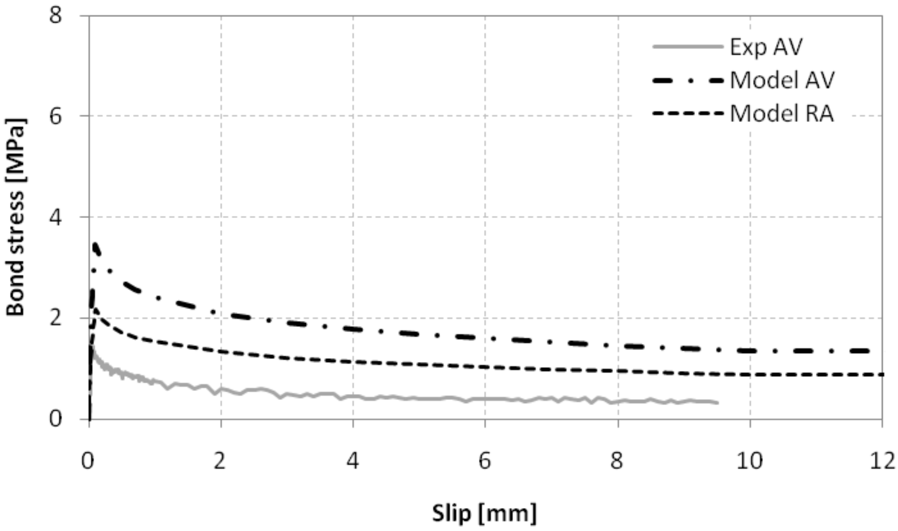

Smooth flat rebars
SS-304L-4x20-S-2B-SCC

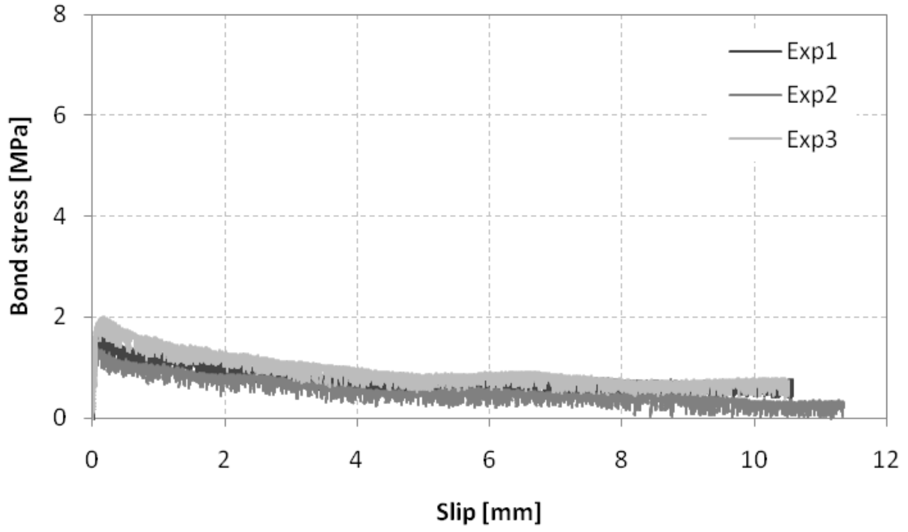

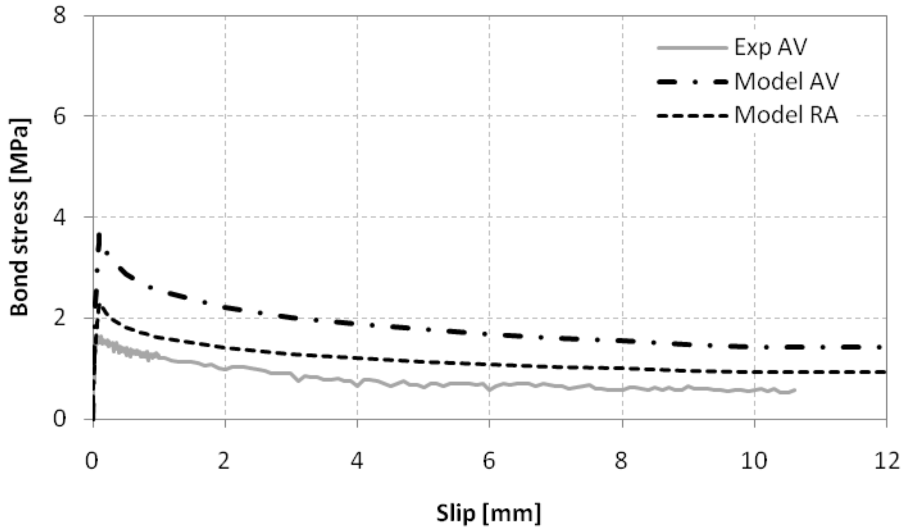

Smooth flat rebars
SS-304L-4x20-S-1D-TC
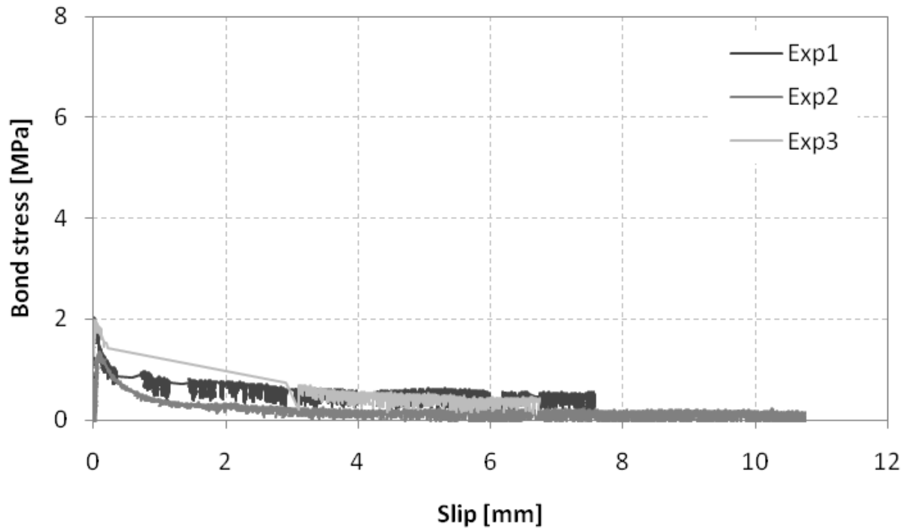
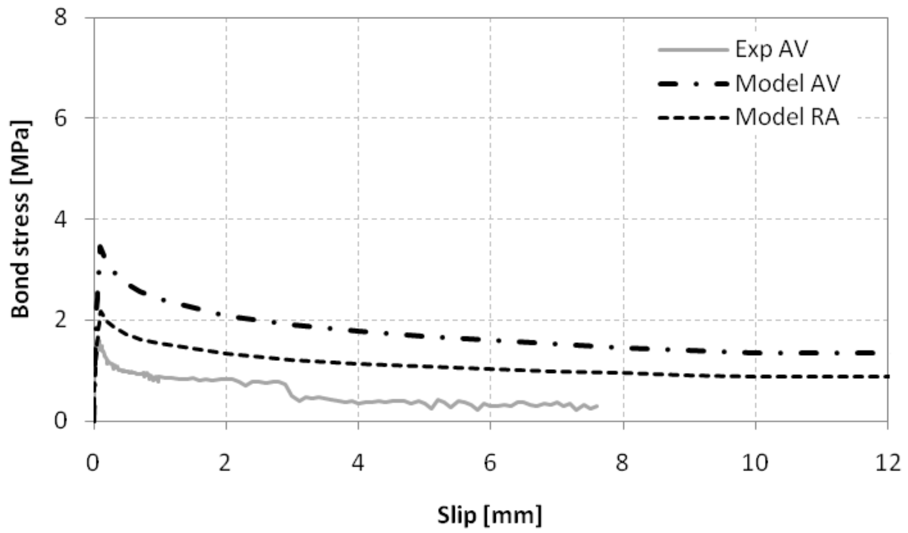

Smooth flat rebars
SS-304L-4x20-S-1D-SCC
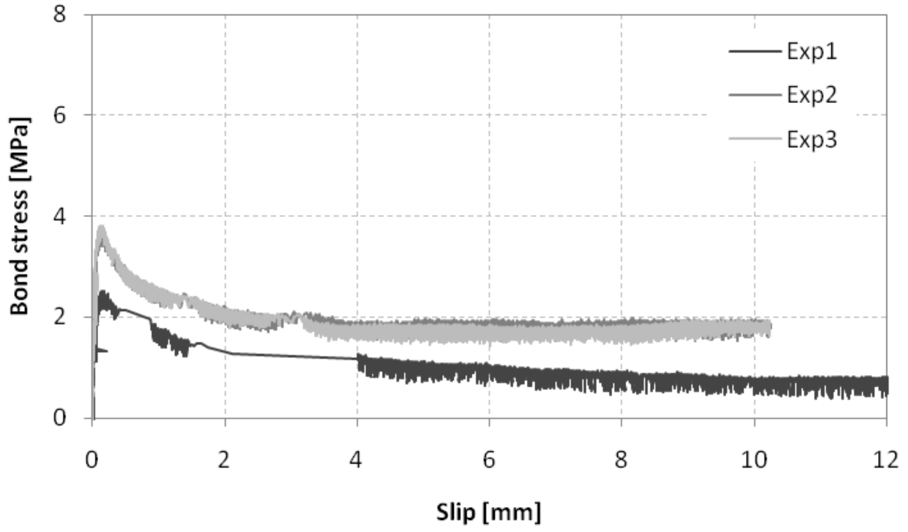
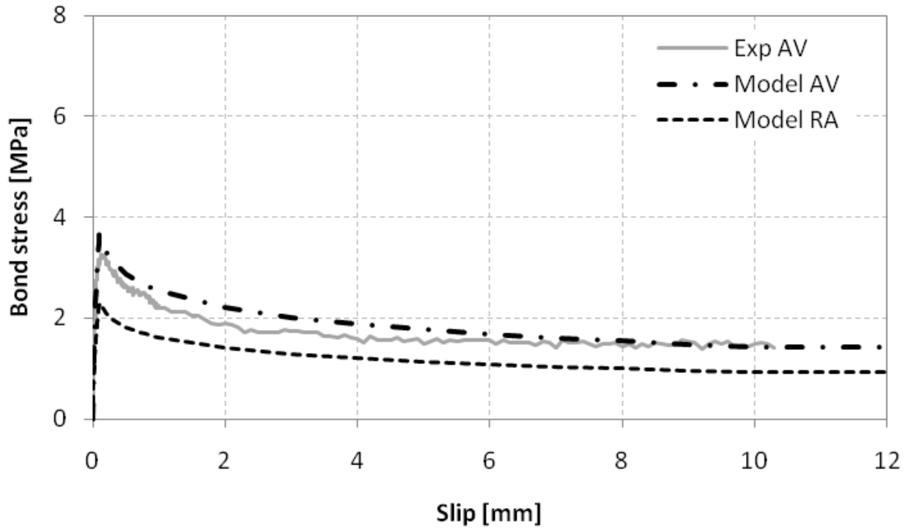

Smooth flat rebars
SS-304L-5x16-S-1D-TC

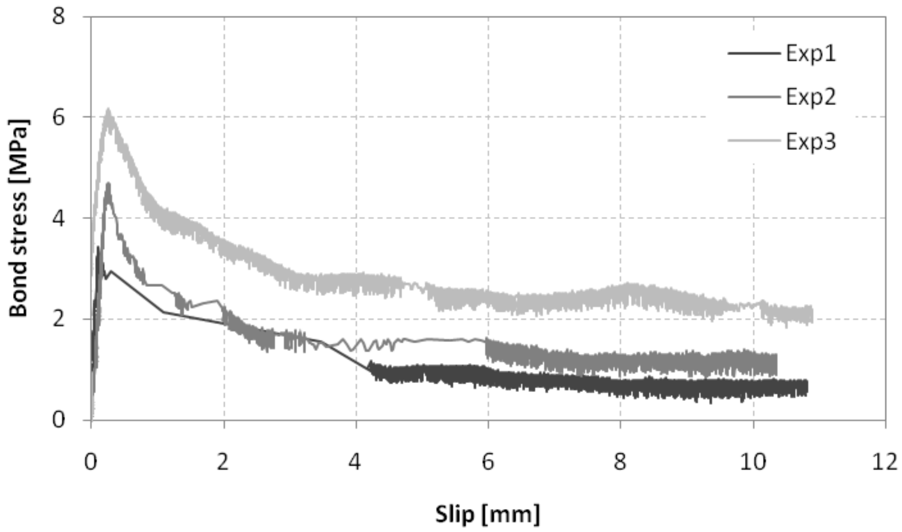

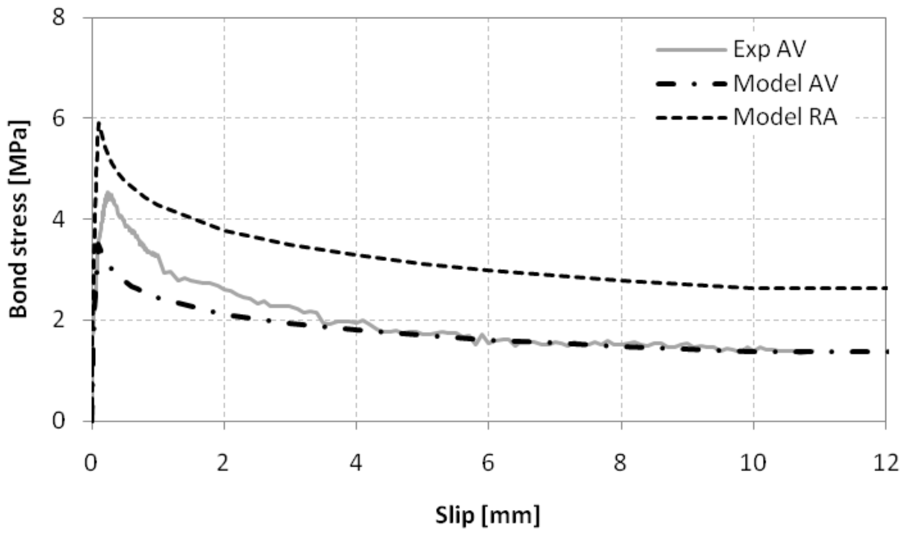

Smooth flat rebars
SS-304L-5x16-S-1D-SCC

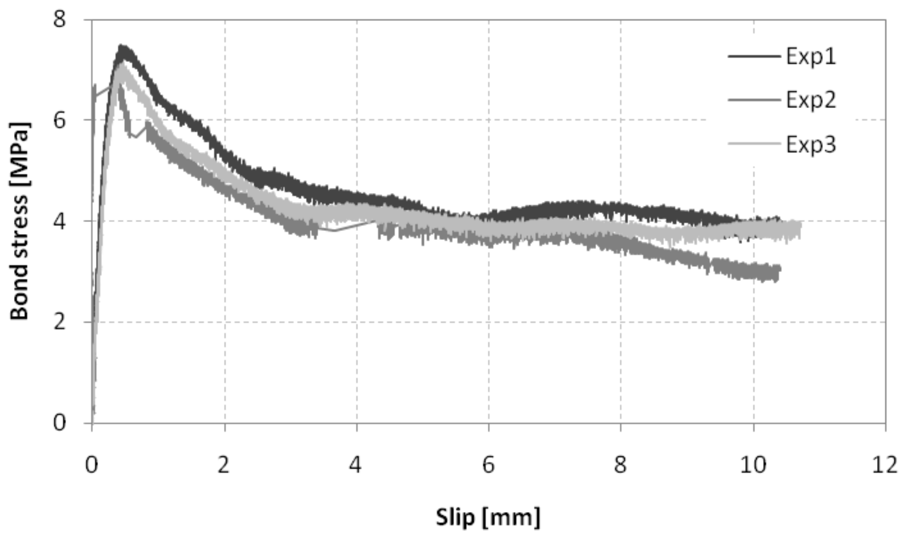

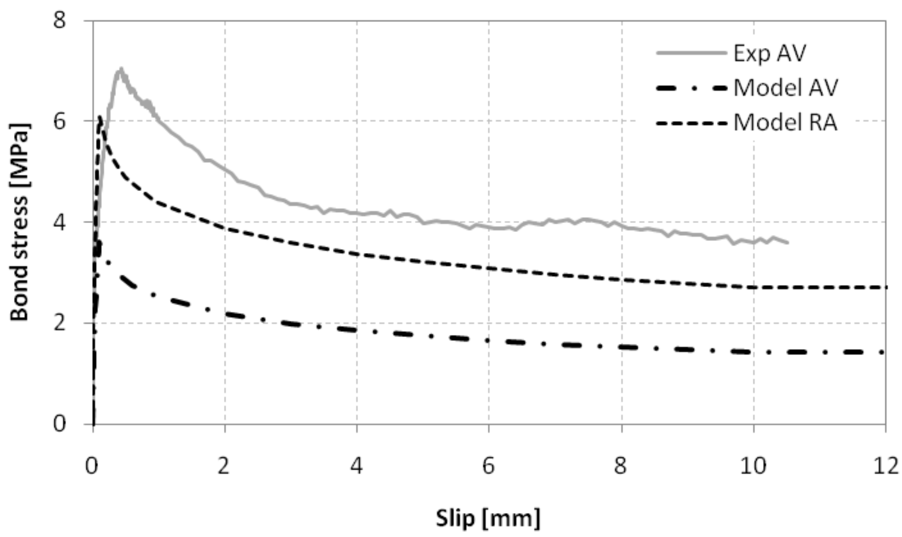

Smooth flat rebars
SS-K31-5x16-S-1D-TC

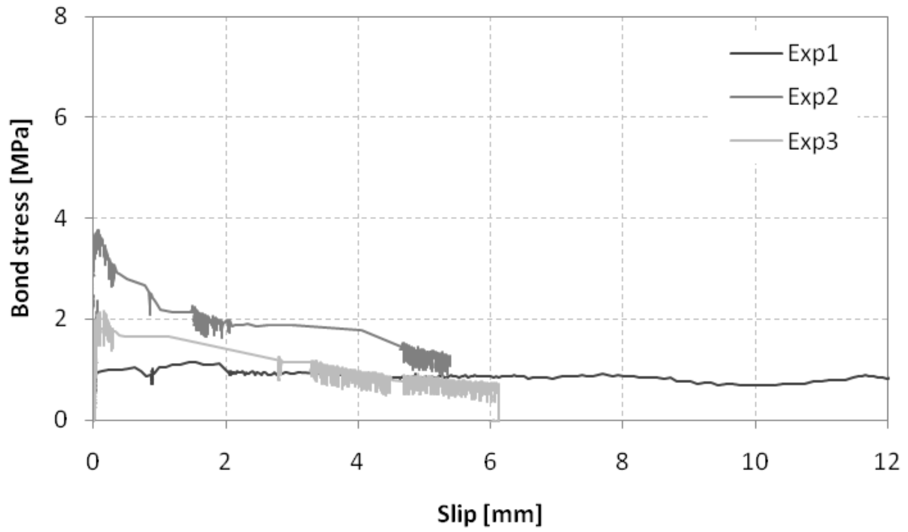

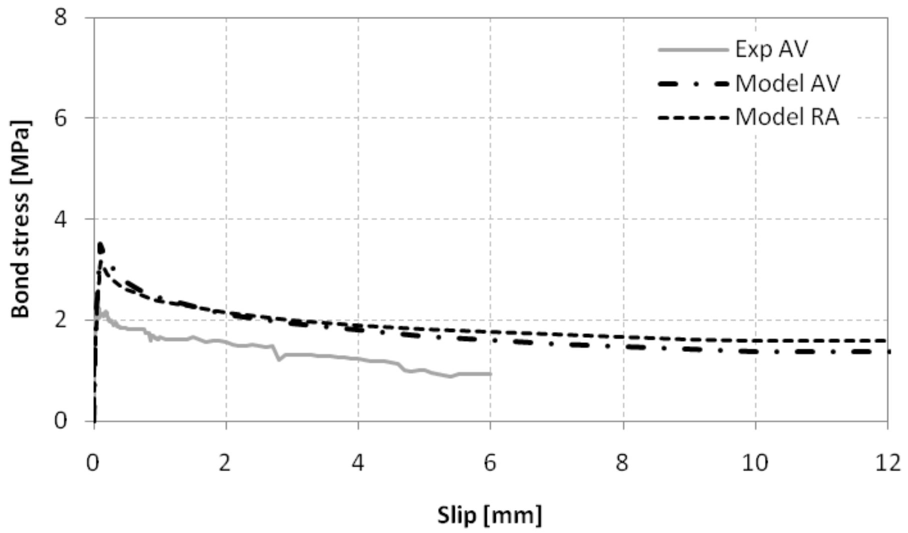

Smooth flat rebars
SS-K31-5x16-S-1D-SCC

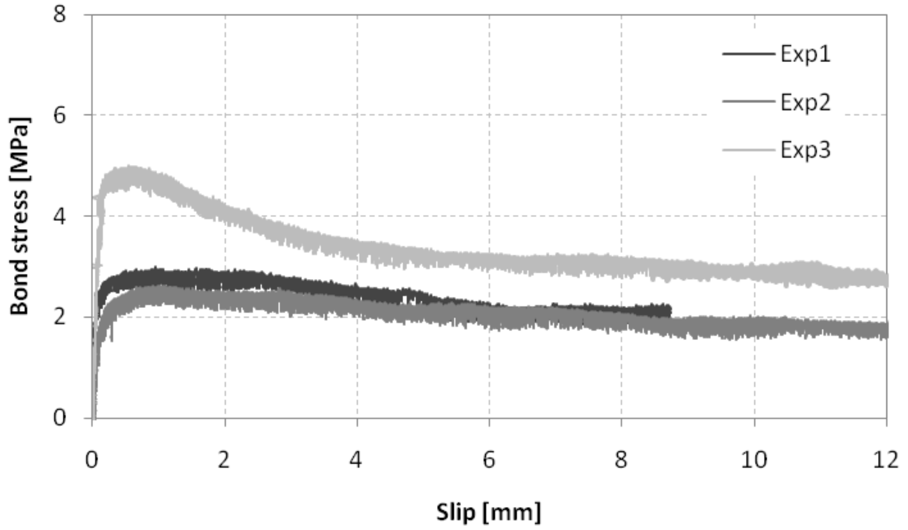

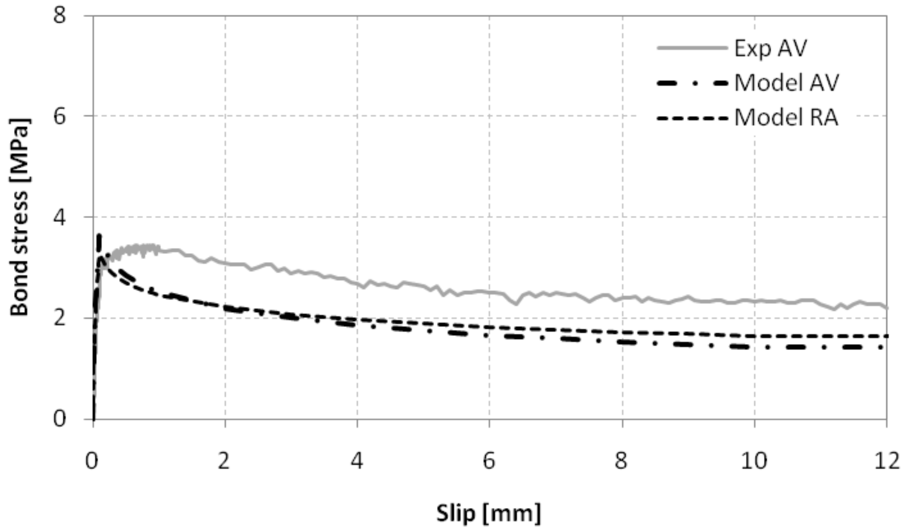

Continuously ribbed flat rebars
CS-3,5x25-CR-TC

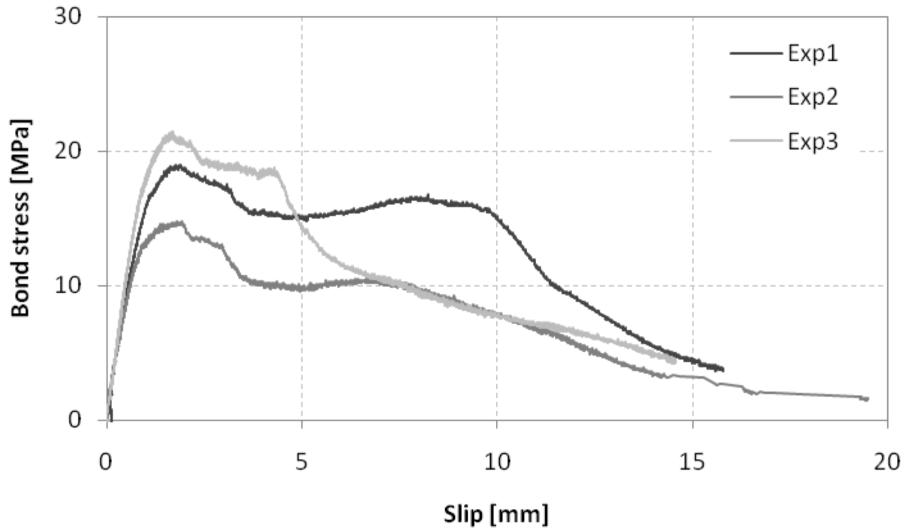

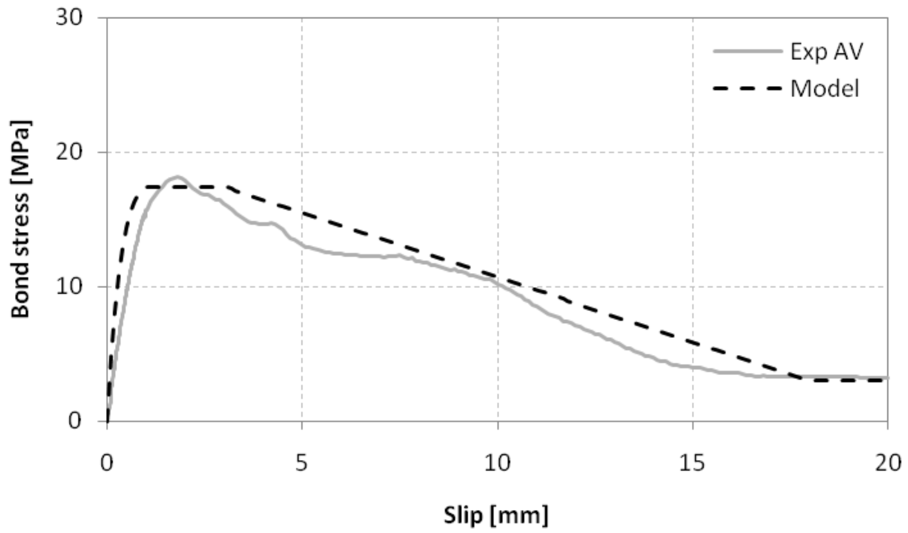

Continuously ribbed flat rebars
SS-5x23-CR-TC
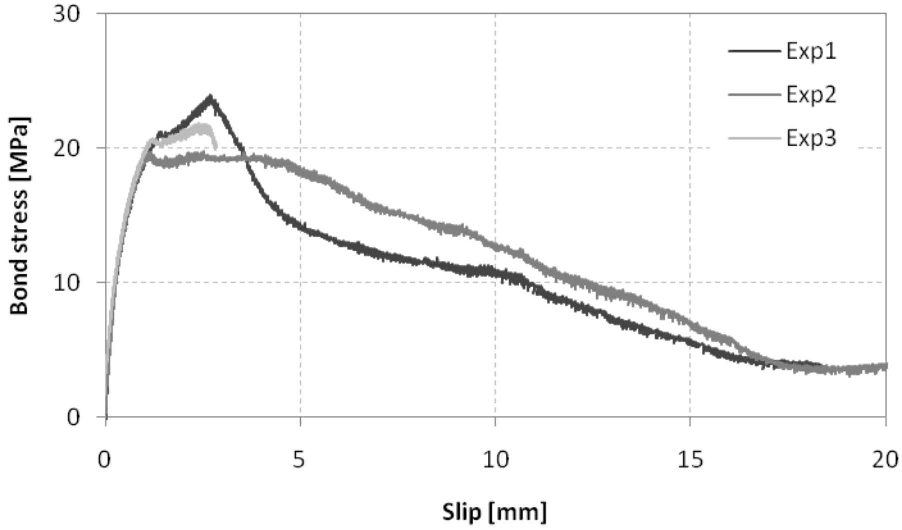
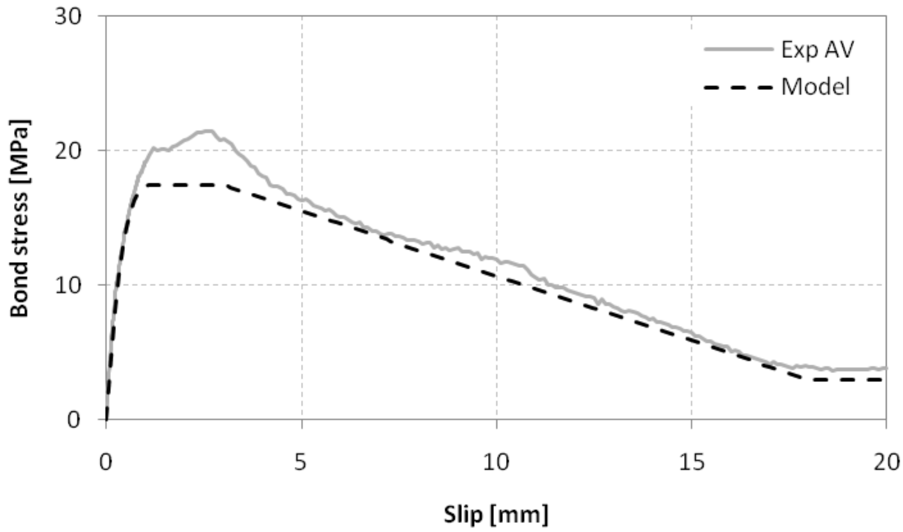

Continuously ribbed flat rebars
CS-3,5x25-CR-SCC
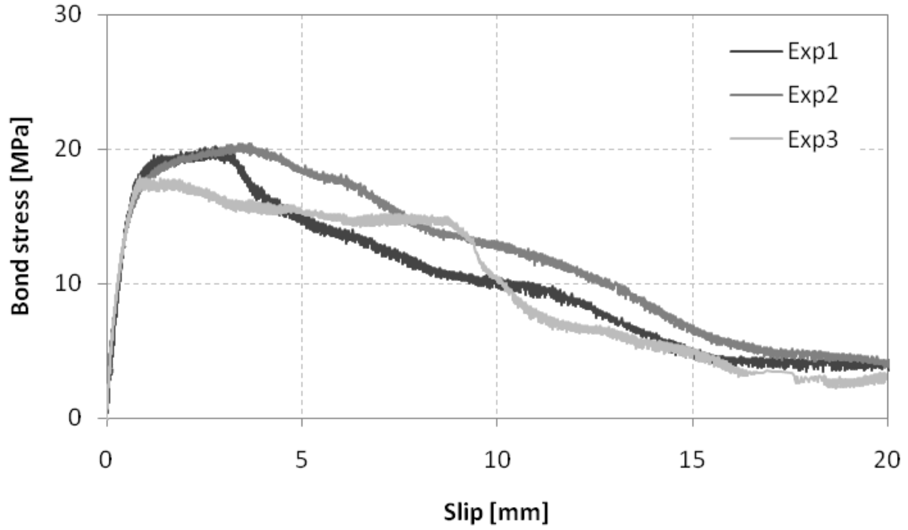
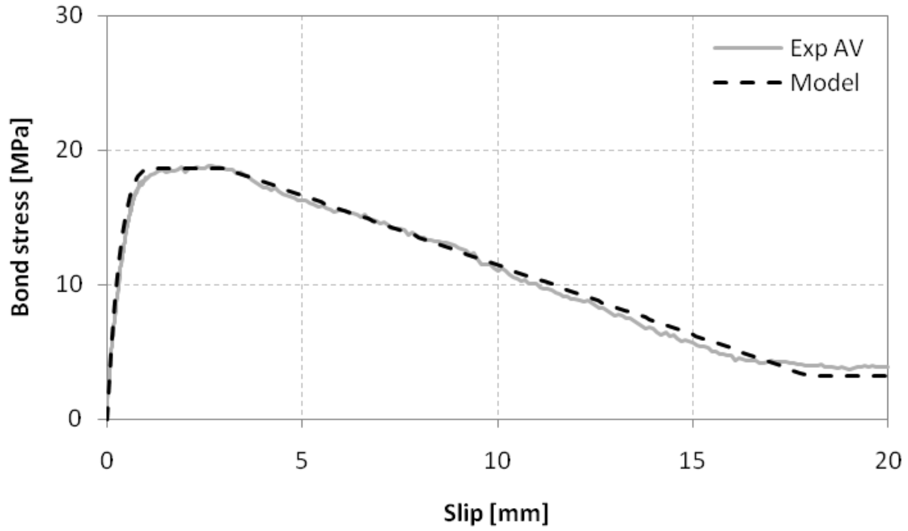

Continuously ribbed flat rebars
SS-5x23-CR-SCC
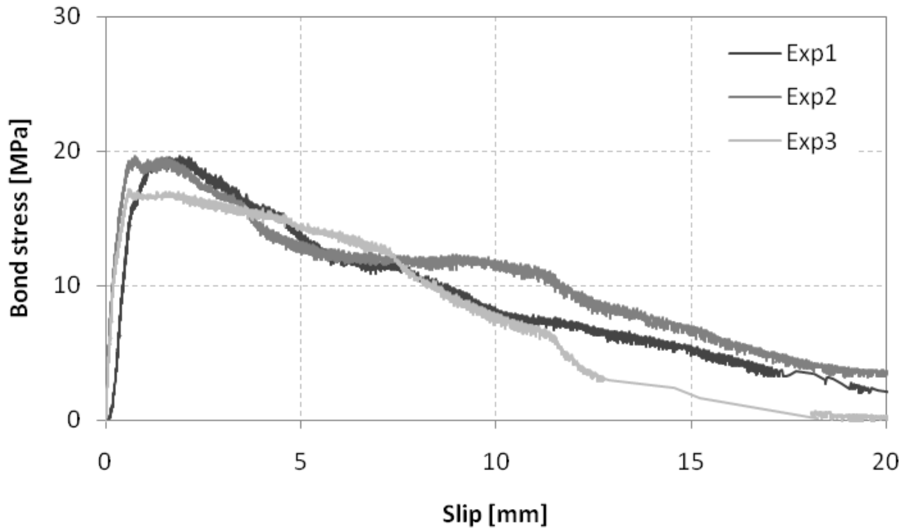
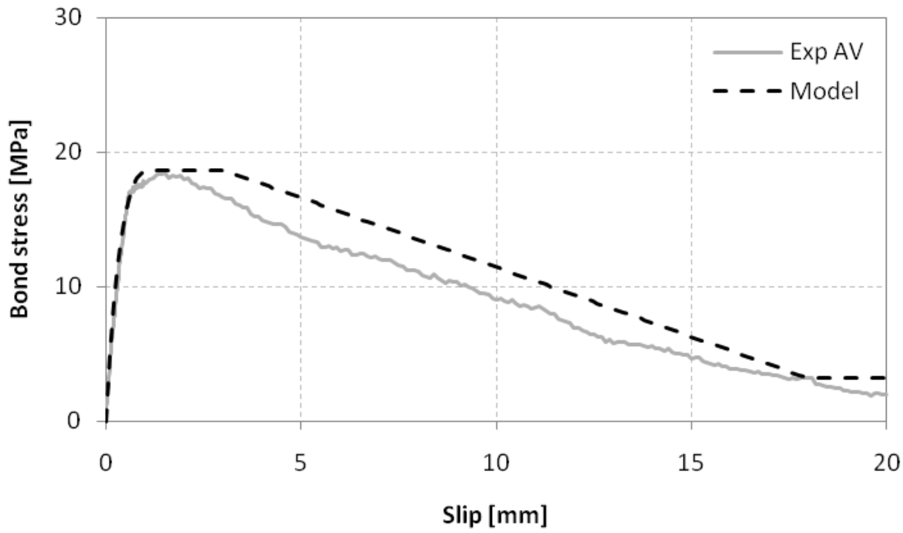

Continuously ribbed flat rebars
CS-3,5x25-CR-TC + confinement stirrups
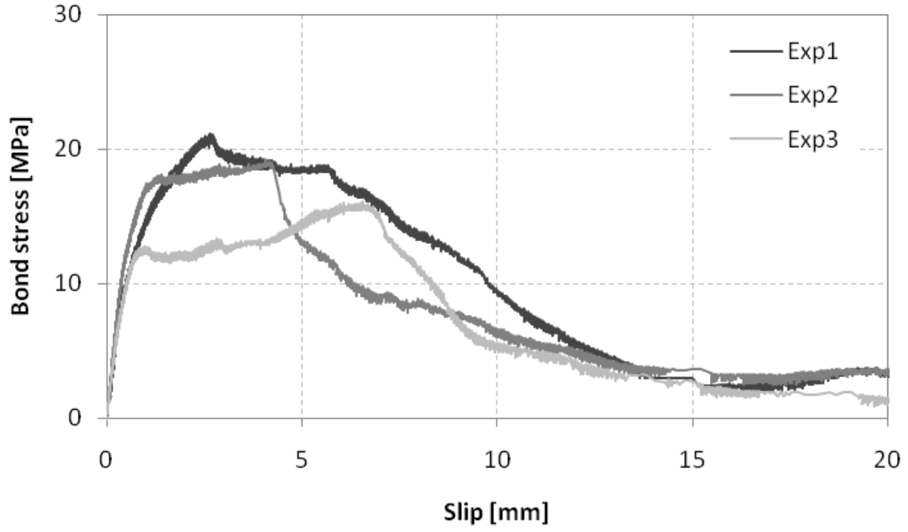
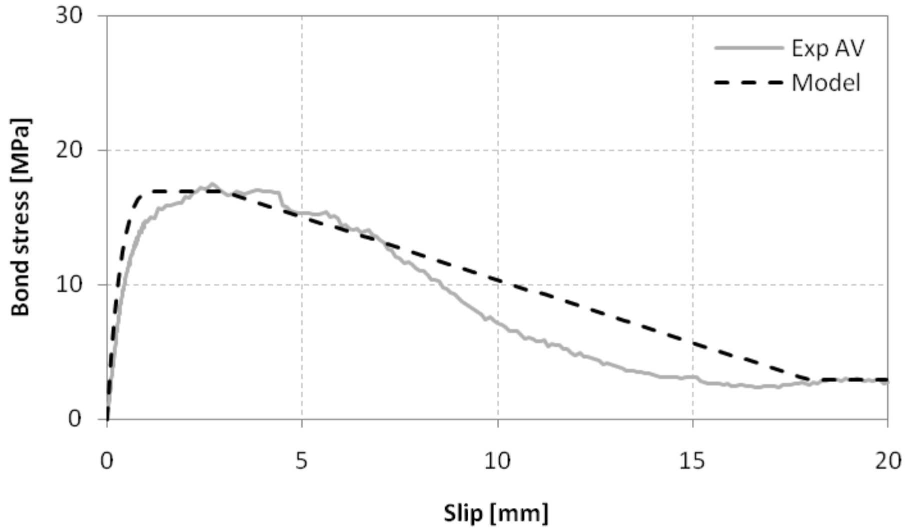

Flat rebars with an alternate rib pattern
CS-3,5x25-15R_10S_15R-TC
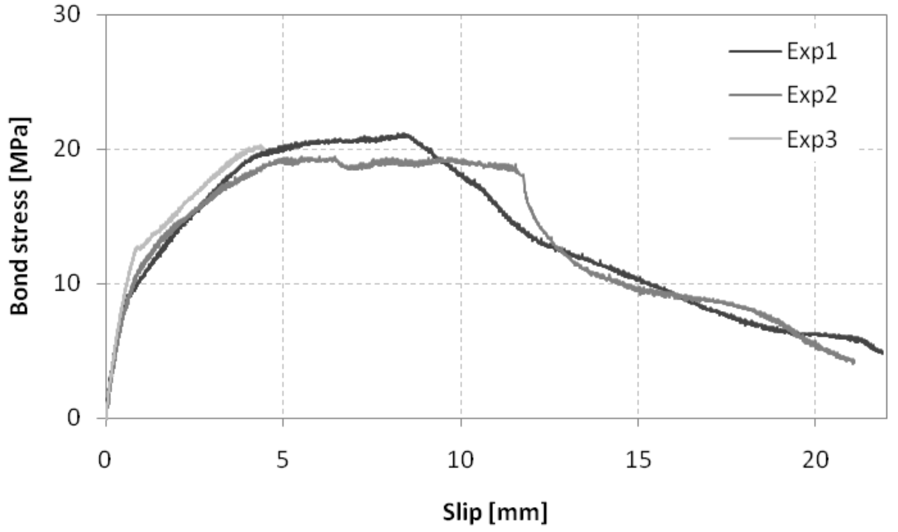
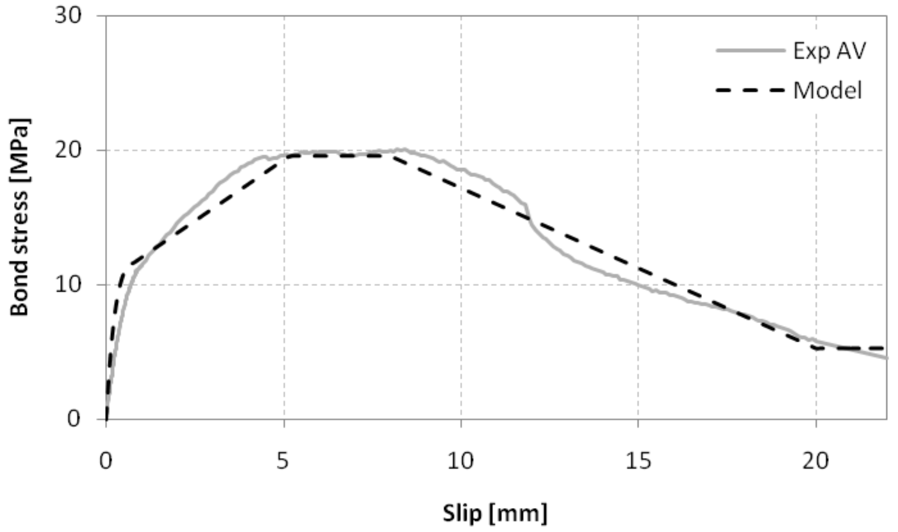

Flat rebars with an alternate rib pattern
SS-5x23-15R_10S_15R-TC
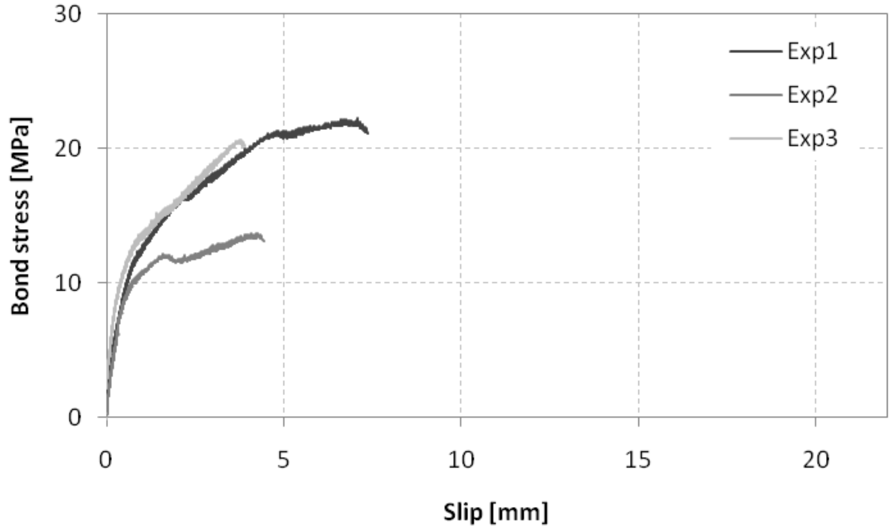
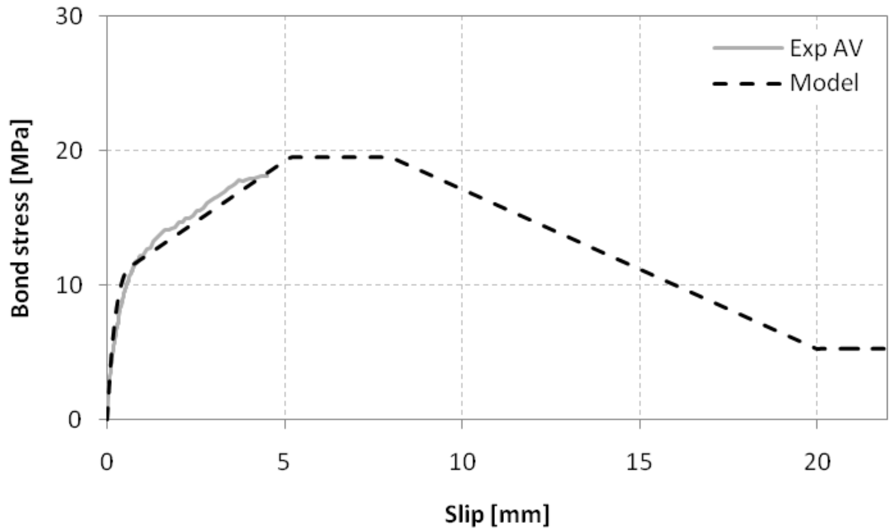

Flat rebars with an alternate rib pattern
CS-3,5x25-15R_10S_15R-SCC

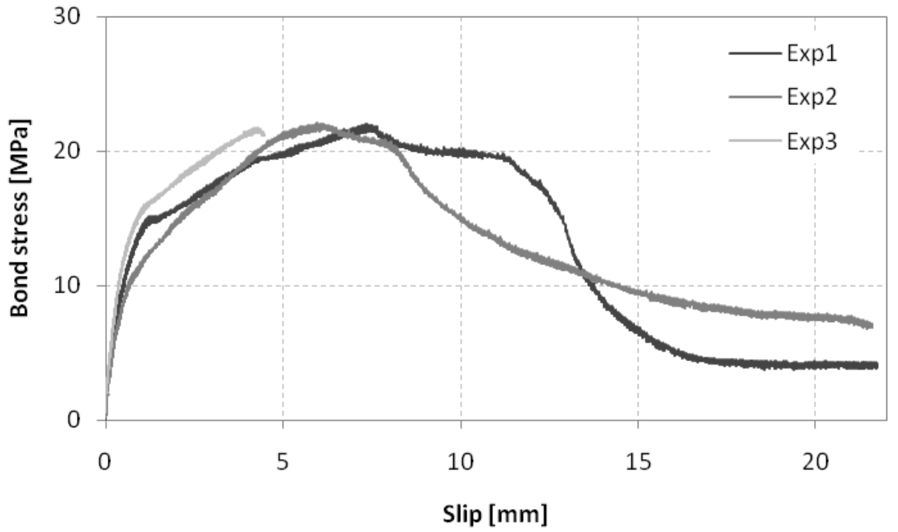

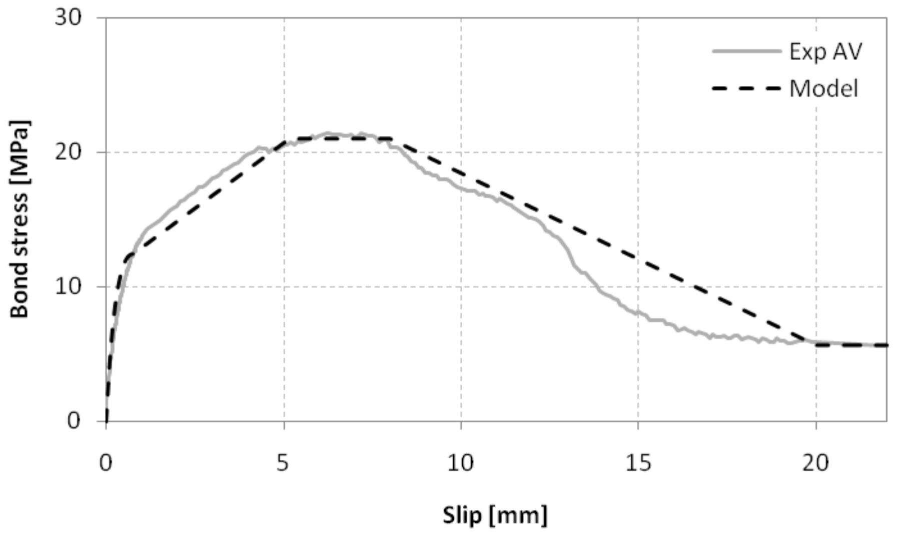

Flat rebars with an alternate rib pattern
SS-5x23-15R_10S_15R-SCC
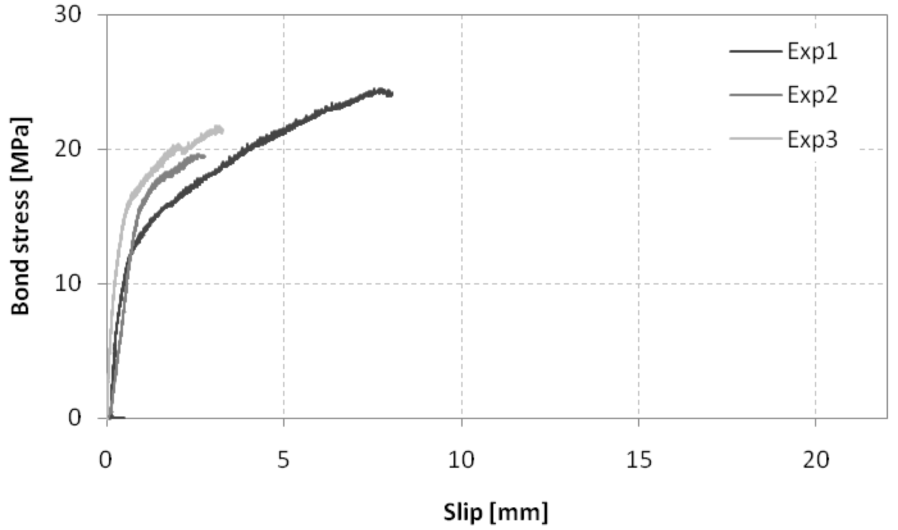
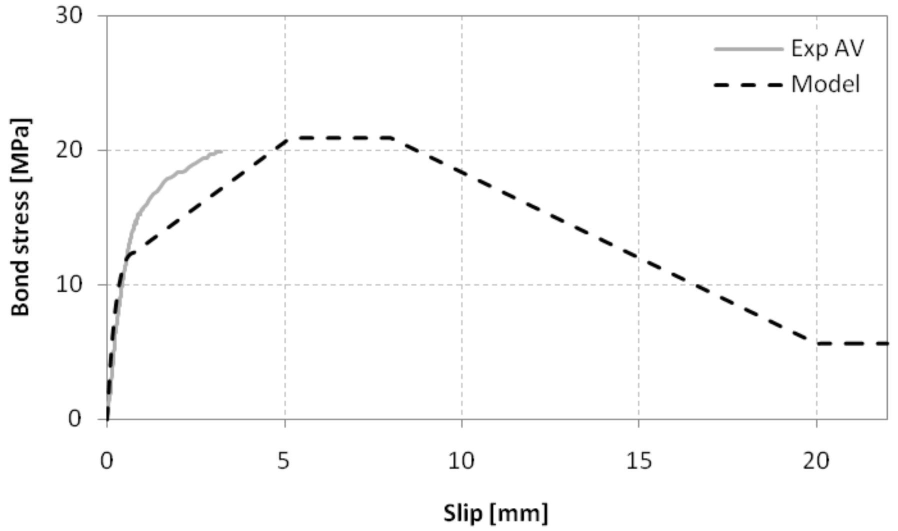

Flat rebars with an alternate rib pattern
CS-3,5x25-15R_10S_15R-TC + confinement stirrups
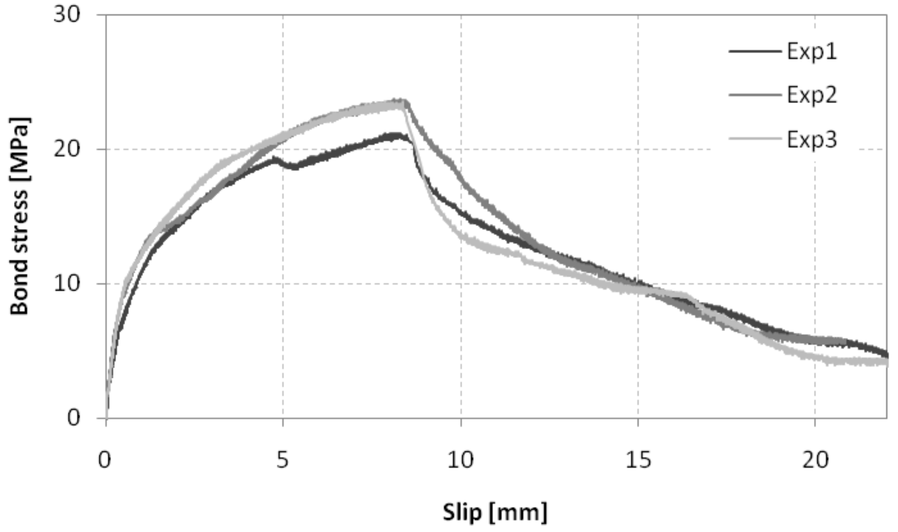
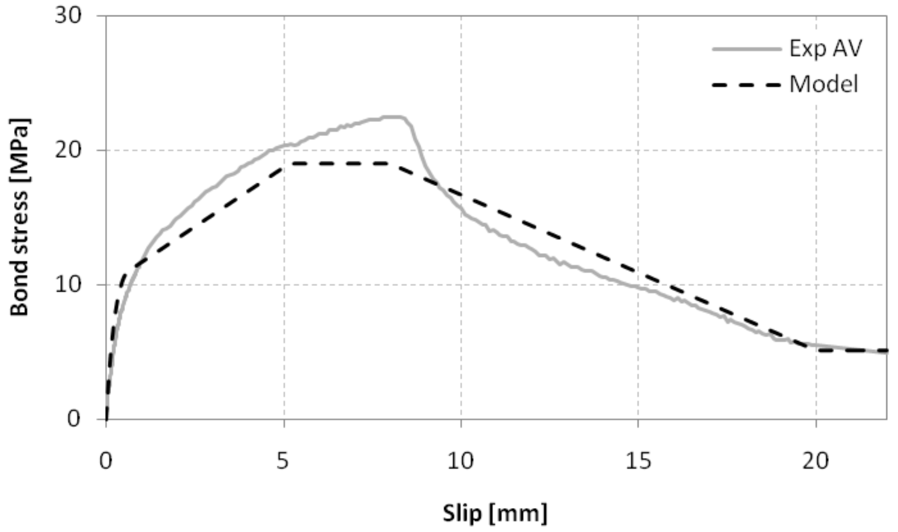

Flat rebars with an alternate rib pattern
CS-3,5x25-15R_20S_15R-TC

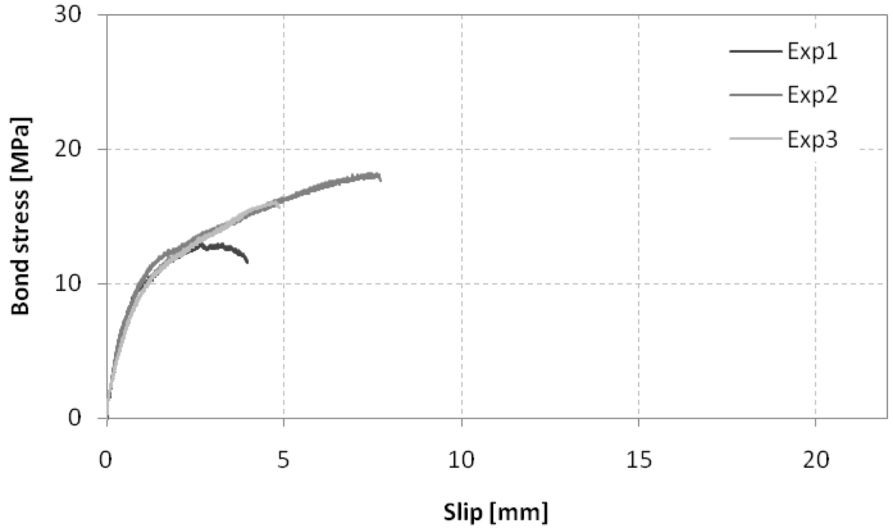

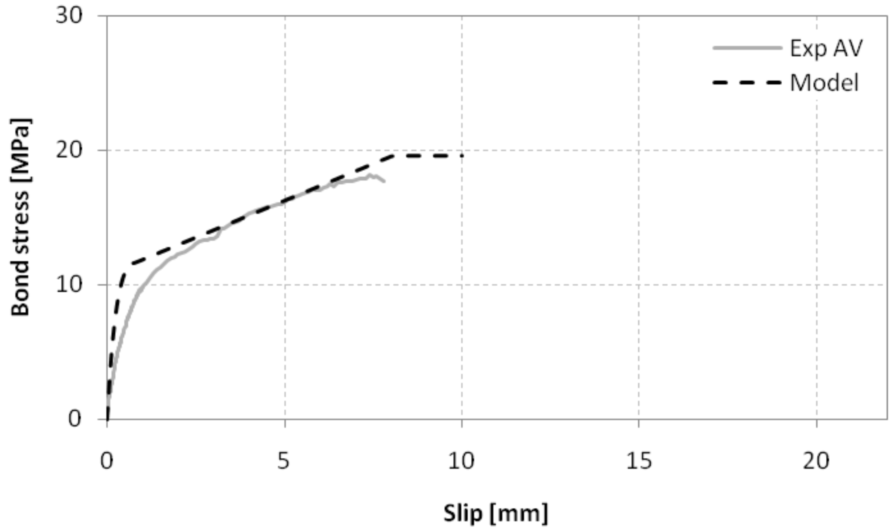

Flat rebars with an alternate rib pattern
SS-5x23-15R_20S_15R-TC
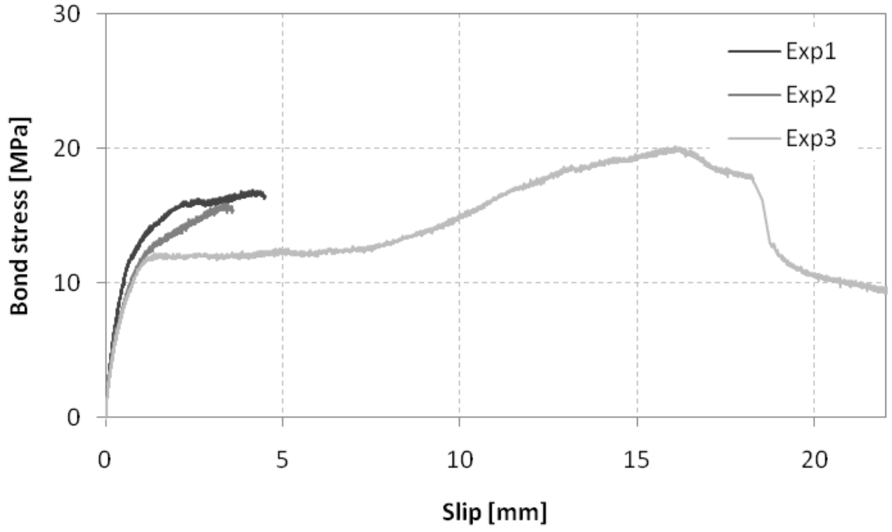
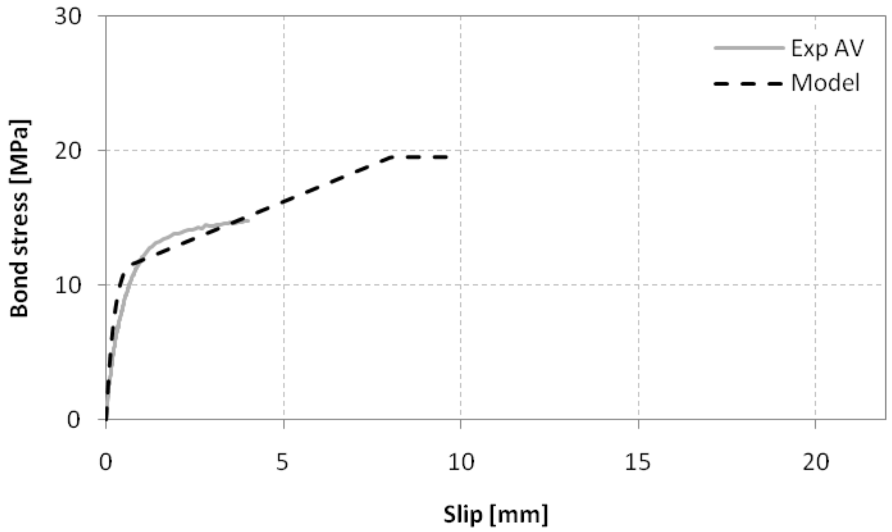

Flat rebars with an alternate rib pattern
CS-3,5x25-15R_20S_15R-SCC

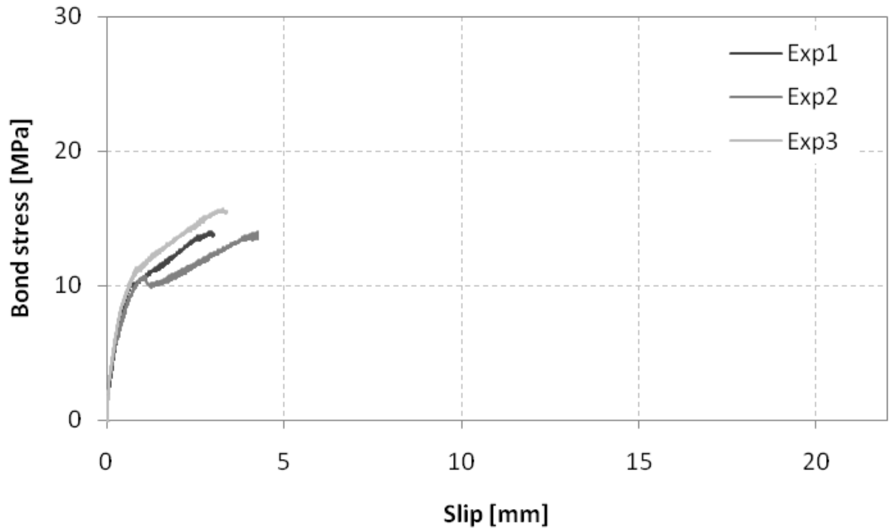

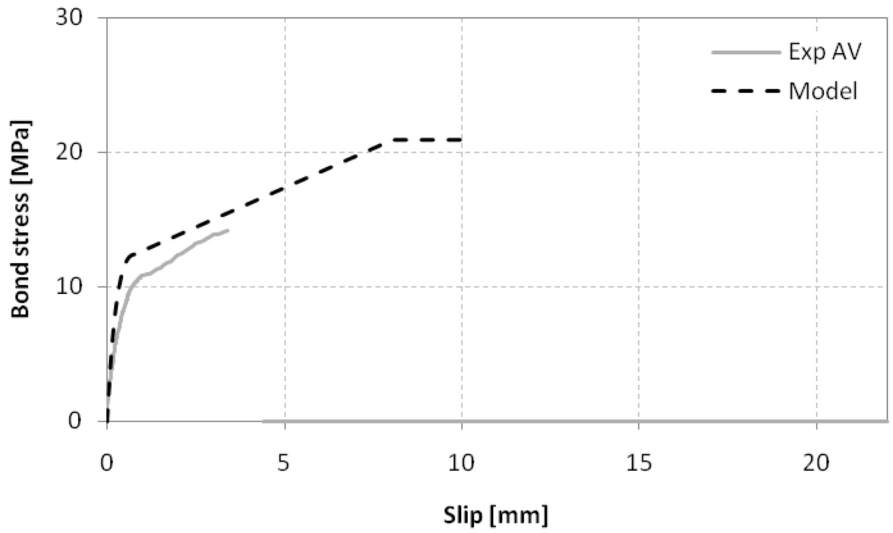

Flat rebars with an alternate rib pattern
SS-5x23-15R_20S_15R-SCC

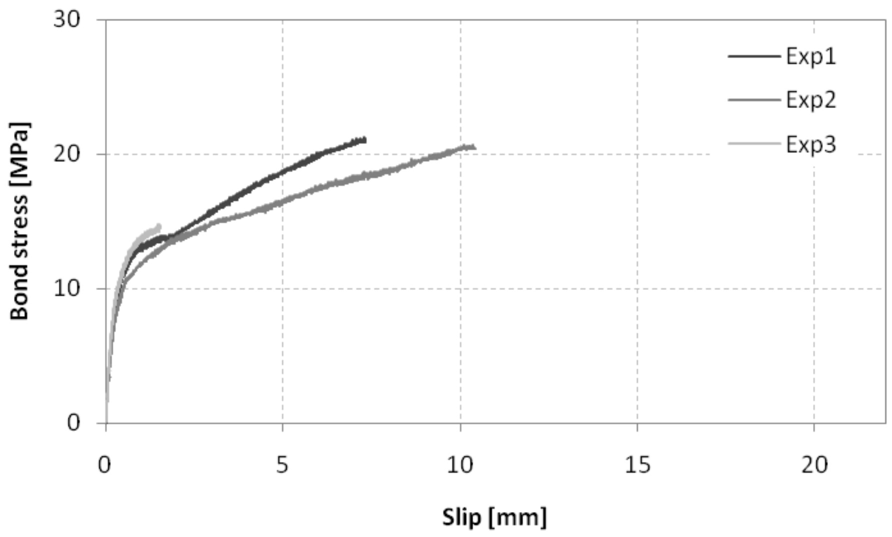

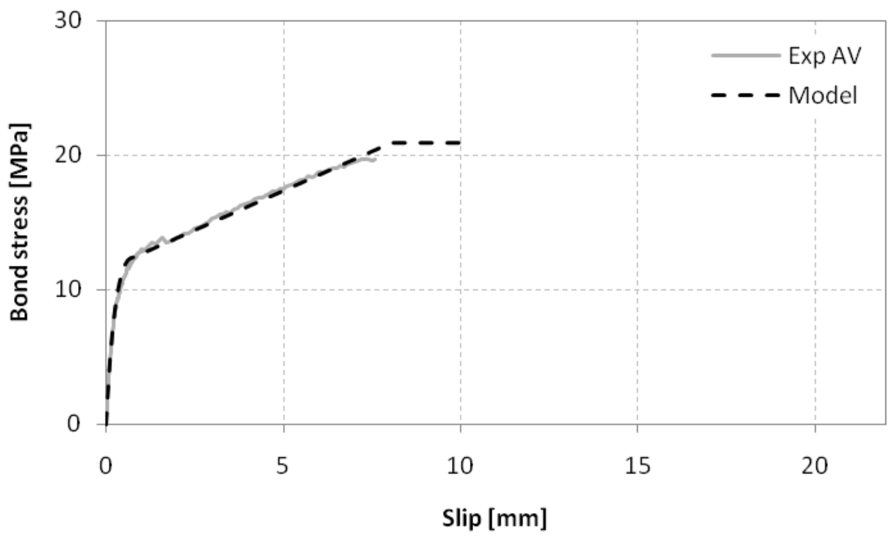

Flat rebars with an alternate rib pattern
CS-3,5x25-15R_20S_15R-TC + confinement stirrups

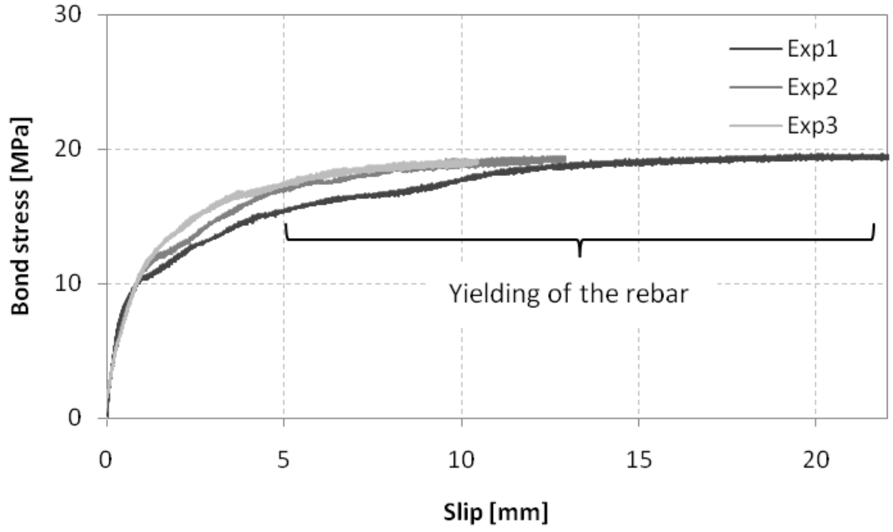

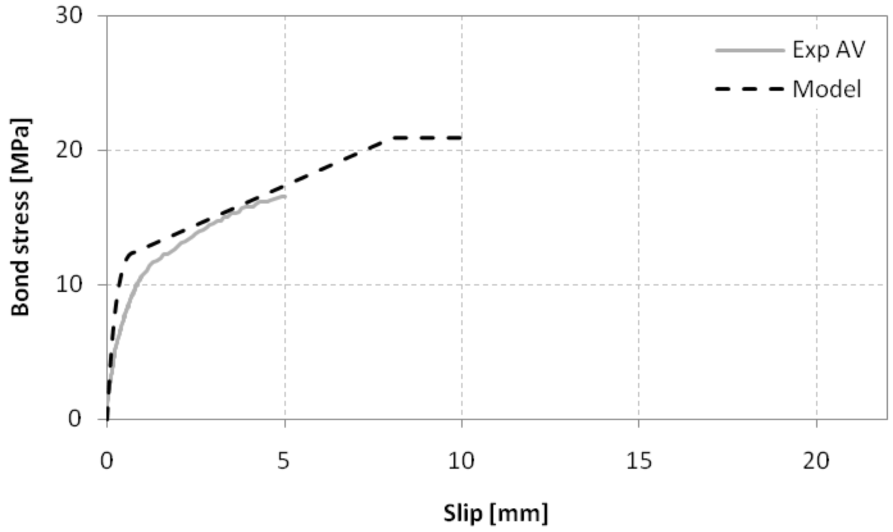

Appendix C Tension Stiffening Tests: Individual Test Results

Individual test results for all the performed 16 tension stiffening tests are given in this section. An individual data sheet is provided for each tested specimen, comprising:

- Denomination
- Geometry
- Concrete compression strength (f_c)
- Concrete tensile strength (f_{ct})
- Cracking stress (σ_{cr})
- Mean crack spacing at 50% of the yielding stress ($s_{rm,50\%y}$)
- Mean crack width at 50% of the yielding stress ($w_{rm,50\%y}$)
- Graphs:
  - Tensile stress - mean strain relationship
  - Cracking behaviour:
    - Tensile stress vs. mean crack width
    - Tensile stress vs. total crack opening
    - Tensile stress vs. maximum crack width
    - Tensile stress vs. mean crack spacing

- Schematic drawing of developed cracks at the end of the test (red dashed lines indicate the position of the middle point of the smooth zone for the alternate patterns)

CS-Ø10-CR-TC	Geom: Ø10 mm	f_c = 55,9 N/mm²	f_{ct} = 3,3 N/mm²
	σ_{cr} = 179,89 N/mm²	$s_{rm,50\%y}$ = 144,00 mm	$w_{rm,50\%y}$ = 0,20 mm

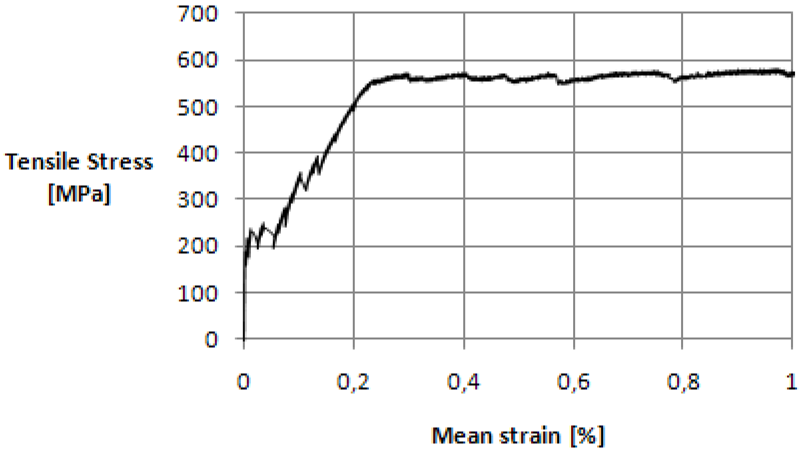

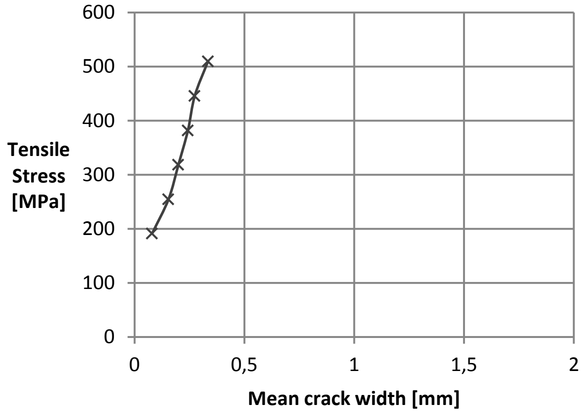

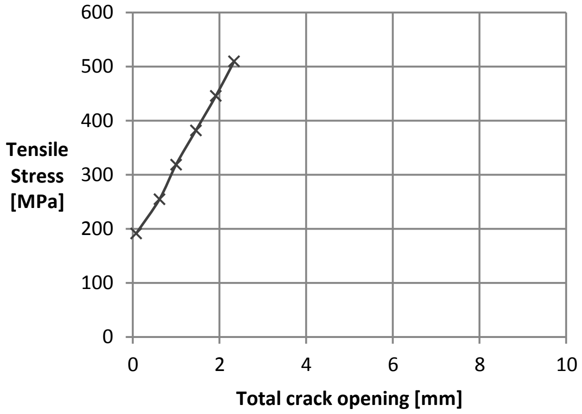

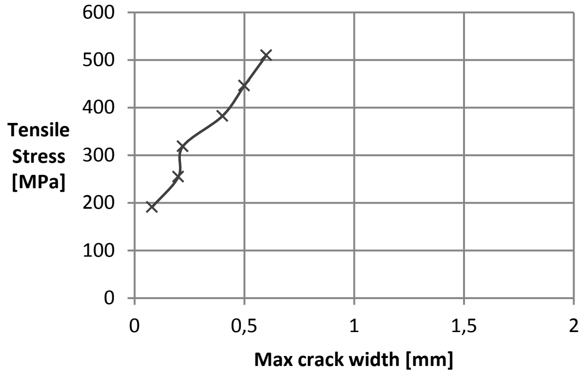

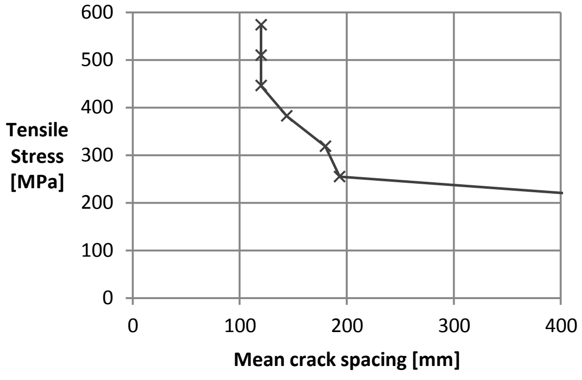

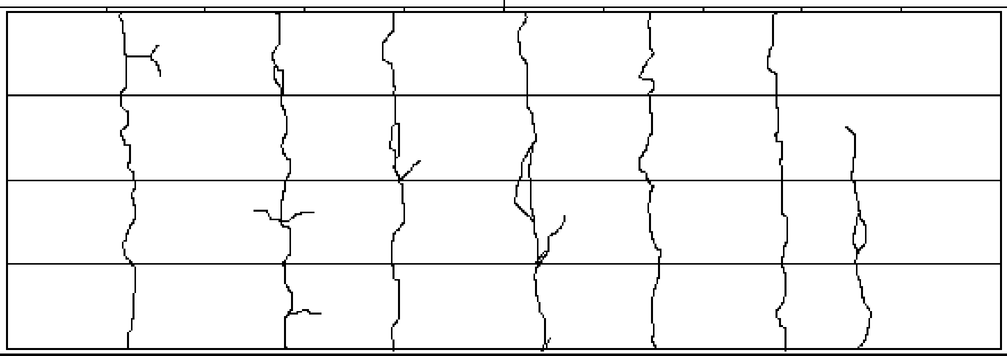

CS-Ø12-CR-TC	Geom: Ø12 mm	f_c = 52,3 N/mm^2	f_{ct} = 3,6 N/mm^2
	σ_{cr} = 170,81 N/mm^2	$s_{rm,50\%y}$ = 134,00 mm	$w_{rm,50\%y}$ = 0,24 mm

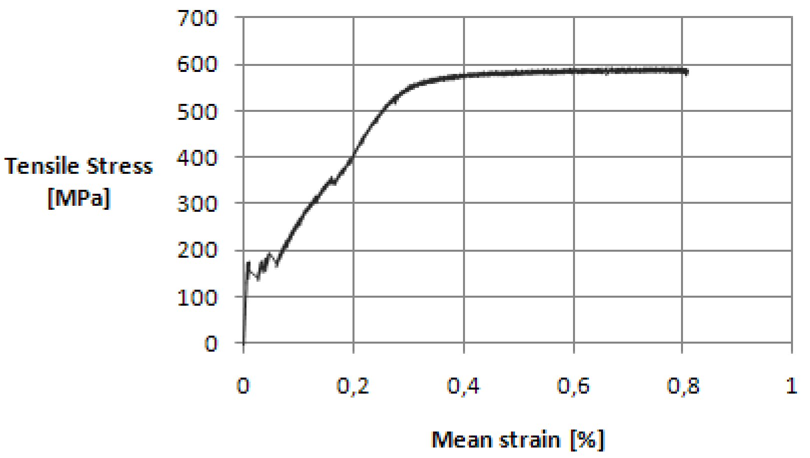

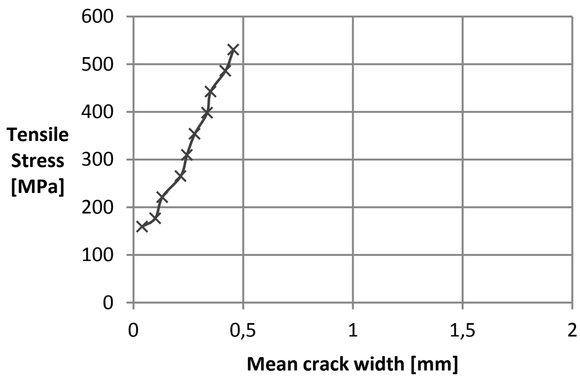

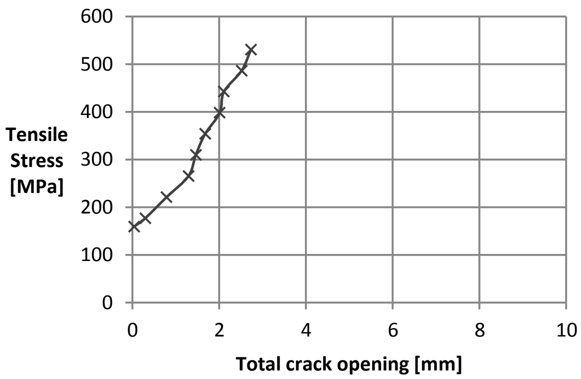

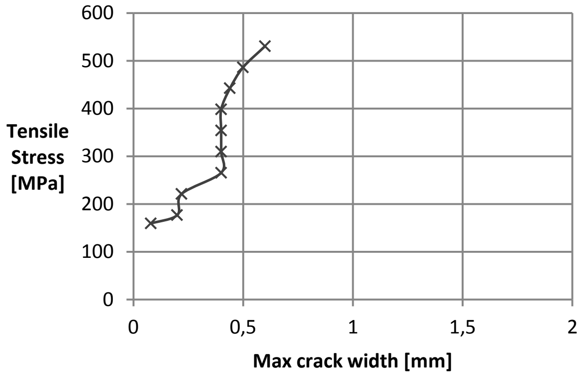

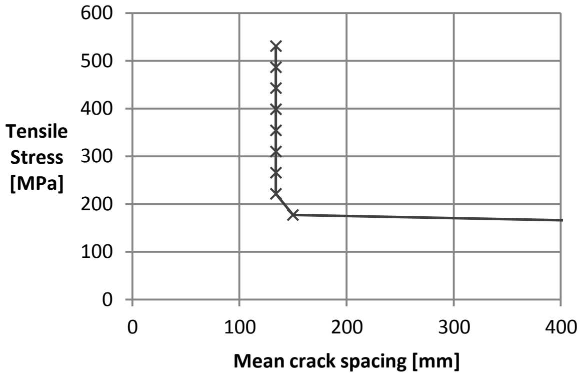

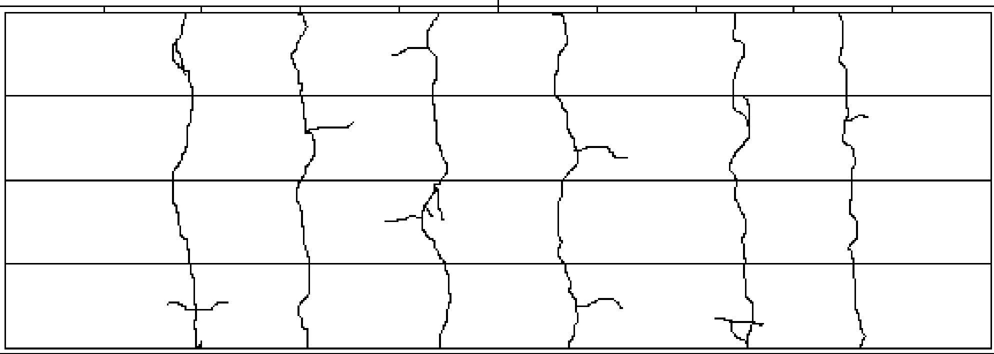

CS-3,5x25-CR-TC	Geom: 3,5x25 mm^2	f_c = 55,9 N/mm^2	f_{ct} = 3,3 N/mm^2
	σ_{cr} = 170,20 N/mm^2	$s_{rm,50\%y}$ = 223,33 mm	$w_{rm,50\%y}$ = 0,55 mm

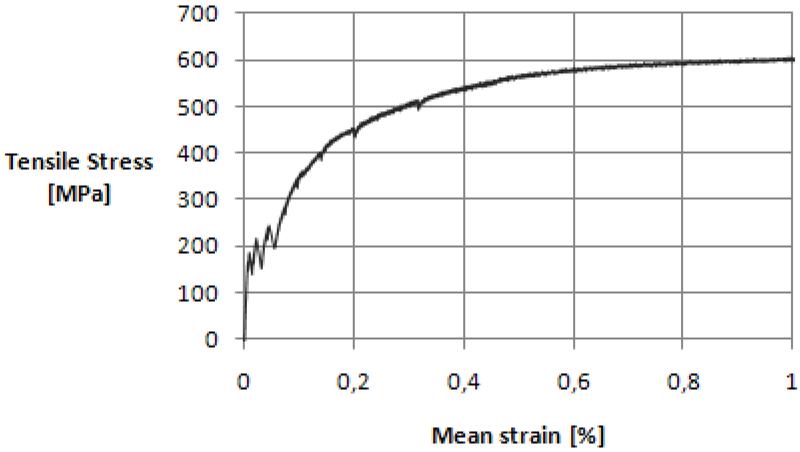

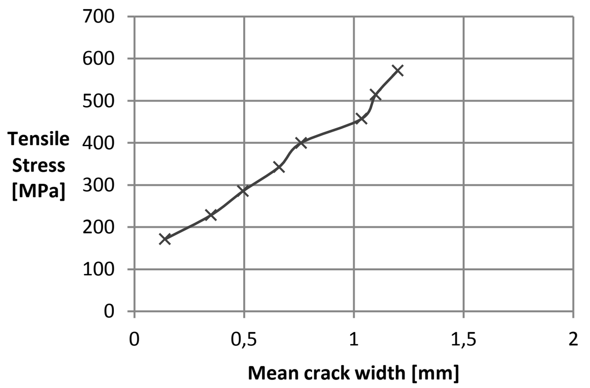

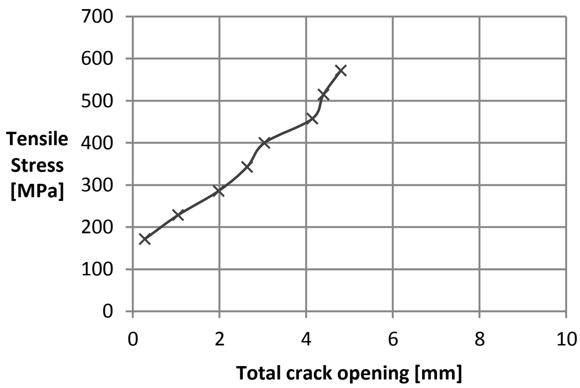

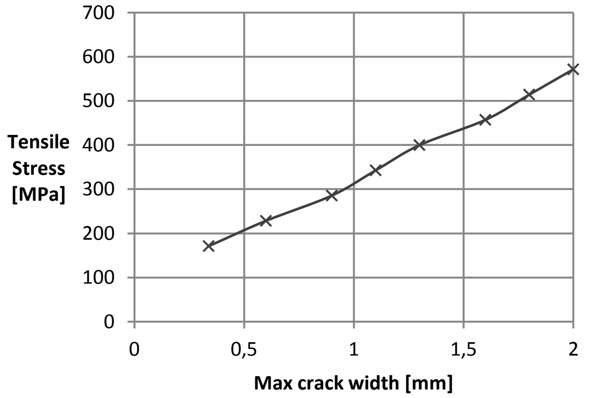

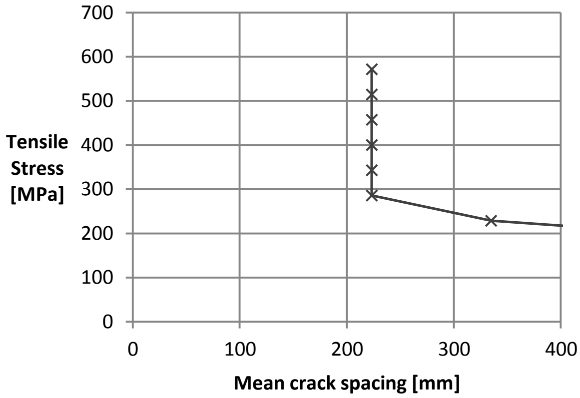

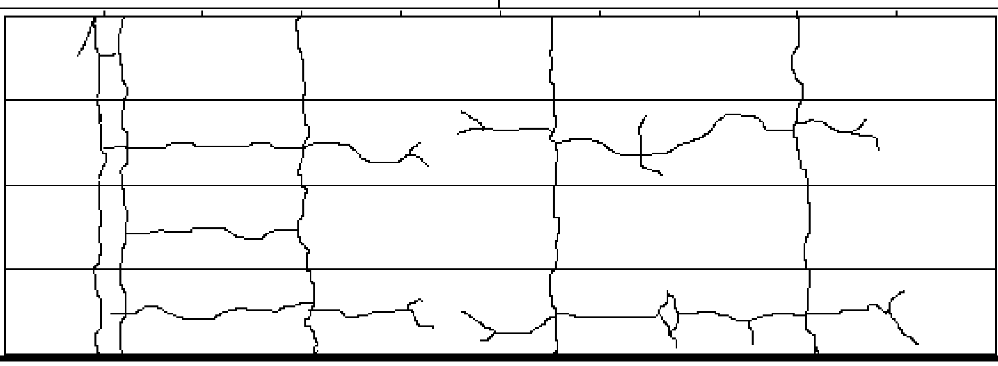

CS-3,5x25-50R_10S-TC	Geom: 3,5x25 mm²	f_c = 55,9 N/mm²	f_{ct} = 3,3 N/mm²
	σ_{cr} = 216,59 N/mm²	$s_{rm,50\%y}$ = 147,50 mm	$w_{rm,50\%y}$ = 0,45 mm

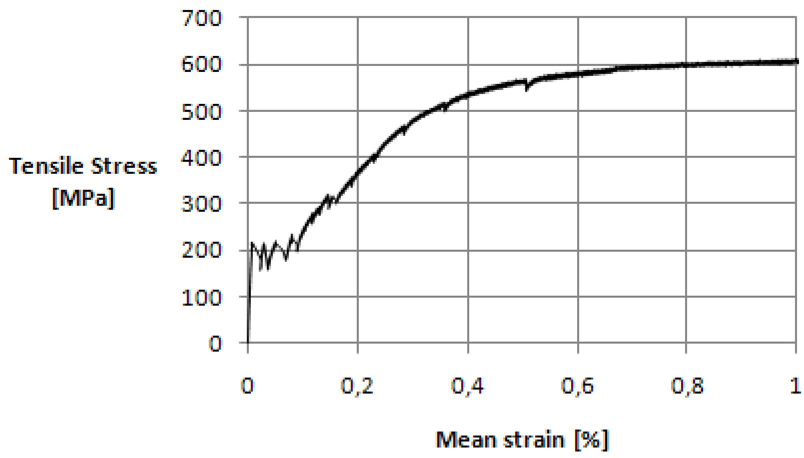

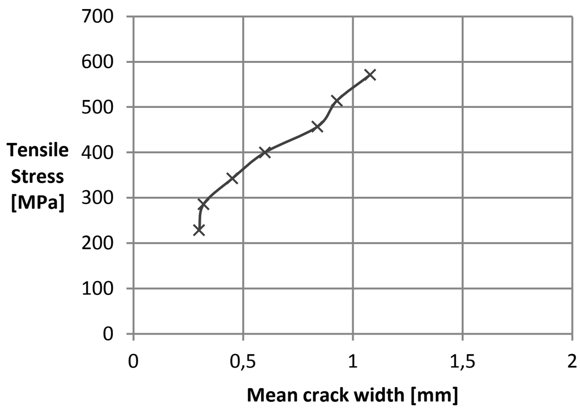

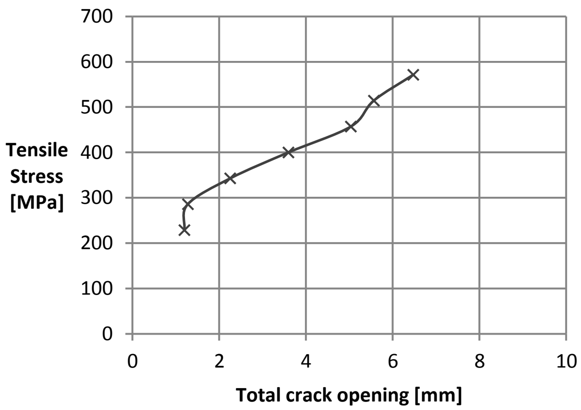

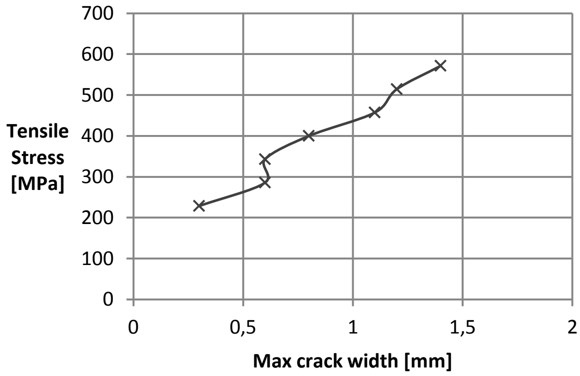

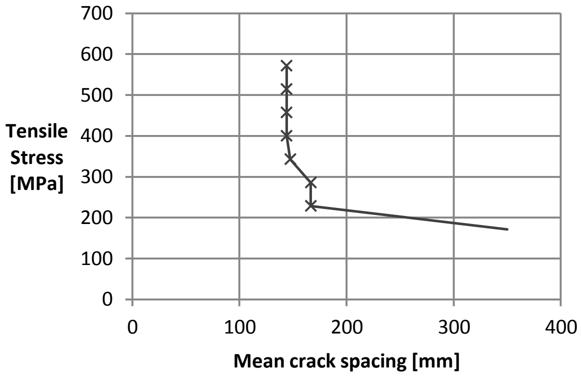

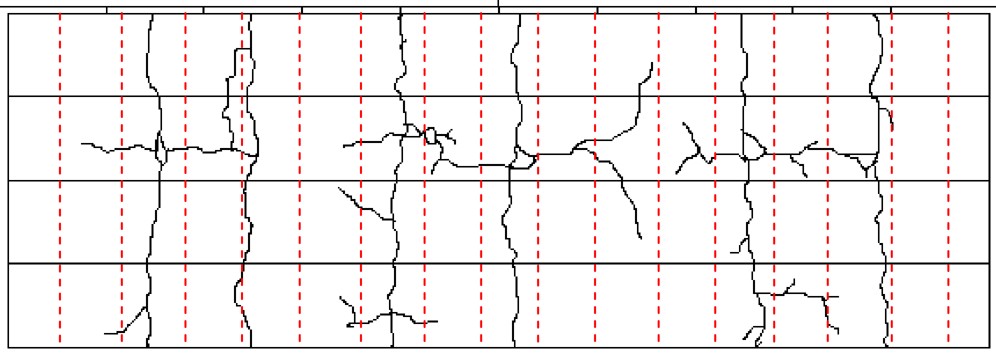

SS-5x23-CR-TC	Geom: 5x23 mm²	f_c = 55,9 N/mm²	f_{ct} = 3,3 N/mm²
	σ_{cr} = 108,79 N/mm²	$s_{rm,50\%y}$ = 165,00 mm	$w_{rm,50\%y}$ = 0,78 mm

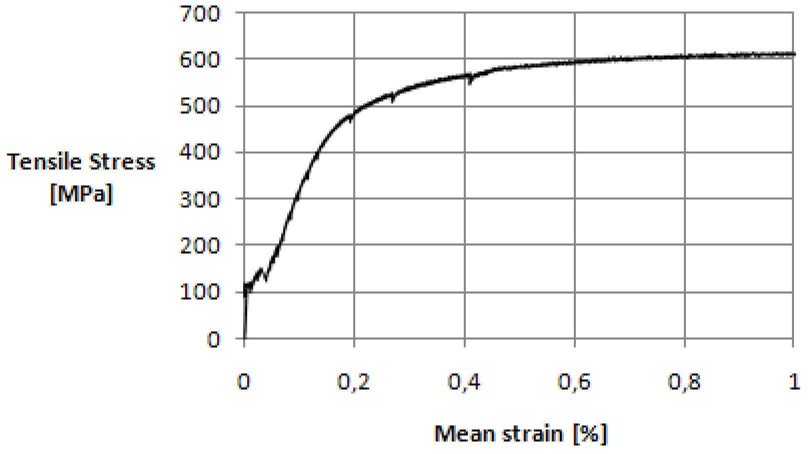

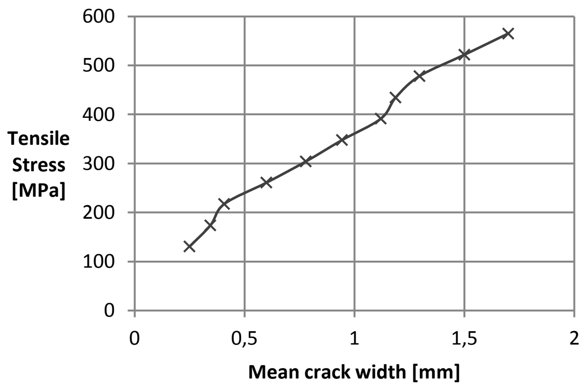

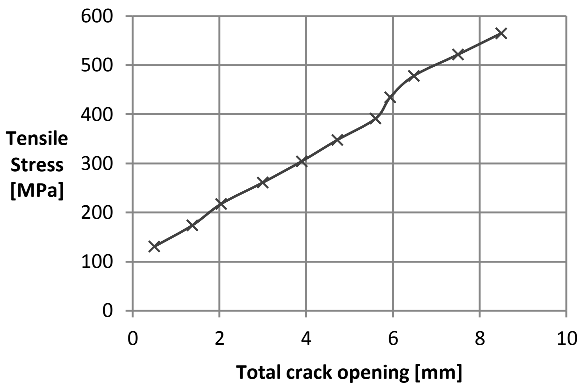

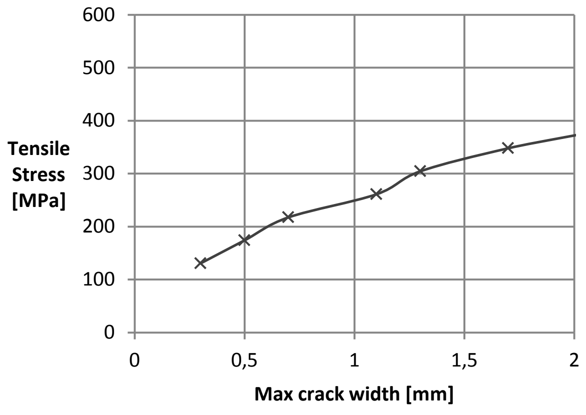

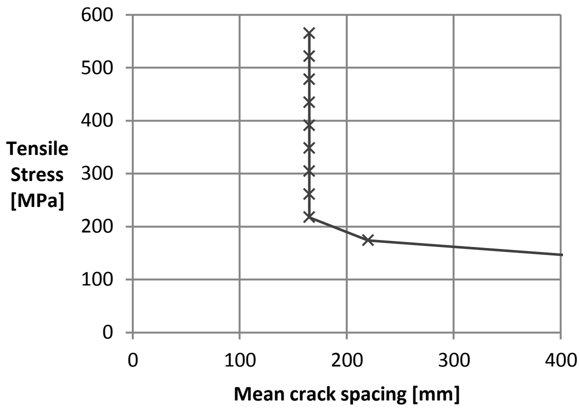

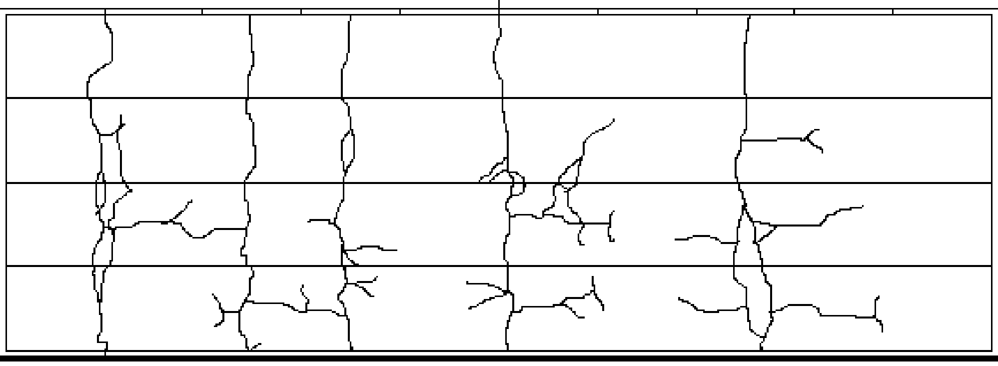

SS-5x23-50R_10S-TC	Geom: 5x23 mm²	f_c = 52,3 N/mm²	f_{ct} = 3,6 N/mm²
	σ_{cr} = 111,18 N/mm²	$s_{rm,50\%y}$ = 134,00 mm	$w_{rm,50\%y}$ = 0,49 mm

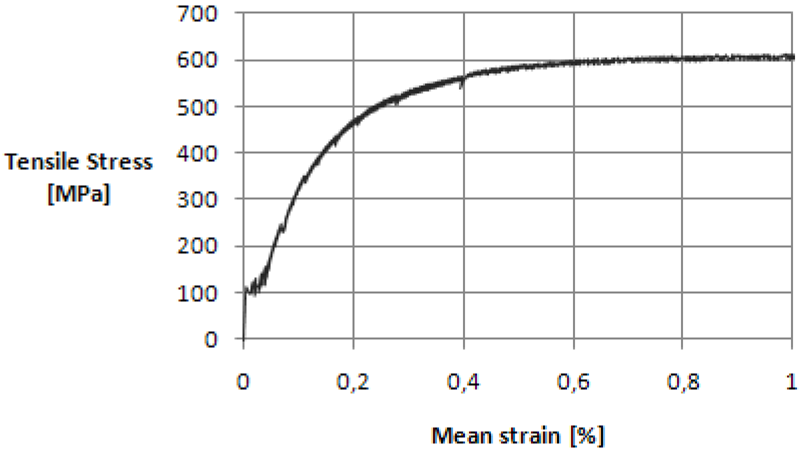

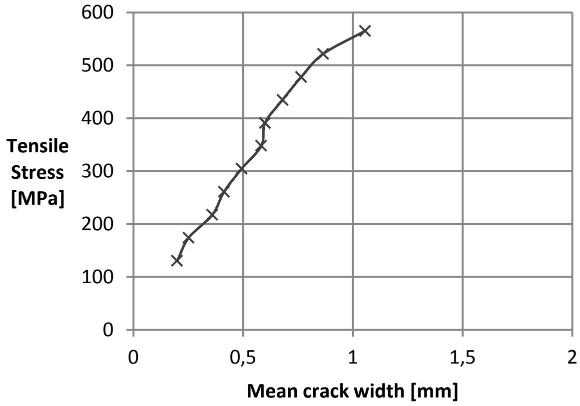

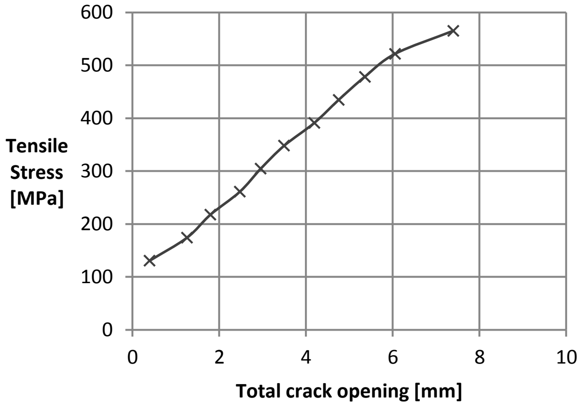

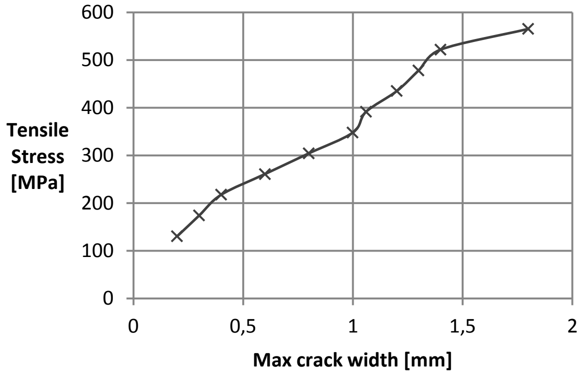

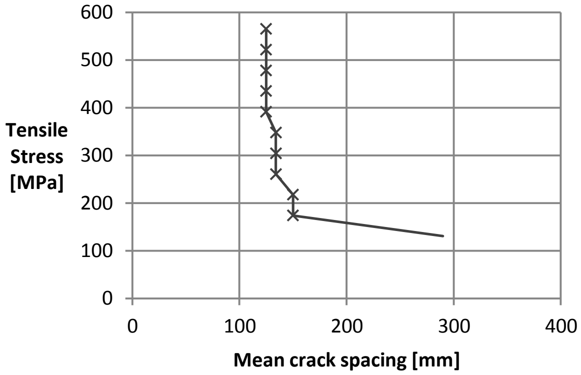

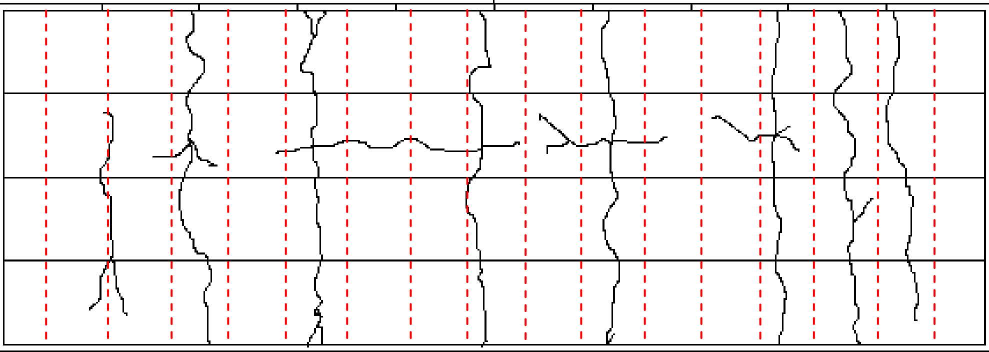

SS-5x23-100R_10S-TC	Geom: 5x23 mm²	f_c = 52,3 N/mm²	f_{ct} = 3,6 N/mm²
	σ_{cr} = 149,93 N/mm²	$s_{rm,50\%y}$ = 170,00 mm	$w_{rm,50\%y}$ = 0,58 mm

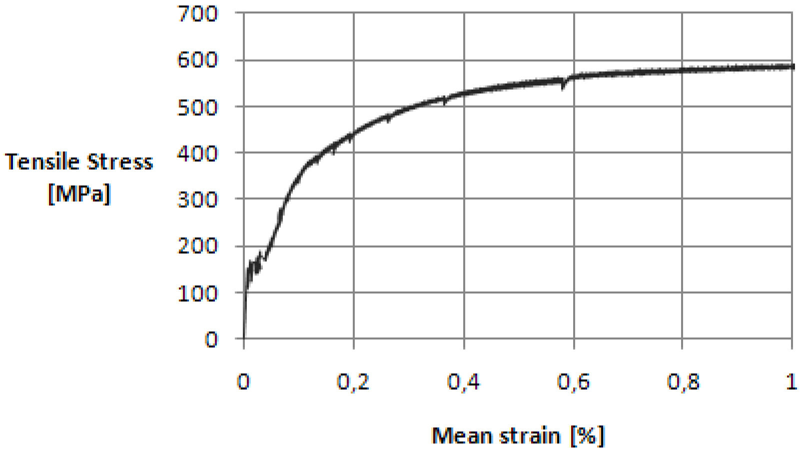

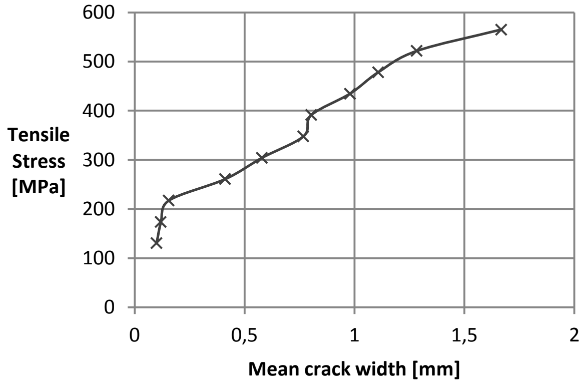

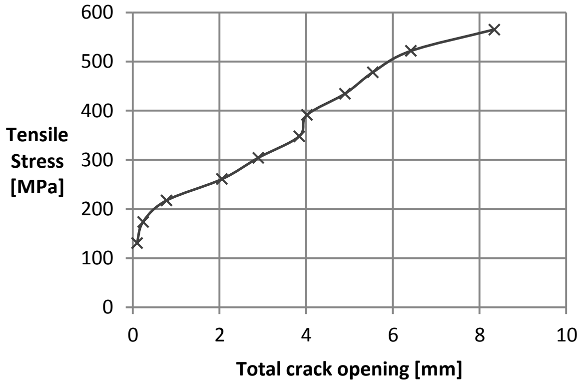

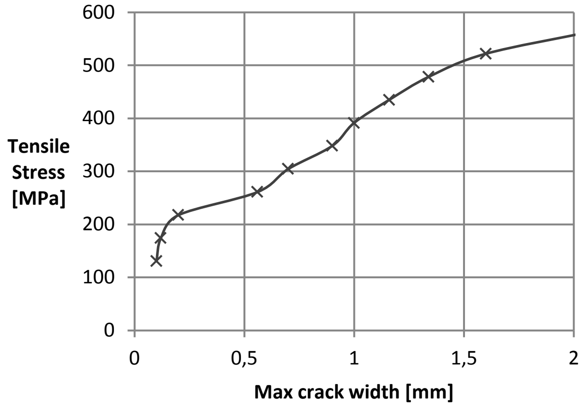

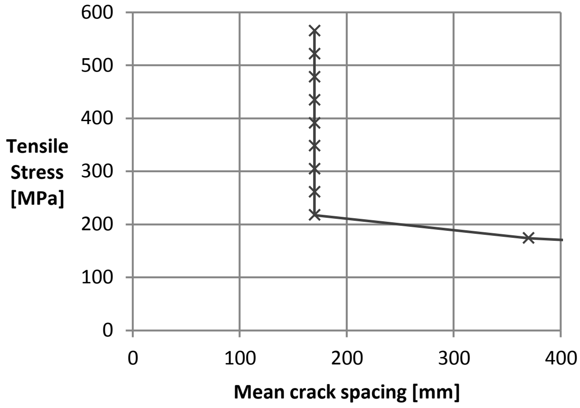

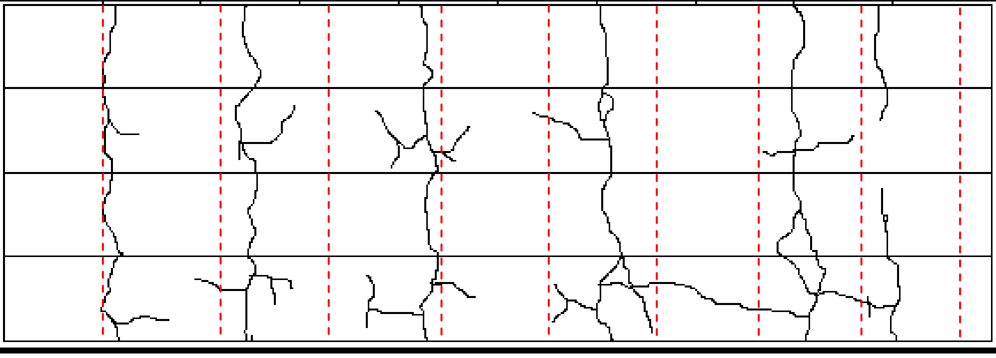

SS-5x23-100R_20S-TC	Geom: 5x23 mm²	f_c = 52,3 N/mm²	f_{ct} = 3,6 N/mm²
	σ_{cr} = 147,93 N/mm²	$s_{rm,50\%y}$ = 175,00 mm	$w_{rm,50\%y}$ = 0,46 mm

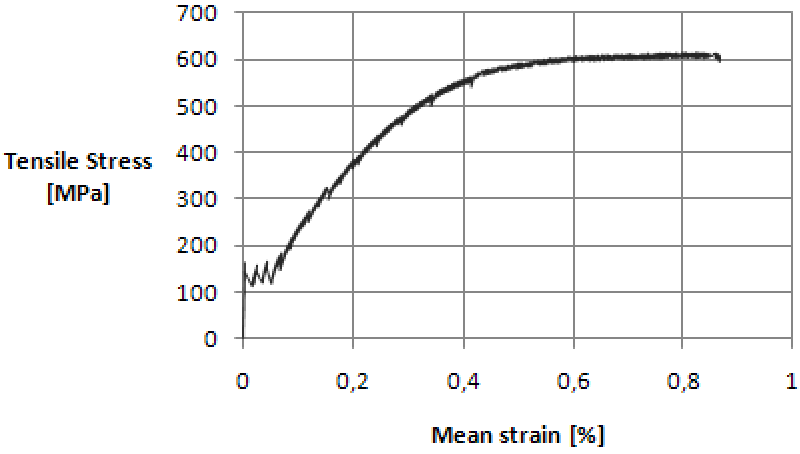

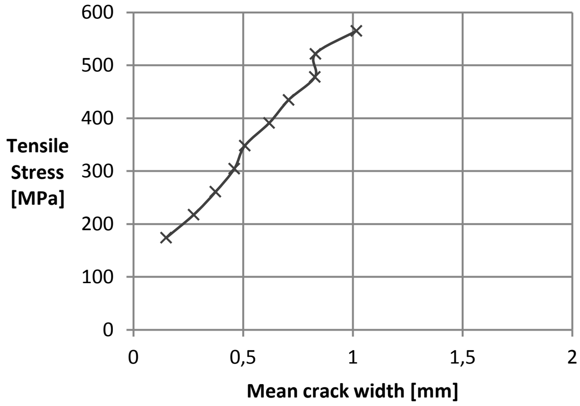

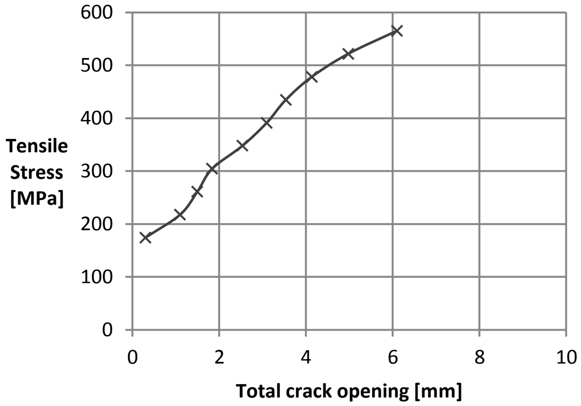

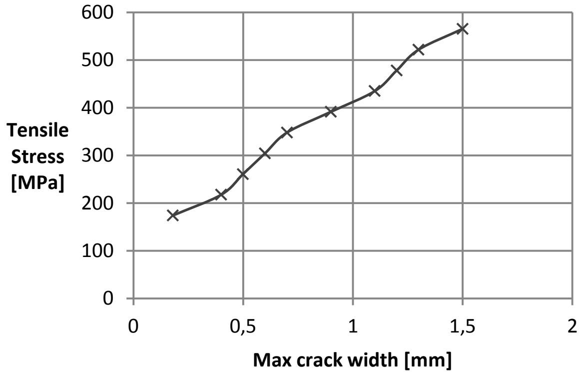

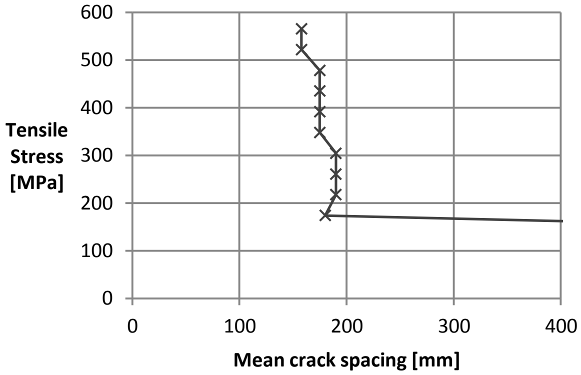

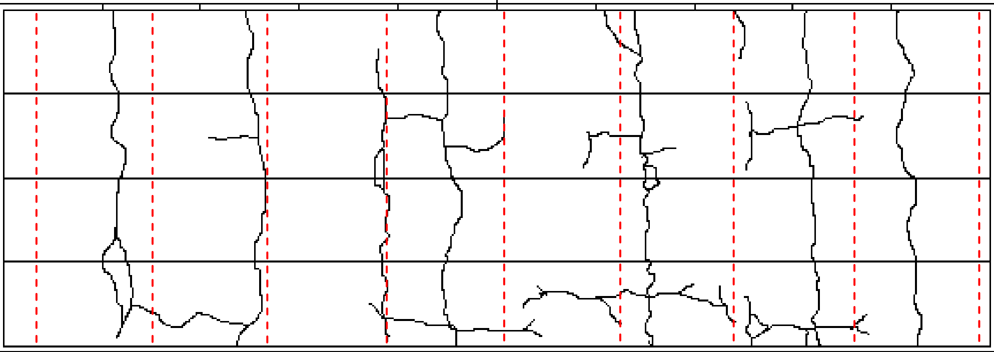

SS-5x23-150R_10S-TC	Geom: 5x23 mm²	f_c = 52,3 N/mm²	f_{ct} = 3,6 N/mm²
	σ_{cr} = 140,91 N/mm²	$s_{rm,50\%y}$ = 187,50 mm	$w_{rm,50\%y}$ = 0,25 mm

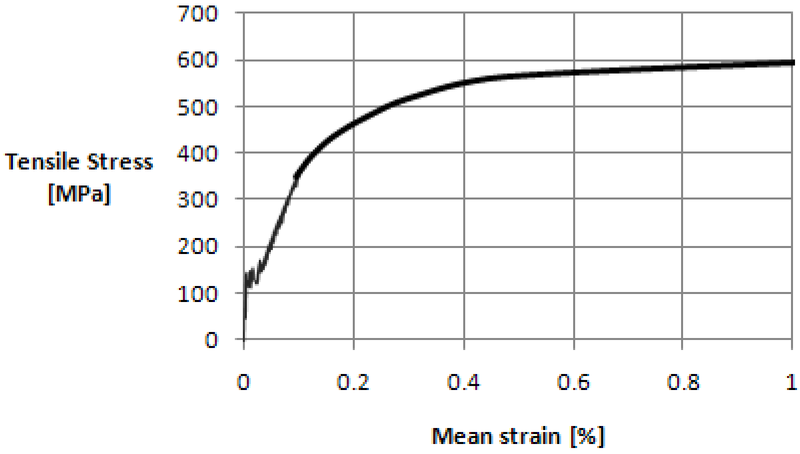

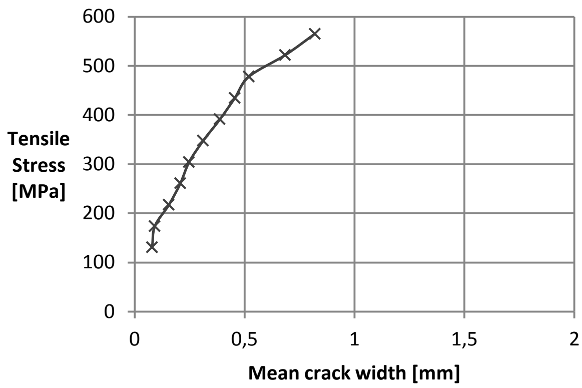

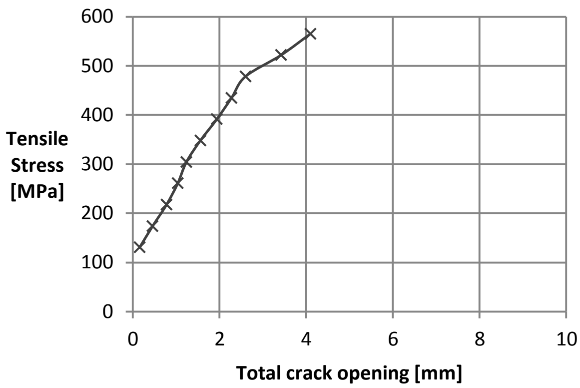

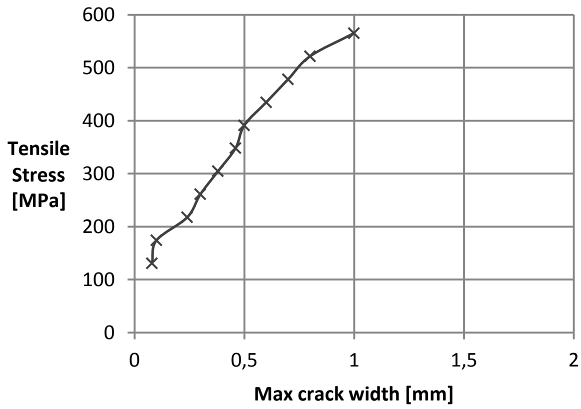

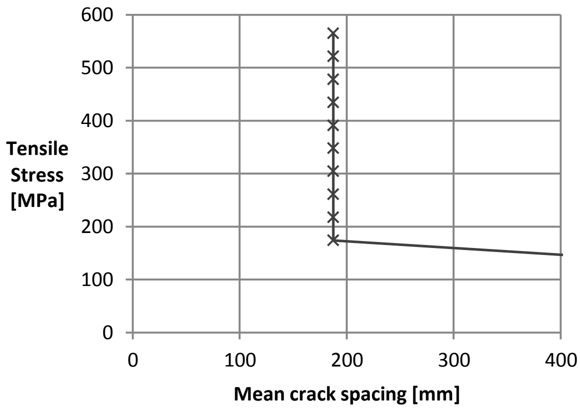

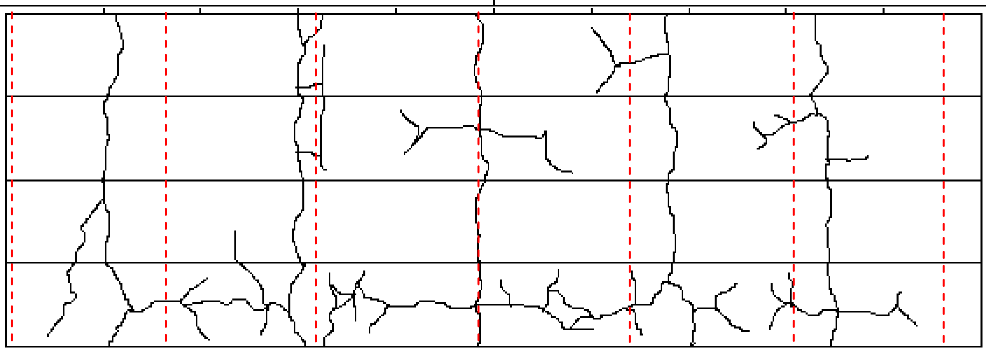

SS-5x23-150R_20S-TC	Geom: 5x23 mm²	f_c= 52,3 N/mm²	f_{ct} = 3,6 N/mm²
	σ_{cr} = 131,35 N/mm²	$s_{rm,50\%y}$= 160,00 mm	$w_{rm,50\%y}$ = 0,39 mm

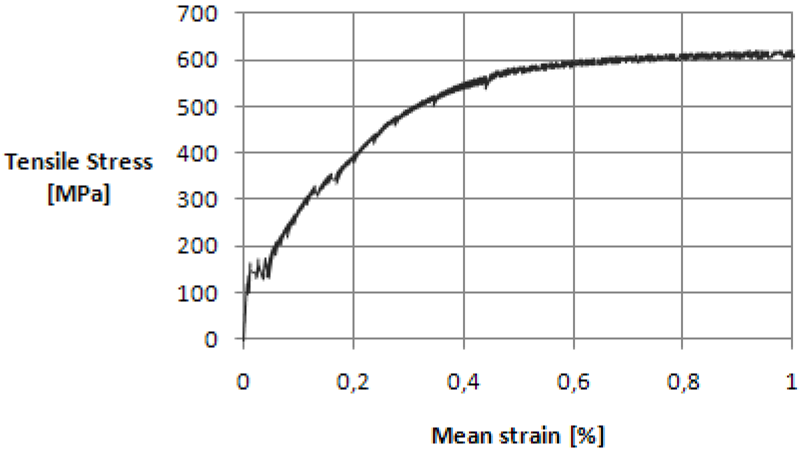

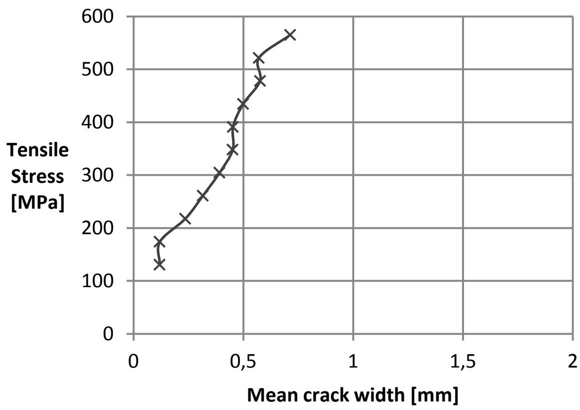

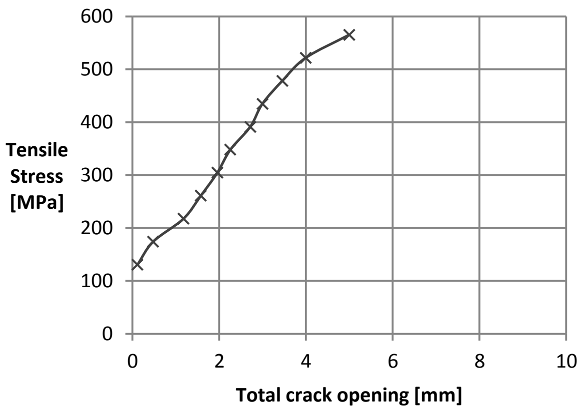

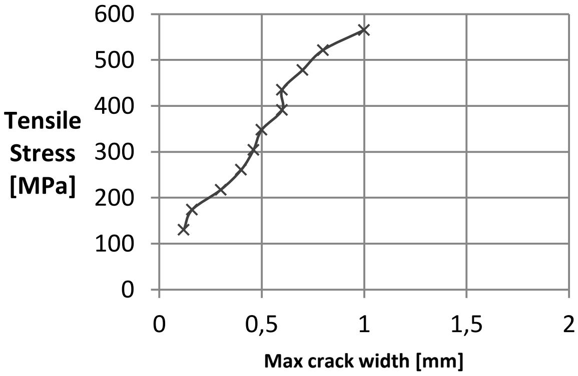

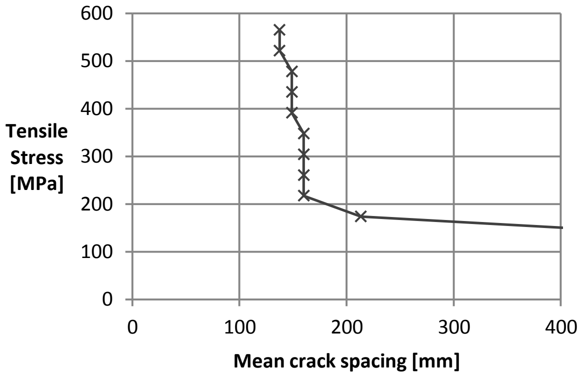

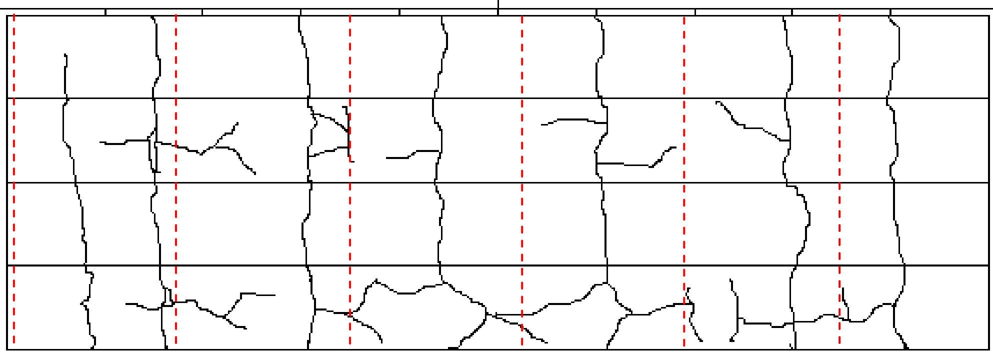

CS-Ø10-CR-SCC	Geom: Ø10 mm	f_c = 55,4 N/mm²	f_{ct} = 3,3 N/mm²
	σ_{cr} = 204,05 N/mm²	$s_{rm,50\%y}$ = 126,67 mm	$w_{rm,50\%y}$ = 0,15 mm

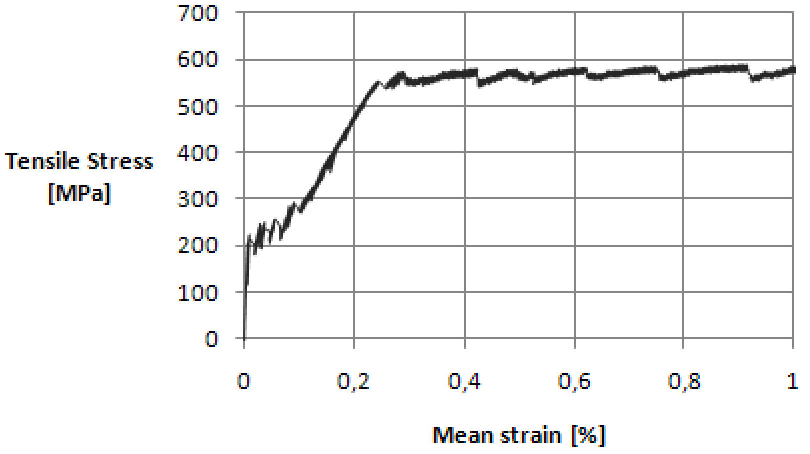

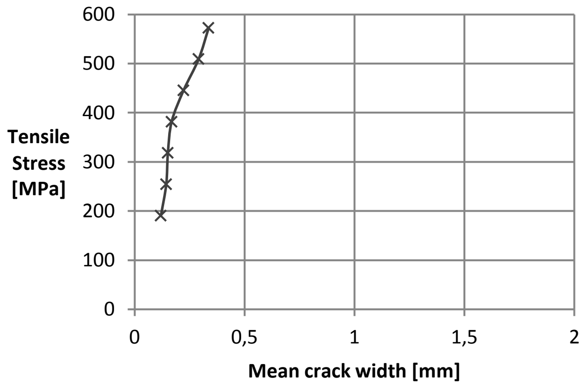

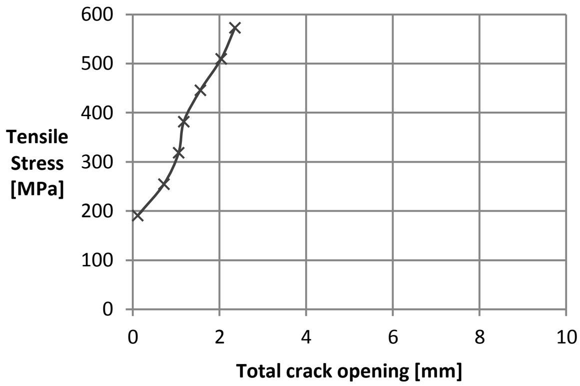

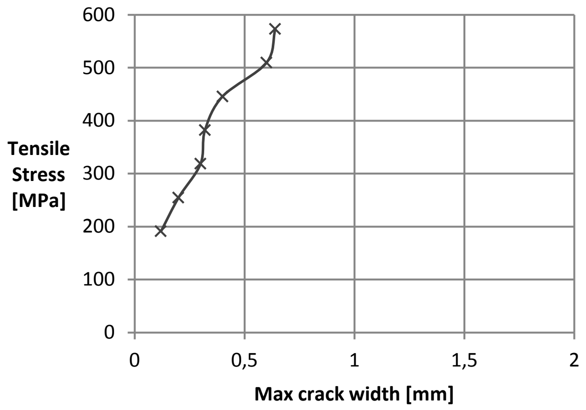

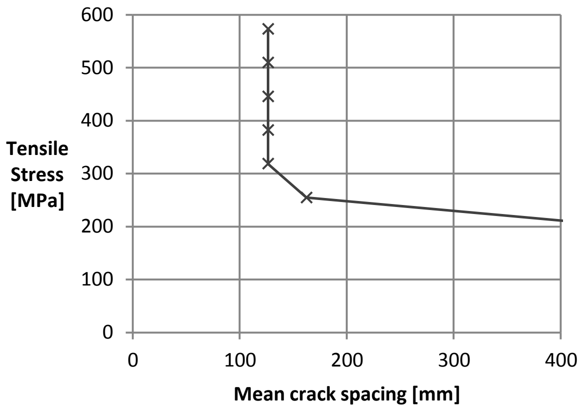

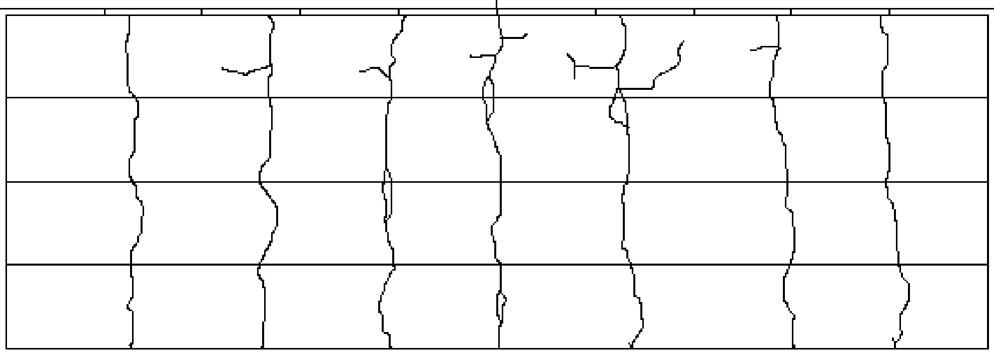

CS-Ø12-CR-SCC	Geom: Ø12 mm	f_c = 55,4 N/mm²	f_{ct} = 3,3 N/mm²
	σ_{cr} = 173,78 N/mm²	$s_{rm,50\%y}$ = 134,00 mm	$w_{rm,50\%y}$ = 0,22 mm

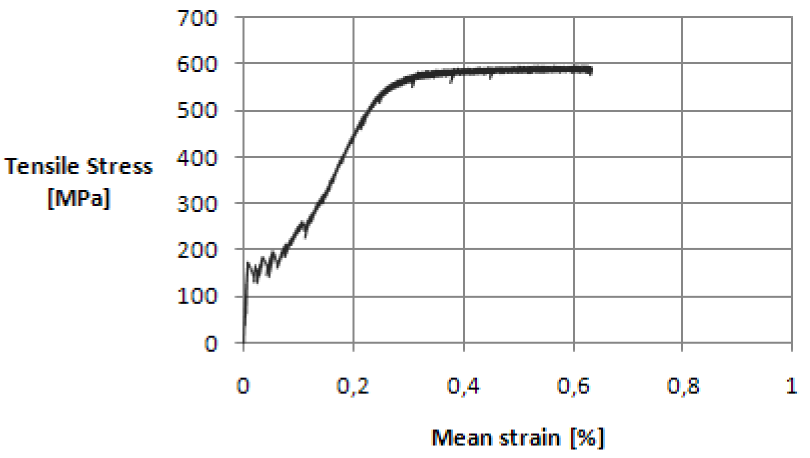

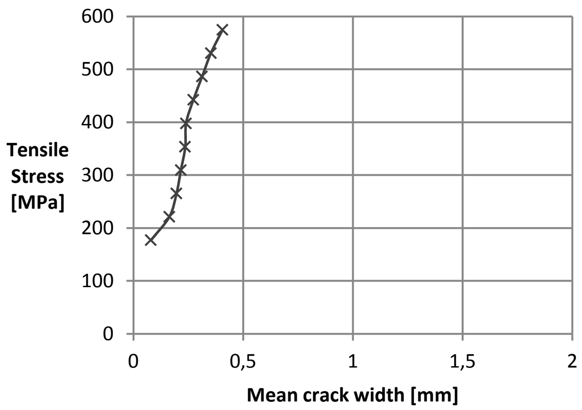

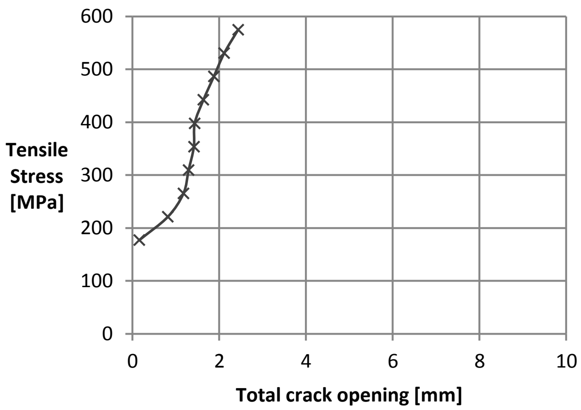

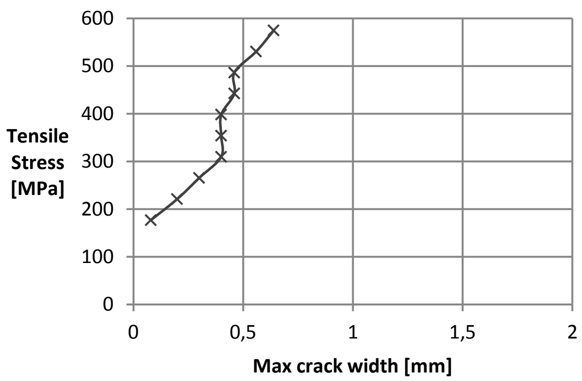

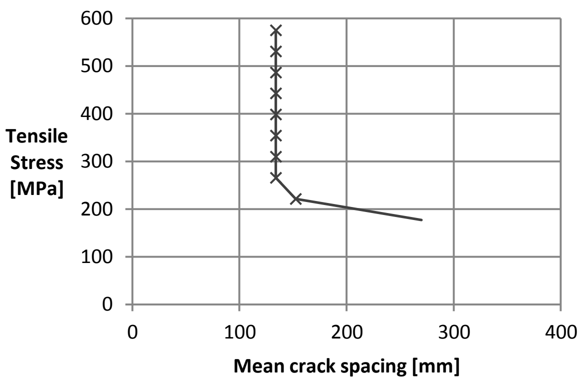

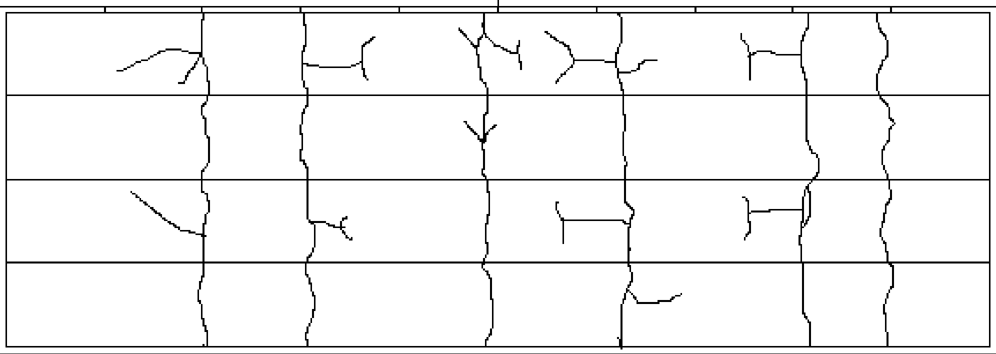

CS-3,5x25-CR-SCC	Geom: 3,5x25 mm²	f_c = 55,4 N/mm²	f_{ct} = 3,3 N/mm²
	σ_{cr} = 206,83 N/mm²	$s_{rm,50\%y}$ = 192,50 mm	$w_{rm,50\%y}$ = 0,50 mm

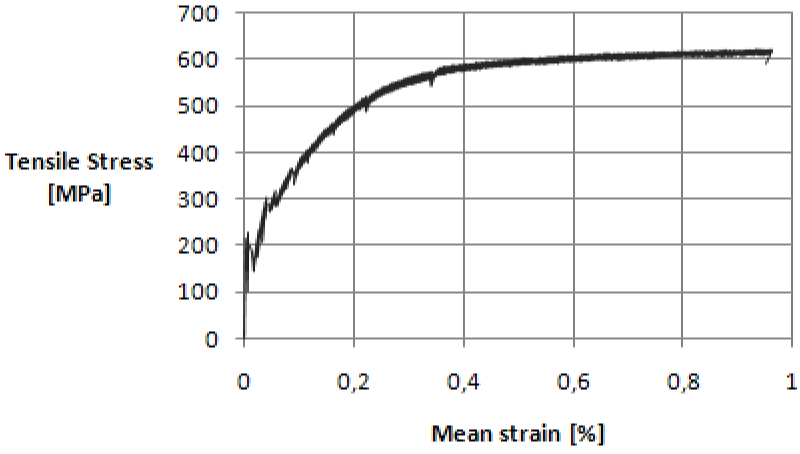

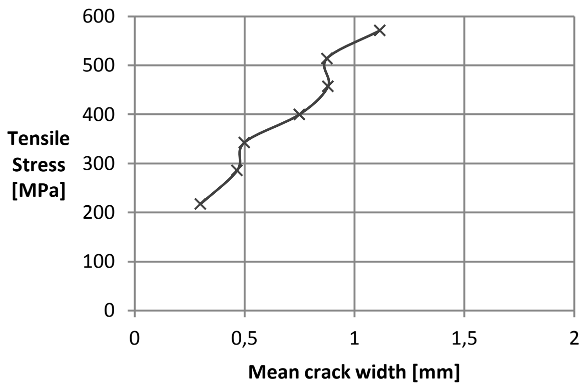

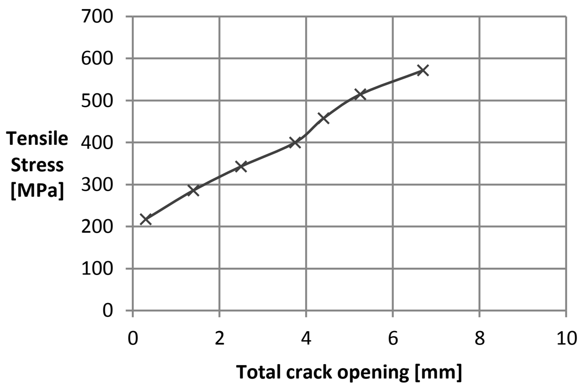

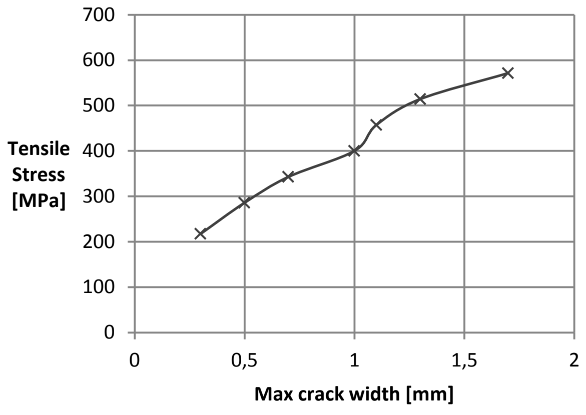

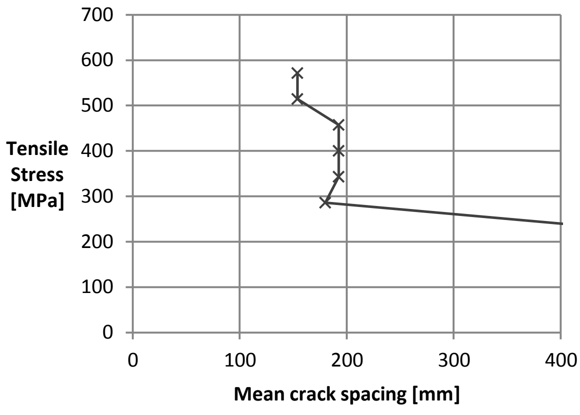

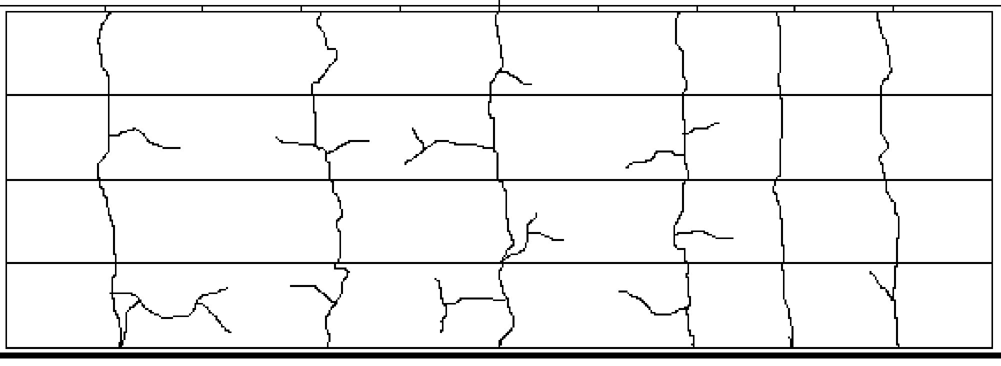

SS-5x23-CR-SCC	Geom: 5x23 mm²	f_c = 55,4 N/mm²	f_{ct} = 3,3 N/mm²
	σ_{cr} = 145,95 N/mm²	$s_{rm,50\%y}$ = 132,00 mm	$w_{rm,50\%y}$ = 0,53 mm

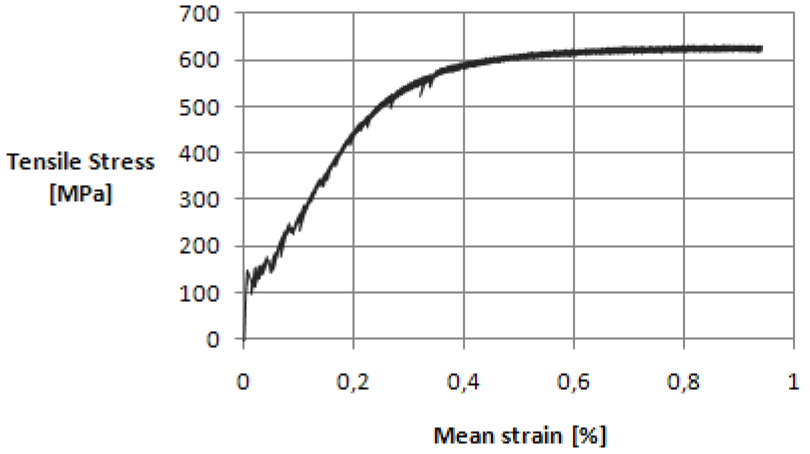

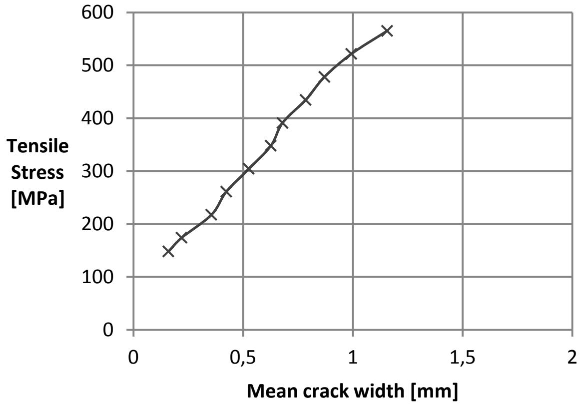

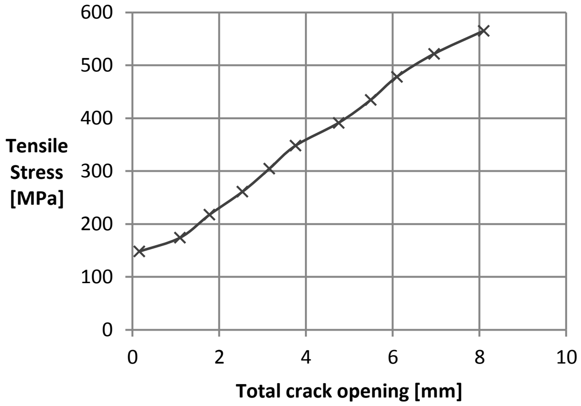

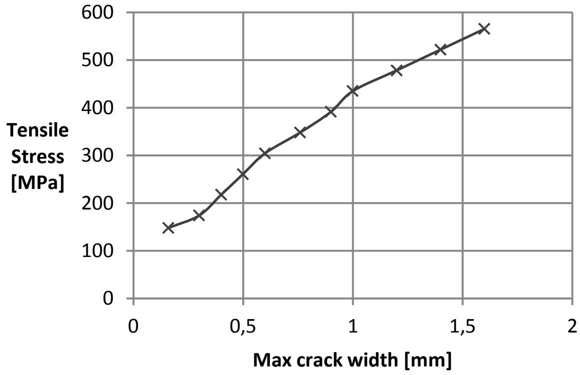

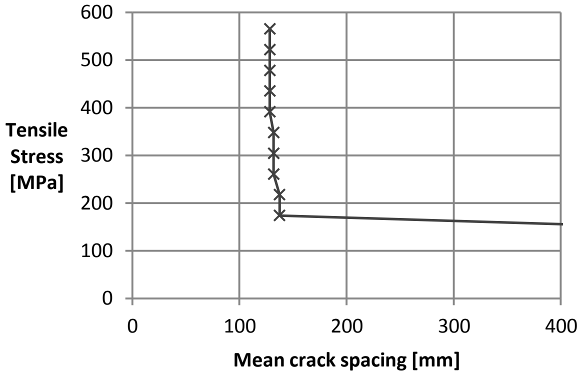

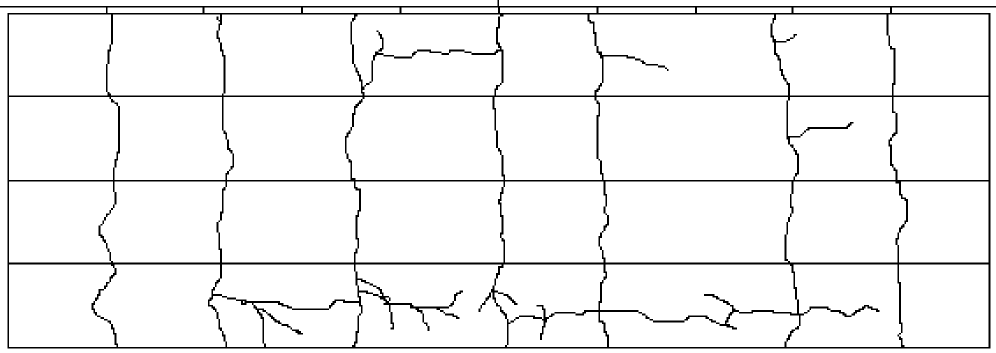

SS-5x23-100R_10S-SCC	Geom: 5x23 mm²	f_c = 55,4 N/mm²	f_{ct} = 3,3 N/mm²
	σ_{cr} = 160,55 N/mm²	$s_{rm,50\%y}$ = 165,00 mm	$w_{rm,50\%y}$ = 0,34 mm

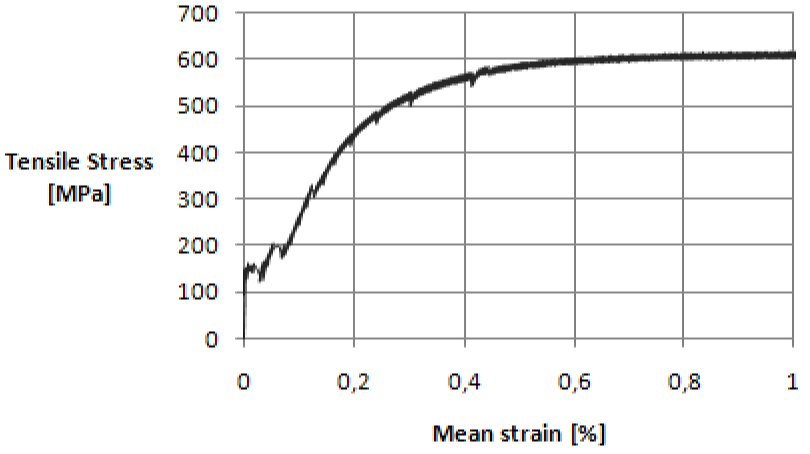

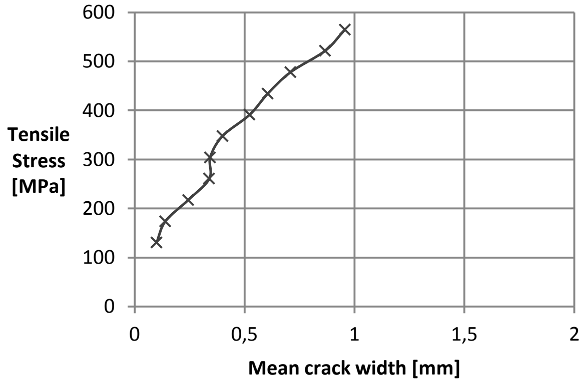

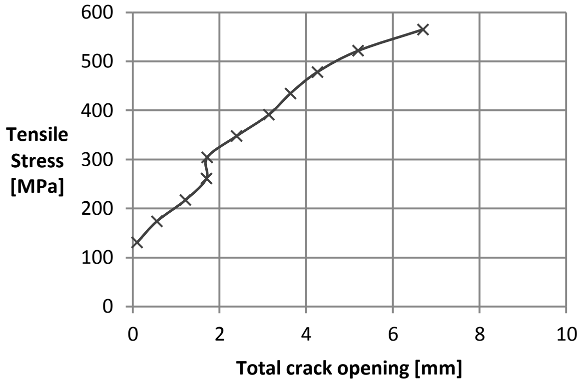

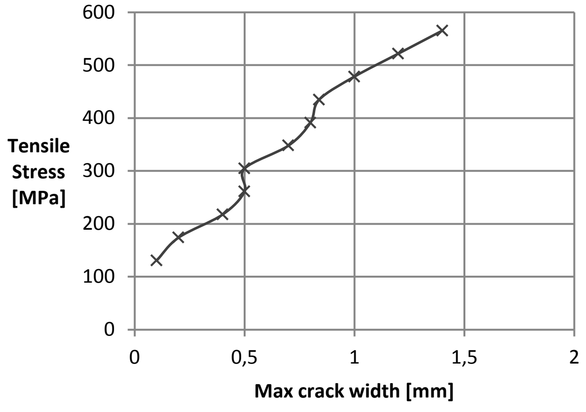

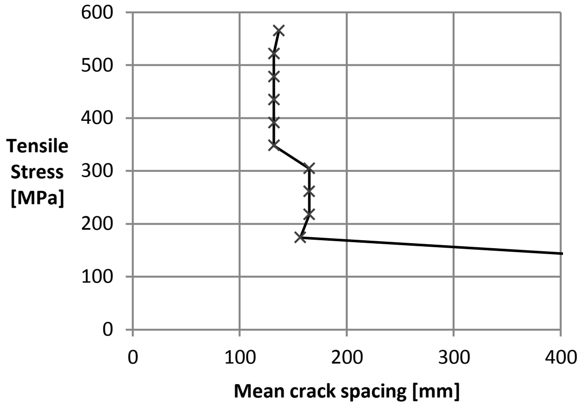

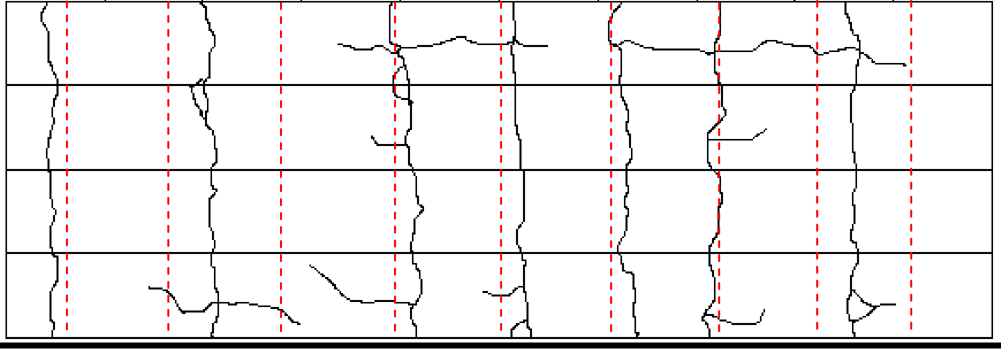

SS-5x23-100R_20S-SCC	Geom: 5x23 mm²	f_c = 55,4 N/mm²	f_{ct} = 3,3 N/mm²
	σ_{cr} = 155,24 N/mm²	$s_{rm,50\%y}$ = 157,50 mm	$w_{rm,50\%y}$ = 0,35 mm